Parametric fuselage design

Integration of mechanics and acoustic & thermal insulation

Parametric fuselage design
Integration of mechanics and acoustic & thermal insulation

Proefschrift

ter verkrijging van de graad van doctor
aan de Technische Universiteit Delft,
op gezag van de Rector Magnificus prof.dr.ir. J.T. Fokkema,
voorzitter van het College voor Promoties,
in het openbaar te verdedigen op vrijdag 4 september 2009 om 12:30 uur

door

Lars Adriaan KRAKERS
ingenieur in de luchtvaart en ruimtevaart
geboren te Hengelo ov

Dit proefschrift is goedgekeurd door de promotoren:
Prof.dr.ir. M.J.L. van Tooren
Prof.ir. A. Beukers

Samenstelling promotiecommissie:

Rector Magnificus,	Voorzitter
Prof.dr.ir. M.J.L. van Tooren,	Technische Universiteit Delft, promotor
Prof.ir. A. Beukers,	Technische Universiteit Delft, promotor
Prof.dr. D.G. Simons,	Technische Universiteit Delft
Prof.dr.ir. A.C. Nilsson,	KTH, Royal Institute of Technology
Prof.ing. M. Gennaretti	Roma Tre University
Prof.ir. E. Gerretsen	Technische Universiteit Eindhoven
Prof.dr.ir.drs. P. Krijgsman	The Odessa State Academy of Refrigeration

KEYWORDS: multidiscipline, parametric, fuselage, DEE

Printed in The Netherlands.

This research was partially financially supported by:
The European Commission, under the GROWTH programme, for the research project: ‘MOB, A computational design engine incorporating Multidisciplinary design and Optimisation for Blended wing body configuration’.
(Contract number G4RD CT1999-0172).

and the ‘Smart panels Project’ co-ordinated by TNO TPD, Department of active noise and vibration control, PO BOX 155, 2600 AD Delft, the Netherlands.

Contents

Acknowledgements

I would like to thank everyone who contributed in some kind of way in making the completion of this PhD possible. But I would like to express special thanks to:

My supervising professors; Michel van Tooren and Adriaan Beukers for the opportunity to do my PhD and for their guidance, inspiration, support and friendship. I have really enjoyed working at their research departments.

My fellow PhD students, with whom I worked in the same room for several years; Gianfranco la Rocca, Paolo Lisandrin and Ton van der Laan and my other colleages of the DAR group; Giampietro Carpentieri, Jochem Berents, Joost Schut, Chiara Cerulli and Marco Nawijn for their friendship and motivation and for creating a nice working atmosphere.

All the people from the structures and materials laboratorium for their support during my noisy measurements. Special thanks to Hans Weerheim and Bertus van de Stok, for their advise on, and the manufacturing of, the test set-up. Furthermore Michiel Haanschoten and Dylan Krul for their IT support and Lin Pijpaert and Lisette Volmer for their friendliness and administrative support.

During my PhD I have worked for the TU Delft in two projects. The first project was the European research project ‘MOB’ and the second was the TNO financed ‘Smart Panel’ project. I would like to thank both the MOB and Smart Panel teams for their cooperation and support.

I would like to thank prof. Pieter Krijgsman for his comments and editorial contribution, which made it possible to bring this dissertation up to the current level. Also I would like to thank prof. Anders Nilsson for his valuable comments on the acoustic subjects.

Last but not least I would like to thank my family for their support and motivation to finish this PhD research.

Summary

Designing a fuselage is a very complex process, which involves many different aspects like strength and stability, fatigue, damage tolerance, fire resistance, thermal and acoustic insulation but also inspection, maintenance, production and repair aspects. It is difficult to include all design aspects from the start of the design process.

In this research it is tried to find an answer to the question whether a Multidisciplinary Design and Optimisation (MDO) approach will lead to a better (lighter) fuselage design compared to the normally practiced sequential approach.

To find an answer to this question, a multidisciplinary design method is developed for fuselage design. Since fuselage design involves many aspects this research is restricted to the mechanical and the thermal and acoustic insulation aspects. Also the fuselage is simplified by excluding detail parts like windows and interior parts. In future research this could easily be extended by including more detail parts and considering other design aspects.

The multidisciplinary design method of a fuselage is given shape in the form of a Design and Engineering Engine (DEE). The DEE is an engineering tool that consists out of different computer tools linked together. The central heart of the DEE is the Multi Model Generator (MMG), which is a flexible parametric description of the fuselage geometry. The MMG consists of building blocks from which any type of fuselage configuration can be constructed. The input to the MMG is the definition of the input parameters that define the fuselage configuration. The user can specify which input parameters will be used as design variables. The outputs of the MMG are the different input models and/or data for the different analysis modules. The current DEE has four analysis modules that are explained briefly:

1.) The structural analysis module can analyse two different structural concepts; the stiffened skin concept and the sandwich skin concept. The stresses are determined with FEM analysis and are evaluated with strength, buckling and wrinkling criteria depending on the structural concept.
2.) The acoustical analysis module, which determines the TL, consists out of three parts. The first part is based on literature equations translated into a MATLAB script. The literature equations cover all insulation concepts that are involved for a fuselage wall. The sound insulation concepts that are involved are the single skin, influence of frames and stiffeners, circular resonance effects, the double wall principle, insulation blankets and visco-elastic damping layers. The second part consists out of a FEM natural frequency analysis and a FEM steady state dynamic analysis to determine the natural frequencies and sound pressure differences over the fuselage wall. Since the second part is quite time consuming this part is only used for the final optimum solution, while the first part of the acoustic analysis module is used during the optimisation loop of the DEE. The third part consists out of an active noise control module using piezoelectric actuators. This part has been developed in cooperation with TNO TPD within the ‘Smart Panel’ project. Unfortunately this part is not fully operational because this project was terminated before the DEE could be linked to the active noise control, prediction algorithms developed by TNO TPD.

3.) The thermal insulation module performs a FEM transient heat analysis on the fuselage wall. The inside surface of the fuselage wall is heated by a constant heat flux. The FEM solution shows equilibrium for the temperature difference between the inside and outside surface of the fuselage wall after a period of time. The magnitude of the equilibrium temperature difference is a measure for the thermal insulation of the fuselage wall.
4.) The weight module uses the geometric dimensions and material properties to determine the weight of each part of the fuselage and sums these weights to the final fuselage weight.

The genetic algorithm concept has been used to optimise the fuselage design. A Design Of Experiments (DOE) method is used to determine, with the DEE, a population of solutions. With this population, response surfaces are created that are used within the optimisation procedures. Validation calculations are performed with the DEE to check the optimum solution. If required a new population is created in the neighbourhood of the optimum solution to perform another optimisation step.

Two fuselage concepts for medium sized civil aircraft have been analysed with the developed DEE; the stiffened skin and the sandwich skin concept. In the analyses, both fuselages concepts were exposed to the same load case and boundary conditions. For the given load and boundary conditions, the DEE showed that the sandwich fuselage concept is slightly lighter compared to the stiffened skin fuselage. When considering minimum weight as the design objective the DEE showed that the MDO solution lies close to the sequentially optimised fuselage.

By using carbon/epoxy instead of aluminium, the largest weight improvement was achieved for the stiffened skin fuselage. These analyses showed that the multidisciplinary design method did not result in a drastically changed fuselage configuration.

The literature equations used in the acoustic module for the influence of the frames and stringers on the sound transmission loss on cylinders suggest that increasing the frame and stringer pitch will improve the sound transmission loss of the fuselage wall. To validate this, sound pressure difference measurements have been performed on cylinder walls with different stiffening. The experiments involved a non-stiffened cylinder, a cylinder with 6 stringers, a cylinder with 12 stringers and a cylinder with 12 stringers and 2 frames. No exact comparison between the measurements and the literature equations could be made. Therefore it is concluded that the literature equations are only indicative. For more accurate predictions more research and experiments are required.

The DEE proved to work successfully. It is a flexible knowledge engineering tool that easily can be extended with new analysis modules. In future work this tool could be updated with new analysis tools for more accurate calculations.

In conclusion the MDO approach did not deliver spectacular weight savings compared to the normally practiced sequential approach. The reason for this is that the design aspects strength and stiffness and the thermal and acoustic insulation showed little correlation. Perhaps by including more design aspects like impact resistance and fatigue into the DEE more advantage can be achieved with the MDO approach.

Nomenclature

Latin symbols

A	Cross section area	m^2
A_{flange}	Cross section area of frame flange	m^2
A_{fr}	Cross section area of frame	m^2
$A_{stiffness}$	Stiffness parameter	-
A_{str}	Cross section area of stringer	m^2
b	Width of a plate	m
b_{fr}	Frame width	m
b_{sk}	Width of skin strip between two adjacent stringers	m
b_{str}	Stringer width	m
C	Speed constant for viscoelastic layers	$m.s^{-1}$
C_{0}	Crimpling parameter	-
c_l	Longitudinal speed of sound of a material	$m.s^{-1}$
c_s	Speed of sound	$m.s^{-1}$
c_v	Specific heat at constant volume	$J.kg^{-1}.K^{-1}$
D	Bending stiffness of a plate per unit area	N.m
D_f	Bending stiffness of a facing	N.m
D_{ijkl}	Elastic stiffness matrix	$N.m^{-2}$
D_{ij}^{φ}	Piezo di-electric matrix	$C^2.N^{-1}.m^{-2}$
d	Total sandwich thickness	m
d_{bl}	Thickness of insulation blanket	m
d_{mkl}^{φ}	Piezo electric strain coefficient matrix	$m.V^{-1}$
d_w	Distance between two walls	m
E	Modulus of elasticity	$N.m^{-2}$
E_c	Core modulus of elasticity	$N.m^{-2}$
E_f	Facing modulus of elasticity	$N.m^{-2}$
E_{gen}	Energy generated within a control volume	J
E_{in}	Energy entering a control volume	J
E_m	Electrical flux vector	$V.m^{-1}$
E_{out}	Energy exiting a control volume	J
E_{skin}	Modulus of elasticity of skin	$N.m^{-2}$
E_{sto}	Energy stored within a control volume	J
E_{str}	Modulus of elasticity of stringer	$N.m^{-2}$
e_{mij}^{φ}	Piezo electric stress coefficient matrix	$C.m^{-2}$
F	Function value	-
f	Frequency	Hz
f_c	Critical frequency	Hz
f_{co}	Coincidence frequency	Hz
f_{max}	Maximum frequency for FEM analysis	Hz
f_{ring}	Ring frequency	Hz
G_c	Core shear modulus of elasticity	$N.m^{-2}$
H	Distance between center of facings	m
H_{fl}	Position of floor with respect to bottom of fuselage	m
H	Convection constant	$W.m^{-2}.K^{-1}$
h_{fr}	Frame height	m
h_{str}	Stringer height	m

$\vec{I}$	Sound intensity	$W.m^{-2}$
I	Moment of inertia	m^4
I_{yy}	Moment of inertia around Cartesian y-axis	m^4
I_{zz}	Moment of inertia around Cartesian z-axis	m^4
K	Extensional stiffness constant	-
K_c	Bulk modulus of sandwich core material	$N.m^{-2}$
K_{cr}	Crimpling constant	-
k	Wave number	$rad.m^{-1}$
k_{con}	Thermal conductivity	$W.m^{-1}.K^{-1}$
k_{cs}	Free propagating cylinder wave number	$rad.m^{-1}$
k_s	Cylinder circumferential wave number	$rad.m^{-1}$
k_{str}	Stringer cross section size factor	-
k_z	Wave number in z-direction	$rad.m^{-1}$
k_σ	Compressive buckling constant	-
k_τ	Shear buckling constant	-
L_{cil}	Cylinder length	m
L_{fr}	Frame pitch	m
L_{fus}	Fuselage length	m
L_I	Sound intensity level	dB
L_{max}	Maximum mesh size	m
L_p	RMS sound pressure level	dB
L_s	Noise spectrum level	$dB.Hz^{-1}$
L_T	Overall sound pressure level	dB
L_w	Fuselage wall thickness	m
M	Bending moment	N.m
M_m	Mach number	-
M_{cr}	Critical bending moment	N.m
m	Mass per unit area	$kg.m^{-2}$
m_{bl}	Mass per unit area of an insulation blanket	$kg.m^{-2}$
m_c	Mass per unit area of a sandwich core	$kg.m^{-2}$
m_f	Mass per unit area of a sandwich facing	$kg.m^{-2}$
N_x	Load at mesh nodes caused by a bending moment	N
$\vec{n}$	Normal vector to a surface	-
n	Number of waves around a circumference	-
$n_{elements}$	Number of mesh elements in circumference	-
n_{fr}	Number of frames	-
n_{min}	Minimum number of mesh elements per half sin wave	-
n_{str}	Number of stringers	-
P	Sound power	W
P_x	Axial load at mesh nodes caused by internal pressure	N
$\widetilde{p}$	Complex acoustic pressure amplitude	$N.m^{-2}$
p	Acoustic pressure	$N.m^{-2}$
p_0	Mean acoustic pressure	$N.m^{-2}$
$p_{pointload}$	Point load divided by outer fuselage surface	$N.m^{-2}$
p_{pore}	Numerical determined pressure at a FEM node	$N.m^{-2}$
p_{ref}	Just audible reference pressure	$N.m^{-2}$
p_{rms}	Root mean square pressure	$N.m^{-2}$
Q	Shear load	N
Q_{cr}	Critical shear load	N

Q_h	Volumetric heating rate	$W.m^{-3}$
Q_y	Shear load at mesh nodes in Cartesian y-direction	N
Q_z	Shear load at mesh nodes in Cartesian z direction	N
q	Heat flux	$W.m^{-2}$
q_s	Constant heat flux	$W.m^{-2}$
R	Fuselage radius	m
R_c	Critical load criteria	-
Re	Reynolds number	-
R_f	Flow resistance of a material	$N.s.m^{-4}$
R_{refl}	Reflection constant	-
R_{skb}	Skin buckling criteria factor	-
R_{skt}	Skin tensile criteria factor	-
R_{sqr}	Square error	-
R_{strb}	Stringer buckling criteria factor	-
R_{strt}	Stringer tensile stress criteria factor	-
S	Surface	m^2
T_{wav}	Wave period	s
T	Temperature	K
T_{tor}	Torsion moment	N.m
T_{cr}	Critical torsion moment	N.m
t	Time	s
t_1	Facing thickness	m
t_2	Facing thickness	m
t_c	Core thickness	m
t_{eq}	Skin thickness plus smeared stringer thickness	m
t_{fr}	Frame thickness	m
t_{plate}	Plate thickness	m
t_{sk}	Skin thickness	m
t_{str}	Stringer thickness	m
t_v	Thickness of visco elastic layer	m
U	Perimeter	m
u	Velocity in Cartesian x-direction	$m.s^{-1}$
V	Velocity	$m.s^{-1}$
V	Volume	m^3
V_c	Crimpling stress ratio	-
V_s	Torsion buckling parameter	-
$\vec{v}$	Particle velocity vector	$m.s^{-1}$
$\tilde{v}$	Complex particle velocity amplitude	$m.s^{-1}$
v	Velocity in Cartesian y-direction	$m.s^{-1}$
v_n	Normal velocity distribution of a panel	$m.s^{-1}$
W_{cil}	Cylinder weight	kg
W_{fus}	Fuselage weight	kg
W_{struc}	Weight of only the fuselage structure	kg
w	Velocity in Cartesian z-direction	$m.s^{-1}$
X	Shear parameter	-
x	Displacement in Cartesian x-direction	m
Y	Geometrical parameter	-
y	Displacement in Cartesian y-direction	m
Z	Coupling parameter	-

Z_{bl}	Characteristic impedance of insulation blanket	$kg.m^{-2}.s^{-1}$
Z_s	Torsion buckling parameter	-
$\tilde{z}$	Complex specific acoustic impedance	$kg.m^{-2}.s^{-1}$
z	Displacement in Cartesian z-direction	m
z_{ac}	Specific acoustic impedance	$kg.m^{-2}.s^{-1}$

Greek symbols

α	Attenuation constant	$dB.m^{-1}$
α_R	Rayleigh mass proportional damping factor	-
β	Circular angle	rad
β	Viscoelastic loss factor	-
β_R	Rayleigh stiffness proportional damping factor	-
δ^*	Boundary layer thickness	m
ε	Emissivity constant	-
ε_{kl}	Strain tensor	-
ϕ	Phase angle	rad
γ	Crimpling constant	-
γ_s	Torsion buckling constant	-
η	Structural loss factor	-
η_c	Sandwich core loss factor	-
η_{eq}	Equivalent loss factor	-
η_p	Plasticity reduction factor	-
φ	Incident angle	rad
φ_m	Microphone position	degrees
λ	Wave length	m
λ_m	Wave length of sound within an insulation blanket	m
ν	Poisson ratio	-
ν_c	Core Poisson ratio	-
θ	Temperature difference	K
ρ	Density	$kg.m^{-3}$
ρ_0	Mean density	$kg.m^{-3}$
ρ_{fr}	Frame material density	$kg.m^{-3}$
ρ_{sk}	Skin material density	$kg.m^{-3}$
ρ_{str}	Stringer material density	$kg.m^{-3}$
ρ_{sw}	sandwich parameter	m
σ	Stefan Bolzman constant	$W.m^{-2}.K^{-4}$
$\sigma_{b\ skin}$	Skin buckling stress	$N.m^{-2}$
σ_{cri}	Crimpling stress	$N.m^{-2}$
σ_{Euler}	Euler buckling stress	$N.m^{-2}$
$\sigma_{flanges}$	Stringer flange buckling stress	$N.m^{-2}$
σ_{Hoop}	Hoop stress	$N.m^{-2}$
σ_{ij}	Mechanical stress tensor	$N.m^{-2}$
σ_{max}	Maximum allowable tensile stress	$N.m^{-2}$
σ_{rad}	Radiation efficiency	-
$\sigma_{skt\ max}$	Maximum allowable skin tensile stress	$N.m^{-2}$
$\sigma_{strt\ max}$	Maximum allowable stringer tensile stress	$N.m^{-2}$

σ_w	Wrinkling stress	$N.m^{-2}$
τ	Transmission loss coefficient	-
$\tau_{b\ skin}$	Skin shear buckling stress	$N.m^{-2}$
τ_{cr}	Critical shear stress	$N.m^{-2}$
τ_d	Transmission loss coefficient under field incidence	-
Ω	Dimensionless frequency	-
ω	Angular frequency	$rad.s^{-1}$
ω_c	Critical angular frequency	$rad.s^{-1}$
ω_{co}	Coincidence angular frequency	$rad.s^{-1}$
ω_{ring}	Angular ring frequency	$rad.s^{-1}$
ξ_i	Critical damping factor of mode i	-

Abbreviations

ABAQUS©	Commercial FEM tool
ANOVA	Analysis of variance
APE	Average percentage error
APU	Auxiliary power unit
CAD	Computer aided design
CFRP	Carbon fibre reinforced plastics
DEE	Design and engineering engine
DOE	Design of experiments
EA	Evolution algorithm
EASA	European aviation safety agency
EP	Evolution programming
ES	Evolution strategy
FAA	Federal aviation administration
FEM	Finite element method
FFT	Fast fourier transform
FML	Fibre metal laminate
FRP	Fibre reinforced plastics
GA	Genetic algorithm
GLARE	Glass fibre reinforced aluminium
GP	Genetic programming
ICAD©	Commercial knowledge based engineering tool
IGES	Initial graphics exchange specification
KBE	Knowledge based engineering
MATLAB©	Commercial numerical computing tool
MDO	Multi disciplinary design and optimisation
MMG	Multi model generator
MTOW	Maximum take of weight of an aircraft
OEW	Operating empty weight of an aircraft
OTL	Overall sound transmission loss
PZT	Lead zirconate titante
RBF	Radial base function
RMAE	Relative maximum absolute error
RMS	Root mean square
RPK	Revenue per passenger kilometer
SA	Stochastic algorithm

SQP	Sequential programming
TL	Sound transmission loss
TNO TPD	Dutch research company

1 Introduction

1.1 History of fuselage design

Since the Wright brothers made their first powered flight on December 17th 1903 (figure 1.1), the fuselage has undergone some drastic design changes. The fuselage of the Flyer I was nothing more than a structure consisting out of wooden struts, steel brackets and diagonal tension wires to accommodate the wing, control surfaces and a place for the pilot. Comfort and safety for the pilot was not an issue during these first attempts to manned, powered flight.

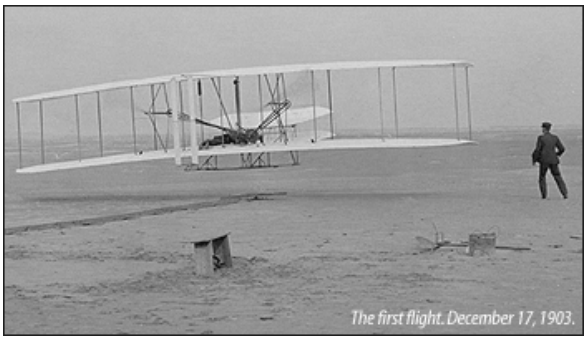

Figure 1.1: *First successful powered flight of Wilbur and Orville Wright on December 17, 1903. [www.aviationhistory.info]*

Figure 1.2*: Fokker D.VII (January, 1918); Steel framework fuselage covered with fabric. [www.aviation-history.com]*

For the aircraft of WW I, which were already capable of flying at considerable speed and altitude, the wooden struts and steel wires were replaced by a welded steel truss structure with a textile fabric as cover material. An example of this type of aircraft is the Fokker D.VII developed in 1918 (figure 1.2).

In the period between 1920 and 1930 flying became a means of transportation for a larger public by the development of the first passenger aircraft of which the Fokker F-7 is an example (figure 1.3). These aircraft also used welded framework structures together with plywood and fabric covering. Comfort and safety were still not very important aspects at that time. The main fuselage design requirements were sufficient strength and stiffness at minimum weight.

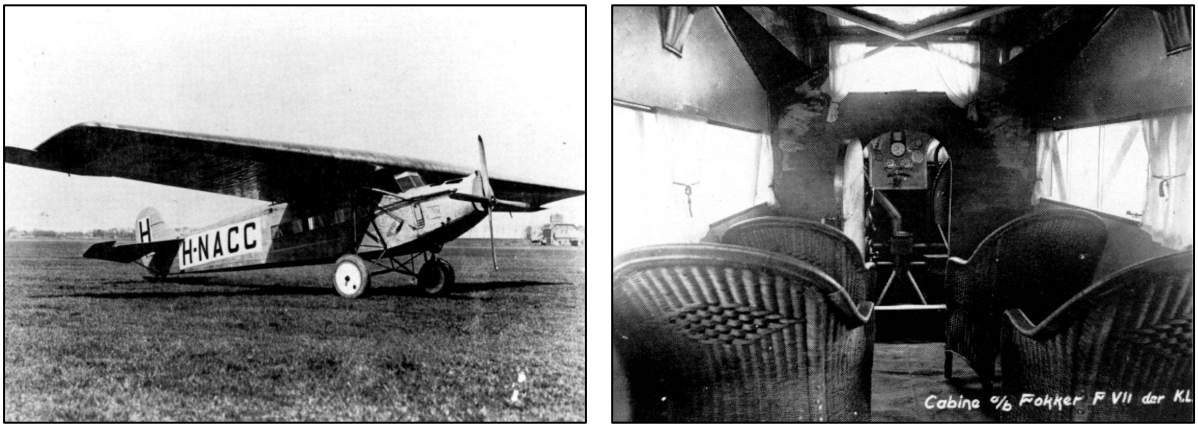

Figure1.3: *Fokker F-7; example of a passenger aircraft with a welded framework structure and a plywood/fabric covering developed in 1924. [www.dutch-aviation.nl]*

At the end of the thirties, aluminium started to take over the role of wood and steel as primary material in aircraft. The all-metal, stressed skin structure became the standard in aircraft industry. Simultaneously, the airplane configuration was adapted to the new structural concept, as were the fabrication methods. A well-known example of the first generation all-metal stiffened skin fuselage aircraft is the Douglas DC-2, 1933 (figure 1.4).

Figure1.4: *DC-2; Example of a first generation aircraft with an aluminium stiffened skin fuselage. [www.stinsonflyer.com]*

Figure 1.5: *Modern aluminium stiffened skin fuselage of a Boeing 747. [www.airplanemart.com]*

The results of the introduction of the pressurised aluminium fuselage concept were rather spectacular. Within a relatively short period of time it became possible to transport more passengers over greater distances, faster, at higher altitudes and, therefore, with more comfort. The first steps to modern air traffic were taken. These steps marked the beginning of a long lasting evolution of the aluminium airplane

structure and resulted in the nowadays aircraft like the Boeing 747 (figure 1.5). A typical interior of a modern passenger aircraft with an aluminium-stiffened skin is shown in figure 1.6.

Figure 1.6: *Typical interior of a modern passenger aircraft with an aluminium stiffened skin fuselage structure. Boeing 747.* [www.wikimedia.org]

This evolution has lead to the current (over)-optimised stiffened skin structure, for which only extensive protection measures, inspection programs and maintenance programs, can guarantee the ever increasing requirements on comfort, reliability and durable safety. Still, it was tried to further optimise the aluminium stiffened skin structures at the cost of large investments by, among other ways, applying new alloys without a clear improvement of the cost efficiency.

Because cost efficiency is the most important drive to switch to new design concepts, a short description is given of the economic situation of airline companies during the last decades. A market study on aircraft utilisation, performed by Boeing, showed that during the seventies, eighties and nineties the airlines were facing a continuous decrease in profit per aircraft seat. This is illustrated in figure 1.7. Reasons for the decrease of the profit per passenger seat during this period were, among others, the increase in competition due to the open-skies-policy and the increased cost of personnel, airports and fuel. Like discussed before, the (over)-optimisation of the stiffened skin fuselage structure resulted in an increase of the maintenance and manufacturing costs. This was highly in contrast with the development of manufacturing costs of most other technical products like cars and consumer electronics, for which the price/performance ratio was continuously improving. Nowadays however, also for these products the room for improving the manufacturing costs by automation is reaching its limits.

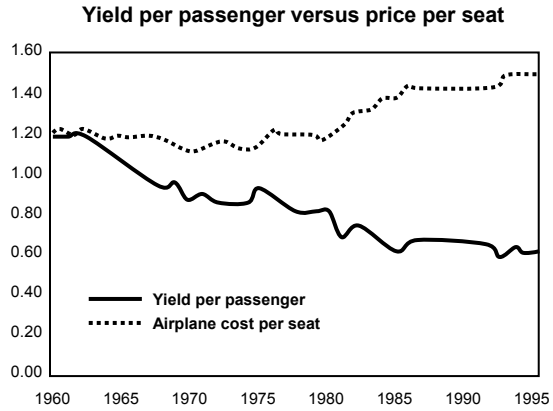

Figure 1.7: *Trend in cost and revenue of passenger transport.*
[Boeing on WAC congress Oct. 1996]

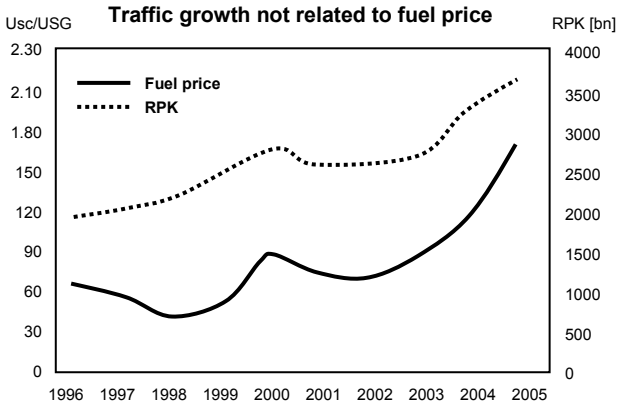

Figure 1.8: *Trend of the fuel price and revenue passenger kilometer.*
[www.rolls-royce.com]

Another market study performed by Rolls-Royce [1] showed that in the last decade, when disregarding the increase in fuel price, the revenue per passenger kilometer (RPK) improved again. The tendency of RPK and the fuel price during the last decade are displayed in figure 1.8. The increase of the RPK can be partly explained by the introduction of the low budget companies, which were able to improve the yield per passenger by reducing the operating costs. This was achieved by the introduction of internet ticket services and by using airports with lower take-off and landing fees. Quite often, communities around local airports make it attractive to airline companies to use their airports because it can boost the local economy. To give head to the explosive increase in fuel price many airline companies introduced fuel surcharges.

Besides reducing the operating cost like the low budget companies do, it can be concluded that to make the aircraft industry more profitable, it will be necessary also to improve the maintenance, manufacturing and purchase cost of that aircraft. This will only be possible when switching to new design concepts using new materials and construction methods.

These developments can be characterised with the product life cycle curve like is shown in figure 1.9, van Tooren [2]. In this figure the technological life cycle of products in general, and of aluminium stiffened skin structures specifically, is presented in a simplified manner. The product life cycle can be divided in four phases, i.e. development, expansion, consolidation and decline.

For aluminium stiffened shell structures the initial development took place around the Second World War. In the following period this combination of material and structural concept found its application in almost all civil aircraft.

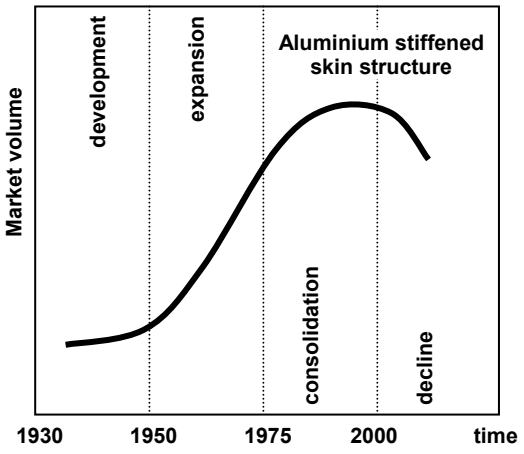

Figure 1.9: *Product life cycle. [2].*

This phase is characterised by a fast development coupled with a large expansion of the number of applications. In the last twenty years, however, the development has reached its consolidation phase. Progress has slowed down considerably and only at the cost of large investments some progress is gained. Considering this development as decline, the final phase of this combination of material and type of structure can be expected in the coming years. Currently attempts are made to achieve a jump to a new product life cycle with the introduction of new materials and construction types. Starting point for this has to be the drive to improve the performance per unit cost of this combination. It is believed, already for quite some time, that new composite materials like Fibre Reinforced Plastics (FRP) and Fibre Metal Laminates (FML) are very good candidates to achieve a jump to a new life cycle curve.

Currently the large aircraft companies are producing the first aircraft that are designed and build with FRPs and/or FMLs. Some illustrations will be given later in this section. First, it will be tried to explain why it took the aircraft industry about thirty years to seriously introduce new materials such as the FRPs and FMLs with corresponding new structural concepts. Compared to the fast introduction of aluminium, several reasons can be identified for the slow introduction of composites in the civil aircraft industry:

- The aluminium alloys entered the aircraft structure in what where still the pioneering days of aviation. Mistakes were made with sometime disastrous results, due to lack of knowledge of the material behaviour and little or no experience with the new structural concept. These mistakes, however, did not frustrate the further development of metal technology. On the contrary, they were accepted and acted as a stimulus for new developments. A characteristic example is metal fatigue. The rather sudden confrontation with this dangerous phenomenon started research on a very large scale. It has contributed much to the improvement of flight safety. In the last few decades, however, aviation has scaled up enormously and modern aviation has become an ordinary, common way of transport like buses and railways. It cannot allow itself risky experiments with new technologies. The phase-in period of a new technology, therefore, has become very long.
- Wood as a structural material persisted until the Second World War, when the ‘Mosquito’ airplane was probably the most sophisticated representative of engineering design with this material. Nevertheless, the first aluminium alloy structures had to compete generally against rather primitive structures. Hence, their starting point was favourable and they could take over easily. The starting point of composite structures, however, is not so favourable. They have to compete against the metal structure, which has become very efficient itself after a long period of development. Moreover the production systems are dedicated to the metal technology. The price of change is not easily paid without a real prospect of immediate reduction of production and operational costs.
- In the twenties, the fabrication techniques and joining methods for thin aluminium sheets were available. The manufacturing processes for composites had (and partly still have) to be developed first. Thermoset-based composites are created simultaneously with the structure, which has complicated the development of manufacturing processes considerably. Also the wide, still increasing variety of composites plays a role in this respect. There is now a tendency to use thermoplastic-based composites. They require completely different fabrication

methods. It is obvious that there are still no widely accepted, easily available processes.

- In the introductory period of metals, there was no well-defined safe design philosophy. It was developed simultaneously and in strong relation with the metal structures themselves. Composites are now confronted with this well-established safety philosophy and related requirements. These requirements, however, are typically metal based and, therefore, cannot simply be applied to composites. An example is the damage tolerance design philosophy, which relies on the concept of slow crack growth, a phenomenon that is characteristic for the metals used in airplane structures. Composites do not show this phenomenon, nevertheless they can be damaged seriously. So questions arise of how to deal with damage and how to guarantee a sufficient safety level for a sufficient period of time. Until now composites have been quite appropriately approached in a very conservative manner, with “knock down’ factors for the strength and limited allowable strains putting these materials in a rather disadvantageous starting position.
- Of course, the limitations of the composites themselves also obstructed a rapid breakthrough of the new technology. Amongst these, the susceptibility to operational impact damage, the large localized damage from lightning strikes, the uncertainties regarding repair techniques, and the price of the material are the most important.
- Finally, there is the predicted structural weight saving itself. Structural weight saving has often been related, almost exclusively, to reduced fuel consumption and not to improvement of flight performance in a more general sense. The required levels of flight performance of future aircraft will, undoubtedly, only be reached due to the application of new technologies. Weight reduction will be an important key in that sense. Structural weight saving for reduced fuel consumption as such, however, is not a convincing argument for the industry to change. The often-predicted 30% weight reduction results in a reduction of the direct operating costs of only 5%. Of course this number depends on the price of fuel; nevertheless, it is not very convincing, especially not if it is easily nullified by a higher purchase price of the airplane.

  It is obvious that a more realistic estimation for the weight reduction, for instance 10% for primary structures such as wings and fuselage, decreases the reduction of the operating costs proportionally. It makes weight reduction an even less convincing argument for the introduction of a new technology. With the development of composite technology, therefore, much more emphasis should be put on two other elements of the operating costs, which can be influenced directly, namely the cost of ownership and the maintenance costs.

Up to recently, most attempts to introduce composites in aircraft structures were limited to the substitution of metals with composites without the introduction of innovated structural concepts and manufacturing methods. The desired and possible jump in price performance ratio, therefore, was only partially achieved. Currently the number of composite components in aircraft is steadily increasing. This is illustrated for the Airbus A380 and the Boeing 787.

Airbus A380:

Figure 1.10 shows the application of composites in the Airbus A380, which is a large sized double deck aircraft that ultimately will be able to accommodate 550 passengers. Like most aircraft up to now, composites are applied in the empennage, the passenger cabin floors, the control surfaces and the high lift devices, which are all non-primary structural parts. However for the A380 also primary structural parts like the central torsion box and the vertical and horizontal stabilizers are made of Carbon Fibre Reinforced Plastics (CFRP). The upper part of the fuselage is made out of GLARE, which is a Fibre Metal Laminate (FML) that consists of alternating layers of thin aluminium alloy sheets (0.2 to 0.5 mm) and prepreg made of glass fibre and epoxy adhesive as illustrated in figure 1.11. Glare is less troubled by metal fatigue and less prone to damage than aluminium on its own. GLARE has been developed at the Delft University of Technology.

The Airbus A380 made its first test flight in April 2006 as is illustrated in figure 1.12 and went into service in 2008. An impression of the economy class interior of the A380 of Singapore Airlines is also illustrated in figure 1.12.

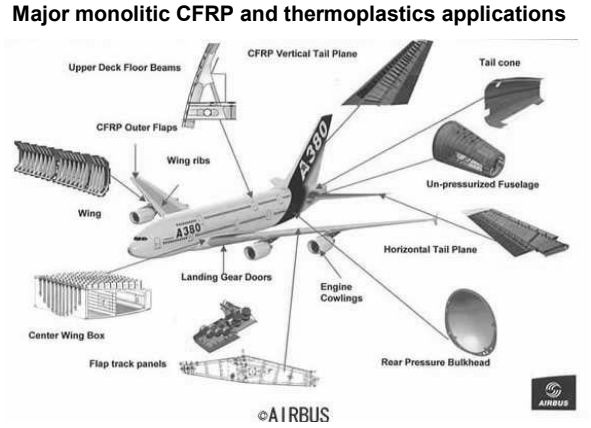

Figure 1.10: *Composite materials used in the Airbus A380.* *[www.carbonfiber.gr.jp]*

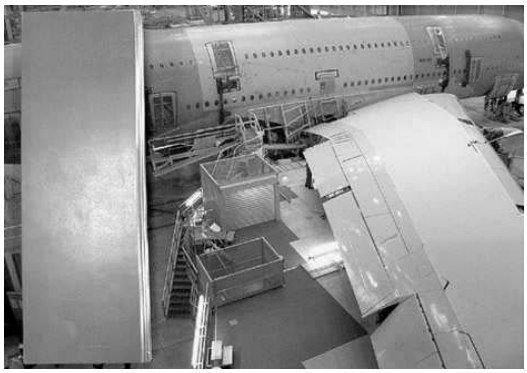

Figure 1.11: *Glare: alternating layers of aluminium and glass epoxy sheets.* *[www.core77.com]*

Figure 1.12: *Singapore Airlines Airbus A380 March 2008 together with an impression of the economy class interior. The fuselage partially made out of GLARE, which is a laminated material made out of aluminium and glass fiber layers.* *[www.hemmy.net]*

Boeing 787:

Boeing is developing the 787, which is an all-new airplane that incorporates lots of new technology in the design [3]. About 50 percent in weight of the primary structure, including the fuselage and wing, will be made of composite materials (Figure 1.13). This makes it possible to manufacture one-piece fuselage sections, as illustrated in figure 1.15, which eliminate 1,500 aluminum sheets and 40,000 - 50,000 fasteners [3]. Boeing expects that the Boeing 787 will have considerable lower maintenance cost as is illustrated in figure 1.14, where the maintenance cost are compared to the all-metal Boeing 767. The Boeing 787 will be fitted with Rolls-Royce and General Electric turbofans that are much more fuel efficient than the engines on earlier widebody aircraft. All in all it is expected that the economics of this new design will be much improved compared to its all-metal competitors.

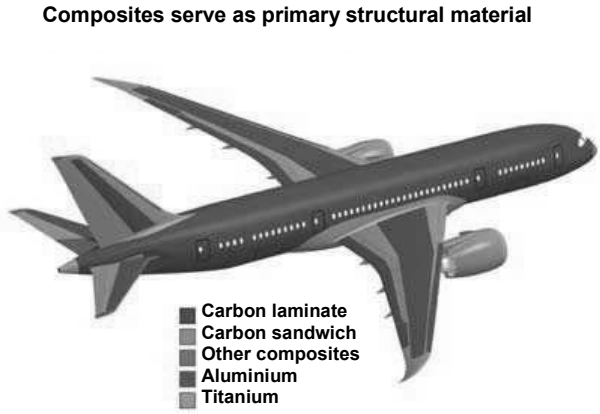

Figure 1.13: *Composite materials used in the Boeing 787.* *[www.specialchem4adhesives.com]*

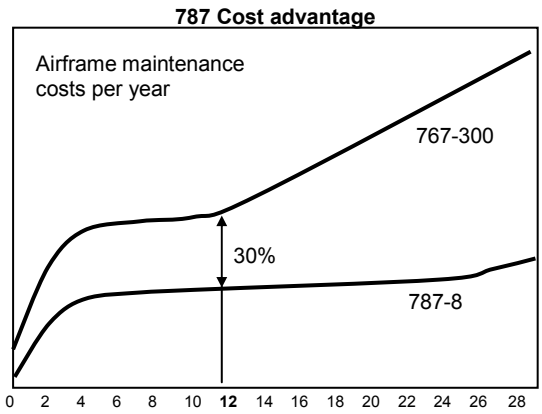

Figure 1.14: *Reduction of maintenance cost predicted by Boeing.* *[www.widebodyaircraft.nl]*

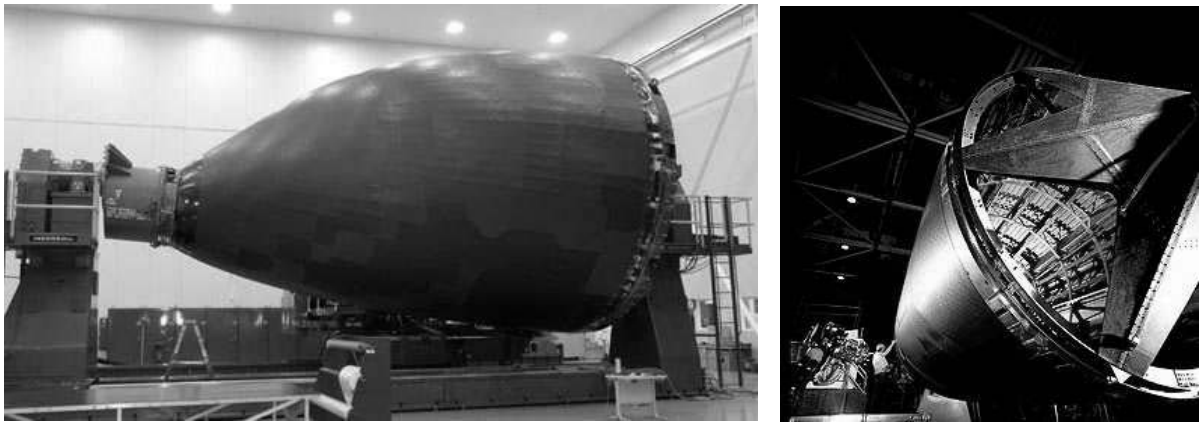

Figure 1.15: *Production of one-piece fuselage parts for the Boeing 787 made of Carbon fiber reinforced plastic.* *[www.boeing.com]*

Besides the weight-advantage of composites also new structural possibilities like larger windows will be possible, which can contribute to the passenger comfort. Figure 1.16 shows a possible interior of the Boeing 787, which also has larger windows.

Figure 1.16: *The Boeing 787, which will have a full composite fuselage. The application of CFRP opens new possibilities like larger windows. [www.boeing.com]*

In other products of the aircraft industry, like helicopters, military aircraft, sailplanes and general aviation, the necessity and attractiveness of a jump onto a new product life cycle curve has been long acknowledged. In these industrial areas the leap from full metal aircraft designs to fully composite ones has already been made. Not only the increase in performance but mainly the improvement in price performance ratio was the main argument for the introduction of composites in these sectors. In the military aircraft industry the necessity of a further technological jump for advancement is always being felt.

The lead of the general aviation is caused by the fact that the manufacturing technology necessary for its jump was already at hand. At the top level of the general aviation market the sandwich concept, autoclave techniques and the thermoset prepregs can be combined. This has lead e.g. to the Beech Starship. (See figure 1.17). The potential of composite materials becomes clear when a traditional fuselage of Beech is put against the fuselage of the Starship, which is illustrated in figure 1.18. It has to be noted that the complexity of the metal solution shown here is limited since it is not a pressurized fuselage, in contrast to the one of the Starship. The Starship concept is also used in the business jet; the Raytheon Premier I, which is manufactured by tape laying.

Figure 1.17: *The Beech Starship. [www.bobscherer.com]*

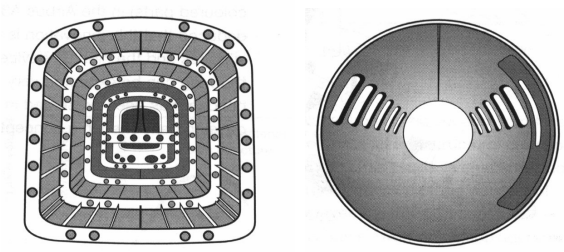

I II

Figure 1.18:
I Traditional fuselage of Beech
II Beech starship fuselage [2]

For the small aircraft industry in general, and also for the sailplane industry, autoclave technology is not common practice. Hand lamination, vacuum bagging and oven curing for this industry is a more cost effective manufacturing method. Main advantages compared to the metal structures are the feasibility of parts integration, the limited tooling cost and the very smooth outer surface. With respect to the first advantages, small composite aircraft look like plastic aircraft model kits.

1.2 Multidisciplinary fuselage design

Like discussed in the previous section the starting point for the choice of new combinations of materials, structural concepts and manufacturing technology has to be the improvement of the cost efficiency. A very good method to achieve this is by integration of functions [4, 5]. For fuselage design one can think of functions like integrety (strength, stiffness & vibrations), durability (fatigue, corrosion & damage tolerance) and survivability (crash & fire damage resistance and thermal & acoustical insulation). Figure 1.19 shows schematically that, compared to metals, new materials like composites are much more suitable for integrating functions.

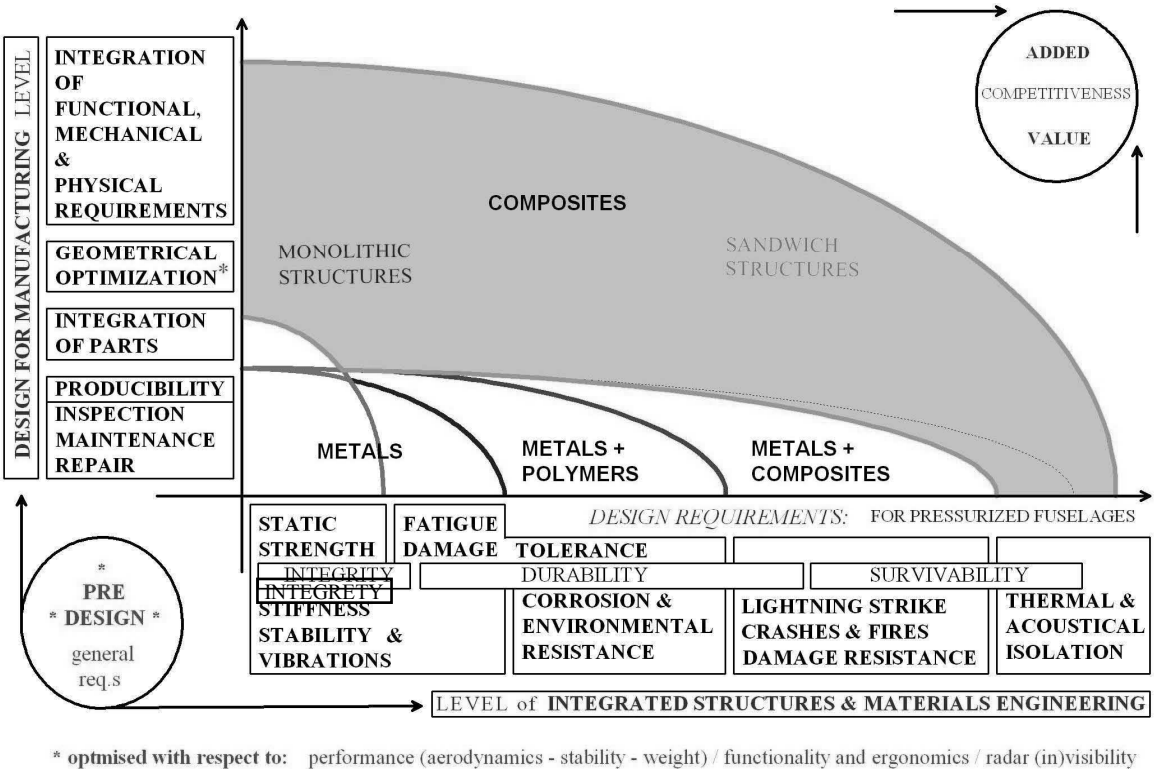

Figure 1.19: *Design requirements for pressurized fuselages. [2].*

Figure 1.19 can be interpreted as follows:

Along the X-axis the most important design requirements for pressurised fuselages are shown. Going from left to right on the X-axis the level of integration of design features in the structure is increasing. To allow for such a representation an arbitrary choice has been made for the integration order. E.g. it is assumed that the

strength and stiffness requirements always need to be fulfilled while thermal and acoustical properties are not necessarily integrated in the design but can be handled separately by adding non-structural items. Integration up to and including the required thermal and acoustical behaviour in the structure is therefore considered advanced, and the integral fulfilment of acoustical requirements is placed right from those of stiffness and strength on the X-axis.

On the Y-axis of figure 1.19 design requirements related to manufacturing are shown. Again a choice has been made for the integration order. The integration of producebility is trivial and therefore the first item on the axis. The other items related to manufacturing are integration of parts, inspectability, maintainability and repairability.

The curves in the diagram illustrate which functions can be integrated in the fuselage design when the fuselage is constructed out of the material mentioned within the areas bounded by the curves. The ultimate integration is considered the fulfilment of all physical requirements during manufacturing together with all stability, durability and survivability requirements.

1.3 Purpose of this research

So far the history of fuselage design has been discussed. It was concluded that the introduction of aluminium, which happened relatively fast, caused a large improvement in performance and comfort. A similar jump for improved operating cost was expected for the introduction of composites. However, the introduction of composites happened relatively slow. Several reasons were identified for this slow introduction. As a result it was concluded that to make the introduction of composites in fuselage design successful, it should be tried to integrate design requirements. Composites are the perfect concept to do this.

In this research it is tried to improve the fuselage design by integrating different design requirements from the start of the design process. Since fuselage design is a comprehensive design process involving many aspects like; strength & stability, corrosion, fatigue, damage tolerance and thermal & acoustic insulation, this research will be limited only to the integration of the trivial strength and stiffness requirements together with the thermal and acoustic insulation requirements. Also the detail parts like windows in interior parts are not included in the fuselage models. The reader should be aware of these limitations and therefore the conclusions have to be considered in this context. Although this research does not include all design requirements it shows the possibility of multidisciplinary design.

A second target of this research is the automation of the design process by using knowledge based engineering principles (KBE) for the development of a computer design tool. It is tried to capture the design process in different computer programs that are linked together with a master script. To be able to do this a general parametric geometrical model of the fuselage structure is defined. From this general model, sub-models are extracted that are used in separate analysis modules. Each module analyses a different design requirement. By using evaluation and optimisation techniques like genetic algorithms and response surfaces an optimum solution can be found for a pre-determined set of design variables.

The content of this research is structured as follows: Because in this research the thermal and acoustic insulation requirements of the fuselage structure are

considered, first a small overview is given of the thermal conditions and acoustic noise sources that act on a fuselage during operation. This is done in chapter 2. Next, the theory of acoustic insulation, thermal insulation and the theory to satisfy the mechanical requirements are discussed in chapters 3, 4 and 5 respectively. Chapter 6 and 7 handle the description of the computer design and engineering tool. Chapter 6 discusses the parametric definition of a fuselage model together with the different analysis modules and chapter 7 discusses the optimisation techniques. Chapters 8 and 9 will verify the Design & Engineering tool with some experimental tests and chapters 10 and 11 give a discussion of two applications. Finally section 12 discusses some future applications and gives some concluding remarks and recommendations.

1.4 Reference

[1] Market Outlook 2006-2025, Rolls Royce, www.rollce-royce.com
[2] Van Tooren, M.J.L., Sandwich fuselage design, 010 publishers Rotterdam, 1998.
[3] www.Boeing.com
[4] Beukers, A., van Tooren, M.J.L., de Jong, Th., Multidisciplinary design philosophy for aircraft fuselages, Part I, Applied composite materials, p 3-11, vol 12, nr 1, Springer, 2005.
[5] De Jong, Th., Beukers, A., van Tooren, M.J.L., Two simple design problems, which illustrate the multidisciplinary design concept, Part II, Applied composite materials, p 13-19, vol 12, nr 1, Springer, 2005

2 Acoustic & thermal requirements

2.1 Introduction

Like discussed in the introduction it used to be common in aircraft fuselage design that the acoustic and thermal requirements are fulfilled after meeting the mechanical requirements. By taking the acoustical and thermal requirements into account already from the beginning, the design could result in a better (lighter) fuselage. Because of the continuously increasing demand on improved passenger comfort, the multidisciplinary approach can offer more opportunities for a more comfortable design.

This chapter gives a short overview of the acoustical and thermal insulation requirements for passenger aircraft. Section 2.2 discusses the noise sources that are important for the noise transmitted through a fuselage wall. An indication of noise comfort levels and the human perception of noise is given in section 2.3. This results in the sound transmission loss requirements for a fuselage wall. Section 2.4 describes the thermal conditions, which an aircraft is subjected to during a flight. In this section also the thermal passenger comfort levels and the resulting thermal insulation requirements are discussed. Finally section 2.5 gives some conclusions with respect to the acoustic and thermal requirements.

2.2 Identification of noise sources

During a flight with an airline aircraft, passengers are subjected to interior noise caused by different noise sources. In this section the focus will be on the noise sources that are important for fuselage cabin interior noise. For convenience, a division is made between noise sources that act from the inside or the outside on the fuselage. A third group is noise caused by the airframe itself. A few examples of these three groups are:

1.) Noise sources that act from within the fuselage on the fuselage wall are the air-conditioning system, APU, hydraulic systems within the fuselage and the retraction and extraction mechanisms of the fuselage landing gears.
2.) Examples of noise sources that act from outside on the fuselage wall are engines, hydraulic systems inside the wing and tail, turning spindles to drive flaps, speed breaks and landing gears located in the wings.
3.) An example of airframe noise is noise caused by the turbulent boundary layer of the air flowing over the fuselage skin.

In this research, the acoustical insulation of the fuselage wall is considered. Therefore the noise sources within the fuselage will be neglected. Also noise sources like the retraction of flaps, speed breaks and landing gears will not be considered. These noise sources are not that annoying to passengers because of their incidental character. This leaves two main noise sources that are important for the sound transmission through the fuselage wall: the turbulent boundary layer noise, which will be discussed in section 2.2.1 and noise generated by the engines, which is discussed in section 2.2.2.

2.2.1 Turbulent boundary layer noise

Fuselage airframe noise is generated by the turbulent boundary layer of the air flowing over the outside fuselage skin. The turbulent boundary layer pressure fluctuations constitute an important source of cabin noise during cruise [4]. Since the late fifties extensive research is performed on turbulent boundary layer noise [1,2,3]. A recent EU research program [4], showed that the current models for modelling the turbulent boundary layer excitation of structures are still inadequate.

A fairly simple model of the turbulent boundary layer noise is given by ESDU [5,6]. This model cannot be used as an excitation model for turbulent boundary layer noise like the models presented by [1,2,3,4], but it gives a first impression of the noise levels generated by a turbulent boundary layer. The ESDU sheets [5,6] give an empirical equation for the turbulent boundary layer noise spectrum:

$$L_s = L_1 - L_2 + L_3 - 10\log_{10} V/\delta^* \qquad (2.1)$$

Where:

- L_s: Noise spectrum level [dB/Hz] of the fluctuating pressure at a certain position in length direction of the turbulent boundary layer.
- L_1: Component depending on the Reynolds and Mach number.
- L_2: Component depending on altitude.
- L_3: Component depending on the Strouhal number ($f\delta^*/V$) where f is the frequency, δ^* is the boundary layer thickness and V the free stream velocity.

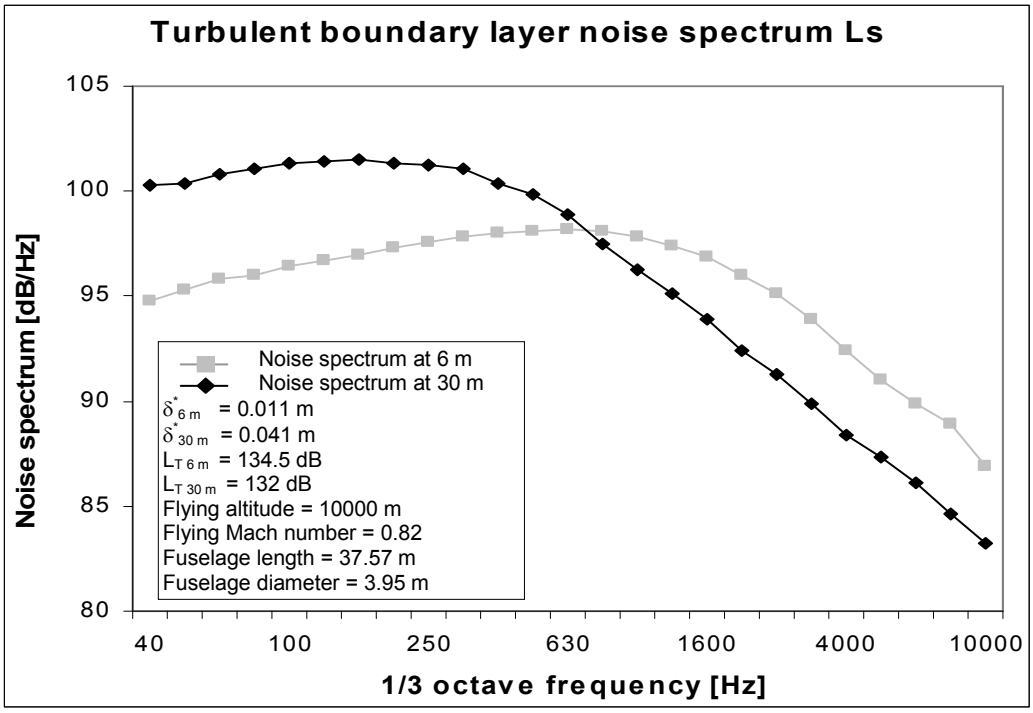

Figure 2.1: *Turbulent boundary layer noise spectrum L_s of an A320 like fuselage at 6 and 30 m from the nose. Dimensions of the A320 are taken from Jane's [7].*

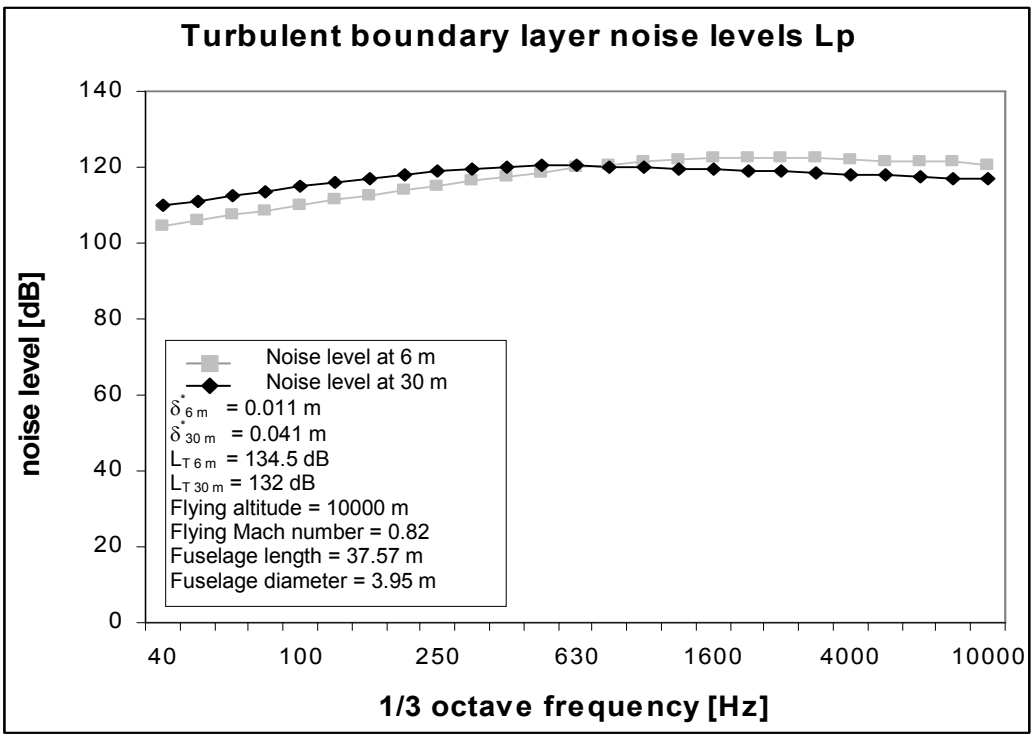

Figure 2.2: *Turbulent boundary layer noise spectrum L_p of an A320 like fuselage at 6 and 30 m from the nose. Dimensions of the A320 are taken from Jane's [7].*

Figure 2.1 shows that the noise level of the turbulent boundary layer along the fuselage is depending on the flying speed, flying altitude, Reynolds number, frequency and the thickness of the boundary layer. The thickness of the boundary layer is dependent on the position along the fuselage

Figure 2.2 gives an illustration of the noise spectrum (L_S) determined with the ESDU sheets. The noise spectrum L_s is determined at two points alongside a fuselage that has dimensions similar to the fuselage of an Airbus A320. The sound pressure level L_{pi} in [dB] can be obtained by integrating the noise spectrum L_{si} over the frequency range i, which results in the following relation:

$$L_{p_i} = L_{s_i} + 10\log_{10}(\Delta f_i) \tag{2.2}$$

Here Δf is the width of the frequency band over which the noise spectrum is integrated. The resulting sound pressure level per one-third octave is displayed in figure 2.3. The overall turbulent boundary noise (L_T) in dB can then be determined by:

$$L_T = 10\log_{10}\sum_{i=1}^{n} 10^{(L_{Pi}/10)} \tag{2.3}$$

Here n is the number of noise sources (In this case equal to the number of one-third centre frequencies that are considered). From the calculations it is found that the overall sound pressure level L_T of the turbulent boundary layer noise decreases a bit from 134.5 dB at the front of the passenger cabin (6 m from the nose) to 132 dB at the end of the passenger cabin (30 m from the nose). The average overall sound pressure level of the turbulent boundary layer noise that acts on an A320 like fuselage can be estimated between 130 and 135 dB.

By comparing the noise spectrum at 6 m from the nose with the noise spectrum at 30 m from the nose, as is illustrated in figure 2.2, it can be observed that the noise spectrum present at the rear of the fuselage is more dominated by the lower frequencies compared to the noise spectrum close to the nose of the fuselage. This can be explained by the increasing boundary layer thickness (0.011 m at 6 m from the nose compared to 0.041 m at 30 m from the nose) allowing larger wavelengths and therefore lower frequencies.

All in all, the turbulent boundary layer noise level can be considered as noise with a relatively constant overall sound pressure level of around 133 dB.

Methods to reduce the turbulent boundary layer noise

Ways to reduce the turbulent boundary layer noise would be to fly at lower speeds and higher altitudes. Normally this is not an option because the flying speed and altitude are important performance criteria that determine the flight time and fuel consumption and therefore the operation costs.

Another possibility to reduce noise of the turbulent boundary layer is the addition of a ‘shark skin’ coating to the outer fuselage surface. The ‘shark skin’ coating is a coating with grooves in the air flow direction. Airbus industry has performed several studies to reduce the turbulent boundary layer noise and the aerodynamic drag by adding high durability plastic films that smooth the airflow or keep it laminar on larger parts of the airframe surfaces [8].

The airflow can also be kept longer laminar with the use of boundary layer suction. This concept is currently tried on sailplanes [9] but has not been proven yet on full scale airline aircraft.

Another large contribution to airframe noise, is noise from extracted landing gears. This noise can be reduced with the addition of fairings.

In this research the addition of a 'shark skin' coating, boundary layer suction and fairings are not considered.

2.2.2 Noise from the engines

Noise generated by the engines can reach the inside of the passenger cabin through several paths as is illustrated in figure 2.3:

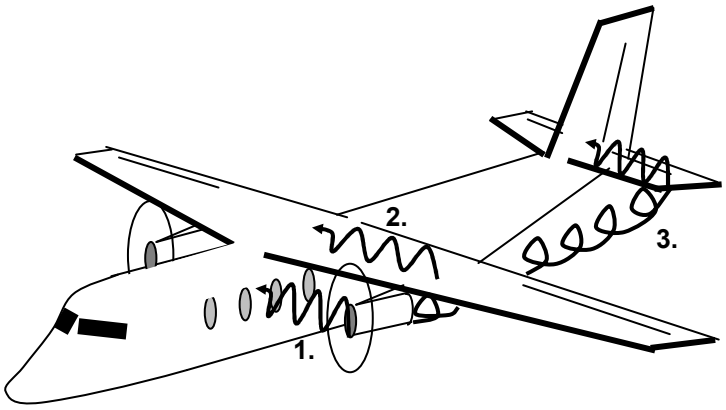

Figure 2.3: *Three noise paths from the engine to the fuselage*.

- Direct excitation of the fuselage by the exhaust noise downstream, and noise from the compressor and propellers upstream, the so-called airborne transmission path. (Path 1).
- Mechanical vibrations of the aircraft engine that are transmitted through the wing structure to the fuselage, the so-called structure borne transmission path. (Path 2).
- Mechanical vibrations that are caused by the impingement of the airborne noise from the engine on the wing and tail surfaces, which are then transmitted through the structure to the fuselage. (Path 3, which is also a structure borne transmission path).

The position of the engines can have several acoustic considerations. For aircraft with a low wing configuration and engines positioned below the wing, the wing can mask a part of the noise from the engines. Similarly the engines could be positioned on top of the wing for high wing configurations. Another common position of the engines is in the empenage, which reduces the excitation of the fuselage by the exhaust noise (path 3 does not exist) and path 1 is not directly near the passenger cabin. However, the structure born transmission path 2, becomes shorter.

There are different types of engines used for passenger aircraft. The two main groups are propeller and jet engines. Both types of engines have different characteristics with respect to noise, which will be discussed separately.

Jet aircraft

Medium range passenger aircraft are usually equipped with turbofan engines with high by-pass ratios. Two main noise sources of the turbofan engine are the 'turbulent mixing' noise and the "buzz saw" noise.

- The turbulent mixing noise is the noise that occurs when the exhaust stream mixes with the external air. The acoustic power of the turbulent mixing noise is approximated by [10]:

$$\frac{\rho_j V_j^{\ 8} D^2}{c_s^5} \tag{2.4}$$

Where: ρ_j: Density of jet stream
V_j: Jet stream velocity
D: Diameter of jet nozzle
c_s: Speed of sound in ambient air

Considering an Airbus A320, the overall sound pressure level of the turbulent mixing noise at cruise speed (M = 0,82) would vary between 130 dB and 145 dB depending on the relative position to the engine. The ESDU sheets [10] describe that also the sound pressure as a function of frequency varies with the relative position to the engine. In general it can be said that the 'amplitude' of the sound incident on the fuselage skin varies along the fuselage and therefore results in areas inside the fuselage, which are relatively quiet or noisy.

- The "buzz saw" noise is caused by the passage of the fan-, compressor- and turbine- blades, which generate pressure waves. The "buzz saw" noise is characterized by a series of pure tones at the Blade Passage Frequencies (BPF), which equals the number of blades times the number of rotations per second and its higher harmonics. The larger size of the fan blades (larger pressure waves) and the lower angular velocity of the fan (BPF of fan in range of the audible frequency range), are the cause that the noise of the fan blades will be dominant compared to the noise of the compressor and the turbine blades. For a turbofan engine with 36 fan blades running at 8000 rpm the BPF becomes 4800 Hz. Roozen [11] showed that in the inlet more pure tones exist besides the ones at the BPF. The extra pure tones in the inlet are caused by the shock waves of the (supersonic) tip speed of the fan blades.

Propeller aircraft

For propeller aircraft, the peaks of the buzz saw noise occur at lower frequencies and are more dominant because of the larger size of the propeller blades and the lower rpm. Also because propellers are not enclosed with any housing, the noise is especially loud in the propeller plane, like is shown in figure 2.6. For example for the propeller engines of the Fokker 50 that have 6 blades and run at 1020rpm the first BPF is 102 Hz (figure 2.4).

Because the blades rotate in a plane perpendicular to the fuselage, the pressure waves that hit the fuselage will be largest in or close to this plane. This is also illustrated in figure 2.5, which shows the interior noise levels of the Fokker 50. Close to the propeller plane the noise levels are the highest. It also can be noticed that the passengers are seated as much as possible in the areas where the noise levels are relatively low. The toilets and galleys are positioned in the noisy areas.

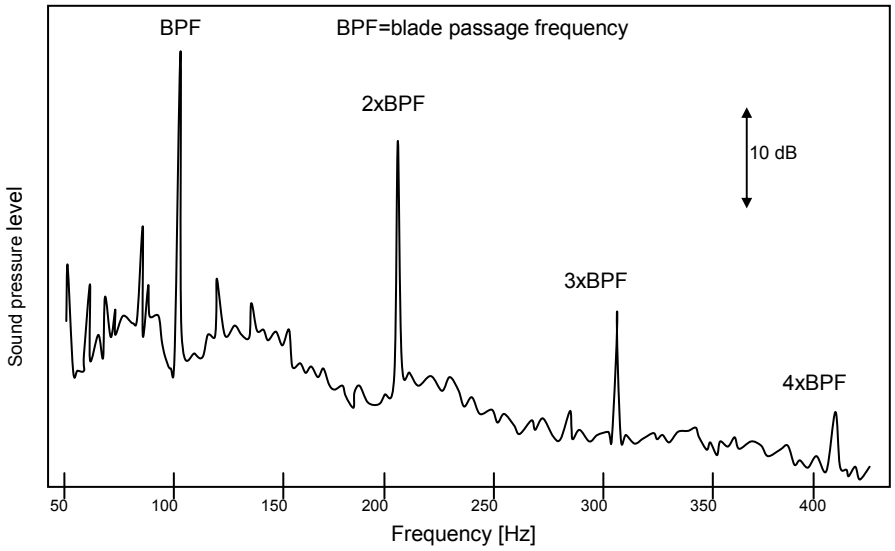

Figure 2.4: *Turboprop noise: pure tones exist at the BPF and its higher harmonics (Fokker 50).* [11].

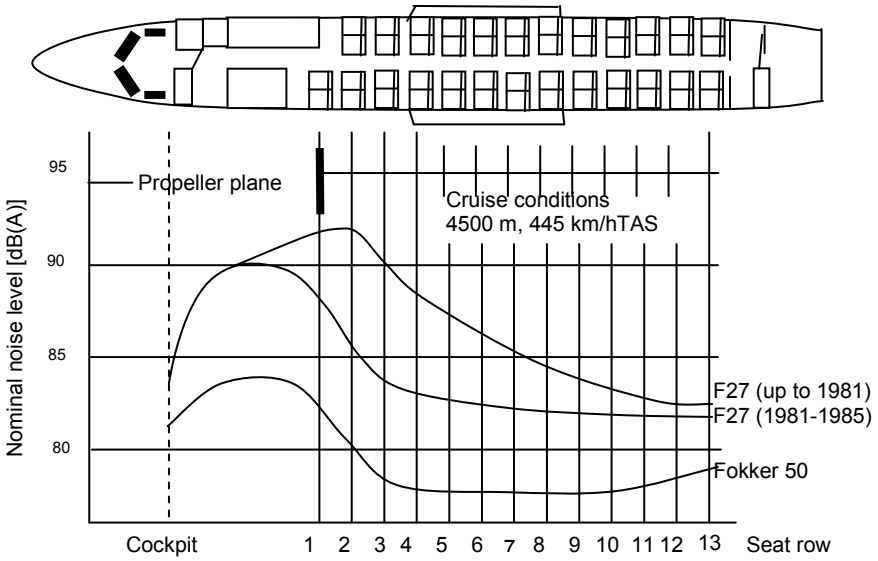

Figure 2.5: *Interior noise levels of the Fokker 50, which is a propeller aircraft).* [11]

Engine silencing techniques

An effective method to reduce the noise levels in the passenger cabin is to reduce the noise levels at its source. Currently there are many techniques to reduce the noise excited from the engines. In this research the objective is to optimise the fuselage wall design. Therefore the focus will not be on the engines themselves. However to get an impression of the current developments in this field a few of these techniques are mentioned here.

New turboprop engines have swept propellers to reduce the tip speed of the blades [12]. The D-27 turboprop engine has counter-rotating propellers, which reduces the noise levels even further. The D-27 engine on an Antanov 70 is shown in figure 2.6. Because of the mechanic complexity of counter-rotating blades this engine never became a commercial success. The swept blade technique is also applied to new turbofan engines. Figure 2.7 shows the swept-fan blade design.

Figure 2.6: *D-27 Turboprop engine with counter rotating swept blades on an An-70.* *[www.wikimedia.org]*

Figure 2.7: *GE Genx turbofan engine with swept blades* *[www.geaviation.com]*

Another method that can be applied on turbofan engines is a nacelle design to improve faster mixing of the jet exhaust and minimise the turbulence creation in the mixing process. The potential noise reduction of the mixing noise with this method is about 2 to 4 dB. An example of a nacelle design for a turbofan engine to reduce noise is given in figure 2.8. This picture shows a modified Rolls Royce Trent 800 engine used in the joint Boeing / Rolls Royce Quiet Technology Demonstrator research program to reduce engine noise [13].

Another method to reduce engine noise is to reduce the vibration levels of the engines themselves, which reduces the noise excited through the structure born path. A possible method is to use active vibration control techniques that can be applied on the inside surfaces of the engine.

From this discussion it is concluded that noise from turbofan and turboprop engines is strongly position and frequency dependent. The noise level of turbofan engines usually is of a higher level than the turbulent boundary layer noise. However due to newly applied technologies, the new generation turbofan engines are becoming more quiet making them less dominant compared to the turbulent boundary layer noise [4].

Figure 2.8: *Turbofan engine (Trent 800) with nacelle design to improve the mixing process between the exhaust and ambient air. Part of the joint Boeing/Rolls Royce Quiet Technology Demonstrator program.* *[www.rolls-royce.com]*

2.3 Perception of noise

The hearing sensibility of the human ear is not constant over the audible frequency range. Figure 2.9 shows a graph with equal loudness curves expressed in phons. Phons are defined as noise with equal loudness as the noise intensity in decibel at 1000 Hz. For example noise of 60 phons at any frequency is perceived just as loud as noise of 60 dB at 1000 Hz. It can be seen that the human ear is very discriminative for low frequency noise. Noise of 50 dB at 30 Hz is not audible while noise of 50 dB at 1000 Hz is very well audible. Because of this phenomenon there are weighting scales that give noise levels a physical meaning. There are four weighting scales: A, B, C and D. Weighting scale A, which follows more or less the 0 phon curve in figure 2.9, is most commonly used because it matches the human perception of noise. From figure 2.11 can be concluded that the human ear is most sensitive to noise (in dB) in the frequencies range of 250 Hz to 8000 Hz. This is also the frequency range of normal speech.

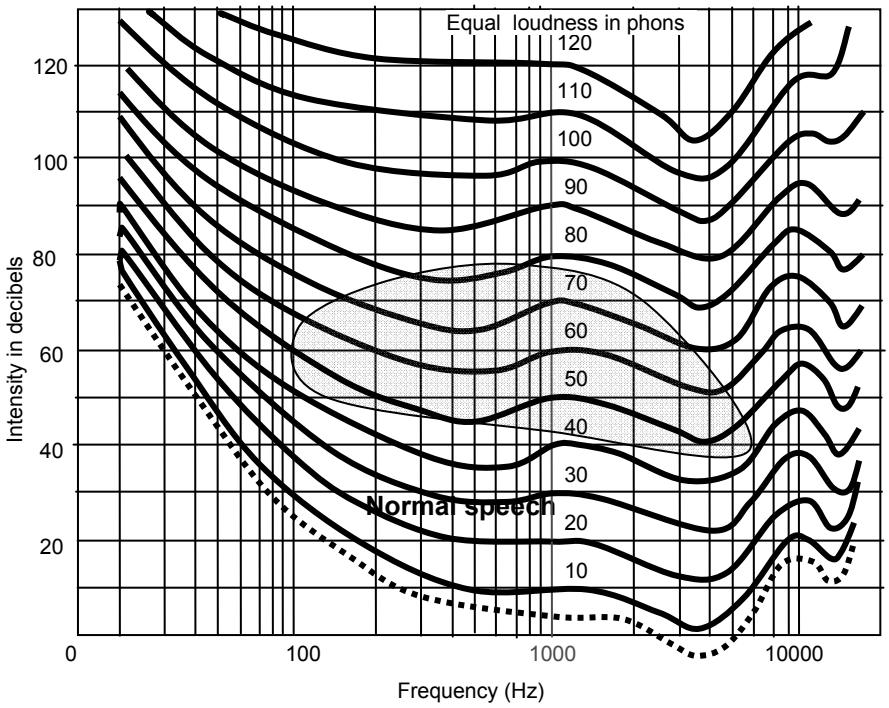

Figure 2.9: *Hearing sensibility of human hearing.*
[http://hyperphysics.phy-astr.gsu.edu/hbase/sound/eqloud.html]

In order to give the reader some feeling for noise levels, table 2.1 gives an indication of noise levels with several practical examples.

Average interior noise levels for transportation vehicles are given in table 2.2. It is seen that the interior noise levels for aircraft are higher than that of cars or trains. However the newer aircrafts have the tendency that the noise levels reduce and come closer to the other transportation vehicles.

Table 2.1: *Noise level examples.*
[http://netvista.net/~hpb/dblevels.html]

Noise source	dB (A)	Noise effect
Jet take-off (at 25m)	150	Eardrum rapture
Aircraft carrier deck	140	
Jet take-off (at 100m)	130	
Chain saw	120	Painful
Turbo-fan takeoff (at 60m)	118	
Live rock music	108	Average human pain threshold
Jackhammer	100	Serious damage (8 hr duration)
Diesel truck	90	Likely damage (8 hr duration)
Propeller plane flyover (at 300m)	88	Possible damage (8 hr duration)
Passenger car (at 100km/h at 7.5m)	77	Annoying
Conversation in restaurant	60	Fairly quiet
Conversation at home	50	
Whisper	20	
Breathing	10	Barely audible

Table 2.2: *Typical noise levels of different means of transportation. [11]*

Transportation	Interior noise level
Fokker 27	84 dB (A)
Fokker 50	78 dB (A)
Fokker 100	74 dB (A)
Passenger car	64-75 dB (A)
Passenger train	60-70 dB (A)
High speed train	63 dB (A)

2.4 Thermal conditions that act on a fuselage

The thermal loading on a fuselage can be characterised by the temperature difference between the temperature inside the fuselage and the outside ambient temperature. The outside air temperature can differ substantially. Weather situations on sea level can change from 50 degrees in the desert of the Sahara to -40 degrees in arctic areas. For airliners that fly at altitudes of 10 to 13 km, the outside air temperature drops during a single flight from average sea level temperature to -55 degrees at cruising altitude as can be seen in figure 2.10. This means that the outside temperature can range from -55 to +50 degrees.

A comfortable temperature inside the passenger cabin would be around 20 degrees, meaning that the fuselage wall has to insulate in both directions. In order to keep a comfortable constant temperature inside the passenger cabin the requirement to the fuselage wall will be that the heat flow through the fuselage wall caused by the difference in temperature between the fuselage inside and outside may not exceed the capacity of the air conditioning system.

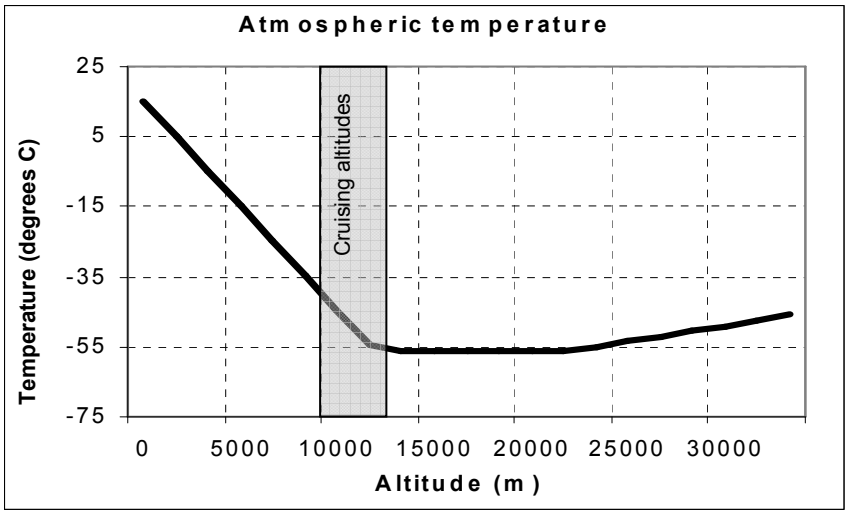

Figure 2.10: *Atmospheric temperature as function of altitude [6].*

2.5 Resulting Acoustic and thermal insulation requirements

In section 2.3 several noise sources have been identified. The two noise sources that are most important for the design of acoustical insulation of a fuselage wall are the turbulent boundary layer noise and noise from the engines. The noise generated by these two sources has an overall noise level that varies around 130 dB with the presence of several peaks at the blade passage frequencies of the engines. The total turbulent boundary layer noise level has a relatively constant character with respect to the position along the fuselage. However, at the front of the fuselage high frequencies are more dominant and at the rear of the fuselage the lower frequencies are more dominant. The engines are responsible for local effects. Especially in the engine-plane, the noise levels are rather high.

The required noise levels inside a passenger cabin are around 75 dB. The tendency is to lower noise levels because of the increasing attention to passenger comfort. The human ear is less sensitive for low frequency noise but because it is difficult to insulate low frequency noise, low frequency noise is still a big issue in sound insulation problems.

In general it can be approximated that the sound transmission loss of the fuselage wall has to span the difference between the outside noise (approximately 130 dB with BPF peaks) and the required weighted inside noise level of approximately 75 dB(A). The required transmission loss can be approximated in figure 2.9 as the difference between the 130 dB line and the 75 phons curve. The fuselage wall also has to be able to insulate noise peaks at certain frequencies.

It should be noted that a lot of research is performed on the modelling of turbulent boundary layer noise. In this section only a few references were considered. More references that could be of use to the reader are given by [14-27].

For passenger comfort the temperature inside the fuselage should be around 20°C. The outside temperature can range from -55°C to +50°C. This gives a

temperature difference (inside minus outside temperature) of 75 or –30 degrees. The minus sign requires insulation in the other direction. The requirement to the fuselage wall is that the heat flow caused by this temperature difference may not exceed the capacity of the air conditioning system. This results in the requirement that the heat flow through the fuselage wall should be minimised.

For the analysis in this research the outside noise levels and the outside temperature will be considered as given facts. The improvements that can be achieved by silencing techniques of the engines and the boundary noise will not be taken into account in the multidisciplinary analysis of the fuselage wall. Only the acoustical and thermal insulation properties of the fuselage wall itself will be considered.

2.6 Reference

[1] Corcos G.M., Liepmann, H.W., 'On the contribution of turbulent boundary layers to the noise inside a fuselage', NACA TM 1420, 1956.

[2] Efimtsov, B.M., 'Characteristics of the field of turbulent wall pressure fluctuations at large Reynolds numbers. Sov. Phys. Acoust. 28 (4) July-August, p. 289-292, 1982.

[3] Rack, R, Weston, A., 'Modelling of turbulent boundary layer surface pressure fluctuation auto and cross spectra verification and adjustments based on TU-144LL data', NASA CR-2005-213938, 2005.

[4] ENABLE, EU Research programme, FP5, Contract No. GR4D-CT-2000-00223, 'Environmental Noise associated with turbulent boundary layer excitation, Final technical report, May 2003.

[5] ESDU 75021, Estimation of the surface pressure fluctuation in the turbulent boundary layer of a flight vehicle, 1975.

[6] ESDU 68046, Atmospheric data for performance calculations, 1968.

[7] Jackson, P. "Jane's, All the world's aircraft 2002-2003".

[8] Bechert, D.W., Bruse, M., Hage, W., Meyer, R., Fluid mechanics of biological surfaces and their technological application, Naturwissenschaften, Springer Berlin, vol 87, nr 4, p157-171, 2000.

[9] Boermans, L.L.M., Research and sailplane aerodynamics at Delft University of Technology, Recent and present developments, Netherlands Association of Aeronautical Engineers (NVvL), June, 2006.

[10] ESDU 74001, An introduction to gas turbine exhaust noise, 1973.

[11] Roozen, N.B., Quiet by design: Numerical acousto-elastic analysis of aircraft structures, 1990.

[12] Dittmar, J.H., Elliot, D.M., Fite, E.B., The noise of a forward swept fan, NASA TM-2003-212208, Glenn Research Center, Cleveland, Ohio, 2003.

[13] www.Rolls-royce.com.

[14] Bhat, W.V., Wilby, J.F., Interior noise radiated by an airplane fuselage subjected to turbulent boundary layer excitation and evaluation of noise reduction treatments, Journal of Sound and Vibration, vol 18, nr 4, p449–464, 1971.

[15] Davies, H.G., Sound from turbulent boundary layer excited panels, Journal of the Acoustical Society of America, vol 49, p878–889, 1971.

[16] Graham, W.R., A comparison of models for the wavenumber-frequency spectrum of turbulent boundary layer pressures, Journal of Sound and Vibration, vol 206, p541–565, 1997.
[17] Han, F., Bernhard, R.J., Mongeau, L.G., A model for the vibro-acoustic response of plates excited by complex flows, Journal of Sound and Vibration, vol 246, nr 5, p901–926, 2001.
[18] Allen, M., Vlahopoulos, N., Noise generated from a flexible and elastically supported structure subject to turbulent boundary layer flow excitation, Finite Elements in Analysis and Design, vol 37, p687–712, 2001.
[19] Wu, S.F., Maestrello, L., Response of finite baffled plate to turbulent flow excitation, AIAA Journal, vol 33, p13–19, 1995.
[20] Finnveden, S., Birgersson, F., Ross, U., Kremer, T., A model of wall pressure correlation for prediction of turbulence-induced vibration, Journal of Fluids and Structures, vol 20, p1127–1143, 2005.
[21] Liu, B., Noise radiation of aircraft panels subjected to boundary layer pressure fluctuations, Journal of Sound and Vibration, vol 314, p693–711, 2008.
[22] Wiken, I.D., Soedel, W., The receptance method applied to ring stiffened cylindrical shells: analysis of modal characteristics, Journal of Sound and Vibration, vol 44, p563–576, 1976.
[23] Liu, B., Feng, L., Sound transmission through curved aircraft panels with stringer and ring frame attachments, Journal of Sound and Vibration, vol 300, p949–973, 2007.
[24] Chase, D.M., Modelling the wavevector-frequency spectrum of turbulent boundary layer wall pressure. J.Sound and Vibration, vol 70, p29-67,1980.
[25] Smolyakov, A.V., Tkachenko. V.M., Model of a field of pseudonic turbulent wall pressure and experimental data. Soviet Physics Acoustics vol 37 nr6, p627-631, 19912SjW70:29-67, 1980.
[26] Ffowcs Williams J.E., Bounday-layer pressures and the Corcos Model. J.Fluid Mechanics, vol 125, p9-25, 1982.
[27] Nilsson, A., Feng, L., Measurements of sound and vibration. P1800 Aircraft Technical note MWL, KTH, October 2008.

3 Acoustic insulation

3.1 Introduction

This chapter gives a literature overview of the theory about acoustical insulation of a fuselage wall. For current passenger aircraft the fuselage wall usually consists out of three layers. On the outside there is the structural layer like a stiffened skin or a sandwich skin. In the middle an insulation layer like the acoustic and thermal insulation blankets and on the inside there are interior panels. Each part has its own contribution to the sound insulation. The interaction between these parts and the influence of the fuselage geometry and interior design on the resonance frequencies and damping properties make the sound insulation of a fuselage wall a very complex subject. Therefore, here already some assumptions will be made:

- It should be noted that a plate excited by a turbulent boundary layer and a plate excited by an acoustic field, in for example a sound transmission room, are not necessarily the same. In this research the sound transmission loss of a fuselage wall will be considered, which is much easier to determine than the radiation from a plate excited by a turbulent boundary layer.
- The sound insulation of a fuselage will be influenced by detailed aspects like windows, seats, floor carpet, kitchen and toilet separation walls, etc. In this research these detailed aspects are not taken into account.

In this chapter, analytical and (semi) empirical relations found from literature for simplified sound transmission loss cases, will be discussed. These relations, from hereon called literature equations, will be included in the acoustical module of the Design & Engineering Engine (DEE). This means that only the bare fuselage skin will be considered in this analysis. In future research, more detailed aspects could be included.

The content of this chapter starts with a general theoretical introduction to the sound transmission loss theory in section 3.2. Sections 3.3 and 3.4 explain, in a more qualitative way, the influence of structural parameters like skin thickness, frame pitch and stringer pitch on the TL. An alternative to the stiffened skin fuselage concept is the sandwich fuselage concept of which the insulation properties are discussed in section 3.5. The influence of interior panels, which create a double wall with the fuselage skin, is described in section 3.6. The influence of the insulation blankets, which are placed in the cavity between the interior panels and the fuselage skin, is discussed in section 3.7. Another insulation method that can be applied, is the addition of viscoelastic layers to improve the damping properties of the fuselage wall. This is discussed in section 3.8. Besides these 'passive' insulation techniques also active techniques can be applied to improve the sound transmission loss. One possible active noise control method is to reduce the noise radiation from the interior panels with active vibration control of these interior panels with the use of piezo-electric actuators. This concept is discussed in section 3.9.

It should be noted that in this chapter only the equations are discussed that are relevant to the acoustic module of the design and engineering engine. More detailed information can be found in appendix A till C and in the relevant references.

3.2 Introduction to Sound transmission loss

The introduction to the sound transmission loss of a fuselage wall is presented in three steps. First a brief introduction is given into the basics of the sound wave theory. Secondly the sound transmission loss of an infinite flat plate is discussed. The sound transmission loss of infinite flat plates is well described in literature and gives a good understanding of the sound transmission loss principle. As a third step the infinite flat plate is closed to form a cylinder. The sound transmission loss of cylinders has close resemblance with a pressurized fuselage cabin of an airliner.

3.2.1 Basic sound wave theory

First, some basics of sound waves in air are discussed. Sound waves in air move along as variations of pressure from the pressure equilibrium without a net displacement of the air particles as is shown in figure 3.1 (The variation of pressure from the equilibrium pressure is called the acoustic pressure: p).

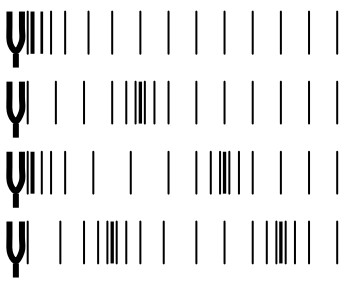

Figure 3.1: *Propagation of sound waves in air. The acoustic pressure is indicated by the density of the vertical lines [1].*

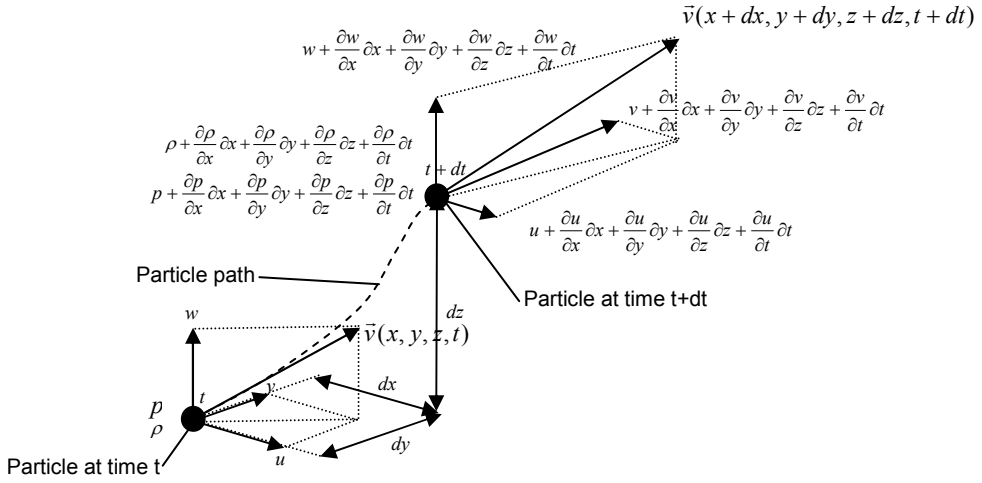

Figure 3.2: *A particle with density ρ, pressure p and velocity $\vec{v}$ at time t in a rectangular Cartesian coordinate system x,y,z moves a distance dx ,dy, dz in time dt. Here is u the velocity component in x-direction, v the velocity component in y-direction and w, the velocity component in z-direction.*

The basic wave equation that describes the propagation of small disturbances through a homogeneous, non viscous, compressible medium in Cartesian coordinates is given by Fahy [1], Maxwell [2], Timoshenko [3]:

$$\frac{\partial^2 p}{\partial x^2} + \frac{\partial^2 p}{\partial y^2} + \frac{\partial^2 p}{\partial z^2} = \frac{1}{c_s}\frac{\partial^2 p}{\partial t^2} \tag{3.1}$$

This wave equation is derived from the linearised* form of the continuity equation:

$$\frac{\partial \rho}{\partial t} + \rho_0\left(\frac{\partial u}{\partial x} + \frac{\partial v}{\partial y} + \frac{\partial w}{\partial z}\right) = 0 \tag{3.2}$$

and the linearised* forms of the momentum equations:

$$\frac{\partial \rho}{\partial x} + \rho_0 \frac{\partial u}{\partial t} = 0 \qquad \frac{\partial \rho}{\partial y} + \rho_0 \frac{\partial v}{\partial t} = 0 \qquad \frac{\partial \rho}{\partial z} + \rho_0 \frac{\partial w}{\partial t} = 0 \tag{3.3}$$

Where:

$c_s = \sqrt{\gamma \frac{p_0}{\rho_0}}$	Speed of sound	p:	Acoustic pressure
		t:	Time
p_0	Mean pressure of the medium	u, v, w:	Particle velocity comp.
ρ_0:	Mean density of the medium	x, y, z:	Cartesian coordinates
γ:	Ratio of c_v/c_p	Adiabatic process is assumed	

*Here, linearised means that products of small quantities are neglected

In nature sound waves rarely occur at a single frequency. However for mathematical and conceptual convenience sound wave equations are often considered as small pressure pertubation equations that are linear and hence the general response may be seen as the superposition of responses to each single frequency. Sound waves in air are usually characterised by the acoustical pressure. For the acoustical pressure of a plane sound wave at a single harmonic frequency usually the complex notation as function of time and position is used, Fahy[1]:

$$p(x,y,z,t) = \mathrm{Re}\{\tilde{p}e^{(-jk_x x - jk_y y - jk_z z)}e^{j\omega t}\} \tag{3.4}$$

Where:

p	Acoustic pressure at position x,y,z and time t
k_x, k_y, k_z:	Wave numbers in respectively the x, y and z direction (According to the wave equation the resultant wave number $k = \omega/c_s = [k_x^2 + k_y^2 + k_z^2]^{0.5}$)
ω:	Angular frequency
$\tilde{p} = \lvert p \rvert e^{-j\phi}$	Complex acoustic pressure amplitude
ϕ	Phase angle

The physical meaning of the angular speed and the wave number are explained in figure 3.3.

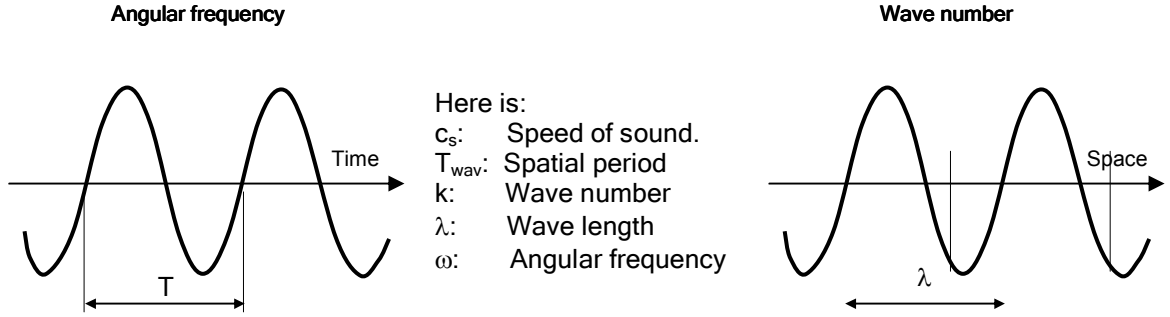

$$\lambda = c_s T_{wav} \qquad \omega = \frac{2\pi}{T_{wav}} \qquad k = \frac{\omega}{c_s} \qquad k = \frac{2\pi}{\lambda}$$

Figure 3.3: *Explanation of the angular frequency and wave number [1].*

The unit for the acoustic sound pressure, also called the sound pressure level (L_p), is decibel. The sound pressure level in decibels is defined by a logarithm of the acoustic rms pressure divided by a reference pressure p_0 where p_0 is the acoustic pressure that is just audible to the human ear.

$$L_p = 20\log_{10}\left(\frac{p_{rms}}{p_{ref}}\right) \tag{3.5}$$

Where: $p_{ref} = 2 \cdot 10^{-5} Pa$

The sound Intensity ($\vec{I}$) of a sound wave is defined as the product of the acoustic pressure (p) with the particle velocity ($\vec{v}$): $\vec{I} = p \cdot \vec{v}$. The sound power ($P$) is defined as the sound intensity normal to a surface (S) multiplied with that surface: $P = \vec{I} \cdot \vec{n} \cdot S$. Here $\vec{n}$ is the normal vector to surface S. For a single frequency, the normal specific acoustic impedance ($\tilde{z}_{ac}$) is defined as the ratio of the complex amplitudes of the acoustic pressure and the normal velocity ($\tilde{v}_n = \vec{\tilde{v}} \cdot \vec{n}$) to any considered surface S: $\tilde{z}_{ac} = \tilde{p} / \tilde{v}_n$. Using the wave and momentum equations, an expression for the normal particle velocity $\tilde{v}_n$ of an acoustic plane wave in a homogeneous, non viscous, compressible medium can be found: $\tilde{v}_n = \tilde{p} / \rho_0 c_s$. The normal specific acoustical impedance of such a medium is: $z_{ac} = \rho_0 c_s$.

3.2.2 Sound transmission loss of infinite flat plates

When a plane sound wave hits a thin infinite flat plate, a part of the incident sound power will be reflected and a part will be transmitted through the plate. This is illustrated in figure 3.4.

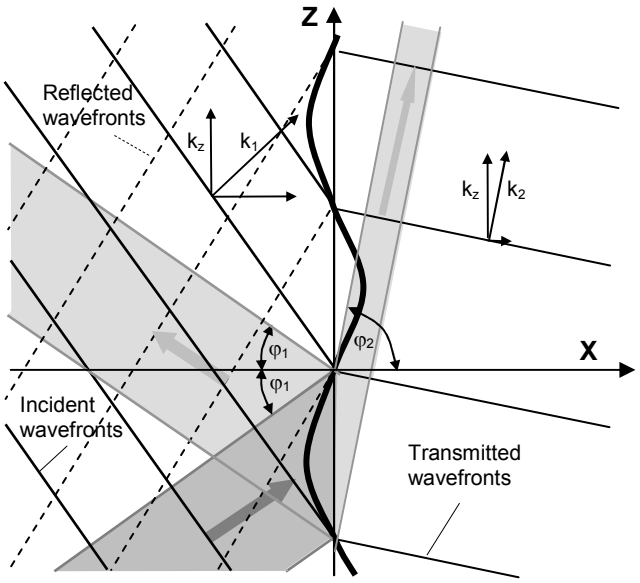

Figure 3.4: *Explanation of wave number and angular speed [1].*

When zooming in, the sound transmission process can be described as follows: The incident plane sound wave acts as a pressure field on the surface of the plate. This pressure field causes the plate to deform perpendicular to the plate surface resulting in a bending wave in the plate.

(It should be noted that bending waves can be described by a combination of in-plane longitudinal waves and shear waves. For flat plates the bending waves can be described with the bending wave equation. Derivation of the complete classical bending wave equation, in which shear deformation and rotary inertia are neglected, can be found in Cremer [4]).

The now vibrating plate on its turn introduces pressure variations in the air on both sides of the plate resulting in a sound wave on the incident side called the reflected sound wave and a sound wave on the other side called the transmitted sound wave. In case of finite plates, also sound would be scattered from the edges. For infinite

uniform plates the effect of scattering can be neglected. During this process a part of the incident sound power will be reflected and absorbed by the plate, resulting in a transmitted sound power lower than the incident sound power.

The sound insulation of a plate is characterised by the so-called transmission loss index (TL). The TL is defined as the quotient, expressed in dB, of the incident sound power (P_{in}), and the transmitted sound power (P_{tr}), Fahy [1]:

$$TL = 10\log_{10}\left(\frac{P_{in}}{P_{tr}}\right) = 10\log_{10}\left(\frac{1}{\tau}\right) \tag{3.6}$$

In equation 3.6, τ is by definition called the sound power transmission coefficient. The sound transmission loss of a plane sound wave on an infinite flexible flat plate, for the case where the air on both sides has the same properties ($c_1 = c_2 = c_s$, $k_1 = k_2 = k$ and $\varphi_1 = \varphi_2 = \varphi$) can be described by equation 3.7, Fahy [1]:

$$\tau = \frac{\left(2\rho_0 c_s / \omega m\right)^2 \sec^2\varphi}{\left[\left(2\rho_0 c / \omega m\right)\sec\varphi + \left(k/k_b\right)^4 \eta \sin^4\varphi\right]^2 + \left[1 - \left(k/k_b\right)^4 \sin^4\varphi\right]^2} \tag{3.7}$$

In this equation:

- k, ω and φ represent respectively the wave number, the angular speed and the incident angle of the incident sound wave
- ρ_0 and c are respectively the density and the speed of sound in air on both sides.
- m, k_b and η represent respectively the mass per unit area of the plate, the free flexural wave number of the plate (dependent on the mass and stiffness of the plate) and the structure loss factor (a kind of damping constant of the plate, η for elastic materials is of order 10^{-2}-10^{-4}).

Figure 3.5 shows TL-curves determined with equation 3.7 for different values of φ as a function of ω. From this figure can be seen that for a certain frequency the TL-curve shows a dip. The reason for this dip is the occurrence of coincidence. At certain frequencies the tangential part of the wave number of the incident wave (k_z in figure 3.4) coincides with the free flexural wave number of the plate, k_b. So coincidence occurs when $k_b = k_z = k \sin\varphi$ ($\varphi = \varphi_1$ in figure 3.4). The frequency at which this occurs is called the coincidence frequency: ω_{co}. When $k_b = k \sin\varphi$ is entered in the transmission coefficient formula one can see that the second term in the denominator vanishes, so the τ becomes larger and therefore the TL smaller

The free flexural wave number of an infinite isotropic plate k_b is given by the following expression:

$$k_b = \sqrt[4]{\frac{\omega^2 m}{D}} \tag{3.8}$$

In equation 3.8, D is the bending stiffness per unit width of the plate and is expressed by:

$$D = \frac{Et^3}{12\left(1-\nu^2\right)} \tag{3.9}$$

If $k_b = k \sin\varphi = \omega/c_s \sin\varphi$ is inserted one finds for the coincidence frequency:

$$f_{co} = \frac{1}{2\pi}\sqrt{\frac{m}{D}}\left(\frac{c_s}{\sin\varphi}\right)^2 \tag{3.10}$$

The lowest coincidence frequency ($\varphi = 90^0$) is called the critical frequency: f_c. Above the critical frequency f_c, there always exists an incident angle at which coincidence will occur.

In practice, sound waves are usually incident upon a partition from many different angles simultaneously. Therefore it is appropriate to weight the transmission coefficient to the directional distribution of the incident intensity and integrate them over the angle of incidence. Fahy [1], gives an appropriate weighting procedure for a diffuse sound field:

$$\tau_d = \int_0^{\pi/2} \tau(\varphi)\sin 2\varphi d\varphi \tag{3.11}$$

From this weighting procedure can be concluded that the coincidence effect is most severe at f_c.

By inserting equation 3.7 into equation 3.11 the TL can be calculated under field incidence. The TL of an infinite flat plate under field incidence can be divided into two sections, which is illustrated in figure 3.5 for an aluminium flat plate:

- Below the coincidence frequency ($f << f_c$): Here the stiffness terms are relatively small compared to the mass terms so the TL expression can be simplified to equation 3.12. (For small η, the damping term can be neglected):

$$TL = 20\log_{10}\left(\frac{\omega m}{2\rho_0 c_s}\right) - 10\log_{10}\left(\ln\left\{1+\left(\frac{\omega m}{\rho_0 c_s}\right)\right\}\right) \tag{3.12}$$

  In literature the first part of equation 3.12 is often referred to as the Mass Law. For frequencies $> f_c/2$ damping may not be neglected.
- Above the coincidence frequency ($f >> f_c$): Here the mass terms are relatively small compared to the stiffness terms so the TL expression again can be simplified:

$$TL = 20\log_{10}\left(\frac{\omega m}{2\rho_0 c_s}\right) + 10\log_{10}\eta + 10\log_{10}\left(\frac{2\left(1-\frac{f_c}{f}\right)}{\pi\frac{f_c}{f}}\right) \tag{3.13}$$

- At the coincidence frequency ($f = f_c$) the TL expression is given by:
  In this case the damping term may not be neglected. It should be noted that for finite plates also losses due to radiation may not be neglected.

$$TL = 20\log_{10}\left(\frac{\omega_c m}{2\rho_0 c}\right) + 10\log_{10}\eta \tag{3.14}$$

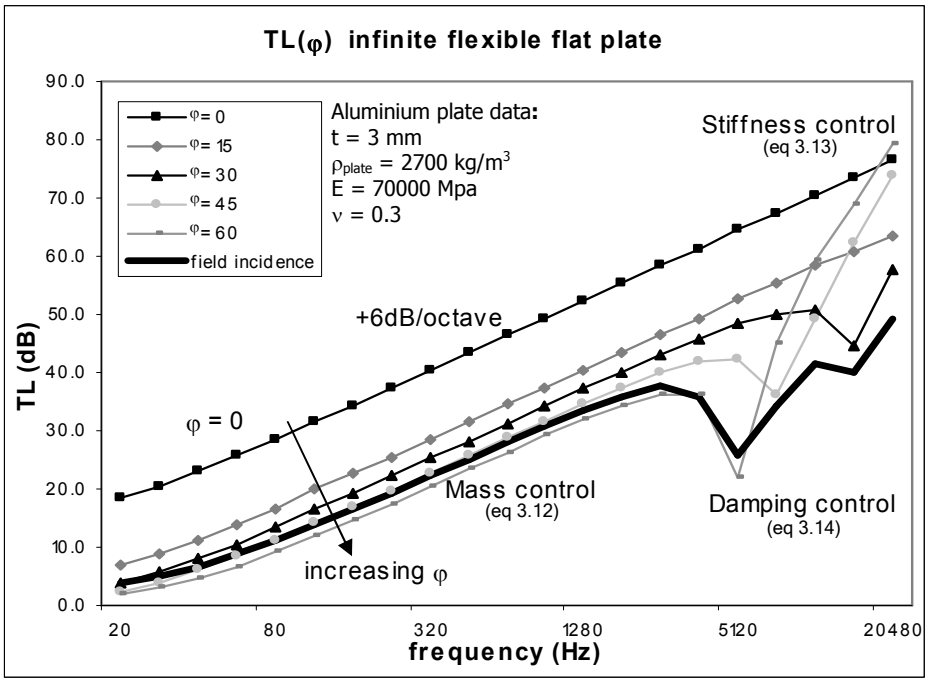

Figure 3.5: *The transmission loss of an infinite 3 mm thick aluminium plate for plane waves at fixed incidence angles and under diffuse incidence according to eqs. 3.7 and 3.11.*

At and above the coincidence frequency damping is important. Equation 3.12 and 3.13 both show that the TL is dependent on the term $20\log_{10}\eta$. (Here η is the structural damping factor). For elastic materials a typical value for η is 0.01, which means that the TL at f_{co} is about 40 dB less compared to the Mass law.

From this discussion can be concluded that for infinite isotropic plates the TL is dependent on the frequency (f), the material properties (density and elasticity) and geometry (thickness). Light, stiff composite structures have a poor acoustic behaviour. (The low mass per unit area causes a low TL below the critical frequency. High stiffness suggests an improved TL above the coincidence frequency. However the low mass per unit area combined with high stiffness lowers the critical frequency, which results in a worsened overall TL).

Within the DEE, which will be discussed in chapter 6, the acoustic module determines the sound transmission loss for infinite isotropic plates by using the combination of equations 3.6, 3.7, 3.8 and 3.11.

3.2.3 Acoustics of cylinders

The difference of cylinders compared to flat plates is that cylinders enclose an air cavity because for a cylinder two opposite edges of a plate are connected. As a result, the cylinder skin has restrictions on the structural and air cavity modes. The interaction of the structural and air cavity modes is important to determine the acoustic behaviour of cylinders. Therefore, first the structural and air cavity modes of thin walled cylinders will be discussed in sections 3.2.3.1 and 3.2.3.2 respectively. The interaction of the structural and cavity modes will be discussed in section 3.2.3.3. Finally section 3.2.3.4 will give some concluding remarks.

3.2.3.1 Structural eigenmodes of thin walled finite cylinders

Converting a flat plate into a cylinder places restrictions on the structural modes and introduces cavity modes. The closure of the shell in the circumferential direction requires that the structural wave variables have to be continuous around the circumference, Fahy [1]. This means that the characteristic circumferential patterns take the form $\cos(k_s s)$ or $\sin(k_s s)$, where $s = R\varphi$ and $k_s = n/R$ (k_s is the circumferential wave number), so that an integer number (n) of complete wave lengths, $\lambda_s = 2\pi R/n$, fit around the circumference. The wave number of a free propagating wave in a cylinder (k), is a combination of the circumferential wave number (k_s) and the axial wave number (k_z), which is illustrated in figure 3.6:

$$k_{cs}{}^2 = k_s^2 + k_z^2 \tag{3.15}$$

Here is: k_{cs}: the wave number of the free propagating wave
k_s: the circumferential wave number
k_z: the axial wave number

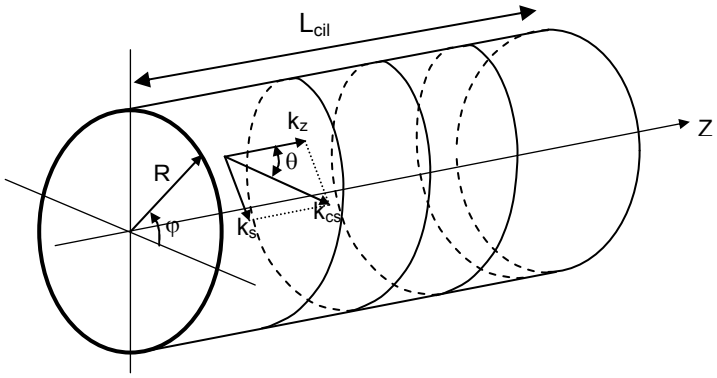

Figure 3.6: *The wave fronts of a free propagating wave of wave number k form a spiral pattern [1].*

For thin flat plates only the flexural bending waves were of interest. Curvature however, couples the radial, axial and tangential motions so the flexural waves will be dependent on all three motion- directions (radial, axial and tangential). There are many thin-shell equations that describe the vibration of cylindrical shells. See for example Leissa [5], Li et al [6], Soedel [7], Junger [8] and Zhang [9].

In this research, use will be made of the equation for natural frequencies of finite thin shell cylinders defined by Li et al [6]. They solved the equations of motion derived by Junger [8] into equation 3.16 for the natural angular frequencies ω:

$$\omega^6 + a_1\omega^4 + a_2\omega^2 + a_3 = 0 \tag{3.16}$$

Where:

$$a_1 = -\frac{1}{\rho t}\left[c_1 + c_2 + c_3\right] \qquad a_2 = \frac{1}{(\rho t)^2}\left[c_1c_3 + c_2c_3 + c_1c_2 - L_{12}^2 - L_{23}^2 - L_{13}^2\right]$$

$$a_3 = \frac{1}{(\rho t)^3}\left[c_1 L_{23}^2 + c_2 L_{13}^2 + c_3 L_{12}^2 - c_1 c_2 c_3 - 2 L_{12} L_{13} L_{23}\right]$$

$$c_1 = L_{11} + \rho t \omega^2 \qquad c_2 = L_{22} + \rho t \omega^2$$

$$c_3 = L_{33} + \rho t \omega^2$$

$$L_{11} = K\left(k_z^2 + \frac{1-\nu}{2} k_s^2\right) - \rho t \omega^2 \qquad L_{12} = L_{21} = \frac{K(1-\nu)}{2} k_z k_s$$

$$L_{13} = L_{31} = \frac{\nu K}{R} k_z \qquad L_{22} = K\left(\frac{1-\nu}{2} k_z^2 + k_s^2\right) - \rho t \omega^2$$

$$L_{23} = L_{32} = \frac{K}{R} k_s \qquad L_{33} = D k^4 + \frac{K}{R^2} - \rho t \omega^2$$

$$k = \sqrt{k_z^2 + k_s^2} \qquad K = \frac{Et}{1-\nu^2}$$

$$k_s = \frac{n}{R} \qquad D = \frac{Et^3}{12(1-\nu^2)}$$

Where:

E	Modulus of elasticity of the cylinder material
t	Thickness of the cylinder skin
ν	Poisson ratio of the cylinder material
ρ	Density of the cylinder material
L_{cil}	Length of the cylinder
R	Radius of the cylinder
k_s	Circumferential wave number
k_z	longitudinal wave number
m	number of half sin waves in longitudinal direction
n	number of half sin waves in circumferential direction

The natural angular frequencies can be determined for different boundary conditions for which the corresponding wave numbers k_z are given in table 3.1.

Table 3.1: *Wavenumbers k_z for different boundary conditions*

Boundary conditions	Wave numbers
Clamped-free	$k_z = (2m-1)\pi/2L_{cil}$
Free-simply supported	$k_z = (4m+1)\pi/4$
Simply supported-simply supported	$k_z = m\pi/L_{cil}$
Clamped-simply supported	$k_z = (4m+1)\pi/4L_{cil}$
Clamped-clamped	$k_z = (2m+1)\pi/2L_{cil}$
Sliding-simply supported	$k_z = (2m-1)\pi/2L_{cil}$
Free-free	$k_z = (2m+1)\pi/2L_{cil}$

There are some restrictions to equation 3.16, Li et al [6]:

1.) The coupling of the vibration between the axial and circumferential direction is neglected. For large ratio R/t (R/t > 30), this assumption is justified, Soedel [7]. For small ratio R/t (R/t < 30), the natural frequencies will be overestimated.
2.) The relative error in the natural frequencies decreases with increasing axial mode number m. For long-thin shells, the effect of the boundary conditions will be small. In that case, the wave propagation in cylindrical shells trends to the form of an approaching wave.

These restrictions indicate that equation 3.16 will be valid for long-thin shells like fuselages. Figure 3.7 illustrates the natural frequencies for a simply supported cylinder.

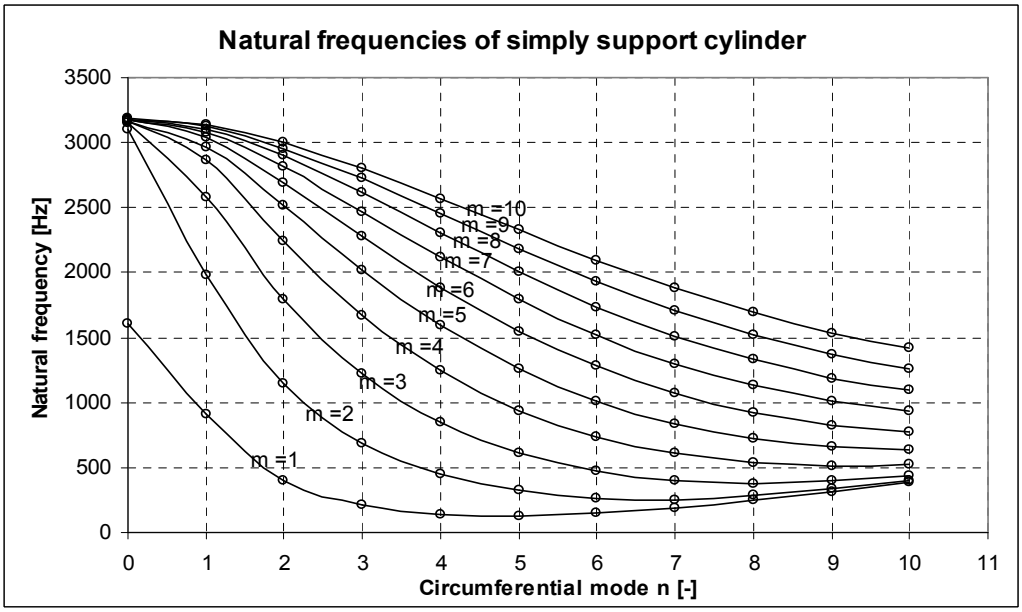

Figure 3.7: *Natural frequencies of a non stiffened simply supported aluminium cylinder with L_{cil} = 970 mm, R = 252.5 mm and t = 1 mm, R/t = 252.5.*

The natural frequencies of thin cylinders are usually made dimensionless by dividing them with the ring frequency and are represented by the parameter $\Omega = \omega/\omega_r$. The ring frequency is defined by:

$$\omega_r = \frac{1}{R}\sqrt{\frac{E}{\rho\left(1-\nu^2\right)}} \tag{3.17}$$

The lowest natural frequencies of a certain circumferential mode that can exist in an infinitely long cylinder are called cut-off frequencies. These cut-off frequencies occur when the axial wavelength is infinite and can be derived from equation 3.16 by setting k_z equal to zero. Figure 3.8 shows the first three cut-off modes of a thin-walled infinite cylinder.

The natural mode restrictions of cylinders that are stiffened with frames and stringers can be implemented in the longitudinal and circumferential wave number definitions. In circumferential direction, the number of circumferential half sin waves n

should be an integer multiple of the number of stringers n_{str}. In longitudinal direction, the boundary conditions of table 3.1 can be applied by setting L_{cil} equal to the frame pitch $L_{fr.}$

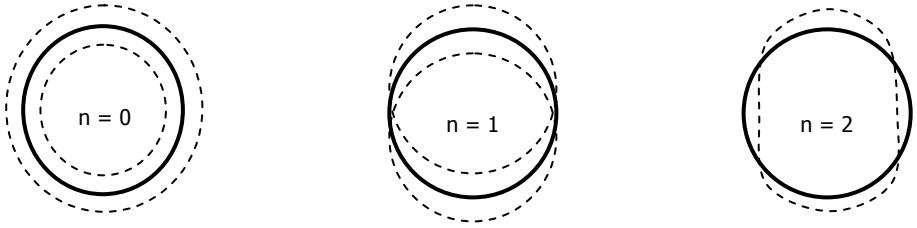

Figure 3.8: *Illustration of the first three structural circumferential resonance modes [1].*

3.2.3.2 Eigenmodes of the air cavity enclosed by a cylinder

The acoustic duct theory by Morse [10] shows that the acoustic modes of the cylinder air cavity that correlate to a rigid-walled cylindrical wave-guide take the form:

$$p_{mn}(r,\varphi,z) = \left|p_{mn}\right| \begin{matrix}\cos\\ \sin\end{matrix} (n\varphi) J_n(k_r r) e^{-jk_z z} \tag{3.18}$$

The first term of this expression represents the circumferential part, which has the form $\cos(n\varphi)$ or $\sin(n\varphi)$. The last term represents the axial part. These two terms match the structural modes of the cylinder wall. The radial part is represented by a Bessel function $J_n(k_r r)$, which is a function of the radial wave number k_r. The Bessel function can be solved with the boundary condition that the particle velocity of the air has to be zero at the cylinder wall:

$$\left[J_n'(k_r r)\right]_{r=R} = 0 \tag{3.19}$$

The characteristic solutions for k_r of this equation are multi-valued for a given n. Therefore the radial wave number is superscripted with np, where n indicates the number of circumferential half waves and p the number of radial half waves. The solutions of k_r^{np} for the first modes n and p are given in table 3.2.

Table 3.2: *Values of k_r^{np} r [1].*

n \ p	1	2	3	4	5
0	0	3.83	7.02	10.17	13.32
1	1.84	5.33	8.53	11.71	14.86
2	3.05	6.71	9.97	13.17	16.35
3	4.20	8.02	11.35	14.59	17.79
4	5.32	9.28	12.68	15.96	19.20
5	6.42	10.63	13.99	17.31	20.58
6	7.50	11.73	15.27	18.64	21.93
7	8.58	12.93	16.53	19.94	23.27
8	9.65	14.12	17.77	21.23	24.59

The radial and axial wave numbers for the air cavity satisfy the acoustic wave equation:

$$k^2 = k_z^2 + \left(k_r^{np}\right)^2 \tag{3.20}$$

The cut-off frequencies of the air cavity are defined as the frequencies at which the axial wavelength is infinite ($k_z = 0$). The dimensionless cut-off frequencies are then determined by:

$$\Omega_{np} = \left(k_r^{np} R\right)\left(\frac{c_s}{c_l^{/}}\right) \tag{3.21}$$

Here is: c_s: the speed of sound of air
$c_l^{/}$: the longitudinal speed of sound in the cylinder material

A few examples of the cross-sectional mode shapes at the cut-off frequencies are given in figure 3.9. Here the + sign indicates a positive pressure and the – sign a negative pressure. In these areas the pressure alternates between equal positive and negative pressure amplitudes. The lines indicate pressure nodes at which the pressure is constant.

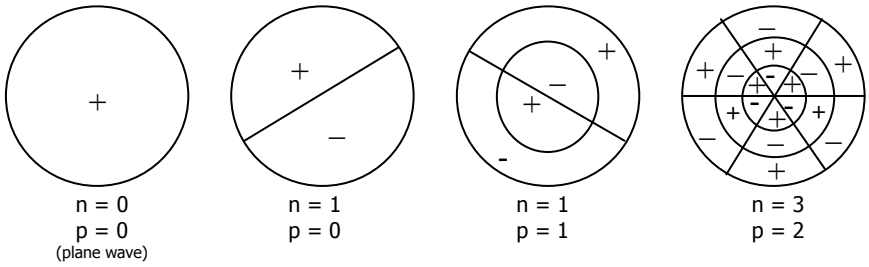

Figure 3.9: *Cross-sectional distribution of the pressure phase and nodal surfaces of the acoustical duct modes of a circular cylinder wave-guide [1].*

3.2.3.3 Acoustics of cylinders

Coincidence occurs when a vibration mode of the cylinder coincides with an acoustical duct mode of the air within the cylinder. Strictly speaking the acoustic duct modes and the shell modes do not exist independently. But in the case of metal/composite ducts filled with air ($c_l^{/} >> c_s$), the coupled modes retain more or less their uncoupled characteristics. In this case the wave number relations can be superimposed. (This is not exactly true but for the qualitative understanding of the coupled characteristics it is allowed, Fahy [1]). By plotting the wave number relationships in figure 3.10 it can be illustrated at which frequencies the coupled eigenmodes occur. In this figure only modes of the same circumferential order n and the same longitudinal mode m may couple.

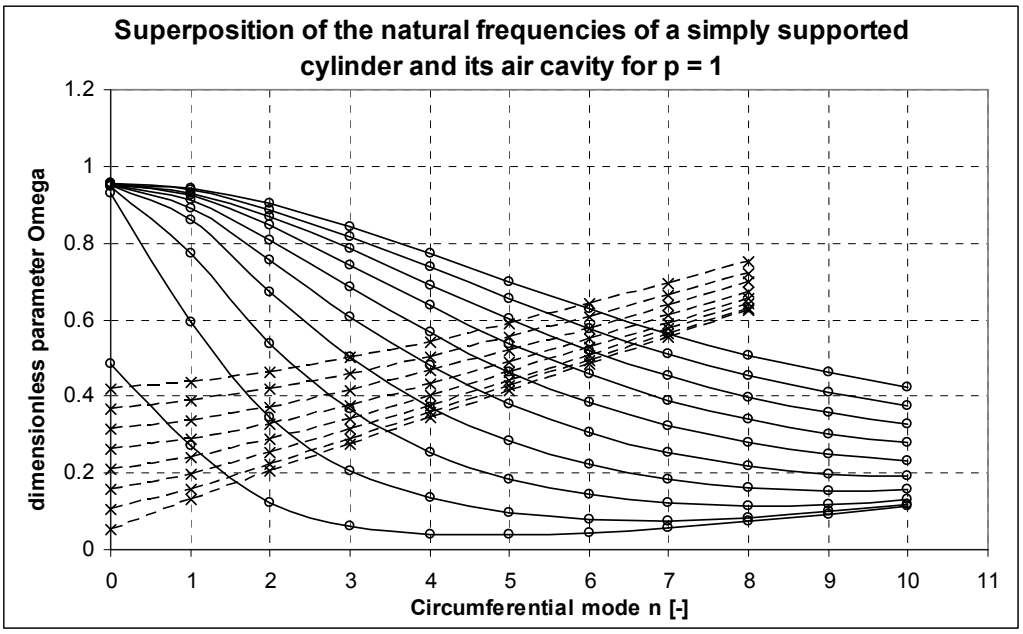

Figure 3.10: *Illustration of coincidence between the cylindrical shell modes (solid lines) and the air cavity modes (dashed lines) for an aluminium simply supported non stiffened cylinder with L_{cil} = 970 mm, R = 252.5 mm and t = 1 mm.*

From figure 3.10 one can see that coincidence, of the low order shell modes and air cavity modes of low radial order p, occur at frequencies close to the air cavity cut-off frequencies. According to Fahy [1], coincidence between the cylindrical shell modes and acoustical duct modes does not occur above the ring frequency because the critical frequency of the wall is always larger than the ring frequency.

The TL of thin cylinders show a low plateau between the lowest acoustic cut-off frequency and the ring frequency caused by coincidence in this region as discussed above. Increasing the cylinder thickness results in less cylinder resonance modes below the ring frequency and therefore less coincidence with the acoustical duct modes, which will increase the TL plateau. Above the ring frequency the TL will increase as it would for flat plates.

3.2.3.4 Concluding remarks on the acoustics of cylinders

By comparing cylindrical thin shells with flat panels it can be concluded that the TL between the lowest acoustical duct mode (n,p = 0,1) and the ring frequency has a low plateau caused by membrane effects. Above the ring frequency, cylindrical shells behave almost like flat panels.

For aircraft with an aluminium fuselage with radius R = 2 m, the ring frequency is: f_r = 400 Hz and f_{01} = 0.12 Hz. So the effects of curvature are only noticeable in the low frequency range.

Since the fuselage interior of an airplane is filled with elements like the floor, lavatory cabins, chairs etc, the fuselage cannot be considered as an empty hollow cylinder and therefore the acoustic duct modes will be disturbed. Some of the interior elements like chairs and floor carpet have high sound absorption coefficients, which also affect the acoustic duct modes. These effects will have a positive influence on the TL.

The acoustic module of the Design & Engineering Engine, which will be discussed in more detail in chapter 6, exists out of two parts. A part that considers the TL for high frequencies based on literature equations and a part that considers the TL for low frequencies based on FEM calculations. Because the cylindrical effects on the sound transmission loss occur in the low frequency range (below the ring frequency) they are not considered in the part based on literature equations, which means that the literature equations used in this module are based on flat plate theory. The coupling effects are taken into account in the low frequency part of the acoustic module.

3.3 Influence of skin thickness

Increasing the skin thickness has according to the infinite flat plate theory (equation 3.7) two consequences:

1.) The mass per unit area of the fuselage panel increases. The increment of the mass per unit area, which is linear with the skin thickness, results in an increment of the TL below the critical frequency of:

$$\Delta TL \approx 20\log_{10}\left(\frac{t_{new}}{t_{old}}\right) \tag{3.22}$$

This means that doubling of the skin thickness results in a 6 dB increase of the TL.

2.) The bending stiffness of the fuselage panel increases. An increase of the skin thickness will result in a decrease of the critical frequency:

$$f_{c\_new} = \frac{t_{old}}{t_{new}} \cdot f_{c\_old} \tag{3.23}$$

At a fixed incident angle the TL above the critical frequency will increase with 18 dB for each doubling of the skin thickness:

$$\Delta TL \approx 20\log_{10}\left(\frac{t_{new}}{t_{old}}\right)^3 \tag{3.24}$$

The resultant TL under field incidence is shown in figure 3.11. Equation 3.24 is also valid under diffuse incidence.

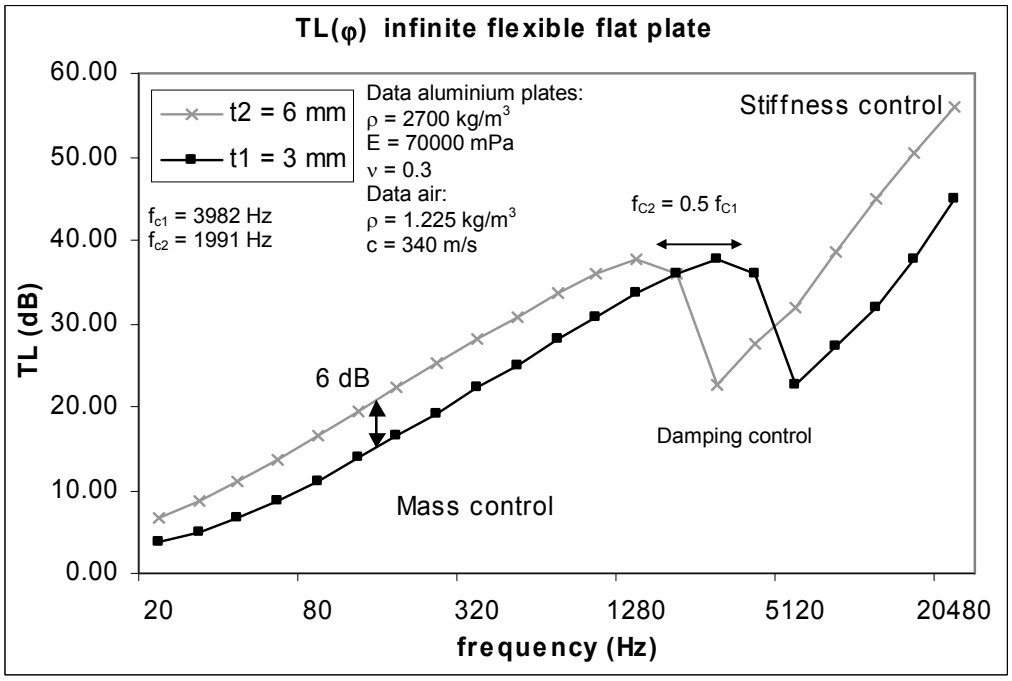

Figure 3.11: *Influence of doubling the skin thickness of an infinite flat plate on the sound transmission loss.*

3.4 Influence of frames and stiffeners

Vér [11] stated that wave motion in finite plates differs from wave motion in infinite plates because of the presence of edges, which reflect waves and cause scattering. Interference between the 'incident' and 'reflected' bending waves can produce standing wave patterns, which may result in transverse panel motions of large amplitudes. The natural frequencies for cylinders were discussed in section 3.2.3.

In order to implement the influence of frames and stringers into the literature equations that are used in the DEE, the TL of stiffened panels can best be discussed in simplified terms of excitation and radiation. When a sound wave hits a panel, this wave will introduce a vibration in that plate. This process is called excitation. The vibration of the plate introduces on its turn sound waves in the air on both sides of the plate. This process is called radiation. Next, both processes are described according to literature equations.

Excitation

Excitation can be expressed with an excitation coefficient. Josse and Lamure [12] estimated the excitation coefficient for a finite stiffened flat panel by:

$$\varepsilon_{ex} = \frac{8\rho_0{}^2 c_s{}^2}{\omega^2 m^2}\left(1+\frac{c_s U\left(1+{f}/{f_c}\right)}{\pi\eta 2S\sqrt{{f}/{f_c}}}\right) \tag{3.25}$$

Figure 3.13 shows the excitation index measured by Von Venzke [13]:

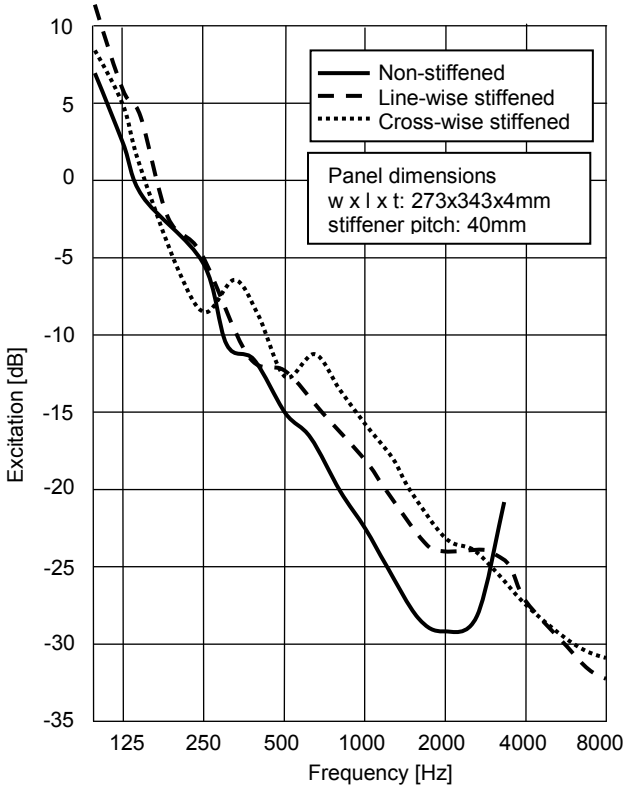

Figure 3.12: *Measured excitation of a non-stiffened, line-wise stiffened and a cross-wise stiffened panel (Identical panels as in figure 3.15 and 3.16) [13].*

Figure 3.12 illustrates that the excitation of the non-stiffened plate is lower than that of the stiffened plate. Equation 3.25 shows that the excitation is dependent on the geometry parameter U/2S. Here U is the perimeter of a sub panel that is defined as a part of the panel surrounded by the stiffeners and S is the sub panel surface. For a skin panel with stringers at stiffener pitch b and frames at frame pitch L_{fr}, U/2S becomes: $(1/b + 1/L_{fr})$. Generally the frame pitch is relatively large compared to the stiffener pitch. Therefore it can be expected that especially an increase of the stiffener pitch will decrease the excitation. Approximately a doubling of the stiffener pitch will result in a 3 dB decrease of the excitation. Note also the presence of the structure loss factor η in the denominator of the equation 3.25.

Radiation

Radiation can be expressed by the radiation efficiency σ_{rad}, Fahy [1]:

$$\sigma_{rad} = \frac{\overline{P}}{\rho_0 c_s \left\langle \overline{v}_n^2 \right\rangle S} \tag{3.26}$$

Where:
$\overline{P}$: Radiated sound power
S: Surface of considered panel
$\left\langle \overline{v}_n^2 \right\rangle$: Time averaged normal velocity and

Fahy [1] gives an approximation of the radiation index of mechanically excited non-stiffened finite panels, which is illustrated in figure 3.13. Other analytical descriptions of the radiation coefficient, are given by Maidanik [14, 15] and Leppinton [16].

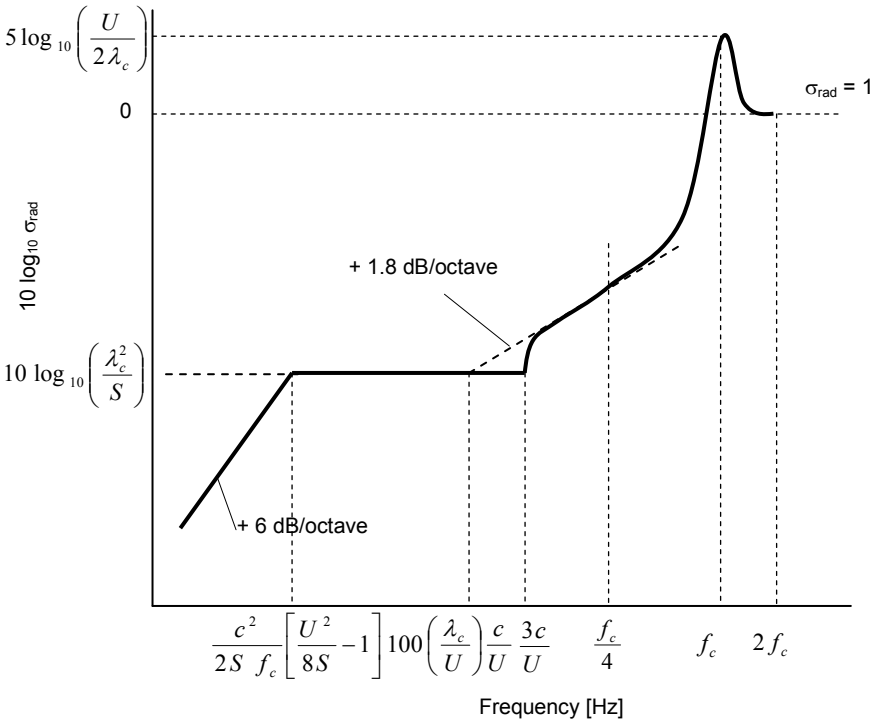

Figure 3.13: *Estimation method of the radiation of a mechanically excited baffled rectangular panel [1].*

In figure 3.13 is:

U:	perimeter of the panel
S:	surface area of the panel
c:	speed of sound in panel material
f_c:	critical frequency of the panel
λ_c:	wave length belonging to critical frequency

Macadams [17] showed that there is a difference in radiation between mechanically excited panels and airborne excited panels. Forssen [18] explained this phenomenon as follows; In case of mechanical (point) excitation almost all modes are equally excited. When a panel is excited by a diffuse sound field, only modes in the panel which are well coupled with the incident field are excited. These modes are in turn efficient sound radiators and thus radiate well into space. Thus, considering two panels, one excited by a diffuse field and one by point excitation, the panel excited by a diffuse field should radiate, below the coincidence frequency, more efficient than the point excited panel. This is illustrated in figure 3.14.

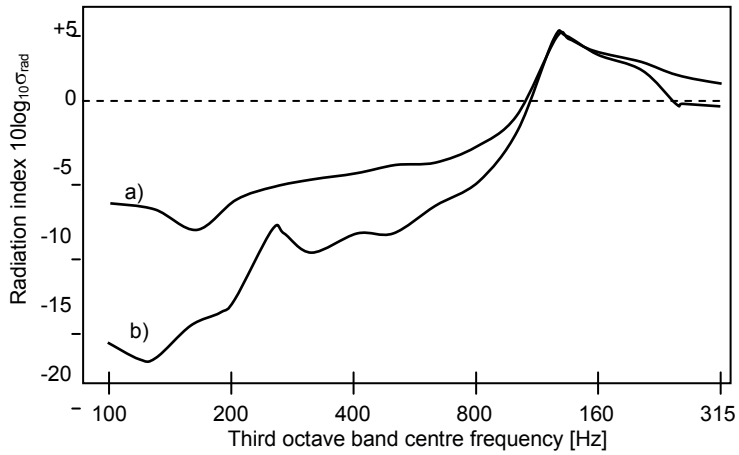

Figure 3.14: *Comparison of radiation efficiencies of a plate under a) airborne excitation and b) mechanical excitation [17].*

Frames and stringers subdivide a large stiffened panel into sub-panels of smaller dimensions. According to the radiation definition given in figure 3.13, small panels with identical thickness and material properties radiate more efficiently than large plates. A more extensive explanation of this effect is given in appendix A. Because a stiffened panel can be considered as an assembly of smaller sub-panels, it is concluded that for identical normal velocity distributions, a stiffened plate will radiate more efficiently compared to a non-stiffened plate. Attention should be paid to the normal velocity distribution that will be influenced by the presence of stiffeners as is expressed by the excitation. An example of radiation of stiffened and non-stiffened panels measured by Von Venzke [13] is shown in figure 3.15. In this case the more stiffened plates radiate slightly more energy.

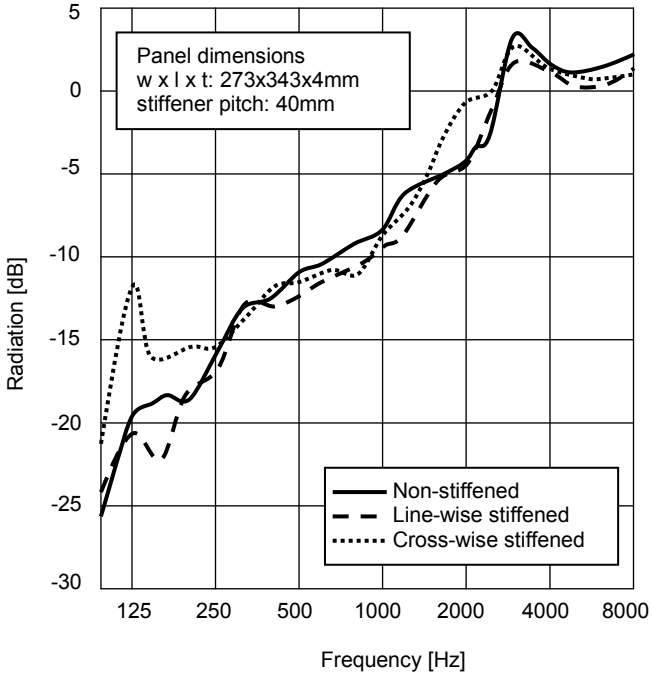

Figure 3.15: *Measured radiation of a non-stiffened, line-wise stiffened and a cross-wise stiffened aluminium panel. (Identical panels as in figure 3.12 and 3.16) [13].*

The resultant sound transmission loss that was measured by Von Venzke [13] for the same panels as for the excitation and radiation measurements shown in figure 3.12 and 3.15, is shown in figure 3.16.

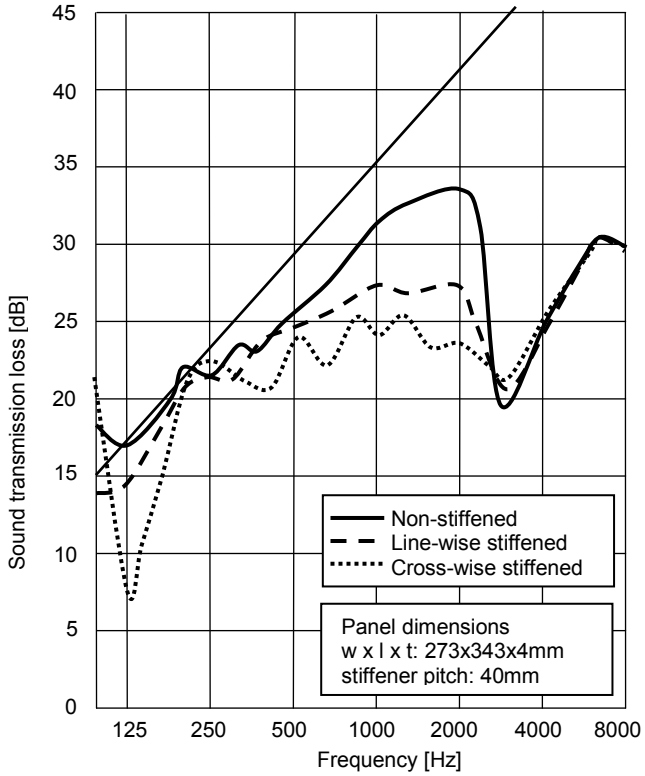

Figure 3.16: *Measured TL of a non-stiffened, line-wise stiffened and a cross-wise stiffened panel. (Identical panels as in figure 3.12 and 3.15) [13].*

In order to implement the influence of frames and stringers into the acoustic module of the DEE a simplification has been made. The influence is estimated by determining the difference in excitation and the difference in radiation with respect to a non-stiffened reference case

$$\Delta TL = -10\log_{10}\left(\frac{\varepsilon_{ex}}{\varepsilon_{ex\,ref}}\right) - 10\log_{10}\left(\frac{\sigma_{rad}}{\sigma_{rad\,ref}}\right) \tag{3.27}$$

In this equation the excitation coefficient ε_{ex} and $\varepsilon_{ex\,ref}$ are determined by equation 3.25 and the radiation efficiency σ_{rad} and $\sigma_{rad\,ref}$ with the equations of figure 3.13. The total TL will be the TL of the non stiffened reference case plus the ΔTL of equation 3.27.

With equation 3.27 some assumptions are made: The estimated radiation efficiency (figure 3.13) is used for mechanically excited panels while in reality a fuselage is airborn excited, which according to figure 3.14 gives a significant difference. However, by determining the difference in radiation to a non-stiffened reference case the absolute difference between airborn and mechanical excitation is

canceled out. Of course this assumption does not give an exact solution but it will show the trends of the influence of frames and stringers. The same assumption counts for the excitation part of equation 3.27. Furthermore the TL_{ref} is determined for infinite flat panels. Therefore the sub-panel reference dimensions in equation 3.27 are chosen to simulate a non stiffened panel.

3.5 Sound transmission loss of sandwich panels

As discussed in section 3.1, the sound transmission of a single panel is characterised by the free flexural deformation mode. For a sandwich panel, the sound transmission is characterised by a combination of the free flexural deformation mode (figure 3.17A) and the shear deformation mode (figure 3.17B). When the core material is compressible also dilatation modes are of influence (figure 3.17C).

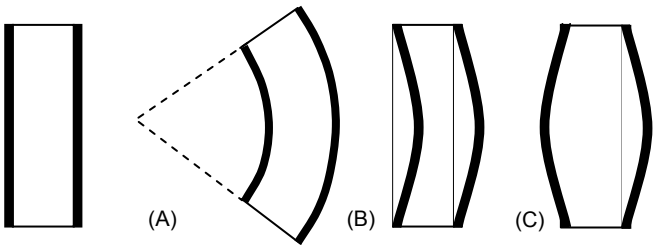

Figure 3.17: *Sandwich deformation modes: Flexural (A), shear (B) and dilatation (C).*

In this section a simplified empirical equation is given [19] (equation 3.28), that is used in the acoustic module of the DEE discussed in chapter 6, to estimate the sound transmission loss for sandwich panels. A more theoretically correct discussion of the sound transmission loss is discussed in appendix B.

Equation 3.28 is a combination of the mass law, a forced and resonant transmission loss term and a dilatation response term. The forced response determines the sound transmission loss below the critical frequency. Above the critical frequency the resonant transmission terms are dominant.

$$TL = TL_0 - 10\log_{10}\left[\frac{2\sigma_{rad\ d}}{\left(1-\left(\frac{f_{11}}{f}\right)^2\right)^2\cdot\left(1-\left(\frac{f}{f_c}\right)^2\right)^2+\eta_{eq}^2}+\frac{\pi\sigma^2 f_c}{2\eta f}\right]+10\log_{10}\left[\left(1-\left(\frac{f}{f_{dil}}\right)^2\right)^2+\eta_{eq}^2\right] \quad (3.28)$$

Mass law | Forced and resonant transmission | Dilatation response

Where:

$$TL_0 = 20\log_{10} m + 20\log_{10} f - 42$$ Mass law

$$f_c = \frac{c_s^{\,2}}{2\pi}\sqrt{\frac{m}{D}}$$ Critical frequency

$$f_{11} = \frac{\pi}{2}\sqrt{\frac{D}{m}} \cdot \left[\left(\frac{1}{b}\right)^2 + \left(\frac{1}{L}\right)^2 \right]$$

First natural frequency of rectangular panel with dimensions b x L

$$f_{dil} = \frac{1}{2\pi}\sqrt{\frac{\frac{4}{3}E_c}{t_c\left(2m_f + \frac{m_c}{3}\right)}}$$

Dilatation frequency

$$\sigma_{rad} = \frac{Uc_s}{\pi^2 S f_c^{3/2}}\sqrt{f}$$

Radiation coefficient for f << f_c

$$\sigma_{rad} = 0.45\sqrt{\frac{Uf_c}{c_s}}$$

Radiation coefficient for f = f_c

$$\sigma_{rad} = 1$$

Radiation coefficient for f >> f_c

$$\sigma_{rad\,d} \cong \frac{1}{2}\left(0.2 + \ln\left(2\pi\frac{f}{c_s}\sqrt{S}\right)\right)$$

Radiation coefficient

$$\eta_{eq} = \sqrt{\eta_c^{\,2} + 0.1\eta_c}$$

Equivalent loss factor

$$D = \frac{1}{2}E_f t_f \left(t_f + t_c\right)^2$$

Sandwich stiffness

$$m = m_c + 2m_f$$

Sandwich surface mass

Furthermore:

S:	Panel area
U:	Perimeter of the panel
c_s:	Speed of sound in air
m:	Mass per unit area
E:	Modulus of elasticity
η_c:	Loss factor of core material

Note: In future use of the DEE the empirical equation 3.28 should be replaced by a more theoretical correct set of equations that are discussed in appendix B. Unfortunately, at the time the DEE was developed this was not yet the case and therefore the calculations of chapter 10 and 11 are still determined with the empirical equation 3.28.

An example of sound transmission loss measurements on three sandwich panels with different core properties is given in figure 3.18 by Ford, Lord and Walker [20]. The material properties, dimensions and the characteristic frequencies of these sandwich panels are given in table 3.3.

Figure 3.19 gives the sound transmission loss for the same three sandwich panels determined with equation 3.28.

Table 3.3: *Material properties of the three sandwich panels described in figure 3.18 and 3.19.*

	Panel A	Panel B	Panel C
Facing:			
Thickness (mm)	4	4	4
Density (kg/m^3)	800	800	800
Elasticity (N/m^2)	1.3e9	1.3e9	1.3e9
Poisson's ratio	0.3	0.3	0.3
Loss factor	0.02	0.02	0.02
Core:			
Thickness (mm)	50	50	50
Density (kg/m^3)	31	104	181
Elasticity (N/m^2)	5.62e6	3.05e7	1.09e8
Shear modulus (N/m^2)	1.2e6	8.7e6	3.02e7
Poisson's ratio	0.3	0.3	0.3
Loss factor	0.041	0.035	0.023
Dimensions			
Length (m)	1	1	1
Width (m)	1	1	1
Characteristic frequencies			
f_{11} (Hz)	97	80	70
f_{dil} (Hz)	741	1590	2800
f_c (Hz)	596	720	831

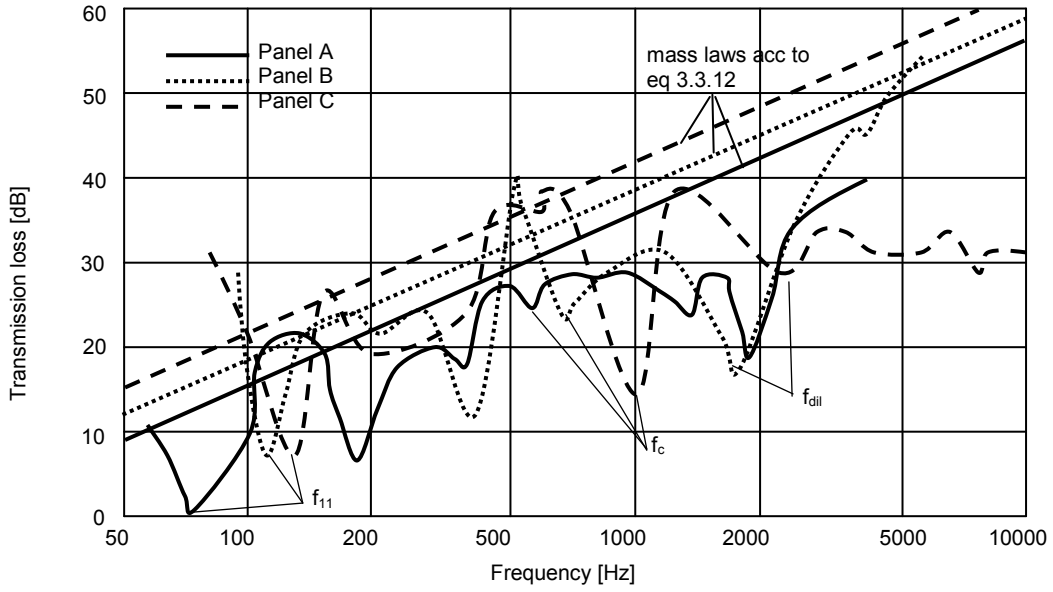

Figure 3.18: *Sound transmission loss measurements of three 1 m^2 sandwich panels with different core properties [19]. The corresponding material properties can be found in table 3.3.*

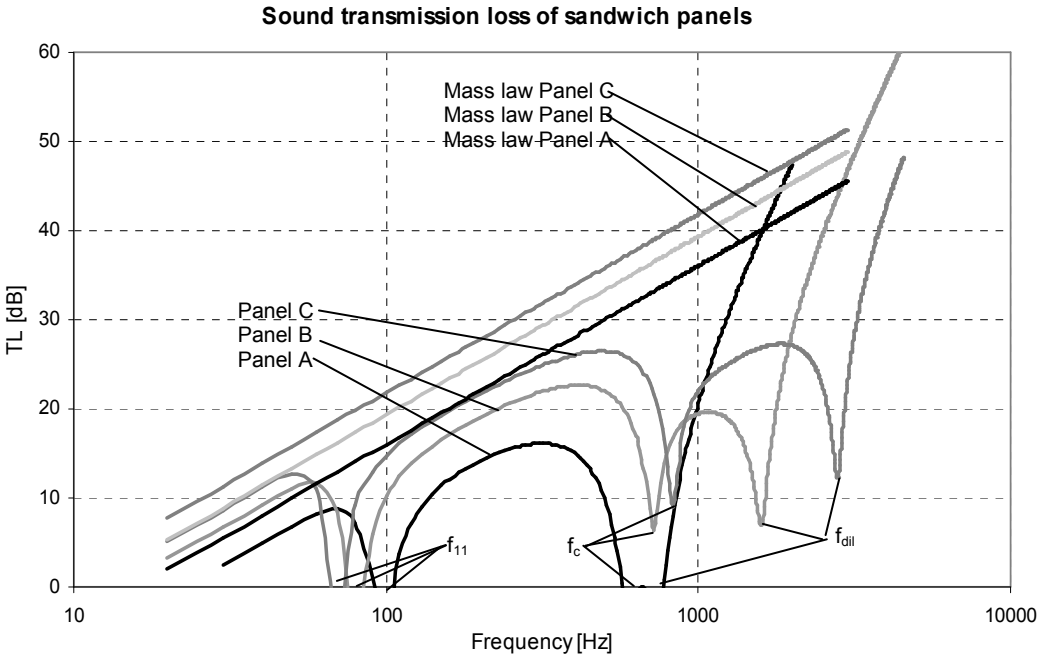

Figure 3.19: *Sound transmission loss of three 1 m² sandwich panels with different core properties determined with equation 3.28. The corresponding material properties are given in table 3.3.*

A comparison of figure 3.18 and figure 3.19 shows that the general tendency predicted with equation 3.28 corresponds with the experimental data taken from Ford, Lord and Walker [20]. However, it is difficult to recognise the different natural frequencies as well as the critical frequency and the dilatation frequency. It should be noticed that for small panels like 1 m^2, the influence of boundary or mounting conditions can be of importance. Therefore, it is difficult to interpret the results of these sound transmission loss measurements.

Depending on the D/m ratio, the f_{11} resonant frequency (in)decreases and the coincidence frequency (de)increases. The dilatation frequency also depends on the core properties. For good sound transmission loss behaviour, it is favourable to have high coincidence and dilatation frequencies, because TL dips in the low frequency range are more difficult to cope with. At high frequencies, it is easier to take acoustic measures like the addition of insulation blankets. This will be discussed in section 3.7. From these relations, it may be concluded that the designer can use the D/m ratio to optimise the sound transmission loss.

Besides the stiffness density ratio, Smolenski and Krokovsky [21] identified several strategies to increase the dilatation frequency:

- Increase the Poisson ratio of the core material (until it reaches the value 0.5). When the Poisson ratio reaches 0.5, the core bulk modulus:

$$K_c = \frac{E_c}{3(1-\nu_c)} \tag{3.29}$$

becomes infinite, which implies that the core becomes incompressible and the dilatational frequency therefore becomes infinite. However, the flexural vibration modes remain almost unchanged.
- The dilatational response of a given panel with a constant bulk modulus is quite sensitive to the thickness of the core. Decreasing the core thickness results in an increased dilatational frequency. Again the flexural vibration modes remain virtually unchanged.

Lang and Dym [22-25], distinguished two sandwich design strategies for optimal integration of mechanics and acoustical insulation:
- The first design strategy is to choose a coincidence frequency as high as possible. In that case the TL follows the mass law as long as possible. For a high coincidence frequency it is necessary to choose a core material with a very low shear modulus. A consequence of this low shear modulus is a dilatation frequency. Conform this strategy it is also tried to have a dilatation frequency as high as possible (preferably also above the frequency range important for speech).
- The second design strategy is to choose a core material with a high shear modulus so the core will behave like an incompressible material. This way the dilatation frequency can even be eliminated. The high shear modulus of the core makes this sandwich more structurally efficient. The major disadvantage of this strategy is that the coincidence frequency will be relatively low.

Which of these two strategies will give the best result depends on the noise source and on the structural requirements for the sandwich panels. Nevertheless a sandwich construction has great potential to combine a high structural efficiency with good acoustical properties.

3.6 The interior panel

The TL of a double wall is larger than the TL of a single wall of the same mass per unit area: $TL(m_1) + TL(m_2) > TL(m_1 + m_2)$. In reality the TL of a double wall is not simply the summation of the TL of the two separate walls because resonance can occur in the air cavity between the two walls.

Fahy [1] gives a theoretical explanation of the TL through two infinite flexible flat plates, which are separated by an air cavity. In case the air on both sides and in between the two plates has the same properties, the ratio between the transmitted to incident complex pressure amplitude is:

$$\frac{\tilde{p}_t}{\tilde{p}_i} = -\frac{2j\rho_0^2 c_s^2 \sec^2\varphi \sin(kd_w \cos\varphi}{\tilde{z}_1\tilde{z}_2 \sin^2\left(kd_w \cos\varphi\right) + \rho_0^2 c_s^2 \sec^2\varphi} \tag{3.30}$$

Here is:

$$\tilde{z}_1 = j\omega m_1 + r_1 + \rho_0 c_s \sec\varphi\left[1 - j\cot(kd_w \cos\varphi)\right]$$
$$\tilde{z}_2 = j\omega m_2 + r_2 + \rho_0 c_s \sec\varphi\left[1 - j\cot(kd_w \cos\varphi)\right]$$

$r_1 = \eta_1\omega_1 m_1$ where ω_1 is the natural frequency of wall 1.
$r_2 = \eta_2\omega_2 m_2$ where ω_2 is the natural frequency of wall 2.

k:	the wave number of the incident wave
d_w:	the distance between the two walls
m:	the mass per unit area
η	structure loss factor
ρ_o	density of air
c_s	speed of sound in air
φ:	the sound wave incident angle

(the indices 1 and 2 refer to respectively wall 1 and wall 2).

Then the TL can be determined according to:

$$TL = 10\log_{10}\left(\frac{\tilde{p}_i^2}{\tilde{p}_t^2}\right) \tag{3.31}$$

The nature of this equation can be explained by considering the equation for low and for high frequencies, Fahy [1]:

Low frequencies:

For very low frequencies: $kd_w\cos\varphi << 1$, $\rightarrow$ the acoustic damping ($\rho_0 c_s \sec\varphi$) and the mechanical damping (r) can be neglected. The transmission coefficient τ is then maximal when the denominator is minimal. This happens at the frequency:

$$\omega_r = \sqrt{\left(\frac{\rho_0 c_s^2}{d_w}\right)\left(\frac{m_1 + m_2}{m_1 m_2}\right)} \cdot \sec\varphi \tag{3.32}$$

This frequency is called the mass-air-mass resonance frequency. The lowest mass-air-mass resonance, called ω_0, occurs at normal incidence ($\varphi = 0$). Above ω_0, there always exists an angle φ at which mass-air-mass resonance occurs.

For low frequencies the transmission behaviour can be classified as follows:

- Below the mass-air-mass frequency: $\omega < \omega_0 \sec\varphi$
  (The wavelength of the incident sound wave is large compared to the cavity width d_w):

$$\frac{\tilde{p}_t}{\tilde{p}_i} \cong \frac{-2j\rho_0 c_s}{\omega(m_1 + m_2)\cos\varphi} \tag{3.33}$$

  In this region the TL follows the mass law for TL($m_1 + m_2$). The two walls act like one.
- Close to the mass-air-mass frequency: $\omega \cong \omega_0 \sec\varphi$:
  In this case the damping terms may not be neglected.

$$\frac{\tilde{p}_t}{\tilde{p}_i} \cong \frac{-2\rho_0 c_s \sec\varphi}{\left(\eta_1\omega_1 m_1 + \eta_2\omega_2 m_2 + \left(\frac{m_1}{m_2} + \frac{m_2}{m_1}\right)\rho_0 c \sec\varphi\right)} \tag{3.34}$$

  It is seen that at the mass-air-mass resonance the TL mainly is determined by the structure loss factors of the two walls.

- Above the mass-air-mass frequency: $\omega > \omega_0 \sec\varphi$:

$$\frac{\tilde{p}_t}{\tilde{p}_i} \cong \frac{2j\rho_0 c_s}{\omega(m_1+m_2)\cos\varphi}\left(\frac{\omega_0 \sec\varphi}{\omega}\right)^2 \tag{3.35}$$

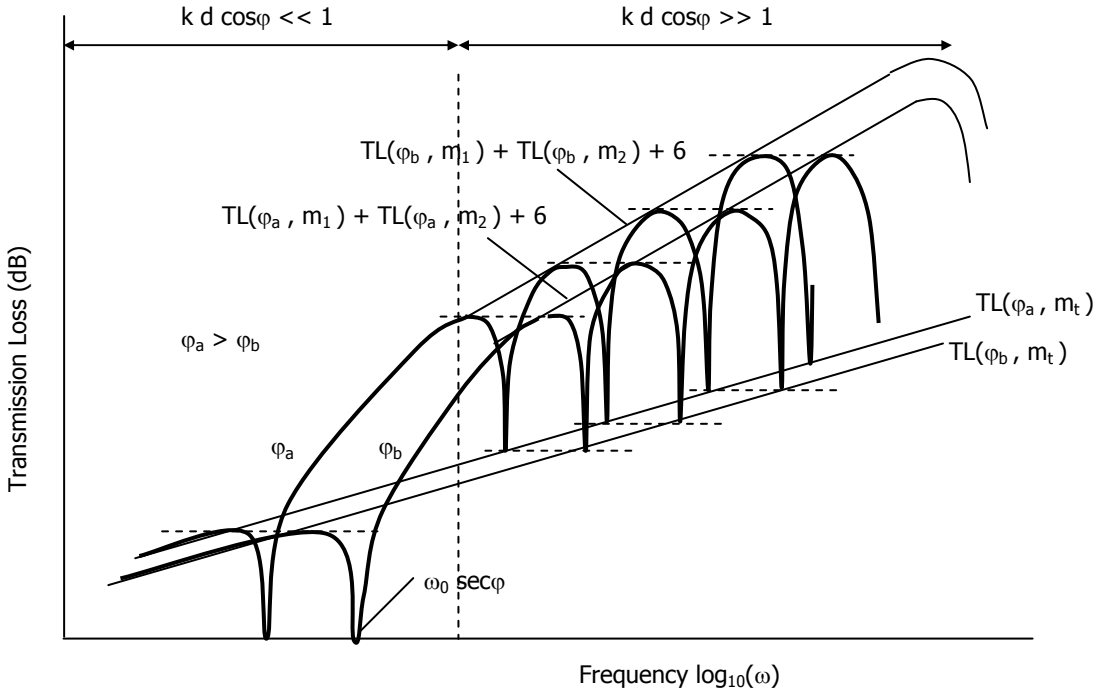

Figure 3.20: *TL of a double wall with air on both sides and in between the two walls with identical properties for two incident angles φ_a and φ_b [1].*

High frequencies:

For higher frequencies $kd_w\cos\varphi << 1$ is no longer valid. Figure 3.20 shows that the general equation for the sound transmission loss at a particular incident angle varies between transmission loss minima at cavity resonance and transmission loss maxima at cavity anti-resonance frequencies.

- The TL at the anti-resonance frequencies $\omega = (2n-1)\pi c_s/(2d_w\cos\varphi)$ are given by the summation of the mass laws of the separate walls plus 6 dB:

$$TL(\varphi) = TL(\varphi, m_1) + TL(\varphi, m_2) + 6 \tag{3.36}$$

  So at the anti resonance frequencies, the total TL is even higher than just the summation of the TL of the two separate walls!

- The TL at the resonance frequencies $\omega = n\pi c_s/(d_w\cos\varphi)$ are given by the mass law where the two walls act like one:

$$TL(\varphi) = TL(\varphi, m_t) \tag{3.37}$$

It is found that the TL at the anti-resonance frequencies is maximal when the mass per unit area of the two walls is the same ($m_1 = m_2$). However the TL close to the mass-air-mass frequency will be minimal for $m_1 = m_2$. Also the TL at the coincidence frequencies of the two walls will be minimal when $m_1 = m_2$ because then the coincidence frequencies of both plates are identical. Therefore, usually a compromise is chosen: $m_1 \neq m_2$ but still of the same order.

3.7 Insulation Blankets

To reduce the resonance effect in the cavity between two walls an absorbent material can be inserted in the cavity. The absorption of the absorbent material will cause the sound wave amplitude to decay with travelled distance through the absorbent material and therefore the reflected wave will be weakened, which decreases the resonance effect.

Beranek [26] discussed the TL of a fibrous absorbent blanket. The TL of such a material can be divided into three frequency regions:

- Region A: This frequency region is bounded by the frequency at which the wavelength of sound within the blanket (λ_m) is one tenth of the thickness of that blanket (d_{bl}). In this frequency region an absorbent blanket possesses insufficient inertia to remain motionless under excitation. The TL of a blanket in this frequency region is given by:

$$TL = 10\log_{10}\left\{1 + \frac{\frac{R_f}{\rho_0 c_s}\left(\frac{\omega m_{bl}}{\rho_0 c_s}\right)^2\left(4 + \frac{R_f}{\rho_0 c_s}\right)}{4\left[\left(\frac{R_f}{\rho_0 c_s}\right)^2 + \left(\frac{\omega m_{bl}}{\rho_0 c_s}\right)^2\right]}\right\} \tag{3.38}$$

Here is: R_f: the flow resistance of insulation blanket with thickness d_{bl}.
m_{bl}: the mass per unit area of the blanket.
$\rho_0 c_s$: the characteristic resistance of air

- Region C: In this frequency region, three different components R_1, R_2 and R_3 contribute to the TL of the blanket. The first contribution R_1, usually the largest of the three, affects the portion of the sound wave that enters and travels through the blanket, and comprises the loss suffered by the wave in a single passage through the blanket:

$$R_1 = 8.69\alpha d_{bl} \tag{3.39}$$

Here is: α: the sound attenuation constant
d_{bl}: the thickness of the blanket

The contributions R_2 and R_3 are caused by the reflection of a part of the wave at the air-blanket interface (R_2) and the blanket-air interface (R_3). These contributions are determined by the ratio of characteristic impedance of the blanket (Z_{bl}) and air

($\rho_0 c_s$) and are shown in figure 3.21. The total TL in this region is: TL = R_1 + R_2 + R_3. When the blanket is attached to a plate the reflection contribution R_2 and/or R_3 will be zero because usually the plate impedance is much greater than the blanket impedance. Region C is the frequency range for which $\alpha d > 1$ dB.

- Region B: Region B is the transition region between regions A and C. For this region no exact TL equation exists. The TL can be determined graphically, by fairing a curve smoothly between the plotted TL curve segments of regions A and C.

When a fibrous insulation blanket is inserted in the cavity of a double wall, the frequency, which separates region A and B, changes according to Beranek [26] from the frequency at which $\lambda_m = 10 d_{bl}$ to 1.5 f_0. Here, $f_0 = (\omega_0/2\pi)$ is the lowest mass-air-mass resonance discussed in section 3.6. In this case the TL in region A will practically be zero. The TL in region C consists then out of the summation of the TL of the wall 1 (as determined in section 3.2), the blanket (calculated according to this section) and wall 2 (also as determined in section 3.2).

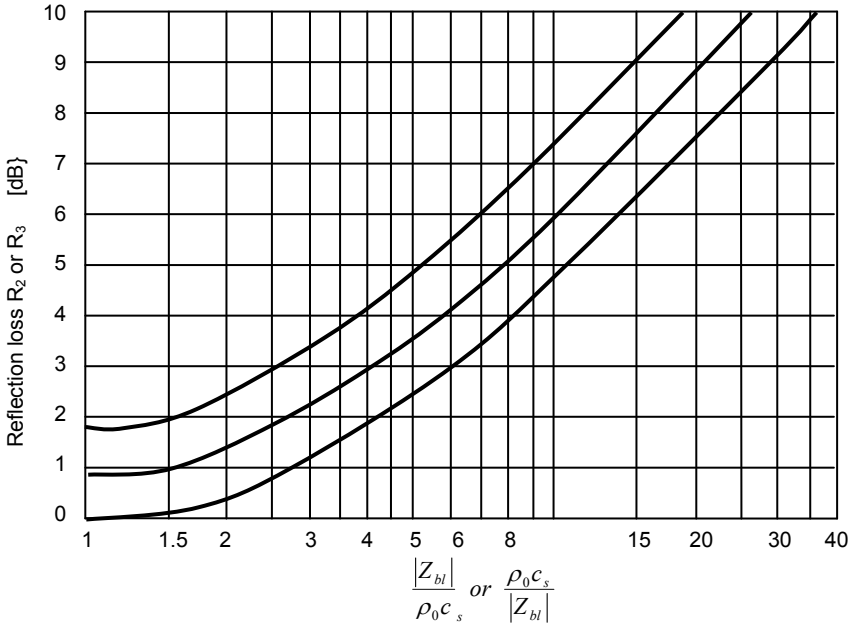

Figure 3.21: *Determination of R_2 and R_3. [26]*

Figure 3.22 shows the TL of a 7.5 cm blanket (9.6 kg/m^3) placed between an aluminium skin (3.55 kg/m^2) and a plywood 'interior' panel (2.5 kg/m^2) calculated according to the method mentioned above. This figure shows that the blanket and the extra wall, that together have a mass per unit area of 3.22 kg/m^2 (little less than the aluminium skin), improve the TL considerably in the for the human ear critical frequency region 250 - 5000 Hz. Therefore this sound insulation method is often used in aircraft fuselages. A demand for the application of this insulation method is that the two walls are not rigidly connected. If the two walls are rigidly connected the second wall will be exited through the rigid connection and radiate sound as much as the first wall did. For this reason the interior panels in aircraft fuselages are attached to the skin by vibration isolators.

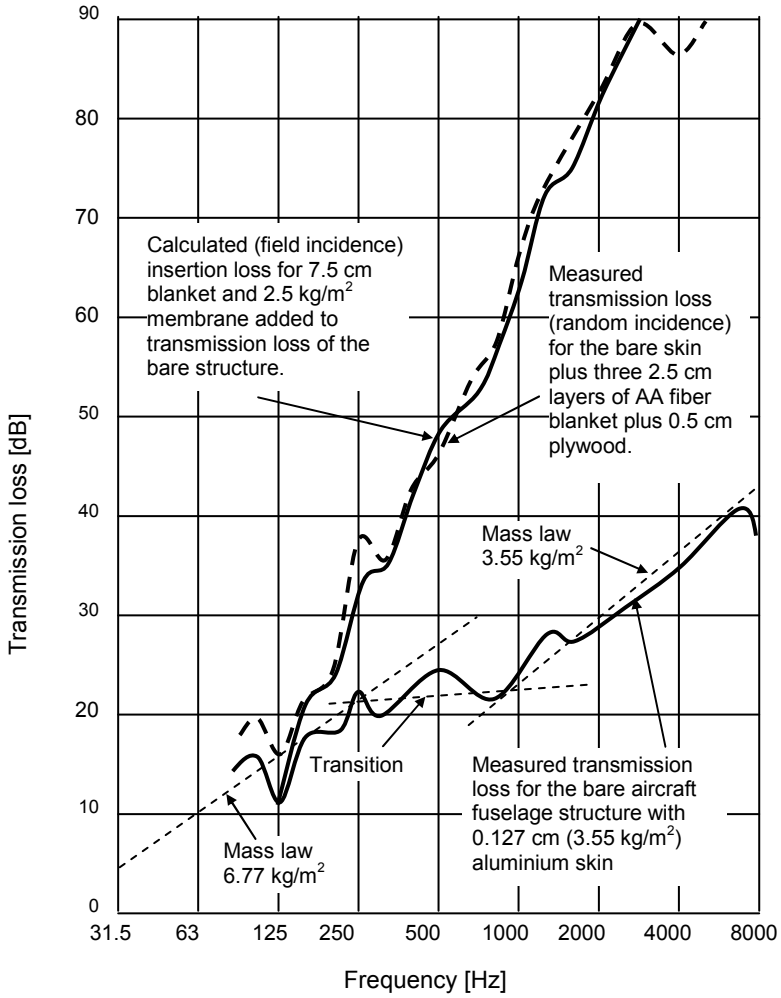

Figure 3.22: *TL of a double wall with an insulation blanket [26]*

3.8 Application of viscoelastic layers

The purpose of inserting a viscoelastic layer in the skin is to improve the acoustic efficiency by increasing the damping factor. In this section the influence of a viscoelastic layer on the transmission loss and the influence on the structural properties will be discussed. Appendix C gives an example of a panel with viscoelastic layers of different thickness.

For a viscoelastic material Hooke's law: $\sigma = E\,\varepsilon$ is no longer valid. According to Cremer [4] a viscosity model is valid: $\sigma = E\,(\varepsilon + \upsilon\, d\varepsilon/dt)$ where υ is strongly frequency dependent. When $\varepsilon = \boldsymbol{\varepsilon}\, e^{i\omega t}$ is inserted in the viscosity model, the following equation is found: $\sigma = E(1 + i\omega\upsilon)\boldsymbol{\varepsilon} e^{i\omega t}$. By defining: $E^* = E(1 + i\beta)$ in which $\beta = i\omega\upsilon$ is the loss factor of the viscoelastic material, the general accepted "complex modulus of elasticity" notation is found. Only the real part of E^* has a physical meaning. The modulus of elasticity E and the loss factor β are material properties that are frequency and

temperature dependent. Usually the manufacturer of the viscoelastic material supplies the material properties as function of frequency.

The damping principle of a viscoelasic layer can be explained by considering the potential energy that is needed to deform a plate with a viscoelastic layer: $U = \int \sigma \, d\varepsilon = 0.5 \, E\varepsilon^2 + 0.5 \, i\beta E\varepsilon^2$. The real part causes the actual deformation and the imaginary part is the part of energy that will dissipate into heat. The incident sound power can be considered as the potential energy that causes a plate to vibrate. Then a part of this energy will dissipate into heat and therefore less energy will be radiated on the other side of that plate.

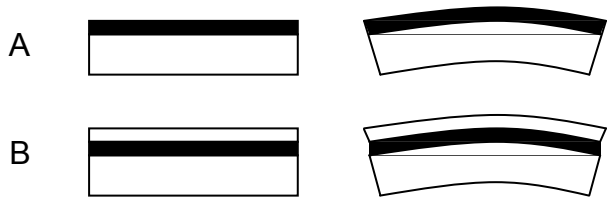

Figure 3.23: *Non-constrained (A) and constrained (B) viscoelastic layer*

There can be distinguished two cases Kerwin [27] to deform a viscoelastic layer like shown in figure 3.23:

- A) A viscoelastic layer attached to a plate without a constraining boundary layer. Here the viscoelastic layer is extensionally loaded so the damping will be a function of $E^* = E(1 + i\beta)$.
- B) A viscoelastic layer attached to a plate with a constraining boundary layer. Here the viscoelastic layer is loaded in shear so the damping will be a function of $G^* = G(1 + i\beta)$.

According to Cremer [4], the constrained boundary layer case has some advantages compared to the non-constrained case:

- Higher loss factors are possible with a relatively thin layer. This means a relatively small amount of extra weight per improved decibel.
- Because in the constrained case a relative small thickness is required to achieve high loss factors, the stiffness and therefore the critical frequency will not increase much.
- The constraining layer is made of a constructive material, which contributes to the structural efficiency.

Because of these reasons, only the constrained viscoelastic layer case is considered. It is assumed that for the constrained viscoelastic layer case, the constraining layer is stiff enough and does not wrinkle under deformation.

Previous sections showed that at resonance frequency, the TL of a panel is strongly dependent on the loss factor. As noticed before the loss factor and the shear modulus are frequency and temperature dependent. The viscoelastic properties: β (loss factor) and the shear modulus of elasticity G, are taken into account in the TL by the structure loss factor η and the (changed) bending stiffness EI. The structure loss

factor η is a factor that combines the influence of the loss factor of the viscoelastic material β, with the geometrical configuration and the material properties of the plate.

Derby and Ruzicka [28] developed a procedure to determine η and EI as a function of frequency (at a certain temperature) for a plate with a constrained viscoelastic layer. The structure loss factor and for the bending stiffness are determined according to the following equations:

$$\eta = \frac{\beta XY}{1 + X(Y+2) + (1+\beta^2)X^2(Y+1)} \tag{3.40}$$

$$EI = EI_0(1+ZY) \tag{3.41}$$

Here is:

β: Loss factor of the viscoelastic material

Y: Geometrical parameter

$$Y = \frac{(EI)_\infty}{(EI)_0} - 1$$

EI_0: Uncoupled bending stiffness per unit width. (Plate and the constraining layer are completely uncoupled).

EI_∞: Coupled bending stiffness per unit width. (Plate and constraining layer are completely coupled).

Z: Coupling parameter

$$Z = \frac{X(1+X) + X^2\beta^2}{(1+X)^2 + X^2\beta^2}$$

X: Shear parameter

$$X = C\left(\frac{G}{f}\right)\sqrt{1+ZY}$$

C: Viscoelastic speed constant

$$C = \frac{b}{2\pi K t_v}\sqrt{\frac{(EI)_0}{m(1-\nu^2)}}$$

K: Extensional stiffness constant (subscript p: plate, c: constraining layer)

$$K = \frac{(EA)_p(EA)_c}{(EA)_p + (EA)_c}$$

b: Width of the plate

m: Mass per unit area (complete panel)

t_v: Thickness of the viscoelastic layer

ν: Poisson ratio of the elastic layers

Because the shear parameter X is dependent on the coupling parameter Z and vice versa an iteration process is required. This iteration process is started with the assumption of a completely uncoupled situation. (Z = 0).

From a parameter study the following can be concluded:

- With increasing β, η increases. For any kind of material, the values of β vary between $0.01 < \beta < 1.5$. The value of β for viscoelastic materials can be found at the high end of this range.
- With increasing Y, η increases for constant values of X and β. Y is maximal when the viscoelastic layer is positioned in the middle. (Thickness of the plate equal to thickness of the constraining layer). Also increasing the viscoelastic layer thickness t_v results in an increased geometrical parameter Y.
- The structural loss factor η is maximal when X varies between 0,1 and 1. This implies the following boundary conditions for the shear modulus of the viscoelastic material:

$$\frac{0{,}1}{C\sqrt{1+Z_{(X=0{,}1)}Y}} \leq \left(\frac{G}{f}\right)_{elastomer} \leq \frac{1}{C\sqrt{1+Z_{(X=1)}Y}} \qquad (3.42)$$

When the lay-up of the plate is determined, the values of the geometrical parameter Y and the viscoelastic speed constant C are set. Because the coupling parameter Z is not strongly dependent on β and it is favourable to have a large β, β is chosen equal to 1.0 to estimate Z at X = 0,1 and X = 1. With the boundaries of equation 3.42 the optimal viscoelastic material can be selected. Note that, since the boundaries that determine the selection area are dependent on Y and C, the optimum viscoelastic material is dependent of the geometry of the skin.

From section 3.2 it is concluded that the TL is only moderately dependent on the loss factor below the coincidence frequency. Above the coincidence frequency the TL improvement caused by the increment of the structure loss factor can be estimated by:

$$\Delta TL = 10\log_{10}\left(\frac{\eta_{new}}{\eta_{old}}\right) \qquad (3.43)$$

Here is η_{old} the structure loss factor of the skin without a viscoelastic layer and η_{new} the structure loss factor of the skin with a viscoelastic layer.

The added damping is of importance to improve the transmission loss at the natural frequencies for each sub panel of a stiffened fuselage skin. However, even a very good damping layer would not improve the sound transmission loss by more than 1 to 2 dB in the frequency range of interest and below the coincidence frequency.

3.9 Application of active noise control

Two major groups of active noise control can be distinguished. The first group is the generation of anti noise: Concealed microphones throughout the interior continuously transmit changing noise patterns to a microprocessor, which creates counterbalanced sound waves that are broadcasted through cabin speakers. The objective is to reduce the noise levels with the produced anti noise. This concept has already successfully been applied at the blade passage frequencies in the ATR 42 and 72, deHavilland Dash 8Q, Canadair Challenger 601 and 604, Saab 2000 and 340B, the Beech King Air 200, 300 and 350 and the Twin Commander, which are all propeller aircraft. For jet powered aircraft these active noise control systems would have been ineffective.

The second group is the generation of anti vibration in the noise radiating structure. This system consists out of monitoring sensors and controlling actuators that are mounted on the structure. The sensors sense the vibration signal. This signal is sent to an electric control unit that determines the required signal to the controlling actuators to counterbalance the vibration.

Within this research only the active vibration control concept is considered, which makes use of piezoelectric actuators.

During this PhD research the author participated in the Smart Panel project of TNO. In this project active noise control with PZT actuators on composite panels was considered. A parametric numerical tool had to be developed that delivers four transfer functions, to calibrate the active noise control prediction algorithms of TNO. Unfortunately this project was terminated before this concept could be successfully applied. Because the prediction algorithms are property of TNO, in this thesis only the parametric tool will be described in chapter 6. To give an impression of piezo electric actuators, a short introduction into piezoelectric materials is given followed by a short description of the linear piezoelectric theory. Finally the working principle of the considered active vibration control concept will be explained.

3.9.1 Piezoelectric material

Actuators for active noise control are usually made of piezoelectric materials. The most common piezoelectric material used in active noise control systems is PZT (Lead zirconate titanate). It has an ABO_3 perovskite type crystal structure (See figure 3.22). Where A is a Zr^{+4} zirconium or Ti^{+4} titanium ion, B is a Pb^{+2} lead ion and O is the O^{-2} oxygen ion.

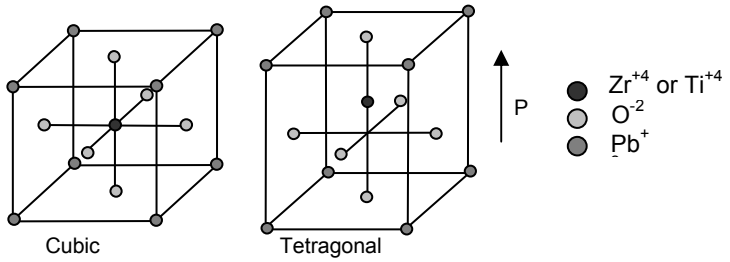

Figure 3.24: *PZT above T_C (cubic) and below T_C (Tetragonal (shown) or Rhombohedral (not shown)).*

The principle of the piezoelectric property of PZT can be visualised by showing the unit cell of PZT. Above the Curie temperature the unit cell is cubic and electrically neutral. Below the Curie temperature the unit cell undergoes a phase transformation to either a tetragonal or rhombohedral structure, depending on the composition. Figure 3.24 shows that for the tetragonal structure the zirconium or titanium ion shifted towards a mid-plane resulting in a polarization of the unit cell.

However, for poly-crystals the polarization of each crystal will be randomly oriented resulting in a zero net polarization as is shown in figure 3.25A. When the temperature is lowered below the Curie temperature while an electrical field is applied, the PZT crystals are forced to be oriented in the field direction as much as possible as is illustrated in figure 3.25B. Such PZT materials can be used for actuator applications.

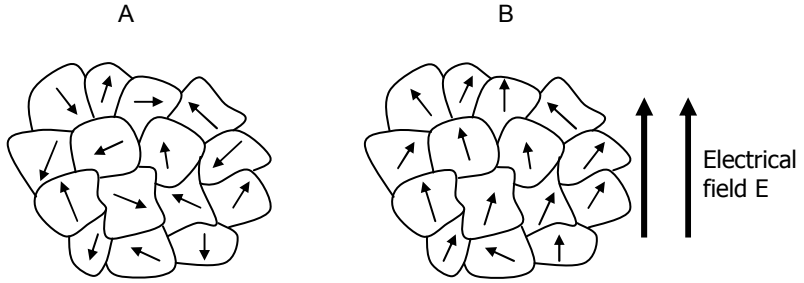

Figure 3.25: *A) Randomly oriented poly-crystal. No net polarization*
B) Electrical field forces the polarization in field direction causing the total poly-crystal to be polarized

The piezoelectric behaviour can be characterised by the piezo electric strain coefficient d and the ultimate strain. The d-coefficient is defined as the gradient between the strain and the applied electrical field. There are two types of PZT: Soft and Hard PZT. Soft PZT switches easier in polarization direction compared to hard PZT. Soft PZT generally has higher values of the d-coefficient but show more hysteresis. Hard PZT behave more linear as is indicated in figure 3.26.

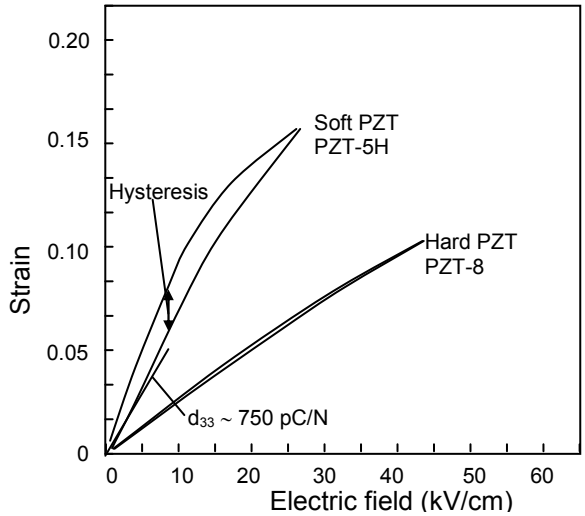

Figure 3.26: *Difference between hard and soft PZT. Soft PZT show large piezoelectric strain coefficients compared to hard PZT but they also show more hysteresis [29].*

Usually soft PZT materials have a relatively large maximum allowable strains but hard PZT materials can develop larger actuator forces. The last decade, single crystals are developed that show superior piezoelectric behaviour, see Park and Shrout [29]. For single crystal PZT ultimate strain levels of 1.7% are reached.

3.9.2 Depolarisation

When the temperature rises above the Curie temperature the piezoelectric material will depolarise because the crystal phase will switch to the electrically neutral cubic structure. When afterwards the temperature is lowered below the Curie temperature the poly-crystal piezoelectric material becomes randomly polarized, which has a zero net polarization. When the piezoelectric material is submitted to high stresses or high strains, the polarization direction of some crystals may also switch, what will result in a reduction of the polarization.

3.9.3 Linear piezoelectric theory

Piezoelectric behaviour can be described with the linear piezoelectric theory. The following equations give the linear piezoelectric relations.

$$\sigma_{ij} = D_{ijkl}\varepsilon_{kl} - e^{\varphi}_{mij}E_m \tag{3.44}$$

$$q_i = e^{\varphi}_{ijk}\varepsilon_{jk} + D^{\varphi}_{ij}E_j \tag{3.45}$$

$$e^{\varphi}_{mij} = D_{ijkl}d^{\varphi}_{mkl} \tag{3.46}$$

Here is:

σ_{ij}	Mechanical stress tensor
D_{ijkl}	Elastic stiffness matrix
ε_{kl}	Strain tensor
e_{mij}^{φ}	Piezo electric stress coefficient matrix
E_m	Electrical potential gradient vector
q_i	Electrical flux vector
D_{ij}^{φ}	Piezo di-electric matrix
d_{mkl}^{φ}	Piezo electric strain coefficient matrix

Equation 3.44 gives Hooke's law with an extra term. This extra term gives the relation between the applied electrical field (E) and the stress in the material by the piezoelectric stress coefficient matrix. The piezoelectric stress coefficient is related to the piezoelectric strain coefficient with the elastic stiffness matrix as shown in equation 3.46. Equation 3.45 gives the electrical charge on the electrodes caused by the applied electrical field or a deformation. With these equations the relation between the required strains for actuation and the required applied electrical fields (the input signal to the actuator) are described.

3.9.4 Active noise control algorithm

The actuators have to receive the right signal to counterbalance the vibrations of the structure. The actuator signal is generated with a prediction algorithm Berkhof [30]. Sensors supply the input to the prediction algorithm.

Within the Smart Panel project of TNO, a parametric panel geometry generator tool was developed that delivers a FEM model for the numerical generation of four transfer functions that would be used to calibrate the prediction algorithms of TNO. These transfer functions are:

1.) The acceleration response at certain points on the panel surface to a prescribed incident impulse sound pressure wave.
2.) The acceleration response at certain points on the panel surface to a prescribed impulse electrical charge on the piezo electric actuators (one by one).
3.) The piezo electric responses to a prescribed incident impulse sound pressure wave.
4.) The piezo electric responses to a prescribed impulse electrical charge on the piezo electric actuators (one by one).

When the prediction algorithms are calibrated for a certain panel, the possible reduction in noise radiation could be determined. Unfortunately the Smart Panel project was terminated just before the tool could successfully generate the transfer functions.

3.9.5 Applications

The advantage of a piezoelectric material is the speed at which it reacts to an applied field. This makes it suitable for active noise control applications. A large disadvantage is the brittleness and the low maximum strain of piezoelectric materials. The low maximum strain levels restrict the application of piezoelectric materials to non-structural parts because the strain levels in structural parts can easily exceed the maximum strain levels of the piezoelectric materials, what could lead to fracture and malfunctioning of the active noise control system.

The strain levels that occur in pressurised fuselages are considerable. For a common aluminium fuselage with: radius R = 1975 mm, thickness t_{sk} = 1.28 mm, modulus of elasticity E_{sk} = 70000 MPa, Poisson ratio ν=0.3, the internal pressure p = 0.055 MPa and maximum tensile stress σ_{max} = 200 MPa, the maximum allowable strain and the Hoop strain caused by pressurisation in a fuselage skin are found with equation 3.47:

$$\varepsilon_{max} = \sigma_{max}/E_{sk}$$
$$\varepsilon_{Hoop} = \sigma_{Hoop}/E_{sk} - \nu\sigma_{axial}/E_{sk} = pR/t_{sk}E_{sk} - \nu pR/2t_{sk}E_{sk} \quad (3.47)$$

Because of the considerable strain levels that can occur in fuselage skins, (i.e. compared to the allowable strain of PZT (See table 3.4)), it is preferable not to use piezo electric elements on the fuselage skin directly but on the non-loaded interior panels.

Table 3.4: *Comparison of allowable strain PZT (Piezo Systems Inc.) to estimated strain levels in pressurised aluminium fuselages.*

Allowable strain PZT (PSI-5A3)	~0.11%
Max allowable strain fuselage skin	~0.28%
Hoop strain in fuselage skin caused by pressurisation	~0.10%

New piezoelectric materials, that have high failure strain levels, could make applications possible where the actuators are mounted directly on loaded structure parts. Single crystal PZN-x%PT [29] has a much higher failure strain compared to common PZT, (1.7% instead of 0.11%), and also possess a much higher piezoelectric strain coefficient (d_{33} = 2500e-12 m/V instead of 650e-12 m/V). Unfortunately the specific density of PZN-x%5PT is almost equal to common PZT.

Another single crystal candidate, Langasite LaGaSi [31, 32], has a density that is about 2/3 of that of PZT and PZN-x%PT. The piezoelectric strain coefficient of Langasite is only 7e-12 m/V. This means that much larger electrical fields are required to achieve similar deformations compared to PZT or PZN-x%PT. This does not necessarily have to be a problem since the power consumption of piezoelectric actuators is very low, even for Langasite actuators that require such high electrical fields. The main question for Langasite to be a promising candidate to replace common PZT is whether it has a high failure strain and a high possible coercive electrical field.

There are many other electro-active materials. However most of them do not possess the energy density of the piezoelectric materials or are not yet mature enough for similar applications. A promising electro active material is the piezoelectric polymer: PVDF-TrFE [33], which can reach electrical induced strains of about 5%. (The failure strain is 50%). The specific density is very low (1770 kg.m^3) but the modulus of elasticity is also relatively low; around 1 GPa. This makes the material not as suitable for integration with structural materials compared to PZT, PZN-x5PT or Langasite.

3.10 Reference

[1] Fahy, F., Sound and structural vibration, radiation, transmission and response, Academic Press, London, 1989.
[2] Maxwell, J.C., On Physical lines of force, philosophical magazine, 1861.
[3] Timoshenko, S.P., Goodier, J.N., Theory of elasticity, Mc Graw Hill, New York, 1951.
[4] Cremer, L., Heckl, M., Ungar, E.E., Structure born sound, Springer Verlag, Berlin, 1973.
[5] Leissa, A.W., Vibration of shells, NASA SP-288, Washington, 1973.
[6] Li, B., Wang, X., Ge, H., Ding, Y., Study on applicability of modal analysis of thin finite length cylindrical shells using wave propagation approach, Journal of Zhejiang University Science, 2005.
[7] Soedel, W., Vibration of shells and plates, 3rd ed., Marcel Dekker, New York, 2004.

[8] Junger, M.C., Feit, D., Sound, Structures, and Their Interaction, 2nd Ed., The MIT Press, 1986.
[9] Zhang, X.M., Liu, G.R., Lam, K.Y., Vibration analysis of thin cylindrical shells using wave propagation approach, Journal of Sound and Vibration, vol 239, nr 3, p397-403, 2001.
[10] Morse, P.M., Vibration and Sound, McGraw-Hill, New York, 1948.
[11] Ver, I.L. and Holmer, C.I., Interaction of Sound Waves with Solid Structures, Noise and vibration control, Mc Graw Hill, p270-361, 1971.
[12] Josse, C., Lamure, R., Transmission of sound through a simple wall, Acoustica, vol 14, p266-280, 1964.
[13] Venzke, G., von, Dammig, P., Fischer, H.W., The effect of stiffeners on the radiation coefficient and damping of metal walls, Acoustica 29, nr 1, 1973.
[14] Maidanik, G., Response of ribbed panels to reverberant acoustic fields, Journal of the Acoustical Society of America, vol 34, p809-826, 1962.
[15] Maidanik, G., Tucker, A.J., Proper and first order solution of regularly ribbed panels, Journal of Sound and Vibration, vol 44, p267-274, 1976.
[16] Leppington, F.G., Broadbent, E.G., Heron, L.H., The acoustic radiation efficiency of rectangular panels, Proc. R. Soc. London, vol 382, p245-271, 1982.
[17] Macadam, J.A., The measurement of sound radiation from room surfaces in leightweight buildings, Journal of Applied Acoustics, vol 9, nr 2, 1976.
[18] Forssen, B., Wang, Y.S., Crocker, M., A study of methods of predictions and measurements of the transmission of sound through the walls of light aircraft, NAG158, NASA semi annual report, 1981.
[19] Technical bulletin, Acoustic behaviour of sandwich panels, DIAB group.
[20] Ford, R.D., Lord, P., Walker, A.W., Sound transmission through sandwich constructions, Journal of sound & vibrations, vol 5, nr 1, 1967.
[21] Smolenski, C.P., Krokosky, E.M., Dilatation-mode sound transmission in sandwich panels, The journal of the acoustical society of America, vol 54, 1973.
[22] Dym, C.L., Lang, M.A., Transmission of sound through sandwich panels, The journal of the acoustical society of America, vol 56, nr 5, 1974.
[23] Dym, C.L., Lang, M.A., Optimal acoustic design of sandwich panels, The journal of the acoustical society of America, vol 57, nr 6, 1975.
[24] Dym, C.L., Ventres, S.C., Lang, M.A., Transmission of sound through sandwich panels: A reconsideration, The journal of the acoustical society of America, vol 59, nr 2, 1976.
[25] Dym, C.L., Lang, D.C., Transmission los of damped asymmetric sandwich panels with orthotropic cores, Journal of sound and vibration, vol 88, nr 3, 1983.
[26] Beranek, L.L., Noise and Vibration control, Institute of noise control engineering, Washington DC, 1988.
[27] Kerwin, E.M., Damping of flexural waves by a constrained viscoelastic layer, Journal of the acoustic society of America, vol 31, nr 7, 1959.
[28] Derby, T.F., Ruzicka, J.E., Loss factor and resonant frequency of viscoelastic shear-damped structural composites, NASA CR-1269, Washington DC., 1969.
[29] Park, S.E., Shrout, T.R., Ultrahigh strain and piezoelectric behavior in relaxor based ferroelectric single crystals, Journal of applied physics, vol 82, nr 4, august 1997.

[30] Berkhof, A.P., Design of actuator arrays for active structural acoustic control, Proc. Active 2002, p611-620, Southampton, 2002.

[31] Bohm, J., Heimann, R.B., Hengst, M., Roewer, R., Schindler, J., "Czochralski growth and characterization of piezoelectric single crystals with Langasite structure: $La_3Ga_5SiO_{14}$ (LGS), $La_3Ga_{5.5}Nb_{0.5}O_{14}$ (LGN) and $La_3Ga_{5.5}Ta_{0.5}O_{14}$ (LGT) Part I", Journal of crystal growth 204, p128-136, 1999.

[32] Bohm, J., Chilla, E., Flannery, C., Frohlich, H.J., Hauke, T., Heiman, R.B., Hengst, M., Straube, U., "Czochralski growth and characterization of piezoelectric single crystals with Langasite structure: $La_3Ga_5SiO_{14}$ (LGS), $La_3Ga_{5.5}Nb_{0.5}O_{14}$ (LGN) and $La_3Ga_{5.5}Ta_{0.5}O_{14}$ (LGT) Part II Piezoelectric and elastic properties", Journal of crystal growth 216, p293-298, 2000.

[33] Wang, D., Li, K., Teo, W.K., "Preparation and characterization of polyvinylidene fluoride (PVDF) hollow fiber membranes", Journal of membrane science, vol 163, p211-220, 1999.

4 Thermal insulation

4.1 Introduction

Most airliners fly at altitudes of about 10 to 12 km. At this altitude the outside air temperature is about -40 to -55 °C. This means that it is necessary to thermally insulate the fuselage. In this section a short overview is given on the heat theory relevant to thermal insulation of a fuselage wall. The thermal heat insulation of fuselage walls can be relatively simply described by the classical heat-conduction equation.

4.2 Classical heat theory

For every structure the thermal behaviour can be described with the energy conservation law. The law of conservation of energy for a certain control volume is given in equation 4.1, Thornton [1].

$$\dot{E}_{in} + \dot{E}_{gen} = \dot{E}_{sto} + \dot{E}_{out} \tag{4.1}$$

Here is:
- E_{in} :The rate of energy entering the control volume
- E_{gen} :The rate of energy generated within the control volume
- E_{sto} :The rate of energy stored within the control volume
- E_{out} :The rate of energy leaving the control volume

For the following equations the fuselage volume V and the fuselage external surface S are taken as control volume and control surface, like is shown in figure 4.1.

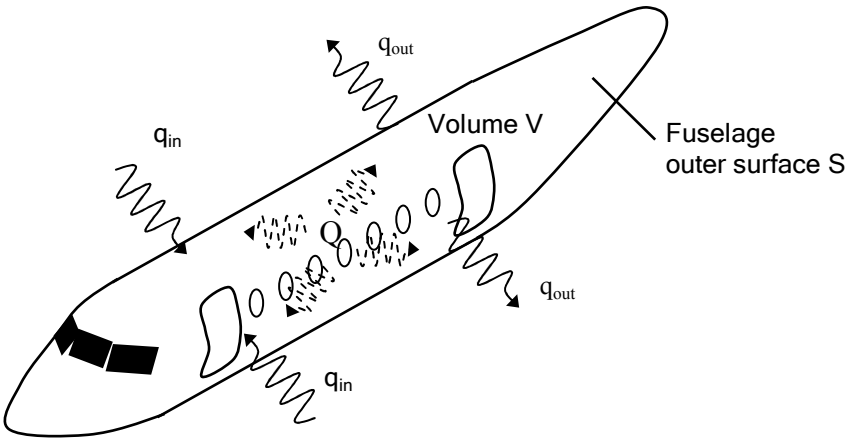

Figure 4.1: *Definition of the control volume around a fuselage.*

The energy entering the fuselage represents external heating like heating by the sun. The external heating is represented by a heat flux entering the fuselage normal to the fuselage surface:

$$\dot{E}_{in} = \int_S q_{in} n dS \tag{4.2}$$

The heat system within the fuselage generates heat, which can be characterised by the volumetric heating rate Q_h. Integrating over the control volume rate of energy generated within the fuselage becomes:

$$\dot{E}_{gen} = \int_V Q_h dV \tag{4.3}$$

When the energy stored in the fuselage structure and cavity caused by deformation is neglected, it may be assumed that the internal energy per unit volume depends only on the temperature of the fuselage material and the material's intrinsic ability to store internal energy by its thermal capacity. The stored internal energy then becomes:

$$\dot{E}_{sto} = \int_V \rho c_v(T) \frac{\partial T}{\partial t} dV \tag{4.4}$$

Like for the energy entering the fuselage, the energy leaving the fuselage can be obtained by integrating the normal component of the heat flux vector over the fuselage surface S:

$$\dot{E}_{out} = \int_S q_{out} n dS \tag{4.5}$$

Rewriting equation 4.1 leads to the classical heat theory:

$$\frac{\partial}{\partial x_i}(q_{in} - q_{out}) + \rho c_v \left(\frac{\partial T}{\partial t} \right) = Q_h \tag{4.6}$$

4.3 Thermal insulation of a fuselage wall

When considering the heat balance of a fuselage wall, one can identify the heat flow incident on the inside surface of the fuselage wall, the heat absorption of the fuselage wall, the heat conduction through the fuselage wall and the heat exiting the fuselage wall by radiation and convection.

In this research the influence of the geometrical and the material parameters on the thermal insulation of the fuselage wall are investigated. The geometrical parameters of the fuselage wall only come to expression in the heat conduction part of the heat balance of the fuselage wall. This means that for this research, heat conduction is the driving heat phenomenon in fuselage wall design concerning thermal insulation.

Therefore, in the remaining part of this section, only heat conduction will be discussed. For the discussion of the other heat phenomenons and its interactions, it is referred to appendix D, Thornton [1], Malloy [2] and many others.

Heat conduction is defined as the energy transfer within a body, or between two bodies in physical contact. The energy transfer is always from a higher temperature region to a lower temperature region.

Because the thickness of a fuselage wall (L_w) usually is quite small compared to its radius (R), conduction through a fuselage wall can, for the sake of simplicity, be considered as a one-dimensional case, which is illustrated in figure 4.2.

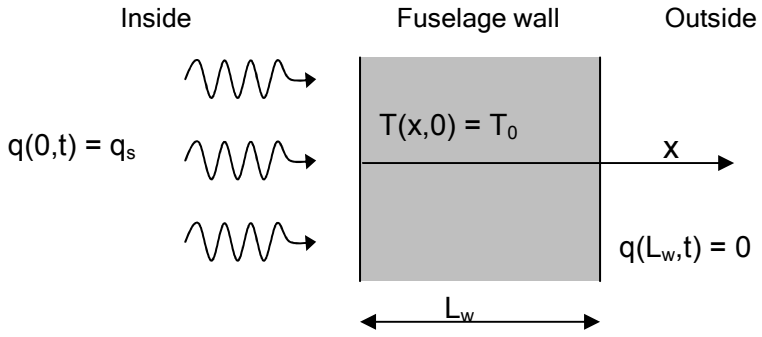

Figure 4.2: *Conduction through a fuselage wall considered as a one-dimensional case*.

In this case the thermal material properties of the fuselage wall will be considered constant. The inside of the fuselage is continuously heated, which results in a constant heat flux acting on the inside of the fuselage wall: $q(0,t) = q_s$. As initial condition the temperature of the whole fuselage wall is considered constant, $T(x,0) = T_0$. Because radiation and convection are not considered here, the fuselage wall can be considered to be perfectly insulated; $q(L_w,t) = 0$. According to Malloy [2], one-dimensional conduction can be described by: $q(x,t) = k_{con}\delta T/\delta x$ where k_{con} is the thermal conduction constant. Rewriting equation 4.6 results in the classical heat conduction equation:

$$\frac{\partial^2 T}{\partial x^2} = \frac{1}{k_{con}} \frac{\partial T}{\partial t} \tag{4.7}$$

Solving the classical heat conduction equation using the boundary conditions as shown in figure 4.2 gives the following equation where n is an integer number, Thornton [1]:

$$T(x,t) = T_0 + \frac{q_s t}{\rho c_v L_w} + \frac{q_s L_w}{k_{con}}\left[\frac{1}{3} - \frac{x}{L_w} + \frac{x^2}{2L_w^2} - \frac{2}{\pi^2}\sum_{n=1}^{\infty}\frac{1}{n^2}\cos\frac{n\pi x}{L_w}\exp\left(\frac{-n^2\pi^2 k_{con} t}{L_w^2}\right)\right] \qquad (4.8)$$

.

From this equation it can be seen that for large period of time the temperature increases linearly with time and that the difference in temperature between the inside surface and outside surface of the fuselage wall remains constant. This difference, T(0,t) – T(L,t), is expressed by:

$$\theta = \frac{q_s L_w}{2k_{con}} \qquad (4.9)$$

Here is L_w the thickness of the fuselage wall and k_{con} the thermal conductivity factor. The temperature as function of time on the inside and outside surface of the fuselage wall for the considered conduction case is illustrated in figure 4.3.

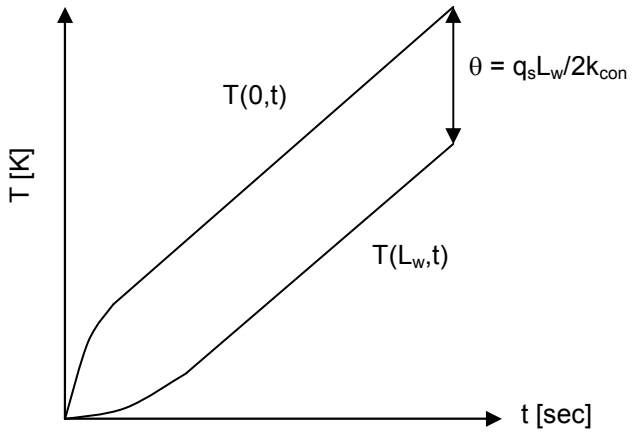

Figure 4.3: *Inside and outside surface temperature for a constant heat flux [1]*

The temperature difference θ, which becomes constant after a long enough period of time is a good indicator to evaluate the heat insulation capability of a fuselage wall. For a predefined specified heat flux, θ of single isotropic skins is simply determined by the ratio of thickness over the material conductivity. So for good thermal insulation a thick wall with a low thermal conductivity factor is favourable. Table 4.1 shows the conductivity constants for several isotropic materials.

Based on table 4.1, it can be concluded that the thermal insulation of a sandwich with a composite honeycomb core, which contains air pockets, will have a much better thermal insulation compared to aluminium skins.

For more complicated skins, like a stiffened skin with insulation blankets and an interior panel, θ cannot be described with equation 4.9. In such cases the aluminium frames can act like heat-bridges in between the insulation blankets because the

thermal conductivity of aluminium is much higher than that of an insulation blanket. Then it is important that the frames are well insulated from the interior panel.

Within the DEE, which is discussed in chapter 6, the temperature difference θ will be determined numerically.

Table 4.1: *Thermal conductivity factors k_{con} for several materials [2]*

Material	Thermal conductivity k_{con} [$W.m^{-1}.K^{-1}$]
Aluminium 6061-T6	170
Aluminium 2024-T4	140
Aluminium 5086-H32	130
Graphite-aluminium	83
Magnesium AZ80A-F	76
Copper G-3	42
Hastelloy-X	19
Stainless steel 17-7PH	17
Carbon-carbon	15
Titanium MIL-T-9047	8.3
Graphite epoxy	1.6
Air	0.024

4.4 Reference

[1] Thornton, E.A., Przemieniecki, J.S., Thermal structures for aerospace applications, AIAA education series, 1996.

[2] Malloy, J.F., Thermal insulation, New York: Van Nostrand Reinhold Company, 1969.

5 Mechanics of fuselage design

5.1 Introduction

This chapter discusses the mechanical aspects of fuselage design. Together with the acoustical and thermal insulation it forms the design aspects that will be integrated in the fuselage DEE, which will be discussed in chapter 6. Nowadays two main structural concepts can be distinguished in fuselage design; the conventional stiffened skin concept and the sandwich skin concept. Both structural concepts will be considered with a design example in section 5.2 and 5.3 respectively. In section 5.4 the concepts are compared.

5.2 Conventional stiffened skin concept

First, the influence of the structural parameters on the structural efficiency of the stiffened skin fuselage will be discussed. The structural efficiency of a stiffened skin fuselage can be judged by the weight required for sufficient strength and stability. To simplify the evaluation of the efficiency of a stiffened skin fuselage, the weight of an idealised fuselage section as a function of its structural parameters will be presented in 'design graphs', (fig 5.2a and b).

For the analysis a cylindrical idealised fuselage section is considered with a length of L_{fus} = 10 m and a radius R = 1.975 m. These dimensions correspond to a civil aircraft with a capacity of about 120 passengers. The idealised fuselage section is stiffened with frames and stringers as illustrated in figure 5.1. The types of stringers that are used are 'hat' stringers, with a height (h_{str}) equal to their width ($b_{str} = h_{str}$). The weight and size of the frames are not included. Furthermore this fuselage has no

doors, windows, floor panels or any other disturbances. The design load case consists out of a bending moment M, a shear load Q and a differential pressure p, which is also indicated in figure 5.1.

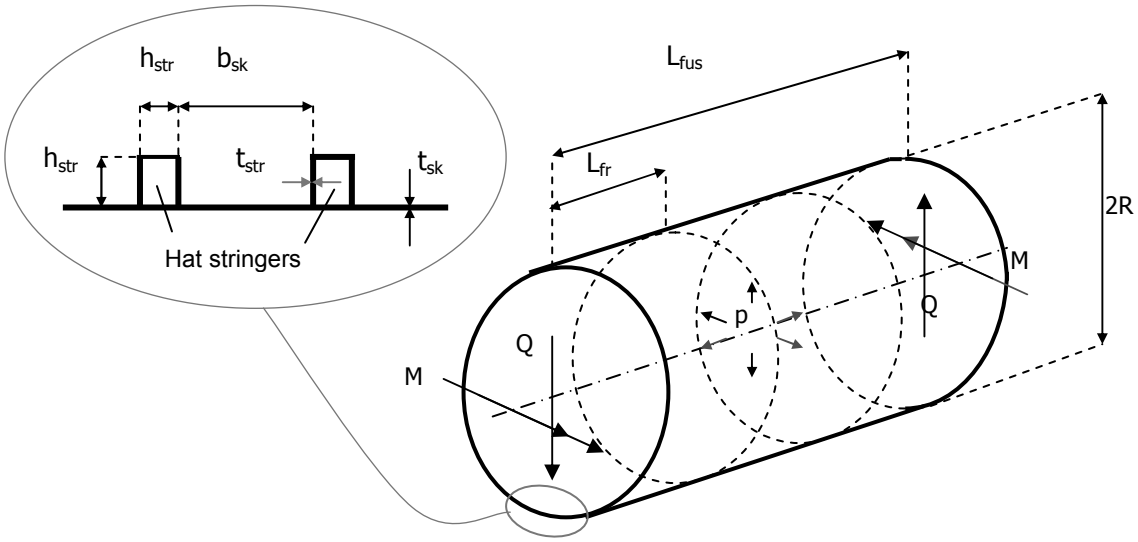

Figure 5.1: *Load case and dimensions of the idealised fuselage.*

Table 5.1: *Numerical values of the load case and the fuselage dimensions used for the parameter study.*

Fuselage dimensions:							
R *(mm)*	**L_{fus}** *(m)*	**A_{fr}** *(mm^2)*					
1975	10	120					
Design load case:							
M *(Nmm)*	**Q** *(N)*	**p** *(N/mm^2)*					
4.4e9	6.0e5	0.055					
Design stresses and material properties of the skin:							
	σ_{Hoop} *(MPa)*	**σ_{max}** *(MPa)*	**E** *(GPa)*	**ν**	**ρ** *(kg/m^3)*	**k_τ**	**k_σ**
aluminium	85	200	70	0.3	2700	5.35	4
carbon/epoxy (Q.I)	100	150	32.1	0.3	1800	5.35	4
Design stresses and material properties of the frames and stringers:							
	σ_{max} *(MPa)*	**E** *(GPa)*	**ρ** *(kg/m^3)*				
aluminium	210	70	2700				
carbon/epoxy (U.D)	160	70	1800				

To visualise the influence of material properties, two structural materials will be compared: aluminium and the composite carbon/epoxy, which is currently introduced in the aircraft industry. The load case, fuselage dimensions and material properties are given in table 5.1. The composite material properties are assumed to be quasi-isotropic, which means that the fibers of the carbon/epoxy skin are placed in such directions that the composite's inplane behaviour is isotropic. The carbon/epoxy stringer is more unidirectional (U.D) resulting in a higher modulus of elasticity. The fiber volume fraction is assumed to be 50 %. k_σ and k_τ are respectively the compressive and shear buckling constants and A_{fr} is the cross-section area of the frames, which remains constant during the parameter analysis.

To determine the 'design graphs' of figure 5.2a and b, the following design criteria are used, according to van Tooren [1] and van Zaal [2]:

- The minimum skin thickness is determined by the Hoop stress:

$$t_{sk\ \min} = \frac{pR}{\sigma_{Hoop}} \tag{5.1}$$

  For aluminium this results in a minimum thickness of t_{sk_min} = 1.28 mm and for carbon/epoxy of t_{sk_min} = 1.10 mm.
- The stresses at which compressive and shear buckling will occur in the skin between two stringers is calculated with:

$$\sigma_{bskin} = k_\sigma \frac{\pi^2 E_{skin}}{12\left(1-\nu^2\right)}\left(\frac{t_{sk}}{b_{sk}}\right)^2 \tag{5.2}$$

$$\tau_{bskin} = k_\tau \frac{\pi^2 E_{skin}}{12\left(1-\nu^2\right)}\left(\frac{t_{sk}}{b_{sk}}\right)^2 \tag{5.3}$$

  The skin buckling criteria is assumed to be:

$$R_{sb} = \frac{\sigma}{\sigma_{bskin}} + \frac{\tau}{\tau_{bskin}} < 1 \tag{5.4}$$

  Where σ and τ are the actual compressive stress and shear stress that exist in the skin between two stringers.
- The stress at which buckling occurs in the flanges of a stringer can be determined similar to equation 5.2, except for the different geometry and material properties:

$$\sigma_{flanges} = k_\sigma \frac{\pi^2 E_{str}}{12\left(1-\nu^2\right)}\left(\frac{t_{str}}{h_{str}}\right)^2 \tag{5.5}$$

- The overall stability of the skin-stringer panel in between two frames (length = L_{fr}) is derived from the Euler buckling load of a stringer-skin panel with a cross section

of one stringer and a skin strip with a width equal to the sum of the distance between two stringers (b_{sk}) and the stringer width (b_{str}):

$$P_{Euler} = \frac{\pi (EI)_{panel}}{L_{fr}^2} \tag{5.6}$$

This leads to a buckling stress of the stringer-skin panel according to:

$$\sigma_{Euler} = E \frac{\pi^2}{L_{fr}^2} \frac{(EI)_{panel}}{(EA)_{panel}} \tag{5.7}$$

- The weight of the fuselage section is estimated by:

$$W_{fus}^{*} = 2\pi R \cdot L_{fus} \cdot t_{sk} \cdot \rho_{sk} + n_{str} \cdot 3h_{str} \cdot t_{str} \cdot L_{fus} \cdot \rho_{str} + n_{fr} \cdot A_{fr} \cdot 2\pi R \cdot \rho_{fr} \tag{5.8}$$

Remark: *These isotropic formulas are used for the dimensioning of both the aluminium and composite fuselage panels*

Using these design criteria, trade off curves can be generated that are displayed in figure 5.2a and b.

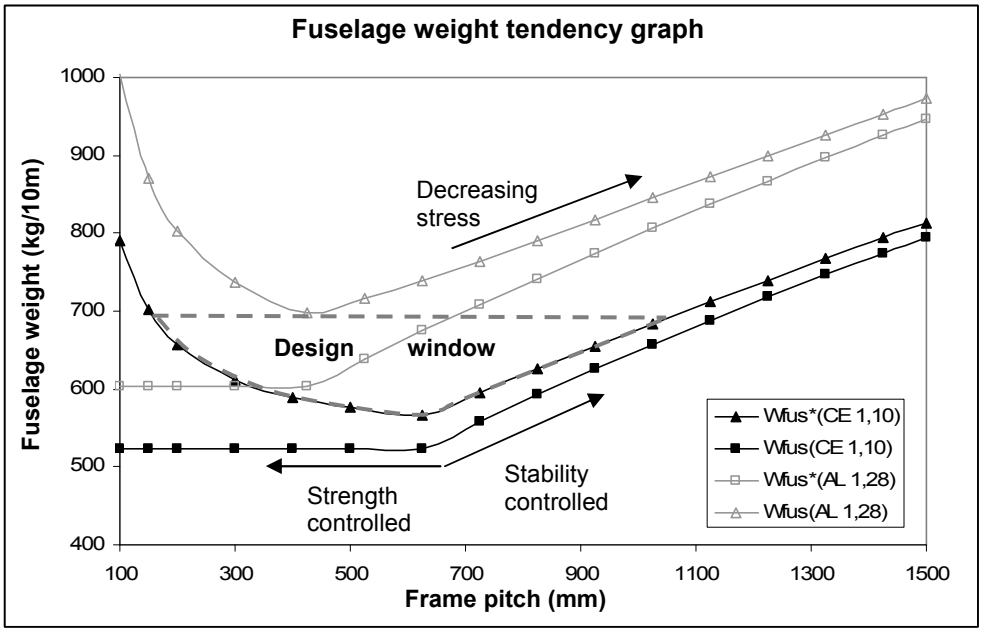

Figure 5.2a: *Fuselage weight (Where for W_{fus}^{*} the weight of the frames is included and for W_{fus} it is excluded) versus frame pitch for the load case and dimensions given in table 5.1 for an aluminium and carbon/epoxy fuselage with minimum skin thickness. The area between the lightest aluminium and the carbon/epoxy solutions is indicated with a dashed line as the design window. One should note that also for the fuselage weight without the weight of the frames the frame pitch is used for Euler buckling criterion, which means that fictively the frames are still present.*

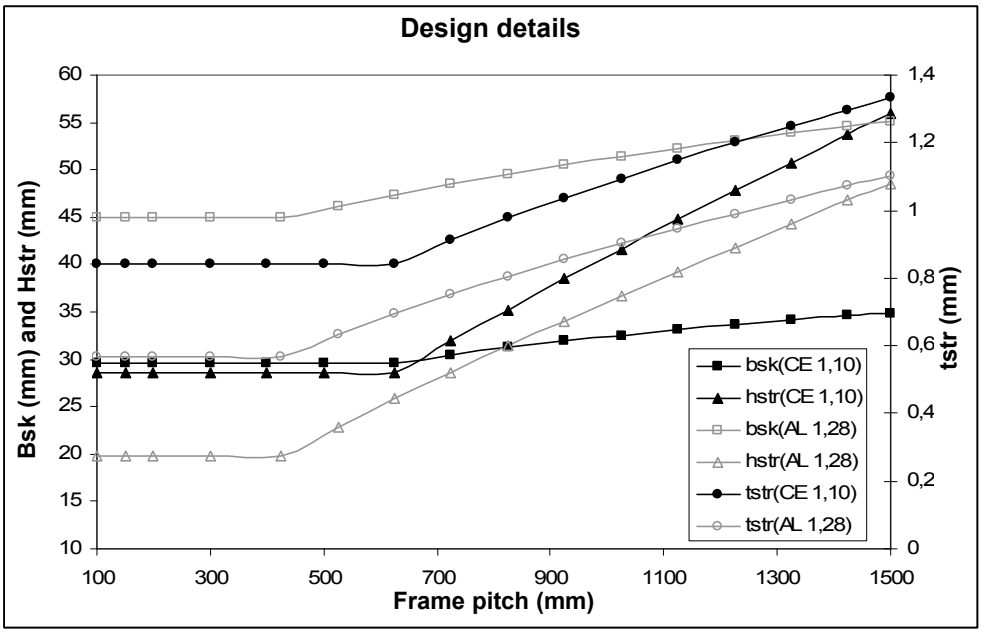

Figure 5.2b: *Hat stringer dimensions belonging to the solutions given in figure 5.2a. b_{sk} is the distance between two stringers, h_{str} is the stringer height, (which is equal to the stringer width) and t_{str} is the stringer thickness.*

All trade off curves have the same characteristic shape. Below a certain frame pitch the fuselage weight without the weight of the frames is constant and determined by the maximum allowable material stress. Above this frame pitch, the fuselage weight is determined by the stability of the skin panels, described by the buckling equations (5.2) - (5.7). The fuselages with minimum weight have minimum skin thickness and the largest allowable frame pitch. According to figure 5.2a the lightest aluminium fuselage (697 kg/10m) is about 23% heavier than the lightest carbon/epoxy fuselage (565 kg/10m). The corresponding dimensions are given in table 5.2.

Table 5.2: *dimensions of lightest aluminium and carbon/epoxy stiffened skin fuselages.*

Material	Aluminium	Carbon/epoxy
Fuselage weight [kg/10m]	697	565
Skin thickness [mm]	1.28	1.10
Frame pitch [mm]	425	625
Stringer pitch [mm]	65	58.5
Stringer height [mm]	20	28.5
Stringer thickness [mm]	0.57	0.84

Figure 5.2b shows the required stiffener dimensions belonging to the solutions shown in figure 5.2a. All these curves show the same tendency; with increasing frame pitch the required stiffener area to avoid panel buckling also increases. Because of the increasing panel cross-section area (in the stability critical region) the stress level

in the panel reduces which allows a lower local buckling stress and therefore an increased stiffener pitch.

With regard to figure 5.2a the following can be noticed: Aircraft designers traditionally choose a frame pitch of 500 mm. This is close to frame pitch of the lightest aluminium solution shown in figure 5.2a. However for fuselages constructed out of composites a frame pitch of 500 mm might not be optimal. Especially for damage control thicker skins are preferred. The figure shows the existence of a design window, that consists out of composite solutions with a frame pitch and skin thickness combination that are lighter than the lightest aluminium solution. The potential weight saving can be either fully exploited or traded off against improved damage control and/or improved acoustical insulation.

5.3 Sandwich fuselage concept

Another promising structural concept for fuselage design is the sandwich concept. Sandwiches consist out of layers. The outer layers are called facings and are generally thin and of high density. These facings are supposed to resist most of the edgewise loads and flat-wise bending moments. The inner layer is called the core and is generally rather thick and of low density. The task of the core is to separate and stabilize the two facings, transmit shear between the facings and provide most of the shear rigidity. The sandwich concept has no stringers. This means that no structural mass is used on stringers, which is favourable for the sound transmission loss properties. Also the core can be made of a material with high insulation properties (acoustic and thermal).

At positions where high concentrated forces have to be introduced (wing, landing gear, etc.) or diverted (from cut-outs), reinforcements will be necessary. In general the sandwich structure will be much cleaner (less parts) compared to the stiffened skin structure. This can reduce the production and maintenance cost.

These characteristics make that the sandwich concept has great potential for multidisciplinary fuselage design.

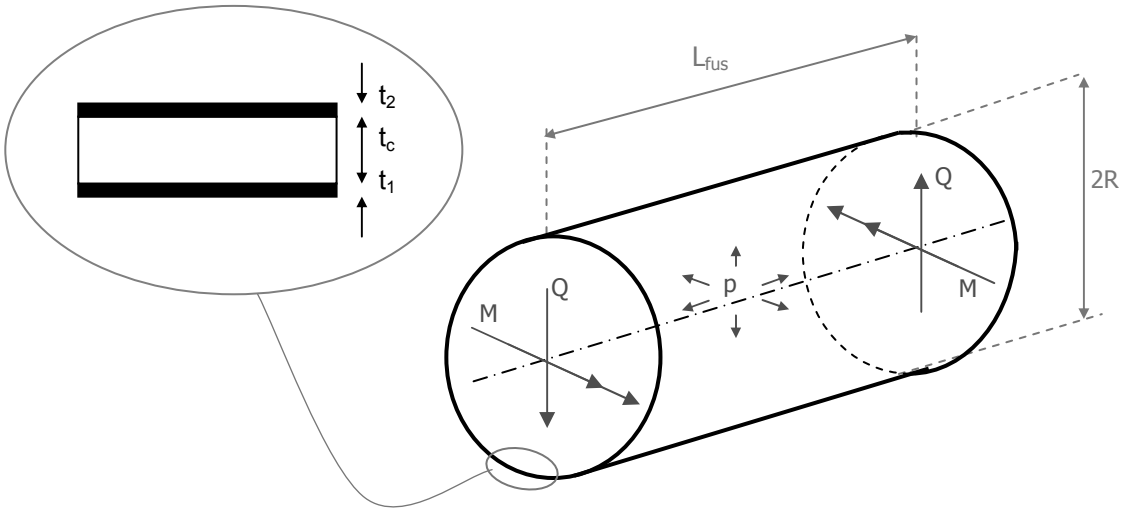

Figure 5.3: *Load case and dimension definition of the idealised sandwich fuselage.*

Like for the stiffened skin concept discussed in section 5.1 an idealised model of a civil aircraft fuselage suitable for approximately 120 passengers will serve as example. (See figure 5.3). The load case consists out of an internal pressure p a shear load Q and a bending moment M. The geometric variables are the facing thickness t_1 and t_2 and the core thickness t_c. These variables are considered constant for the entire fuselage section. The material properties are given in table 5.3.

Table 5.3: *Load case, dimensions and material properties used to determine the sandwich fuselage dimensions.*

Load case			
M	[Nm]	4.4e6	
T_{tor}	[Nm]	0	
Q	[N]	6.0e5	
p	[Mpa]	0.055	
Dimensions			
R	[m]	1.975	
L_{fus}	[m]	10	
material properties core			
E_c	[Mpa]	420	
G_c	[Mpa]	91	
ν_c		0.3	
minimum thickness	[mm]	5	
density	[kg/m^3]	96	
maximum thickness	[mm]	50	
material properties facing		**Carbon/epoxy**	**Aluminium**
E_{xf}	[Mpa]	32100	70000
E_{yf}	[Mpa]	32100	70000
ν_{xyf}		0.318	0.3
density	kg/m^3]	1800	2700
minimum thickness	[mm]	0.3	0.3
Maximum allowable stresses			
$\sigma_{Hoop\ max}$	[Mpa]	100	
$\sigma_{max\ tensile}$	[Mpa]	150	

To determine the geometric variables (t_1, t_2 and t_c) for minimum weight of a fuselage that is able to carry the defined load case, Van Tooren [1] described the following procedure:

1.) Define a minimum thickness for both facings and the core.
2.) If necessary modify the required thickness for wrinkling.
3.) If necessary modify the required thickness for static strength based on:
   - Maximum allowable strain due to internal pressurization.
   - Maximum allowable strain for tensile loads (other than those from internal pressurization).
   - Maximum allowable strain for compression loads
4.) Check on bending buckling of the sandwich cylinder.
5.) Check on torsion buckling of the sandwich cylinder.
6.) Check on shear buckling of the sandwich cylinder.
7.) Check on interaction of bending, torsion and shear buckling.

8.) If necessary increase the thickness of the core. If the core thickness is larger than the maximum value allowed, then increase the facing thickness and set the core thickness back to the minimum allowable thickness.

By iterating steps 2 to 8, the minimum thicknesses are found for which the cylinder meets the strength and stability requirements.

Next, the equations are given to determine the necessary stresses in the previously mentioned steps. (van Tooren [1], Sullins [4])

Wrinkling

Wrinkling is a local failure mode of the facings as is shown in figure 5.4. Wrinkling occurs when the stress in the facing exceeds the wrinkling stress. Allen [3], gives a conservative equation for wrinkling stress:

$$\sigma_{wr} = \frac{1}{2}\sqrt[3]{E_f E_c G_c} \tag{5.9}$$

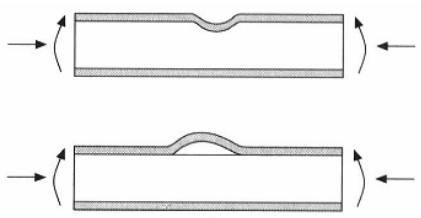

Figure 5.4: *Wrinkling of the sandwich facings [1].*

Internal pressure

Van Tooren [1] showed that for sandwich cylinders with large radius and small E_c the ratio between the stresses in the facing becomes similar to the ratio of the facing stiffness E_2t_2/E_1t_1. For small radii, the ratio between the stresses in the inner and outer facing is dependent on the non dimensional stiffness parameter $A_{stiffness}$:

$$A_{stiffness} = \frac{R^2 E_c}{t_c}\frac{1-\nu^2}{E_1 t_1} \tag{5.10}$$

When A is larger than 100, the radius and E_c can be considered large enough to assume that the ratio between the stresses in the inner and outer facing will be equal to the stiffness ratio E_2t_2/E_1t_1. For example the parameter A for the A320 like fuselage varies between 500 and 16500. For this case the total minimum facing thickness is defined by:

$$(t_{tot})_{\min} = (t_1 + t_2)_{\min} = \frac{pR}{\sigma_{Hoop}} \tag{5.11}$$

Where σ_{Hoop} represents the allowable stress in circumferential direction. For the stress ratio at smaller values of A is referred to: van Tooren [1].

Bending buckling

In case of bending loads, the sandwich cylinder may fail in different buckling modes. These buckling modes may also interact. In this case only shear crimpling and cylinder bucking will be considered. For the analysis of cylinders loaded in bending only the peak axial compression stress needs to be taken into account. The effect of this peak compression stress can be analysed with the classical small deflection theory applied to axially loaded sandwich cylinders. It is common design practice, to use the results of this classical theory in combination with an empirical knock-down factor. When the method for axially loaded cylinders is applied for the analysis of bending loaded cylinders a knock-down factor for bending buckling loads has to be used. The knock-down factor is empirical and based on test results, Sullins [4]. Figure 5.5 shows the knock-down factor, which is a function of R/ρ_{sw}. Where ρ_{sw} is given by equation 5.12

$$\rho_{sw} = \frac{h\sqrt{E_1 t_1 E_2 t_2}}{E_1 t_1 + E_2 t_2} \tag{5.12}$$

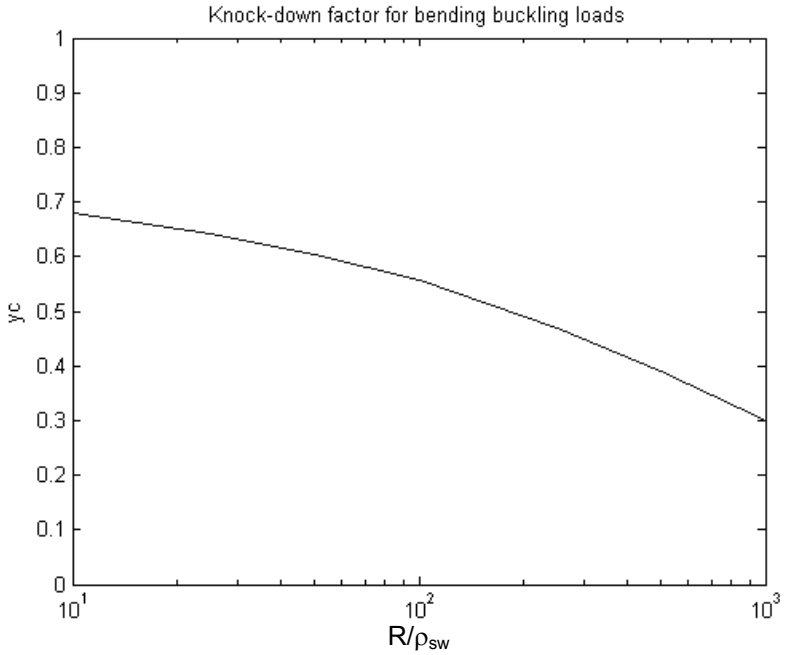

Figure 5.5: *Knock-down factor for bending buckling loads [1,4].*

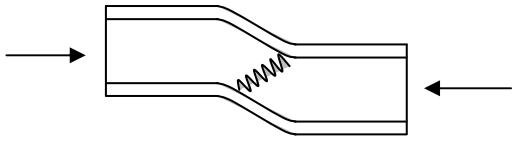

Figure 5.6: *Shear crimping of the sandwich core [1].*

The critical stress for bending buckling can be calculated with the equations 5.13 to 5.17. In the analysis, the interaction between shear crimping, which is a local failure mode shown in figure 5.6, and bending buckling is taken into account.

$$\sigma_{cri} = \gamma_c K_{ci} \sigma_{0i} \tag{5.13}$$

$$\sigma_{0i} = \eta_p E_i C_0 \tag{5.14}$$

$$C_0 = \frac{h}{R} \frac{2\sqrt{(E_1 t_1)(E_2 t_2)}}{\sqrt{1-\nu_c^2}\left[(E_1 t_1)+(E_2 t_2)\right]} \tag{5.15}$$

$$h = \frac{t_1}{2} + \frac{t_2}{2} + t_c \tag{5.16}$$

$$\sigma_{crimpi} = \frac{h^2}{\left[t_i + \left(\frac{E_j}{E_i}\right) t_j\right] t_c} G_{xz} \tag{5.17}$$

$$V_{ci} = \frac{\sigma_{0i}}{\sigma_{crimpi}} \tag{5.18}$$

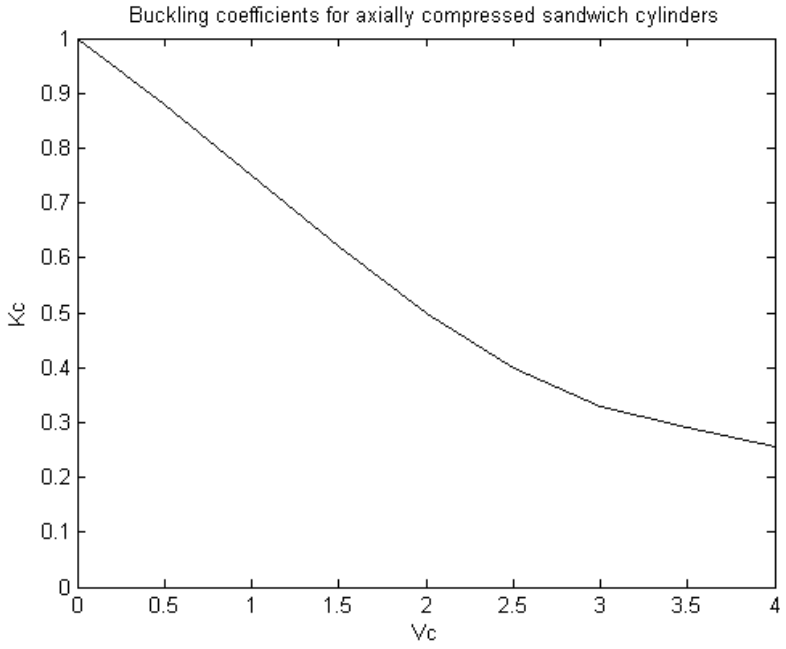

Figure 5.7: *Buckling coefficients for axially compressed sandwich cylinders. Sullins [4]*

The appropriate value of K_c can be taken from figure 5.7. The value V_c defines what failure mode will dominate. If $V_c > 2$ then shear crimping is dominant and the result will be accurate, regardless the length of the cylinder L. In the region $V_c < 2$ the accuracy of the results depends on the length of the cylinder. Results are only valid if the length of the cylinder is larger than the length of a single axial half wavelength in the buckle pattern of the corresponding infinite-length cylinder. This can be expressed with the following formula:

$$\frac{L}{R} \geq 1.57\sqrt{C_0\left(2 - V_c\right)} \tag{5.19}$$

For shorter cylinders the above formulas give conservative results [1].

The critical bending moment can be found from the buckling stresses with the following equation:

$$M_{cr} = \pi R^2\left[\sigma_{cr1}t_1 + \sigma_{cr2}t_2\right] \tag{5.20}$$

Torsion buckling

The value of the shear stress at which torsion buckling will occur can be estimated with the following equations:

$$\tau_{cr} = \gamma_s K_s \eta_p E_f \frac{d}{R} \tag{5.21}$$

$$\gamma_s = 0.80 \tag{5.22}$$

The value of the buckling coefficient can be found from figure 5.8 when the following values are known:

$$Z_s = \frac{L^2}{dR} \tag{5.23}$$

$$V_s = \frac{16t_c t_1 t_2 \eta E_f}{15\left(t_1 + t_2\right)RdG_{xz}} \tag{5.24}$$

$$d = t_1 + t_2 + t_c \tag{5.25}$$

The critical torsion moment can be computed from the critical shear stress with the following equation:

$$T_{cr} = 2\pi R^2\left(t_1 + t_2\right)\tau_{cr} \tag{5.26}$$

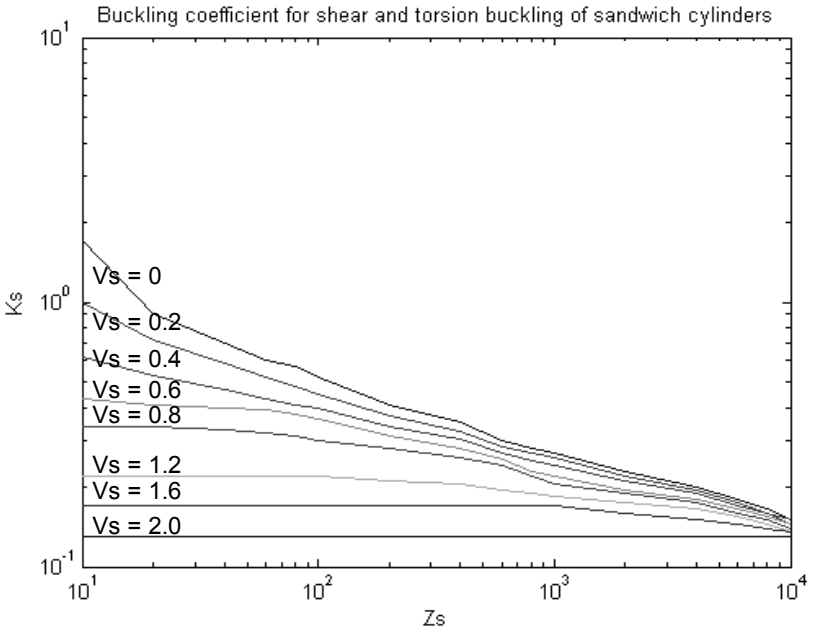

Figure 5.8: *Buckling coefficient for shear and torsion buckling of sandwich cylinders for $t_c/d=1$ and $G_{xz}/G_{yz}=1$, Sullins [4].*

Shear buckling

For cylinders loaded with a transverse shear force Q the critical shear stress can be computed from the following equations:

$$\tau_{cr} = 1.25 K_s \eta_p E_f \frac{d}{R} \tag{5.27}$$

The critical buckling coefficient can be taken again from figure 5.7. The critical shear force can be calculated from the critical shear stress with:

$$Q_{cr} = \pi R(t_1 + t)\tau_{cr} \tag{5.28}$$

Buckling interaction

The critical load for the three buckling loads described before will be lowered when a combined loading is applied. The interaction is assumed to be described by:
(Buckling will occur when $R_c \geq 1$)

$$R_c = \frac{M}{M_{cr}} + \frac{T_{tor}}{T_{cr}} + \frac{Q}{Q_{cr}} \tag{5.29}$$

Parameter study

In order to be able to perform a parameter study on the sandwich fuselage described in figure 5.4 and table 5.3 the previous equations are implemented in a Matlab program. The Matlab program determines the minimum core thickness as

function of t_1 for fixed ratios t_2/t_1. In this parameter study the facing and core thickness are determined for minimum weight of a fuselage that is still able to carry the specified loads. The resultant core thickness as function of t_1 for fixed t_2/t_1 ratios is given in figure 5.9a for the carbon/epoxy facings and in figure 5.9b for the aluminium facings.

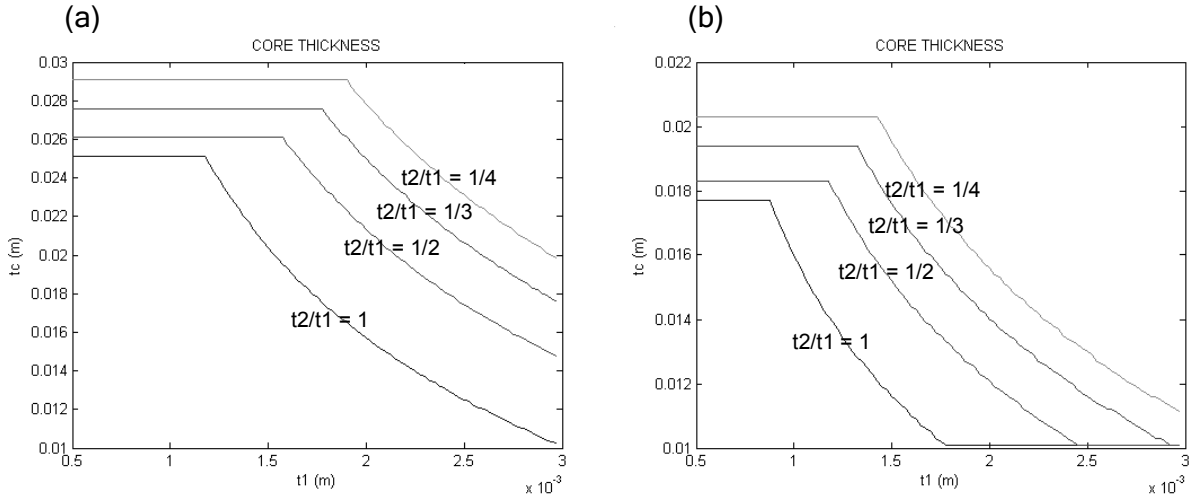

Figure 5.9: *Core thickness as function of the thickness of facing 1 for fixed facing thickness ratios:*
a) Fuselage with carbon/epoxy facings
b) Fuselage with aluminium facings.

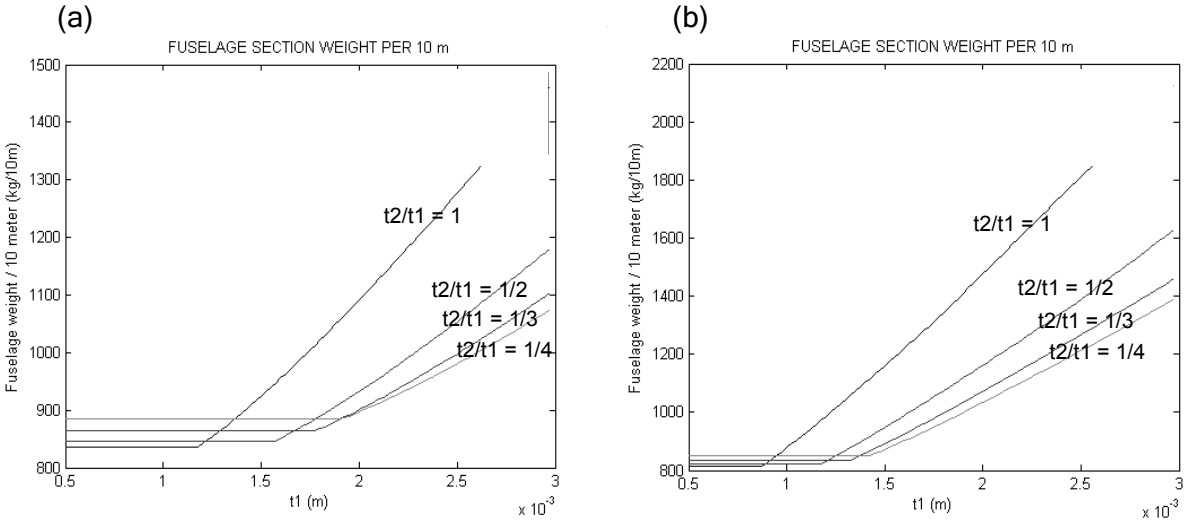

Figure 5.10: *Fuselage weight as function of the thickness of facing 1 for fixed facing thickness ratios*
a) Fuselage weight for sandwich with carbon/epoxy facings corresponding to dimensions given in figure 5.9a.
b) Fuselage weight for sandwich with aluminium facings corresponding to dimensions given in figure 5.9b.

Once the dimensions are known the corresponding fuselage weight per 10 meter length can be determined with the following formula:

$$W_{fus} = \left((t_1 + t_2)\rho_f + t_c\rho_c\right) \cdot 2\pi R \cdot L_{fus} \tag{5.30}$$

The weight per 10 m fuselage length is shown in figure 5.10a for the sandwich with carbon/epoxy facings and 5.10b for the aluminium facings.

The horizontal parts of figure 5.9a and b have no physical meaning. The intersection of the horizontal parts with the curved lines only indicate the minimum facing thickness t_1 and the corresponding minimum core thickness t_c. With increasing facing thickness the minimum core thickness decreases until the minimum core thickness is reached.

Figure 5.10 shows the fuselage weight per 10 meter fuselage length as function of facing thickness t_1 for fixed thickness ratios t_2/t_1, corresponding to the geometric variables given in figure 5.9. Again the horizontal parts of the curves in figure 5.10 only indicate the fuselage weight at minimum facing thickness.

It is noted that in this case the minimum sandwich fuselage weight occurs at the minimum facing thickness. The minimum fuselage weights and corresponding dimensions are given in table 5.4.

Table 5.4: *dimensions of lightest aluminium and carbon/epoxy sandwich fuselages excluding frame weights..*

Facing material		Aluminium	Carbon/epoxy
Fuselage weight	[kg/10m]	814	835
Facing 1 thickness	[mm]	0.90	1.21
Facing 2 thickness	[mm]	0.90	1.21
Core thickness	[mm]	17.7	24.8
Frame pitch	[mm]	10	10

5.4 Comparison of the sandwich and the stiffened skin fuselage concepts

Since the load case was chosen similar as for the stiffened fuselage discussed in section 5.1 the two fuselage concepts can be compared. The resultant weights and corresponding dimensions were summarised in table 5.2 and 5.4.

It is noted that for the specified load case the sandwich fuselages are heavier compared to the stiffened skin fuselages. This is caused by the minimum required thickness for maximum tensile stress. For the stiffened skin fuselage all material is used to carry the tensile load. For the sandwich fuselage only the facings are able to carry tensile and compressive loads. The core has to be added to increase the buckling resistance resulting in added weight. For cases where the minimum fuselage weight is not determined by the minimum facing thickness, the sandwich fuselage may be lighter than the stiffened skin fuselage.

It should be noted that for the sandwich fuselage the length without a reinforcing frame was chosen 10 meters. To see the influence of reinforcement frames in the sandwich fuselage, the lightest sandwich fuselage is determined for several values of fuselage length L_{fus}. The weight per 10 meter is then determined by multiplying the calculated fuselage weight with the ratio $10/L_{fus}$. For the fuselage with aluminium facings aluminium frames are used and for the fuselage with carbon/epoxy facings carbon/epoxy frames are used. The cross section area of the frames is chosen equal to the frames used in the stiffened skin fuselage; A_{fr} = 120 mm^2, which results in 2.6 kg/frame for the carbon/epoxy frame and 4.02 kg/frame for the aluminium frame. The resultant fuselage weight as function of L_{fr} is given in figure 5.11. It can be seen that now the carbon/epoxy sandwich fuselage with a frame pitch of 2m is a little bit lighter (802 kg/10m), compared to the aluminium sandwich fuselage with a frame pitch of 3m (804 kg/10m).

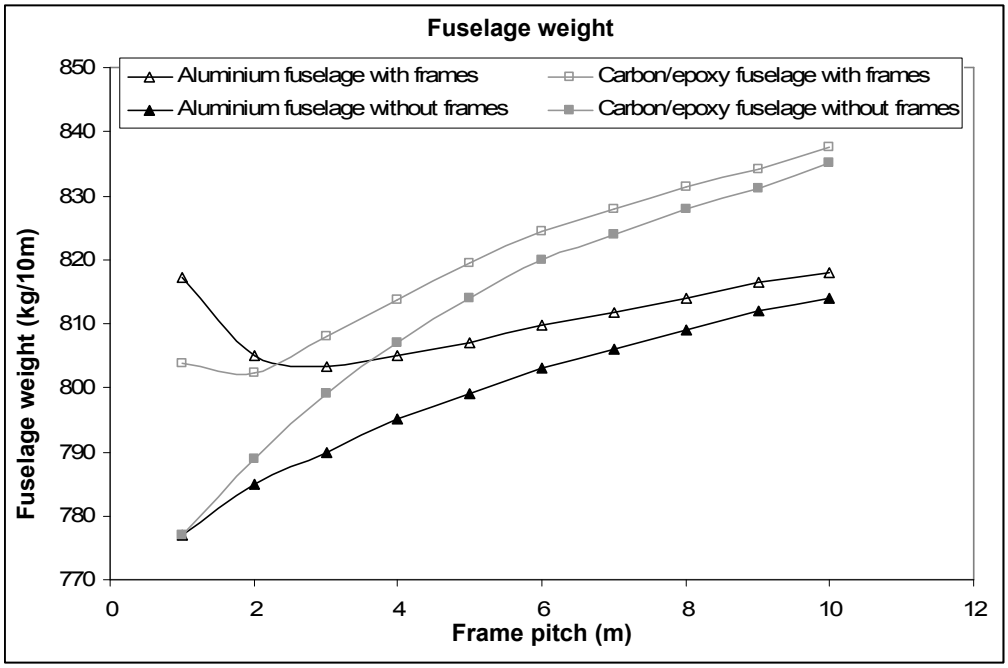

Figure 5.11: *Sandwich fuselage weight as function of frame pitch for carbon/epoxy and aluminium facings with the frame weight in- and excluded.*

The fact that the carbon/epoxy sandwich solution lies close to the aluminium sandwich solution can be explained with the material properties. The modulus of elasticity of the selected carbon/epoxy prepreg (quasi isotropic) is about half of that of aluminium. (See table 5.1 and 5.3). Also the maximum allowable tensile stress for the aluminium facings is much higher than for the carbon/epoxy facings, which results in a smaller minimum facing thickness requirement. By adding more unidirectional carbon fibers in the fuselage length-direction, the modulus of elasticity and maximum tensile stress in that direction can be increased, what would result in a lighter solution.

The structural weights calculated for the different fuselage concepts and the geometry and material properties given in table 5.1 and 5.4 are summarised in table 5.5.

Table 5.5: *Summary of the lightest calculated fuselage weights considering the geometry and material properties given in table 5.1 and 5.3.*

Concept	Stiffened skin	
Material	Aluminium	Carbon/epoxy
Weight/10m	697 kg/10m	565 kg/10m
Skin thickness	1.28 mm	1.10 mm
Frame pitch	425 mm	625 mm
Stringer pitch	65 mm	58.5 mm
Concept	**Sandwich**	
Material	Aluminium	Carbon/epoxy
Weight/10m	804 kg/10m	802 kg/10m
Frame pitch	3 m	2 m
Facing 1 thickness	0.90 mm	1.21 mm
Facing 2 thickness	0.90 mm	1.21 mm
Core thickness	17.7 mm	24.8 mm

For the considered case, the carbon/epoxy stiffened fuselage will be the lightest option. The optimum solution will depend on the load case, material properties and the chosen fixed geometric variables like the area of the frame cross sections.

Weight is of course not the only design criteria to select the fuselage structure concept. Also design aspects like the thermal and acoustical insulation, impact resistance will play a role in the decision of structural concept.

5.5 References

[1] van Tooren, M.J.L., Sandwich fuselage design, PhD thesis, Structures and Materials Laboratory, Delft University of Technology, Delft University press, 1998.

[2] Zaal, K., de Jong, Th., Beukers, A., Tooren, M.J.L. van, Structure effectiveness of aircraft, Discussion notes, Airbus Industry, Toulouse, 19 Dec, 1996.

[3] Allen, H.G., Analysis and design of structural sandwich panels, Pergamon Press, 1969.

[4] Sullins, R.T., Smith, G.W., Spier, E.E., Manual for structural stability analysis of sandwich plates and shells, NASA report, CR-1457, Langley, 1969.

6 The design & engineering engine

6.1 Introduction

Designing an aircraft is a very complex process because of its multidisciplinary nature. Requirements important in aircraft design involve structural, safety, performance, maintenance, manufacturing, passenger comfort and inspection aspects. Most of these requirements are documented in the FAA and EASA regulations. These regulations also describe the requirements for pressurised fuselages. Like discussed in previous chapters, the fuselage structure is usually designed and optimised only for primary requirements like strength, stiffness and fatigue. Secondary requirements like thermal and acoustical insulation are met afterwards. To be able to include also secondary design requirements from the start a Design & Engineering Engine is developed.

The Design & Engineering Engine (DEE) can be considered as a linkage of computer tools, each automating a part of the preliminary design process. See for other DEE examples developed at the TU Delft, reference [1-6]. The DEE enables the user to investigate relations between chosen design variables and the performance in satisfying the selected requirements. This implies that the DEE has to include a parametric model generator that can link the geometric design variables defined in input files to the analysis tools that calculate the performance on the specific design requirements.

With the use of the 'Design Of Experiments (DOE) [7-11]' concept a set of smartly chosen combinations of design variables can be selected for which the performance in satisfying the requirements can be calculated. With these results the response surfaces of the boundary constraints for each requirement can be determined. A generic optimisation tool then is able to find the optimum design. The optimisation process will be discussed in chapter 7.

The large advantage of the DEE concept is that it is suitable for automation. A scripting file controls the in- and output between the different computer tools within the DEE. The automated DEE is capable of performing many recurring calculations in a relatively short period of time. That is an advantage for the DOE concept. Based on response surfaces the designer can evaluate the chosen design. This makes the DEE a very suitable tool for the preliminary design phase.

The DEE concept also has some limitations. The DEE is not capable of capturing the creative part of the design process, meaning: choosing a design concept that could meet the design requirements. Therefore the designer remains responsible for choosing a design concept. Usually the concepts are chosen based on the designers experience and on company know how. Once the designer has chosen a concept the DEE can be used to evaluate and optimise the chosen concept.

The difficulty of a well-developed DEE is that it has to be able to handle all the different concepts the designer comes up with. This requires a very general approach of the geometric model generator keeping all possible design options open. The level of this general approach then determines the possibilities of capturing the concept of the designer. A high level generalisation is realised with the use of primitives and 'IF-THEN' parameters as will be explained in section 6.4.

The DEE will only be able to handle design disciplines that are represented within the DEE. Because each design discipline is represented by a computer tool that can be considered as modules, the design disciplines can be switched 'on' or 'of' within the DEE. This means that when it is desired to include a new design discipline in the design process a new module can be created without changing the already existing parts of the DEE.

Figure 6.1 shows a schematic overview of a DEE for aircraft design [6]. It starts with the definition of the customer requirements that have to be satisfied by the design. (Indicated as the '*Requirements*'). Then the designer has to think of possible concepts that could satisfy these requirements. This concept has to be initiated by the *'Initiator'* with the so-called parametric primitives. The primitives are considered as the building blocks with which a generic product model of the concept is build. (The primitives will be discussed in more detail in section 6.4). From this generic product model specific models are extracted by the *'Multi Model Generator (MMG)'* that serve as an input model for the different '*Discipline modules'* and '*Analysis tools'*. The outcome of these modules is stored in a database '*data files*'. By chosing some input parameters as design variables the DOE method together with the DEE and a genetic optimisation method can be used to find the optimum design variable configuration for the chosen concept. The validity of the outcome of the '*Discipline modules'* is represented by the 'Converger'. The solution is evaluated by the value of the objective function, which is represented by the *'Evaluator'*. Changing the design variables to find the optimum configuration is represented by decision switch '1'. With decision switch '2' the user decides whether the optimised solution is accepted to be the 'final configuration' or rejected, meaning that a new concept has to be chosen.

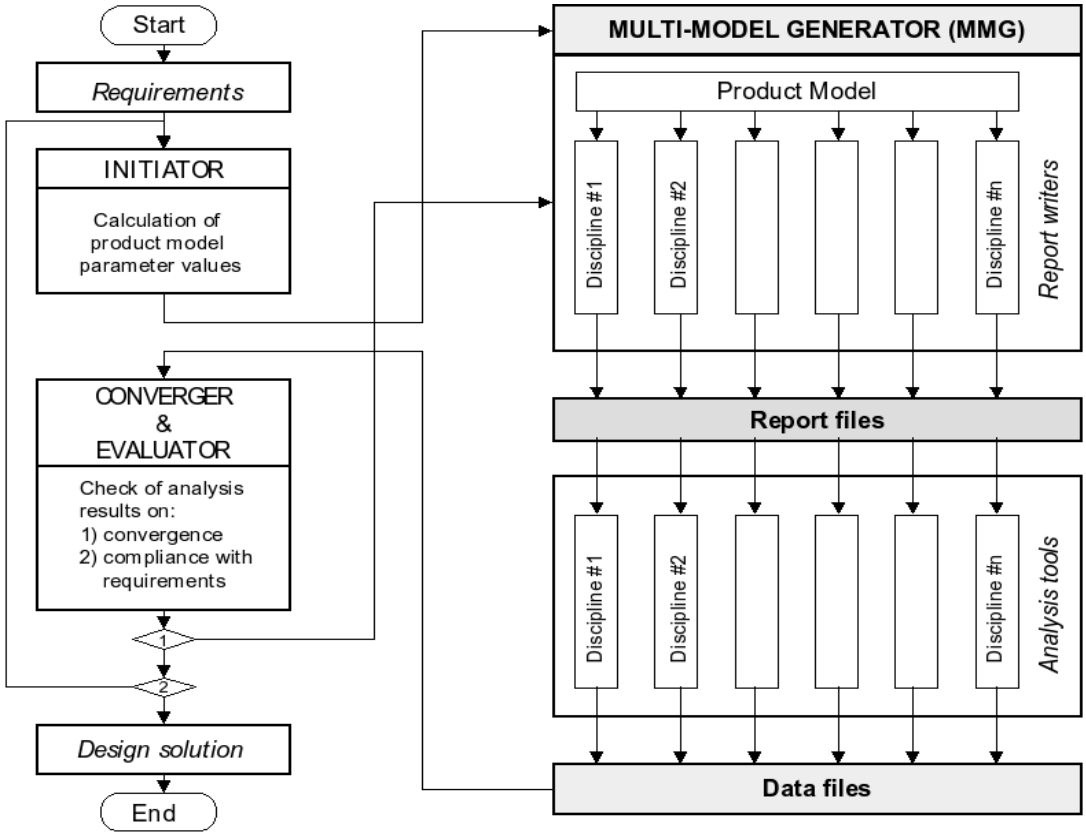

Figure 6.1: *Paradigm of a Design & Engineering Engine (DEE).*

In this research a DEE is developed for the design and optimisation of fuselages that will take into account the structural and acoustical & thermal insulation requirements. This chapter describes how this DEE is developed and how it meets the requirements that are set to the DEE. The requirements, which the DEE needs to fulfill are summarized in table 6.1.

First of all, the DEE will need a general fuselage model generator that is able to generate every kind of fuselage that the user comes up with. This means that the fuselage model generator has to be very flexible. In order to be able to implement the fuselage model generator in an automated tool it has to be defined in a parametrical way.

The fuselage model generator has to supply models for four discipline silos; for structural analysis, acoustic and thermal insulation analysis and a weight evaluator. All discipline silos are represented by computer tools that require input from the fuselage model generator. These computer tools must be able to run batchwise and evaluate the discipline requirements in the shape of evaluation parameters. This DEE makes use of three different commercial computer packages; the fuselage model generator is programmed within the knowledge based engineering environment of the computer package: ICAD, the thermal insulation, low frequency acoustical analysis and mechanical analysis are performed with the FEM package ABAQUS and the acoustical insulation analysis and evaluation tools are performed with the computer package: MATLAB. The steering scripts that link all tools together are written with the

open source code Python. The Python scripts make it possible to communicate between different computers. This makes it possible to enable access to special calculation computers for heavy analysis jobs.

Table 6.1: *Summation of requirements that the DEE needs to fulfil.*

- Contain a parametric description of the fuselage models
- Generate different types of fuselage models (Geometric flexibility)
- Start with a set of input parameters from which the user can select design variables.
- Contain a Design Of Experiments tool to generate smartly chosen combinations of design variables that will be analysed
- Generate input models for acoustic analysis
- Evaluate acoustic insulation
- Generate input models for thermal analysis
- Evaluate thermal insulation
- Generate input models for mechanical analysis
- Evaluate strength and stiffness requirements
- Evaluate fuselage weight
- Run autonomously
- Communicate between different computers to enable access to required computer programs
- Store results in data files for further analysis
- Determine response surfaces for the different analysis models
- Flexible definition of the design objective function
- Contain an optimisation tool

MATLAB is also used to perform the design of experiments and the optimization. Within this MATLAB environment it is easy to define the objective function for the optimization analysis and store the discipline analysis and optimization results.

A schematic overview of the DEE that is developed within this research is given in figure 6.2. It has the same structure as the DEE described in figure 6.1. Figure 6.2 shows that the process starts with the customer requirements for which the designer has to initiate a concept. The ideas to generalise a parametric description of a fuselage concept are discussed in section 6.2. All design parameters are summarised in section 6.3. The user chooses which design parameters will be design variables. With the DOE method different sets of input variables are defined for the chosen concept. The ICAD model generator generates for each set a generic model by making use of the so-called primitives. (The concept of the primitives is further explained in section 6.4 and the required set of input parameters is described in appendix E).

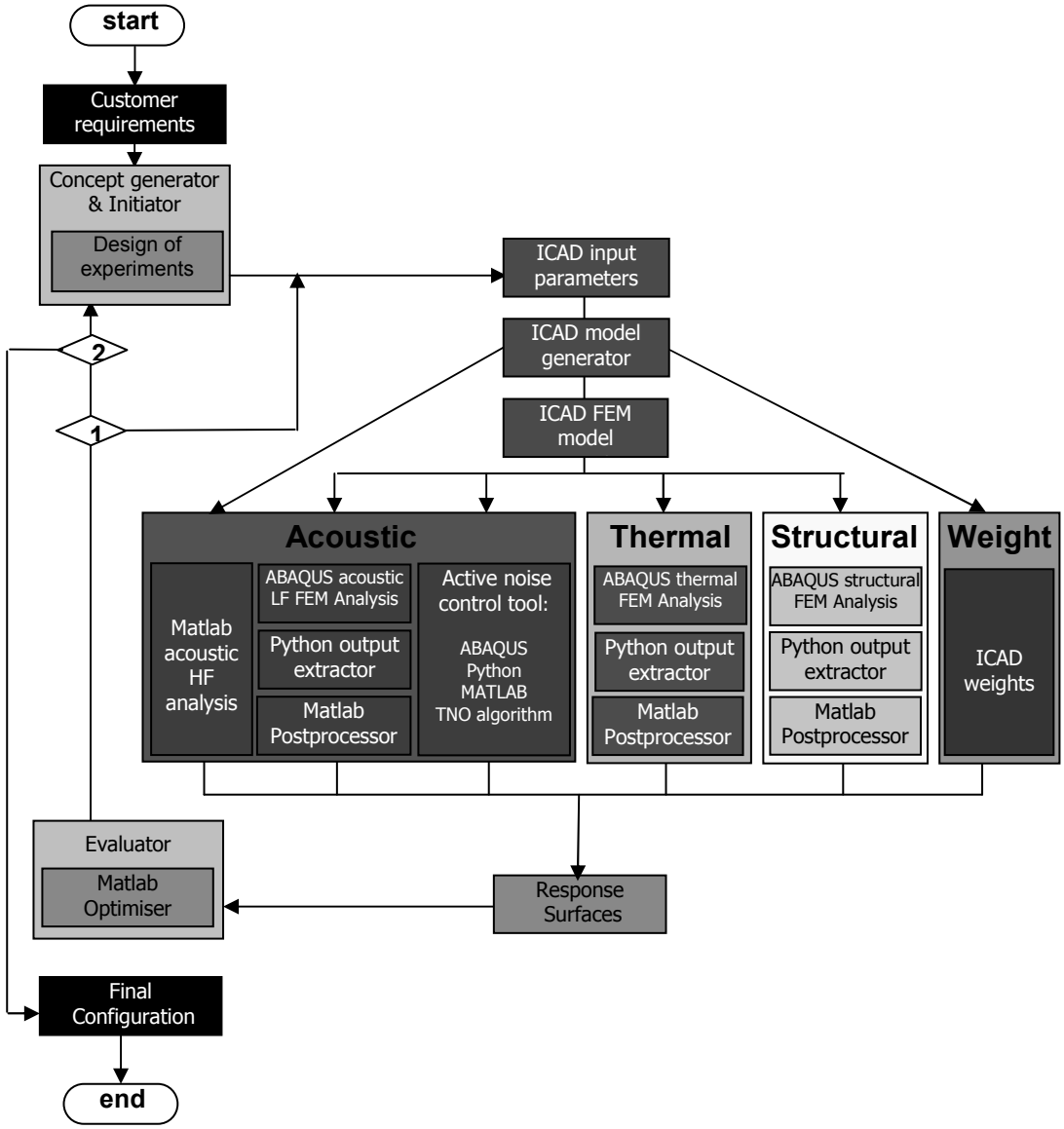

Figure 6.2: *Schematic overview of the DEE used for the design of pressurised fuselage taking into account the structural and the thermal & acoustical insulation aspects. (see also colour section)*

From the generated generic model, models are extracted for the four different modules that are used in this DEE; 1) the acoustic module, 2) the thermal module, 3) the structural module and 4) the weight module. The fourth module determines the weight of the configuration that will be used as an objective function in the optimisation. As is shown in figure 6.2 some modules require finite element models, which are generated with the ICAD FEM model generator discussed in section 6.5. The details of the four different modules, (the acoustic, thermal, structural and weight modules), are discussed in section 6.6 to 6.9. The DOE method and the link with the optimisation procedure are explained in chapter 7.

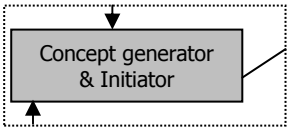

6.2 Concept generator

To be able to define a fuselage in a parametric way first the characteristics of a fuselage have to be defined. One of the geometrical requirements of a fuselage is that it has to encapsulate a space that can host passengers. For passenger comfort it must be possible that this space can be pressurised and for thermal and acoustical comfort, that it can be insulated. The most effective way to encapsulate a space that can be pressurised is with a load carrying skin construction. The most effective shapes of fuselage skins that are capable of carrying pressurisation loads are spherical or cylindrical shapes. Some examples are given below:

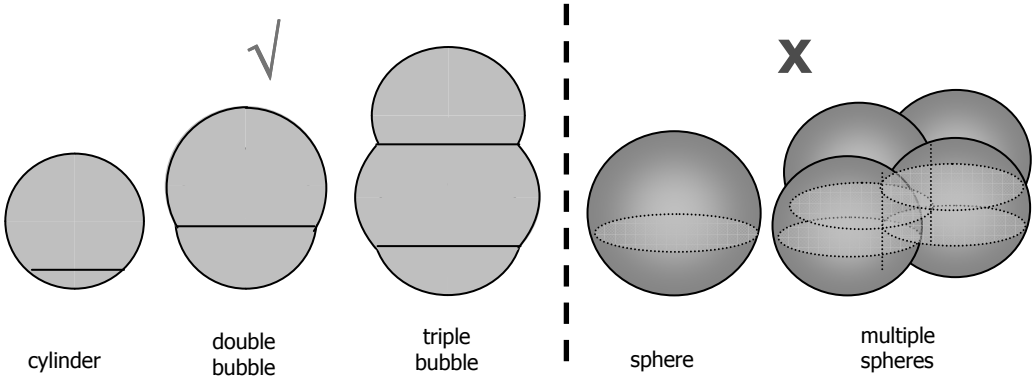

Figure 6.3: *Several fuselage shapes effective to carry pressurised loads.*

These shape solutions can be grouped into 2-dimensional shapes like the single cylinder, the double and the triple bubble cylinder, and 3-dimensional shapes like a sphere and multiple sphere combinations. In this research only (Quasi) 2-dimensional shapes are considered. That means, the configuration of the cross-section (single, double or triple bubble cylinders) is not allowed to change, while within a configuration the size and shape is allowed to change along the longitudinal axis. This group of shapes is most common for all existing aircraft because it has the optimal possibility to increase the volume, while keeping the frontal area constant, by elongating the fuselage. (A small frontal area is important for low drag). Only for more exotic aircraft like a blended wing body, where a pressurised fuselage has to be fitted inside a wing shape, spherical solutions can be more effective.

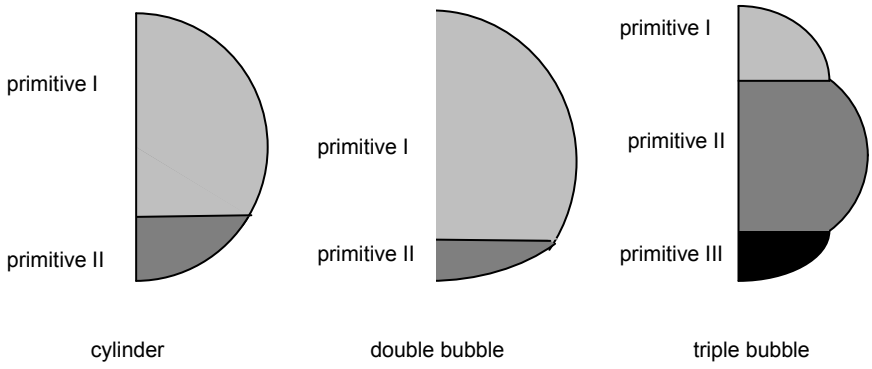

Figure 6.4: *Definition of fuselages constructed with building blocks*.

To accommodate the passengers, or in case of a freighter aircraft the cargo, floors are required inside the 2-dimensional shapes. The 2-dimensional shapes always have the mid-plane as plane of symmetry. When the single cylinder, the double bubble or triple bubble shapes are cut at the floor planes a general building block can be identified as is shown in figure 6.4.

From here on, these building blocks will be called fuselage primitives. There is no separate building block defined for the floor. The floors are included in the fuselage primitive by the possibility to have a floor on the 'bottom' and/or 'top' side of the building block.

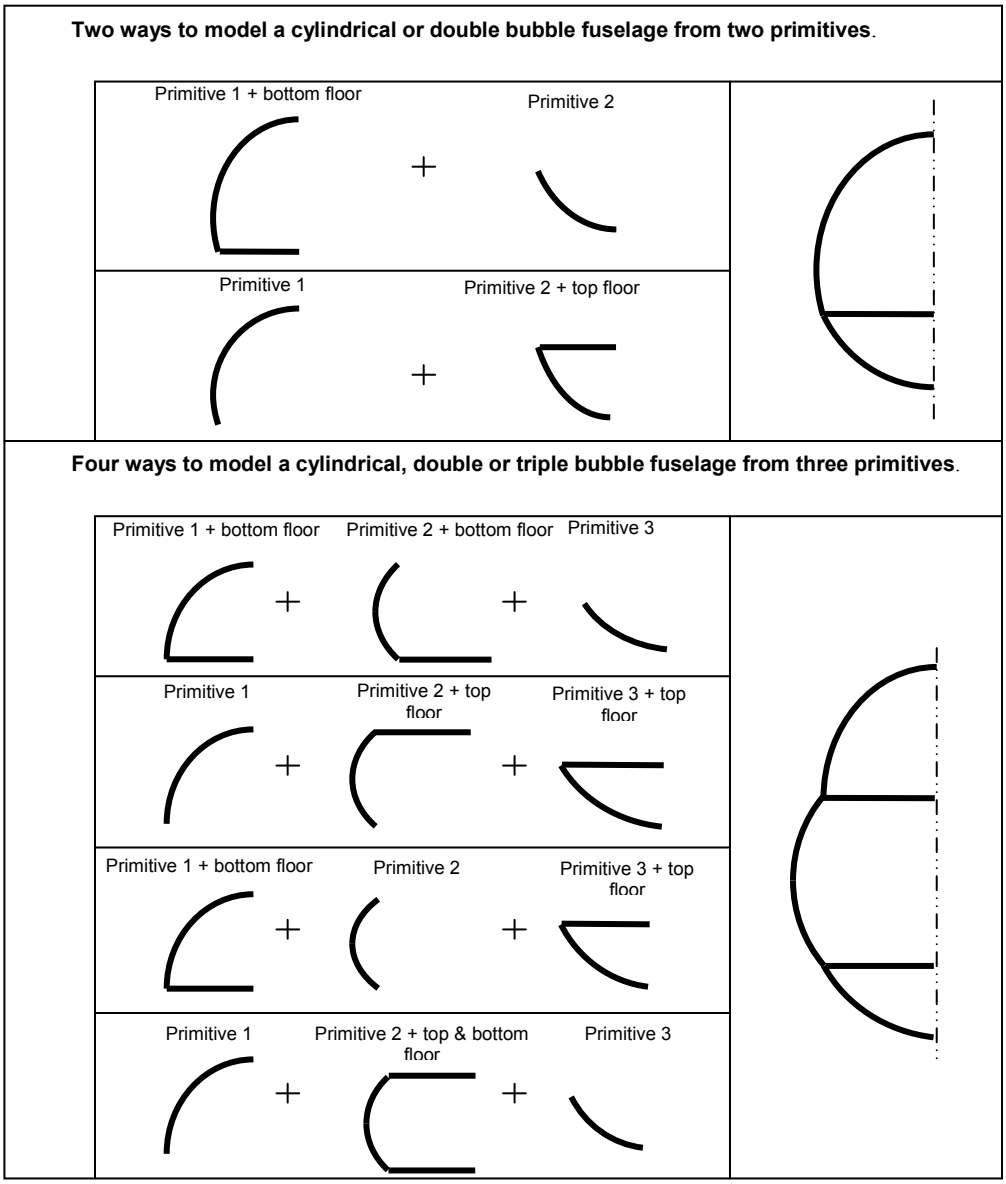

Figure 6.5: *Definition of fuselages constructed with the fuselage primitives*.

Figure 6.5 illustrates that with the choice of a 'top floor' and/or 'bottom floor', there are many different ways to define 2 dimensional fuselage concepts. For the final model either way will be fine. The structural concepts are enclosed within the

fuselage primitive. The user can choose for a stiffened skin or a sandwich skin concept. The exact definition of the fuselage primitive and its structural concepts are discussed in section 6.4

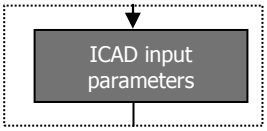

6.3 ICAD input parameters

The fuselage primitives are parametrically described with a rule base. The parametric description of a fuselage primitive starts from a set of input parameters. All input parameters, necessary to define the different elements of the fuselage primitive, are given in appendix E. From the list of input parameters a set of parameters can be chosen as design variables. The design variables will be used in an optimisation procedure while the remaining input parameters will remain fixed.

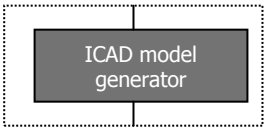

6.4 ICAD multi model generator

The multi model generator is an ICAD program that describes the fuselage parametrically. To generalise the parametric fuselage description the fuselage is constructed with parametrical described fuselage primitives. Each fuselage primitive starts with the same set of input parameters. The whole parametric fuselage model is called the generic product model. From the generic product model different models can be extracted depending on the kind of analysis they are used for. By always using the ICAD generic product model as a basis, consistency between the extracted models is ensured.

The whole fuselage is described by meta-level parameters such as the number of primitives and the primitive connections, and lower level parameters that define the fuselage primitives. The complexity in parametrically describing a fuselage is incorporated in the fuselage primitives. Therefore, in the next sub sections first the parametric description of the fuselage primitive will be given. Because the model required for the active noise control analysis has some special requirements, it will be discussed separately in section 6.4.2.

6.4.1 Parametric description of the fuselage primitive

The fuselage primitive describes a part of the fuselage that consists out of the fuselage wall including the skin, frames, stringers, interior wall and insulation elements. Also the air inside the fuselage is part of the fuselage primitive. Because fuselages usually have a plane of symmetry in the longitudinal-vertical plane, only half of the fuselage part is considered. Figure 6.6 shows an example of a fuselage primitive.

The fuselage primitive is described with parameters that can be categorized in two levels; High level parameters that define the configuration of the fuselage primitive and middle level parameters that define the shape, material and position of the different elements within a fuselage primitive. A third type of parameters are the parameters that describe the load case and boundary conditions required for the different discipline modules within the DEE. These parameters are considered low level parameters.

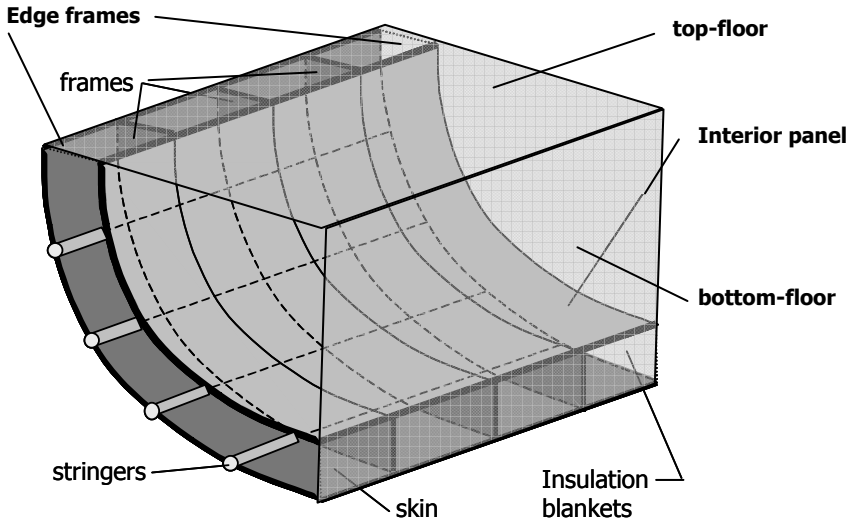

Figure 6.6: *The fuselage primitive with its basic elements.*

In this section the high and middle level fuselage primitive parameters will be discussed. The low-level parameters will be partly discussed within the sections that describe the different discipline modules.

High level fuselage primitive parameters

Each fuselage primitive consists out of set of basic elements. The basic elements are the skin (sandwich or single layer), frames, stringers, interior panels (sandwich or single layer), visco-elastic layers, insulation blankets and floor elements. To achieve a high level of flexibility, the fuselage primitive contains 14 high-level primitive parameters that define whether the fuselage primitive contains the basic elements or not. The high level parameters are all IF-THEN parameters.

Table 6.2 shows the high-level parameters of the fuselage primitive. By assigning the high-level primitive parameters to '**t**' for true, the basic element is created and by assigning the parameter to '**nil**' the basic element is not created.

The first four parameters from table 6.2 give the possibility to choose if the fuselage primitive contains a 'bottom' floor, 'top' floor, both or no floor at all with the corresponding floor beams. The *':single-skin'* parameter defines whether the fuselage skin consists out of a single or a sandwich skin. The *':frames'*, *':edge-frames'* and *':stringers'* parameters define whether the single or sandwich skin is reinforced with frames and/or stringers. The *':insulation'* parameter defines the insulation blankets, that are positioned between the fuselage skin and the interior panels. The *':interior-panel?'* parameter defines whether or not there is an interior panel and the *':interior-shell?'* parameter defines whether it is modeled as a single skin or as a sandwich. The two *':visco-elastic-xxx'* parameters define whether there is a visco-elastic layer within the skin or interior panel or not. Finally, the *':air-inside?'* parameter defines whether the air inside the fuselage will be modelled or not. The fuselage primitive does not (yet) take into account doors, windows or any other irregularities.

Table 6.2: *The 14 high-level parameters of the fuselage primitive.*

Parameter	t	nil
:top-floor?	top floor	no top floor
:bottom-floor?	bottom floor	no bottom floor
:top-floor-beams?	floor has beams	no top floor beams
:bottom-floor-beams?	bottom floor has beams	no bottom floor beams
:single-skin?	single skin	sandwich skin
:skin-visco?	skin has viscoelastic layer	no viscoelastic layer
:frames?	frames	no frames
:edge-frames?	frames at edge of fuselage primitive	no edge frames
:stringers?	stringers	no stringers
:insulation?	insulation blanket	no insulation blanket
:interior-panel?	interior panel	no interior panels
:interior-shell?	single interior panel	sandwich interior panel
:interior-visco?	interior panel has viscoelastic layer	no viscoelastic layer
:air-inside?	air inside the fuselage modelled	no air modelled

Middle level fuselage primitive parameters

The middle level fuselage primitive parameters define the shape, material and position of the different basic elements within the fuselage primitive and are indicated in appendix E with the level ML. The shape of the fuselage primitive is defined with a starting surface that represents the outside surface of the fuselage skin.

Next, the starting surface will be described followed by the description of some of the main middle level fuselage primitive parameters.

Definition of the starting surface

The definition of the parametric fuselage primitive starts with the definition of the surface that represents the outside of the fuselage skin. This surface can be defined within the ICAD environment or it can be delivered from other CAD packages. In both cases a starting surface is created in IGES format that can be imported into the ICAD fuselage primitive program with the same IGES reader. Within the ICAD environment the starting surface is currently created from four edge curves that are defined with sets of points.

For the special case of a simple straight circular fuselage with a single floor, the fuselage is defined with the use of two fuselage primitives; an upper part including a bottom floor and a lower part as is illustrated in figure 6.7. In this case the two starting surfaces can be defined by only specifying a radius, floor-height and a fuselage length.

Besides the definition of the starting surface, also two construction ‘end lines’ are required, which are illustrated in figure 6.8. With these construction ‘end lines’ and the upper and lower edges of the starting surface, the connection surfaces of the fuselage primitives to other fuselage primitives are defined. These connection surfaces are also used to define the floors.

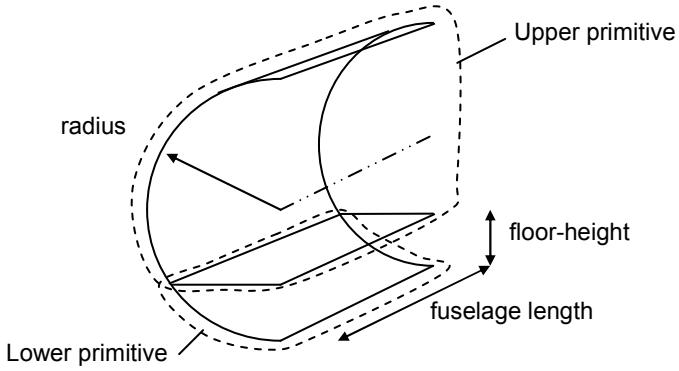

Figure 6.7: *Three parameters define the starting surfaces for a fuselage with a single floor.*

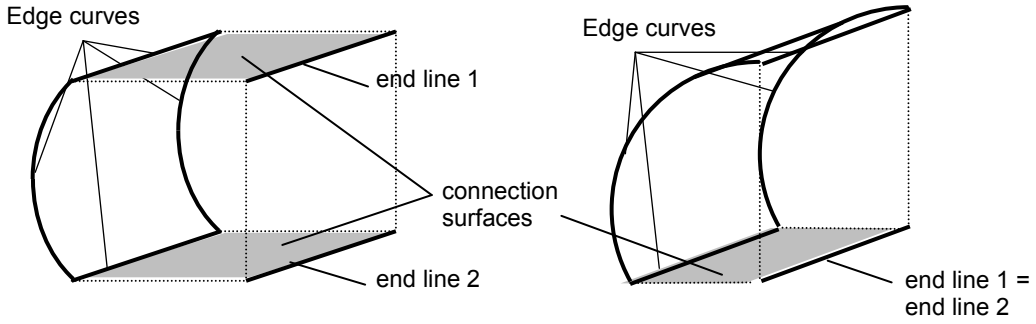

Figure 6.8: *End line principle to define two different forms of fuselage primitives.*

Explanation of some of the main middle level fuselage primitive parameters

The middle level fuselage primitive parameters define the dimensions, positions and material properties of the basic elements. These middle level fuselage primitive parameters are given in appendix E indicated with ML.

All plate-like elements like the skin, frame webs, interior panels and floors have a *'thickness-list'* and a *'material-list'* parameter that define the thickness of the different layers and the materials assigned to each layer.

For the frames and stringers additional shape and positioning parameters are defined. The frame flange cross-sections are represented by area equivalent circular cross-sections. Also the stringer cross-section can be simplified using equivalent models. The definition of the equivalent models for the frame flanges and stringers is explained in more detail in appendix F.

The positioning of the frames and stringers is based on the u-v parameterisation of the starting surface. See figure 6.9. Every surface defined in ICAD has a u-v parameterisation, where the u-direction is pointed along a surface edge and the v-direction is pointed along a second surface edge that intersects the first edge at u equals zero. The direction of the boundary curves is always from the first defined curve-point to the last defined curve-point. Direction v is then pointed along the boundary curve that crosses the first boundary curve in the starting point.

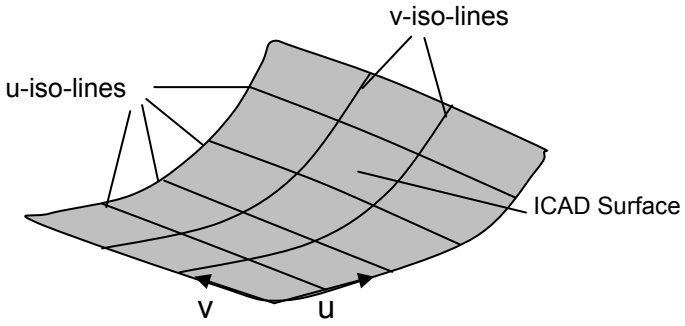

Figure 6.9: *u-v parameterisation of an ICAD Surface*

The u-v parameterisation defines the directions of the frames and stringers. The frames, respectively the stringers, always follow the v-iso-lines, respectively the u-iso-lines. This implies a restriction on the direction of the frames and stringers. The positions of the frames and stringers are defined in a percentage of the u-parameter respectively the v-parameter with the *':frame-position-list'* and the *':stringer-position-list'* parameters.

In general the skin surface edges are straight lines or single curved lines resulting in a parameterisation that perfectly fits the desired direction of the frames and stringers. If the skin surface has double curved edges, attention has to be paid to the parameterisation of the starting surface. When necessary the fuselage skin can be represented with multiple starting surfaces. This can also be useful when stiffeners are not continuous along the entire length of the fuselage like is common in the empenage of the fuselage. This concept is explained in figure 6.10.

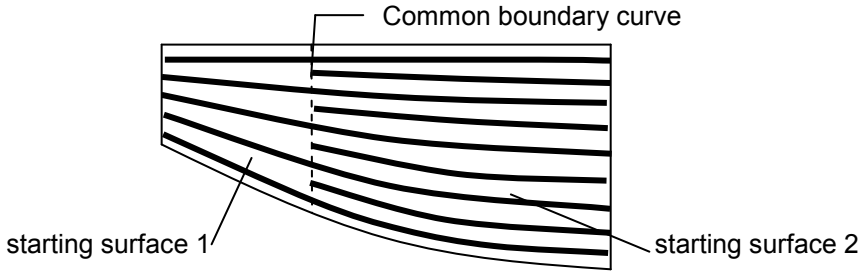

Figure 6.10: *Example of two starting surface to model non-continuous stringers.*

In the case shown in figure 6.10, both starting surfaces have one boundary curve in common. Because the stringer position is defined in percentage of the boundary curve length, continuity of the long stringers is guaranteed between the two parts.

The interior panels are attached to the frames which means that the distance between the skin and the interior panel is defined by the *':frame-web-height'* parameter.

The space between the interior panels and the fuselage skin can be defined as an insulation blanket. In that case this space is completely filled with insulation blanket.

With the high and middle level parameters of the fuselage, the configuration, dimensions and material properties of the fuselage primitive are defined. In the next sub section the definition of the parametric active noise control model is discussed.

6.4.2 Parametric description of the active noise control models

For the analysis of the sound transmission loss with the active noise control concept separate models are generated. The models for the active noise control analysis differ from the fuselage primitive because of the presence of piezoelectric actuators. In this study the piezoelectric actuators are represented as rectangular PZT actuators that have electrodes on the top and bottom side as shown in figure 6.11. This type of actuator makes use of the d_{31} and d_{32} piezoelectric strain coefficients, (which are explained in equation 3.46 of chapter 3).

Figure 6.11: *Example of a rectangular piezo electric actuator.*

The actuators are modeled with solid elements where the amount of FEM elements in thickness direction is variable. The electrodes are simply represented by the top and bottom surface of the actuator elements.

Because of the fact that the actuators are modeled as solids the active noise control models are difficult to integrate with the fuselage primitive models. The integration of the actuators in the fuselage primitive requires extra effort because the actuators disturb the smooth connection between the structural surfaces and the air or insulation volumes. This full integration has not been completed in this research. However the current active noise control models are sufficient to analyse the effects of an active noise control concept on (interior) skin panels.

For active noise control analysis the amount of actuators as well as the actuator size, position and material properties are input parameters. This is achieved by representing the actuators as extra layers that are added to a skin panel. In the current model, up to three layers can be added on both sides of the skin panel. Each layer has a thickness that is constant through the whole layer. However, a layer can consist out of different elements that have different positions and size. By using three different layers, actuators with three different thicknesses can be modeled in the same model. The three layers can also be used to model stringers in 3D. Figure 6.12 illustrates the additional layer concept with a few examples:

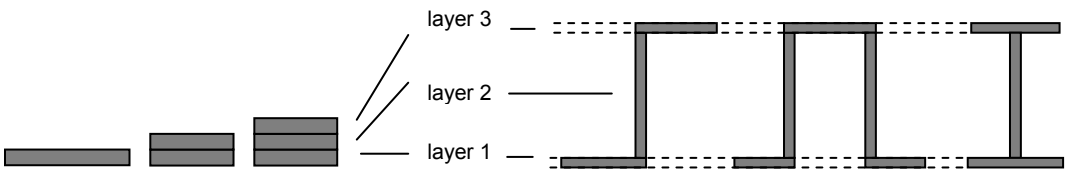

Figure 6.12: *Examples of 3D stiffener models modeled with 3 layers of elements.*

The active noise control model is modeled similar to the fuselage primitive. Also in the active noise control model the skin panel is modeled with a starting surface. The skin panel thickness and the skin material properties are defined in an identical manner as for the fuselage primitive. However for the active noise control model there are no structural parts like the frames, stringers and floors. Also the air is not modeled. For the active noise control model the structural elements are modeled with the additional layer concept.

Also for the active noise control model the parameters can be divided into high, middle and low level parameters. The high-level choice parameters define whether a layer exists or not, the middle level parameters define the position, size and material properties of the layers and the low level parameters define the load case and boundary conditions. The high level parameters and the middle level parameters for layer 1 are summarized in table 6.3. (The middle level parameters for layer 2, 3, 1b, 2b, and 3b are identical to middle level parameters of layer 1).

Table 6.3: *The high- and middle-level parameters of the active noise control model primitive.*

High level parameter	**Description**	
	't'	**'nil'**
:layer-1?	Extra layer 1 top side	no extra layer 1 top side
:layer-2?	Extra layer 2 top side	no extra layer 2 top side
:layer-3?	Extra layer 3 top side	no extra layer 3 top side
:layer-1b?	Extra layer 1 bot side	no extra layer 1 bot side
:layer-2b?	Extra layer 2 bot side	no extra layer 2 bot side
:layer-3b?	Extra layer 3 bot side	no extra layer 3 bot side
Middle level parameter	**Description**	
:x1-list	List with x-coord of middle points of all elemts of layer 1	
:y1-list	List with y-coord of middle points of all elemts of layer 1	
:t1-thickness	Thickness of layer 1	
:l1-list	List with lengths of all elements of layer 1	
:b1-list	List with widths of all elements of layer 1	
:layer-1-material-list	List with material identifiers of all elements of layer 1	

The elements of each layer are positioned with their middle point. The middle point is defined with the u and v surface parameters defined in percentage of the skin panel width (u-direction) and the skin panel length (v-direction). A vertical positioning coordinate is not required because the active noise control model automatically places the layers on top of each other. The size of the elements is defined with the length and width of each element. The width of the elements is defined in the u-direction and the length in the v-direction. The positioning principle of layer elements is illustrated in figure 6.13. Similar layers are defined for the bottom side of the panel. Whether an element inside a layer is piezoelectric or not depends on the material property definition.

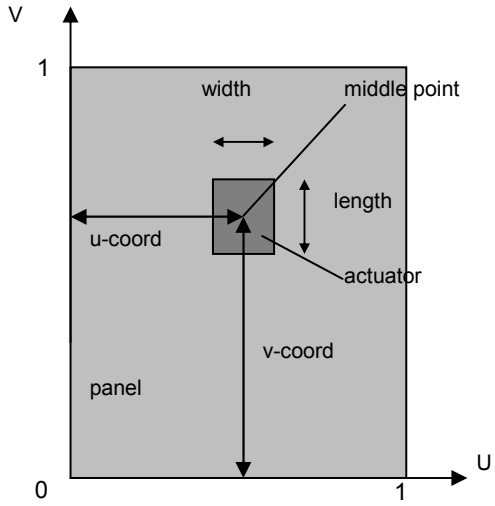

Figure 6.13: *Positioning of elements for active noise control panels.*

Figure 6.14 shows two examples of active noise control panels. The first example shows a panel with 9 activated rectangular piezo elements. The second example illustrates the modeling of stringers with the layer concept. This panel has one piezo element in the middle, which is also activated by an electrical field.

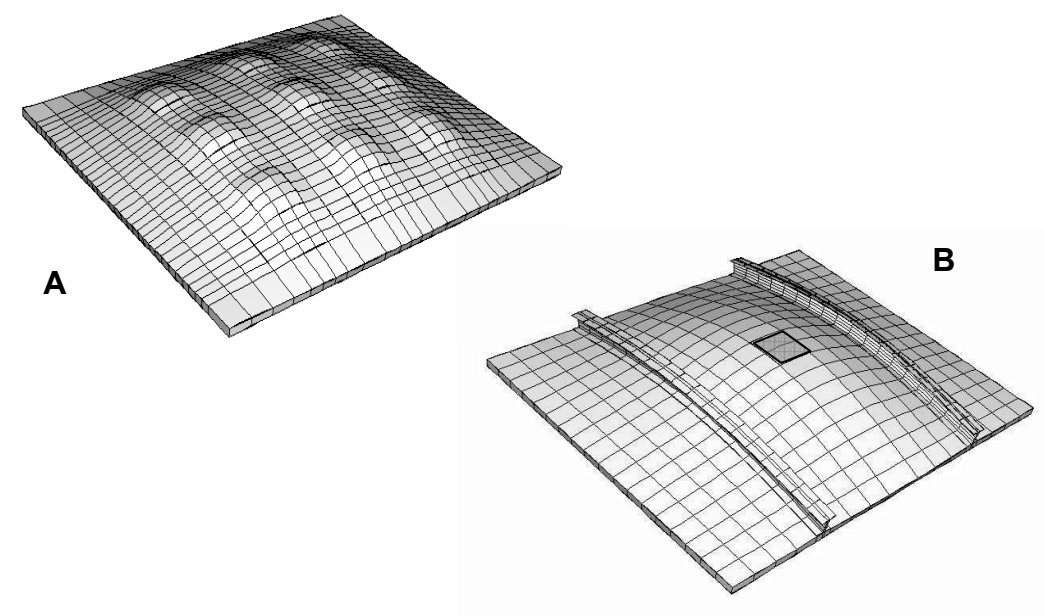

Figure 6.14: *Two examples of active noise control panels;*
A) A panel with 9 rectangular piezo electric actuators.
B) A panel with one actuator in the middle with I-type stringers.

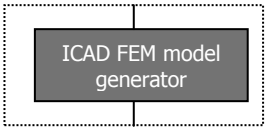

6.5 ICAD FEM model generator

The structural, thermal and the sound transmission loss analysis for the low frequency range as well as the active noise control analysis are performed with the finite element program ABAQUS. This implies that an interface is required between ICAD and ABAQUS. This interface is realised with the ICAD model meshing procedure, which will be explained in section 6.5.1 for the fuselage primitive. Because the active noise control model has a different set-up its meshing procedure will be discussed separately in section 6.5.2. The FEM models are exported from ICAD to ABAQUS in the format of; ready to use text input files. The required material properties are extracted from a material database.

6.5.1 ICAD fuselage primitive meshing procedure

For the finite element analysis the commercially available FEM package ABAQUS is used. The ICAD FEM model generator generates a FEM input file for fuselage primitive. This FEM input file is a text file that contains all the nodes, elements, material properties and load case definitions of the considered fuselage primitive.

Within ABAQUS it is possible to assemble a model from different parts (fuselage primitives). Each part of an assembled model is independent from other parts. This means that identical node and element numbering is allowed for different parts in an assembly.

The assembly option of ABAQUS makes it possible to call the ICAD program multiple times to generate the separate fuselage primitives of the assembly. This process is controlled within a Python DEE script file. The Python DEE script calls the ICAD model and the FEM model generator routines what results in the FEM input files for each fuselage primitive of the assembly. A concatenating command within the Python script adds the separate FEM input files into one overall ABAQUS input file for the complete fuselage model.

The multiple parts concept discussed in section 6.2 results in an extra loop in the DEE. This is illustrated in figure 6.15. The multiple parts concept also has the consequence that the designer has to specify multiple ICAD input parameter files, (One ICAD input file for each fuselage primitive). These ICAD input files also contain parameters that define if the fuselage primitive is connected with neighbouring fuselage primitives.

In the remaining part of this section the mesh size control of the fuselage primitive will be discussed. The mesh of the fuselage primitive forms the basis of the mesh definition for the stringers, the frames, the air inside the fuselage, the interior panels and the insulation blankets an the floors that are discussed in appendix F.1. The material properties are linked through a material library system within the ICAD environment. This is discussed in appendix F.2. The ICAD FEM generator generates text files as output. These text files are generated with so-called ‘report writers’. The various report-writers of the ICAD FEM generator are described in appendix F.3.

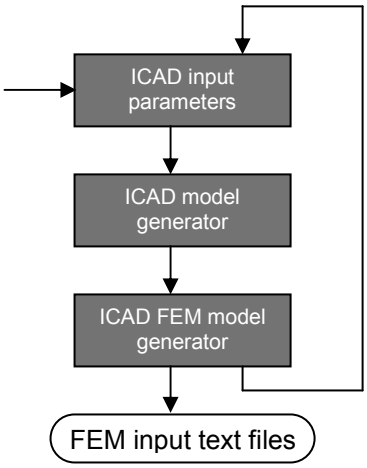

Figure 6.15: *The addition of the loop in the DEE illustrates the generation of the assembly models that consists out of multiple fuselage primitive models. For each analysis discipline a separate FEM input file is generated that contains analysis specific data.*

Mesh size control

The user has full control on the number of mesh elements within a fuselage primitive by setting 5 mesh-parameters. These 5 mesh-parameters are given in the table 6.5.

Table 6.5: *Meshing parameters for the fuselage primitive.*

Mesh-parameters
:inbetween-frame-mesh-nr
:inbetween-stringer-mesh-nr
:frame-z-mesh
:air-inside-mesh-nr
:air-mesh-factor

The first two parameters define the rectangular mesh of the fuselage skin between two frames and two stringers. The number of mesh elements is identical between each two frames and two stringers. The parameter '*:inbetween-frame-mesh-nr*' defines the number of mesh elements between two frames and the parameter '*:inbetween-stringer-mesh-nr*' defines the number of mesh elements between two stringers. The parameter '*:frame-z-mesh'* defines the number of elements in the frame height direction and the parameter '*:air-inside-mesh-nr'* defines the number of elements in radial direction of the air inside the fuselage primitive. This is illustrated in figure 6.16.

In order to be able to match a course mesh for the air inside of the fuselage with a fine mesh of the fuselage wall, the fine mesh of the fuselage wall has to be an integer multiple of the air mesh. This integer is defined as the *':air-mesh-factor'* parameter. Figure 6.17 illustrates the match between the fuselage wall mesh and the air inside mesh for an ':air-mesh-factor' of 1, 2 and 3. Air-mesh factors smaller than 1 are not possible. In that case the mesh of the skin has to be refined.

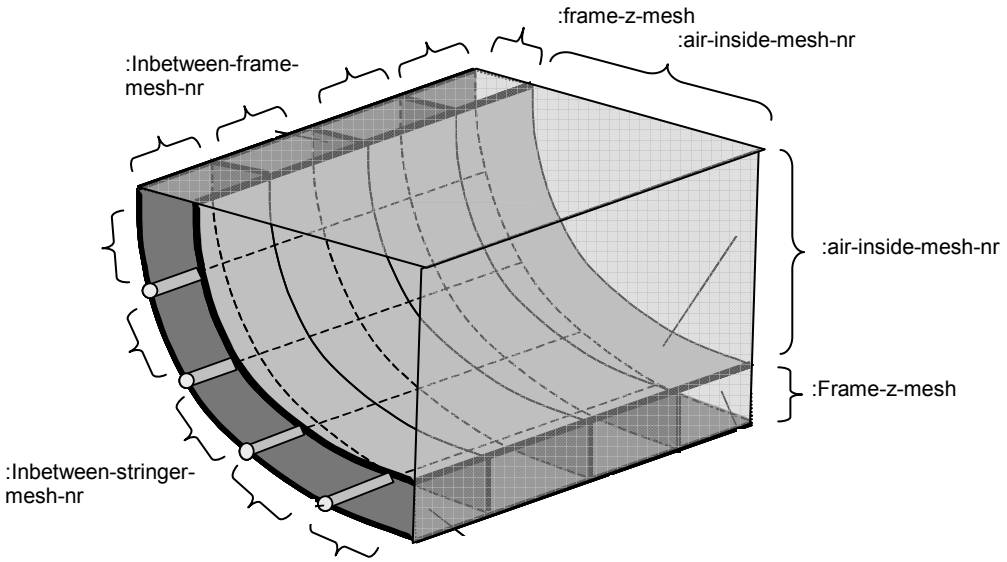

Figure 6.16: *Illustration of the mesh parameters.*

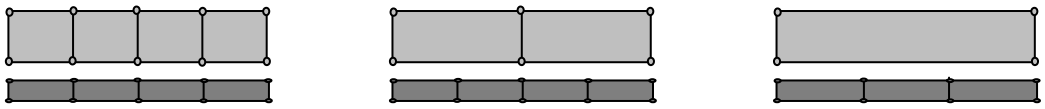

Figure 6.17: *Illustration of the air-mesh-factor, which defines the match of the mesh between the fuselage wall and the air inside.*

Depending on the purpose of the FEM model (structural, thermal or acoustical analysis) the skin is modeled with 8 node solid brick elements (thermal and acoustical analysis) or with 4 node shell elements (structural analysis).

When the skin is modeled with solid elements the length of the parameter *':skin-thickness-list'* controls the number of layers in the skin. By assigning different material properties to the different layers, laminates or sandwich skins can be specified. By assigning identical material properties to different layers, the mesh in thickness direction of a skin layer can be controlled.

In case the sandwich skin is modeled with shell elements the ':skin-thickness-list' parameter defines the thickness of each layer through a 'shell section' property definition.

Figure 6.18 gives an illustration of a meshed fuselage model with a single skin, 3 frames, multiple stringers and a floor. Also the mesh of the air inside the fuselage is shown.

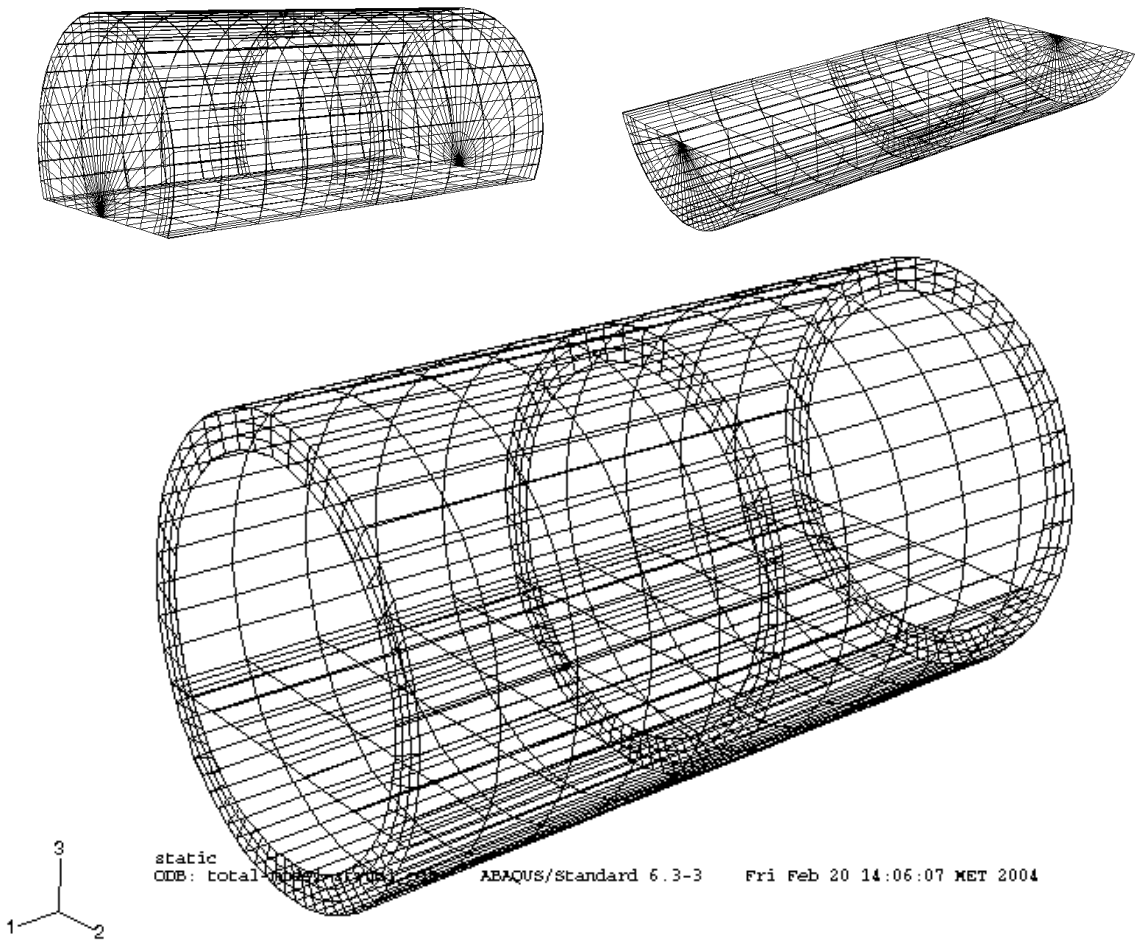

Figure 6.18: *Illustration of the mesh of a circular fuselage that consists out of two fuselage primitives. The fuselage has 3 frames, multiple stringers and a floor. The inserts show the meshing of the air inside the fuselage parts.*

6.5.2 Meshing of the active noise control model

The active noise control model consists out of a panel with added layers. The positions of the mesh lines of the active noise control model are dependent on the added layer elements. Along each boundary line of the added layer elements a mesh line is created. In between these 'master' mesh lines more mesh lines are positioned when the space between the 'master' mesh lines is larger than the maximum mesh size. This means that for the active noise control model two mesh control parameters are defined; a maximum mesh size parameter in u-direction and a maximum mesh size parameter in v-direction. Figure 6.19 shows an example of a meshed active noise control model. The model has multiple layers with 9 equally distributed rectangular piezoelectric elements.

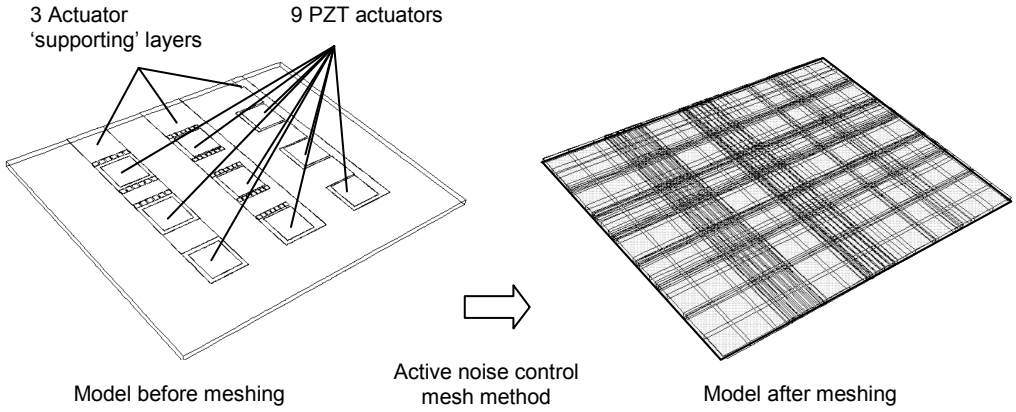

Figure 6.19: *Example of the active noise control mesh method for a panel with 9 rectangular piezo electric actuators attached to 3 actuator 'supporting' layers.*

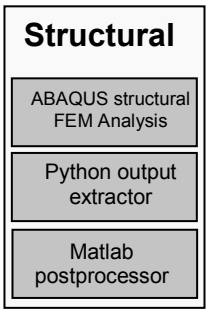

6.6 The structural module

The structural module consists out of three parts; the structural FEM analysis, the Python output extractor and the Matlab postprocessor. The commercially available computer package ABAQUS is used for the structural FEM analysis consisting out of a static stress analysis to determine the stresses and displacements. A Matlab postprocessing routine searches the elements with the highest stresses and determines the corresponding stress factors. The stress factors indicate whether the structure will fail or remain in tact.

The remaining of this section consists out of the discussion of; the structural model definition, the load case definition, the result extraction routines and post processing routines.

Structural model definition

For the structural analysis only the load carrying parts of the model are required. This means that the structural model only includes the skin, frames, stringers, floor and floor beams.

Load case definition

The load case that is defined for the structural analysis is a simple load case definition that is characteristic for fuselages. The load case exists out of an internal overpressure p, a bending moment M, and a shear force Q, which is explained in figure 6.20. The load case is introduced in the meshed model by defining a surface pressure on the skin elements and resultant longitudinal, horizontal and vertical loads on the nodes of the fuselage boundary elements. In the current ICAD FEM model generator the resultant longitudinal, horizontal and vertical loads are calculated with a simple routine only suitable for circular stiffened fuselages. For arbitrary shaped fuselages the load case definition should be generalised.

At the faculty of aerospace engineering at the TU Delft an overall DEE is developed for complete aircraft. In case the DEE that is developed in this research, would be integrated in the overall DEE for complete aircraft, the load case and boundary conditions should be extracted from the complete aircraft model that is subjected to manoeuvre and gust loads. Although work has been done in this direction at the faculty of aerospace engineering, this is not part of this research.

In the remaining of this section the basic rules are given below for the load case definition acting on circular stiffened fuselages. The internal pressure p, the axial loads P_x and N_x and the shear loads Q_x and Q_z are determined as indicated in figure 6.20.

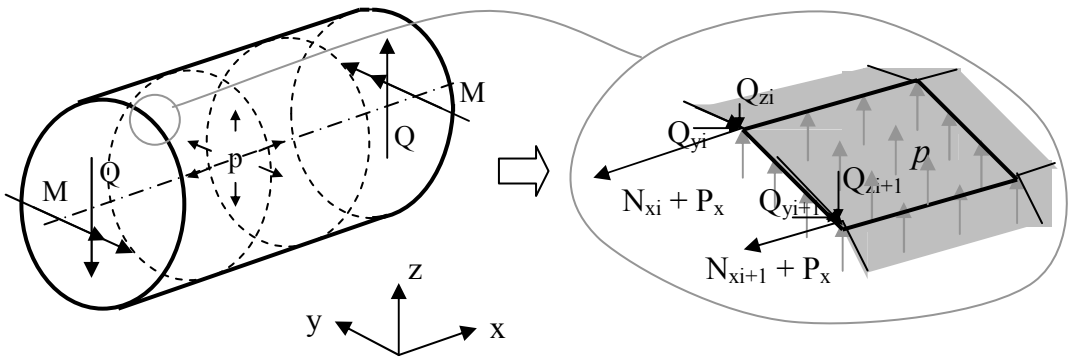

Figure 6.20: *Load case definition.*

Internal overpressure p

The internal overpressure in N/m^2 applied to the skin surface elements:

$$p \tag{6.1}$$

Axial loads P_x and N_x

Axial loads in N caused by the internal overpressure at nodes *in between* stringer positions:

$$P_x = \frac{p\pi R^2}{2t_{sk}\pi R E_{sk} + A_{str}E_{str}n_{str}} \cdot \frac{2\pi R t_{sk} E_{sk}}{n_{elements}} \tag{6.2}$$

Here is n_{str} the number of stringers and $n_{elements}$ the number of FEM elements in circumferential direction.

Axial loads caused by the internal overpressure at nodes *at* stringer positions:

$$P_x = \frac{p\pi R^2}{2t_{sk}\pi R E_{sk} + A_{str}E_{str}n_{str}} \cdot \left(\frac{2\pi R t_{sk} E_{sk}}{n_{elements}} + A_{str}E_{str} \right) \tag{6.3}$$

Axial loads caused by the bending moment at node i along the circumference *in between* stringer positions:

$$N_{xi} = \frac{MR\cos\varphi_i}{EI_{yy}} \cdot \frac{2\pi R t_{sk} E_{sk}}{n_{elements}} \tag{6.4}$$

Axial loads at node i along the circumference because of bending moment *at* stringer positions:

$$N_{xi} = \frac{MR\cos\varphi_i}{EI_{yy}} \cdot \left(\frac{2\pi R t_{sk} E_{sk}}{n_{elements}} + A_{str} E_{str} \right) \tag{6.5}$$

Shear loads Q_y and Q_z

Shear load at node i along the circumference:

$$Q_{zi} = \frac{Q}{EI_{zz}} \cdot R^2 E \bar{t} \sin\varphi_i \cdot R(\varphi_{i+1} - \varphi_i)\sin\varphi_i \tag{6.6}$$

$$Q_{yi} = \frac{Q}{EI_{yy}} \cdot R^2 E \bar{t} \sin\varphi_i \cdot R(\varphi_{i+1} - \varphi_i)\cos\varphi_i \tag{6.7}$$

Where:

$$EI_{zz} = EI_{yy} = \pi R^3 E t_{eq} \tag{6.8}$$

$$Et_{eq} = Ekt_{sk} + \frac{E_{str} A_{str} n_{str}}{\pi R} \tag{6.9}$$

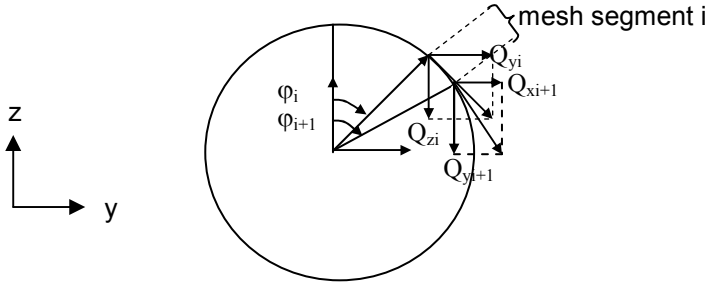

Figure 6.21: *Illustration of the horizontal and vertical shear load definition.*

For the previous load case definition the following assumptions are made:

- The moment of inertia of the fuselage is estimated according to equation 6.8, which means that the stringers are considered as an equivalent thickness. The shear load is introduced as if the stringers are smeared over the skin, meaning that the shear flow has a sinus shape without interruptions at stringer positions.

- The segment shear loads Q_{yi} and Q_{zi} are applied on the first node of the mesh segment i. For mesh segments that are small compared to the radius this assumption is allowed.

Figure 6.22 shows an example of a structural FEM model consisting out of two mirrored fuselage primitives for a circular fuselage with one floor.

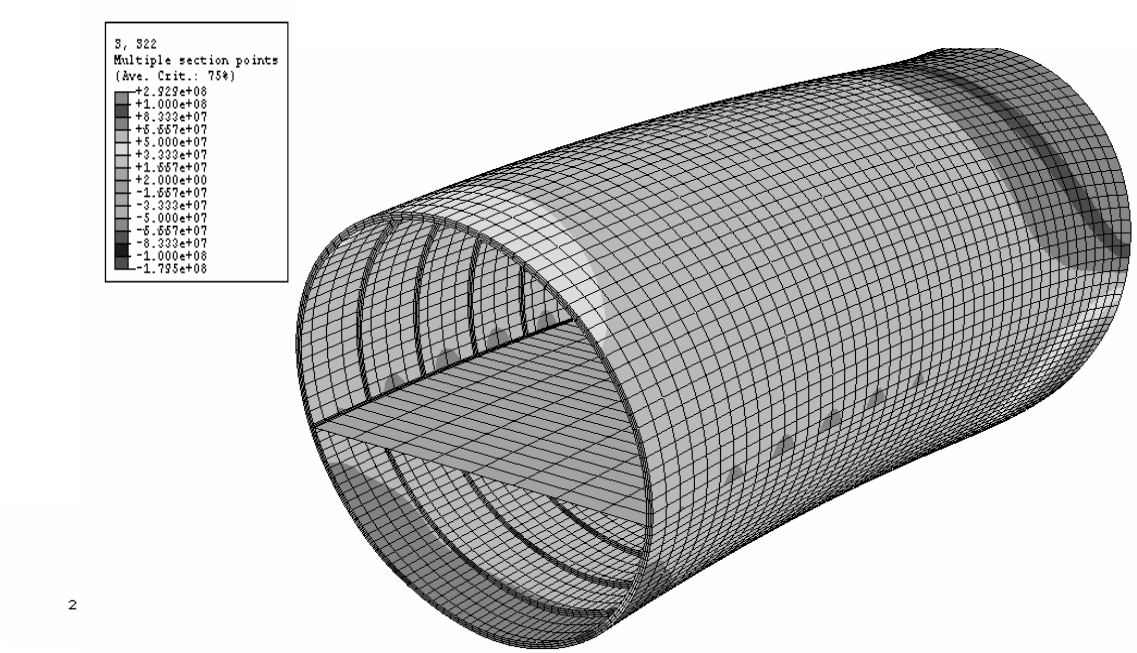

Figure 6.22: *Example of the stress distribution of a stringer stiffened fuselage loaded with an internal pressure, a bending moment and a shear load.(See also colour section).*

Result extraction

The ABAQUS structural FEM analysis determines the stresses at the integration points of each mesh element. The structural FEM model consists out of shell and beam elements. The positions of the integration points in the cross section of these elements are illustrated in figure 6.23.

For shell elements the stresses are extracted at 5 integration points through the thickness of each layer. This means that for a sandwich consisting out of 3 layers, stresses are extracted at 15 integration points.

For circular beam elements the stresses are extracted at integration point 3, 7, 11 and 15 for circular cross section beams and for z-stringers at integration point 1, 3, 5 and 7 as is illustrated in figure 6.23.

With the extraction of the stresses at these integration points for each mesh element a good approximation of the stress distribution in the mesh element cross section can be estimated. Besides the stresses also the mesh element numbers are extracted. The mesh element numbers are used to identify the element in which the stresses occur. The stresses are used in the failure criteria that are discussed in the next section about the post processing routine.

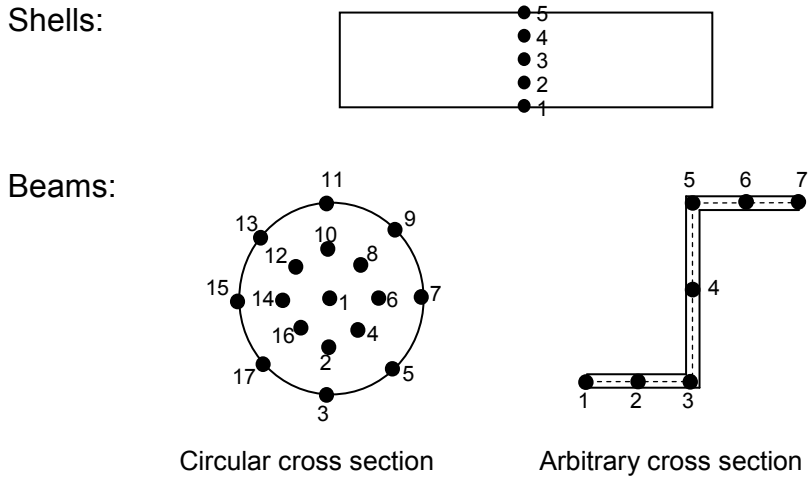

Figure 6.23: *Cross sectional integration points for the ABAQUS shell and beam elements*

Post processing routine

The Matlab post processing part of the structure module investigates whether or not the fuselage structure has sufficient strength and stiffness to carry the specified load case. The procedure of this post processing part can be considered to exist out of three steps. First the theoretical buckling stresses using the equations of chapter 5 and the maximum allowable tensile stresses (material property) are determined for reference for each type of element (skin, frame, stringer). Secondly, the maximum stresses from the stresses extracted from FEM analysis are determined for each element group. The third step determines whether or not the fuselage structure satisfies the buckling criteria and the tensile stresses do not exceed the maximum allowable material stresses. The considered failure criteria are:

skin buckling criteria:

$$R_{skb} = \frac{\sigma}{\sigma_{b\,skin}} + \frac{\tau}{\tau_{b\,skin}} < 1 \qquad (6.10)$$

stringer buckling criteria:

$$R_{strb} = \frac{\sigma}{\sigma_{Euler}} < 1 \qquad (6.11)$$

skin max tensile stress criteria:

$$R_{skt} = \frac{\sigma}{\sigma_{skt\,\max}} < 1 \qquad (6.12)$$

stringer max tensile stress criteria:

$$R_{strt} = \frac{\sigma}{\sigma_{strt\,\max}} < 1 \qquad (6.13)$$

Where σ and τ are the FEM stresses that occur in the elements, $\sigma_{b\ skin}$ and $\tau_{b\ skin}$ the theoretical buckling stresses and σ_{sktmax} and $\tau_{strtmax}$ the maximum allowable material stresses. The results of these four criteria are used in the optimisation process that will be explained in chapter 7.

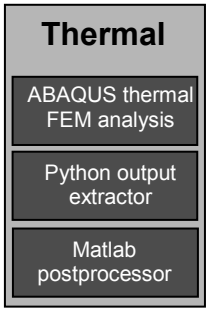

6.7 The thermal insulation module

The thermal insulation module determines the thermal insulation capacity of the fuselage wall. Like discussed in chapter 4 the thermal insulation of a fuselage wall can be characterised by the equilibrium that exists in time in the temperature difference between the inside and outside surface of the fuselage wall when the inside surface is heated with a constant heat flux.
In this section first the FEM model used for the thermal analysis is discussed followed by the description of the applied thermal load case. Finally the results extraction and the post processing routines are discussed.

Thermal model definition

Because of symmetry the FEM model that is used for thermal analysis only consists out of half a fuselage model including the fuselage structure, insulation blankets and interior panels. The fuselage skin, insulation blankets and interior panels are all modeled with 8 node solid brick elements.

The type of ABAQUS FEM analysis that is used is an uncoupled transient heat transfer analysis. Uncoupled because in this case there is no interest in the deformations caused by the temperature distributions. Transient analysis is selected because the temperature distribution in the fuselage wall has to reach equilibrium between the incident energy and the exiting energy over a period of time.

Load case definition

The thermal load case is defined as a constant heat flux incident on the inside surface of the fuselage wall as is illustrated in figure 6.24. The constant incident heat flux causes the inside surface of the fuselage to heat up. Because of conduction the rest of the material, which is in physical contact, will also heat up. Since the incident heat flux is constant, the thermal model will reach a semi steady state when the temperature difference between the inside and outside fuselage surface remains constant although the absolute temperature of the fuselage wall is continuously rising. The reached constant temperature difference is taken as the characteristic measure of the thermal insulation of the fuselage wall.

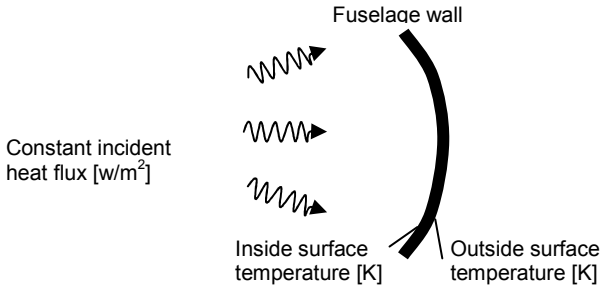

Figure 6.24: *Thermal load case definition*.

Result extraction

For a thermal heat transfer analysis the temperatures are determined as function of time at each integration point of the solid elements. To determine the characteristic

temperature difference only the temperatures on the inside and outside surface of the fuselage wall are of interest. Therefore the time dependent temperatures are extracted at predefined opposite points on the inside and outside surface of the fuselage wall.

Post processing routine

The Matlab post processing routine simply consists out of determining the average temperature on the fuselage wall inside surface and the average temperature at the outside surface for each time step. The difference between these two temperatures at the semi steady state gives the characteristic representation of the thermal insulation of the fuselage wall.

Figure 6.25 gives an example of the results of a thermal insulation analysis for a fuselage wall consisting out of a single aluminum skin. The temperature distribution in the FEM models is illustrated in figure 6.26. Figure 6.25a shows the absolute average temperatures and figure 6.25b shows the temperature gradient of the inside and outside surfaces. Finally figure 6.25c shows the temperature difference between the inside and outside surface. From these figures it can be seen that after a period of time the temperature difference remains constant. This temperature difference is taken as the characteristic measure of the thermal insulation of the fuselage wall, which is used in the optimisation procedure as will be explained in chapter 7.

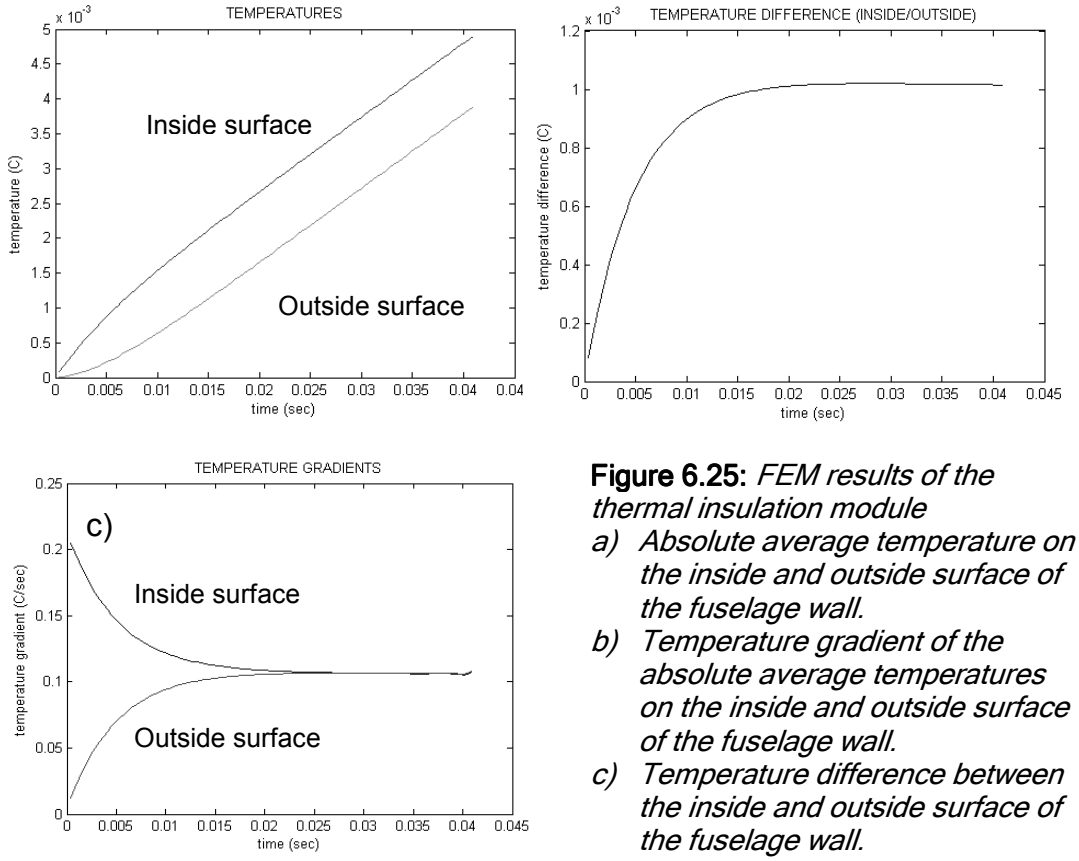

Figure 6.25: *FEM results of the thermal insulation module*

a) Absolute average temperature on the inside and outside surface of the fuselage wall.

b) Temperature gradient of the absolute average temperatures on the inside and outside surface of the fuselage wall.

c) Temperature difference between the inside and outside surface of the fuselage wall.

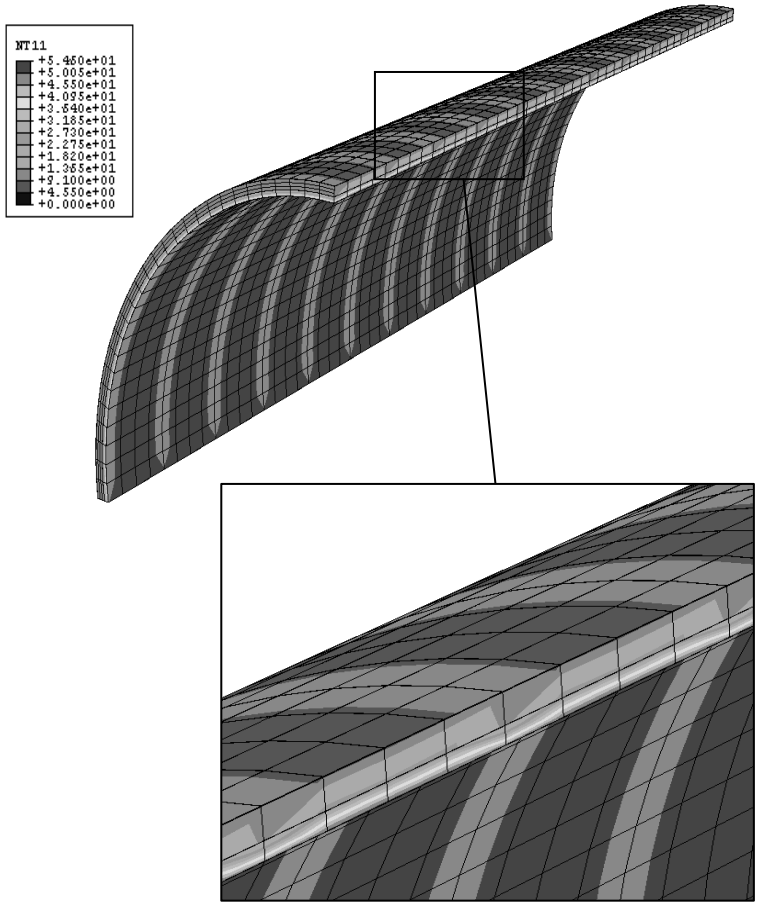

Figure 6.26: *Illustration of FEM results of the thermal insulation module corresponding to the results in figure 6.25. (See also colour section).*

For a simple fuselage wall, which only consists out of a single skin the temperature difference can also simply be determined from the conduction constants. However when the fuselage model includes insulation blankets, frames and interior panels the heat transfer analysis becomes more complex because in that case it is expected that the frames, which connect the interior panels to the fuselage skin, will act as heat transfer bridges.

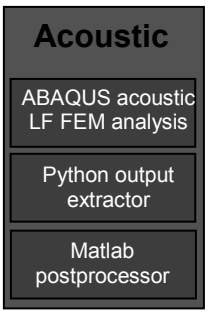

6.8 The acoustic insulation module

The acoustic module consists out of three sub modules. The first sub module determines the sound pressure levels for the low frequency range by performing an acoustic FEM analysis. The second sub module determines the sound transmission loss with a Matlab script file that is based on the literature formulas described in chapter 3. The third sub module determines the improvement of the sound transmission loss in the low frequency range when applying the active noise control concept. This analysis is performed with a FEM model and can only be performed on panel level. In the following three sections each of these sub modules will be discussed shortly.

6.8.1 Low frequency acoustic module

The low frequency acoustic module determines the sound pressure levels of the fuselage wall by means of an acoustic FEM analysis. This FEM analysis consists out of a coupled structural-acoustic eigenmode analysis. The determined natural frequencies are used in a frequency response analysis of the sound pressure levels inside the fuselage cabin, excited by an acoustic point load on the outside of the fuselage wall. Since the acoustic FEM analysis is very time consuming, it is more practical to use this module only for the analysis of the final solution and not for each iteration step with the DEE. The FEM package ABAQUS is used for this analysis.

This section is subdivided into four parts; first the acoustic FEM model and it s restrictions are discussed followed by the definition of the acoustic load case that is used for the acoustic FEM analysis. In the last two sections the result extraction and the post processing routines are discussed.

Acoustic model definition

In the acoustic FEM model the skin, insulation blankets, interior panels and the air inside the fuselage that are all modeled with solid brick elements. The air on the outside of the fuselage is not included in the acoustic FEM model. This means that the acoustic load will be applied directly on the fuselage skin. The frames are modeled with shell elements and the stringers and frame flanges are modeled with beam elements.

The air and insulation elements are different from the structural elements because they are not capable of carrying any stresses. To enable ABAQUS to perform a coupled structural-acoustic analysis these different elements have to be connected with each other with the ABAQUS specific '*TIE' definition.

For the frequency response analysis, the ABAQUS non-linear steady state dynamic analysis procedure is used to determine the frequency dependent pressure distribution of the air inside the fuselage. From this pressure distribution and the applied load the sound transmission loss of the fuselage wall is determined as will be discussed in the post processing routine section.

Because of computational limitations, the FEM analysis of the sound transmission loss is not suitable for the high frequency range. For high frequencies the model would require very small mesh elements resulting in heavy models (in memory size) and extremely long calculation times. As a rule of thump the element size has to be smaller than:

$$L_{\max} < \frac{c_s}{n_{\min}} \cdot f_{\max} \tag{6.14}$$

Here is L_{max} is the maximum element size, c_s the speed of sound in the considered material at ambient temperature, n_{min} the minimum amount of mesh elements and f_{max} the maximum frequency.

To be able to properly represent a sinus wave with linear mesh elements a minimum of at least 6 mesh elements is required; $n_{min} = 6$. This means that for a FEM analysis up to frequencies of 2000 Hz, the maximum mesh size of an aluminium skin would be $L_{max} = 420$ mm ($c_{s\_aluminium} = 5054$ m/s).

Load case definition

The steady state dynamic analysis is a mode-based analysis. This means that the steady state dynamic analysis has to be preceded with an natural frequency analysis. With the eigenmode analysis all natural frequencies of the frequency range of interest are determined. In reality the fuselage is loaded by a pressure distribution resulting from the turbulent boundary layer and the noise from the engines. The turbulent boundary layer noise covers the complete frequency spectrum. This means that all eigenmodes of the fuselage model in the considered frequency range will be of interest.

In this research the acoustic load case definition has been simplified to a simple point force excitation. To ensure that all eigenmodes are excited during the frequency sweep analysis, the point load is applied with an out of phase component.

Results extraction

During the steady state dynamic FEM analysis the acoustic pressure of the air is recorded at all mesh nodes and written to an output database. A Python routine selects the pressures at user specified positions, called the recording nodes, from the output database and writes them in an ASCII text file. This ASCII file serves as input file for the post processing routine

An example of a calculated pressure distribution of the air inside the fuselage for one time frame of the dynamic analysis is given in figure 6.27.

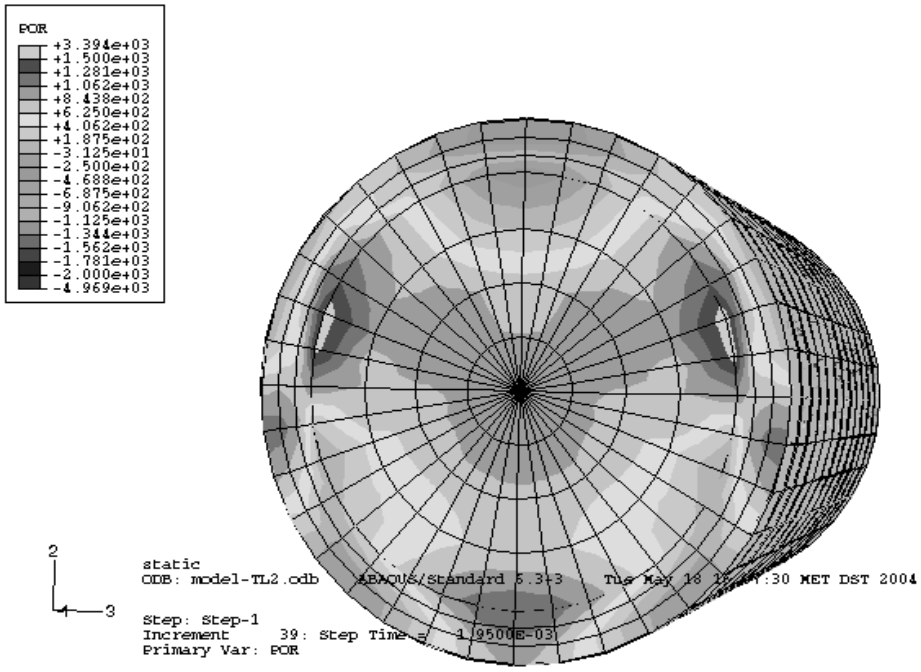

Figure 6.27: *Resultant pressure distribution at a time step of the acoustical FEM analysis in the low frequency range. (See also colour section).*

Post processing routine

The post processing routine determines the sound pressure level inside the fuselage. The sound pressure level inside the fuselage is determined by determining the average air pressure at each frequency increment. With a reference pressure p_{ref} = $2 \cdot 10^{-5}$ Pa the acoustic sound pressure level of the air inside is determined according:

$$L_p = 20 \log_{10} \left(\frac{p_{rms}}{p_{ref}} \right) \tag{6.15}$$

Here is p_{rms} the RMS pressure inside the fuselage.

For the optimisation as discussed in chapter 7 the sound transmission loss defined with equation 6.16 is used.

6.8.2 High frequency acoustic module

The MATLAB sound transmission loss module for the high frequency range makes use of the literature formulas explained in chapter 3. The Matlab sound transmission loss module requires two input data text files. These input text files are generated by the ICAD model generator.

The first input data file contains all geometry, choice parameters and non-frequency dependent material data. The second input data file contains all frequency dependent data like the frequency dependent material properties of insulation blankets.

The choice parameters are linked to the IF-THEN parameters in the ICAD input file and specify whether or not there are interior panels, insulation blankets, frames, stringers, sandwich skin or single skin, viscoelastic layers, etc within the fuselage model. With these choice parameters the Matlab script file can identify which TL formulas to use. Figure 6.28 shows a schematic overview of the formula selection procedure with a reference to the involved formula of chapter 3.

A brief explanation to figure 6.28: When the parameter *wall2?* is set to *'t'* then there is an interior panel. In that case the equations of wall1 and the equations of wall 2 are combined in equation 3.30 for a double wall. The parameter *visco?* determines the visco-elastic loss factor and the parameter *sand?* determines whether the wall is a sandwich wall or a single skin wall. The influence of frames and stringers is implemented by the parameter *stiffened?* that determines a ΔTL with respect to a reference stiffening case by equation 3.27. Insulation blankets are added by the parameter *blanket?* That determines a ΔTL by equation 3.38.
It should be noted, that the way the equations are interconnected, depends on the combination of the equations.

An example of a resultant TL as function of frequency for a single stiffened skin is given in figure 6.29.

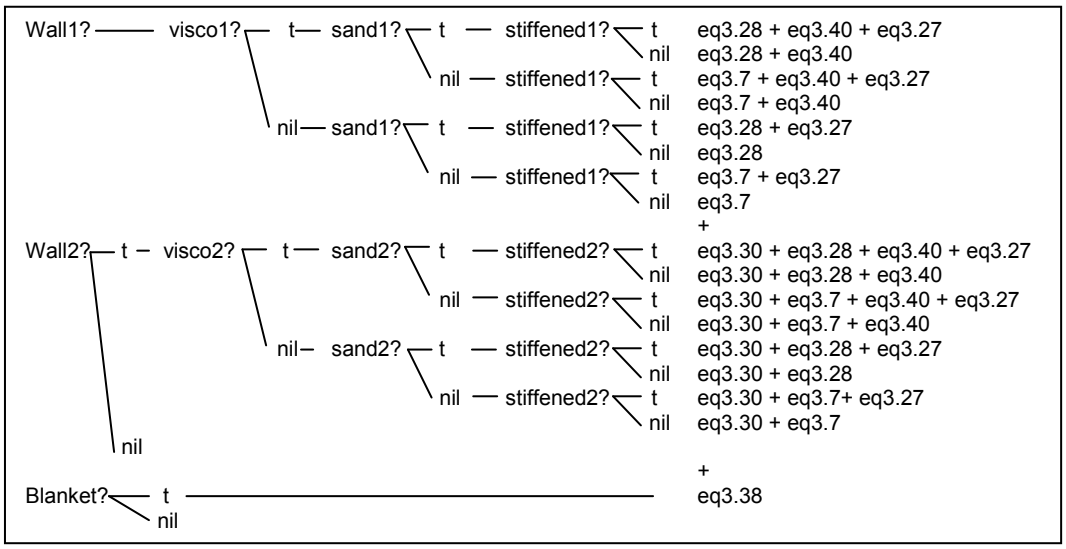

Figure 6.28: *Selection parameters that specify the literature formulas that are used to determine the TL.*

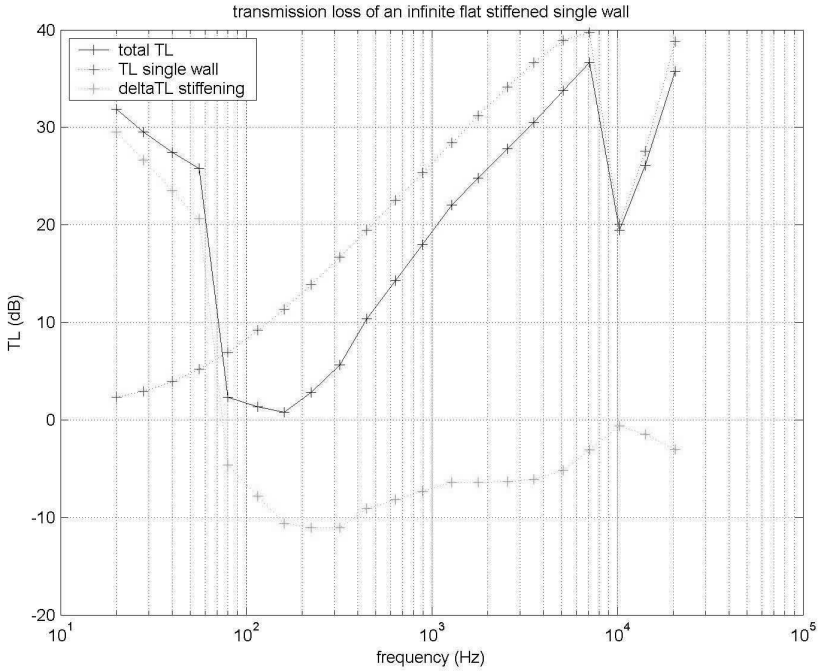

Figure 6.29: *Illustration of the TL determined with literature formulas. (See also colour section).*

It is difficult to evaluate the TL curves determined with the Matlab sound transmission module. Here it is chosen to determine the absolute overall TL at three different frequency ranges: [0 – 500 Hz], [500 – 5000Hz] and [5000 – 20000 Hz]. These three overall sound transmission loss numbers serve as input for the optimisation procedure. A good alternative can be found from the field of building acoustics. In this

field the TL usually is evaluated with one TL value that is defined as the overall TL corrected for human hearing (dBA) over the relevant frequency range of the noise source.

6.8.3 Active noise control module

For the active noise control analysis a different procedure is used. The goal of the FEM analysis for the active noise control concept is to determine four transfer matrices of a panel with multiple rectangular piezoelectric actuators. These transfer matrices serve as input to a sound transmission loss prediction algorithm developed by TNO TPD. The prediction algorithm then is able to determine the achievable sound transmission loss of the panel using active noise control.

The required four transfer matrices are:

1.) Three dimensional matrix *h_sec(Nh x Nsens x Nact)* that describes the transfer functions between actuator drive signals (voltage or current) and near field sensor signals (piezo charge or acceleration), with Nh the number of time samples of the responses, Nsens the number of sensors and Nact the number of actuators.
2.) Three dimensional matrix *h_sec_ff(Nh x Nsens_ff x Nact)* that describes the transfer functions between the actuator drive signals (voltage or current) and farfield sensor signals (sound pressure), with Nh the number of time samples of the responses, Nsens the number of sensors and Nact the number of actuators.
3.) Two dimensional matrix *h_prim(Nh x Nsens)* that describes the responses of the nearfield sensors (piezo charge or acceleration) due to the primary acoustical field, with Nh the number of time samples of the responses, Nsens the number of sensors.
4.) Two dimensional matrix *h_prim_ff(Nh x Nsens_ff)* that describes the responses of the farfield sensors (sound pressure) due to the primary acoustical field, with Nh the number of time samples of the responses, Nsens_ff the number of farfield sensors.

To determine these transfer matrices two different load cases are defined: The first load case is defined as an impulse electrical charge on one of the piezoelectric actuators. Then the electrical response from the remaining actuators and the vertical accelerations at chosen points on the panel are recorded. This procedure is repeated sequentially by defining the impulse electrical charge on the other actuators. With this load case the first two transfer matrices are determined. The second load case is defined as an impulse acoustic pressure wave traveling over the panel at a certain incident angle. Again the same electrical and vertical acceleration responses are recorded determining the last two transfer matrices.

A Fortran user routine collects the required responses and writes them in a data file. The post-processing of the transfer functions is performed with the TL algorithms of TNO TPD. Because the prediction algorithms are property of TNO TPD they are not discussed here.

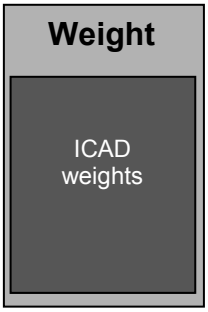

6.9 The weight module

The last module determines the weight of the considered fuselage section including, when required, the insulation blankets and interior panels. Since all the required data to determine the considered fuselage section weight is available within the ICAD environment this module is completely integrated in the ICAD program. The volume of the different parts is extracted from the geometry model that is defined in ICAD. The material densities are extracted from the material library, which also is defined within the ICAD environment. The weights of the different parts are determined with a simple multiplication of the volume with the corresponding material density. The results are listed in a weight data text file. The total weight is used in the optimisation routine as discussed in chapter 7.

6.10 Reference

[1] Emberey, C.L., Milton, N.R., Berends, J., Van Tooren, M., and Van Der Elst, S., Vermeulen, B., Application of knowledge engineering methodologies to support engineering design application development in aerospace, 7th AIAA Aviation Technology, Integration and Operations Conference (ATIO), AIAA-2007-7708, Belfast, Ireland, 2007.

[2] La Rocca, G., van Tooren, M.J.L., A knowledge based engineering approach to support automatic generation of FEM models in aircraft design, 45th AIAA Aerospace Sciences Meeting and Exhibit, AIAA-2007-0967, Reno, NV, USA, 2007.

[3] Schut, E.J., van Tooren, M.J.L., A knowledge based engineering approach to automation of conceptual design option selection, 45th AIAA Aerospace Sciences Meeting and Exhibit, AIAA-2007-0968, Reno, NV, USA, 2007.

[4] Nawijn, M., van Tooren, M.J.L., Arendsen, P., Berends, J.P.T.J., Automated finite element analysis in a knowledge based engineering environment, 44th AIAA Aerospace Sciences Meeting and Exhibit, Reno, Nevada, USA, 2006.

[5] La Rocca, G., and van Tooren, M.J.L., Development of design and engineering engines to support multidisciplinary design and analysis of aircraft, Delft Science in Design - A congress on Interdisciplinary Design, Faculty of Architecture, ISBN 90-5269-327-7, Delft, NL, 2005 .

[6] La Rocca G., Krakers L., van Tooren, M.J.L., Development of an ICAD Generative Model for Blended Wing Body Aircraft Design, Proceedings of the 9th AIAA/ISSMO Symposium on MDO, Atlanta, Georgia, USA, 2002.

[7] Krakers, L.A., M.J.L. van Tooren, M.J.L., Beukers, A., Bergsma, O.K., Multidisciplinary fuselage design: Integration of mechanics & acoustics, Sampe-JEC 2000 conference, Paris, France, 2000.

[8] Krakers, L.A., van Tooren, M.J.L., Beukers, A., A design engine to evaluate sound damping of flat panels in the low frequency range ECCM 10 conference, Brugge, Belgium, 2002.

[9] Krakers, L.A., van Tooren, M.J.L., Beukers, A., La Rocca, G., Lisandrin, P., A design & engineering engine to investigate acoustics in preliminary fuselage design, 9th AIAA/CEAS conference, Hilton Head Island USA, May 2003.

[10] Krakers, L.A., van Tooren, M.J.L., Zaal, K., Vermeeren, C.A.J.R., Integration of Acoustics and Mechanics in a stiffened shell Fuselage. Part III, Applied Composite Materials Vol. 12, p21-35, Springer 2005.

7 Optimisation procedure

7.1 Introduction

Optimisation is a very extensive field of research on which a lot of literature can be found. For example Swisher [1], Azadivar [2], Andradottir [3], Fu [4] and Carson [5] all present general summaries on simulation optimisation techniques. Swisher [1] described simulation optimisation as a technique that provides a structured approach to determine optimal input parameter values, where the optimum is measured by a function of output variables associated with a simulation model. According to Omran [6], simulation optimisation techniques can be divided into several groups, which will be discussed shortly:

- First of all there is the brute force method. This method determines all possible objective solutions and memorises the maximum or minimum solution. This is a very inefficient method because it requires quite some time.
- More efficient methods are path search based methods involving some kind of gradient estimation technique imbedded in a stochastic approximation (SA) algorithm. SA algorithms are used to find near optimal solutions. For the SA algorithms it is assumed that good solutions are close to each other. This is true for most real world problems, Lovberg [7]. Examples of SA algorithms are the Hooke and Jeeves method, Hooke [8], random methods and integral methods. More advanced methods are hill climbing, Michalewicz [9], simulated annealing, Laarhoven [10], and tabu search, Glover [11, 12]. These more advanced methods are described briefly.
  - For the hill climbing method, a potential solution is randomly chosen. The algorithm then searches the neighbourhood of the current solution for a better solution. If a better solution is found, then it is set as the new potential solution. This process is repeated until no more improvements can be made.

  - Simulated annealing is similar to hill climbing in the sense that a potential solution is randomly chosen. A small value is then added to the current solution to generate a new solution. If the new solution is better than the original one, then the solution moves to the new location. Other wise, the solution will move to the new location with a probability that decreases as the run progresses.
  - Tabu search is a heuristic search algorithm where a tabu list memory of previously visited solutions is maintained in order to improve the performance of the search process. The tabu list is used to guide the movement from one solution to the next one to avoid cycling, thus avoid being trapped in a local optimum. Tabu search starts with a randomly chosen current solution. A set of test solutions is generated through moves from the current solution. The best test solution is set as the next current solution if it is not in the tabu list. When the best test solution it is in the tabu list, but satisfies an aspiration criterion it will also be set as next current solution. A test solution satisfies an aspiration criterion when it is the best solution found so far. This process is repeated until a stopping criterion is satisfied.
- Evolutionary algorithms. Evolutionary algorithms (EAs) are general purpose stochastic search methods simulating natural selection and evolution in the biological world. EAs maintains a population of potential solutions to a problem and not just one solution, Engelbrecht [13]. Generally, EAs work as follows: a population of individuals is initialised where each individual represents a potential solution to the problem at hand. The quality of each solution is evaluated using a fitness function. A selection process is applied during each iteration of an EA in order to form a new population. The selection process is biased towards the fitter individuals to ensure that they will be part of the new population. Individuals are altered using transformation (mutation) and higher order transformation (crossover). This procedure is repeated until convergence is reached. The best solution found is expected to be a near optimum solution. There are four major evolutionary techniques:
  - Genetic programming (GP) Koza [14], which is used to find the fittest program to solve a specific problem.
  - Evolutionary programming (EP) Fogel [15], EP uses selection and mutation operators.
  - Evolutionary strategies (ES), Back et al. [16]. ES uses selection, crossover and mutation operators. ES optimises both the population and the optimisation process by evolving strategy parameters.
  - Genetic algorithms (GA) Goldberg [17], Holland [18], GA uses mutation and crossover.

Implementation of optimisation techniques within the DEE

As discussed in chapter 6 the DEE is able to automatically determine the performance with respect to several design requirements for specified sets of input parameters. The performance of a design with respect to the design requirements are evaluated with the design requirement evaluation parameters. In this research the considered design requirement evaluation parameters are:

- The structural design requirement parameters: Defined as the maximum actual stresses that occur in the skin and stringers divided respectively by the theoretical

maximum allowable skin and stringer tensile stress, skin and stringer buckling stress and the skin hoop stress.
- The thermal insulation design requirement parameter: Defined as the average temperature difference between the inside and outside surface of the fuselage wall when the inside surface is constantly heated by a heat source.
- The acoustic insulation design requirement: Defined as the overall sound transmission loss for the fuselage wall over three frequency ranges.

Because the DEE runs automatically, it is able to determine the design requirement evaluation parameters for many different sets of input parameters. By plotting the design requirement evaluation parameters as function of the design variables, response surfaces can be created. By applying an optimisation routine on the response surfaces the optimal set of design variables can be found. In this research is chosen to use the Genetic Algorithm method because it is very suitable for multi variable optimisation problems where the variable relations are defined in response surfaces. In this thesis, the genetic algorithm based Matlab program; 'L_GOPT' developed by Lanzi [19] is used for optimisation.

Note: The statistical analysis method ANOVA (Analysis Of Variance) Miller [20], Montgomery [21] is a widely spread tool for analysing experimental data from carefully designed experiments. The usual objective is to find out which factors contribute most or not at all. This method is a useful analysis method, what would be perfect for the considered optimisation cases. However this method was not familiar to the author at the time of research and therefore was not applied. In this research the correlation between the design variables are qualitatively evaluated. Future analysis using the developed DEE could well profit from the ANOVA analysis method.

In section 7.2 the working principle of Genetic Algorithms will be shortly explained. The position of the optimisation routine within the DEE is discussed in section 7.3. For illustration purposes, section 7.4 discusses the optimisation of a stiffened aluminium cylinder. This stiffened aluminium cylinder is the same cylinder as used for the experimental evaluation discussed in chapter 8. Finally section 7.5 gives some conclusions.

7.2 The optimisation process incorporated in the DEE

As discussed in the previous section it was decided to use the genetic algorithm method within the DEE. Figure 7.1 gives a short overview of the position of the optimisation process in the DEE. In this figure, the DEE is represented as a black box. As discussed in chapter 6 the DEE consists out of a parametric description of the fuselage and the evaluation tools for the weight, structural and thermal- and acoustic-insulation analyses. This means that the black box in figure 7.1 is capable to evaluate the design requirement parameters for the various design disciplines for a set of input parameters that define the fuselage configuration.

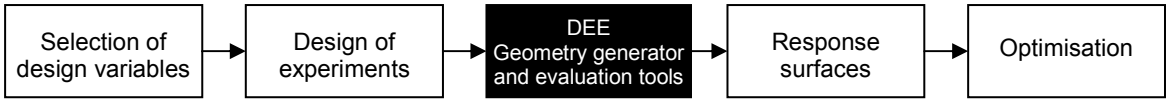

Figure 7.1: *Overview of the optimisation process using the DEE.*

In the following text, each box of the optimisation process shown in figure 7.1, except for the DEE, which was discussed in chapter 6, will be discussed somewhat more in detail:

Selection of design variables

To optimise the fuselage design the user has to decide which of the input parameters will be selected as design variables. Also the design space that marks the boundaries of the design variables, has to be defined by the user. Once the design variables are chosen, the optimisation process will start with a design of experiments

Design of Experiments DOE

The DOE is in fact nothing more than the creation of a set of smartly chosen sample points, where each sample point represents a set of values for the selected design variables. The definition of sample points can be captured in Latin hypercubes. Tang [22] defines a Latin hypercube as an m x n size matrix where each row m represents a sample point and where each sample point is a set of values for n selected design variables. The sample points are chosen in such a way, that they cover the complete design space in the most efficient way, meaning with the least amount of sample points.

In this research the DOE is performed using the L_GOPT program developed by Lanzi [19]. The MaxMin criterion is used to select the sample points. The MaxMin criterion searches to maximise the minimum distance between any pair of the sample points.

Response surfaces

The DEE evaluates the design requirement parameters for each sample point for the weight, structural, thermal insulation and acoustical insulation disciplines. These evaluations are used to build response surfaces on which the actual optimisation will be performed. In order to find the correct optimum design, an accurate description of the response surfaces is required. The G_OPT program uses 4 types of Radial Basis Function (RBF) approximations to determine the response surfaces (linear, cubical, thin plate spline and Gaussian). The program selects automatically the RBF approximation that has the best fit. The best fit is determined using 5 error estimators.

Response surface error estimators

To evaluate the quality of the response surfaces, 5 error estimators are determined by using some sample points as verification points. The error can be determined by comparing the exact value for the verification point with the response surface value.

The five error estimators are:

1.) The absolute maximum error (indicated as MAX), which is the maximum error when all verification points are compared with the response surface.

2.) The absolute mean error (indicated as MEAN), which is the mean error when all verification points are compared with the response surface.

3.) The third error estimator is called R square error (R_{sqr}) and indicates the overall accuracy of the response surfaces. The R square error is computed for M verification points as:

$$R^2 = 1 - \frac{\sum_{i=1}^{m} \left(F(\vec{x}_i) - f(\vec{x}_i)\right)^2}{\sum_{i=1}^{m} \left(F(\vec{x}_i) - \overline{F}\right)^2} \tag{7.1}$$

Where:

$$\overline{F} = \frac{1}{m} \sum_{i=1}^{m} F(x_i)$$

$F(x_i)$ is the exact value of the i^{th} verification point, $f(x_i)$ is the corresponding value obtained by the response surfaces and F denotes the mean value of the whole set of m verification points.

4.) The fourth error estimator is a global measure of the Average Percentage Error (APE) and is defined as:

$$APE = \frac{\sum_{i=1}^{m} \left(\left| F(\vec{x}_i) - f(\vec{x}_i) \right| \right)}{\sum_{i=1}^{m} \left| F(\vec{x}_i) \right|} \cdot 100\% \tag{7.2}$$

5.) Since an overall accuracy does not necessarily mean a good local accuracy, the fifth index is related to the maximum local errors. To determine the maximum local error the Relative Maximum Absolute Error (RMAE) is computed as:

$$RMAE = \frac{\max_{i=1,\ldots,m} \left(\left| F(\vec{x}_i) - f(\vec{x}_i) \right| \right)}{\sqrt{\frac{1}{2} \sum_{i=1}^{m} \left(F(\vec{x}_i) - \overline{F} \right)^2}} \tag{7.3}$$

Once the response surfaces for objective and constraint functions have been defined with satisfying accuracy, the actual optimisation procedure can be started.

Optimisation

For the optimisation the Genetic Algorithm (GA) routine is used. With this routine, the response surfaces are used to maximise or minimise a selected objective with taking into account several constraints. The GA routine can also be used for the maximisation or minimisation of multi objectives. This will result in a Pareto set of solutions where the objective functions are plotted against each other. Another

optimisation option is the Sequential Programming (SQP) routine. With this option the user will have to select a valid starting point from which the solution will travel in sequential steps to the optimum solution of a single objective. This routine is only suitable for real variables. Integer or discrete variables have to be fixed to a chosen value. All three optimisation routines are illustrated in the next section that gives the optimisation example of a stiffened aluminium cylinder.

7.3 Optimisation example of a stiffened aluminium cylinder

To illustrate the optimisation process and the usage of the DEE, a stiffened aluminium test cylinder will be optimised for minimum weight. (This cylinder is the same cylinder as is used in the experiments discussed in chapter 8). The main objective is to determine the lightest stiffened aluminium cylinder under the constraint of several strength and stiffness criteria. Secondary objectives are to maximise the thermal and acoustic insulation of the cylinder wall. This means that the structural, thermal and the acoustic modules of the DEE will be used. It should be noted, that for the aluminium stiffened cylinder no additional insulation materials are added. Therefore the thermal and acoustic insulation will be very small. Nevertheless this example will illustrate how the optimisation process works.

7.3.1 Definition of the aluminium test cylinder

The aluminium stiffened test cylinder, which will be subject of chapter 8, has a length L_{cil} = 970 mm and a radius R = 250 mm and consists out of an aluminium skin with aluminium C-frames of a fixed size and aluminium z-stringers with a fixed shape. The frames and stringers are illustrated in figure 7.2 and are attached to the cylinder skin at their connection nodes.

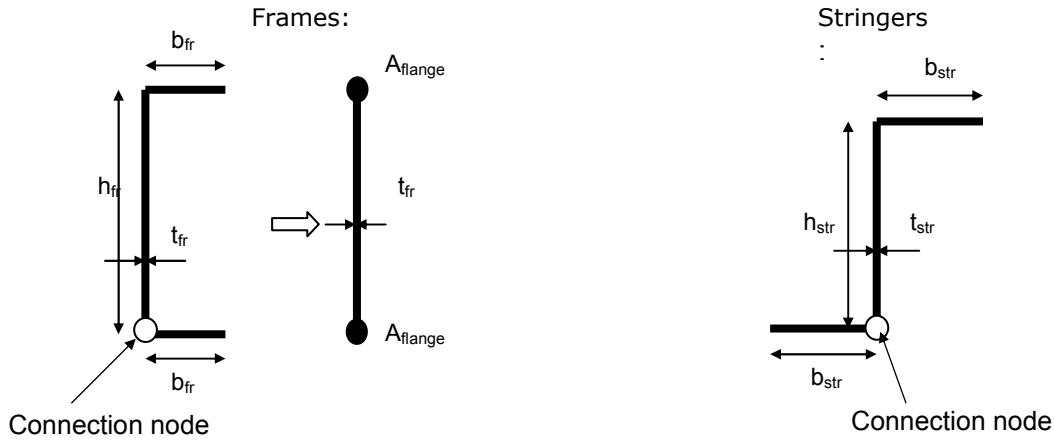

Figure 7.2: *Geometry of the frames and stringers of the aluminium cylinder.*

The strength and stiffness criteria are evaluated with the structural analysis module of the DEE. In this case the structural module consists out of a static FEM analysis that determines the stress levels in the different elements of the stiffened

cylinder for a specified load case. For this analysis a FEM model is required. Within the FEM model the skin and the frame webs are represented by 4-node shell elements and the stringers and frame flanges by beam elements. The beams of the frame flanges have circular cross sections as is illustrated in figure 7.2. The stringers are represented by beam elements of which the cross section has the properties of the actual thin walled Z-shape stringer cross-section, which is illustrated in figure 7.2. The Basic dimensions and material properties are given in table 7.1.

Table 7.1: *Basic dimensions and material properties of the aluminium stiffened cylinder*

Basic dimensions			
Radius (R)	0.25 m	Stringer height (h_{str})	20 mm
Cylinder length (L_{cil})	0.97 m	Stringer width (b_{str})	15 mm
Skin thickness (t_{sk})	1 mm	Stringer thickness (t_{str})	1 mm
Frame height (h_{fr})	40 mm	Nr of stringers ref (n)	10
Frame width (b_{fr})	20 mm	Nr of frames ref (m)	1
Frame thickness (t_{fr})	1.2 mm		
Material properties of the aluminium skin, frames and stringers			
Modulus of elasticity	68.9 GPa	Allowable skin tensile stress	210 MPa
Density	2710 kg/m^3	Allowable stringer tensile stress	200 MPa
Poisson ratio	0.3	Allowable hoop stress	85 MPa
Thermal conductivity	140 W/mK		
Specific heat	900 J/kgK		
Load case			
Internal pressure (p)	55000 N/m^2	Applied heat flux	100 W/m^2
Bending moment (M)	4000 Nm		
Shear load (Q)	600 N		

The load case applied on the aluminium test cylinder is similar as discussed in chapter 5 for the stiffened skin and sandwich fuselage (See figure 5.1) except for the magnitude, and consists out of an internal pressure p = 55000 N/m^2, a bending moment M = 4000 Nm and a shear load Q = 600 N

The cylinder is optimised for minimum weight with the requirement that it has to fulfil the strength and stiffness criteria. The strength criterion is simply defined by the restriction that the tensile stresses have to be smaller than the maximum allowable material stresses and the Hoop stress. The stiffness criteria's are represented by restriction that the compressive stresses have to be lower than the stringer (Euler) and skin buckling stresses. The maximum allowable material stresses are given as material properties in table 7.1. The Euler and skin buckling stresses are determined using the buckling formulas for flat skins. These equations are explained in chapter 5. The radius of the cylinder is not taken into account in the buckling formulas. This will give a conservative solution.

7.3.2 Choosing the design variables

In this section the design variables are chosen. The parameters that are most important for the strength and stiffness criteria are the parameters that determine the dimension of the cylinder cross section. For Euler buckling also the frame pitch is of importance. Therefore the following four design variables are chosen:

1.) The cylinder skin thickness: t_{sk}
2.) The number of frames: n_{fr}

3.) The number of stringers: n_{str}
4.) The stringer factor k_{str}

The stringer factor k_{str} indicates the multiplication factor of the cross sectional area of the stringers. The new cross section of the stringer A_{str}^* is defined by:

$$A_{str}^* = k_{str} A_{str} = \left(h_{str}\sqrt{k_{str}} + 2b_{str}\sqrt{k_{str}}\right) t_{str}\sqrt{k_{str}} \tag{7.4}$$

Where A_{str} is a cross secttion area of the reference stringer illustrated in figure 7.2.

7.3.3 Objective functions

The weight of the aluminium test cylinder is chosen as the primary objection function. To illustrate the dependence of the cylinder weight on the chosen design variables the weight function is given below:

$$W_{cil} = 2\pi R L_{cil} t_{sk} \rho_{sk} + n_{fr} 2\pi R A_{fr} \rho_{fr} + n_{str} L_{cil} A_{str}^* \rho_{str} \tag{7.5}$$

Secondary objection functions are the thermal and acoustic insulation. The thermal insulation is represented by the temperature difference (θ) between the inside and outside surface of the cylinder aluminium skin and the acoustic insulation is represented by the overall sound transmission loss (OTL).

7.3.4 Constraints

The strength and stiffness criteria are translated into the following five constraints:

1.) Stress has to be smaller than the maximum skin material tensile stress:

$$R_{skt} = \sigma/\sigma_{skt\ max} < 1 \tag{7.6}$$

2.) Stress has to be smaller than the maximum stringer material tensile stress:

$$R_{strt} = \sigma/\sigma_{strt\ max} < 1 \tag{7.7}$$

3.) Stress has to be smaller than the maximum Hoop stress:

$$R_{Hoop} = \sigma/\sigma_{Hoop\ max} < 1 \tag{7.8}$$

4.) Stress has to be smaller than the maximum stringer buckling stress:

$$R_{strb} = \sigma/\sigma_{Euler} < 1 \tag{7.9}$$

5.) Stress has to be smaller than the maximum combined buckling shear/compressive stress of the skin:

$$R_{skb} = \tau \cdot \sigma_{skb} + \sigma \cdot \tau_{skb} < 1. \tag{7.10}$$

Where σ_{skb} and τ_{skb} are the buckling stresses of the cylinder and σ and τ are the compressive stress and the shear stress respectively that occur in the cylinder skin.

7.3.5 Setting up the design space

For the stiffened aluminium cylinder the following boundaries of the design space are chosen around the basic dimensions that are given in table 7.1. This resulted in the design space as mentioned in table 7.2.

Table 7.2: *Definition of the design space*

Design variable	Min value	Max value
Cylinder skin thickness (t_{sk})	0.5 mm	1.5 mm
Number of frames (n_{fr})	0	4
Number of stringers (n_{str})	6	16
Stringer size factor (k_{str})	0.5	1.2

7.3.6 Design of experiments

The Latincube 'MaxMin' criterion is used to generate a set of sample points The DEE is run 60 times to generate the function values for the strength and stiffness constraints and the objective function values for the cylinder weight, the thermal and acoustic insulation. The results are given in table G.1.1 of Appendix G.

7.3.7 Response surfaces

The response surfaces for R_{skt}, R_{strt}, R_{hoop}, R_{strb}, R_{skb}, Weight, θ and OTL are given in appendix G.2. As a first conclusion, it can be noted from these response surfaces that for this case within the chosen design space, R_{skt}, R_{strt} and R_{Hoop} are not critical. The response surfaces for the more critical constraints like the Euler and skin buckling, and the objective functions; minimum weight and maximum thermal and acoustical insulation are shortly discussed below:

Euler buckling

The response surface for stringer Euler buckling is illustrated in figure G.2.1 of appendix G. The response surface for R_{strb} has a relatively large maximum error of 58.5%. This error can be reduced by adding more sample points. To reduce this error a second optimisation step can be performed on a part of the design space, which lies close around the first estimated optimum solution of minimum cylinder weight. This smaller design space will have a higher sample point density and therefore the response surface for stringer Euler buckling will become more accurate. The large maximum error can also be explained by the fact that the value for R_{strb} is very small for a large range of the design variables; n_{str} and n_{fr} as is illustrated in figure G.2.1C. In this area the maximum error of the response surface easily becomes large when comparing the response surface with the actual sample point values.

It is assumed that the response surface is accurate enough in the area that is critical for the optimisation (The response surface area where R_{strb} is close to 1). The first optimisation step to minimise the cylinder weight while satisfying the structural constraints will prove that this assumption is justified when determining a first estimate of the minimum cylinder weight.

The resultant response surfaces illustrated in figure G.2.1 show that the R_{strb} is only slightly dependent on the skin thickness. The frame and stringer pitch and the stringer cross section area are more important parameters for the stringer buckling criteria. This corresponds with the Euler buckling theory.

Skin Buckling

When all sample points are considered to determine the response surfaces for the skin buckling criterion also a large error is found. This large error in creating the response surface, is caused by sample points that result in very large values for R_{skb}. By excluding data points for which $R_{skb} > 4$ the maximum response surface error decreases to 15.5%. The exclusion of data points can be justified because the design space for which R_{skb} is larger than 4 will not be of interest for the optimisation.
Figure G.2.2 illustrates the response surfaces for R_{skb}. It can be seen that R_{skb} decreases with increasing skin thickness and decreasing stringer pitch. For skin buckling, the number of frames and the stringer size are not of significance.

Cylinder weight

Figure G.2.6 illustrates the response surface for the cylinder weight. Because the weight is a straightforward function of the design parameters, this response surface is relatively accurate.

Thermal insulation

The resultant response surfaces for the thermal insulation are illustrated in figure G.2.7. Because the FEM model for the heat transfer analysis does not take any stringers into account the response surfaces as function of the number of stringers and the stringer factor are of no physical meaning. Also the number of frames is not of real importance because the heat transmission is only applied on the cylinder skin. However thermal leakage will occur untill a steady state is reached (i.e. constant θ is reached).

Acoustical insulation

The response surfaces for the overall sound transmission loss are shown in figure G.2.8. It is noticed that the maximum error in creating these response surfaces is relatively small (A maximum error of 2% is found). It can be seen from figure G.2.8 that the overall sound transmission loss has only a small dependency on the design parameters in the considered design space. It can be noted that an increase of the skin thickness (Mass Law) and a decreasing of the 'Number of stringers' and a decreasing 'Number of frames' has a positive influence on the overall sound transmission loss. The dependency on the stringer factor is fictive because the stringer factor is not taken into account in the sound transmission loss analysis.

7.3.8 Optimisation: Genetic Algorithms

Once the response surfaces have been determined, a Genetic Algorithm can be used to determine the minimum cylinder weight while taking the five structural constraints into account. The G_OPT program is used to perform the optimisation. Table 7.3 gives the solutions for minimum cylinder weight with different program settings.

The minimum cylinder weight varies between 4.39 and 4.55 Kg. To validate the solutions, the solutions are re-evaluated with the DEE. These results are presented in table 7.4.

Table 7.3: *Four optimised solutions for minimum cylinder weight determined with the genetic algorithm (GA) option of the G_OPT program using four different program settings.*

		Solution 1	Solution 2	Solution 3	Solution 4
G_opt program settings					
Number of members for each generation		100	100	100	100
Number of generations		200	500	200	500
Cross-over probability		0.75	0.75	0.85	0.85
Mutation probability		0.15	0.15	0.15	0.15
Design variables					
t_{sk}	[mm]	0.7235	0.7941	0.7196	0.7353
n_{fr}	[-]	0	0	0	0
n_{str}	[-]	16	14	16	16
k_{str}	[-]	0.7278	0.6839	0.6757	0.6565
Final performances:					
R_{skb}	[-]	0.9535	0.9986	0.9755	0.9144
R_{skt}	[-]	0.1409	0.1351	0.1436	0.1417
R_{strb}	[-]	0.7143	0.9670	0.8501	0.9127
R_{strt}	[-]	0.0986	0.1028	0.0980	0.0965
R_{Hoop}	[-]	0.3704	0.3472	0.3758	0.3696
W_{cil}	[kg]	**4.51**	**4.55**	**4.39**	**4.42**
θ	[K]	2.62e-4	2.86e-4	2.58e-4	2.62e-4
OTL	[dB]	28.88	28.93	28.88	28.88

Table 7.4: *Re-evaluation of the four solutions found with the GA optimisation for minimum cylinder weight given in table 7.3.*

Sol. nr	t_{sk}	n_{fr}	n_{str}	k_{str}	R_{skb}	R_{skt}	R_{strb}	R_{strt}	R_{Hoop}	W_{cil}	θ	OTL
1	0.7235	0	16	0.7278	0.8933	0.1376	0.7296	0.1108	0.3561	**4.4805**	2.61e-4	28.77
2	0.7941	0	14	0.6839	0.9625	0.1346	0.9867	0.1097	0.3407	**4.5131**	2.87e-4	29.04
3	0.7196	0	16	0.6757	0.9290	0.1407	0.8517	0.1137	0.3618	**4.3590**	2.60e-4	28.75
4	0.7353	0	16	0.6565	0.8847	0.1393	0.9112	0.1129	0.3567	**4.3856**	2.66e-4	28.83

By comparing the objective function and constraint values of table 7.4 with table 7.3 it can be seen that they correspond reasonably well. Maximum deviations occur of around 5%. To find a more accurate optimum solution a second optimisation step will be necessary. For the second optimisation step a new design space is chosen close around the optimum solutions of table 7.4. Since all solutions have zero frames the design variable 'Number of frames' was set to zero for the second optimisation step meaning that only three design variables are left.

Table 7.5: *Accuracies of the response surfaces for the zoomed in design space*

Validation criteria error	R_{skb}	R_{skt}	R_{strb}	R_{strt}	R_{Hoop}	θ	OTL	W_{cil}
MaxMin	1.2144	0.8481	0.9515	0.5959	0.5301	0.7157	0.2889	0.1298
MEAN	0.5149	0.4924	0.6515	0.3261	0.2946	0.4859	0.1302	0.0543
Rsqr	0.9993	0.9961	0.9994	0.9978	0.9993	0.9976	0.9494	0.9998
RMEA	0.0480	0.0978	0.0425	0.0830	0.0438	0.0690	0.4002	0.0245
APE	0.6258	0.4922	0.6858	0.3316	0.2891	0.4751	0.1303	0.0560

To determine the new response surfaces a new design of experiments is performed to determine 40 new sample points. The sample points and the DEE evaluations are given in table G.1.2 of appendix G. The error estimators of these response surfaces are given in table 7.5. It is noticed that these response surface are much more accurate.

Again the Genetic Algorithm of the G_OPT program is used to determine the minimum cylinder weight. The results are given in table 7.6 and the re-evaluations with the DEE are given in table 7.7.

Table 7.6: *Four optimised solutions of the second optimisation step for minimum cylinder weight determined with the genetic algorithm (GA) option of the G_OPT program using four different program settings.*

		Solution 1	Solution 2	Solution 3	Solution 4
G_opt program settings					
Number of members for each generation		100	100	100	100
Number of generations		200	500	200	500
Cross-over probability		0.75	0.75	0.85	0.85
Mutation probability		0.15	0.15	0.15	0.15
Design variables					
t_{sk}	[mm]	0.7076	0.7049	0.7063	0.7063
n_{fr}	[-]	0	0	0	0
n_{str}	[-]	16	16	16	16
k_{str}	[-]	0.6333	0.6392	0.6333	0.6294
Final performances:					
R_{skb}	[-]	0.9924	0.9998	0.9976	0.9997
R_{skt}	[-]	0.1440	0.1440	0.1442	0.1444
R_{strb}	[-]	0.9822	0.9613	0.9818	0.9955
R_{strt}	[-]	0.1159	0.1158	0.1162	0.1162
R_{Hoop}	[-]	0.3693	0.3700	0.3699	0.3703
W_{cil}	[kg]	**4.22**	**4.22**	**4.22**	**4.21**
θ	[K]	2.55e-4	2.54e-4	2.55e-4	2.55e-4
OTL	[dB]	28.74	28.72	28.73	28.73

Table 7.7: *Re-evaluation of the four solutions found with the GA optimisation for minimum structural fuselage section weight given in table 7.6.*

Sol. nr	t_{sk}	n_{fr}	n_{str}	k_{str}	R_{skb}	R_{skt}	R_{strb}	R_{strt}	R_{Hoop}	W_{cil}	θ	OTL
1	0.7076	0	16	0.6333	0.9922	0.1447	0.9779	0.1172	0.3705	4.2235	2.55e-4	28.69
2	0.7049	0	16	0.6392	0.9995	0.1447	0.9698	0.1171	0.3711	4.2242	2.54e-4	29.67
3	0.7063	0	16	0.6333	0.9972	0.1449	0.9775	0.1174	0.3711	4.2181	2.55e-4	28.68
4	0.7063	0	16	0.6294	0.9990	0.1450	0.9915	0.1174	0.3713	4.2102	2.55e-4	28.68

From table 7.6 and 7.7 can be concluded that the minimum weight of the aluminium cylinder under the defined load case and satisfying the five structural constraints is 4.21 kg. It is also noted that the re-evaluations are very close to the solutions defined by the response surfaces.

7.3.9 Optimisation: Sequential Quadratic Programming

Another possibility to find the cylinder with minimum weight is the use of the Sequential Quadratic Programming technique. The SQP option of the G_OPT program can only handle real variables. Therefore the integer variables n_{str} and n_{fr} have to be preset. These variables are chosen equal to the previous optimisation solution; n_{str} = 16 and n_{fr} = 0. Furthermore a starting point has to be chosen for the k_{str} and t_{sk}. Table 7.8 shows three SQP optimisations with different starting points.

Table 7.8: *Three SQP optimisations with different starting points.*

		Solution 1	Solution 2	Solution 3
G_OPT program settings				
Tol on design variable		1e-5	1e-5	1e-5
Tol on objective function		1e-5	1e-5	1e-5
Max number of iterations		25	25	25
Fixed design variables				
n_{fr}	[-]	0	0	0
n_{str}	[-]	16	16	16
Start design variables				
t_{sk}	[mm]	0.9	0.8	0.71
k_{str}	[-]	0.75	0.7	0.65
Optimised design variables				
t_{sk}	[mm]	0.7843	0.7489	0.7051
k_{str}	[-]	0.6343	0.6318	0.6376
Final performances				
R_{skb}	[-]	0.7505	0.8524	1.0000
R_{strb}	[-]	1.0000	1.0000	0.9666
θ	[K]	2.83e-4	2.71e-4	2.54e-4
OTL	[dB]	29.00	28.89	28.73
W_{cil}	[kg]	4.54	4.39	4.22

It can be concluded that for the three starting points different solutions are found. Apparently, the skin and stringer Euler buckling constraints reach the boundary (R_{strb} = 1) before the global optimum is found. Only when the starting point is chosen close to the global optimum the correct optimum is found. This example illustrates that the Genetic Algorithm optimization is more robust than the SQP optimization.

7.3.10 Optimisation: Multi objective genetic algorithm

Genetic algorithms can also be used for multi objective optimisations. In that case, a Pareto set of solutions, which shows the relations between the objective functions, is generated for which the objective functions are optimal. For the aluminium cylinder two multi objective optimisations are performed; one for minimum W_{cil} with respect to maximum OTL and one for minimum W_{cil} and maximum θ. The results are presented in figure 7.4 and 7.5. The first 20 solutions of the corresponding Pareto set are given in table G.3.1 and G.3.2 of appendix G.

The multi objective optimisations give a trade off between the objective functions. Figure 7.4 shows the weight penalty for improved sound transmission loss and figure 7.5 shows the weight penalty for improved thermal insulation. The gaps in these figures represent a jump in the number of frames and/or stringers.

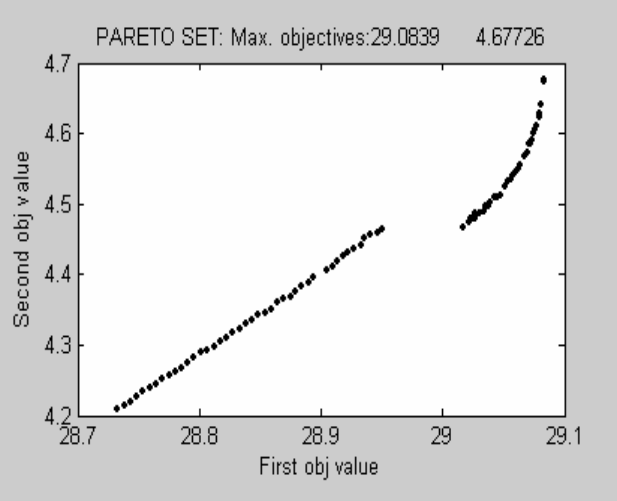

Figure 7.4: *Pareto set of solutions for minimum cylinder weight (2nd objective) and maximum overall sound transmission loss (1st objective). The corresponding design variables of the first 20 points are given in table G.3.1 of appendix G.*

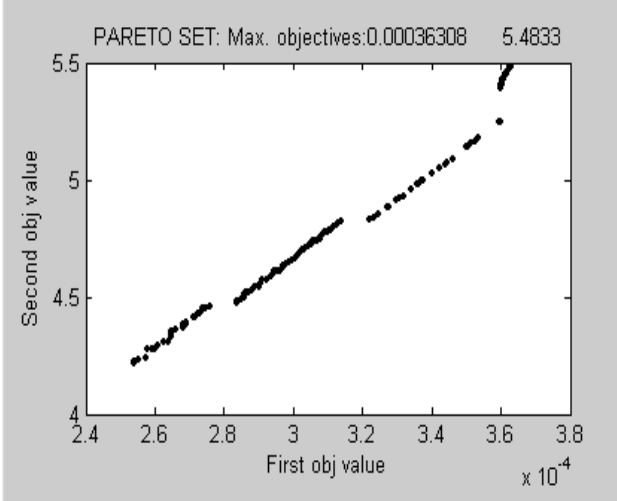

Figure 7.5: *Pareto set of solutions for minimum cylinder weight (2nd objective) and maximum thermal insulation (1st objective). The corresponding design variables of the first 20 points are given in table G.3.2 of appendix G.*

7.4 Discussion

To evaluate the results of the optimisation example discussed in section 7.3 a comparison is made to an analytical determined solution of the stiffened cylinder. The dimensions, material properties and load case definition for the analytical solution are chosen as close as possible to the aluminium cylinder analysed in section 7.3 and are given in table 7.9.

Table 7.9: *Material properties, dimensions and load case definition that are used to determine an analytical solution for the aluminium test cylinder with hat stringers.*

Fuselage dimensions:

R [mm]	L_f [m]	A_{fr} [mm^2]
252.5	0.975	96

Design load case:

M [Nm]	Q [N]	p [N/m^2]
4000	600	55000

Design stresses and material properties:

	σ_{hoop} [Mpa]	σ_{max} [Mpa]	E [Gpa]	ν	ρ [kg/m^3]	k_τ	k_σ
skin	85	200	70	0.3	2700	5.35	4
frames/stringers		210	70	0.3	2700		

The cross section area of the frames for the analytical analysis is chosen identical to the frames used in the DEE analysis. It should be noted that the analytical tool

described in section 5.1 was programmed for stringers with a hat cross section with identical height and width (h_{str} = b_{str}), instead of the Z shaped stringers that where used in the optimisation analysis with the DEE. Nevertheless a comparison can be made to evaluate the DEE and optimisation tools. When the minimum weight of the cylinder is determined with the analytical tool a weight of 2.28 kg is found. The corresponding dimensions are shown as solution 1 in table 7.10.

Table 7.10: *Three analytical results with different starting points.*

		Solution1	Solution 2	Solution 3
t_{sk}	[mm]	0.17	0.71	0.87
h_{str}	[mm]	17.43	20.56	21.98
t_{str}	[mm]	0.21	0.20	0,19
b_{sk}	[mm]	31	93	95.8
n_{fr}	[-]	0	0	0
n_{str}	[-]	51	17	16
W_{cil}	[kg]	2.28	3.62	4.21

It can be noticed that the skin thickness for solution 1 in table 7.10 is the minimum skin thickness determined by the maximum Hoop stress (t_{sk} = 0.17 mm). The skin thickness determined with the DEE was according to table 7.7: t_{sk} = 0.71 mm, which means that higher stresses occur in the model used in the DEE. A reason for this can be found in the boundary condition that was applied to the FEM model used in the DEE. For the FEM model the cylinder edges were clamped. This introduces stress concentrations near the cylinder edges.

Because the analytical solution has such a thin skin thickness, a high number of stringers are required. The fames, which are identical in both cases, have a weight of 0.45 kg. This weight is so large that it is not worth to add a frame to reduce the length of the stringers the stringer Euler buckling stress the required number of stringers.

When it is assumed that the stress in the skin is of equal amplitude as for the DEE analysis the skin thickness should also be equal. Solution 2 in table 7.10 gives the analytical results in case the skin thickness is fixed to 0.71 mm. This results in a cylinder weight of 3.62 kg with 0 frames and 17 stringers. It can be seen that n_{fr} and n_{str} lie much closer to the solution found with the DEE given in table 7.7. The difference in weight can be explained by the different type of stringers that were used. The hat shaped stringers are connected to the skin at two ‘points’ while the z-stringers only connected at one point as is illustrated in figure 7.6. This means that the width between two stringers (b_{sk}) is smaller for hat-stringers than for z-stringers, which results in higher allowable skin buckling stresses.

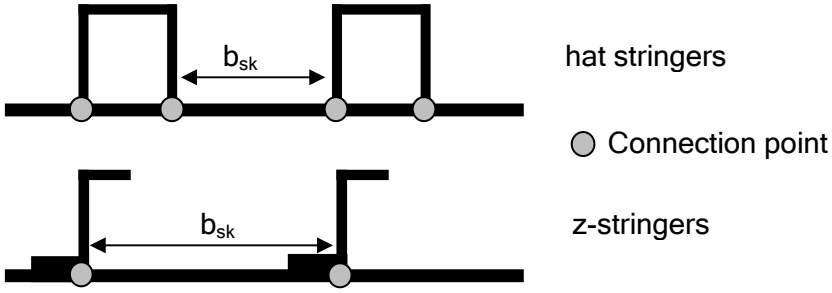

Figure 7.6: *Difference between hat and Z stringer shape*

Solution 3 in table 7.10 gives the optimum result when the skin thickness is chosen such that the cylinder weight is identical to the optimum cylinder weight that was found with the DEE in table 7.7. It is seen that in this case the number of stringers is identical to the number of stringers found with the DEE.

In conclusion it can be said that the DEE and the genetic optimisation tool work properly. Attention should be paid to the boundary conditions that are applied to the FEM models for structural analysis within the DEE. When stress concentrations occur, the DEE will result in heavier solutions. To some extend this will give conservative solutions. One can avoid that the solution will be determined by stress concentrations, by excluding the FEM elements, in which the stress concentrations occur, from the evaluation area. The evaluation area consists out of all FEM elements for which the highest stresses are searched that are used to determine the stress criteria R_{skb}, R_{skt}, R_{strb} and R_{strt}.

Furthermore it can be concluded that the genetic algorithm optimisation is a robust optimisation tool that is very suitable for optimisation with a DEE. A two step optimisation proved successful for the stiffened aluminium cylinder example. The first optimisation step will give a first estimate of the optimum solution. From this result, a new smaller design space can be defined around the estimated solution. Then a second optimisation step is performed on the new design space. The two step optimisation process requires less sample points to achieve more accurate response surfaces near the optimum solution.

7.5 References

[1] Swisher JR, Jacobson SH, Hyden PD, Schruben LW, “A survey of simulation optimisation techniques and procedures”, Proceedings of the 2000 Winter Simulation Conference, pp 119-128.

[2] Azadivar F., Simulation optimisation methodologies. Proceedings of the 1999 Winter Simulation Conference, 93-100.

[3] Andradottir S, “A review of simulation optimisation techniques”, Proceedings of the 1998 Winter Simulation Conference, 151-158.

[4] Fu M., “Optimization via simulation: a review” Anneals of Operations Research 53, 1994, pp199-247.

[5] Carson Y, Maria A, “Simulation optimisation: methods and applications”, Proceedings of the 1997 Winter simulation Conference, 118-126.

[6] Omran MGH, “Particle swarm optimisation for pattern recognition and image processing” Phd thesis, University of Pretoria, 2005

[7] Lovberg M., Krink T., “Extending Particle Swarm Optimisers with Self-Organized Criticality”, Proceedings of the IEEE Congress on Evolutionary Computation, volume 2, p1588-1593, 2002.

[8] Hooke R, Jeeves TA., ”Direct search solution of numerical and statistical problems”, Journal Assoc. Comp. Mach; 1961:8 (2), pp 221-9.

[9] Michalewicz Z, Fogel DB, “How to solve it: Modern Heuristics, Springer-Verlag, Berlin 2000

[10] Laarhoven, PJM, Aarts EHL, “Simulated Annealing: theory and applications”, Wiley, New York 1987

[11] Glover F., “Tabu search Part I”, ORSA Journal on computing, 1 (3), 190-206, 1989.
[12] Glover F., “Tabu-search Part II”, ORSA Journal on Computing, 2, 4-32, 1990
[13] Engelbrecht, A.P., “Computational Intelligence, an introduction”, Chichester, John Wiley, 2002
[14] Koza J.R., “Genetic programming”, MIT Press, 1992
[15] Fogel L.J., Owens A., Walsh M.J., “Artificial Intelligence Through Simulated Evolution”, John Wiley & Sons, Inc., New York, 1966.
[16] Back T., Hofmeister, F., Schefel, H.P., “A survey of evolution strategies”, In Proceedings of fourth International Conference on Genetic Algorithms, p2-10, 1991
[17] Goldberg, D.E., Deb, K., “A Comparative Analysis of Selection Schemes Used in Genetic Algorithms”, Urbana, 1991
[18] Holland J.H., “Adaptation in natural artificial systems”, University of Michigan Press, Ann Arbor, 1975.
[19] Lanzi, L., “Optimisation of composite stiffened panels under post buckling constraints”, PhD thesis, Polytecnico di Milano, 2004
[20] Montgomery, D.C., “Design and Analysis of Experiments”, JohnWiley & Sons, New York, 3rd edition, 1991.
[21] Miller R.G., Jr., “Beyond ANOVA” ,Chapman and Hall, London, 1997
[22] Tang, B., “Selecting latin hypercubes using correlation criteria”, Statistica Sinica, Vol 8, pp 965-977, 1998.

8 Experimental verification of an aluminium test cylinder

8.1 Introduction

In this research it is tried to make a multidisciplinary fuselage design, which incorporates mechanical and acoustic & thermal insulation aspects. Since many aircraft have a stiffened skin structural fuselage concept there is a special interest in the influence of frame and stringer pitches on the sound transmission loss of a fuselage wall. Therefore experiments are performed to validate the sound transmission loss theory of stiffened skins, which was discussed in section 3.4.

In the ideal case the sound transmission loss measurements would be performed in a reverberation noise sending room and an anechoic noise receiving room as is illustrated in figure 8.1. In such a case the sound transmission loss can be determined according to the ISO standard 15186-1 [1]:

$$TL = L_{p\,send} - 6 - L_{I\,recieved} - 10\log_{10}\left(\frac{S_m}{S}\right) \tag{8.1}$$

In this equation $L_{p\,send}$ is the sound pressure level in the sending room (in dB, p_{ref} = $2{\cdot}10^{-5}$ Pa), measured with a microphone on a rotating boom, $L_{I\,recieved}$ the sound intensity level (in dB, I_{ref} = $1{\cdot}10^{-12}$ W/m^2), normal to, and averaged over the measuring surface S_m, and S the area of the test specimen (i.e. the part radiating sound to the receiving room). Often S and S_m are chosen equal and of order 1 m^2.

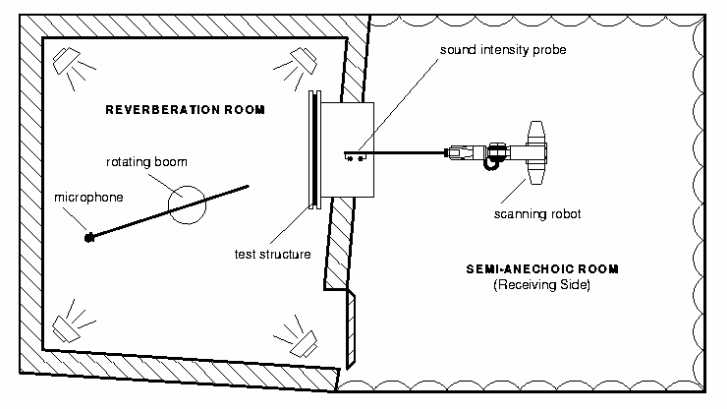

Figure 8.1: *Ideal testing facility for sound transmission loss measurements [2]*

For the measurements in this research no ideal testing facility was available. Therefore the tests have been performed on complete test cylinders, (not on a part of the cylinder wall, as would be the case in an ideal testing facility), that were positioned inside a single rectangular room with dimensions; width 4m, height 3m and a length of 10m. The test cylinder is excited by noise produced from sound speakers and the sound pressure levels were measured inside and outside the test cylinder. With this test set-up it is not possible to measure the correct sound transmission loss because of influences of sound reflection on the test cylinders on the outside microphone and the influence of absorption inside the test cylinder on the inside microphone. This means that for the sound measurements discussed in this chapter only the sound pressure level difference between the inside and outside of the test cylinder could be determined.

The sound pressure differences have been determined for four different test cylinders. First, a non-stiffened cylinder is considered as a reference case. Then two stringer stiffened cylinders are tested; one with six and one with twelve stringers. (The stringers are equally spaced in circumferential direction). Finally, two frames are added to the cylinder stiffened with twelve stringers.

The remaining of this chapter has the following structure: Section 8.2 discusses the experimental test set-up. In section 8.3, the characteristic frequencies are determined of the test cylinders that will help to interpret the sound pressure level measurements discussed in section 8.4. Section 8.5 presents some concluding remarks. A numerical modal analysis of the four test cylinders will be discussed in chapter 9.

8.2 Experimental test set-up

This section discusses the test equipment, the calibration of the microphones and the used noise signal.

Test equipment

The experimental set-up is shown in figure 8.2. The noise is generated with two (*Stage Accompany*) speakers. A pink noise sound signal is played with a standard windows program. This signal is amplified with a two-channel high efficiency power amplifier (*Stage Accompany SA800*). The two ¼ inch diameter condenser microphones from *Bruel & Kjaer* are connected to a matching *Bruel & Kjaer* microphone power supply. The signals from the microphones are processed with a 4-channel analyser (*Difa D-TAC 100 version 3.31A*).

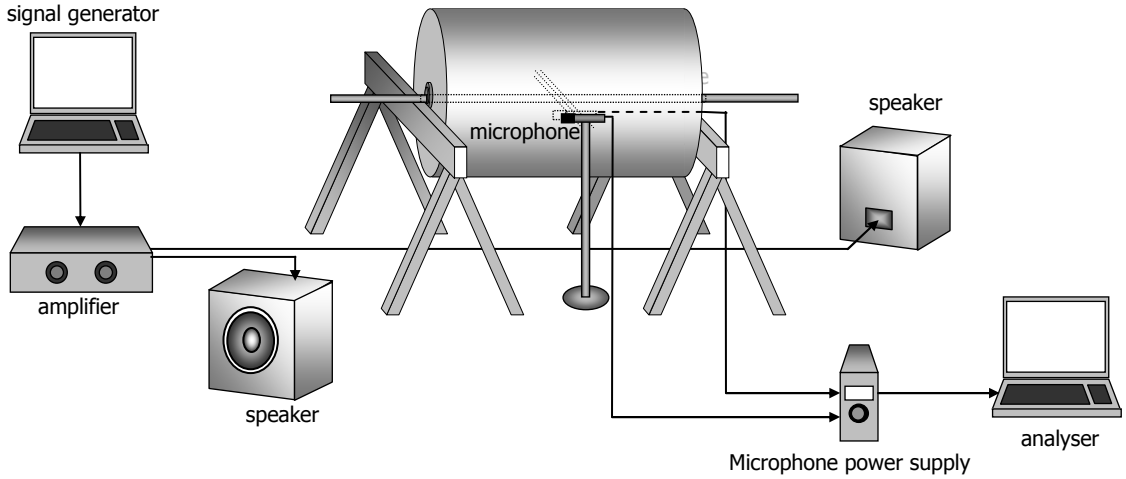

Figure 8.2: *Experimental set-up.*

The design of the aluminium test cylinder is based on the aluminium cylinder tested by NASA, Wilby [3]. There are a few differences with the NASA test cylinder:

- Because of manufacturing limitations the length of the cylinder is 1 meter, which is 20 cm shorter than the NASA test cylinder.
- Because of material availability the cylinder skin thickness is chosen 1 mm instead of the 1.63 mm thickness of the NASA test cylinder.

The complete dimensions and material properties are given in table 8.1. Figure 8.3 shows a drawing of the aluminium test cylinder.

The aluminium skin is made from one single sheet resulting in one lengthwise seem. This lengthwise seem is bonded and riveted with an aluminium overlap strip with a width of 50 mm and a thickness of 1 mm. The adhesive ensures an airtight connection. The end caps of the cylinder have to be heavy to ensure that the noise measured inside the cylinder is transmitted through the skin and not through the end caps. The end caps are made to have a perfect fit with the cylinder skin. The cylinder skin is clamped to the end caps with a steel strap. To ensure air tightness, the two connections between the cylinder skin and the end caps are sealed with silicone kit.

Table 8.1: *Dimensions and material properties of the test cylinder*

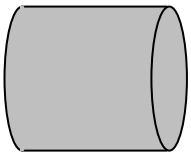

Cylinder

Diameter	0.505 m
Length	1.000 m
Thickness	0.001 m
Material: aluminium	E = 6.89e10 N/m^2, ν = 0.3, ρ =2710 kg/m^3

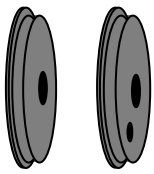

End cap

Diameter	0.505 m (diameter outside lip: 0.515m)
Thickness	0.015 m (including thickness outside lip: 0.005m)
Material: steel	E = 2.00e11 N/m^2, ν = 0.3, ρ = 7900 kg/m^3
Diameter hole for end cap support	0.055 m
Diameter hole microphone wire	0.025 m (positioned 0.1 m form center end cap)

End cap support

Inner diameter	0.025 m
Outer diameter outside rings	0.055 m
Outer diameter middle ring	0.105 m
Thickness outside rings	0.015 m
Thickness middle ring	0.025 m
Material: aluminium	E = 6.89e10 N/m^2, ν = 0.3, ρ =2710 kg/m^3

Support pole

Diameter	0.025 m
Length	2.5 m
Material: steel	E = 2.00e11 N/m^2, ν = 0.3, ρ = 7900 kg/m^3

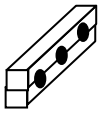

Microphone support

(Two length wise symmetric parts clamping the pole)

Length x width x height	0.03 x 0.03 x 0.48 m (one half)
Microphone support holes at r/R	0.2, 0.53, 0.87
Material:	trovidure

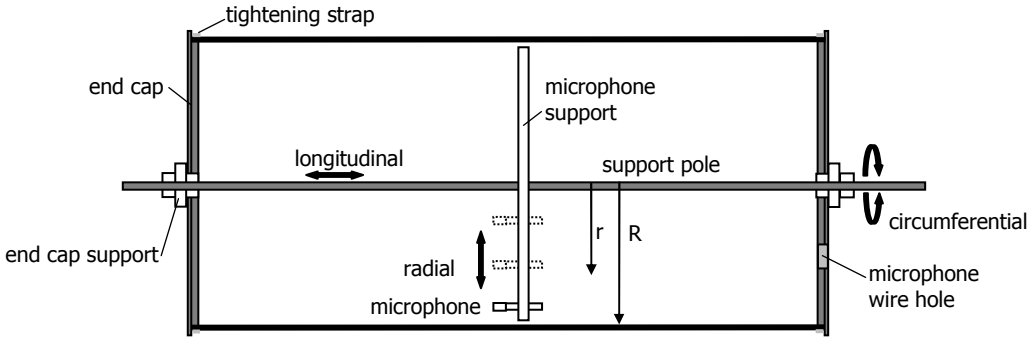

Figure 8.3: *Details of the non-stiffened test cylinder.*

A simple check using the mass law for flat panels showed that the steel end caps with a thickness of 15 mm are sufficient to guarantee that the sound pressure difference through the end caps is at least 10 dB less than the sound pressure difference through the skin for all frequencies as is recommended in ASTM E90 [4]. One of the end caps has a hole for the wire to connect the inside microphone. This hole is closed with clay during the measurements. The end caps are positioned with two identical aluminium end cap supports. The function of the end cap supports is to

be able to place the cylinder on two wooden abutments and still have the possibility to freely move the steel support pole in longitudinal and circumferential direction. The free movement of the steel support pole is necessary to be able to freely position the inside microphone between the front and end cap. The steel support pole has a length of 2.5m. The inside microphone is fixed to the steel support pole with a 'trovidure' support that has three fixed radial microphone positions at r/R = 0.20, 0.53 and 0.87. Because only one microphone was available to place inside the cylinder, the cylinder had to be opened and closed each time when the radial position of the microphone had to be changed. The outside microphone is positioned on a microphone standard.

Calibration of the microphones

Condenser microphones measure voltage levels. To determine the sound pressure levels in decibels, the microphones have to be calibrated. This is done with a calibrator (*Bruel & Kjaer*) that generates a pure tone at 996 Hz of 94 dB. By measuring the voltage level at this pure tone the calibration factor for each microphone is determined to express the measured voltages in decibels.

The noise signal

A well-known noise signal is white noise. White noise is noise that contains every frequency within the human hearing range in equal amounts. Most people perceive white noise as noise that contains relatively more high-frequency noise, which in fact is not the case. This perception occurs because each successive octave has twice as many frequencies as the one preceding it.

Pink noise is a variant of white noise. Pink noise is white noise that has been filtered to reduce the volume at each octave. This is done to compensate for the increase in the number of frequencies per octave. Each octave is reduced by 6 decibels, resulting in a noise sound wave that has equal energy at every octave.

NASA [3] used pink noise as the incident noise signal for their sound transmission loss tests. For comparability reasons pink noise is also used during these measurements. The pink noise signal is extracted from an internet source [5]. This pink noise is acquired by sampling a high quality analogous noise generator (Wandel & Gottermann). Some characteristic values of the noise signal are given in table 8.2.

Table 8.2: *Characteristics of the pink noise signal [5].*

Sampling rate:	19.98 kHz
A/D:	16 bit
Pre-filter:	anti-liasing filter
Pre-emphasis:	none
Filter:	none
Duration:	235 seconds

A representation of the first 3 seconds of this pink noise signal and its power spectrum are illustrated in figure 8.4 and 8.5. The power spectrum represents the frequency content of the pink noise signal in the range from DC to the Nyquist frequency.

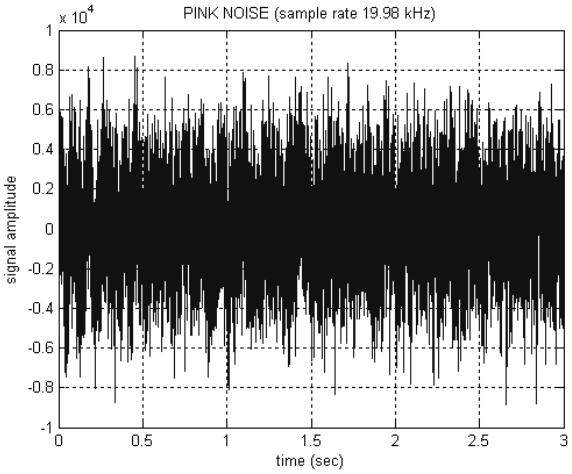

Figure 8.4: *First 3 seconds of the Pink noise signal [3] (Sampling frequency 19.98 kHz).*

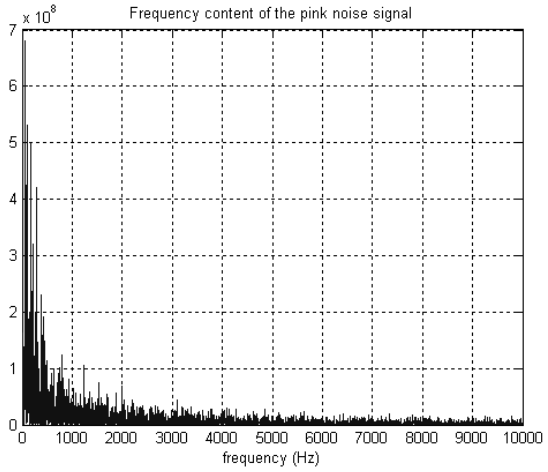

Figure 8.5: *Frequency content of the pink noise signal [3] shown in figure 8.4.*

Signal processing

The sound pressure level measurements are performed with a sampling frequency of 12.8 kHz and a bandwidth of 6125 Hz. One measurement consists out of the average of ten measurements of 1.28 seconds. The *Difa D-TAC* analyser determines the FFT signal of the sound pressure level using a Hanning filter with overlap. For the sound pressure graphs presented in this chapter, a linear frequency averaging is carried out with an averaging frequency of 125Hz.

8.3 Analytical determination of characteristic frequencies

To understand the measurements of the inside and outside sound pressure levels first some characteristic frequencies are determined:

Ring frequency

The ring frequency is given by equation 8.3. The ring frequency is independent of the amount of stiffeners.

$$f_{ring} = \frac{1}{2\pi R}\sqrt{\frac{E_{sk}}{\rho_{sk}\left(1-\nu_{sk}^{\ 2}\right)}} \tag{8.2}$$

Here, R is the radius of the cylinder, E_{sk} the modulus of elasticity of the cylinder material, ν_{sk} the Poisson ratio and ρ_{sk} the material density. For the aluminium test cylinders the ring frequency is 3332 Hz.

Coincidence frequency

The coincidence frequency is given by equation 8.3. Also the coincidence frequency is independent of the amount of stiffeners

$$f_c = \frac{c_s^2}{2\pi}\sqrt{\frac{12(1-\nu_{sk})\rho_{sk}}{E_{sk}t_{sk}^2}} \tag{8.3}$$

Here, c_s is the speed of sound in air and t_{sk} the thickness of the cylinder wall. The coincidence frequency of the aluminium test cylinder is 12058 Hz, which is well above the measured frequency range.

Structural and acoustic natural frequencies

The structural natural frequencies were discussed in section 3.2.3.1 and the acoustic duct modes were discussed in section 3.2.3.2. The superposition of the structural natural frequencies for the non-stiffened simply supported test cylinder on the air cavity modes for radial mode number p = 1 and p = 2, are shown in figure 8.6A and 8.6B respectively. Because, for the experiments the boundary conditions appear to be a combination of simply supported and clamped conditions, also the superposition for a clamped non-stiffened cylinder are shown in figure 8.7A and 8.7B.

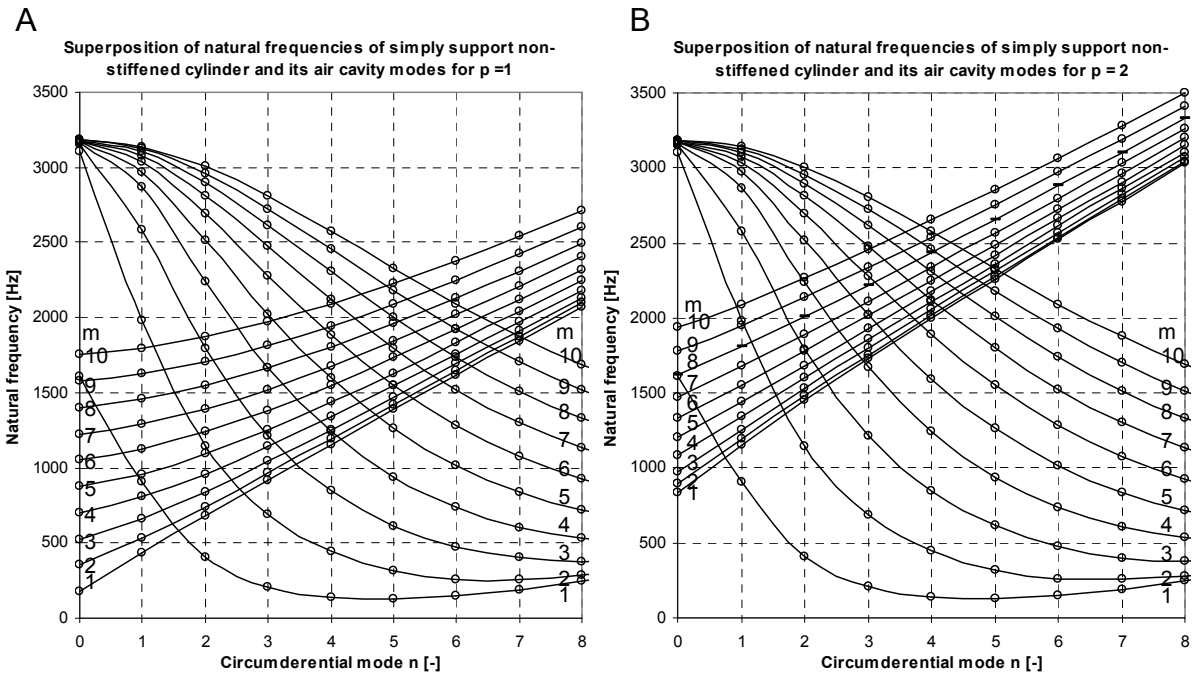

Figure 8.6: *Superposition of acoustic modes with; A) radial mode p = 1 and B) radial mode p = 2, on the structural modes of a simply supported unstiffened cylinder. Only modes with identical circumferential and identical longitudinal wave numbers will give strong resonance.*

When it is assumed that the addition of frames and stringers will introduce simply supported boundary conditions at the frame and stringer positions, the natural frequencies of the stiffened cylinders can be extracted from the natural frequencies of the non-stiffened simply supported and clamped cylinders. An overview of the non-stiffened natural mode numbers relevant for the stiffened cylinders is given in table 8.3.

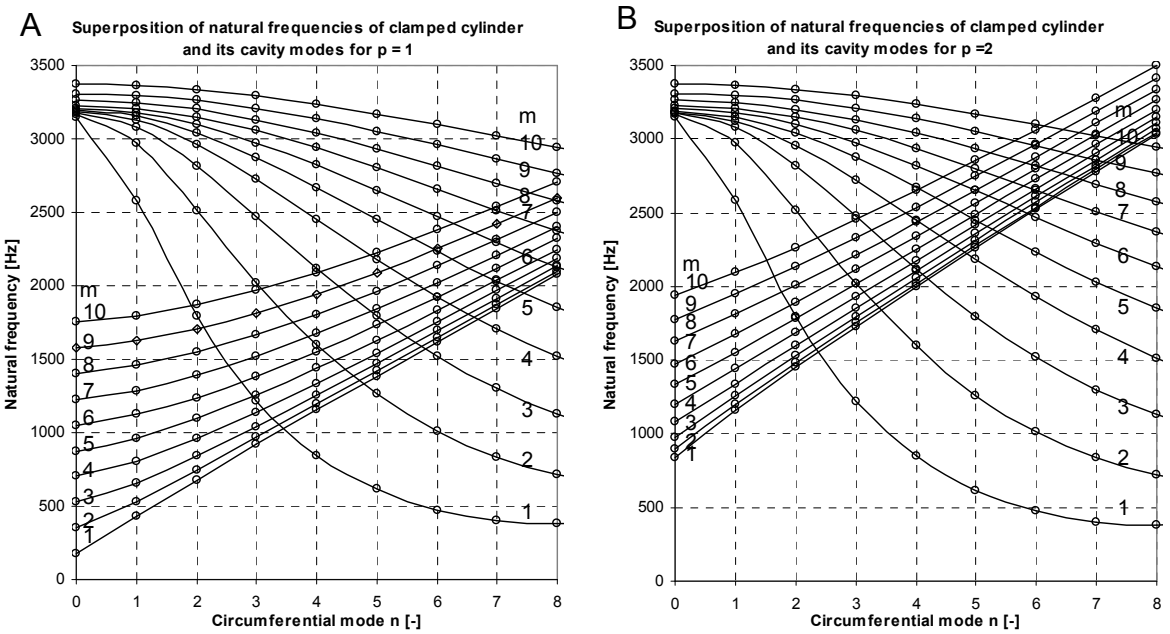

Figure 8.7: *Superposition of acoustic modes with; A) radial mode p = 1 and B) radial mode p = 2; on the structural modes of a clamped unstiffened cylinder. Only modes with identical circumferential and identical longitudinal wave numbers will give strong resonance.*

Table 8.3: *Non stiffened cylinder mode numbers from figure 8.6 important for stiffened cylinders*

Cylinder with 6 stringers								
m	1	2	3	4	5	6	7	8
n	0	6	12	18	24			
Cylinder with 12 stringers								
m	1	2	3	4	5	6	7	8
n	0	12	24					
Cylinder with 12 str and 2 fr								
m	1	3	5	7	9			
n	0	12	24					

Coupled structural and acoustical natural frequencies

To find out which eigenmodes are of importance for the ΔL_p measurements of thin walled cylinders it has to be checked which structural and acoustical eigenmodes couple. An approximate method is to check, which structural and acoustical eigenmodes with identical longitudinal and identical circumferential mode numbers are (almost) coincident with one another. These modes can easily be found by superpositioning the plot of the structural and acoustic natural frequencies like is shown in figure 8.6 and 8.7.

Table 8.4 shows some coupled eigenmodes that are found from figure 8.6A and B for the non-stiffened simply supported aluminium test cylinder.

Table 8.4: *Coupled eigenmodes that can be of interest for the ΔL_p measurements of a non-stiffened simply supported aluminium test cylinder. The modes are extracted from figure 8.6A/B.*

Circumferential mode n	Longitudinal mode m	Radial mode p	Frequency (Hz)
5	7	1	1795
5	8	1	2004
3	5	2	2020
4	8	2	2304
4	9	2	2452

Table 8.5 shows the coupled eigenmodes that are found from figure 8.7A and B for the non-stiffened clamped aluminium test cylinder.

Table 8.5: *Coupled eigenmodes that can be of interest for the ΔL_p measurements of a non-stiffened clamped aluminium test cylinder. The modes are extracted from figure 8.7A and B.*

Circumferential mode n	Longitudinal mode m	Radial mode p	Frequency (Hz)
7	5	1	2031
8	7	1	2369
4	3	2	2118
5	5	2	2450
6	9	2	2958

Sub panel natural frequencies

The sub panels are the parts of the fuselage skin surrounded by two adjacent stringers and two adjacent frames. The natural frequency of flat plates with dimensions stringer pitch b and frame pitch L_{fr} can be determined with equation

$$f_{pq} = \frac{1}{2\pi}\left(\frac{D}{m}\right)^{1/2}\left[\left(\frac{p\pi}{b}\right)^2 + \left(\frac{q\pi}{L_{fr}}\right)^2\right] \qquad (8.4)$$

Some sub panel natural frequencies for the stiffened test cylinders are given in table 8.6.

Table 8.6: *Some sub panel natural frequencies of the different stiffened test cylinders with frame pitch L_{fr} and stringer pitch b.*

Cylinder with 6 stringers	p	q	f_{pq} [Hz]	p	q	f_{fq} [Hz]
L_{fr} = 970mm	1	1	37	2	1	140
b = 264mm	1	2	44	2	2	147
	1	3	57	2	3	160
	1	4	75	2	4	178
Cylinder with 12 stringers	p	q	f_{pq} [Hz]	p	q	f_{fq} [Hz]
L_{fr} = 970mm	1	1	140	2	1	551
b = 132 mm	1	2	147	2	2	559
	1	3	160	2	3	571
	1	4	178	2	4	589
Cylinder with 12 str + 2 fr	p	q	f_{pq} [Hz]	p	q	f_{fq} [Hz]
L_{fr} = 323 mm	1	1	160	2	1	571
b = 132 mm	1	2	229	2	2	640
	1	3	343	2	3	755
	1	4	504	2	4	915

For comparison: Characteristic frequencies of a typical real size fuselage

The material properties and dimensions of the considered real size fuselage are given in table 8.7. The corresponding ring frequency and coincidence frequency are given in table 8.8 together with the sub-panel natural frequencies.

Table 8.7*: Basic dimensions of the considered fuselage*

Radius (R)	1.98 m	E_{sk}	70e9 N/m^2
Frame pitch (L_{fr})	0.5 m	ρ_{sk}	2700 kg/m^3
Stringer pitch (b)	80 mm	ν_{sk}	0.3
Skin thickness (t_{sk})	1.28 mm		

Table 8.8: *Ring and coincidence frequency together with the sub panel natural frequencies of the considered fuselage*

f_{ring}	429 Hz						
f_c	9329 Hz						
Sub panel frequencies [Hz]	p	q	f_{pq} [Hz]		p	q	f_{fq}
L_{fr} = 500mm	1	1	114	2	1	123	
b = 80mm	1	2	449	2	2	458	
	1	3	1007	2	3	1015	

The fuselage structural natural frequencies superpositioned on the air cavity natural frequencies for radial mode p = 1 and p = 2, are given in figure 8.8A and B respectively.

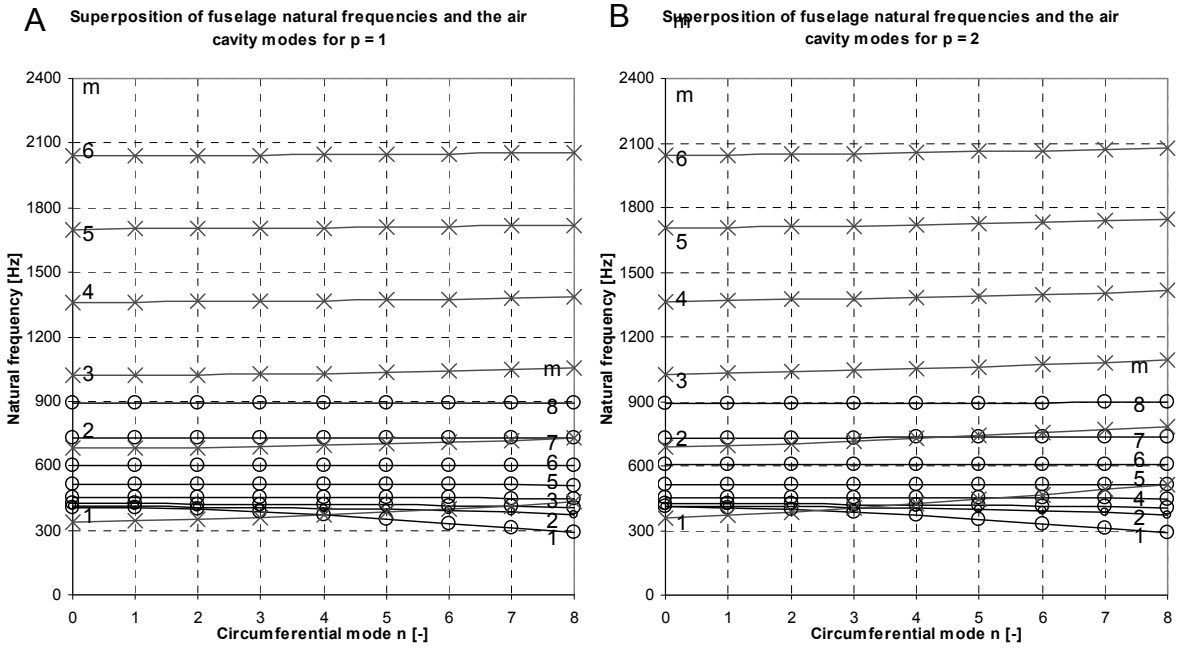

Figure 8.8: *Superposition of acoustic modes with; A) radial mode p = 1 and B) radial mode p = 2, on the structural modes of a clamped unstiffened cylinder. Only modes with identical circumferential and identical longitudinal wave numbers will give strong resonance.*

Table 8.9: *Coupled eigenmodes that can be of interest for the ΔL_p measurements of a fuselage with radius of 1.98m. The modes are extracted from figure 8.8A and B.*

Circumferential mode n	Longitudinal mode m	Radial mode p	Frequency (Hz)
3	1	1	386
4	1	1	370
2	1	2	398
3	1	2	386

From figure 8.8 and table 8.9 can be concluded that coupled structural-acoustic modes are only possible below the ring frequency. This means that, for the considered fuselage, the coupled structural-acoustic modes occur below 429 Hz. Above the ring frequency the fuselage will behave like flat panels. There, the sub-panel modes are of influence. Also the coincidence frequency remains relatively large.

8.4 Measurements

The sound pressure differences of four cylinders have been measured. First, the non-stiffened cylinder is discussed, followed by a cylinder with 6 stringer, one with 12 stringers and finally a cylinder with 12 stringers and 2 frames.

8.4.1 Non-stiffened reference cylinder

Figure 8.9 shows the non-stiffened cylinder in the test set-up. First, the test procedure is described. A noise signal is transmitted through a speaker system in the 'non-perfect reverberation room' such that a diffuse sound field, where the sound pressure level is constant at all points, is approximated. For every measurement the same noise signal is used. The sampling rate of the measurements is set at 12.8 kHz and the bandwidth at 6125 Hz. The measurements are controlled with the DIFA analyser software. Each measurement takes 1.28 seconds and is performed ten times, after which the analyser determines the average. The analyser software directly performs an FFT transformation on the measured microphone signals and saves it in a Matlab file format.

Figure 8.9: *Experimental test set-up at $\varphi_m = 0$ and $x/L_{cil} = 0.2$*

Sound pressure level measurements are performed at different microphone positions. The inside microphone is positioned at every combination of φ_m = 0, 90, 180 and 270 degrees, x/L_{cil} = 0.2, 0.4, 0.6, and 0.8 and r/R = 0.20, 0.53 and 0.87. Definitions of the parameters: φ_m, x/L_{cil} and r/R are illustrated in figure 8.10. The outside microphone is positioned 30 mm from the cylinder skin in the φ_m = 0 position at the same x/L_{cil} position as the inside microphone. Also when the inside microphone is positioned at φ_m = 90 or φ_m = 270 the outside microphone is positioned at the φ_m = 0 position. Only when the inside microphone is positioned at φ_m = 180 the outside microphone is also positioned at φ_m = 180 degrees.

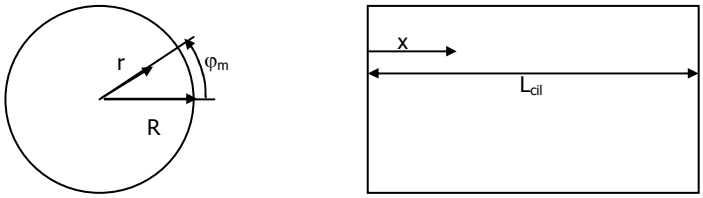

Figure 8.10: *Definition of r/R, x/L_{cil} and φ_m.*

First it is verified if the room approximates a reverberation room by comparing the sound pressure levels with the outside microphone at different x/L_{cil} positions along the outside of the cylinder. Figure 8.11 shows the sound pressure levels of the outside microphone measured at positions along the right side (φ_m = 0) of the cylinder. Figure 8.12 compares the average sound pressure level of the left (φ_m = 180) and right side of the cylinder.

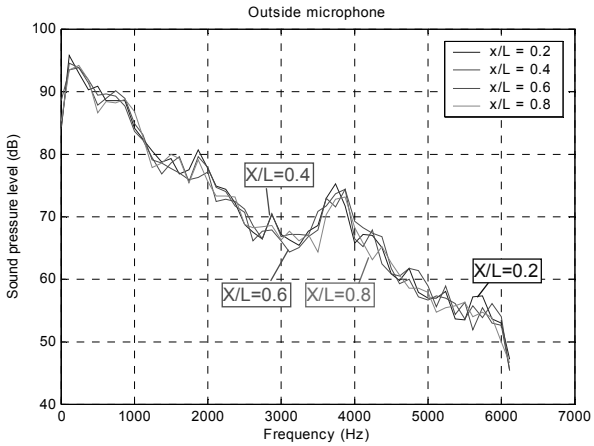

Figure 8.11: *Sound pressure levels for the outside microphone at r/R = 0.87, φ_m = 0 and variable x/L_{cil} position.*

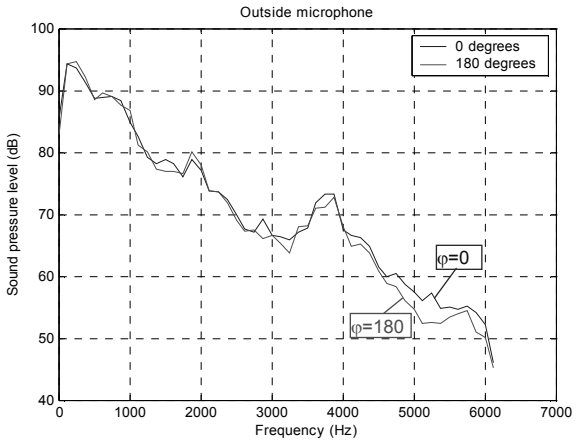

Figure 8.12: *Sound pressure levels for the outside microphone at r/R = 0.87, averaged x/L_{cil} and φ_m = 0, 180 position.*

Both figures show the general decreasing trend of the sound pressure level with frequency that is characteristic for pink noise. From figure 8.11, it is concluded that the general L_p distribution is quite similar for all positions along side the cylinder with a maximum variation of $\pm$ 2 dB for some frequencies. From figure 8.12 it is concluded that the average left and right sound pressure level distribution are also quite similar except for the higher frequencies where the sound pressure levels at φ_m = 180 is up to 4 dB less than for φ_m = 0. The differences in sound pressure levels around the cylinder can be explained by room acoustics and reflections from the test cylinder.

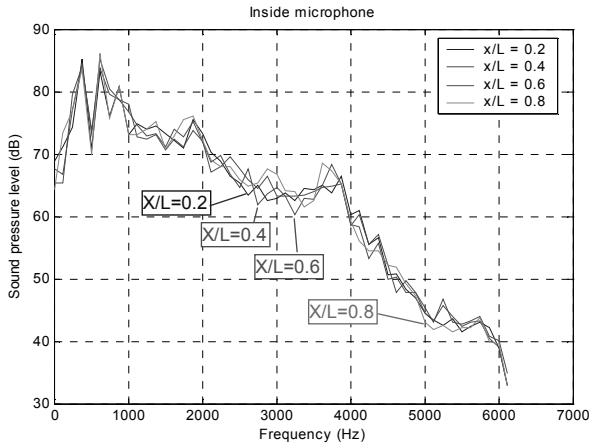

Figure 8.13: *Sound pressure levels for the inside microphone at r/R = 0.87, φ_m = 0 and variable x/L_{cil} position.*

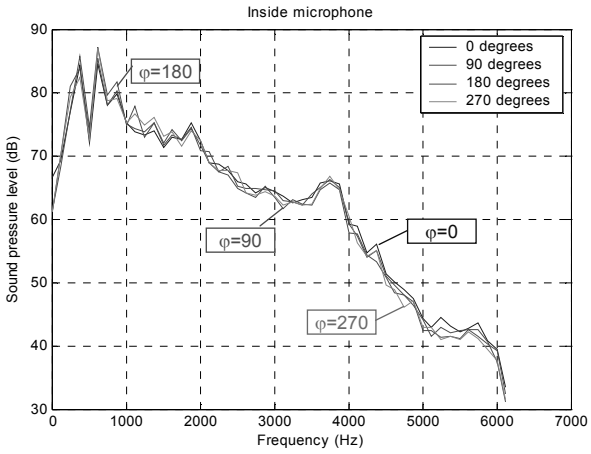

Figure 8.14: *Sound pressure levels for the inside microphone at r/R = 0.87, averaged x/L_{cil} and variable φ_m position.*

Figure 8.13 shows the sound pressure levels measured with the inside microphone for different longitudinal positions x/L_{cil} at φ_m = 0, and r/R = 0.87 and figure 8.14 shows the inside sound pressure levels for variable position of φ_m at r/R = 0.87 and averaged x/L_{cil}. From figure 8.13 is concluded that the general distribution is quite similar. However maximum variations of +/- 3 dB do occur. These variations can be explained by the different contributions of the different acoustic modes at different positions inside the cylinder and by the effect of absorption inside the cylinder. From figure 8.14 is concluded that when the longitudinal sound pressure levels are averaged, little variation is shown. This can be explained by the fact that a cylinder is rotation symmetrical and therefore all acoustic modes will contribute equally in circumferential direction.

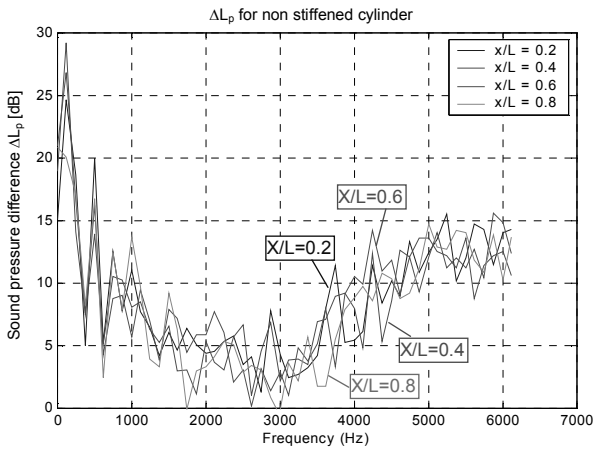

Figure 8.15: *Sound pressure difference for the inside microphone at r/R = 0.87, φ_m = 0 and variable x/L_{cil} position. (See also colour section).*

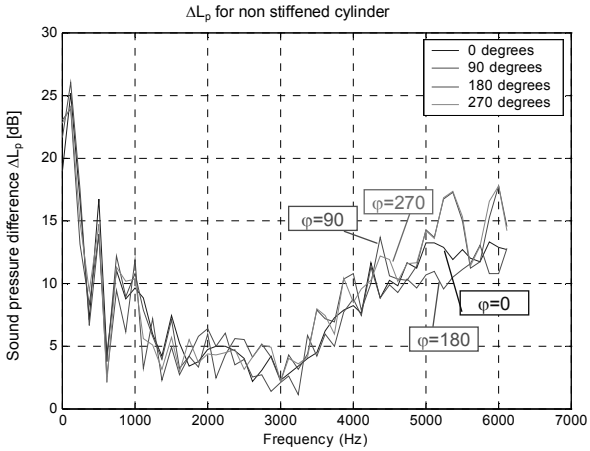

Figure 8.16: *Sound pressure difference for the inside microphone at r/R = 0.87, average x/L_{cil} and variable φ_m position. (See also colour section).*

The sound pressure difference level ΔL_p of the cylinder wall is calculated by subtracting the L_p of the inside microphone from the L_p measured with the outside microphone. Figure 8.15 shows the sound pressure difference for variable x/L_{cil} at r/R = 0.87 and φ_m = 0 and figure 8.16 shows the sound pressure difference for variable φ_m at r/R = 0.87 and averaged x/L_{cil}. The variations in the sound pressure difference are caused by the summary of the variations in the measurements of the outside and inside microphone. Comparison of figure 8.16 with figure 8.15 shows that the variations are smaller when the sound pressure difference is averaged in longitudinal direction. It can be concluded that the testing room cannot be compared to an ideal testing facility. Therefore, it is not possible to determine the actual TL. Only the ΔL_p can be measured. The variations in ΔL_p from figure 8.15 and 8.16 have to be taken into account in discussing the results from measurements.

Because the outside microphone is always positioned at φ_m = 0 it is most correct to also use the sound pressure difference averaged over x/L_{cil} at φ_m = 0. In the remainder of the text, when it is referred to the sound pressure difference level of the cylinder, it is referred to the sound pressure difference at averaged x/L_{cil} at φ_m = 0.

Table 8.10 shows the overall sound pressure levels (L_T) in decibel of the outside and inside microphone for φ_m = 0 at different positions along side the cylinder (x/L_{cil} = 0.2, 0.4, 0.6 and 0.8) and different radial positions at r/R=0.2, 0.53 and 0.87. The overall sound pressure level L_T is determined from the measured frequency dependent sound pressure levels according to equation 8.5:

$$L_T = 10\log_{10}\left(10^{L_{p1}/10} + 10^{L_{p2}/10} + etc...\right) \qquad (8.5)$$

Where: L_T is the overall sound pressure level for the complete considered frequency range
L_{p1} is the sound pressure level for frequency range 1
L_{p2} is the sound pressure level for frequency range 2

It is noticed that the overall outside sound pressure level remains almost constant at 100.4 dB with a variation of +/- 0.25 dB.

Table 8.10: *Overall sound pressure levels and corresponding sound pressure difference at 20, 40, 60 and 80 % along side the non-stiffened cylinder measured at radial positions R1, R2 and R3 and φ_m = 0.*

Position	r/R=0.87		r/R=0.53		r/R=0.20	
	L_T (dB)	ΔL_p (dB)	L_T(dB)	ΔL_p(dB)	L_T(dB)	ΔL_p(dB)
0.2m						
Inside	90.12		87.71		84.84	
Outside	100.63	10.51	100.35	12.64	100.19	15.35
0.4m						
Inside	90.21		87.94		86.28	
Outside	100.41	10.20	100.61	12.67	100.68	14.40
0.6m						
Inside	90.54		87.79		86.75	
Outside	100.46	9.92	100.39	12.60	100.63	13.88
0.8m						
Inside	90.65		87.92		84.79	
Outside	100.19	9.54	100.13	12.22	100.32	15.53
Average						
Inside	90.38		87.84		85.67	
Outside	100.42	10.04	100.37	12.53	100.46	14.79

Also the overall inside sound pressure levels are almost constant at a fixed radial position. The variations of the inside microphone measurements are respectively 0.27dB, 0.13dB and 1.08dB for respectively r/R = 0.87, 0.53 and 0.20. From table 8.10 also can be concluded that the sound pressure difference increases with decreasing r/R meaning moving away from the cylinder wall. This is in agreement with TL measurements performed by NASA [3] as is illustrated in figure 8.17. NASA tested a cylinder with almost similar size but with a cylinder wall thickness of 1.63 mm instead of 1 mm in this case. According to the mass law this thickness difference should give an increase in the sound pressure difference of 2.12 dB, compared to the current tested cylinder. It should be noted that NASA determined the real TL, while for

the measurements only the sound pressure difference was measured. Nevertheless the measurements have the same trend as the NASA experiments as shown in figure 8.17.

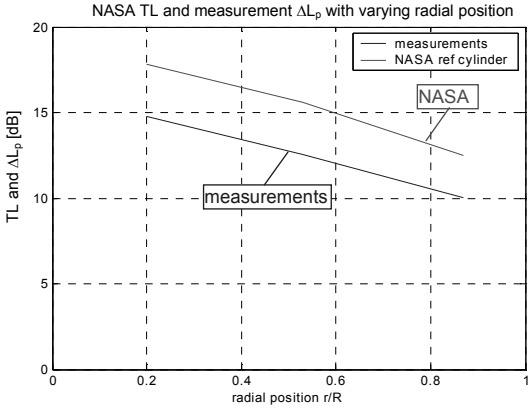

Figure 8.17: *Noise reduction versus radial position [3].*

In order to cancel out the radial dependence of the sound pressure difference, in the remaining text the overall sound pressure difference is considered to be the sound pressure difference at r/R = 0.87 and φ_m = 0 averaged over the x/L_{cil} position. This gives the resultant sound pressure levels for the inside and outside microphones and the corresponding pressure difference as shown in figure 8.18 and 8.19.

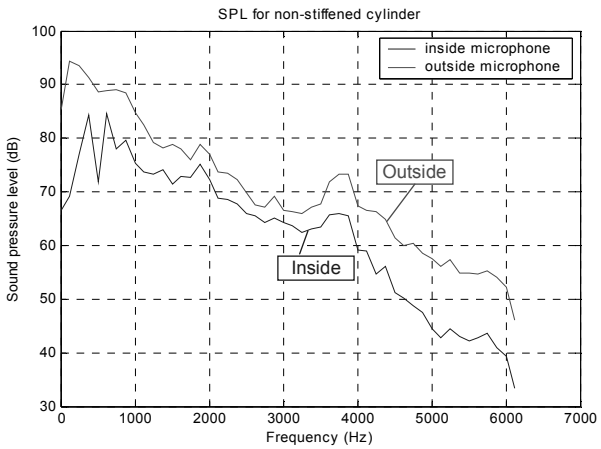

Figure 8.18: *Average sound pressure levels for the inside and outside microphone at r/R = 0.87, φ_m = 0.*

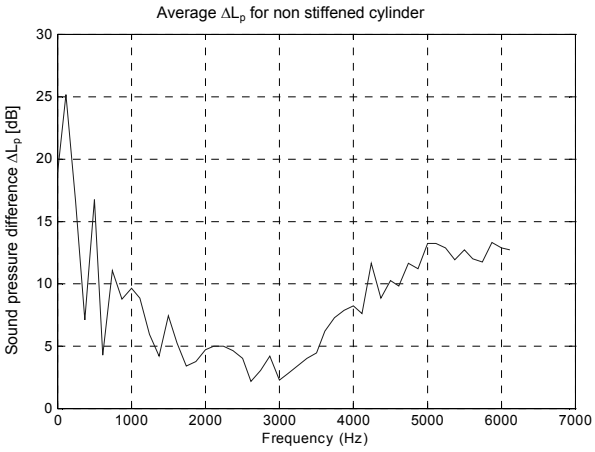

Figure 8.19: *Average sound pressure difference at r/R = 0.87, φ_m = 0.*

8.4.2 Cylinder with 6 stringers

Figure 8.20 illustrates the z-stringers that are used to stiffen the cylinder. Figure 8.21 shows the cylinder with 6 stringers in the test set-up. The test procedure, including the test settings, is identical to that of the measurements of the non-stiffened cylinder.

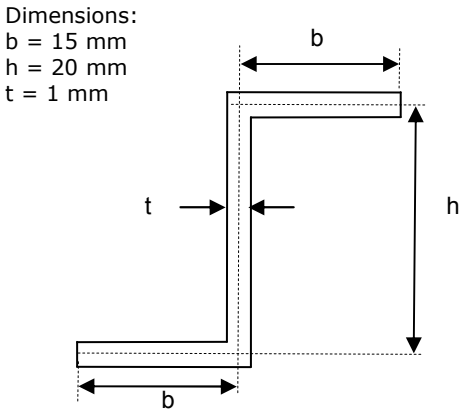

Figure 8.20: *Stringer dimensions.*

Figure 8.21: *Test set-up of the cylinder with 6 stringers.*

Because of the presence of stringers there might be a difference in the ΔL_p measured between two stringers and the ΔL_p measured at stringer positions.

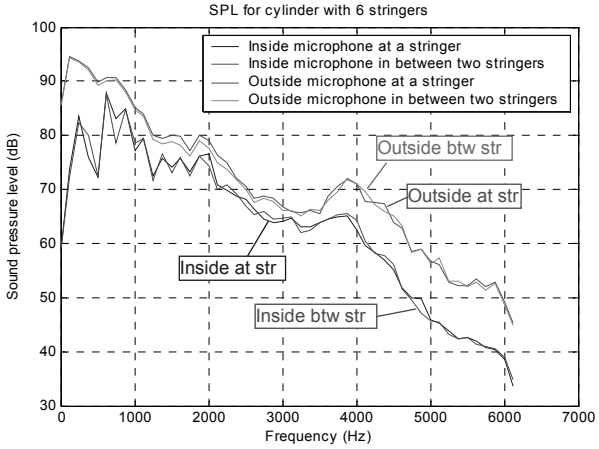

Figure 8.22: *Sound pressure levels for the inside and outside microphone at and in between stringers at r/R = 0.87, φ_m = 0 and averaged x/L_{cil} position. (See also colour section).*

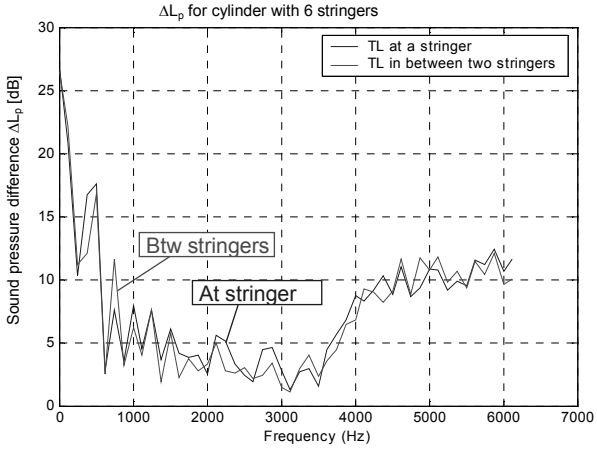

Figure 8.23: *Sound pressure difference at and in between stringers at r/R = 0.87, φ_m = 0 and averaged x/L_{cil} position. (See also colour section).*

Figure 8.22 shows the inside and outside sound pressure levels measured at a stringer position and between two stringers and figure 8.23 shows the corresponding ΔL_p. Apparently the measuring position (in between or at a stringer) is not relevant for the resultant ΔL_p.

Averaging the measurements at and in between stringers gives the results shown in figure 8.24 and 8.25. The averaged sound pressure levels and corresponding ΔL_p for different radial positions are given in table 8.11.

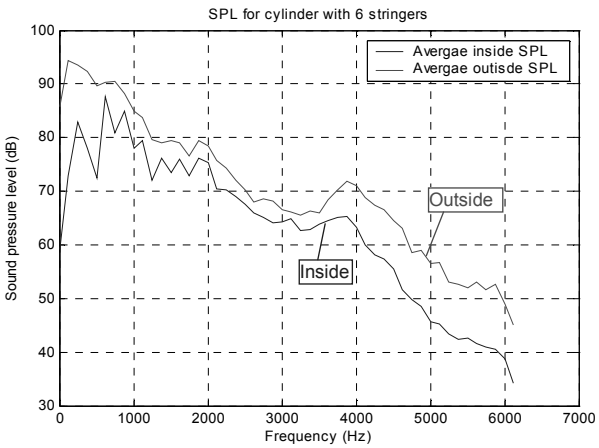

Figure 8.24: *Average sound pressure levels for the inside microphone at r/R = 0.87, φ_m = 0 and averaged x/L_{cil} position.*

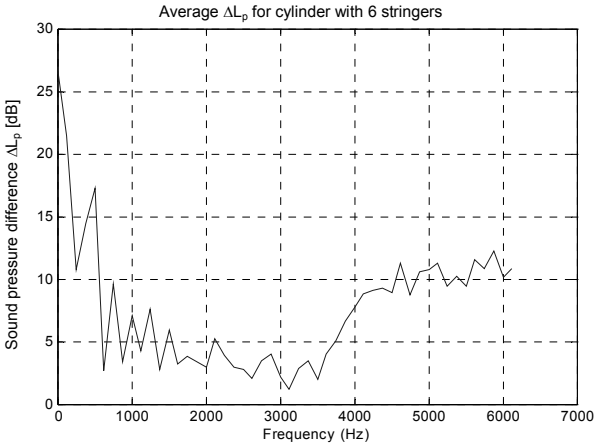

Figure 8.25: *Average sound pressure difference for the test cylinder with 6 stringers at r/R = 0.87, φ_m = 0 and averaged x/L_{cil} position.*

Table 8.11: *Inside and outside overall sound pressure levels and corresponding sound pressure difference for the test cylinder with 6 stringers for φ_m = 0 at x/L_{cil} = 0.2, 0.4, 0.6, at radial positions R1, R2 and R3. (The sound pressure levels shown in this table are averaged over the measurements at and in between stringers).*

Position	r/R=0.87		r/R=0.53		r/R=0.20	
	L_T(dB)	ΔL_p(dB)	L_T(dB)	ΔL_p(dB)	L_T(dB)	ΔL_p(dB)
0.2m						
inside	92.40		88.87		87.55	
outside	100.91	8.51	101.37	12.57	100.05	13.46
0.4m						
inside	94.10		93.11		90.92	
outside	101.07	6.97	101.28	8.17	101.16	10.24
0.6m						
inside	92.78		92.37		89.47	
outside	100.84	8.07	100.93	8.56	100.95	11.48
0.8m						
inside	92.48		90.01		87.72	
outside	100.95	8.48	101.25	11.24	100.99	13.25
average						
inside	92.94		91.09		88.92	
outside	100.94	8.01	101.22	10.14	101.03	12.11

Comparing the sound pressure difference for the cylinder with 6 stringers with the sound pressure difference of the non-stiffened cylinder it is concluded that the sound pressure difference of the stiffened cylinder is less than that of the non-stiffened cylinder, which was to be expected according to section 3.4. Section 8.5 will discuss the results in more detail.

8.4.3 Cylinder with 12 stringers

The cylinder with 12 stringers is manufactured by placing 6 new z-stringers in between the stringers of the cylinder with 6 stringers. The dimensions of the 6 added stringers are identical to the 6 stringers that were already attached. See figure 8.21. The testing procedure is again similar as for the non-stiffened cylinder and the cylinder with 6 stringers.

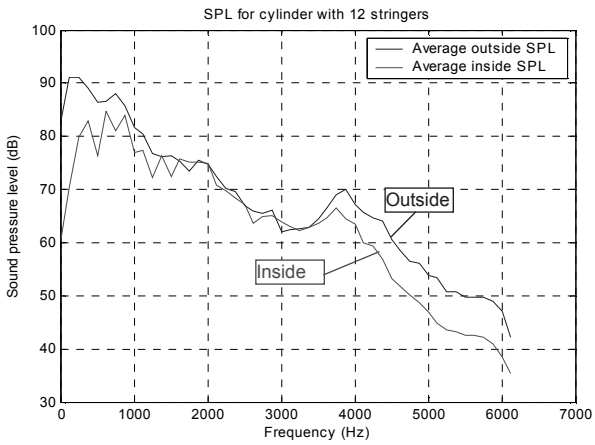

Figure 8.26: *Average sound pressure levels for the inside microphone at r/R = 0.87, φ_m = 0 and averaged x/L_{cil} position.*

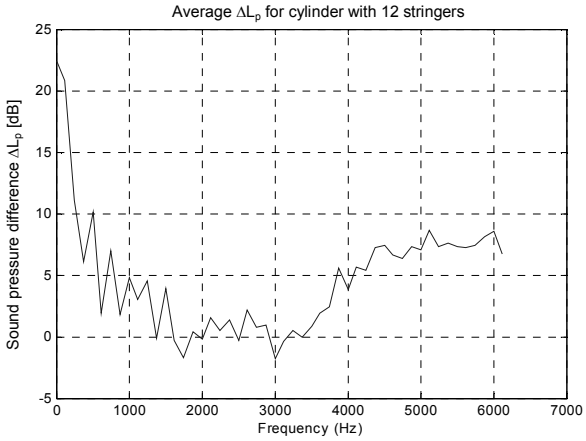

Figure 8.27: *Average sound transmission loss for the test cylinder with 12 stringers at r/R = 0.87, φ_m = 0 and averaged x/L_{cil} position.*

Table 8.12: *Inside and outside overall sound pressure levels and corresponding sound pressure difference for the test cylinder with 12 stringers at x/L_{cil} = 0.2, 0.4, 0.6 at radial positions R1, R2 and R3. (The sound pressure levels shown in this table are averaged over the measurements at and in between stiffeners).*

Position	r/R=0.87		r/R=0.53		r/R=0.20	
	L_T(dB)	ΔL_p(dB)	L_T(dB)	ΔL_p(dB)	L_T(dB)	ΔL_p(dB)
0.2m						
inside	91.40		88.10		86.17	
outside	98.09	6.69	98.18	10.08	97.80	11.63
0.4m						
inside	91.87		88.37		86.10	
outside	97.71	5.85	97.72	9.36	97.73	11.63
0.6m						
inside	91.21		88.36		86.14	
outside	98.38	7.18	97.99	9.63	97.61	11.47
0.8m						
inside	91.54		87.93		86.24	
outside	98.20	6.65	98.15	10.22	98.10	11.86
average						
inside	91.51		88.19		86.17	
outside	98.10	6.59	98.01	9.82	97.81	11.64

Figure 8.26 and 8.27 show the sound pressure levels for the inside and outside microphone and the corresponding sound pressure difference. Again the sound pressure levels are averaged for positions at and in between stringers like for the cylinder with 6 stringers. The averaged sound pressure levels and corresponding sound pressure difference for different radial positions are given in table 8.12.

It is concluded that the sound pressure difference is again lower than that of the cylinder with 6 stringers. At two frequencies the sound pressure difference is even negative, which would mean that the noise inside is higher than the noise outside. This indicates that sound reflections from the outside cylinder surface and the sound absorption inside the cylinder play a role in the sound pressure measurements.

8.4.4 Cylinder with 12 stringers and 2 frames

Figure 8.28 illustrates the C-shaped frames that are added to the cylinder with 12 stringers. The frames are positioned on the outside of the cylinder. The frames have cut-outs at positions where the stringers pass. The dimensions of the C-shaped frames are also given in figure 8.28.

Figure 8.29 shows the cylinder with 12 stringers and 2 frames in the test set-up. The test procedure, including the test settings, is identical to that of the measurements of the non-stiffened cylinder.

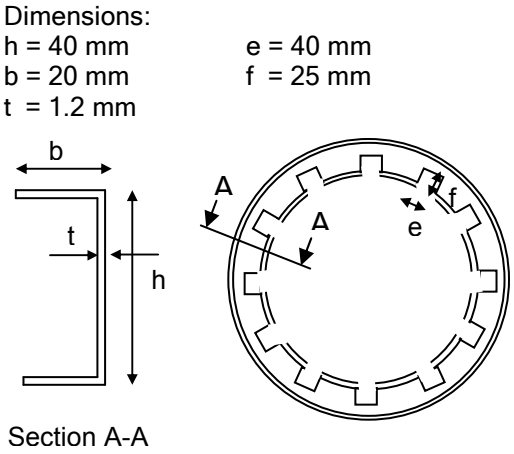

Figure 8.28: *C-shaped frame*

Figure 8.29: *Test set-up of the cylinder with 12 stringers and 2 frames.*

The sound pressure difference is measured at x/L_{cil} = 0.16, 0.33, 0.5, 0.67 and 0.84. The positions x/L_{cil} = 0.33 and 0.67 are at frame positions and the positions x/L_{cil} = 0.16, 0.5 and 0.87 are between frame positions. The measurements are taken at and in between stringers and only for r/R = 0.87.

Figure 8.30 shows the average in- and outside sound pressure levels at and between frame positions for r/R = 0.87. These sound pressure levels are averaged over the 'at and between' stringer positions for x/L_{cil} = 0.16, 0.5 and 0.87 (between frames) and x/L_{cil} = 0.33 and 0.67 (at frames). Figure 8.31 shows the corresponding sound pressure difference for the 'at and between' frame measurements. It is noted that the measurements 'at and between' frame positions do not differ much. Figure 8.32 and 8.33 show the overall averaged sound pressure and ΔL_p levels.

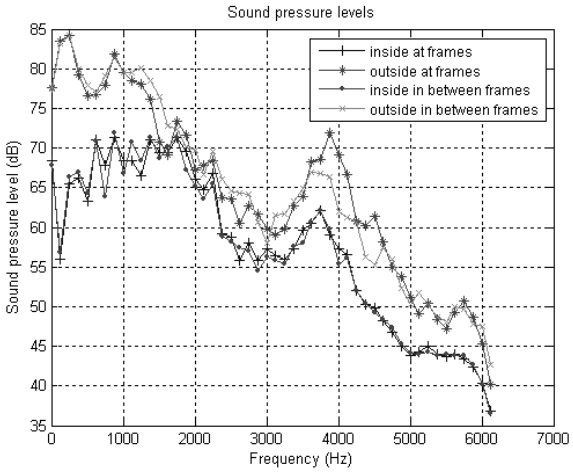

Figure 8.30: *Average sound pressure levels at and in between frame positions. (Averaged over x/L_{cil} = 0.33 and 0.67, at and in between stringers at r/R = 0.87). (See also colour section).*

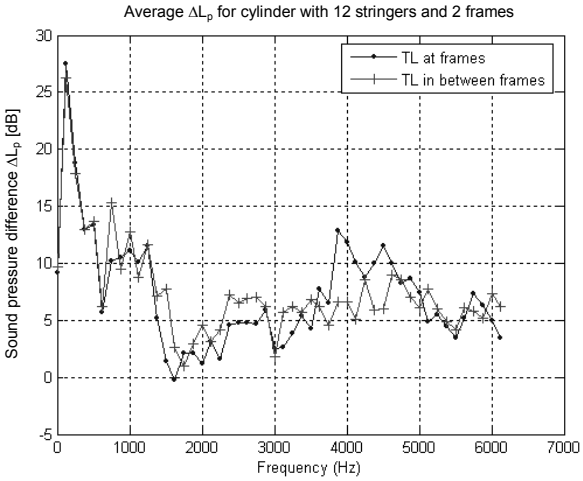

Figure 8.31: *Average sound pressure difference at and in between frame positions (Averaged over x/L_{cil} =0.33 and 0.67 at and in between stringers at r/R =0.87). (See also colour section).*

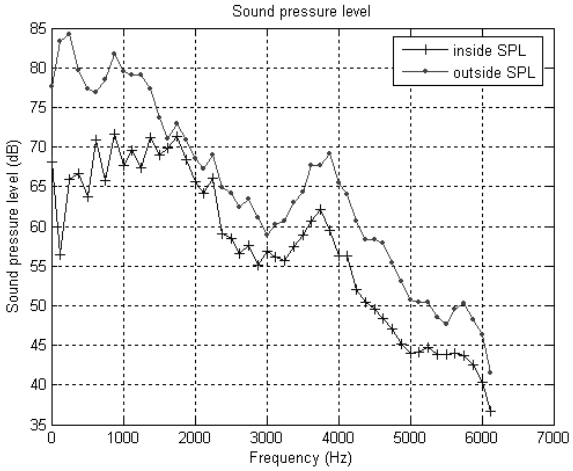

Figure 8.32: *Overall sound pressure levels. (Averaged over x/L_{cil} = 0.33 and 0.67, at and in between stringers, at and in between frames at r/R = 0.87).*

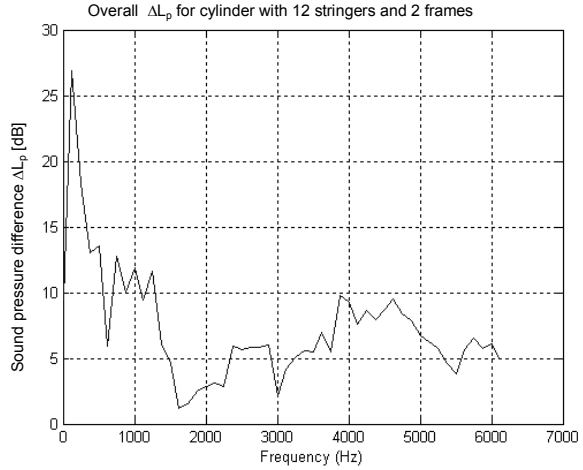

Figure 8.33: *Overall sound pressure difference (Averaged over x/L_{cil} =0.33 and 0.67 at and in between stringers, at and in between frames at r/R =0.87).*

The averaged sound pressure levels and corresponding sound pressure difference for different axial positions are given in table 8.13.

Table 8.13: *Inside and outside overall sound pressure levels and corresponding sound pressure difference for the test cylinder with 12 stringers for φ_m = 0 at x/L_{cil} = 0.2, 0.4, 0.6 at radial position R1. (The sound pressure levels shown in this table are averaged over the measurements at and in between stiffeners).*

Position	r/R=0.87 at stringer position		r/R=0.87 in between stringers	
	L_T(dB)	ΔL_p(dB)	L_T(dB)	ΔL_p(dB)
0.17m	(between end plate and frame)			
inside	82.06		81.60	
outside	90.59	8.54	90.03	8.43
0.33m	(at frame position)			
inside	81.86		81.72	
outside	89.75	7.88	89.87	8.15
0.5m	(between the two frames)			
inside	82.29		81.96	
outside	90.14	7.86	89.62	7.66
0.67m	(at frame position)			
inside	81.64		81.93	
outside	89.19	7.55	89.11	7.18
0.84m	(between end plate and frame)			
inside	81.23		81.98	
outside	89.05	7.83	89.05	7.07
Average				
Inside	81.82		81.84	
Outside	89.74	7.93	89.54	7.70

8.5 Discussion of the sound pressure difference measurements

In this section the measurements of the four cylinders are compared to each other. Figure 8.34 gives an overview of the sound pressure differences measured for the non-stiffened cylinder, the cylinder stiffened with 6 and with 12 stringers and the cylinder stiffened with 12 stringers and 2 frames. In this figure also the resonance frequencies are identified. First of all it can be recognized that the measured ring frequency occurs at 3000 Hz. Above this frequency the ΔL_p increases again. Below the ring frequency structural and coupled acoustic structural frequencies can occur. Especially, the frequency range between 1800 and 3000 Hz shows a low ΔL_p. From the discussion in section 8.3, it is known that this is the range of the coupled acoustic structural resonance frequencies. Below 1500 Hz sub panel natural frequencies are the cause for the dips in the ΔL_p. Coupled resonance modes are more severe than only structural modes. Therefore the region with the coupled eigenmodes, between 1800 and 3000 Hz, shows the lowest ΔL_p.

However it is noticed that, like for the measured ring frequency, the measured resonance frequencies do not exactly coincide with the analytically determined resonance frequencies. This can be explained by the fact that the support condition of the test cylinders is probably a combination of a clamped and simply supported boundary condition. Also, it should be noted that the averaging frequency was set to 125 Hz, so the ΔL_p dips that occur in between frequency steps of 125 Hz are not

shown at the real frequency at which they occur. This may give a maximum offset of 62.5 Hz. Figure 8.34 also indicates that for frequencies above 4800 Hz, the sound pressure difference decreases when the number of stringers increases. This is expected according to the theory explained in section 3.4.

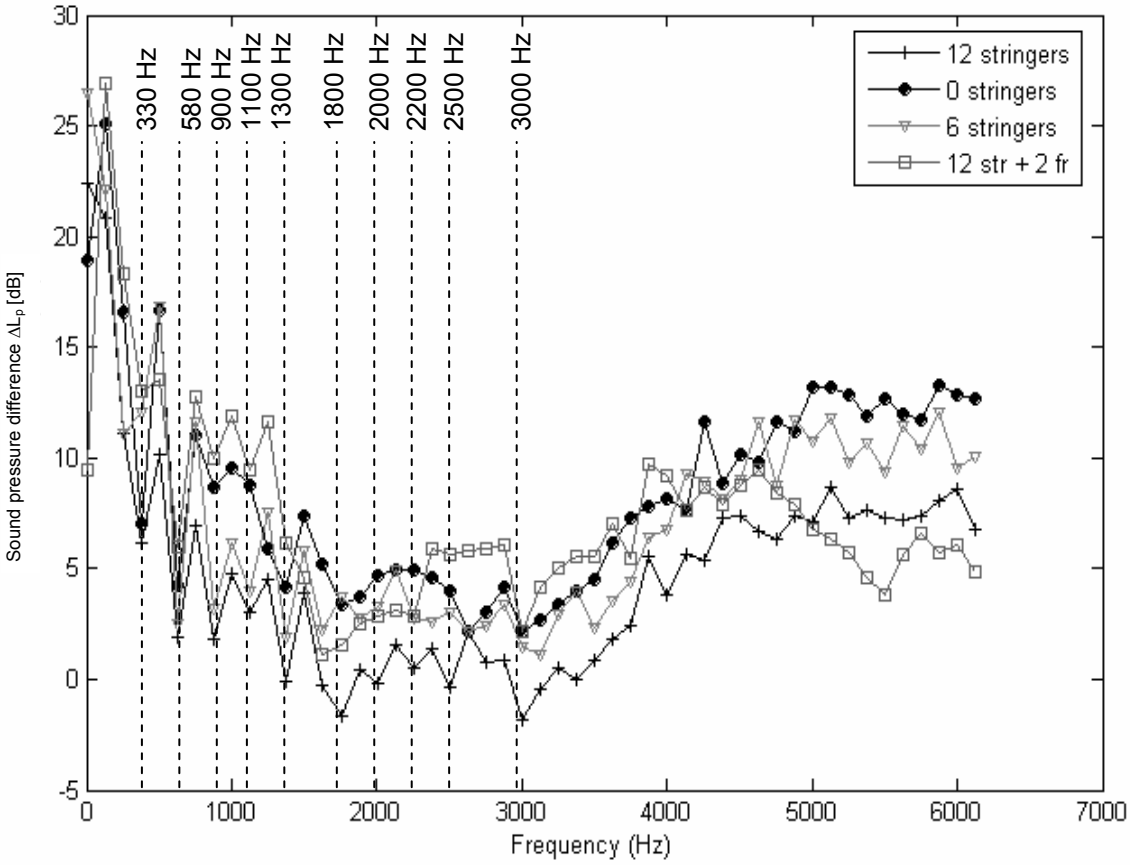

Figure 8.34: *Comparison of the measured sound pressure difference for the non-stiffened cylinder and the cylinders stiffened with 6 and 12 stringers.*

However, below 5000Hz the ΔL_p of the cylinder with 12 stringers is lower than the ΔL_p for the cylinder with 12 stringers and 2 frames. This behaviour was not expected according to the theory of section 3.4. A possible explanation could be that the addition of frames, that were mounted on the outside of the cylinder, cause more reflection. (In addition to the cylinder skin, also the webs of the frames will reflect noise to the microphone). Therefore the sound pressure levels measured with the outside microphone could have been relatively larger compared to the case without frames.

Also it is noted that for the cylinder with 12 stringers there are two frequency regions at which the ΔL_p has negative values. The frequencies at which this occurs are around the ring frequency and around the first coupled structural-acoustic modes. At these resonant frequencies the sound pressure level can increase inside the cylinder because there is no absorption material mounted inside the test cylinders. (For a TL measurement in an ideal test facility no negative TL can be measured).

The coincidence frequency was determined to be 12864 Hz, which is out of range of the measured frequency range.

Figure 8.35 shows the measured influence on the overall ΔL_p of adding stiffeners to a cylinder for different values of r/R. (Only the dots represent measured values). The number of stringers is related to the stringer pitch according to equation 8.6.

$$b = \frac{2\pi R}{n_{str}} \tag{8.6}$$

Here is b the stringer pitch, R is the radius of the cylinder and n_{str} the number of stringers.

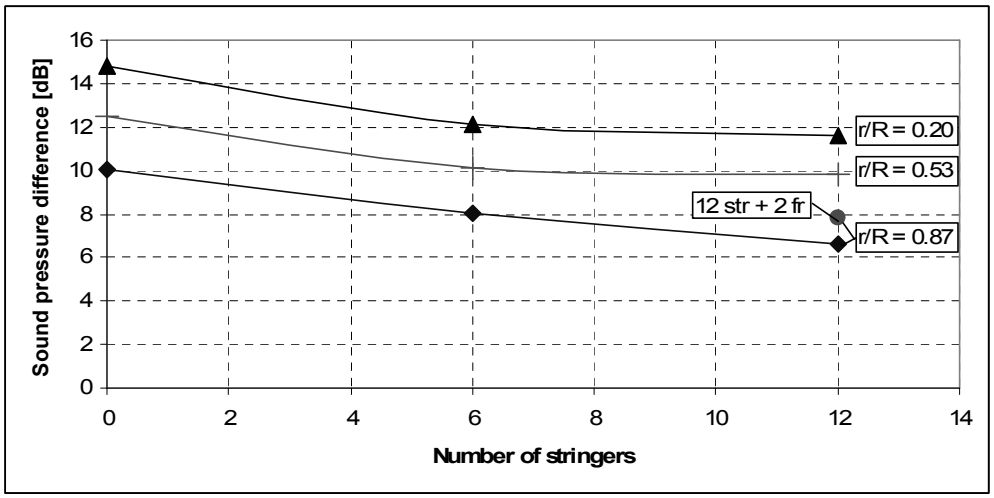

Figure 8.35: *Average sound pressure difference as function of the number of stiffeners for r/R = 0.87, 0.53 and 0.20 at φ = 0 and averaged x/L position.*

Figure 8.35 shows that the ΔL_p decreases when r/R increases, which means that the inside noise levels are measured further away from the skin. This is similar to the measurements performed by NASA [3].

Figure 8.35 also shows that the overall ΔL_p decreases by adding stringers, except for the case of adding 2 frames to the cylinder with 12 stringers. This behaviour was explained by means of the non ideal test set-up.

In section 3.2 it was concluded that below the ring frequency cylinders behave different compared to flat plates. In this region coupling of air cavity modes and structural modes are of importance. Above the ring frequency cylinders do behave like flat plates. Figure 8.34 showed, that the experiments confirmed this theory.

The tested cylinder does have a small radius and therefore a relatively high ring frequency. As discussed in section 8.3, an aircraft with a radius of 1.98 m does have a ring frequency of about 429 Hz. Because most fuselages have a relatively large radius the ring frequency will be low. This means that for a large part of the frequency range the literature equations are valid for the TL of fuselages. Because the module based on the literature equations is not very time consuming while the numerical model is very time consuming, the first analysis and optimisation steps are always performed with the module based on the literature equations. Only when more

detailed information of the sound pressure difference in the low frequency range is required, the numerical module can be used.

The results in this section are based on only few non ideal tests. To validate the tests and to get more insight in the influence of adding stringers and frames to cylinders the sound transmission loss should be measured in an ideal test facility.

8.6 Reference

[1] ISO 15186, “Acoustics -- Measurement of sound insulation in buildings and of building elements using sound intensity. -- Part 1: 2000, Laboratory measurements. -- Part 2: 2003, Field measurements. -- Part 3: 2002, Laboratory measurements at low frequencies.

[2] Van der Wal, H.M.M, Nilsson, A.C, Sound transmission measurements on composite and metal fuselage panels for different boundary conditions, NLR report NLR TP 2005-570, 2005.

[3] Wilby E.G., Wilby, J.F., Application of stiffened cylinder analysis to ATP interior noise studies, NASA CR-172384, 1984.

[4] ASTM E90-04 Standard Test Method for Laboratory Measurement of Airborne Sound Transmission Loss of Building Partitions and Elements, ASTM, 2004

[5] http://spib.rice.edu/spib/data/signals/noise/pink.html.

9 Numerical analysis of the aluminium test cylinder

9.1 Introduction

In chapter 8 it was concluded that below the ring frequency the literature equations discussed in section 3.2 are not valid to determine the sound transmission loss. As discussed in section 3.4 the sound transmission loss in the frequency range below the ring frequency is dominated by the coupled structural-acoustic natural modes and by the sub-panel natural modes. To validate the experimental results below the ring frequency, the numerical acoustic module of the DEE for the low frequency range is used. The definition of the numerical acoustic module was discussed in section 6.8.1.

The ring frequency for the aluminium test cylinders was measured at 3000 Hz. The numerical acoustic module of the current DEE can only be used up to 500 Hz. When it is desired to analyse the sound transmission loss up to higher frequencies more detailed FEM models and more powerful computers are required. For fuselages with radius larger than 2 m the ring frequency will be lower than 400 Hz.

In section 9.2 the results from the analysis with the numerical acoustic module are discussed for the unstiffened cylinder, the cylinder with 6 and 12 stringers and the cylinder with 12 stringers and 2 frames. Section 9.3 gives some concluding remarks.

9.2 Numeric analysis of the ΔL_p of the aluminium test cylinders

The numerical acoustic analysis module of the DEE that determines the ΔL_p characteristics, makes use of the commercially available FEM package ABAQUS. The analysis module consists out of a steady state dynamic analysis based on the coupled structural acoustic natural frequencies. This means that the FEM analysis consists out of two steps. First, the determination of the coupled structural-acoustic natural frequencies and secondly the steady state dynamic analysis, which determines the frequency response of the sound pressure levels at user specified recording nodes.

In section 9.2.1 the FEM model definitions are described followed in sub-section 9.2.2 by the results of the steady state dynamic analysis for the four aluminium test cylinders.

9.2.1 Model definition

A description of the FEM models that represent the four aluminium test cylinders is given in Appendix H.1.

In the remaining of this section only a short description is given of the load case definition, the definition of damping, the definition of the acoustic boundary conditions at the end caps and the definition of the recording nodes at which the sound pressure levels will be determined.

Load case definition

During the measurements discussed in chapter 8 the test cylinders were excited by pink noise generated with loudspeakers. It is very difficult to define a load case that simulates a pink noise pressure field. Therefore, for simplicity reasons, a simplified load case is considered. Because a constant pressure field applied on the whole outside surface of the cylinders would suppress certain eigenmodes, it is chosen to define the simplified load case as a point load that is partly in phase and partly out of phase with the excitation frequency of the steady state dynamic analysis. The point load has a magnitude of 1 N that is in phase, and 0.06 N that is out of phase with the excitation frequency. This point load definition is chosen identical to a reference case of the ABAQUS example problem manual [1], which discusses a coupled structural-acoustic steady state dynamic analysis of a passenger cabin of a pick-up truck. The point load is applied at a point that coincides with a FEM model node positioned on the outer surface of the test cylinders. The position of this point is identical for all four test-cylinders and is illustrated in figure 9.1. It should be noted that radiation from a cylinder excited by a point is much less compared to the radiation from a cylinder excited by an acoustic field like was explained in section 3.4. Therefore, the steady state dynamic analysis with a point load excitation will give different results compared to the experiments. Only a qualitative comparison with the experiments will be possible.

Definition of damping in the test cylinder models

The frequency response of the sound pressure levels at the recording nodes will depend on the damping definition. Within ABAQUS, for a natural frequency based steady state dynamic analysis, damping can be defined as the fraction of the critical damping factor ξ_i for a given natural frequency mode i. This is called Rayleigh

damping. Rayleigh damping is specified with two damping factors: the mass damping factor α_R that is proportional to the mass matrix of the FEM model and a stiffness damping factor β_R that is proportional to the stiffness matrix of the FEM model. The critical damping factor ξ_i can then be determined by equation 9.1 [2]:

$$\xi_i = \frac{\alpha_R}{2\omega_i} + \frac{\beta_R \omega_i}{2} \tag{9.1}$$

Here is ω_i the natural frequency of mode i.

Like for the pick-up truck example discussed in the ABAQUS example problem manual [1] only a stiffness proportional damping factor is used in the FEM analysis of the four test cylinders. For these test cylinder models a critical damping of 1% is chosen at 300 Hz. This results in a damping factor definition of α_R = 0 and β_R = 1.061e-5. However, with this definition the absorption inside the cylinder is not modeled like in reality.

Definition of the acoustic boundary conditions at the end caps

The test cylinder end caps are manufactured from a 15 mm thick steel plate. These end caps can be considered as rigid boundaries. A boundary is considered rigid when the impedance of the boundary material (medium 2) is much larger than the impedance of origin medium (medium 1). For the aluminium test cylinders the air cavity is medium 1 (Impedance of air is Z_1 = 415 kg/m^{2}s) and the steel end caps are medium 2 (Impedance of steel is Z_2 = 45e6 kg/m^{2}s). The normal reflection coefficient is defined by [3]:

$$R_{refl} = \frac{(Z_2/Z_1) - \sqrt{1 - [n-1]\tan^2 \varphi_i}}{(Z_2/Z_1) + \sqrt{1 - [n-1]\tan^2 \varphi_i}} \tag{9.2}$$

Here is $n = (c_{s2}/c_{s1})^2$ where c_{s1} and c_{s2} are respectively the speed of sound of the steel end caps (c_{s1} = 5800 m/s) and the speed of sound in air (c_{s2} = 340 m/s) and φ_i is the angle of incidence of the wave ray. For rigid walls the reflection at normal incidence is almost 100 % ($R_{refl} \approx 1$). For the ABAQUS models of the test cylinders the steel end caps are not modeled themselves. Instead a rigid boundary condition is assumed at the end cap positions.

For the experiments discussed in chapter 8 noise reflections on the outside microphone play a role. Also this effect is not taken into account in the numerical model.

Definition of the nodes at which the acoustic pressure is recorded

The air of the non-stiffened cylinder and the two stringer stiffened cylinders is modeled as a perfect non-disturbed solid cylinder. The FEM models for these three cylinders have an equal amount of FEM elements in longitudinal direction. Because the amount of stringers does not influence the node position in the vertical direction of the vertical symmetry plane of these three cylinders, the recording nodes are chosen in this vertical symmetry plane. The fourth test cylinder has two frames of which the webs are modeled with shell elements. The existence of the frame webs, influence the node position in the vertical symmetry plane. This means that for the cylinder with frames the positions of the recording nodes are slightly different compared to the

cylinders without frames. The definition of the 16 recording nodes for the four cylinders are illustrated in figure 9.1. All nodes are positioned in the lower half of the vertical symmetry plane of the air cavity.

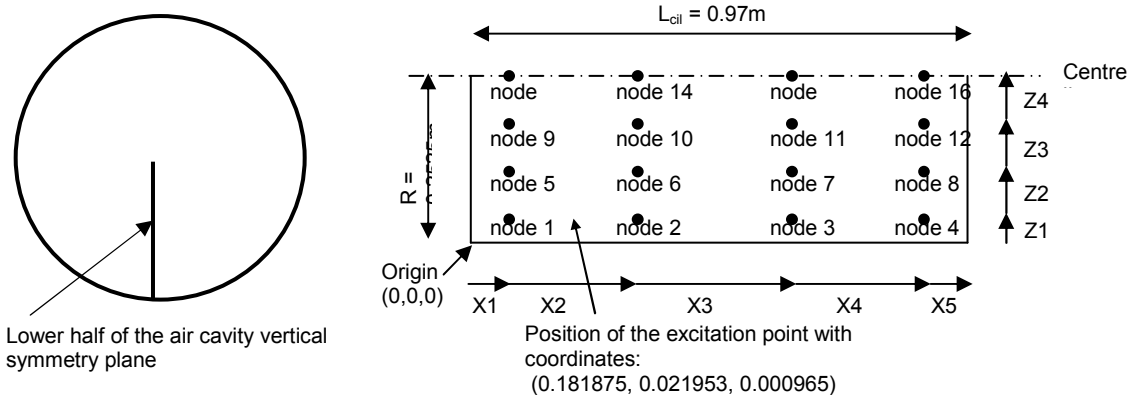

Non-stiffened and stringer stiffened cylinders:

X1 = 0.080833m	Z1 = 0.063875m
X2 = 0.323333m	Z2 = 0.126750m
X3 = 0.646667m	Z3 = 0.189625m
X4 = 0.889167m	Z4 = 0.252500m
X5 = 0.970000m	

Cylinder stiffened with 12 stringers and 2 frames:

X1 = 0.080833m	Z1 = 0.041000m
X2 = 0.323333m	Z2 = 0.093875m
X3 = 0.646667m	Z3 = 0.146725m
X4 = 0.889167m	Z4 = 0.199625m
X5 = 0.970000m	

Figure 9.1: *Definition of the node positions at which the acoustic pressure is recorded. Because of the existence of the frames the positions of the recording nodes of the cylinder with frames is different from the cylinders without frames.*

9.2.2 Results of the numerical ΔL_p analysis of the test cylinders

The acoustic frequency response of the test cylinders is determined by performing a steady state dynamic analysis over a frequency range of 100 to 500 Hz. As stated in the previous section, the steady state dynamic analysis is based on the coupled structural-acoustic natural frequencies. These numerically determined coupled structural-acoustic natural frequencies for the four test cylinders are listed in table 9.1. The separate and coupled structural and acoustical natural frequencies are also given in appendix H.

The acoustic frequency response is defined as the pore pressure at the recording nodes in the air inside the test cylinders. The positions of the recording nodes were defined in figure 9.1. From the recorded pore pressures the resultant sound pressure levels are determined with equation 9.3 [1]:

$$L_p = 20\log_{10}\left(\frac{p_{rms}}{p_{ref}}\right) \tag{9.3}$$

In equation 9.3 is p_{rms} the root mean square pressure of the recorded pore pressure, ($p_{rms} = p_{pore}/\sqrt{2}$) and p_{ref} is the reference pressure that is just audible by the human ear ($p_{ref} = 2 \cdot 10^{-5}$ Pa).

Table 9.1: *Numerically determined coupled acoustic-structural natural frequencies of the non-stiffened cylinder, the cylinder with 6 and 12 stringers and the cylinder with 12 stringers and 2 frames.*

	Unstiffened Cylinder	Cylinder with 6 stringers	Cylinder with 12 stringers	Cylinder with 12 stringers and 2 frames
1	0.0000	0.0000	0.0000	0.0000
2	176.27	104.62	101.46	174.02
3	178.59	105.49	102.60	345.32
4	178.71	105.52	102.60	394.15
5	186.58	107.15	105.42	396.84
6	186.76	107.18	105.46	429.09
7	204.09	107.86	107.86	431.56
8	204.25	176.27	107.86	479.60
9	240.27	177.90	109.18	479.65
10	241.68	181.59	109.20	484.44
11	250.79	185.14	109.78	484.52
12	250.94	185.29	109.78	487.19
13	298.19	202.99	109.94	487.28
14	298.43	203.20	176.28	493.08
15	307.89	226.81	177.24	493.41
16	307.89	227.76	183.82	508.47
17	311.17	235.97	184.09	515.10
18	311.40	236.25	184.22	516.78
19	327.58	236.31	203.26	517.50
20	328.23	238.95	203.47	517.73
21	346.44	238.99	218.03	517.84
22	346.69	241.02	218.78	518.92
23	349.87	249.40	229.19	522.42
24	357.90	249.52	230.17	529.19
25	358.68	274.33	230.18	541.47
26	382.05	310.75	234.37	543.08
27	382.30	327.52	234.38	543.19
28	389.33	329.64	241.03	546.92
29	397.34	330.40	241.03	547.01
30	405.30	338.43	247.41	549.25
31	405.36	338.44	247.54	549.32
32	405.55	346.09	251.26	552.96
33	405.93	349.88	251.50	553.58
34	422.13	349.89	251.75	561.45
35	422.36	354.97	251.75	561.53
36	424.52	365.80	253.19	565.05
37	424.82	366.11	274.31	565.29
38	425.61	381.94	274.32	568.23
39	432.96	389.30	326.88	568.31
40	458.50	397.31	336.22	574.80
41	458.74	404.28	336.88	576.71
42	459.15	404.29	345.78	576.82
43	459.56	404.74	346.72	582.54
44	462.09	410.29	347.04	582.64
45	462.37	410.33	347.60	585.24
46	478.63	414.51	349.88	586.67
47	478.92	415.31	382.25	587.74
48	514.65	419.46	382.37	587.76
49	516.30	420.24	389.18	590.46
50	516.50	425.64	396.52	590.50

In the remaining of this section the frequency responses of the recorded sound pressure levels for the four test cylinders are described:

The non-stiffened cylinder

Figure 9.2 shows the sound pressure levels recorded at node 1, 2, 3 and 4 at a z is constant position as defined in figure 9.1. The peaks correspond to the coupled

natural frequencies as illustrated in the first column of table 9.1. The strongest peaks occur at 176 Hz and 399 Hz which are the first and the third acoustical modes. The second (350 Hz) and fourth (434 Hz) acoustic modes are less dominant. The other peaks occur at coupled natural frequencies that are originated by the structural modes given in table H.5 of appendix H.

By averaging L_p over the four recording nodes the average L_p at z-position 1 is determined. Similar average L_p levels can be determined for the nodes 5, 6, 7 and 8 at z-position 2 and nodes 9, 10, 11 and 12 at z-position 3. The average L_p are illustrated in figure 9.3. Figure 9.3 shows that the L_p decreases when the recording nodes are further away from the cylinder wall except for the strong resonance modes.

It can be concluded that the L_p within the point load excited unstiffened test cylinder in the considered frequency range is dominated by the coupled structural-acoustic natural frequencies.

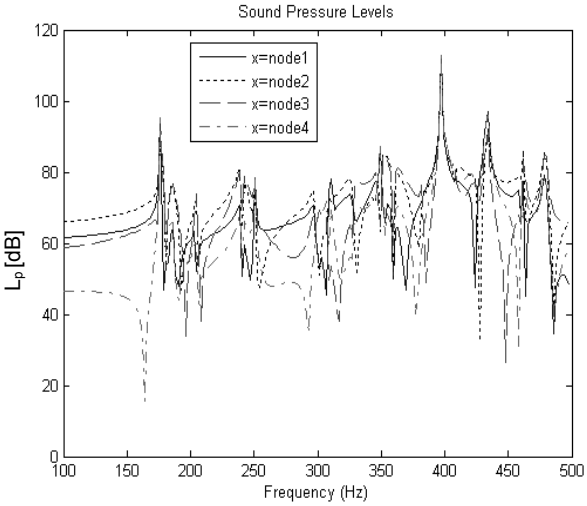

Figure 9.2: *Numerically determined sound pressure levels at node 1, 2, 3 and 4 for the non-stiffened cylinder exited by a concentrated point load. The excitation and recording nodes are defined in figure 9.1. (See also colour section).*

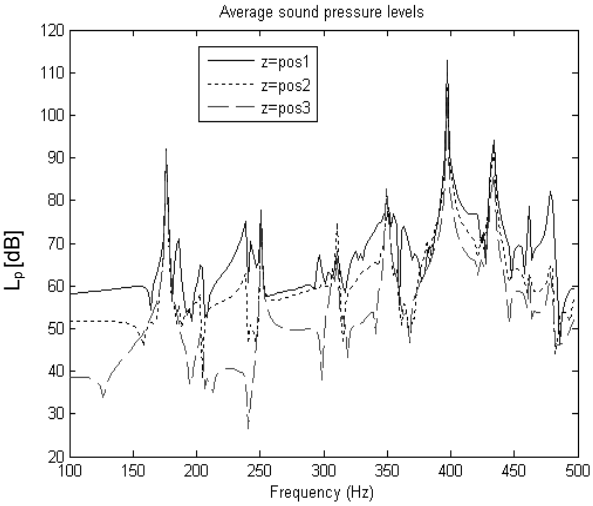

Figure 9.3: *The averaged sound pressure levels at three z-positions for the non-stiffened cylinder exited by a concentrated point load. The L_p are averaged over the x-positions. The excitation and recording nodes are defined in figure 9.1. (See also colour section).*

The cylinder stiffened with 6 stringers

The calculated sound pressure levels for the cylinder with 6 stringers are shown in figure 9.4. The average L_p for the different radial z-positions are given in figure 9.5. From figure 9.4 and 9.5 it can be seen that also for the cylinder with 6 stringers the first and third acoustic modes are the most dominant. (The first acoustic mode occurs at 176 Hz and the third at 399 Hz). Compared to the non-stiffened cylinder fewer resonance modes are recorded in the frequency range of [100-500 Hz]. Also the average sound pressure levels are a little lower comparable to the non-stiffened cylinder. This can be explained by the fact that the stringers suppress (partly) the modes that do not fit six sinusoidal nodes in circumferential direction at the positions of the stringers. Figure 9.5 shows again that the sound pressure levels decrease when measuring further away form the cylinder wall.

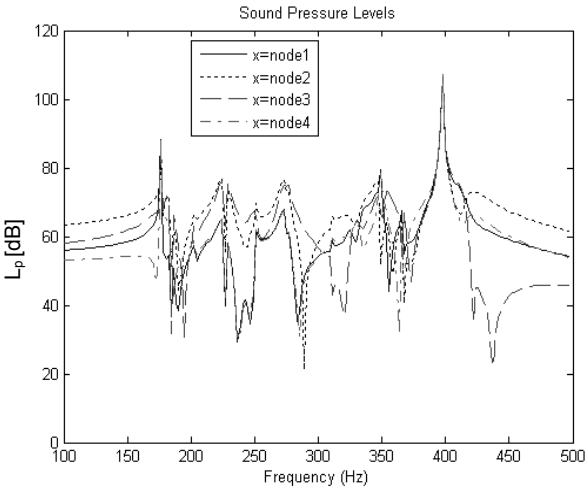

Figure 9.4: *Numerically determined sound pressure levels at node 1, 2, 3 and 4 for the cylinder with 6 stringers exited by a concentrated point load. The excitation and recording nodes are defined in figure 9.1. (See also colour section).*

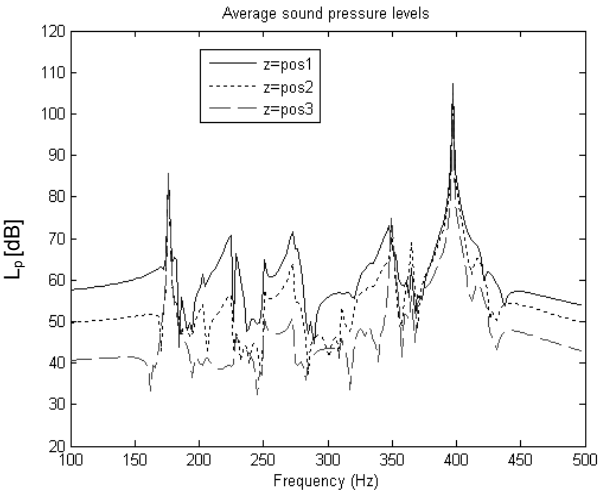

Figure 9.5: *The averaged sound pressure levels at three z-positions for the cylinder with 6 stringers exited by a concentrated point load. The SPL are averaged over the x-positions. The excitation and recording nodes are defined in figure 9.1. (See also colour section).*

The cylinder stiffened with 12 stringers

The calculated sound pressure levels for the cylinder with 12 stringers are illustrated in figure 9.6 and 9.7. Again the first and third acoustic modes at 176 Hz and 399Hz can be recognized. Compared to the non-stiffened and the cylinder with 6 stringers again fewer resonance modes were recorded in the considered frequency range [100-500 Hz], which again also can be seen in table 9.1. Compared to the non-stiffened and the cylinder with 6 stringers the overall sound pressure levels for the cylinder with 12 stringers are a somewhat higher.

The cylinder stiffened with 12 stringers and 2 frames

The calculated sound pressure levels for the cylinder with 12 stringers and 2 frames are shown in figure 9.8 and 9.9. It should be noted that the position of the recording nodes is slightly different from the other three cylinders. Recording nodes 5, 6, 7 and 8 are positioned somewhat more to the center of the cylinder compared to nodes 1, 2, 3 and 4 of the other three cylinders. The recording nodes were illustrated in figure 9.1. By comparing the L_p with that for the other three cylinders it is seen that it is considerable lower. This can be explained by the fact that the two frames suppress the degree of freedom of the cylinder skin that much that the excitation is much lower. In this case all four acoustic modes that exist in the considered frequency range can be recognized. (See table H.4 of appendix H). The first structural induced modes were expected to occur around 479 Hz. (See table H.1 of appendix H). Apparently these structural modes are weak and do not cause resonance of the pore pressure at the recording nodes.

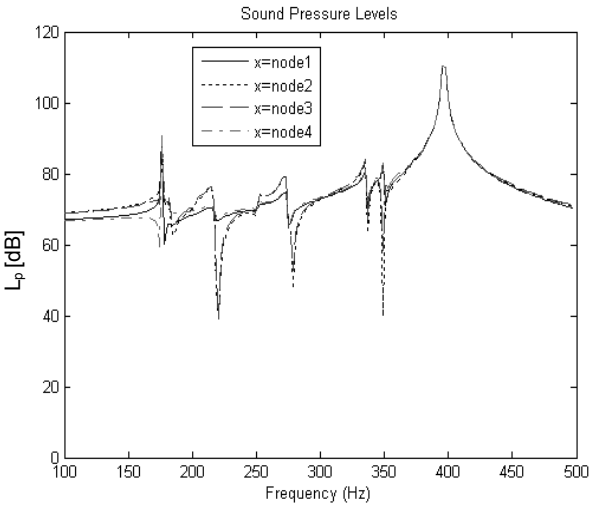

Figure 9.6: *Numerically determined sound pressure levels at node 1, 2, 3 and 4 for the cylinder with 12 stringers exited by a concentrated point load of 1N at node 108. The excitation and recording nodes are defined in figure 9.1. (See also colour section).*

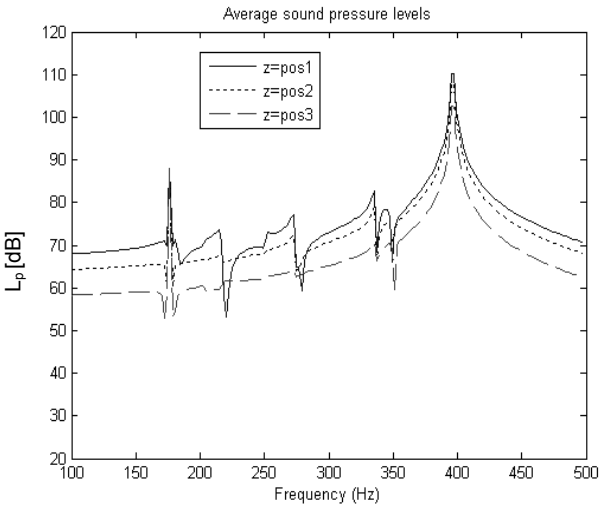

Figure 9.7: *The averaged sound pressure levels at three z-positions for the cylinder with 12 stringers exited by a concentrated point load of 1N at node 108. The L_p are averaged over the x-positions. The x- and z-positions of the recording nodes and the excitation node are defined in figure 9.1. (See also colour section).*

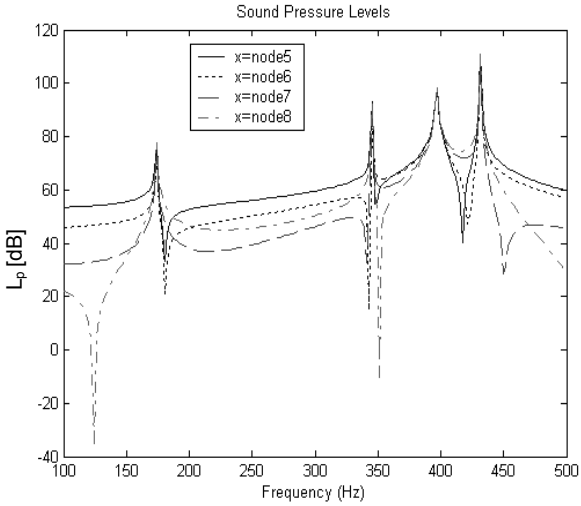

Figure 9.8: *Numerically determined sound pressure levels at node 5, 6, 7 and 8 for the cylinder with 12 stringers and 2 frames exited by a concentrated point load of 1N at node 108. The excitation and recording nodes are defined in figure 9.1. (See also colour section).*

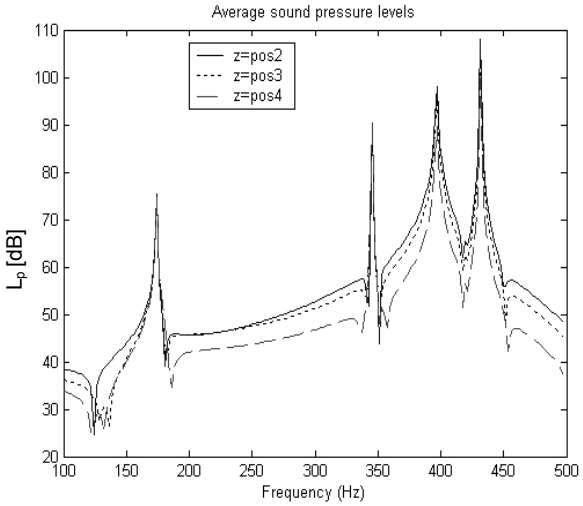

Figure 9.9: *The averaged sound pressure levels at three z-positions for the cylinder with 12 stringers and 2 frames exited by a concentrated point load of 1N at node 108. The L_p are averaged over the x-positions. The x- and z-positions of the recording nodes and the excitation node are defined in figure 9.1. (See also colour section).*

9.3 Comparison of the experimental, analytical and numerical results

The experimentally measured sound transmission loss for the non-stiffened cylinder, the cylinders stiffened with 6 and 12 stringers and the cylinder with 12 stringers and 2 frames were presented in figure 8.34 of section 8.5. The ring frequency was identified at 3000 Hz. It is not possible to make a proper comparison between the experimental and numerical results. Several reasons can be identified:

- The numerical FEM model does not have a correct representation of the absorption inside the cylinder and of the reflection influences on outside microphones.
- The edges of the cylinder FEM model are simple supported while for the real test cylinder the boundary conditions appear to be a mixture of a simply supported and a clamped boundary condition.
- The FEM model is excited by a point force while the cylinders in the experiments were excited by an acoustic field.
- The FEM analysis only determines results up to 500 Hz, which is only a small region of the tested frequency range.

Because of these modelling limitations it is suggested that the numerical acoustic module of the DEE is only used to compare results with identical model definitions.

The numerically determined average sound pressure levels for the four test cylinders over the frequency range of 0 till 500 Hz are presented in figure 9.10.

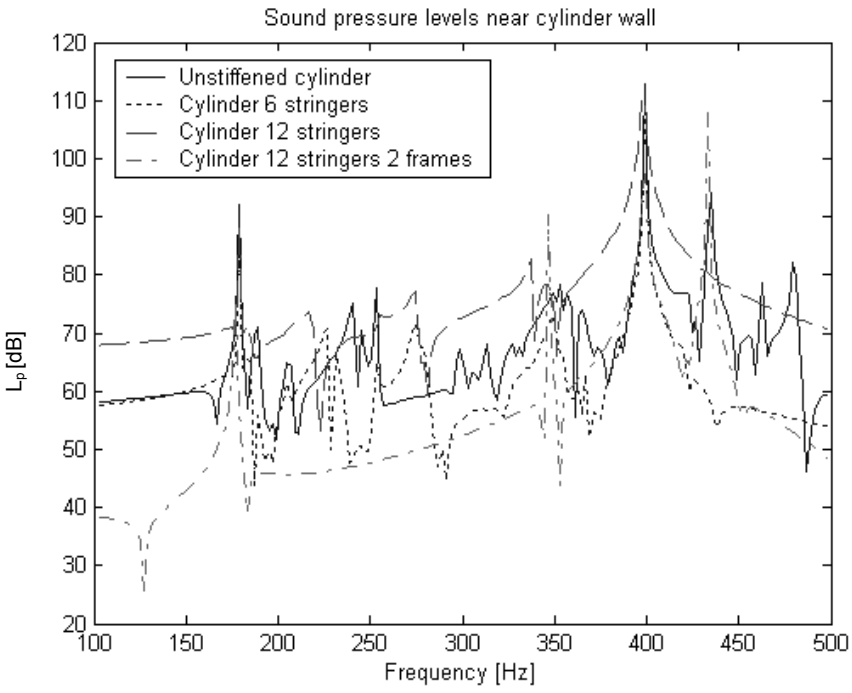

Figure 9.10: *Comparison of the numerically determined sound pressure levels in the frequency range of [100-500 Hz] for the non-stiffened cylinder and the cylinders stiffened with 6 and 12 stringers and the cylinder stiffened with 12 stringers and 2 frames. (See also colour section).*

For all four cylinders the first (176 Hz) and third (399 Hz) acoustic modes can be recognized in figure 9.10. Furthermore it can be seen that in the considered frequency range the sound pressure levels for the cylinder with 12 stringers are the highest, followed by the non-stiffened cylinder and the cylinder with 6 stringers. The cylinder with 12 stringers and 2 frames shows the lowest sound pressure levels. However for this cylinder it should be noted that the position of the recording nodes is slightly different from the other cylinders. (The positions of the recording nodes are given in figure 9.1).

In general it can be carefully concluded that stiffening an aluminium cylinder increases the sound transmission loss below the ring frequency but decreases the sound transmission loss for the higher frequencies. The sound transmission loss below the ring frequency is mainly dominated by the coupled structural-acoustic natural frequencies. Especially the acoustic natural frequencies will have an impact on the TL.

This leads to the recommendation to use the literature equation TL module as the default TL module in the DEE because this module is very fast and gives a good impression of the TL over a large frequency range. It is difficult to represent reality with numerical models. Therefore it is suggested to use the numerical TL tool only to compare solutions that have identical numerical model definitions.

9.4 Reference

[1] ABAQUS Example problem manual, version 6.4.
[2] ABAQUS Theoretical manual, version 6.4.
[3] Fahy, F., Sound and structural vibration, radiation, transmission and response, Academic Press, London, 1989.

10 Design of a stiffened skin fuselage for a mid size civil aircraft

10.1 Introduction

In this chapter the DEE, which was discussed in chapter 6, will be used to perform a multidisciplinary design analysis of a fuselage for an approximately 120 passenger civil aircraft. Only the passenger cabin of the fuselage will be considered. The main dimensions of this fuselage will remain fixed during this analysis and are illustrated in figure 10.1.

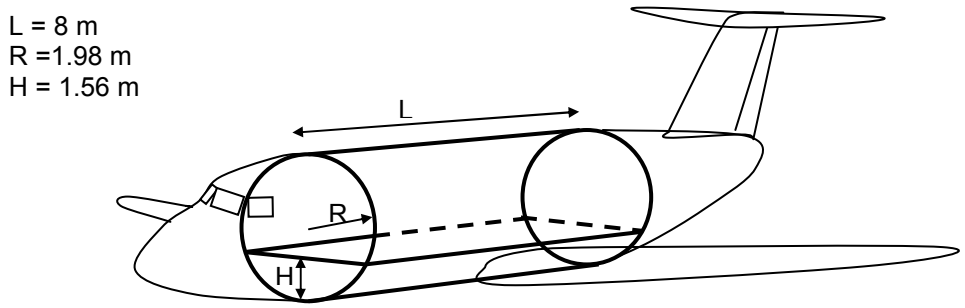

Figure 10.1: *Illustration of the fuselage of medium size civil aircraft.*

To include the floor in the analysis, the DEE has to use two building blocks. This means that for each run the ICAD model generator will be used twice; once to generate the lower fuselage part including the floor and once to generate the upper fuselage part.

The multidisciplinary analysis considers the acoustical and thermal insulation as well as the structural design. The current DEE is capable of considering two different structural concepts. This chapter will focus on the conventional stiffened skin concept. Chapter 11 will discuss a similar design analysis with a sandwich fuselage structure.

The fuselage will be optimised for minimum weight and maximum thermal and acoustical insulation with the constraints that it has to fulfil the strength and stiffness criteria. To validate the multidisciplinary designed fuselage it will be compared to a reference fuselage, which is optimised for minimum structural weight without considering the thermal and acoustic insulation performances.

For the optimisation genetic algorithms (GA) and sequential programming routines (SQP) will be used. Also multi-objective optimisations will be considered.

The remaining of this section is structured as follows: First the model definition of the fuselage is described in section 10.2. Then the FEM models for the structural, thermal and acoustic analysis are discussed in section 10.3. Section 10.4 describes the applied load cases and boundary conditions and in section 10.5 the design variables are chosen, the constraints are determined and the objective functions are defined. Section 10.6 presents the resultant response surfaces of the analysis with the DEE. Section 10.7 discusses the different optimisations that are performed and section 10.8 discusses the results of multi-objective optimisations. In section 10.9 a second optimisation step is performed by zooming in on the design space around the optimum solutions found in section 10.7. Section 10.10 discusses the final results.

10.2 Model definition of the fuselage section of a medium size civil aircraft

The model of the fuselage with the stiffened skin concept consists out of an aluminium skin stiffened with circumferential aluminium C-frames and longitudinal aluminium z-stringers. The floor of the passenger cabin is constructed as a sandwich. The model also includes interior panels and insulation blankets that cover the whole skin of the fuselage. (This means that the passenger cabin and the cargo-bay have similar interior panels and insulation blankets). Figure 10.2 gives an illustration of the conventional stiffened fuselage model concept with some detailed cross sections of the interior and floor panels as well as the C-frames and Z-stringers.

Dimensions

The considered fuselage section has a length of 8 meters. The radius of the fuselage section and the floor position are chosen similar to the fuselage of an A320 aircraft. The circular cross section is assumed to remain constant for the whole fuselage section. The radius is set to 1.98 m and the floor is positioned at a height of 1.56m measured from the bottom side of the fuselage.

Reference dimensions for details like the stringer, frame, insulation blankets, interior panels and floor panels are chosen fictively and given in table 10.1. The thickness of the insulation blankets is identical to the height of the frames.

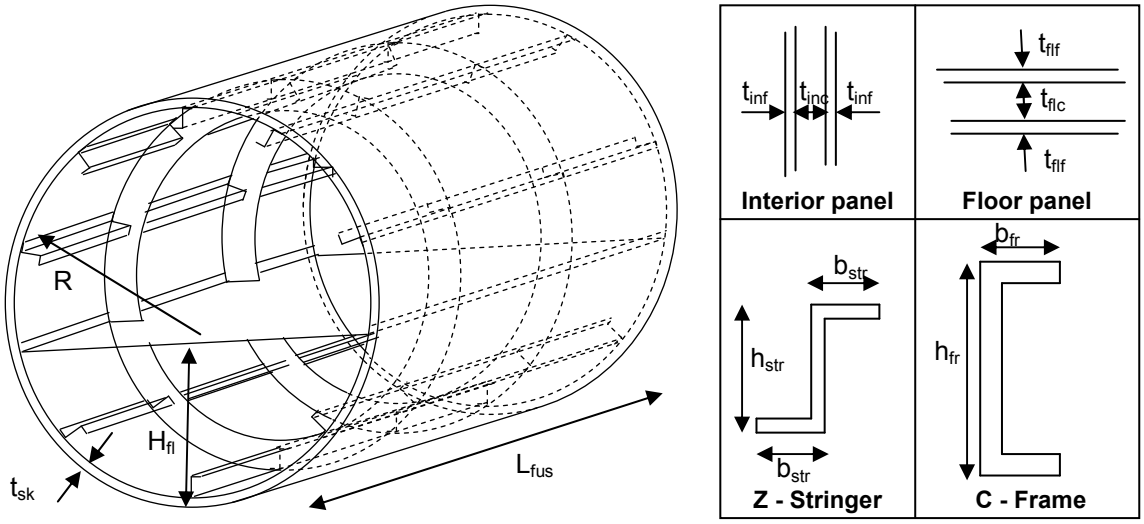

Figure 10.2: *Illustration of the conventional stiffened skin fuselage concept with detailed cross sections.*

Table 10.1*: Basic dimensions of the conventional stiffened A320 like fuselage*

Radius (R)	1.98 m	Stringer height (h_{str})	35 mm
Fuselage section length (L_{fus})	8.0 m	Stringer width (b_{str})	20 mm
Skin thickness (t_{sk})	1 mm	Stringer thickness (t_{str})	1 mm
Floor height (H_{Fl})	1.56 m	Interior facing thickness (t_{inf})	0.5 mm
Floor facing thickness (t_{flf})	0.8 mm	Interior core thickness (t_{inc})	4 mm
Floor core thickness (t_{flc})	8 mm	Nr of stringers top ($n_{str\ top}$)	8
Frame height (h_{fr})	120 mm	Nr of stringers bottom ($n_{str\ bot}$)	6
Frame width (b_{fr})	50 mm	Nr of frames (n_{fr})	15
Frame thickness (t_{fr})	1.2 mm		

Material properties

The relevant material properties of the different parts in the fuselage section model are given in table 10.2. The skin, frames and stringers are made of aluminium. The floor and interior panels are constructed as sandwich panels. In this example typical aircraft materials from HEXCEL Composites [3] are chosen; Fibrelam® type 6100 Grade 1 for the floor panels and Fibrelam® type 1100 Grade 2 for the interior panels. Fibrelam® type 6100 Grade 1 consists out of carbon phenolic facings and aramid phenolic honeycomb with a density of 139 kg/m^3 and a cell size of 1/8". Fibrelam® type 1100 Grade 2 has an aramid phenolic honeycomb core with a density of 64 kg/m^3 and a cell size of 1/8" and glass phenolic facings.

Table 10.2: *Chosen material properties. References: Zaal [1], Beranek [2], Hexcel composites [3], ABAQUS example manual [4]*

Aluminium [1]: (skin, frames and stringers)		**Glass phenolic [3]:** (Interior panel facings)	
Modulus of elasticity	68.9 GPa	Modulus of elasticity	4 GPa
Density	2710 kg/m^3	Density	2550 kg/m^3
Poisson ratio	0.3	Poisson ratio	0.3
Thermal conductivity	140 W/mK	Thermal conductivity	0.24 W/mK
Specific heat	900 J/kgK	Specific heat	1110 J/kgK
Allowable material stress	210 MPa	Allowable material stress	100 MPa
Allowable hoop stress	85 MPa		
Carbon phenolic [3]: (Floor facings)		**Air [4]:**	
Modulus of elasticity	18 GPa	Bulk modulus	144120 MPa
Density	1800 kg/m^3	Density	1.225 kg/m^3
Poisson ratio	0.3		
Thermal conductivity	1 W/mK		
Specific heat	600 J/kgK		
Allowable material stress	150 MPa		
Fibrelam® 6100 Aramid phenolic honeycomb HRH-10-1/8-9.0 [3] (Floor core)		**Fibrelam® 1100 Aramid phenolic honeycomb HRH-10-1/8-4.0 [3]** (Interior core)	
Modulus of elasticity	620 MPa	Modulus of elasticity	193 MPa
Shear modulus L-direction	120 MPa	Shear modulus L-direction	59 MPa
Shear modulus W-direction	76 MPa	Shear modulus W-direction	32 MPa
Density	139 kg/m^3	Density	64 kg/m^3
Thermal conductivity	0.0675 W/mK	Thermal conductivity	0.0675 W/mK
Specific heat	1300 J/kgK	Specific heat	1300 J/kgK

Glass fibre blanket [2]: (Insulation blankets)

Bulk modulus	118300 N/m^2
Density	9.6 kg/m^3
Thermal conductivity	0.036 W/mK
Specific heat	1005 J/kgK
Volumetric drag	1

Frequency dependent properties:

Frequency [Hz]	**20**	**28**	**40**	**56**	**80**	**116**	**160**	**224**	**320**	**447**	**640**
Sound attenuation [dB]	2	3	4	6	8	10	15	23	35	55	90
Blanket impedance	1190	1189	1188	1186	1184	1181	1176	1170	1130	1080	1000
Blanket wave length	2.25	2.00	1.75	1.5	1.25	1.03	0.81	0.60	0.45	0.33	0.024
Frequency [Hz]	**891**	**1280**	**1778**	**2560**	**3548**	**5120**	**7079**	**10240**	**14125**	**20480**	
Sound attenuation [dB]	140	210	285	350	400	450	490	520	545	560	
Blanket impedance	900	800	710	630	560	520	510	506	505	504	
Blanket wave length	0.17	0.13	0.10	0.08	0.06	0.05	0.045	0.043	0.041	0.039	

Both the floor and interior panels are fabricated with phenolic resin instead of epoxy because of its excellent low fire, smoke and toxic gas emission features as well as good corrosion and impact resistance properties. Because it is difficult to find a complete set of material properties for insulation blankets, the material properties of the glass fibre blankets as mentioned by Beranek [2] are used.

10.3 Fem models of the fuselage section

As discussed in chapter 6 the DEE generates three ABAQUS FEM models; one for the structural analysis, one for the thermal insulation analysis and one for the acoustical insulation analysis. Next the characteristics of the three FEM models are shortly described:

Structural FEM model

The structural FEM model only contains the structural parts of the fuselage section. The structural parts are the skin, frames, stringers and the floor. The skin, floor and frame web are modelled with ABAQUS specific 'S4R' shell elements. The floor has a sandwich structure. ABAQUS has the possibility to assign different layer properties to shell elements, which makes it possible to model also the sandwich floor with shell elements.

The stringers are modelled with three-dimensional ABAQUS specific 'B31' beam elements. ABAQUS has the possibility to assign the exact cross sectional properties to the beam elements by specifying the exact shape of the cross-section. Also the frame flanges are modelled with 'B31' beam elements only with a circular cross section. An example of a structural FEM model is given in figure 10.3A

Thermal insulation FEM model

To determine the characteristics of the thermal insulation of the fuselage wall only a part of the fuselage wall needs to be considered. The part of the fuselage wall that is considered for the thermal insulation analysis is the right upper part of the passenger cabin as is illustrated in figure 10.3B. The fuselage part includes the skin (single skin or sandwich) and the frame webs as well as the insulation materials like the insulation blankets and the interior panels. Because within ABAQUS the heat transfer analysis can only be performed on models that consist out of diffusive shell and continuum elements, the stringers and frame flanges which are modelled with beam elements are ignored. Also the influence of the floor is neglected. (It is assumed that the floor is isolated from the fuselage wall in such a way that no heat bridge is created). The frame webs connect the interior panels to the fuselage skin, which means that the frame webs do create a heat bridge. This heat bridge will decrease the insulating effect of the insulation blankets.

To be able to investigate variations in skin thickness, the skin is modelled with 8 node three-dimensional ABAQUS specific 'C3D8' solid elements. Also the interior panel and the insulation blankets are modelled with 'C3D8' solid elements where each layer of the sandwich interior is represented by a separate layer of solid elements. An example of a thermal insulation FEM model is given in figure 10.3B.

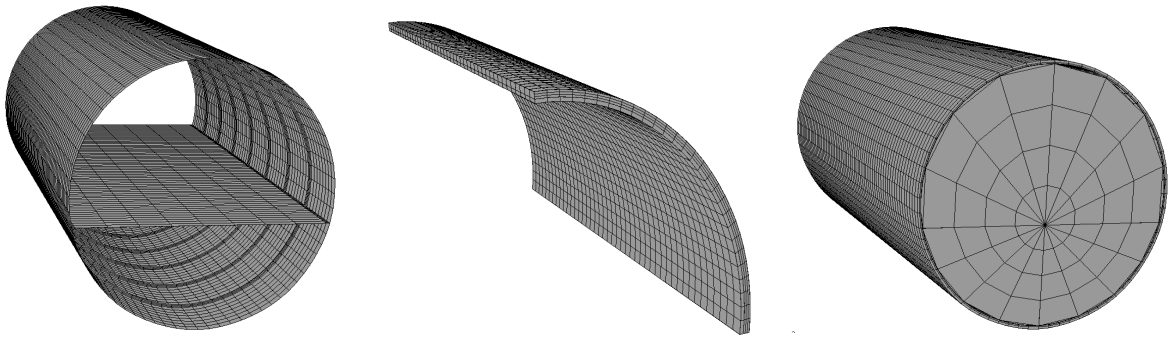

A) Example of a FEM model for the structural analysis

B) Example of a FEM model for the thermal analysis

C) Example of a FEM model for the acoustical analysis

Figure 10.3*: Illustration of the ABAQUS FEM models for the structural, thermal insulation and acoustical insulation analysis of the A320 like fuselage.*

Acoustical insulation FEM model

The acoustical insulation FEM model is the most complete FEM model. Like for the thermal FEM model it includes 'C3D8' solid elements for the skin, interior panel and insulation blankets. Also the 'B31' beam elements for the frame flanges and stringers and the 'S4R' shell elements for the floor and frame webs that were used in the structural FEM model are included. Furthermore the air inside the fuselage section is included. The air is modelled with 8 and 6 node three-dimensional acoustic elements ('AC3D8' and 'AC3D6'). An example of an acoustical insulation FEM model is given in figure 10.3C. However it is noted that in this analysis only the literature equation module will be used for the acoustic analysis. The acoustical insulation FEM model would be used only for a more detailed analysis of the final optimum solution.

10.4 Definition of load cases and boundary conditions

Because of the different nature of the three analysis types a different set of load case and boundary conditions has to be defined for each FEM model. First the load case definition is discussed for all three FEM models followed by the boundary conditions:

Load case definitions

1.) Load definition for the structural analysis

The structural load case consists out of a bending moment M, an internal pressure p and a shear load Q. Figure 10.4 gives an illustration of the definition of the load case.

The internal pressure p is applied as a distributed pressure on the inside surface of the whole fuselage skin. This means that both the passenger cabin and the cargo compartment are pressurised resulting in zero pressure difference on the floor. The fuselage section model does not include pressure bulkheads. To simulate pressure bulkheads axial forces are applied on the skin, stringers and floor at the end cross-sections of the fuselage model.

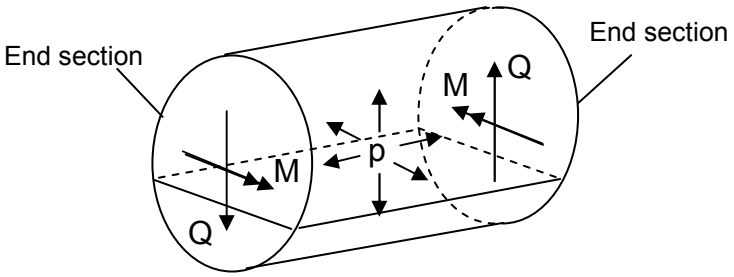

Figure 10.4: *Illustration of the structural load case definition on the fuselage section model.*

Table 10.3: *Structural load case definition*

p	55000 N/m^2
M	4400000 Nm
Q	600000 N

Also the bending moment is introduced in the skin, stringers and floor by axial forces applied at the end sections of the fuselage model.

The shear load is introduced in the skin by forces applied in circumferential direction of the end sections of the fuselage model.

A more detailed description on how the loads are introduced in the FEM elements is given in chapter 6.

2.) Definition of the load case for the thermal insulation analysis
A constant heat flux of 100 Watt/m^2 is applied on the inside surface of the interior panel of the fuselage wall of the passenger cabin. The resultant temperature difference over the fuselage wall will be the measure for thermal insulation.

3.) Definition of the load case for the acoustic insulation analysis
In this analysis the TL of the fuselage wall, for noise at field incidence, is determined using the literature equations discussed in chapter 3

Boundary conditions

1.) Boundary conditions applied to the FEM model for the structural analysis
For a static structural analysis the free rigid body modes have to be fixed. It is assumed that at the end sections of the fuselage model a frame is positioned. Because the frames have a rather high in-plane stiffness the end sections are assumed to remain perfectly round. This means that the in-plane degrees of freedom of the end sections are restraint. The longitudinal degree of freedom of the frames is not restrained. Because the load case is anti-symmetric with respect to the middle section of the fuselage model the longitudinal degree of freedom is restraint in the middle section. This is illustrated in figure 10.5. The rotational degrees of freedom are restraint for the complete model.

2.) Boundary conditions applied to the FEM model for the thermal insulation analysis
For the uncoupled heat transfer analysis, (no coupling between temperature and stresses), where only heat conduction is considered only a starting temperature is required.

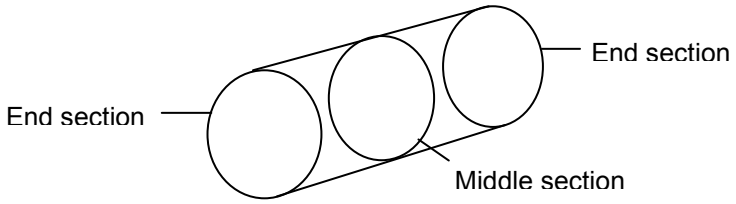

Figure 10.5: *Illustration of the middle and end sections.*

3.) Boundary conditions applied to the FEM model for the thermal insulation analysis
For the uncoupled heat transfer analysis, (no coupling between temperature and stresses), where only heat conduction is considered only a starting temperature is required.

4.) Boundary conditions applied to the FEM model for the acoustical insulation analysis
For the acoustical insulation analysis identical boundary conditions can be chosen as for the structural analysis.

10.5 Definitions of the design variables, objective function and constraints

The DEE will be used to search for the optimum configuration of the fuselage wall of a medium size civil aircraft with a conventional stiffened skin structure. First a selection of the design variables has to be made. For the optimisation of the structure of the aluminium test cylinder, which was discussed in chapter 7, four design variables were chosen; the skin thickness, the number of frames, the number of stringers and the area of the stringer cross section.

Because the stiffened skin fuselage has a similar structure as the aluminium test cylinder, similar design variables are chosen for the structural optimisation of the fuselage model. To include the thermal and acoustic insulation in the optimisation process, the core thickness of the sandwich interior panel is chosen as fifth design variable. The thickness of the insulation blanket is linked to the interior panel core thickness and the skin thickness by assuming that the total fuselage wall thickness and the interior panel facing thickness remain constant. This is expressed in equation 10.1.

$$t_{tot} = t_{sk} + 2t_{\inf} + t_{inc} + h_{fr} \tag{10.1}$$

Where:

t_{tot}	: thickness of the whole fuselage wall, which is a fixed parameter
t_{sk}	: thickness of the fuselage skin, which is a design variable
t_{inf}	: thickness of the interior panel facings, which is a fixed parameter
t_{inc}	: thickness of the interior panel core, which is a design variable
h_{fr}	: thickness of the insulation blanket, which is equal to the frame height and dependent on the design variables t_{sk} and t_{inc}

In total this gives five design variables:

Table 10.4: *Definition of the five design variables*

t_{sk}	Skin thickness
n_{fr}	Number of frames
n_{str}	Number of stringers
k_{str}	Stringer cross-section area factor
t_{inc}	Interior panel core thickness

The design space

Like discussed in chapter 7, the optimisation will be performed in two steps. As a first step the optimisation is performed on a design space that is chosen large enough to ensure that the optimum feasible solution is captured. With this optimisation step, it can be decided whether or not the design space was chosen correctly and the requirements were realistic. In a second step, the design space is reduced to a smaller design space around the optimum solution found in the first optimisation step. This results in more solutions near the optimum solution, which increases the accuracy of the optimum.

The mechanical analysis of the stiffened skin fuselage structure, which was discussed in chapter 5, is used to determine the design space for the structural

design variables. The dimensions of the optimised stiffened skin structure as discussed in chapter 5, are shown in table 10.5. Also the corresponding design variables for the current design, if it would have similar dimensions as the fuselage discussed in chapter 5, are given in table 10.5.

Table 10.5: *Dimensions of the optimal stiffened skin fuselage determined with the mechanical analysis described in chapter 5 and the corresponding design variables for the current design.*

Dimensions of the fuselage structure as discussed in chapter 5			Corresponding design variables for the current design	
Skin thickness	1.28 mm	→	t_{sk}	1.28 mm
Frame pitch	450 mm	→	n_{fr}	18
Stringer pitch	65 mm	→	n_{str}	95*
Stringer area	36 mm^2	→	k_{str}	0.5

Note: The design variable n_{str} indicates the number of stringers in a half model of the fuselage.*

The minimum skin thickness of the fuselage described in chapter 5 was limited by the maximum allowable Hoop stress. This resulted in a minimum skin thickness of 1.28 mm. It should be noted that compared to the mechanical analysis described in chapter 5, now a floor is included. This can result in a small influence on the Hoop stress. Because the current analysis has an identical internal pressure, it is assumed as a reasonable first guess that the optimum skin thickness will be found within the range of 1 and 2 mm. Compared to the structural optimal solution it is expected that the multidisciplinary solution will have larger frame and stringer pitches. As a result, to maintain the required stiffness, a larger stringer cross-section area will be required. Commonly the total fuselage wall thickness of a medium size civil aircraft is around 100 mm. Characteristic dimensions for interior panels are: a facing thickness of around 0.5 mm and a core thickness of around 4 mm. The interior panel core thickness of 4 mm is assumed to be the minimum thickness. The optimisation will show whether or not it is useful to transfer insulation blanket thickness to the interior panel core thickness. Therefore the range of the interior panel core thickness is defined between 4 and 40 mm. The total fuselage wall thickness and the interior panel facing thickness are set at 100 and 0.5 mm respectively. This discussion results in a chosen design space as mentioned in table 10.6.

Table 10.6: *Definition of the design space*

t_{sk}	1 - 2 mm
n_{fr}	8, 9, 10, 11, 12, 14, 16, 18, 20, 22, 25
n_{str}	20, 30, 40, 50, 60, 70, 80, 90, 100
k_{str}	0.5 - 1.5
t_{inc}	4 - 40 mm

The definition of the design space for the second step will be discussed after the first analysis and optimisation step has been completed.

Objective functions

For the structural optimisation the weight of the fuselage structure is assigned as objective function. This objective function can be expressed as equation 10.2:

$$W_{fus\_struc} = \rho_{skin} 2\pi RLt_{skin} + \rho_{stringer} nA_{stringer} f_{stringer} + \rho_{frame} m2\pi RA_{frame} \quad (10.2)$$

Where:

Objective:

W_{struc} : The fuselage structure weight

Fixed parameters:

L : Fuselage section length

R : Radius of the fuselage section (Assumed constant over fuselage section length)

A_{fr} : Frame cross-section area

A_{str} : Stringer cross-section area

ρ_{xxx} : Density of respectively the skin, stringers and frames

Design variables:

t_{sk} : Skin thickness

k_{str} : Multiplication factor for the stringer cross-section area

n : Number of stringers

m : Number of frames

For the multidisciplinary optimisation (structural including the acoustic and thermal insulation) also the total fuselage section weight is assigned as objective function, except in this case the weight of the insulation materials is included. This objective function is expressed by equation 10.3:

$$W_{fus} = \rho_{sk} 2\pi RL_{fus} t_{sk} + \rho_{str} n_{str} A_{str} k_{str} + \rho_{fr} n_{fr} 2\pi RA_{fr} + 2\pi RL_{fus} \rho_{bl} h_{fr} + 2\pi RL_{fus} (\rho_{\inf} 2t_{\inf} + \rho_{inc} t_{inc}) \quad (10.3)$$

Where:

Objective:

W_{tot} : The total fuselage weight

Fixed parameters:

L_{fus} : Fuselage section length

R : Radius of the fuselage section (Assumed constant over fuselage section length)

A_{fr} : Frame cross-section area

A_{str} : Stringer cross-section area

ρ_{xxx} : Density of respectively the skin, stringers, frames, blanket, interior panel facing and core

t_{inf} : Interior panel facing thickness

h_{fr} : Frame height, which is equal to the insulation blanket thickness. The frame height is indirect dependent on interior panel core thickness and skin thickness

Design variables:

t_{sk}	: Skin thickness
k_{str}	: Multiplication factor for the stringer cross-section area
t_{core}	: Interior panel core thickness
n_{str}	: Number of stringers
n_{fr}	: Number of frames

Secondary objectives will be the temperature difference between the inside surface of the interior panels and the outside surface of the fuselage skin and the sound transmission loss in the low, middle and high frequency range.

Constraints

There are two types of constraints in this analysis. The first type of constraint restricts the geometrical degrees of freedom of the fuselage model and the second type defines the performance requirements.

There are two geometric constraints applied on the fuselage model:

- The first geometric constraint is the restriction that the total fuselage wall thickness has to remain constant at 100 mm with the assumption that the facing thickness of the interior panels remains fixed at 0.5 mm. This restriction is made to keep the number of design variables at five. In principle there is no restriction to the number of design variables other than the increase of required size of the DOE and therefore the computation time.
- The second geometric constraint keeps the stringer pitch constant in the upper and lower part of the fuselage section. Because of the existence of the floor the stringer pitch can be different for the upper and lower part of the fuselage. The geometric constraint will always divide the number of stringers in such a way that the constant stringer pitches of the upper and lower part match each other as much as possible.

Both these geometric constraints are implemented in a Matlab routine, that translates the set of design variables into the input parameters of the DEE.

The constraints of the second type are formulated by the performance requirements, which the fuselage section has to fulfil. The performance requirements are divided in structural and thermal- and acoustical insulation requirements.

- The structural requirements are:
  - 1) $R_{skt} < 1$: The tensile stress in the skin has to be smaller than the allowable material stress
  - 2) $R_{skb} < 1$: The combination of the compressive and shear stress has to be smaller than the combination of the allowable compressive and shear buckling stress.
  - 3) $R_{strt} < 1$: The tensile stress in the stringers has to be smaller than the allowable material stress
  - 4) $R_{strb} < 1$: The compressive stress in the stringers has to be smaller that the Euler buckling stress
  - 5) $R_{Hoop} < 1$: The tensile stress in circumferential direction has to be smaller than the maximum allowable hoop stress

- The thermal insulation requirement can be described as the required minimum temperature difference over the fuselage wall for a certain applied heat flux.

$$\theta = T_{inisde} - T_{outside} > T_{\min} \tag{10.4}$$

- The acoustical insulation requirement can be described as the required minimum overall sound transmission losses for three frequency ranges [0-500Hz], [500-5000Hz] and [5000-20000Hz].

$$TLHF_{0-500} > TLHF_{0-500\min} \qquad TLHF_{500-5k} > TLHF_{500-5k\min} \qquad TLHF_{5k-20k} > TLHF_{5k-20kin} \tag{10.5}$$

It should be noted that in this analysis only the literature equation module to determine the TL is used to save computation time.

Note: The statistical analysis method ANOVA (Analysis Of Variance) Miller [5]; Montgomery [6] is a widely spread tool for analysing experimental data from carefully designed experiments. The usual objective is to find out which factors contribute most or not at all. This method is a useful analysis method, which would be perfect for the considered optimisation cases. However this method was not familiar to the author at the time of research and therefore was not applied. In this research the correlation between the design variables are qualitatively evaluated. Future analysis using the developed DEE could well profit from the ANOVA analysis method.

10.6 Results of the DEE

So far the design space, objective function and constraints are determined. The next step is to determine the response surfaces for the objective functions and the structural, acoustic and thermal insulation requirements. To achieve this with a least amount of DEE runs a design of experiments (DOE) is performed.

The DOE is performed with the Latin hypercube routine of the genetic optimisation program G_OPT developed by Lanzi [7]. (The DOE is generated by using the max-min criteria option of the G_OPT program). For the first optimisation step a set of 100 data points are generated, which are given in table I.1 of Appendix I. Also the evaluations of the objective functions and the structural, acoustical and thermal requirements are given in table I.1. The evaluations given in table I.1 are used to generate the response surfaces shown in appendix I.2. In the following section each of these response surfaces will be discussed.

Discussion of the response surfaces

1) *R skin tensile stress*: Figures I.2.1A, B and C show response surfaces for R_{skt}. From these figures can be seen that R_{skt} decreases with increasing skin thickness and increasing number of stringers and increasing cross section area of the stringers. The number of frames does not have much influence on R_{skt}. These results show the same tendency as the structural analysis presented in chapter 5.

2) *R skin buckling stress*: When all data points are considered to determine the response surfaces for the skin buckling stress a maximum error of 65% was found. By excluding data points for which $R_{skb} > 3$ the maximum response surface error decreased to 3.4%. (See figure I.2.2). This exclusion leaves only 47 out of the 100 data points but results in a more accurate response surface for which $R < 3$. The exclusion of data points can be justified because the design space for which R_{skb} is larger than 3 will not be of interest for the optimisation.
   Figure I.2.2 illustrates the response surfaces for R_{skb} based on 47 data points. Like for the R_{skt}, R_{skb} decreases with increasing skin thickness and stringer cross-section area and decreasing stringer pitch. For skin buckling the number of frames is not of significance. This will be true as long as the frame pitch is larger than the stringer pitch.

3) *R stringer tensile stress:* The response surfaces for the R_{strt} are given in figure I.2.3. These response surfaces show similar tendencies as the R_{skt} and R_{skb}.

4) *R stringer buckling stress:* In creating the response surface for R_{strt} a maximum error of 55% was found. By excluding data points with R_{strb} larger than 2 the maximum error was reduced to 26.2%. This remaining large error can be explained by the fact that the maximum compressive stresses in the stringers are found near the fuselage edge sections. The large stresses in the stringers near the edge sections are introduced by the applied boundary conditions. To exclude the effect of the applied boundary conditions, a region of 15 FEM elements counted from the fuselage edge sections is excluded from the area of which the stresses are extracted for the structural analysis. This is illustrated in figure 10.6. In average, the fuselage FEM model had 80 FEM elements in length direction. However, because of the changing number of frames the number of FEM elements can also change somewhat. This will result in a small variation in the position of the boundary line of the 15 FEM elements zone. When the maximum stresses occur on this boundary line, the shifting of this boundary line will introduce some inaccuracy in the response surfaces. However for a constant number of frames, this inaccuracy should disappear.

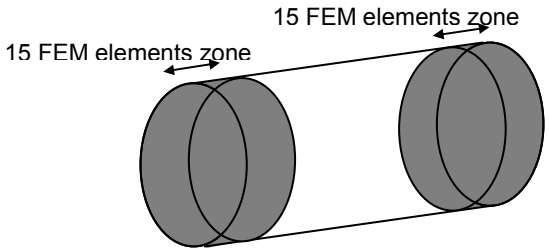

Figure 10.6: *Illustration of the 15 FEM elements zone that is excluded in determining the R_{strb} to exclude the influence of the applied boundary conditions on the fuselage section edges.*

The resultant response surfaces are illustrated in figure I.2.4. They show that the R_{strb} is only slightly dependent on the skin thickness. The frame and stringer pitch and the stringer cross section area are more important parameters for the stringer buckling criteria. This corresponds with the Euler buckling theory.

5) R Hoop stress: Figure I.2.5 shows two response surfaces for the Hoop stress criteria. It can be concluded that the skin thickness and the number of frames are the two most important parameters.

6) Thermal insulation θ: The resultant response surfaces for the thermal insulation are illustrated in figure I.2.6. Because the FEM model for the heat transfer analysis does not take any stringers into account, the response surfaces as function of the number of stringers and the stringer factor are of no physical meaning. It is noted that the thermal insulation increases with decreasing number of frames and interior panel core thickness and increasing skin thickness.

7) Sound transmission loss in the low frequency range [0-500Hz]: The response surfaces for the sound transmission loss in the low frequency range represented as TLHF1 are shown in figure I.2.7. It is noticed that the maximum error in creating these response surfaces is relatively small (A maximum error of 1.9% is found). It can be seen from figure I.2.7 that the sound transmission loss in the low frequency range has a dependency on all design parameters. It should be noted that in the low frequency range an increasing number of stringers and a decreasing number of frames is favourable.

8) Sound transmission loss in the middle frequency range [500-5000Hz]: The response surfaces for the sound transmission loss in the middle frequency range represented as TLHF2 are illustrated in figure I.2.8. From these response surfaces can be concluded that the sound transmission loss in the middle frequency range is dominated by the thickness of the insulation blankets. It should be noted that for the middle frequency range a decreasing number of stringers is favourable. Also an increase of the skin thickness will have a positive influence on the sound transmission loss as is expected from the Mass law.

9) Sound transmission loss in the high frequency range [5000-20000Hz]: The response surfaces for the sound transmission loss in the high frequency range represented as TLHF3 are shown in figure I.2.9. It is noted that the TLHF3 varies between 110 and 125 dB while the maximum response surface error is around 9.4%. This makes these response surfaces somewhat unreliable. The large error is created by the existence of the coincidence frequency in this frequency range.

10) Structural fuselage section weight: Figure I.2.10 shows the response surfaces of the structural fuselage section weight. This weight does not include the weight of the interior panel and the insulation blankets. Because the weight is a straightforward function of the design parameters, these response surfaces are relatively accurate.

11) Total fuselage section weight: Figure I.2.11 shows the response surfaces of the complete fuselage section weight, which means that the weight of the interior panels and insulation blankets is added to the structural fuselage weight.

10.7 Optimisation of the fuselage section design

In section 10.6 the response surfaces were determined. These response surfaces can now be used for the optimisation of the fuselage section design. The optimisation is performed with the genetic algorithm option of the G_OPT program developed by Lanzi [7]. To explore the design space for optimum configurations several optimisations with different objective functions are performed. In all cases the structural constraints are taken into account.
The six optimisation cases that are considered are:

1) Minimise the structural weight of the fuselage section for a fixed applied load case, which means that only the structural parts are considered.
2) Minimise the total fuselage section weight for a fixed applied load case including the interior panels and insulation blankets.
3) Maximise the temperature difference between the inside surface of the interior panel and the outside surface of the skin for a fixed applied heat source.
4) Maximise the sound transmission loss in the low frequency range for fixed applied incident noise level.
5) Maximise the sound transmission loss in the middle frequency range for a fixed applied incident noise level.
6) Maximise the sound transmission loss in the high frequency range for a fixed applied incident noise level.

Case 1: Minimise the structural fuselage section weight

Several genetic optimisations are performed with different program settings to determine the minimum structural fuselage section weight taking the structural constraints into account.
The results are presented in table 10.7A. The interior panel is not part of the load carrying structure. Therefore the interior panel core thickness has been fixed to the minimum thickness of 4 mm.

From the optimisation results presented in table 10.7A it can be seen that the minimum structural fuselage section weight lies between 800 and 810 kg. For the four solutions the skin thickness varies between 1.60 and 1.63 mm, the number of frames between 13 and 14, the number of stringers is 90 and the stringer factor varies between 0.51 and 0.58. As a first check the four solutions are re-evaluated using the corresponding parameters as input to the DEE. The results are presented in table 10.8.

It is noted that for all four solutions the skin buckling criterion is violated by 5 to 10 %. Apparently the response surface is not accurate enough to find the optimum fuselage configuration with minimum weight. To find a more accurate solution for the minimum fuselage section weight, a second optimisation step will be performed where is zoomed in on the design space close to the optimum solutions given in table 10.8. This second optimisation step will be discussed in section 10.8.

By performing a sequential programming (SQP) optimisation with the G_OPT program solutions can be found that do not violate any structural constraint. The results of the SQP optimisation are presented in table I.3.1 of appendix I.3. The SQP program is only able to optimise continuous variables. Therefore, the integer variables have to be preset manually. The preset variables are the number of frames, which are preset to 11, 12 or 13, and the number of stringers (preset to 90 or 100). The interior panel core thickness was fixed to 4mm like discussed previously. The

new optimum solutions show a minimum structural weight of 812 kg and a total weight of 1166 kg for a skin thickness of 1.48mm and a stringer factor of 0.66.

Table 10.7: *A) Four optimised solutions for minimum structural fuselage weight determined with the genetic algorithm (GA) option of the G_OPT program using four different program settings. The design variable Interior Core thickness is fixed at 4 mm.*

B) Four optimised solutions for minimum total fuselage section weight using the genetic algorithm (GA) option of G_OPT for four different program settings. In this case all design variables including the Interior Core Thickness are unbound.

A	**Solution 1**	**Solution 2**	**Solution 3**	**Solution 4**
G_opt program settings				
Number of members for each generation	100	100	100	100
Number of generations	200	500	200	500
Cross-over probability	0.75	0.75	0.85	0.85
Mutation probability	0.15	0.15	0.15	0.15
Design variables				
t_{sk}	1.6118	1.6118	1.6039	1.6314
n_{fr}	13	13	14	14
n_{str}	90	90	90	90
k_{str}	0.5118	0.5784	0.5157	0.5118
t_{inc}	4	4	4	4
Final performances:				
R_{Hoop}	0.8484	0.8373	0.8445	0.8333
R_{skt}	0.9266	0.9018	0.9302	0.9194
R_{strt}	0.7917	0.7685	0.7952	0.7864
R_{skb}	1.0251	1.0233	1.0257	0.9714
R_{skt}	1.0109	0.8197	0.8641	0.8824
θ	108.55	108.79	106.40	106.81
TLHF1	38.28	38.30	37.92	37.96
TLHF2	82.63	81.95	81.62	82.04
TLHF3	117.44	117.08	117.51	117.48
W_{tot}	1155.34	1174.42	1162.55	1168.73
Objective function				
W_{struc}	800.45	813.22	805.29	811.90

B	**Solution 1**	**Solution 2**	**Solution 3**	**Solution 4**
G_OPT program settings				
Number of members for each generation	100	100	100	100
Number of generations	200	500	200	500
Cross-over probability	0.75	0.75	0.85	0.85
Mutation probability	0.15	0.15	0.15	0.15
Design variables				
t_{sk}	1.6353	1.6157	1.6588	1.6275
n_{fr}	14	13	10	13
n_{str}	90	90	90	90
k_{str}	0.5157	0.5588	0.7078	0.5078
t_{inc}	7	4	4	5
Final performances				
R_{Hoop}	0.8181	0.8386	0.8274	0.8377
R_{skt}	0.9200	0.9075	0.8336	0.9229
R_{strt}	0.7877	0.7740	0.7045	0.7891
R_{skb}	0.9639	1.0167	0.9751	0.9949
R_{strb}	0.8722	0.8736	0.9074	1.0277
θ	103.63	108.78	116.2	107.65
TLHF1	37.98	38.30	39.58	38.31
TLHF2	80.44	82.21	83.18	82.41
TLHF3	118.11	117.18	116.71	117.62
W_{struc}	813.67	810.26	835.60	803.90
Objective function				
W_{tot}	1185.85	1169.90	1199.17	1163.63

By comparing the solutions from the GA and the SQP optimisations it can be concluded that so far solution 4 of the SQP optimisation is the best solution because it does not violate any structural constraint.

Case 2: Minimise the total fuselage section weight

In this case the total fuselage section weight is chosen to be the objective function. The constraints are similar as for case 1. Except in this case the interior panel core thickness is left unbound to see whether the optimum will move away from the minimum interior panel core thickness of 4 mm.

The results of four GA optimisations with different program settings are given in table 10.7B. It can be seen that the minimum total fuselage weight varies between 1160 and 1200 kg. The skin thickness varies between 1.61 and 1.66 mm, the number of frames between 10 and 14, the stringer factor between 0.50 and 0.70 and the interior panel core thickness between 4 and 7 mm. The optimum number of stringers is found to be 90. Also these four solutions are re-evaluated using the DEE and the results are presented in table 10.9.

Table 10.8: *Re-evaluation of the four solutions found with the GA optimisation for minimum structural fuselage section weight given in table 10.7A.*

Solution nr	t_{sk}	n_{fr}	n_{str}	k_{str}	t_{inc}	R_{Hoop}	R_{skt}	R_{skb}	R_{strt}	R_{strb}	θ	TLHF1	TLHF2	TLHF3	W_{tot}	W_{struc}
A1	1.6118	13	90	0.5118	4	0.8542	0.9313	1.1028	0.7926	1.0508	110.64	38.09	78.22	108.81	1156.9	804.6
A2	1.6118	13	90	0.5784	4	0.8516	0.9053	1.0688	0.7678	0.7741	110.64	38.09	78.22	108.81	1175.6	823.4
A3	1.6039	14	90	0.5157	4	0.7914	0.9208	1.0894	0.7901	0.8843	107.11	37.74	78.01	108.74	1163.5	811.2
A4	1.6314	14	90	0.5118	4	0.7804	0.9101	1.0416	0.7812	0.8895	107.51	37.78	78.17	109.01	1169.8	817.5

Table 10.9: *Re-evaluation of the four solutions found with the GA optimisation for minimum structural fuselage section weight given in table10.7B.*

Solution nr	t_{sk}	n_{fr}	n_{str}	k_{str}	t_{inc}	R_{Hoop}	R_{skt}	R_{skb}	R_{strt}	R_{strb}	θ	TLHF1	TLHF2	TLHF3	W_{tot}	W_{struc}
B1	1.6353	14	90	0.5157	7	0.7800	0.9073	1.0335	0.7786	0.8854	111.2	37.82	78.82	125.29	1185.8	818.0
B2	1.6157	13	90	0.5588	4	0.8506	0.9110	1.0714	0.7734	0.8785	104.6	38.10	78.24	108.85	1171.1	818.9
B3	1.6588	10	90	0.7078	4	0.8591	0.8445	0.9324	0.7086	0.9055	94.7	39.35	78.74	109.17	1201.6	849.4
B4	1.6275	13	90	0.5078	5	0.8481	0.9263	1.0763	0.7885	1.0616	106.4	38.12	78.30	111.07	1164.6	807.1

It can be concluded that the re-evaluated weights correspond quite well to the solutions determined with the response surfaces and that solution B4 gives the lightest configuration. Solution B4 shows similar fuselage section weights as solutions A2 and A4 discussed in the previous case. However the stringer buckling criteria is again violated with 7%.

Another point of attention is the interior panel core thickness. Now a thickness varying between 5 and 7 mm is found, which is somewhat larger than the minimum 4 mm. Because the optimisation is performed for minimum weight and the density of

the interior panel is larger than that of the insulation blankets (and both the interior panel and the insulation blankets do not contribute to the structural performance) it is expected that the minimum total fuselage section weight would also have the minimum interior panel core thickness. The fact that a slightly larger thickness is found for the interior panel core thickness can be explained by an inaccurate definition of the response surfaces with respect to the interior panel core thickness near the optimum solution. This will be verified during the second optimisation step by zooming in on the design space in the area of the optimum solution, which will be discussed in section 10.8.

Case 3: Maximise the temperature difference between the interior panel inside surface and the fuselage skin outside surface

In this case 'θ' is selected as the objective function. θ is the resultant constant temperature difference between the inside and outside surface of the fuselage wall when a constant heat flux of 100 Watt/m^2 is applied on the inside surface. A large θ corresponds to good thermal insulation properties of the fuselage wall.

The GA solution is given in the first column of table 10.10. The GA resulted in a maximum temperature difference between the inside and outside surface of the fuselage wall of 127.5 °C.

Table 10.10: *Four solutions found with the GA optimisation for maximum θ, maximum TLHF1, maximum TLHF2 and maximum TLHF3.*

	θ	**TLHF 1**	**TLHF 2**	**TLHF 3**
G_opt program settings				
Number of members for each generation	100	100	100	100
Number of generations	200	200	200	200
Cross-over probability	0.75	0.75	0.75	0.75
Mutation probability	0.15	0.15	0.15	0.15
Design variables				
t_{sk}	2.0000	1.9922	2.0000	1.8471
n_{fr}	8	8	12	20
n_{str}	80	100	90	80
k_{str}	1.2765	1.0765	0.6137	0.8333
t_{inc}	4	7	5	6
Final performances:				
RHoop	0.7440	0.7671	0.7246	0.7199
R_{skt}	0.5891	0.5728	0.7387	0.7686
R_{strt}	0.4835	0.4672	0.6269	0.6502
R_{skb}	0.3529	0.2956	0.6008	0.8459
R_{strb}	0.4603	0.5130	0.9958	0.1609
θ	**127.46**	122.75	115.40	97.49
TLHF1	39.59	**41.62**	38.99	35.60
TLHF2	82.20	81.35	**87.58**	76.21
TLHF3	119.02	120.25	117.31	**123.49**
W_{tot}	1387.23	1415.21	1283.52	1347.53
W_{struc}	1032.41	1044.35	918.22	972.90

Solution 1 of table 10.11 shows the results of the numerical re-evaluation of the fuselage configuration for maximum θ. This solution matches the solution found with the GA optimisation quite well. Figure 10.7 illustrates the detailed results of the heat transfer analysis for the numerical determined optimum fuselage configuration. Because of the constant applied heat flux on the inside surface the temperature of the

fuselage wall is constantly increasing. The temperature is constantly rising because no radiation and no convection are considered. Only the conduction of the fuselage wall is considered. The time scale in figure 10.7 is a computational unit and has no physical meaning. The optimum configuration for thermal insulation has a maximum skin thickness and a least amount of frames. It is obvious that a least amount of frames will reduce the number of heat bridges and therefore increase 'θ'.

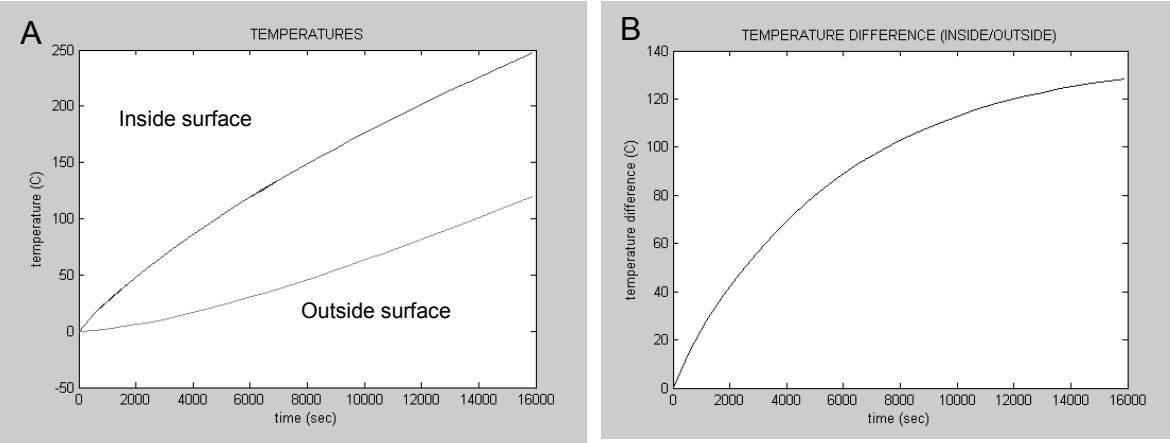

Figure 10.7: *A) Temperatures calculated at the inside and outside surface of the fuselage wall. Note that the temperatures constantly increase because no radiation and no convection are considered. B) Temperature difference between the inside and outside surface of the fuselage wall. The maximum reached temperature difference characteristic for the thermal insulation property of the fuselage wall.*

Table 10.11: *Numerical re-evaluations of the four solutions found with the GA optimisation for maximum θ, maximum TLHF1, maximum TLHF2 and maximum TLHF3.*

Solution nr	t_{sk}	n_{fr}	n_{str}	k_{str}	t_{inc}	R_{Hoop}	R_{skt}	R_{skb}	R_{strt}	R_{strb}	θ	TLHF1	TLHF2	TLHF3	W_{tot}	W_{struc}
1	2.0000	8	80	1.2765	4	0.7363	0.6399	0.6166	0.5383	0.4414	128.5	40.38	82.59	126.36	1397.3	1045.4
2	1.9922	8	100	1.0765	7	0.7397	0.6317	0.3832	0.5192	0.4860	123.9	42.53	86.76	108.81	1427.9	1060.5
3	2.0000	12	90	0.6137	5	0.6753	0.7511	0.5765	0.6410	0.8584	115.9	39.66	74.32	119.26	1286.4	929.3
4	1.8471	20	80	0.8333	6	0.7380	0.7645	0.8862	0.6484	0.1768	97.6	35.38	77.40	110.20	1346.4	984.0

The optimum interior panel thickness is found to be the minimum of 4 mm, which means, according to equation 10.1 a maximum blanket thickness. This is the expected thickness for the case when the fuselage wall would have no frames because the thermal conductivity of the glass fibre insulation blanket is about half of the thermal conductivity of the interior panel core. However, in this case there are frames present. The frames act like heat bridges through which the heat can 'by-pass' the insulation blankets. This would suggest that a thick interior panel core thickness would be preferable for optimal heat insulation. These two phenomena are counteracting with each other. Apparently in this case a thick insulation blanket is more favourable than a thicker interior panel core thickness.

The other two design variables: 'number of stringers' and 'stringer area' are arbitrary for optimum thermal insulation, because the stringers are not considered in the heat transfer analysis.

Case 4: Maximise the overall sound transmission loss in the low frequency range

In this case the overall sound transmission loss in the low frequency range [0-500Hz], indicated as 'TLHF1', is selected as the objective function. The optimum configuration for maximum TLHF1 is shown in the second column of table 10.10.

The GA resulted in a maximum TLHF1 of 41.62 dB, which is found for a skin thickness of 1.99mm, a minimum amount of frames (8), a maximum amount of stringers (100) and an interior panel core thickness of 7 mm. Solution 2 of table 10.11 gives the numerical re-evaluation of the configuration for maximum TLHF1 determined with the DEE. Figure 10.8A gives a detailed view of the sound transmission loss for solution 2 of table 10.10 as function of frequency determined with the DEE.

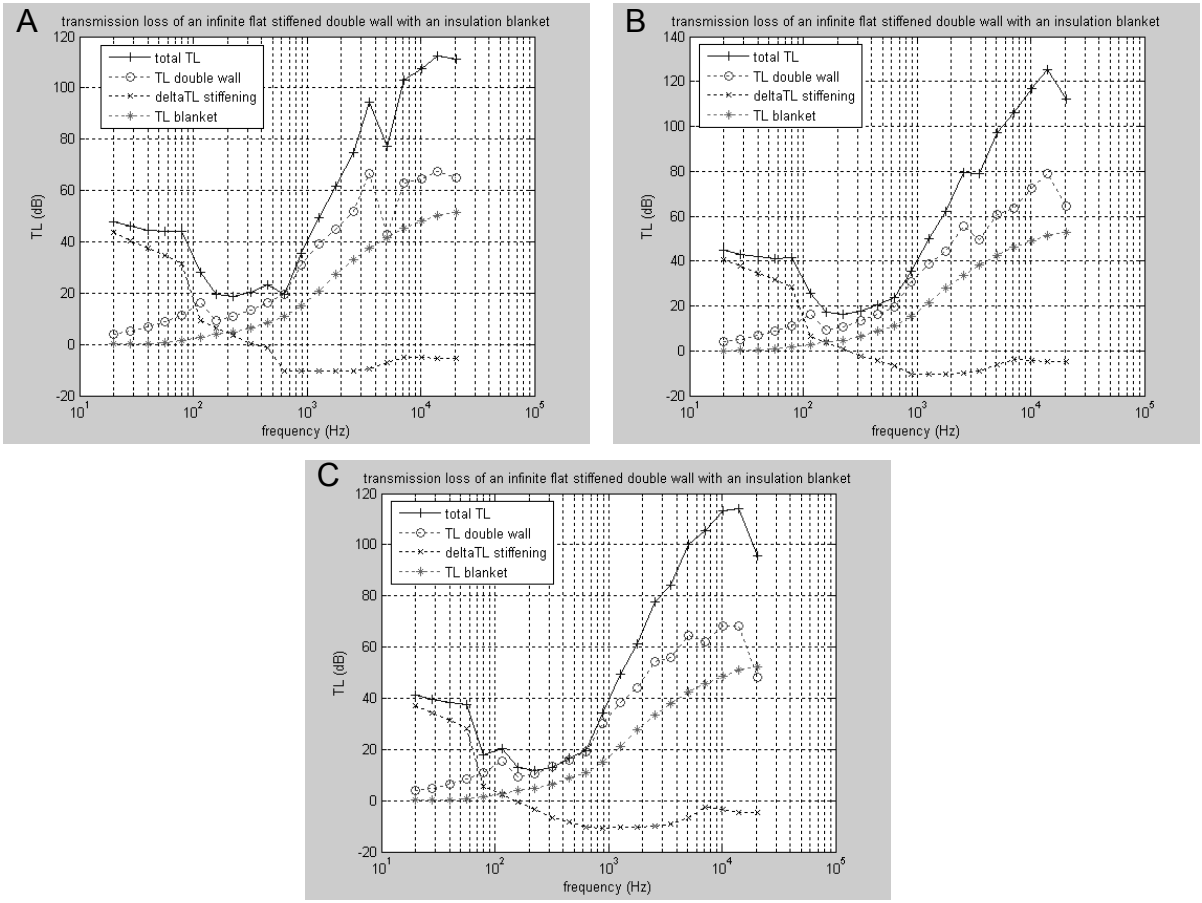

Figure 10.8:
A) Sound transmission loss for the fuselage configuration optimised for maximum TLHF1.
B) Sound transmission loss for the fuselage configuration optimised for maximum TLHF2.
C) Sound transmission loss for the fuselage configuration optimised for maximum TLHF3.

It can be seen that in the low frequency range till about 100 Hz, the stiffening of the fuselage with frames and stringers has a positive effect on the sound transmission loss. Above 200 Hz this effect becomes negative. Apparently for the overall sound transmission loss over the frequency range of 0 - 500 Hz a minimum amount of frames and a maximum amount of stringers is optimal. The dimensions of the stringers are of no importance since they are not considered in the Matlab script based on literature formulas that determine the sound transmission loss. It can also be seen that an increase of the insulation blanket thickness has a more positive effect on the overall sound transmission loss in the frequency range [0-500Hz] than an increase of the interior panel core thickness. Therefore a minimum interior panel core thickness is found.

Case 5: Maximise the sound transmission loss in the middle frequency range

In this case the sound transmission loss in the middle frequency range [500-5kHz] indicated as 'TLHF2' is selected as the objective function. The optimum configuration for maximum TLHF2 is shown in the third table 10.10. The maximum overall sound transmission loss in this frequency range is 87.58 dB. The corresponding design variables are: a skin thickness of 2.00 mm, 12 frames, 90 stringers and an interior panel core thickness of 5 mm. Again the dimensions of the stringers of not considered in the sound transmission loss analysis. Solution 2 of table 10.11 gives the re-evaluation of the configuration for maximum TLHF2 determined with the DEE. Figure 10.8B gives the corresponding detailed presentation of the sound transmission loss as function of frequency. It is noticed that compared to case 4 the number of frames has increased from 8 to 12 and the number of stringers decreased from 100 to 90. Apparently, stiffening the fuselage has a less negative effect in the middle frequency range.

Case 6: Maximise the sound transmission loss in the high frequency range

In this case the sound transmission loss in the high frequency range [5-20kHz] indicated as 'TLHF3' is selected as the objective function. The optimum configuration for TLHF3 is also shown in table 10.10. It can be seen that a maximum overall sound transmission loss of 123.49 dB is found. The corresponding configuration has a skin thickness of 1.85 mm, 20 frames, 80 stringers in half the circumference of the fuselage and an interior panel core thickness of 5 mm. Again the re-evaluation is given as solution 4 of table 10.11 and figure 10.8C gives the corresponding detailed view of the sound transmission loss as function of frequency. The coincidence frequency for this configuration of the fuselage is 7295 Hz. Above the coincidence frequency the influence of stiffeners, like the frames and stringers, is very small. This can be confirmed by the response surfaces for TLHF3 given in figure I.2.9 of appendix I. The strange response surfaces of TLHF3 as function of the stringer factor and the number of frames and stringers are caused by inaccuracies.

10.8 Multi-objective optimisations

To find out whether it is useful to sacrifice weight for improved sound transmission loss and improved thermal insulation multi-objective optimisations are performed using the G_OPT program of Lanzi [5]. This optimisation procedure results in a Pareto set of solutions for which the objectives are optimal. Next four multi-objective

optimisation cases are performed for maximum θ, TLHF1, TLHF2 and TLHF3 all in combination with minimum total fuselage section weight. The results are given in figure 10.9A, B, C and D. The corresponding Pareto sets are given in tables I.4.1 to I.4.4 of appendix I.

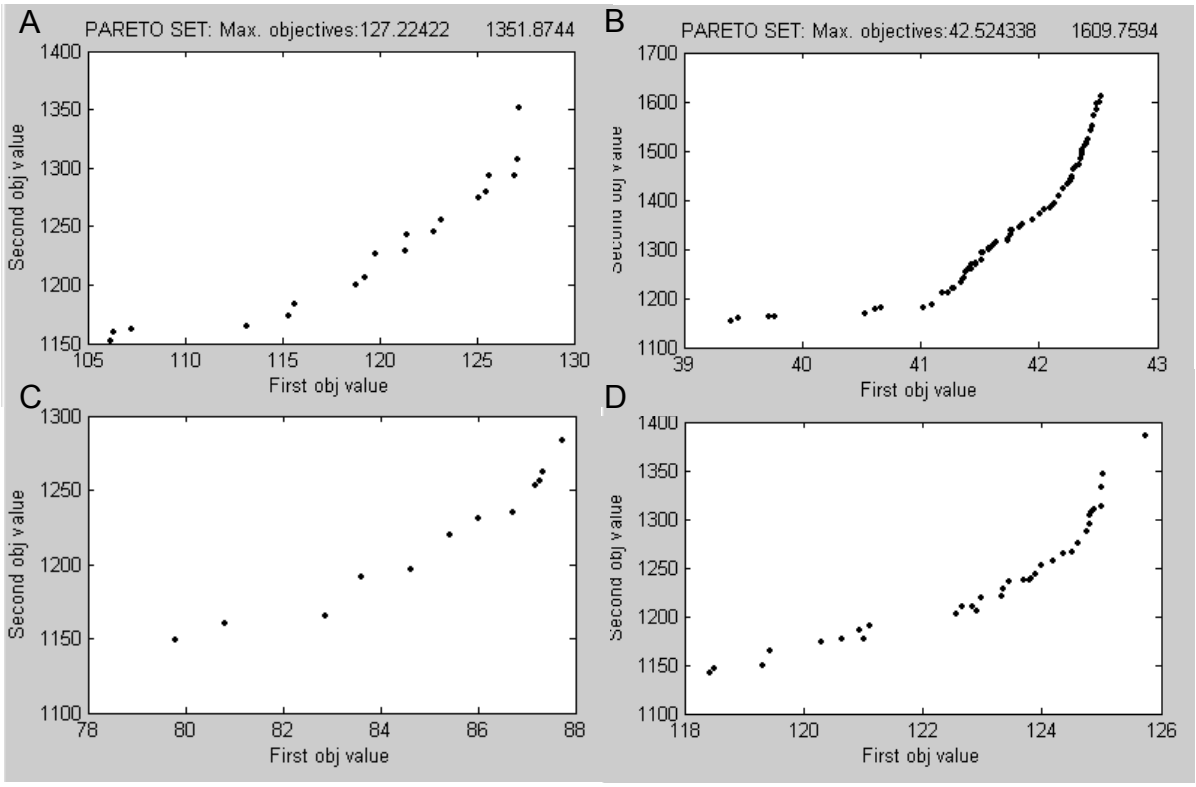

Figure 10.9: *Multi objective optimisations using two objectives: A) Maximising θ and minimising the total fuselage section weight. B) Maximising TLHF1 and minimising the total fuselage section weight. C) Maximising TLHF2 and minimising the total fuselage section weight. D) Maximising TLHF3 and minimising the total fuselage section weight. In all four figures the total fuselage section weight is every time presented on the vertical axis and the other objective on the horizontal axis.*

Case 1: Minimum total fuselage weight and maximum θ

From figure 10.9A can be concluded that an improvement the characteristic temperature difference for the thermal insulation of 20 degrees is possible at the cost of 200 kg. The reason that only such a small improvement is possible at such a great weight cost is the constraint that the total fuselage wall thickness has to remain constant. From the Pareto set belonging to figure 10.9A given in appendix I.4.1 can be seen that all configurations have a minimum interior panel core thickness and therefore a maximum insulation blanket thickness. The increase of 'θ' is mainly dominated by the decreasing number of frames and increasing skin thickness. A decreasing number of frames requires a thicker skin and larger stringers to fulfil the structural constraints. From the Pareto set of appendix I.4 can be seen that for a jump from 12 to 10 frames an increase of θ of 7 degrees is possible at the cost of about 13 kg. (Comparing Pareto set nr 1 with 4 of table I.4.1).

Case 2: Minimum total fuselage weight and maximum TLHF1

Figure 10.9B shows that an increase of the overall sound transmission loss in the low frequency range can be increased by 3 dB at the cost of 400kg. However, by decreasing the number of frames from 12 to 8 and increasing the skin thickness and stringer factor to fulfil the structural requirements already an increase of the overall sound transmission loss of 1.6 dB is possible at the cost of 29 Kg. (Comparing Pareto set nr 6 with 5 of table I.4.2 of appendix I).

Case 3: Minimum total fuselage weight and maximum TLHF2

Figure 10.9C shows the possible increase of the overall sound transmission loss in the middle frequency range. It can be seen that an increase of the overall sound transmission loss of 8 dB is possible at the cost of 150kg. Again, by decreasing the number of frames from 14 to 13 and the number of stringers from 100 to 90 and increasing the skin thickness from 1.51 mm to 1.75mm, an increase of TLHF2 is possible of 4.8 dB at the cost of 47.5 Kg. (Comparing Pareto set nr 1 with 5 of table I.4.3 of appendix I).

Case 4: Minimum total fuselage weight and maximum TLHF3

Figure 10.9D shows the weight penalties for increasing the sound transmission loss in the high frequency range. By decreasing the number of frames from 12 to 10 an increase of TLHF3 of 4.4 dB is possible at the cost of 60 Kg. (Comparing Pareto set nr 3 with 1 of table I.4.4 of appendix I).

In conclusion it can be said that based on the current response surfaces an improvement of the θ and the overall sound transmission loss in the whole frequency range is possible at the cost of a relatively small weight penalty by decreasing the number of frames and increasing the number of stringers and the skin thickness.

In section 10.9 a second optimisation step is performed to find a more accurate result of the optimum fuselage configuration by zooming in on the design space around the current optimum solution. In this zoomed-in design space also the lower number-of-frames are included to validate the small weight penalty for a possible improvement of the thermal and acoustical insulation.

10.9 Optimisation step 2: Zooming in on the design space around the structural optimum solution

To improve the accuracy of the fuselage configuration with minimum total weight a second optimisation step is performed. For the second optimisation step the design space is limited around the optimum solution so more data points will be positioned around the optimum solution. The optimum configuration found in the first optimisation step had a total weight of 1160 kg and was presented in table 10.10A. The definition of the new design space is presented in table 10.12.

The Latin Hypercube routine was used to generate 50 data points in this design space. The 50 data points together with the evaluations for the constraints and objective functions are shown in table I.1.2 of appendix I. The G_OPT program is used to determine the response surfaces again. The errors of these new response surfaces are presented in table 10.13. It should be noticed that the maximum error margin does not exceed 5.3%!

Table 10.12: *Definition of the refined design space*

t_{sk}	1.45 - 1.7 mm
n_{fr}	8 - 14
n_{str}	80, 100
k_{str}	0.5 - 0.8
t_{inc}	4 - 8 mm

Table 10.13*: Accuracies of the response surfaces for the zoomed in design space*

Validation criteria error	R_{Hoop}	R_{skt}	R_{skb}	R_{strt}	R_{strb}	θ	TLHF1	TLHF2	TLHF3	W_{tot}	W_{struc}
MaxMin	3.7024	1.5604	1.5016	1.4888	5.2972	0.9683	0.1626	2.9079	4.1727	0.4631	0.3938
Mean	2.0145	0.7545	0.6123	0.7463	3.6029	0.5340	0.0839	1.3758	1.8292	0.2517	0.1910
Rsqr	0.6584	0.9586	0.9988	0.9698	0.9881	0.9811	0.9979	0.9106	0.4747	0.9943	0.9971
Rmea	1.0081	0.3744	0.0714	0.2826	0.2381	0.2109	0.0709	0.5543	1.3589	0.1185	0.0964
APE	2.0262	0.7674	0.5908	0.7461	3.8559	0.5433	0.0837	1.3737	1.8530	0.2475	0.1927

Table 10.14: *Minimised total fuselage section weight and minimised structural fuselage section weight determined with the GA optimisation procedure.*

	Wtot	**Wtot**	**Wstruc**	**Wstruc**
G_opt program settings				
Number of members for each generation	100	100	100	100
Number of generations	200	200	200	200
Cross-over probability	0.75	0.85	0.75	0.85
Mutation probability	0.15	0.15	0.15	0.15
Design variables				
t_{sk}	1.5294	1.5078	1.5167	1.5255
n_{fr}	13	11	12	13
n_{str}	100	100	100	100
k_{str}	0.5071	0.5753	0.5388	0.5071
t_{inc}	4	4	4	4
Final performances:				
R_{Hoop}	0.8685	0.9103	0.8897	0.8697
R_{skt}	0.9466	0.9247	0.9370	0.9483
R_{strt}	0.8042	0.7788	0.7928	0.8058
R_{skb}	0.9897	0.9929	1.0002	0.9963
R_{strb}	0.9963	1.0019	0.9930	0.9952
θ	108.90	113.59	111.45	108.79
TLHF1	38.99	39.77	39.37	38.98
TLHF2	79.03	77.62	78.33	79.07
TLHF3	108.23	107.40	107.84	108.21
W_{tot}	1149.15	1151.95	1149.44	1148.01
W_{struc}	794.48	795.81	793.99	793.37

Again the genetic algorithm option of the G_OPT program is used to determine the minimum total weight of the fuselage section and the minimum structural weight based on the newly defined response surfaces. The results are presented in table 10.14. It can be seen that for all optimisations the minimum total fuselage section

weight is about 1149 kg and the minimum structural weight is 794 kg. From table 10.14 it can also be seen that the number of frames can be decreased from 13 to 11 at an almost zero weight penalty. The four solutions are validated by a re-evaluation using the DEE. The results are presented in table 10.15. It can be concluded that the actual minimum structural weight is 796 kg and the minimum total weight is 1150 kg.

Table 10.15: *Re-evaluation of the four solutions found with the GA optimisation for minimum structural fuselage section weight given in table 10.2.10.*

Sol. nr	t_{sk}	n_{fr}	n_{str}	k_{str}	t_{inc}	R_{Hoop}	R_{skt}	R_{skb}	R_{strt}	R_{strb}	θ	TLHF1	TLHF2	TLHF3	W_{tot}	W_{struc}
1	1.5294	13	100	0.5071	4	0.8900	0.9494	0.9976	0.8037	0.9393	109.1	38.97	76.94	107.59	1149.6	797.2
2	1.5078	11	100	0.5753	4	0.9010	0.9275	0.9942	0.7812	0.9566	112.5	39.71	76.92	107.13	1149.8	797.4
3	1.5167	12	100	0.5388	4	0.8536	0.9335	0.9916	0.7929	0.9331	110.0	39.32	76.98	108.65	1148.4	796.1
4	1.5255	13	100	0.5071	4	0.8918	0.9512	1.0045	0.8052	0.9392	109.0	38.97	76.92	107.67	1148.5	796.2
5*	1.5186	12	100	0.5235	4	0.8649	0.9398	0.9988	0.7992	0.9935	110.1	39.32	76.69	108.39	1144.0	792.2
6*	1.5186	12	100	0.5235	4	0.8533	0.9395	0.9964	0.7987	1.0555	110.0	39.33	76.99	108.19	1144.1	791.8

Table 10.16: *Four optimised solutions for minimum structural fuselage weight determined with the sequential programming (SQP) option of the G_OPT program with different number of frames. (Only continuous variables can be considered. Therefore, the design variables t_{inc} , n_{fr} and n_{str} have to be fixed).*

	Solution 1	**Solution 2**	**Solution 3**	**Solution 4**
G_OPT program settings				
Tol value on design variable	1e-5	1e-5	1e-5	1e-5
Tol value on obj function	1e-5	1e-5	1e-5	1e-5
Max number of iterations	25	25	25	25
Fixed design variables				
n_{fr}	11	10	9	8
n_{str}	100	100	100	100
t_{inc}	4	4	4	4
Start design variables				
t_{sk}	1.7	1.7	1.7	1.7
k_{str}	0.8	0.8	0.8	0.8
Design variables				
t_{sk}	1.5064	1.5579	1.6232	1.6870
k_{str}	0.5677	0.6294	0.7078	0.7844
Final performances				
R_{Hoop}	0.8987	0.9023	0.8764	0.8416
R_{skt}	0.9303	0.8978	0.8368	0.7709
R_{strt}	0.7849	0.7388	0.6926	0.6583
R_{skb}	1.0000	0.8927	0.7680	0.6660
R_{strt}	0.9857	1.0000	1.0000	1.0000
θ	112.41	116.43	119.47	121.76
TLHF1	39.71	40.21	40.77	41.41
TLHF2	76.86	76.98	76.70	75.63
TLHF3	107.24	107.57	108.74	110.33
W_{tot}	1147.03	1172.62	1206.68	1238.91
Objective function				
W_{struc}	794.88	819.52	854.34	886.64

To find out the weight penalty for better thermal and acoustic insulation by decreasing the number of frames from 11 to 8 a SQP optimisation is performed for 11, 10, 9 and 8 frames. The results are given in table 10.16. (New response surfaces are used for the SQP optimisation, which include the re-evaluated optimum solutions of table 10.15). The newly determined lightest solution using the GA is also given in table 10.15 as solution nr 5* and the re-evaluation with the DEE of this solution as solution nr 6*.

Table 10.16 illustrates the weight penalty for improved θ, TLHF1, TLHF2 and TLHF3 by decreasing the number of frames.

10.10 Discussion of results

When regarding only the structural requirements a minimum structural weight of 792 kg/8m was found, which equals to 990 kg/10m. For the analytical analysis discussed in chapter 5, of the stiffened skin fuselage with similar dimensions and load case definitions but without a floor, a minimum weight of 697 kg/10m was found. The optimum design variables are summarised in table 10.17.
The difference can be explained by the following points:

- First of all there was no floor included in the analytical analysis. For the DEE analysis, the floor has a weight of 150 kg/10m. For comparison the analytical detrmined weight becomes 697+150= 847 kg/10m as indicated in table 10.17.
- Secondly the way the boundary and load conditions are introduced in the FEM model is different from the analytical case. On the FEM model a boundary condition was applied that the fuselage has to remain perfectly round at the section edges. This has the result that higher stresses occur near the edges compared to the undisturbed stresses that are found in the analytical case. This is confirmed by the fact that for the analytical case the skin thickness was limited by the hoop stress while for the FEM analysis the skin thickness is limited by the bucking stresses. This means the skin thickness has increased from the minimum skin thickness limited by the hoop stress of 1.28 mm to a skin thickness of 1.52 mm.
- The third difference is the fact that the fuselage used in the DEE analysis has z-stringers while the analytical case had hat-stringers. The z-stringers have a stringer pitch of $\pi R/n_{str}$ while the hat-stringers have a stringer pitch of $\pi R/n_{str} - b_{str}$. This means that fewer stiffeners are required for the fuselage with hat-stringers, which results in the remaining weight difference.

Improvement of the thermal and acoustical insulation properties were possible at the cost of considerable weight penalties, which means that there is little correlation between the design variables for the structural and acoustic and thermal insulation requirements. This would mean that the advantage of the multidisciplinary design method compared to the normally practiced sequential design method is little. Of course more optimisation cases can be defined. For instance by varying the total fuselage wall thickness. This could be part of a following research. Also the inclusion of more design disciplines like fatigue and impact tolerance could give results that show the advantages of MDO over sequential design methods

Table 10.17: *Final optimum solutions for the stiffened skin fuselage and the sandwich fuselage.*

	Stiffened skin DEE	Stiffened skin analytical
Design variable:		
t_{sk}	1.5186	1.28
n_{fr}	12	22
n_{str}	100	191
k_{str}	0.5235	
t_{inc}	4	
Final performances:		
R_{Hoop}	0.8649	1
R_{skt}	0.9398	1
R_{strt}	0.7992	1
R_{skb}	0.9988	1
R_{strb}	0.9935	1
θ	110.1	
TLHF1	39.32	
TLHF2	76.69	
TLHF3	108.39	
W_{tot}/10m	1430	
W_{struc}/10m	990	847

10.11 References

[1] Zaal, K., de Jong, Th. Beukers, A., Tooren M.J.L., Structure effectiveness of aircraft, Discussion noted, Airbus Industry, Toulouse, 19 Dec, 1996.

[2] Beranek, L.L., Noise and Vibration control, Institute of noise control engineering, Washington DC, 1988.

[3] Hexcel composites.

[4] ABAQUS Example manual version 6.4.

[5] Montgomery, D.C., Design and Analysis of Experiments, JohnWiley & Sons, New York, 3rd edition, 1991.

[6] Miller R.G., Jr., Beyond ANOVA ,Chapman and Hall, London, 1997.

[7] Lanzi, L., Optimisation of composite stiffened panels under post buckling constraints, PhD thesis, Polytecnico di Milano, 2004.

11 Design of a sandwich fuselage for a mid size civil aircraft

11.1 Introduction

This chapter discusses the optimisation of a mid size civil aircraft fuselage that has a sandwich structural concept. Like discussed in chapter 10, the developed DEE will be used to perform a multidisciplinary analysis including the structural, the thermal insulation and the acoustic insulation aspects.

Again several optimisations will be performed. First, the primary objectives will be optimised like the fuselage structure weight and the fuselage total weight with the constraints that it has to fulfil the strength and stiffness criteria. Secondly, secondary objectives like the thermal and acoustical insulation are optimised also by taking into account the structural constraints. This will give an idea of the behaviour of the design space. With multi-objective optimisations, a multidisciplinary designed fuselage can be evaluated. A second optimisation step for the structural optimisation, which zooms in on the design space around the optimum solution found in the first optimisation step, will give a more accurate final solution.

The structure of this section is similar to chapter 10. Section 11.2 gives the model definition of the mid size civil aircraft fuselage with a sandwich structure. The load case definitions and the boundary conditions are discussed in section 11.3 and the

definition of the design variables, the constraints and the objective functions are discussed in section 11.4. Section 11.5 presents the results of the analysis with the DEE and section 11.6 and 11.7 give the results of the optimisations. The second optimisation step to find the final solution is presented in section 11.8. The final solutions will be evaluated in section 11.9

11.2 Model definition of the sandwich fuselage structure

The main difference compared to the stiffened skin concept discussed in section 10.2 is that the considered sandwich concept has no stringers. Furthermore the single aluminium skin is replaced with a sandwich skin that consists out of carbon/PEI facings and a Hexcel HRH-10 1/8" honeycomb core. The sandwich concept still includes frames. The frames are required to attach the interior panels to the sandwich structure and to improve the buckling behaviour. In fact the buckling theory for sandwich cylinders, discussed in section 5.3, is used as part of the structural analysis. This theory does not directly take any frames into account. However the length of the cylinder is of importance for the buckling of sandwich cylinders. By setting the frame pitch L_{fr} equal to the cylinder length considered in the sandwich buckling analysis, the frames are included in the structural analysis of sandwich fuselages. The used aluminium C-frames will have similar dimensions as the frames used in the stiffened skin concept discussed in section 10.2. Also the sandwich floor has similar dimensions and material properties. Figure 11.1 gives an illustration of the sandwich fuselage model concept.

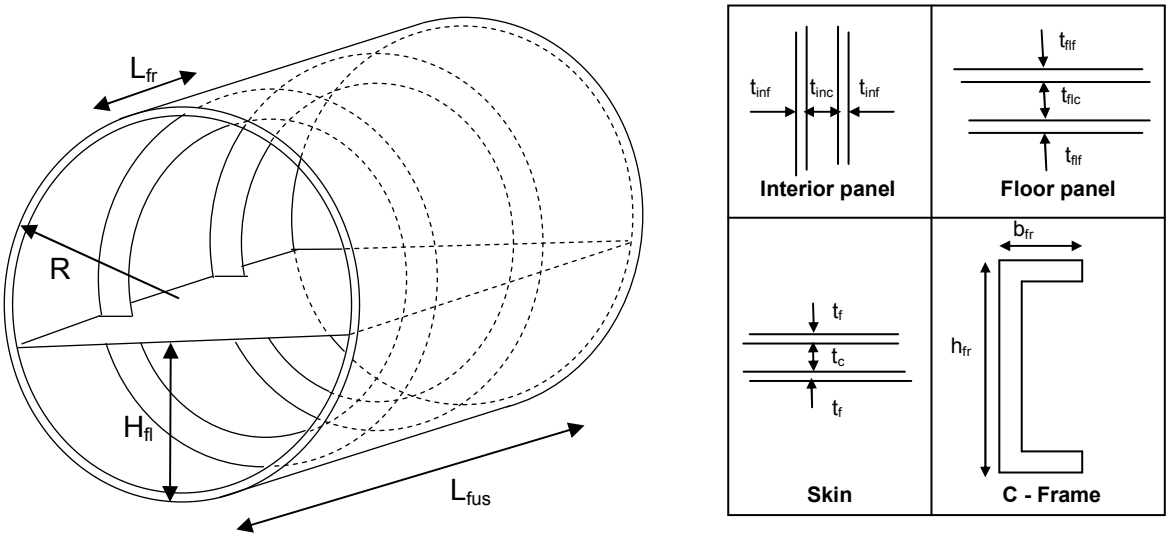

Figure 11.1: *Illustration of the sandwich fuselage concept*

The reference dimensions are presented in table 11.1 and the material properties were presented in table10.2 of section 10.2. Additional material properties are presented in table 11.2.

Table 11.1: *Reference dimensions of the sandwich mid size civil aircraft fuselage*

Radius (R)	1.98 m	Frame height (h_{fr})	120 mm
Fuselage section length (L_{fus})	8.0 m	Frame width (b_{fr})	50 mm
Floor height (H_{fl})	1.56 m	Frame thickness (t_{fr})	1.2 mm
Skin facing thickness (t_f)	0.6 mm	Floor facing thickness (t_{flf})	0.8 mm
Skin core thickness (t_c)	10 mm	Floor core thickness (t_{flc})	8 mm
Nr of frames (n_{fr})	3		

Table 11.2: *Material properties additional to table 10.2 that are relevant for the analysis of the mid size civil aircraft fuselage.*

Carbon PEI [0/90/±45]$_s$: (Skin facings)		**Hexcel HRH-10-1/8-6.0:** (skin core)	
Modulus of elasticity	3.96 GPa	Modulus of elasticity	413 MPa
Density	1800 kg/m^3	Shear modulus L-direction	89.6 MPa
Poisson ratio	0.34	Shear modulus W-direction	44.8 MPa
Thermal conductivity	1 W/mK	Density	93 kg/m^3
Specific heat	600 J/kgK	Thermal conductivity	0.068W/mK
Allowable tensile stress	150 MPa	Specific heat	1300 J/kgK
Allowable hoop stress	100 MPa		

11.3 Definition of load cases and boundary conditions

The definition of the load cases and boundary conditions are similar to that of the stiffened skin fuselage concept discussed in chapter 10. The skin of the FEM model that is used for the structural analysis of the sandwich fuselage consists out of shell elements just like the model for the stiffened skin concept. The sandwich properties, like layer thicknesses and material properties, are defined using the ABAQUS specific "*SHELL SECTION" option. The fact that the sandwich skin is also modelled with shell elements makes it possible to use the same boundary conditions and load case definitions to introduce the loading into the structure as for the stiffened skin fuselage.

11.4 Definitions of the design variables, objective function and constraints

For the optimisation of the sandwich fuselage four design variables are chosen; the skin facing thickness, the skin core thickness, the number of frames and the interior panel core thickness, which are listed in table 11.3. Again the insulation blanket thickness, which is identical to the frame height, is linked to the skin and interior panel sandwich thickness by the assumption that the total fuselage wall thickness remains constant. This is expressed in equation 11.1.

$$t_{bl} = t_{tot} - \left(2t_f + t_c\right) - \left(2t_{inf} + t_{inc}\right) \tag{11.1}$$

Where:

t_{bl} : thickness of the insulation blanket
t_{tot} : thickness of the whole fuselage wall, which is fixed during the optimisation
t_f : thickness of both the fuselage sandwich skin facings, which is a design variable
t_c : thickness of the fuselage sandwich skin core, which is a design variable
t_{inf} : thickness of the interior panel facings, which is fixed during the optimisation
t_{inc} : thickness of the interior panel core, which is a design variable

Table 11.3: *Definition of the four design variables*

t_f	Skin facing thickness
t_c	Skin core thickness
n_{fr}	Number of frames
t_{inc}	Interior panel core thickness

Setting up the design space

The next step is to choose a design space of which it is likely that it will capture the optimum configuration. From the mechanical analysis of the sandwich fuselage structure discussed in chapter 5, an optimum structural design was found for the structural design variables as given in table 11.4. Also the translation of this optimum structural design dimensions into the current design variables is listed.

Table 11.4: *Dimensions of the optimal sandwich fuselage determined with the mechanical analysis described in chapter 5 and the corresponding design variables.*

Dimensions from chapter 5			Design variable	
Skin facing thickness	1.2 mm	→	t_f	1.2 mm
Skin core thickness	25 mm	→	t_c	25 mm
Frame pitch	10 m	→	n_{fr}	2

It should be noted that compared to the mechanical analysis described in chapter 5 now a floor is present, which will have its influence on the stress distribution in the structure. Because of the nature of the sandwich concept a relatively large frame pitch can be expected (At least compared to the frame pitch of the stiffened skin concept). Therefore, for a mid size aircraft fuselage a minimum frame pitch of 0.89 m is chosen. Another reason to choose 0.89 m as minimum frame pitch is the fact that the used sandwich buckling analysis is not valid for very short cylinders. The height of the frame web is identical to the thickness of the insulation blankets. Like for the stiffened skin fuselage, the total wall thickness is set at 100 mm and the facing thickness of the interior panels is chosen 0.5 mm. The range of the interior panel core thickness is selected again between 4 and 40 mm. Therefore an initial design space is defined as mentioned in table 11.5.

Table 11.5: *Definition of the design space*

t_f	0.5 - 2 mm
t_c	5 - 30 mm
n_{fr}	1 - 8 (frame pitch: 8m - 0.89m)
t_{inc}	4 - 40 mm

Objective functions

For the structural optimisation the weight of the fuselage structure is assigned as objective function. This objective function can be expressed as given in equation 11.2:

$$W_{struc} = 2\pi RL_{fus}(2\rho_f t_f + \rho_c t_c) + \rho_{fr} n_{fr} 2\pi RA_{fr} \tag{11.2}$$

Where:

Objective:

W_{struc} : The fuselage structure weight

Design variables:

t_f : Skin facing thickness
t_c : Skin core thickness
n_{fr} : Number of frames

Fixed parameters:

L_{fus} : Fuselage section length
R : Radius of the fuselage section
A_{fr} : Frame cross-section area
ρ_{xxx} : Density of respectively the skin and frames

For the multidisciplinary optimisation (structural including the acoustic and thermal insulation) the total fuselage section weight is assigned as an objective function, which means that in this case the weight of the insulation materials is included. This objective function is expressed by equation 11.3:

$$W_{tot} = 2\pi RL_{fus}(2\rho_f t_f + \rho_c t_c) + \rho_{fr} n_{fr} 2\pi RA_{fr} + 2\pi RL_{fus}\rho_{bl} h_{fr} + 2\pi RL_{fus}(\rho_{\inf} 2t_{\inf} + \rho_{inc} t_{inc}) \tag{11.3}$$

Where:

Objective:

W_{tot} : The total fuselage weight

Design variables:

t_f : Skin facing thickness
t_c : Skin core thickness
t_{inc} : Interior panel core thickness
n_{fr} : Number of frames

Fixed parameters:

L : Fuselage section length
R : Radius of the fuselage section
(Assumed constant over fuselage length)
A_{fr} : Frame cross-section area
ρ_{xxx} : Density of respectively the skin, frames, blanket, interior panel facing and core
t_{inf} : Interior panel facing thickness
h_{fr} : Frame height

Secondary objectives will be, to maximize the temperature difference between the inside surface of the interior panels and the outside surface of the fuselage skin and to maximize the sound transmission loss in the low, middle and high frequency range.

Constraints

Like discussed in chapter 10 there are geometric and performance constraints:

- In this case only one geometric constraint is applied, which is the restriction that the total fuselage wall thickness has to remain constant at 100 mm where the facing thickness of the interior panels are fixed at 0.5 mm. This constraint is implemented in the Matlab routine that transforms the set of design variables into the ICAD input file of the DEE.
- The performance requirements are divided into structural requirements and thermal- and acoustical insulation requirements.
  - The structural requirements are:
    1.) $R_{swt} < 1$: The tensile stress in the sandwich skin has to be smaller than the allowable material stress
    2.) $R_{swb} < 1$: The combination of the compressive and shear stress has to be smaller than the combination of the allowable compressive and shear buckling stress.
    3.) $R_{wr} < 1$: The compressive stress in the facings has to be smaller than the wrinkling stress
    4.) $R_{Hoop} < 1$: The tensile stress in circumferential direction in the skin has to be smaller that the maximum allowable Hoop stress
  - The thermal insulation requirement can be described as the required minimum temperature difference over the fuselage wall for a certain applied heat flux.

$$\theta = T_{inisde} - T_{outside} > T_{min} \tag{11.4}$$

  - The acoustical insulation requirement can be described as the required minimum overall sound transmission losses for three frequency ranges TLHF1 [0-500Hz], TLHF2 [500-5000Hz] and TLHF3 [5000-20000Hz].

$$TLHF1 > TLHF1_{min} \qquad TLHF2 > TLHF2_{min} \qquad TLHF3 > TLHF3_{min} \tag{11.5}$$

    Note: Like in chapter 10, in this analysis only the literature equation module of the DEE is used for the TL analysis to save computation time.

For each run of the DEE the objective functions and the constraints will be evaluated, which are converted into response surfaces that are used for the optimisation analysis.

11.5 Results of the DEE

Like for the stiffened skin concept a design of experiments (DOE) with the Latin hypercube routine of the optimisation program G_OPT is performed, Lanzi [1]. For the first optimisation step a set of 100 data points is generated, which are given in table J.1 of Appendix J. Also the evaluations of the corresponding performance requirements and the objection functions determined with the DEE are given in table J.1. Subsequently, the response surfaces of the constraints and objective functions are discussed separately.

Discussion of the response surfaces

1) *Sandwich buckling*: Figures J.2.1A and B of Appendix J show the response surfaces for R_{swb}. These figures show that the buckling stress that occurs in the fuselage section decreases with increasing skin facing and core thickness. The number of frames has only a small influence on the sandwich buckling stress. The maximum response surface error is 17.7%. This is still quite large. One possible reason can be the fact that the buckling criteria consists out of two criteria: sandwich cylinder buckling and crimpling, which can cause some discontinuity.

2) *Sandwich wrinkling*: Figures J.2.2A and B of Appendix J show the response surfaces for R_{wr}. It can be seen that sandwich wrinkling is mainly dependent on the skin facing thickness and not on the skin core thickness and the number of frames.

3) *Hoop stress:* The response surfaces for the R_{Hoop} are given in figure J.2.3. They show that also the Hoop stress is also mainly dependent on the skin facing thickness.

4) *Sandwich tensile stress, R_{swt}:* Like for the Hoop stress, also the sandwich tensile stress is mainly dependent on the skin facing thickness.

5) *Thermal insulation, θ:* The resultant response surfaces for the thermal insulation are illustrated in figure J.2.5. It can be seen that for increasing skin facing, skin core and interior panel core thickness the thermal insulation improves. Also a decrease of the number of frames is positive for the thermal insulation.

6) *Sound transmission loss in the low frequency range, TLHF1 [0-500Hz]:* The response surfaces are shown in figure J.2.6. The influence of the skin facing and core thickness is irregular. This is probably caused by the influence of the mass-air-mass resonance of the double wall. When the sound transmission loss as function of frequency is examined in more detail (An example is given in figure 11.3), the mass-air-mass resonance of the double wall contribution can be clearly identified in the frequency range between 100-500 Hz. Furthermore it can be seen that decreasing the number of frames has a positive influence on the sound transmission loss in the low frequency range, which was expected according to equation 3.32.

7) *Sound transmission loss in the middle frequency range, TLHF2 [500-5000Hz]:* The response surfaces are shown in figure J.2.7. From these response surfaces can be concluded that in general the sound transmission loss in the middle frequency range increases for increasing skin facing and core thickness, increasing interior panel core thickness and decreasing number of frames.

8) *Sound transmission loss in the high frequency range, TLHF3 [5000-20000Hz]:* The response surfaces are illustrated in figure J.2.8. Like for the sound transmission loss in the low frequency range the sound transmission loss in the high frequency range is quite irregular. In this frequency range the dilatation frequencies of the sandwich skin and interior panel have their influence.

9) *Structural fuselage section weight:* Figure J.2.9 shows the response surfaces of the structural fuselage section weight. This weight does not include the weight of the interior panel and the insulation blankets. Because the weight is a straight forward function of the design parameters these response surfaces are relatively accurate.

10) *Total fuselage section weight:* Figure J.2.10 shows the response surfaces of the complete fuselage section weight, which means the structural fuselage weight added with the weight of the interior panels and insulation blankets.

11.6 Optimisation of the sandwich fuselage section design

In section 11.5 the response surfaces are determined. These response surfaces can now be used for the optimisation of the fuselage section design. The optimisation is performed with the genetic algorithm option of the G_OPT program developed by Lanzi [1]. To explore the design space for optimum configurations, optimisations are performed for the same six objective functions as discussed in section 10.7. In all cases the structural constraints are taken into account.

1.) Minimise the structural weight of the fuselage section for a fixed applied load case, which means that only the structural parts are considered.
2.) Minimise the total fuselage section weight for a fixed applied load case including the interior panels and insulation blankets.
3.) Maximise the temperature difference between the inside surface of the interior panel and the outside surface of the skin for a fixed applied heat source.
4.) Maximise the sound transmission loss in the low frequency range for fixed applied incident noise level.
5.) Maximise the sound transmission loss in the middle frequency range for a fixed applied incident noise level.
6.) Maximise the sound transmission loss in the high frequency range for a fixed applied incident noise level.

Case 1: Minimise the structural fuselage section weight

Like for the stiffened skin concept several genetic optimisations are performed with different program settings to determine the minimum structural fuselage section weight taking the structural constraints into account.

The results are presented in table 11.6A. Because the interior panel core thickness has no influence on the structural weight of the fuselage section this design variable has been fixed to the minimum thickness of 4 mm. It can be concluded that for all settings the same solution is found:

The minimum structural fuselage section weight is about 723 kg. This fuselage configuration has a skin facing thickness of about 1.33 mm, a skin core thickness of 12 mm and 1 or 2 frames. As a first check, the four solutions are re-evaluated using the corresponding parameters as input to the DEE. The results are presented in table 11.7. It can be concluded that the sandwich buckling and tensile criteria are slightly violated.

Table 11.6: *A) Four optimised solutions for minimum structural fuselage weight determined with the genetic algorithm (GA) option of the G_OPT program using four different program settings. The design variable Interior Core thickness is fixed at 4 mm.*

B) Four optimised solutions for minimum total fuselage section weight using the genetic algorithm (GA) option of G_OPT for four different program settings. In this case all design variables including the Interior Core Thickness are unbound.

A	**Solution 1**	**Solution 2**	**Solution 3**	**Solution 4**
G_opt program settings				
Number of members for each generation	100	100	100	100
Number of generations	200	500	200	500
Cross-over probability	0.75	0.75	0.85	0.85
Mutation probability	0.15	0.15	0.15	0.15
Design variables				
t_f	1.3471	1.3294	1.3235	1.3471
t_c	12	12	12	12
n_{fr}	1	2	2	1
t_{inc}	4	4	4	4
Final performances:				
R_{swb}	0.9902	0.9572	0.9611	0.9902
R_{wr}	0.1934	0.1933	0.1941	0.1934
R_{Hoop}	0.4203	0.4223	0.4242	0.4203
R_{swt}	1.0093	1.0131	1.0175	1.0093
θ	126.68	125.16	125.06	126.68
TLHF1	41.33	39.15	39.14	41.33
TLHF2	93.94	92.85	92.79	93.94
TLHF3	116.26	116.70	116.75	116.26
W_{tot}	1063.78	1064.53	1062.55	1063.78
Objective function				
W_{struc}	723.99	724.63	722.55	723.99
B	**Solution 1**	**Solution 2**	**Solution 3**	**Solution 4**
G_OPT program settings				
Number of members for each generation	100	100	100	100
Number of generations	200	500	200	500
Cross-over probability	0.75	0.75	0.85	0.85
Mutation probability	0.15	0.15	0.15	0.15
Design variables				
t_f	1.3412	1.3353	1.3529	1.3471
t_c	12	12	12	12
n_{fr}	2	2	1	2
t_{inc}	4	4	4	4
Final performances				
R_{swb}	0.9496	0.9534	0.9865	0.9459
R_{wr}	0.1917	0.1925	0.1926	0.1909
R_{Hoop}	0.4186	0.4204	0.4183	0.4167
R_{skt}	1.0044	1.0087	1.0048	1.0001
θ	125.35	125.26	126.78	125.45
TLHF1	39.18	39.16	41.34	39.19
TLHF2	92.97	92.91	94.03	93.03
TLHF3	116.61	116.66	116.23	116.57
W_{struc}	728.80	726.72	726.08	730.89
Objective functions				
W_{tot}	1068.68	1066.61	1065.86	1070.76

To find a more accurate solution for the minimum fuselage section weight, a second optimisation step will be performed where is zoomed in on the design space close to the optimum solutions given in table 11.7. This second optimisation step will be discussed in section 11.8.

Table 11.7: *Re-evaluation of the four solutions found with the GA optimisation for minimum structural fuselage section weight given in table 11.6A.*

Solution nr	t_f	t_c	n_{fr}	t_{inc}	R_{swb}	R_{wr}	R_{Hoop}	R_{swt}	θ	TLHF1	TLHF2	TLHF3	W_{Tot}	W_{struc}
A1	1.3471	12	1	4	1.0004	0.1931	0.4166	1.0075	126.9	41.38	91.34	115.21	1063.81	723.98
A2	1.3294	12	2	4	1.0060	0.1944	0.4231	1.0227	125.1	39.17	90.33	113.85	1064.69	724.83
A3	1.3235	12	2	4	1.0100	0.1953	0.4250	1.0272	125.0	39.16	90.35	113.75	1062.60	722.74
A4	1.3471	12	1	4	1.0004	0.1931	0.4166	1.0075	126.9	41.38	91.34	115.21	1063.81	723.98

It is seen that both the fuselage configurations with 1 and 2 frames have almost similar weight. With a sequential programming (SQP) optimisation with the G_OPT program, the influence of the frame pitch can be examined. The results of the SQP optimisation are presented in table J.3.1 of appendix J.3. The program is only able to optimise continuous real variables. Therefore, the discontinuous integer variables have to be set by the user. It can be remarked that the configuration with 1 frame gives the lightest weight as well as the best acoustical performance in the low and middle frequency range as well as the best thermal insulation. It is noted that now a minimum structural weight is found of 728 kg. This weight is a slightly larger than found in table 11.7 since the structural constraints are less violated.

Case 2: Minimise the total fuselage section weight

In this case the total fuselage section weight is chosen to be the objective function. The constraints are similar as for case 1. The results of four GA optimisations with different program settings are given in table 11.6B.

It can be seen that the minimum total fuselage weight varies between 1065 and 1070 kg. The skin facing thickness varies between 1.33 and 1.35 mm, the number of frames between 1 and 2 and the interior panel core thickness is the minimum 4 mm. The re-evaluations using the DEE are presented in table 11.8.

Table 11.8: *Re-evaluation of the four solutions found with the GA optimisation for minimum total fuselage section weight given in table 11.6B.*

Sol. nr	t_f	t_c	n_{fr}	t_{inc}	R_{swb}	R_{wr}	R_{Hoop}	R_{swt}	θ	TLHF1	TLHF2	TLHF3	W_{tot}	W_{struc}
B1	1.3412	12	2	4	0.9979	0.1928	0.4193	1.0138	125.33	39.19	90.32	114.05	1068.86	729.03
B2	1.3353	12	2	4	1.0019	0.1936	0.4212	1.0183	125.23	39.18	90.32	113.95	1066.77	726.93
B3	1.3529	12	1	4	0.9965	0.1923	0.4148	1.0032	127.02	41.39	91.36	115.28	1065.86	726.04
B4	1.3471	12	2	4	0.9940	0.1919	0.4174	1.0095	125.43	39.19	90.33	114.14	1070.95	731.12

It can be concluded that the re-evaluated weights correspond quite well to the solutions determined with the response surfaces and that solution B3 gives the lightest configuration. It can also be noted that the minimum fuselage weights (Structural and total) correspond to case 1 and to the solutions found with the SQP routine given in appendix J.3 by considering the small violations of the buckling and tensile stress criteria. This was to be expected, because the insulation and interior panel materials are lighter than the structural materials.

Case 3: Maximise the temperature difference between the interior panel inside surface and the fuselage skin outside surface

In this case 'θ' is selected as the objective function, where the total fuselage wall thickness is fixed to 100 mm. The resultant solution is given in the last column of table 11.9. It can be seen that a maximum temperature difference between the inside and outside surface of the fuselage wall is found of 134.5 °C. Solution 4 of table 11.10 gives the re-evaluation of the fuselage configuration for maximum θ.

Figure 11.2 illustrates the detailed results of the heat transfer analysis for the re-evaluated fuselage configuration. Again it is noted that the temperature of the fuselage wall is constantly increasing. This is because a constant heat flux is applied on the interior panel inside surface while no radiation and no convection are considered. Only the conduction of the fuselage wall is considered. The time scale in figure 11.2 is a numerical time scale and cannot be considered as real time.

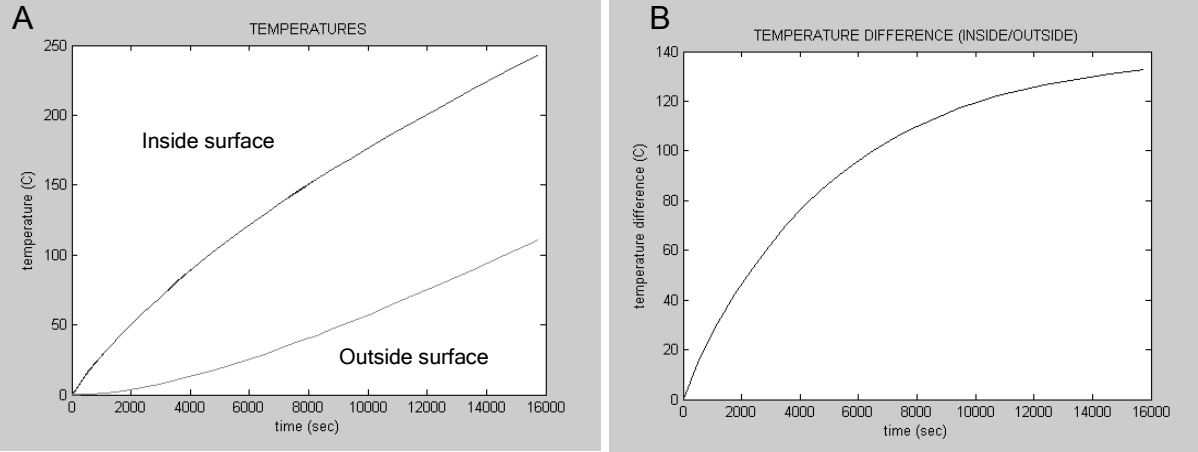

Figure 11.2*: A) Temperatures calculated at the inside and outside surface of the fuselage wall. Note that the temperatures constantly increase because no radiation and no convection are considered.*
B) Temperature difference between the inside and outside surface of the fuselage wall. The maximum reached temperature difference characteristic for the thermal insulation property of the fuselage wall.

The optimum configuration for thermal insulation has a maximum skin thickness and a least amount of frames just like for the stiffened skin concept discussed in section 10.7. It is obvious that a least amount of frames will reduce the number of heat bridges and therefore increase 'θ'. Not so obvious is the fact that a thicker sandwich facing thickness also increases 'θ'. A thicker facing thickness results in a thinner core thickness, which means that with the fixed total fuselage wall thickness

the insulation blankets will have maximum thickness. Because the insulation blankets have the lowest thermal conductivity of all fuselage wall materials the thicker facing thickness result in a lower total thermal conductivity of the fuselage wall and therefore higher 'θ'.

The optimum interior panel thickness is found to be at the minimum of 4 mm. This is the expected thickness for the case when the fuselage wall would have no frames because the thermal conductivity of the glass fibre insulation blanket is about half of the thermal conductivity of the interior panel core. However, in this case there are 2 frames. The frames act like heat bridges through which the heat can by pass the insulation blankets. Because of the existence of heat bridges, a thick interior panel core thickness would be preferable for optimal heat insulation. Apparently in this case a thick insulation blanket is more favourable than a thicker interior panel core thickness.

Table 11.9: *Four solutions found with the GA optimisation for maximum θ, maximum TLHF1, maximum TLHF2 and maximum TLHF3.*

GA	**TLHF 1**	**TLHF 2**	**TLHF 3**	**θ**
G_opt program settings				
Number of members for each generation	100	100	100	100
Number of generations	200	200	200	200
Cross-over probability	0.75	0.75	0.75	0.75
Mutation probability	0.15	0.15	0.15	0.15
Design variables				
t_f	1.9941	2.0000	1.9941	1.9941
t_c	9	10	24	13
n_{fr}	1	1	7	1
t_{inc}	6	4	8	4
Final performances:				
R_{swb}	0.9271	0.8150	0.2989	0.5844
R_{wr}	0.1316	0.1300	0.1300	0.1290
R_{Hoop}	0.2778	0.2756	0.2669	0.2775
R_{swt}	0.6806	0.6712	0.6754	0.6666
θ	131.84	134.78	117.41	**134.56**
TLHF1	**44.17**	43.93	32.07	42.88
TLHF2	103.59	**107.04**	83.41	106.55
TLHF3	117.04	116.28	**132.63**	118.39
W_{tot}	1279.73	1279.13	1447.99	1301.06
W_{struc}	927.71	938.68	1100.31	963.43

Table 11.10: *Re-evaluations of the four solutions found with the GA optimisation for maximum TLHF1, maximum TLHF2, maximum TLHF3 and maximum θ.*

Sol. nr	t_f	t_c	n_{fr}	t_{inc}	R_{swb}	R_{wr}	R_{Hoop}	R_{swt}	θ	TLHF1	TLHF2	TLHF3	W_{tot}	W_{struc}
1	1.9941	9	1	6	0.9422	0.1324	0.2789	0.6864	132.58	**44.02**	94.05	114.11	1278.96	926.96
2	2.0000	10	1	4	0.8458	0.1317	0.2783	0.6832	132.55	43.82	**93.63**	117.97	1278.78	938.17
3	1.9941	24	7	8	0.3282	0.1309	0.2740	0.6810	116.73	31.97	82.46	**127.01**	1447.85	1099.79
4	1.9941	13	1	4	0.6430	0.1312	0.2800	0.6821	**135.26**	42.54	94.10	118.40	1300.66	962.93

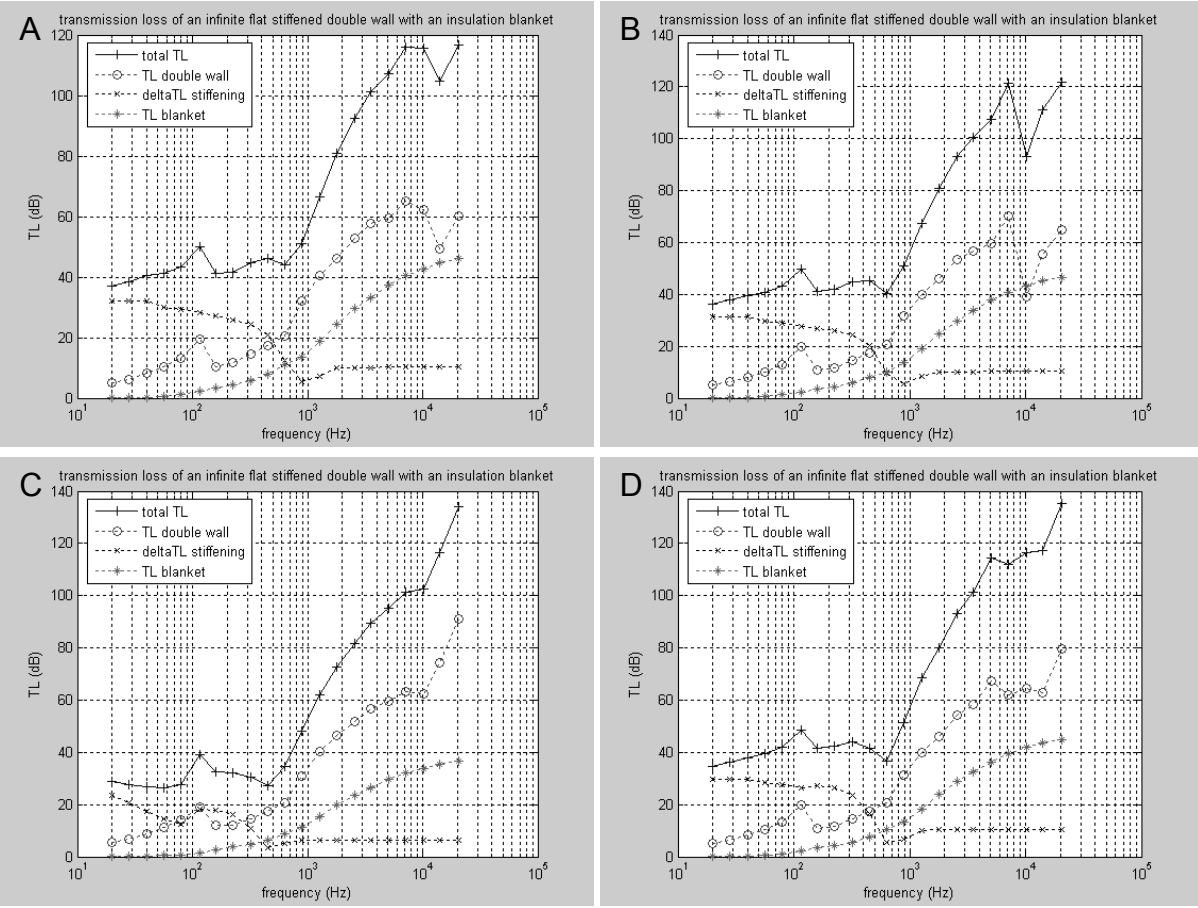

Figure 11.3:
A) Sound transmission loss for the fuselage configuration optimised for maximum TLHF1.
B) Sound transmission loss for the fuselage configuration optimised for maximum TLHF2.
C) Sound transmission loss for the fuselage configuration optimised for maximum TLHF3.
D) Sound transmission loss for the fuselage configuration optimised for maximum θ.

Case 4: Maximise the overall sound transmission loss in the low frequency range

In this case 'TLHF1' is selected as the objective function, considering a fixed total fuselage wall thickness of 100 mm. The optimum configuration for maximum overall sound transmission loss in the low frequency range [0-500Hz] is shown in the first column of table 11.9.

It can be seen that a maximum overall sound transmission loss of 44.17 dB is found for a skin facing thickness of 1.9941 mm, which is the maximum allowed within the design space. Furthermore a skin core thickness is found of 9 mm, a minimum amount of frames (1) and an interior panel core thickness of 6 mm. The maximum facing thickness can be explained with the mass law, which prescribes that more mass is most effective in the low frequency range, knowing that the facings have the highest specific weight.

Solution 1 of table 11.10 gives the re-evaluation of the configuration for maximum TLHF1 determined with the DEE. Figure 11.3A gives a detailed view of the sound transmission loss as function of frequency. It can be noted that in the low frequency range till about 400 Hz, a low amount of frames has a positive effect on the sound transmission loss. Above 400 Hz this effect becomes smaller. It has also to be noted that the TL effect of stiffeners like frames and stringers is determined as difference to

a stiffened reference case that has a frame pitch of 8m and a stringer pitch of 3.96m). It is questionable if this contribution will be valid for sandwich fuselages.

The influence of the insulation blankets is not so large in the low frequency range. Therefore a minimum interior panel core thickness is found. The contribution of the double wall shows the influence of the mass-air-mass resonance.

Case 5: Maximise the sound transmission loss in the middle frequency range

In this case 'TLHF2' is selected as the objective function. The optimum configuration for maximum overall sound transmission loss in the middle frequency range [500-5000Hz] with fixed total fuselage wall thickness is shown in the second column of table 11.9. The maximum overall sound transmission loss in this frequency range is 107.04 dB. It can be seen that the re-evaluations shown in table 11.10 give a completely different result as the solution found with the response surfaces. It has to be concluded that the response surfaces in the area around this solution is not accurate enough. In fact it is noted that solution 1 and 4 of table 11.10 give a much better TLHF2 compared to solution 2 of table 11.10.

Case 6: Maximise the sound transmission loss in the high frequency range

In this case 'TLHF3' is selected as the objective function. The optimum configuration for maximum overall sound transmission loss in the high frequency range [5000-20.000Hz] with fixed total fuselage wall thickness is also shown in table 11.9. It can be seen that a maximum overall sound transmission loss of 132.63 dB is found. The corresponding configuration has the maximum skin facing thickness of 1.99 mm, a skin core thickness of 13 mm, 1 frame and a minimum interior panel core thickness of 4 mm. Again the re-evaluation is given as solution 3 of table 11.10 and Figure 11.3D gives the corresponding detailed view of the sound transmission loss as function of frequency. In this frequency region the coincidence and the dilatation frequencies are of influence, which are represented in the contribution of the double wall.

11.7 Multi-objective optimisations

To find out whether or not it is useful to sacrifice weight for improved sound transmission loss and improved thermal insulation, multi-objective optimisations are performed using the G_OPT program of Lanzi [1]. This optimisation procedure results in a Pareto set of solutions for which the objectives are optimal. Next, four multi-objective optimisations are performed for maximum θ, TLHF1, TLHF2 and TLHF3 all in combination with minimum total fuselage section weight. The results are given in figure 11.4A, B, C and D. The corresponding Pareto sets are given in tables J.4.1 to J.4.4 of appendix J.

Case 1: Minimum total fuselage weight and maximum θ

From figure 11.4A can be concluded that an improvement of the characteristic temperature difference for the thermal insulation of 18 degrees is possible at the cost of 230 kg. The reason that only such a small improvement is possible at such a great weight cost is the constraint that the total fuselage wall thickness has to remain constant. From the Pareto set belonging to figure 11.4A given in appendix J.4.1 can be seen that all configurations have a minimum interior panel core thickness and therefore a maximum insulation blanket thickness and a minimum number of frames.

The increase of 'θ' is mainly dominated by the increasing skin facing thickness. This results in a linear relation of θ with the skin facing thickness.

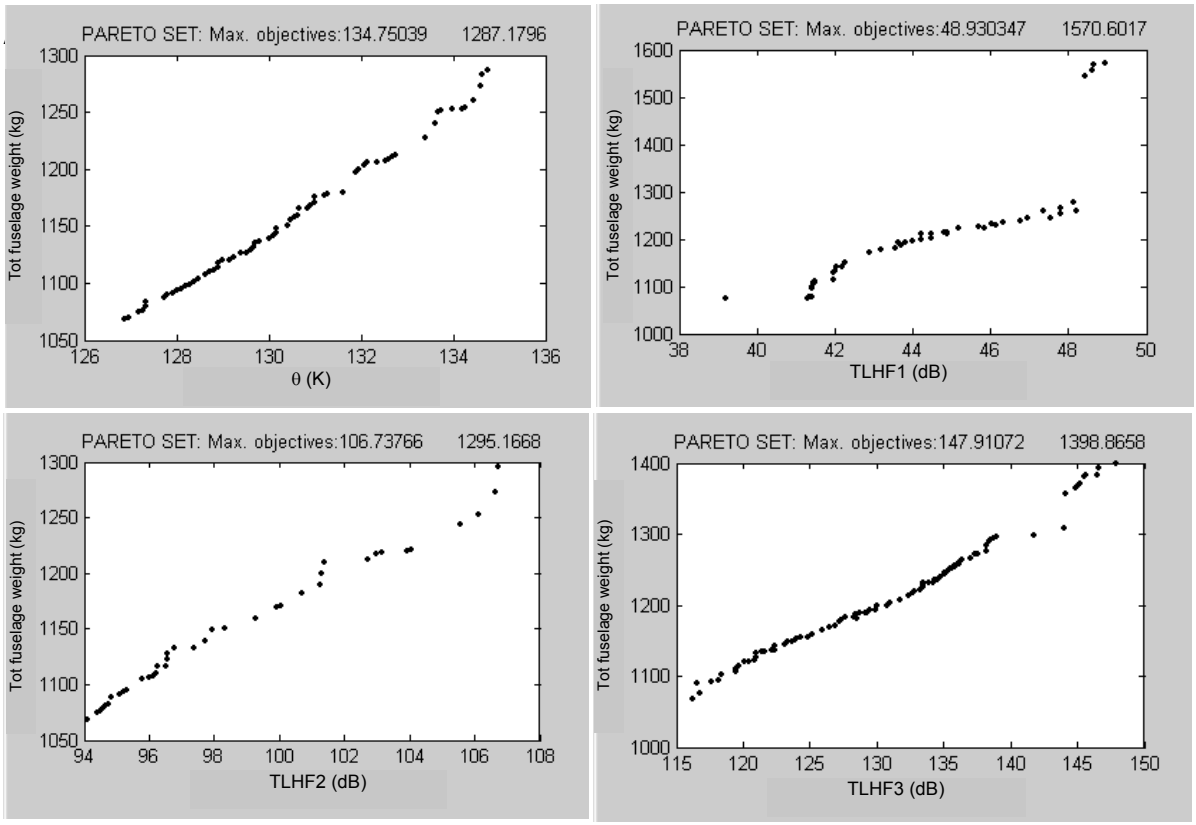

Figure 11.4: *Multi objective optimisations using two objectives: A) Maximising θ and minimising the total fuselage section weight. B) Maximising TLHF1 and minimising the total fuselage section weight. C) Maximising TLHF2 and minimising the total fuselage section weight. D) Maximising TLHF3 and minimising the total fuselage section weight. In all four figures the total fuselage section weight is every time presented on the vertical axis and the other objective on the horizontal axis.*

Case 2: Minimum total fuselage weight and maximum TLHF1

Figure 11.4B shows that an increase of the overall sound transmission loss in the low frequency range can be increased by 7 dB at the cost of 150kg. By comparing the lightest solutions (Pareto set nr 18, 19 and 3 of table J.4.2 of Appendix J), it can be seen that they all have 1 frame and a skin core thickness of 12 mm. A small TLHF1 improvement can be achieved by increasing the interior panel core thickness. Larger improvements are possible by increasing the sandwich facing and core thickness but at the expense of larger weight penalties. Figure 11.4B shows that after the addition of a first 100 kg the increase in TLHF1 becomes larger at the expense of a smaller weight increase.

Case 3: Minimum total fuselage weight and maximum TLHF2

Figure 11.4C shows the possible increase of the overall sound transmission loss in the middle frequency range. It can be seen that an increase of the overall sound transmission loss of 13 dB is possible at the cost of 230kg. The improvements are

mainly established by increasing the skin facing thickness. This results in the more or less linear relation. (The corresponding Pareto set is given in table J.4.3 of appendix J).

Case 4: Minimum total fuselage weight and maximum TLHF3

Figure 11.4D shows the weight penalties for increasing the sound transmission loss in the high frequency range. Again an almost linear relation is found for the increment of TLHF3 with respect to the total fuselage section weight. The increment is achieved at the cost of increasing skin and interior core thicknesses. (The corresponding Pareto set is given in table J.4.4 of appendix J).

In conclusion it can be said that the improvement of the thermal and acoustical insulations is linear with the total fuselage weight. Unlike the stiffened skin fuselage there is no region at which the thermal and acoustical insulation can be improved at the cost of a small weight penalty. It should be noted that it is possible that by using different constraints, (for example variable total fuselage wall thickness), different results will be found.

11.8 Optimisation step 2: Zooming in on the design space around the structural optimum solution

To improve the accuracy of the fuselage configuration with minimum total weight a second optimisation step is performed. For the second optimisation step the design space is limited around the optimum solution. In other words, more data points will be positioned around the optimum solution. The optimum configuration found in the first optimisation step had a total weight between 1065 and 1070 kg and was presented in table 11.8. The definition of the new design space is presented in table 11.11.

Table 11.11*: Definition of the refined design space*

t_f	1.25 – 1.40 mm
t_c	11, 12, 13 mm
n_{fr}	1, 2, 3
t_{inc}	4, 5, 6 mm

The Latin Hypercube routine was used to generate 50 data points in this design space. The 50 data points together with the evaluations for the constraints and objective functions are shown in table J.2 of appendix J. The G_OPT program is used to determine the response surfaces again. The errors of these new response surfaces are presented in table 11.12. It can be noticed that the maximum error margin does not exceed 3.6%.

Again the genetic algorithm option of the G_OPT program is used to determine the minimum total weight of the fuselage section and the minimum structural weight based on the newly defined response surfaces. The results are presented in table 11.13. It can be seen that for both optimisations the minimum total fuselage section weight is about 1067 Kg and the minimum structural weight is 727.5 Kg. The final fuselage configuration is validated by a re-evaluation using the DEE. The result is also presented in table 11.13. It can be concluded that the response surfaces around

the optimum are quite accurate. The final fuselage configuration with a sandwich structure has a minimum structural weight of 727.5 Kg and a total weight of 1067 Kg.

Table 11.12: *Accuracies of the response surfaces for the zoomed in design space*

Validation criteria error	R_{swb}	R_{wr}	R_{Hoop}	R_{swt}	θ	TLHF1	TLHF2	TLHF3	W_{tot}	W_{struc}
Max	2.8100	2.4371	2.0140	1.6120	0.3116	0.2884	3.5676	1.8343	0.1812	0.1222
Mean	1.6571	1.0180	1.2341	0.7770	0.1441	0.1183	1.7214	0.8106	0.0763	0.0536
Rsqr	0.9319	0.8391	0.8121	0.9612	0.9757	0.9992	0.6418	0.6921	0.9959	0.9977
Rmea	0.3996	0.6843	0.6236	0.3427	0.2624	0.0538	1.0045	1.0330	0.1207	0.0866
APE	1.6763	1.0101	1.2309	0.7726	0.1442	0.1149	1.7358	0.8056	0.0768	0.0537

The weight penalties to improve the thermal and acoustic insulation were given in figure 11.4 of section 11.7. Table J.4.5 of appendix J gave the Pareto set of fuselage section configuration for minimised total fuselage section weight and maximised θ, TLHF1, TLHF2 and TLHF3.

Table 11.13: *Minimised total fuselage section weight and minimised structural fuselage section weight determined with the GA optimisation procedure.*

	Wtot	**Wstruc**	**Re-evaluation**
G_opt program settings			
Number of members for each generation	100	100	
Number of generations	200	200	
Cross-over probability	0.75	0.75	
Mutation probability	0.15	0.15	
Design variables			
t_f	1.3571	1.3571	1.3571
t_c	12	12	12
n_{fr}	1	1	1
t_{inc}	4	4	4
Final performances:			
R_{swb}	0.9946	0.9946	0.9937
R_{wr}	0.1917	0.1917	0.1917
R_{Hoop}	0.4135	0.4135	0.4134
R_{swt}	1.0001	1.0001	1.0001
θ	127.06	127.06	127.10
TLHF1	41.40	41.40	41.40
TLHF2	91.82	91.82	91.38
TLHF3	115.07	115.07	115.32
W_{tot}	1067.33	1067.33	1067.34
W_{struc}	727.52	727.52	727.54

11.9 Discussion of results

The two-step optimisation with the DEE of the structural sandwich fuselage weight resulted in a minimum structural weight of 727 kg/8m, which is 909 kg/10m. The analytical analysis of the structural sandwich fuselage weight, which was discussed in chapter 5, resulted in a minimum weight of 804 kg/10m. Next, the two results will be compared.

It should be noted that the analytical analyses did not include a floor, which has an estimated weight of 150 kg/10m. The addition of a floor results in an analytically determined structural fuselage weight of 954 kg/10m. The corresponding design variables are listed in table 11.14. As a first simple conclusion it can be concluded that the DEE analysis resulted in a structural sandwich fuselage weight that is 45 kg/10m or 5% lighter than the structural sandwich fuselage weight determined with the analytical analysis. When looking into the results more closely several reasons can be pointed out that can explain this difference:

- The boundary conditions and the introduction of loads applied on the FEM model are different from the analytical case. This results in a different stress distribution and therefore a different skin facing and core thickness. For the analytical case a facing thickness of 1.2 mm and a core thickness of 25 mm were found. For the analysis with the DEE a skin facing thickness of 1.36 mm and a core thickness of 12 mm are found. This means that the weight of the sandwich skin alone for the analytical case is 126 kg/10m heavier than for the sandwich skin found with the DEE analysis.
- The second difference is the fact that the weight of the frames considered in the DEE analysis is different from the weight of the frames considered in the analytical case because of the changing frame height. However only few frames are present in the sandwich concept so this will have only a small influence on the difference in fuselage weight.

Table 11.14: *Final optimum solutions for the stiffened skin fuselage and the sandwich fuselage.*

	Sandwich DEE	**Sandwich Analytical**
Design variable:		
t_f	1.36	1.2
t_c	12	25
n_{fr}	1	1
t_{inc}	4	
Final performances:		
R_{swb}	0.9937	1
R_{wr}	0.1917	1
R_{Hoop}	0.4134	1
R_{swt}	1.0001	1
θ	127.10	
TLHF1	41.40	
TLHF2	91.38	
TLHF3	115.32	
W_{tot}/10m	1334	
W_{struc}/10m	909	954

Finally it is concluded that the lightest structural configuration found with the DEE lies relatively close to the analytically found solution. The existing differences can be explained by the different definitions of the boundary conditions. This means that a proper definition of the of the boundary conditions is very important when using the DEE.

Like for stiffened skin fuselage improvements of the thermal and acoustical insulation properties were only possible at the cost of considerable weight penalties, which means that also for the considered sandwich fuselage there is little correlation

between the design variables for the structural and acoustic and thermal insulation requirements. This would mean that the advantage of the multidisciplinary design method compared to the normally practiced sequential design method is little. Of course more optimisation cases can be defined. For instance by varying the total fuselage wall thickness. This could be part of future research. Also the inclusion of more design disciplines like fatigue and impact tolerance could give results that show the advantages of MDO over sequential design methods.

Comparison the sandwich fuselage with the stiffened skin fuselage concept

The final optimum solutions for the stiffened skin and sandwich fuselage determined with the DEE are presented in table 11.15. First of all it can be concluded that the total fuselage weight of the optimal sandwich concept is 96 kg/10m lighter than the optimal stiffened skin concept. The difference in structural weight is 81 kg/10m also in favour of the sandwich concept.

All the thermal and acoustic performances of the sandwich concept are slightly better than that of the stiffened skin concept. However the stiffened skin concept had some room to improve the thermal and acoustic insulation performance at the cost of a lower weight penalty compared to the sandwich concept.

Table 11.15: *Final optimum solutions for the stiffened skin fuselage and the sandwich fuselage.*

	Stiffened skin DEE	**Sandwich skin DEE**	
Design variable:			
t_{sk}	1.5186	t_f	1.36
n_{fr}	12	t_c	12
n_{str}	100	n_{fr}	1
k_{str}	0.5235	t_{inc}	4
t_{inc}	4		
Final performances:			
R_{Hoop}	0.8649	R_{Hoop}	0.4134
R_{skt}	0.9398	R_{swt}	1.0001
R_{strt}	0.7992	R_{swb}	0.9937
R_{skb}	0.9988	R_{wr}	0.1917
R_{strb}	0.9935		
θ	110.1	θ	127.10
TLHF1	39.32	TLHF1	41.40
TLHF2	76.69	TLHF2	91.38
TLHF3	108.39	TLHF3	115.32
W_{tot}/10m	1430	W_{tot}/10m	1334
W_{struc}/10m	990	W_{struc}/10m	909

Of course these are results only valid for the restrictions made on these fuselage concepts. In reality there are many more aspects that are of influence on the structural, thermal insulation and acoustical insulation performance of the fuselage. Examples are; the existence of windows, seats, carpet, galleys, etc.

Meaning of fuselage weight saving in the overall picture

A typical mid size passenger aircraft like the Airbus A320 has a total operating empty weight (OEW) of 41000 kg, a load capacity of 13500 kg and a maximum fuel weight of 20000 kg, which gives a maximum take of weight of 74500 kg. The OEW

can be divided into the weight distribution of the different parts, as is illustrated in table 11.16, Beukers [2]. From this table can be concluded that the structural weight of the fuselage shell is only 16% of the OEW. From table 11.15 was concluded that for the considered cases a weight saving of 81 kg/10m is possible when using the sandwich concept instead of the stiffened skin concept. This is a structural weight saving on the considered fuselage section of 8%. This weight saving can be extrapolated to a 8% weight saving of the complete fuselage shell. From table 11.16 can be concluded that a 8% weight saving on the structural fuselage shell can be translated into 1.3% weight saving of the OEW.

Table 11.16: *Weight breakdown of a typical mid size passenger aircraft [2]*

Total aircraft	100%
Wing structure	31%
Wing control surfaces	9%
Interior	16%
Equipment	7%
Fuselage structure	37%
Fuselage structure	100%
Shell; Skin, stiffeners, frames	43%
Keel; wheel wells etc	16%
Floor assemblies	12%
Door assemblies	11%
Bulkheads	10%

According to Helms [3], a 100 kg weight saving for a long distance aircraft results on average to a fuel consumption saving of 190 liter/kg per year. The weight saving of 1.3% of the OEW for the Airbus A320 is 533kg. This results in a fuel consumption reduction of 101270 liters/year. (In percentage this would mean a fuel cost saving of 1% per year). When considering a fuel price of $100/158liter (barrel), this would mean a fuel cost saving of $64100 per year. The fuel consumption reduction also means an emission reduction. With future plans to tax emission, this would mean additional cost savings.

In conclusion it can be said that a 8% fuselage structure weight reduction will result only in a 1% fuel consumption reduction. Although in percentage this seems low, in absolute values it is still quite considerable.

11.10 Reference

[1] Lanzi, L., "Optimisation of composite stiffened panels under post buckling constraints", PhD thesis, Polytecnico di Milano, 2004.

[2] Beukers, A., Bersee, H., Bergsma, O., Koussios, S., van Tooren, M., Future aircraft structures, from metal to composite structures, IMAST, Capri, 2008.

[3] Helms, H., et al., Energy savings by light weighting-II, IFEU, Heidelberg, 2004.

12 Conclusions & Recommendations

12.1 Conclusions

This research was conducted in order to answer the question whether the design of a fuselage in the preliminary design phase could be improved, (i.e. lighter), by applying a MDO approach instead of the normally practiced sequential design approach.

The MDO approach is given shape with the development of a Design & Engineering Engine (DEE). The DEE is a parametric computer tool that can automatically analyse many different fuselage configurations for different design disciplines. Based on the results of these analyses, the fuselage configuration can be optimised. In fuselage design, many different design disciplines are involved. Examples are strength and stiffness, vibrations, fatigue, corrosion, damage tolerance, fire resistance and thermal & acoustic insulation. Besides these design disciplines, also other aspects are involved like; the geometric shape for aerodynamics, manufacturing, maintenance, inspection and repair. During this research it was not possible, time wise, to include all design aspects in the DEE. Because thermal and acoustic insulation requirements are usually met after the structure has been optimised, it was chosen to include these aspects in the DEE as a first step. The DEE is set up in such a way that it can easily be extended with additional analysis modules for other design requirements.

The current DEE contains a parametric fuselage model generator that is capable to handle fuselage structures with a stiffened skin or a sandwich skin concept. These fuselage models include the skin, frames, stringers, floors, insulation blankets and interior panels.

The DEE has been used to study two design cases;

1.) A stiffened skin the design variables that were chosen for the stiffened skin concept were the skin thickness, the frame and stringer pitch and the insulation blanket and interior panel thickness with a fixed total fuselage wall thickness.
2.) A sandwich fuselage concept where the core and facing thickness of the sandwich skin and the insulation blanket and interior panel thickness were chosen as design variables also with a fixed total fuselage wall thickness.

Optimisation of both design concepts for minimum weight, resulted in solutions very similar to the sequential design approach. This means that there is little correlation between the design variables for structural optimisation and for thermal & acoustic optimisation. Compared to the lightest structural solutions, which also include insulation blankets and interior panels because of the fixed total fuselage wall thickness, the only way to improve the thermal and acoustical insulation is at the cost of extra weight.

It has to be noted that this conclusion is based on only two design concepts and model definitions. Possibly, different solutions will be found when the design problems are defined differently. For example the total fuselage wall thickness was fixed in both considered design cases. Adding the total fuselage wall thickness as a new design variable could result in thinner and perhaps lighter, fuselage walls with similar or perhaps better, thermal and acoustical insulation properties. However these design cases were not considered in this research because of time limitations.

In order to fully exploit the advantages of the MDO design approach, the inclusion of other design requirements like damage tolerance and fatigue also might lead to more efficient fuselage wall concepts. Damage tolerance and fatigue, both favour more weight to the fuselage skin and less to the interior panels. Also, other combinations of design variables, material properties and boundary conditions should be considered to explore all possible configurations.

The developed DEE proved to work effectively. The current DEE is capable to analyse overnight, about fifty fuselage configurations on a pentium IV machine. This makes it a useful tool to analyse many different fuselage configurations in the preliminary design stage, where it is still possible to change to a different design concept.

The definition of fuselage primitives used in the multi model generator enables the DEE to handle many different fuselage configurations. The way the DEE is structured, (different analysis modules for different design disciplines), makes it easy to implement new design modules. This makes the DEE a very flexible tool that can easily be adjusted to the needs of the user.

Acoustic measurements of the sound pressure difference between the inside and outside of four differently stiffened test cylinders have been performed to validate the influence of frames and stringers on the sound transmission loss of fuselage walls. The measurements showed a partial agreement with the theoretical predictions of the literature equations that are implemented in the DEE. The tests showed, that above the ring frequency, the sound transmission loss of the curved cylinder walls can be predicted with the literature equations for flat panels. For fuselages of mid size commercial aircraft with a radius of 2 m the ring frequency is about 400 Hz.

As a final conclusion it can be said that so far the MDO approach in this research did not lead to spectacular changes in the fuselage wall configuration. The conventional fuselage wall configuration designed with the normally practiced sequential design approach is very effective as it is.

12.2 Recommendations

From this research was concluded that the MDO approach did not result in weight saving in fuselage design compared to the conventional sequential design approach when only the structural and thermal & acoustic insulation requirements are considered. However, the DEE proved to be a very effective and flexible analysis tool, which can easily be extended with other design modules. Therefore it is recommended to extend the DEE with other analysis disciplines like fatigue, damage tolerance, corrosion, fire resistance and aerodynamics. This will result in a more integrated, more realistic fuselage design.

Besides extending the DEE with more analysis modules also the current DEE should be better explored by adding and/or changing design variables and/or defining different constraints and objective functions. For example, the fixed total fuselage wall thickness could be made variable. Also different optimisations could be performed where minimum thermal insulation and minimum sound transmission loss are set as constraints. By performing more of these kind of analyses, a better understanding of the correlations between the design variables and the objective functions can gained.

In this perspective it is also recommended to implement the statistical analysis method ANOVA (Analysis Of Variance). The usual objective of ANOVA is to find out what factors contribute most or not at all to the objective functions.

Another aspect which needs attention is the effect that boundary conditions have on the solutions. In chapter 10, already was stated that the occurrence of stress concentrations because of the applied boundary conditions can strongly influence the solution.

So far only the geometric shape of the fuselage wall has been investigated. When different material properties are chosen, different solutions can be expected. Therefore, it is also recommended to perform more optimisation studies with different materials like for example carbon fibre reinforced composites.

For the analyses discussed in chapter 10 and 11 only the literature equation acoustic insulation module was used in the DEE. The application of the literature equations module implies that simplifying assumptions have to be made. When computational times can be reduced, specialised numerical acoustic tools could be implemented to determine the sound transmission loss for each step in the optimisation loop. This will lead to more accurate results.

The active noise control part of the acoustic insulation module, which was developed during the “Smart panel” project in cooperation with TNO TPD, has never been used in the discussed optimisation examples. The “Smart panel” project was terminated before the developed tools were completely finished. The current DEE is able to deliver the required noise transfer matrices but whether these matrices comply with the TNO TPD optimisation algorithms is uncertain. More work should be done to validate this module.

Until now the developed DEE was considered as an independent design tool. Since the fuselage is part of a complete aircraft, the developed fuselage DEE can also be placed in a larger DEE of a complete aircraft. At the chair “Design of aircraft and rotorcraft” a DEE is being developed for complete aircraft [1-5]. A major part of this aircraft DEE was developed as part of the European research project MOB “Multidisciplinary design and Optimisation of a Blended wing body” (Contract number G4RD-CT1999-0172) in which the author participated. Implementation of the fuselage DEE into the aircraft DEE may result in a more integrated, more realistic fuselage design.

Implementation of the fuselage DEE in the aircraft DEE

Figure 12.1 shows a paradigm of the aircraft DEE. Starting point of the DEE are the customer requirements. Next, models of the various design concepts invented by the designer have to be generated. This is given shape with the ICAD aircraft Multi Model Generator (MMG). The MMG has to be capable to handle all the possible aircraft configurations the designer can come up with. This is achieved by the development of parametrically described aircraft primitives. These primitives are the building blocks to construct the various aircraft configurations. An aircraft can be considered as a composition of typical parts like the fuselage, wings, vertical and horizontal tails, canards etc. All wing shaped parts can be considered to be member of one family and therefore they can be represented by one aircraft primitive; the wing trunk. An example of the wing trunk is given in figure 12.2. A second aircraft primitive is defined for the fuselage. The fuselage primitive can almost be considered to be similar to the wing trunk (with circular airfoils) except for a different structural definition. A third and fourth primitive are the nose and the engines. Procedures are available to connect multiple parametric wing trunks, on different angles to allow winglets and vertical tails.

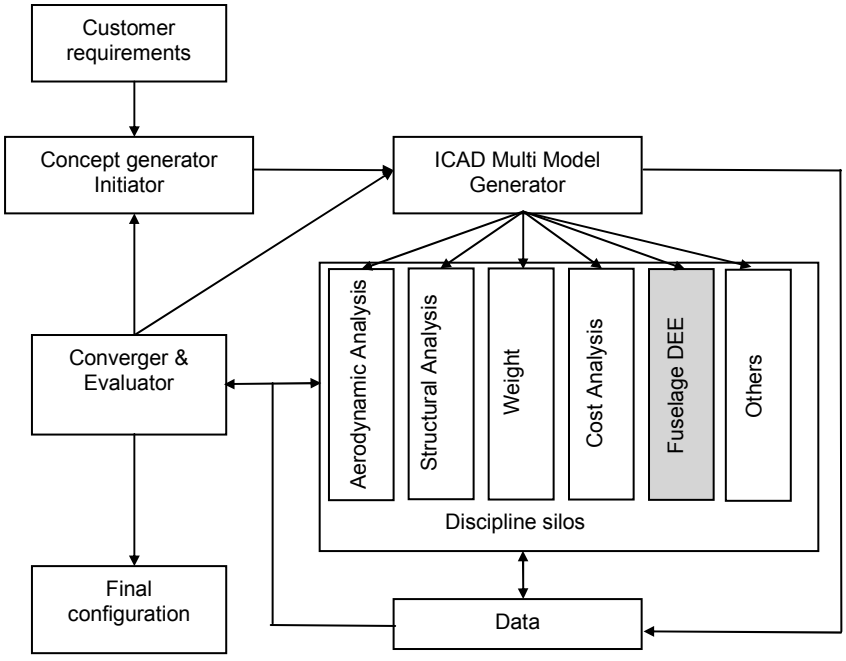

Figure 12.1: *Paradigm of a Design & Engineering Engine (DEE).*

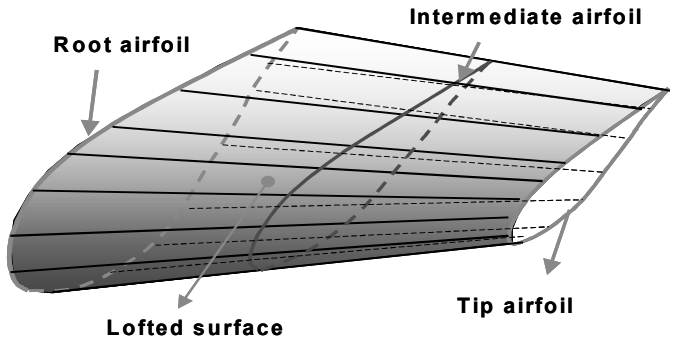

Figure 12.2: *The wing trunk definition*

With just these four types of building blocks, geometric models of many different aircraft concepts can be generated. A few examples are given in figure 12.3.

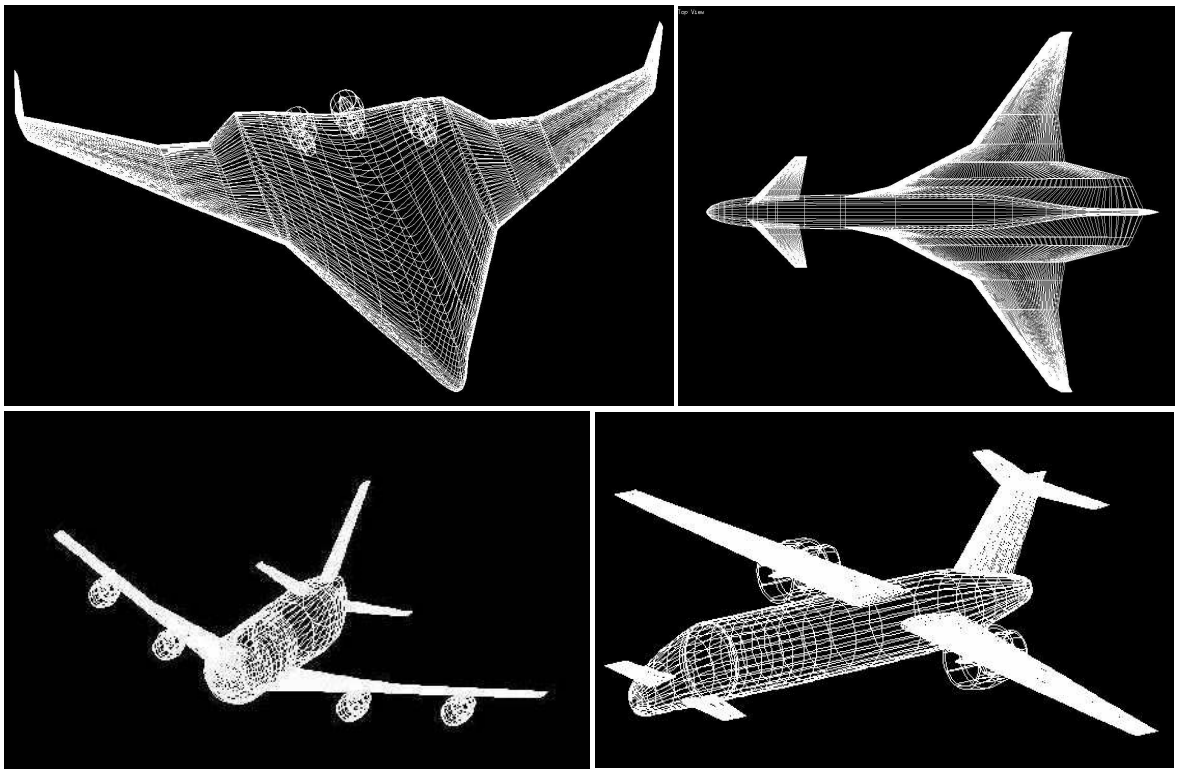

Figure 12.3: *parametric models of different configuration aircraft, generated with the ICAD multi model generator.*

According to the paradigm of figure 12.1, the MMG has to deliver special models to each of the discipline silos. Usually, specialised commercially available software tools are available for the different disciplines. Each of these tools need their own specific input. For example, CFD tools for aerodynamic analysis only need a model of the outer surface. For mechanical analysis, models are required that include the structure. Figure 12.4 gives an example of the models used for aerodynamic, mechanical, flutter, weight and balance and a detail analysis for a blended wing body.

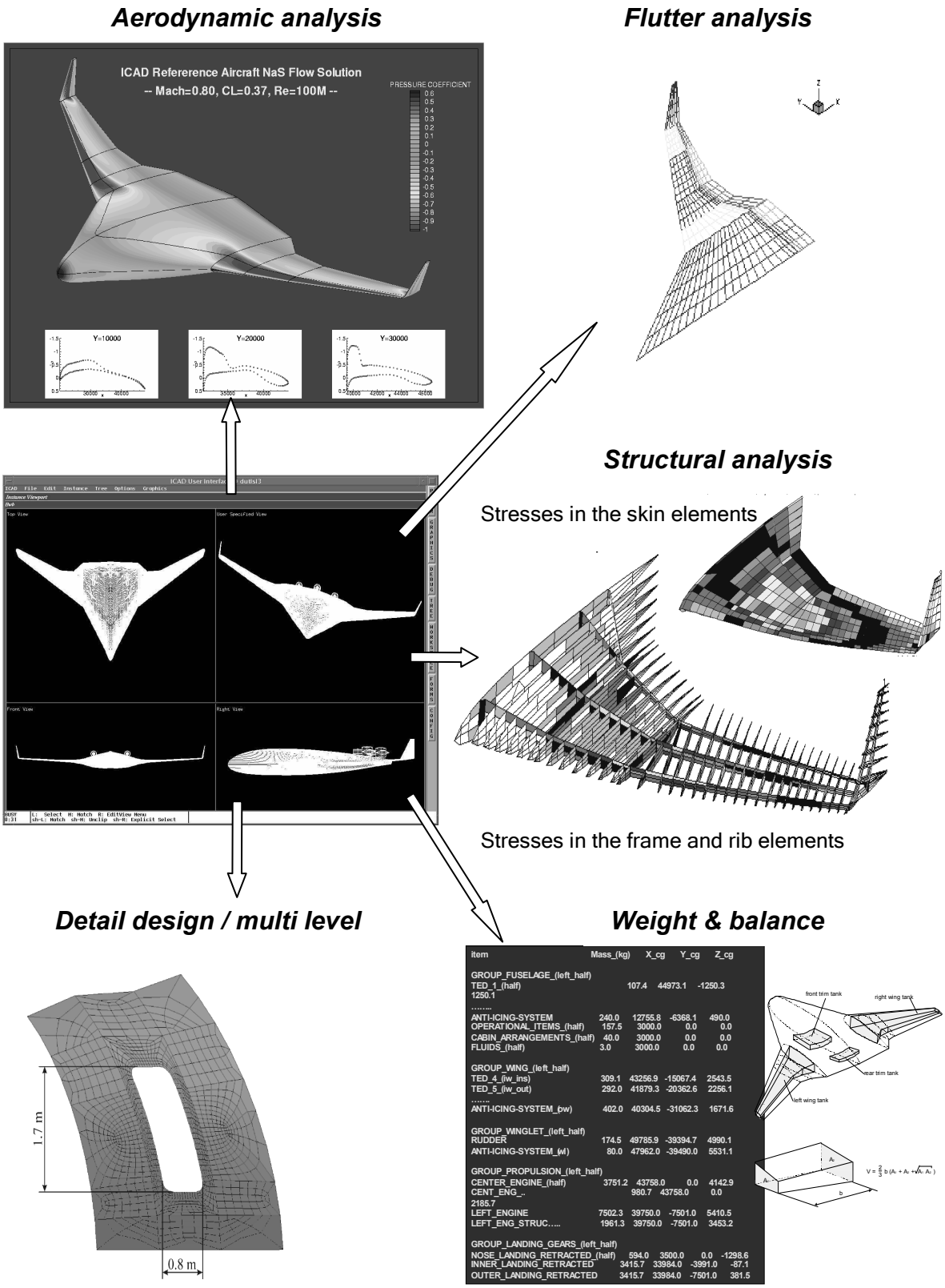

item	Mass_(kg)	X_cg	Y_cg	Z_cg
GROUP_FUSELAGE_(left_half)				
TED_1_(half)		107.4	44973.1	-1250.3
1250.1				
……..				
ANTI-ICING-SYSTEM	240.0	12755.8	-6368.1	490.0
OPERATIONAL_ITEMS_(half)	157.5	3000.0	0.0	0.0
CABIN_ARRANGEMENTS_(half)	40.0	3000.0	0.0	0.0
FLUIDS_(half)	3.0	3000.0	0.0	0.0
GROUP_WING_(left_half)				
TED_4_(iw_ins)	309.1	43256.9	-15067.4	2543.5
TED_5_(iw_out)	292.0	41879.3	-20362.6	2256.1
……..				
ANTI-ICING-SYSTEM_(w)	402.0	40304.5	-31062.3	1671.6
GROUP_WINGLET_(left_half)				
RUDDER	174.5	49785.9	-39394.7	4990.1
ANTI-ICING-SYSTEM_(wl)	80.0	47962.0	-39490.0	5531.1
GROUP_PROPULSION_(left_half)				
CENTER_ENGINE_(half)	3751.2	43758.0	0.0	4142.9
CENT_ENG_..		980.7	43758.0	0.0
2185.7				
LEFT_ENGINE	7502.3	39750.0	-7501.0	5410.5
LEFT_ENG_STRUC…..	1961.3	39750.0	-7501.0	3453.2
GROUP_LANDING_GEARS_(left_half)				
NOSE_LANDING_RETRACTED_(half)	594.0	3500.0	0.0	-1298.6
INNER_LANDING_RETRACTED	3415.7	33984.0	-3991.0	-87.1
OUTER_LANDING_RETRACTED	3415.7	33984.0	-7501.0	381.5

Figure 12.4: *Example of the aircraft DEE with the different disciplines; aerodynamics, structure, flutter, weight and balance and detailed design, which has been developed for the European research project MOB. (See also colour section).*

The results of the analysis disciplines have to be evaluated by an optimiser, which decides for new input parameters and will lead to an improved design. This creates an iteration loop that has to converge to the optimum design solution.

The fuselage DEE could be implemented as a new discipline silo as was illustrated in figure 12.1. From interaction with other discipline silos realistic load cases and boundary conditions can be defined that act on the fuselage models defined within the fuselage DEE. For example, from the aerodynamic module of the aircraft DEE, aerodynamic loads can be determined for any kind of flying manoeuvre, that serve as an input load case for the structural analysis of the wings, tail and fuselage. Similarly, using the weight and stability module of the aircraft DEE the gravitational forces can be determined that act on the different aircraft components. Through the position definitions of the landing gear, loads introduced by taxiing manoeuvres can be simulated. The determination of these realistic load cases would result in a more realistic analysis of the fuselage structure. In conclusion, the developed fuselage DEE can considered as a small part of the overall aircraft DEE that contributes to the overall aircraft design.

12.3 Reference

[1] La Rocca, G., van Tooren, M.J.L., A knowledge based engineering approach to support automatic generation of FEM models in aircraft design, 45th AIAA Aerospace Sciences Meeting and Exhibit, AIAA-2007-0967, Reno, NV, USA, 2007.

[2] Schut, E.J., van Tooren, M.J.L., A knowledge based engineering approach to automation of conceptual design option selection, 45th AIAA Aerospace Sciences Meeting and Exhibit, AIAA-2007-0968, Reno, NV, USA, 2007.

[3] Nawijn, M., van Tooren, M.J.L., Arendsen, P., Berends, J.P.T.J., Automated finite element analysis in a knowledge based engineering environment, 44th AIAA Aerospace Sciences Meeting and Exhibit, Reno, Nevada, USA, 2006.

[4] La Rocca, G., and van Tooren, M.J.L., Development of design and engineering engines to support multidisciplinary design and analysis of aircraft, Delft Science in Design - A congress on Interdisciplinary Design, Faculty of Architecture, ISBN 90-5269-327-7, Delft, NL, 2005.

[5] La Rocca G., L. Krakers and M.J.L. van Tooren, Development of an ICAD generative model for blended wing body aircraft design, Proceedings of the 9th AIAA/ISSMO Symposium on MDO, Atlanta, Georgia, USA, 2002.

A Radiation of stiffened panels

This appendix gives a more elaborated discussion about the radiation behaviour, which was discussed in section 3.4.

According to Fahy [1], the radiated power $\overline{P}$ from a simple supported unstiffened panel (in the one-dimensional case) of width: b (finite length!), with a given normal velocity distribution $v_n(x,t)$ is:

$$\overline{P} = \frac{\rho_0 c k}{4\pi} \int_{-k}^{k} \frac{\left|\overline{V}(k_x)\right|^2}{\left(k^2 - k_x{}^2\right)^{1/2}} dk_x \qquad \text{(A.1)}$$

Here is:
- k: the acoustic wave number.
- k_x: the wave number in the plate in x-direction.
- $V(k_x)$: the Fourier wave number transform of the given normal velocity distribution $v_n(x,t)$ of the plate:

$$v_n(x,t) = \tilde{v}_p \sin\left(\frac{p\pi x}{b}\right) e^{i\omega t} \qquad 0 < x < b$$

Here p is the number of half waves present in the plate.

From equation A.1 can be seen that $\overline{P}$ is dependent of $|V(k_x)|^2$, which is known as the energy spectrum. Evaluation of $|V(k_x)|^2$ gives a spectrum as shown in figure A.1. (The shaded area ($\int|V(k_x)|^2 dk_x$) is a measure for the radiated sound power). The normal velocities are maximal at the resonant modes (standing waves of mode p) so radiation is mostly determined by the resonant modes.

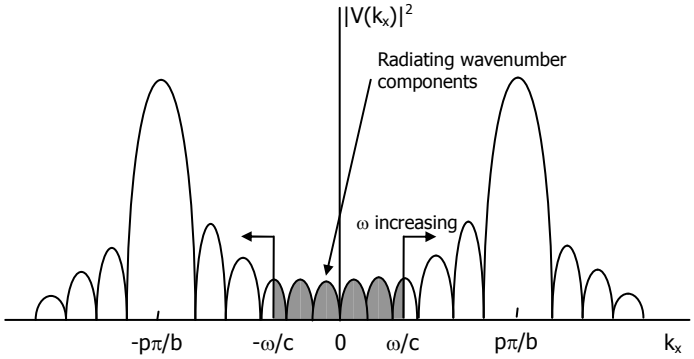

Figure A.1: *Fourier wave number transform of a given normal velocity distribution. Fahy [1]*

The plate radiates only sound energy into the air when $|k_x| < k$. In this case the equation of $\overline{P}$ is real. The case that $|k_x| > k$, is physically not possible because k_x must equal the component of the 'radiated' acoustical wave number k parallel to the plate. When the acoustical wave number increases, the amount of wave numbers in the plate that participate in the radiation also increases. Therefore the radiation increases with increasing frequency. (The radiation includes more and more resonant modes with increasing frequency).

Physically, this means that at the first resonant modes (below the critical frequency) only the edges of the plate radiate because there the air particles cannot cancel out the 'positive and negative displacements of the plate by moving from the positive peaks to the negative peaks, which is visualised in figure A.2. Fahy [1] found that at and above the critical frequency the whole plate will participate in the radiation resulting in an approximately constant radiation coefficient $\sigma_{rad} = 1$.

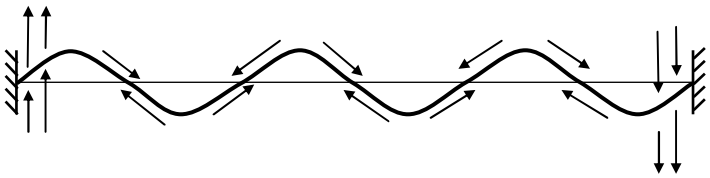

Figure A.2: *Visualisation of the radiation of a 1-dim plate at resonance mode p=6 below the critical frequency. The air particles level out the positive and negative peaks of the plate. At the edges this is not possible resulting in radiation into the air.*

The vibration power of the plate is $\rho_0 c S v_n^2$, where S is the surface area of the vibrating object (S = b, for 1-dim plate). So the radiation coefficient of a 1-dim plate with a given normal velocity distribution v_n is:

$$\sigma_{rad} = \frac{\overline{P}}{\rho_0 c_s S v_n^2} \tag{A.2}$$

Next, two 1-dim plates are considered, which are made of the same material and have similar thickness but different width. When these plates vibrate at modes of the same structural wavelength λ the corresponding natural frequencies will be similar. Although the spectra are different in the region of the main peaks because of the different width, the heights of the other peaks at low frequencies are approximately the same. Therefore it can qualitatively be concluded that for the same velocity amplitude, the smaller plate will radiate more effectively. (So σ_{rad} of a small plate is greater than σ_{rad} of a large plate).

For the two-dimensional case the natural frequencies and its normal velocity distribution are given by:

$$\omega_{pq} = \left(\frac{D}{m}\right)^{1/2}\left[\left(\frac{p\pi}{b}\right)^2 + \left(\frac{q\pi}{L}\right)^2\right] \tag{A.3}$$

$$v_n(x,z) = \tilde{v}_{pq}\sin\left(\frac{p\pi x}{b}\right)\sin\left(\frac{q\pi z}{L}\right) \qquad 0 < x < b \qquad 0 < z < L \tag{A.4}$$

Similar to the one-dimensional case a two dimensional plate can only radiate if $|k_x^2 + k_z^2| < k^2$. So for a two-dimensional plate three cases can be distinguished as is explained in figure A.3:

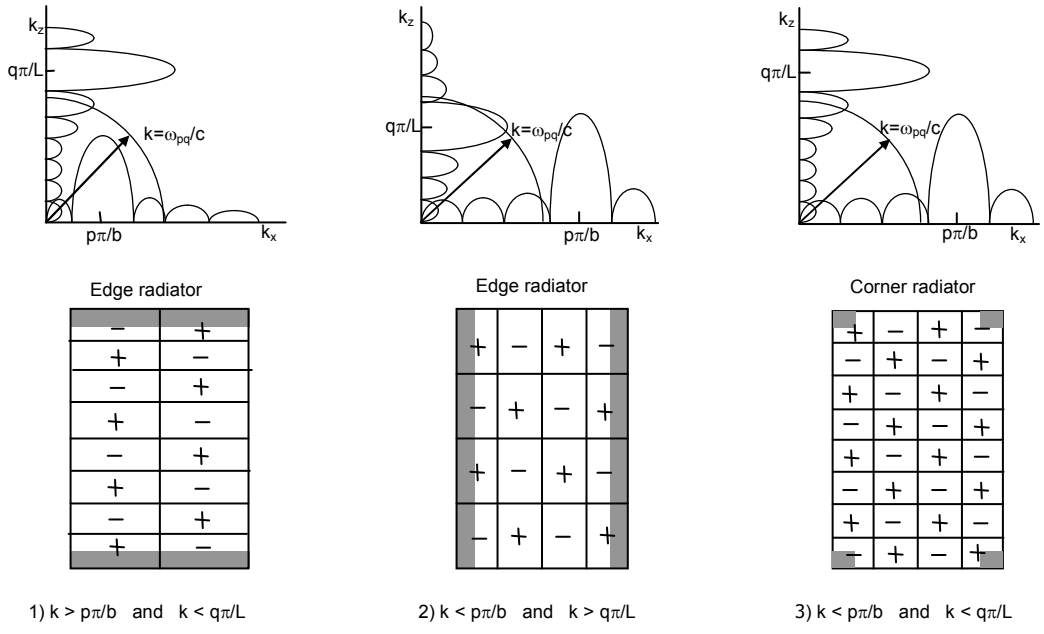

Figure A.3: *Visualisation of the radiation of a 2-dim plate below the critical frequency. The air particles level out the positive and negative peaks of the plate. Depending on the wave number the edges or the corners radiate into the air. [1]*

Only wave numbers in the shaded area radiate sound. Case 1) and 2) correspond to edge radiators and case 3) to a corner radiator. Edge radiators radiate more than corner radiators. With increasing frequency more resonant modes participate in the radiation process and therefore increasing the radiation coefficient σ_{rad}. At and above the critical frequency the whole plate is 'involved' in the radiation process and the radiation coefficient σ_{rad} will reach 1.

For the same reason as in the one dimensional case it can be concluded that of two plates of the same material and thickness but with different dimensions (b and L) the smaller plate radiates more effectively for the same normal velocity distribution.

Reference

[1] Fahy, F., Sound and structural vibration, radiation, transmission and response, Academic Press, London, 1989.

B Acoustic insulation of sandwich skins

This appendix gives some background information to the acoustic behaviour of sandwich panels. The sound transmission of a sandwich panel differs from that of single panel because of the presence of a core layer. As discussed in section 3.1 the sound transmission of a single panel is characterised by the free flexural deformation mode. For a sandwich panel the sound transmission is characterised by a combination of the free flexural deformation mode and the shear deformation mode. When the core is compressible also dilatation modes are of influence.

The free flexural wave speed of a panel with a bending stiffness D and a total mass per unit area m is given by, Fahy [1]:

$$c_b = \sqrt{\omega}\sqrt[4]{\frac{D}{m}} \tag{B.1}$$

The transverse shear wave speed is, Kurtze and Watters [2]:

$$c_{sh} = \sqrt{\frac{G}{\rho}} \tag{B.2}$$

Here G is the shear modulus of elasticity and ρ the density. Notice that the transverse wave speed is independent of the frequency. (Shear waves show no dispersion). Therefore coincidence will not occur as long as the velocity of the propagation of shear waves is appreciably less than the speed of sound in air. This gives a restriction for the optimal acoustic core material. The core should be soft but incompressible (e.g. rubber), sandwiched between two stiff skins.

The combination of the flexural and shear modes, gives the opportunity to increase the coincidence frequency. This can be explained with the dispersion curve for sandwich panels.

The dispersion curve of a sandwich panel was determined by Kurtze and Watters [2]:

$$\frac{c_s^4}{c_b^4}c^6 + c_s^2 c^4 - c_s^4 c^2 - c_{bf}^4 c_s^2 = 0 \qquad \text{(B.3)}$$

Here is:

$$c_b = \sqrt{\omega}\sqrt[4]{\frac{D}{m}}$$

$$c_{bf} = \sqrt{\omega}\sqrt[4]{\frac{2D_f}{m}}$$

$$c_s = \sqrt{\frac{G_c t_c}{m}}$$

In this equation, the total sandwich bending stiffness D can be estimated by:

$$D = \frac{1}{2}E_f t_f \left(t_f + t_c\right)^2 \qquad \text{(B.4)}$$

And the bending stiffness of a separate facing D_f by:

$$D_f = \frac{E_f t_f^3}{12\left(1-\nu^2\right)} \qquad \text{(B.5)}$$

m is the total mass per unit area of the sandwich panel:

$$m = 2\rho_f t_f + \rho_c t_c \qquad \text{(B.6)}$$

G_c is the shear modulus of the core and E_f the modulus of elasticity of the facing and t_c and t_f are the thickness of the core and the facing.

Equation B.3 results in the dispersion curve as shown in figure B.1. For low frequencies, the wave speed of the sandwich panel approaches the flexural bending wave speed of the complete sandwich (c_b), while for high frequencies the wave speed approaches the flexural bending wave speed of the separate facings (c_{bf}). The difference between these two wave speeds, indicates the possible shift of the coincidence frequency. The possible shift in coincidence frequency can be determined by two characteristic frequencies:

for $c_s = c_b$ $$\omega_1^2 = \frac{\left(G_c t_c\right)^2}{mD} \qquad \text{(B.7)}$$

for $c_s = c_{bf}$ $$\omega_2^2 = \frac{\left(G_c t_c\right)^2}{2mD_f} \qquad \text{(B.8)}$$

When the speed c_{sh} is kept well below the speed of sound in air c_s, say $c_{sh} \leq 0.66\ c_s$, the coincidence frequency will increase approximately by a factor of $\omega_2/\omega_1 = D/2D_f$. Depending on the panel material and dimensions, coincidence frequency increment factors of about 1000 are possible

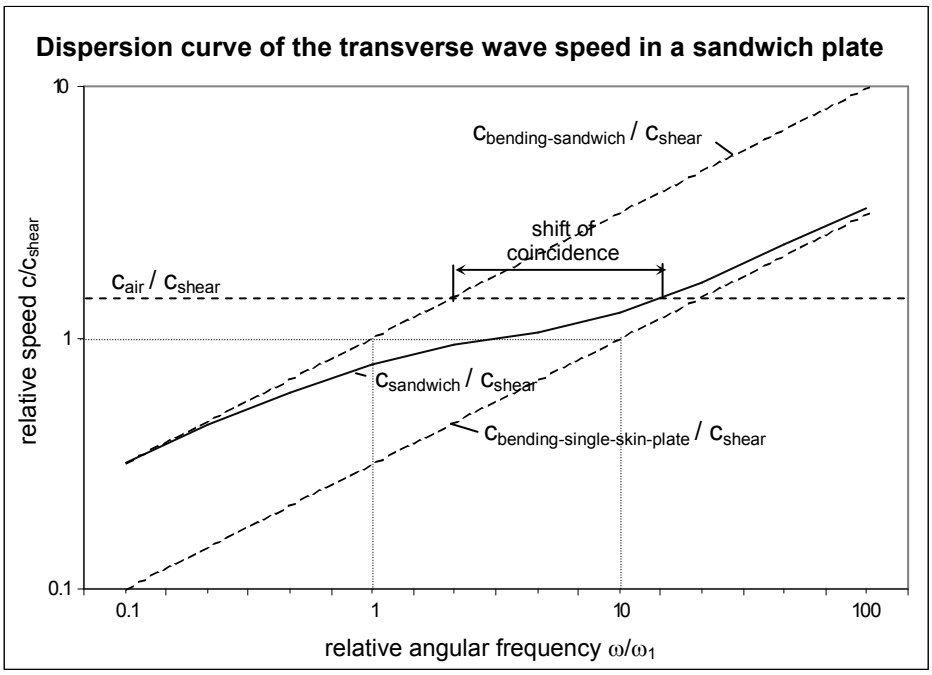

Figure B.1: *Dispersion curve of the transverse wave speed in a sandwich plate, with total static bending stiffness equal to 20 times the stiffness of a single skin plate. (ω_2/ω_1)*

This discussion gives two design rules for the sandwich materials and dimensions when a high coincidence frequency is desired:

1.) The velocity of the transverse shear wave may not exceed two-thirds of the speed of sound in air, Kurtze and Watters [2]:

$$c_{sh} = \sqrt{\frac{G_c t_c}{m}} \leq \frac{2}{3} c_{s\,air} \tag{B.9}$$

This implies that the shear modulus of elasticity of the core should be low.

2.) When the coincidence frequency is chosen just above the upper bound of the frequency range important for speech; $\pm$ 4000 Hz a restriction is found to the allowable materials and dimensions, Kurtze and Watters [4]:

$$\frac{c_{s\,air}^{\;2}}{2\pi}\sqrt{\frac{m}{2D_f}} \geq f_c \tag{B.10}$$

It should be avoided that the core material is compressible because in that case the spacing between the two skins will not remain constant. According to Ford [3] and Smolenski [4], then the dilatation frequency will be of influence.

The dispersion equation B.3 of Kurtze and Waters has later been improved using Hamiltons principle. It can be found that the apparent bending stiffness of a sandwich is the real solution of equation B.11:

$$\frac{A}{f} D^{\frac{3}{2}} - \frac{B}{f} D^{\frac{1}{2}} + D - C = 0 \qquad \text{(B.11)}$$

Where:

$$A = \frac{G_c t_c}{2\pi D\sqrt{m}} \qquad B = \frac{G_c t_c}{2\pi\sqrt{m}} \qquad C = 2D_f$$

Figure B.2 gives an example of the frequency dependent bending stiffness of a sandwich with properties given in table B.1

Table B.1: *Dimensions and material properties of example sandwich panel*

Facing			Core		
E_f	70e9	N/m^2	G_c	1e7	N/m^2
t_f	1	mm	t_c	10	mm
ν_f	0.3	(Poisson ratio)	ρ_c	100	kg/m^3
ρ_f	2700	kg/m^3			

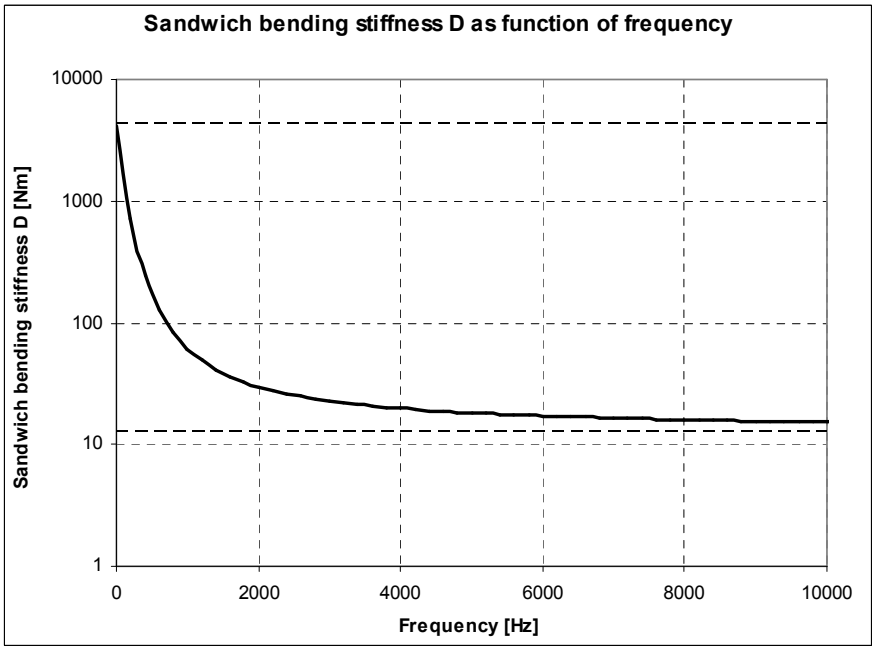

Figure B.2: *Illustration of the frequency dependency of the bending stiffness of a sandwich panel with properties stated in table B.1.*

The sound transmission loss of a sandwich panel now can be determined by using the solution of D from equation B.11 in equation 3.6, 3.7 and 3.8 from chapter 3 and intergrating over the incidence angle with equation 3.13. It should be noted that the coincidence frequency of equation 3.9 is also dependent on the frequency dependent bending stiffness D.

Reference

[1] Fahy, F., Sound and structural vibration, radiation, transmission and response, Academic Press, London, 1989.
[2] Kurtze, G., Watters, B.G., New wall design for high transmission loss or high damping, The journal of the acoustical society of America, vol 31, nr 6, 1959.
[3] Ford, R.D., Lord, P., Walker, A.W., Sound transmission through sandwich constructions, Journal of sound & vibrations, vol 5, nr 1, 1967.
[4] Smolenski, C.P., Krokosky, E.M., Dilatation-mode sound transmission in sandwich panels, The journal of the acoustical society of America, vol 54, 1973.

C Acoustic insulation with visco elastic layers

Demmenie [1] experimentally showed that an addition of a viscoelastic layer on a fuselage structure improves the TL. Figure C.1 shows an example of the TL of a fuselage skin section compared to the TL of the same fuselage section with an added constrained viscoelastic layer 'Y' that consists out of a 0.05 mm viscoelastic layer and 0.125 mm constraining layer. The TL for the panel without a viscoelastic layer shows a decrease of the TL gradient above 1000 Hz caused by coincidence. The panel with a visco-elastic layer (+ 1 layer Y) shows an improvement of the TL caused by the increased structural loss factor and the added mass. Especially above the coincidence frequency range the TL improvement is large as can be expected.

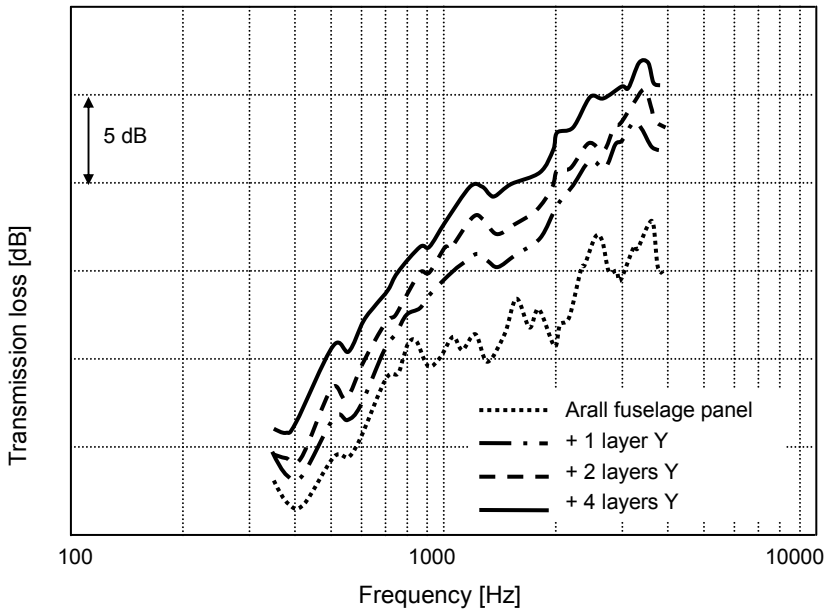

Figure C.1: *Experimentally determined TL [1] of an Arall fuselage section with a skin thickness of 0.8mm. Layer Y consist out of a 0.05 mm elastomer layer and a 0.125 mm constraining layer.*

Demmenie [1] found that the addition of extra viscoelastic layers becomes less efficient. The improvement from one layer Y to two layers Y is approximately the same as the improvement from two layers Y to four layers Y. (See figure C.1). The physical reason for this is that the viscoelastic layers will be less loaded in shear when more viscoelastic layers are present in the panel.

Reference

[1] Demmenie, E.A.F.A., Transmissieverlies van rompwandpanelen, NLR TP 94476 L, Amsterdam, 1994.

D Additional heat transfer theory

This appendix discusses the heat and convection phenomenons in section D.1 and D.2. In section D.3 the interaction of heat conduction, radiation and convection on a fuselage wall is described.

D.1 Heat radiation

Radiation is the transfer of energy from a higher temperature body, through space, to another lower temperature body or bodies some distance away. True radiation is the transfer of heat between these bodies without raising the temperature of the medium through which the heat passes. Radiation is expressed as $\sigma\varepsilon T^4 - \alpha q_r$ where σ is the Stefan-Boltzman constant and ε is the surface emissivity, which is the ability of an opaque material to emit radiant energy as a result of its temperature. It is measured by the ratio of the radiant emission of the material to the corresponding emission of a thermally black body at the same temperature (ε = 1.0). α is the surface absorbtivity.

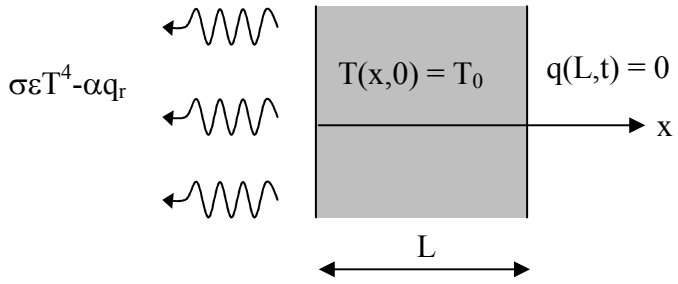

Figure D.1: *Radiation from a fuselage surface.*

Filling the boundary condition for radiation into the equation for conservation of energy the following relation is found:

$$\rho c L \frac{dT}{dt} + \sigma\varepsilon T^4 = \alpha q_r \qquad \text{(D.1)}$$

As time becomes large the fuselage wall temperature will approach the ambient air temperature T_a. Therefore αq_r can be set equal to $\sigma\varepsilon T_a^4$. This means there is as much heat radiated into the fuselage wall surface as is radiated into the ambient air. This leads to the following equation:

$$\frac{\sigma\varepsilon}{\rho cL}dt = \frac{dT}{T_a^4 - T^4} \tag{D.2}$$

By solving this equation with the boundary condition $T(x,0) = T_0$ the following equation is found, Thornton [1]:

$$\frac{\sigma\varepsilon}{\rho cL}t + \frac{1}{4T_a^3}\left[\ln\frac{(T_a - T)(T_a + T_0)}{(T_a + T)(T_a - T_0)} + 2\arctan\left(\frac{T_0}{T_a}\right) - 2\arctan\left(\frac{T}{T_a}\right)\right] = 0 \tag{D.3}$$

Equation D.3 does not give the temperature as function of time explicitly but the time can simply be calculated for different temperatures between T_0 and T_a. This results in a temperature time distribution as is shown in figure D.2.

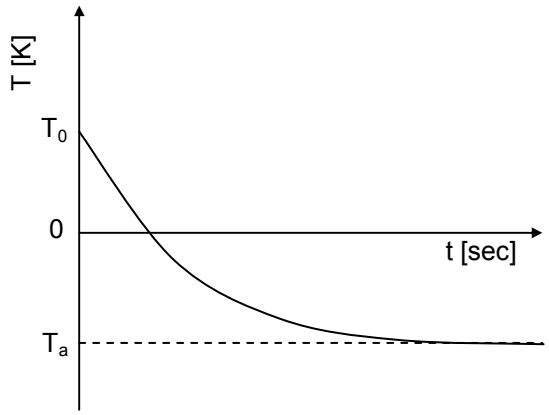

Figure D.2: *Outside surface temperature versus time*.

D.2 Convection

Convection can be considered as the movement of heat energy from one location to another. Convection is expressed by the equation: $h(T_a-T)$ where h is the convective constant and T_a is the ambient air temperature. For aircraft at cruise speed the outside air moves with cruise speed along the fuselage. This gives the outside air almost no chance to heat up. In a simplified case it is assumed that the outside air remains at a constant temperature T_a. The case that the heated air is moved away is called forced convection.

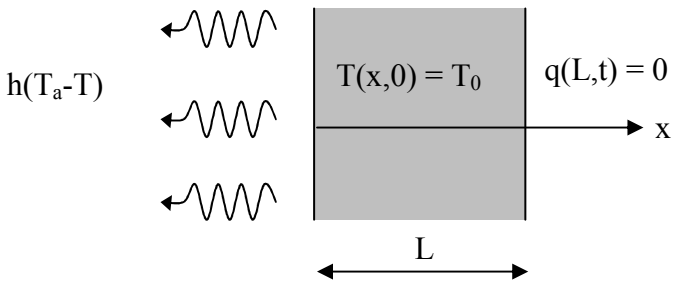

Figure D.3: *Convection from a fuselage surface*.

Figure D.3 considers forced convection for a fuselage wall with a initial temperature $T(x,0)=T_0$, a perfectly insulated inside surface and a constant ambient air temperature T_a at the outside surface. For this situation the energy balance becomes:

$$h(T_a - T)A = \left(\rho c \frac{dT}{dt}\right)AL \tag{D.4}$$

The solution to this equation is:

$$T(t) = T_0 e^{-\left(\frac{h}{\rho cL}\right)t} + T_a\left(1 - e^{-\left(\frac{h}{\rho cL}\right)t}\right) \tag{D.5}$$

This relation shows that the fuselage wall temperature will gradually approach the ambient air temperature just like in the case of radiation.

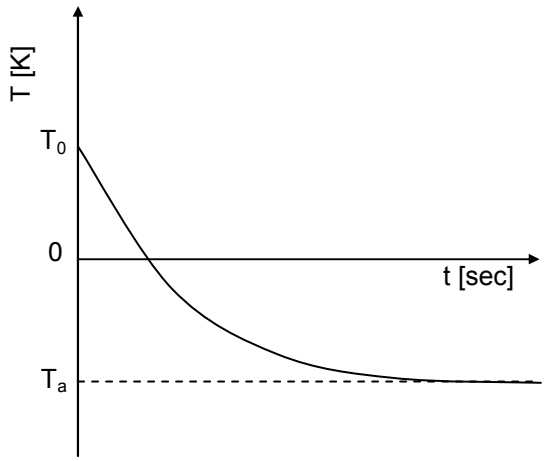

Figure D.4: *Outside surface temperature versus time*.

D.3 Relation between conduction, radiation and convection

In reality conduction, radiation and convection occur at the same time. However combining the boundary conditions for all three aspects makes it very difficult to analytically solve the heat transfer equations.
Malloy [2], considered a simplified case where only the temperature equilibrium is considered that would exist at the outer surface of the fuselage wall after a certain amount of time. This means that the time parameter is taken out of the equations. At the outside surface of the fuselage skin, the transmitted heat q_t (which equals the conduction through the fuselage wall) must equal the heat that disappears into the air outside the fuselage by radiation and convection. This equilibrium is expressed by the following equation in Brittish units by Malloy [2]:

$$\frac{T_{in}-T_s}{\sum\frac{t_n}{k_n}}=0.174\varepsilon\left[\left(\frac{T_s+459.6}{100}\right)^4-\left(\frac{T_a+459.6}{100}\right)^4\right]+0.296\left(T_s-T_a\right)^{5/4}\sqrt{\frac{V+68.9}{68.9}} \tag{D.6}$$

Where: T_{in}: Temperature inside the fuselage [°F]
T_s: Temperature at the outside fuselage wall surface [°F]
T_a: Ambient air temperature outside the fuselage [°F]
t_n: Thickness of nth layer of the fuselage wall [inch]
$k_{con\text{-}n}$: Conduction factor of n^{th} layer of the fuselage wall [BTU/inch°Fft^2hr]
ε: Fuselage outside surface emissivity
V: Flying speed [ft/min]

Because the conduction constants $k_{con\text{-}n}$ are dependent on temperature an iteration process is needed to determine the transmitted heat. This iteration process has the following steps:

1. Estimate the mean temperatures of the fuselage wall layers and determine the conduction constants $k_{con\text{-}n}$. (Usually the conduction constants as a function of temperature for a material are given by the manufacturer).
2. Determine the surface temperature, T_s, from the transmitted heat equation.
3. Determine with the now known surface temperature T_s the new mean temperatures and its conduction constants $k_{con\text{-}n}$ of each wall layer and return to step 2.

This process can be repeated until the outside surface temperature T_s has converged. Once T_s is known the transmitted heat can be determined:

$$q_t=\frac{T_{in}-T_s}{\sum\frac{t_n}{k_{con-n}}} \tag{D.7}$$

The energy needed per hour (E) to keep the fuselage temperature at a constant comfortable temperature equals the transmitted heat (q_t) times the fuselage surface (S):

$$E=q_tS \tag{D.8}$$

When the fuselage wall is optimised for thermal insulation the only parameters that are of interest for different fuselage configurations are the conduction factors and the thicknesses of the fuselage wall. The emissivity, which depends on the fuselage painted colours (predetermined for each airline company), and the flying speed can be considered as constants. As a result the optimising procedure of the DEE only has to take the conduction into account. The fuselage wall will be most efficient for thermal insulation when the heat transfer caused by conduction is minimised.

D.4 Reference

[1] Thornton, E.A., Przemieniecki, J.S., Thermal structures for aerospace applications, AIAA education series, 1996.
[2] Malloy, J.F., Thermal insulation, New York: Van Nostrand Reinhold Company, 1969.

E List of input parameters for the ICAD Multi Model Generator

The ICAD Multi Model Generator starts with the definition of the input parameters. By defining the input parameters, a fuselage concept of the designers choice can be generated. For the analyses, the designer has to choose what input parameters will be selected as design variables.

The input parameters can be divided into three groups:

1.) Geometric model parameters, that define the geometrical model and assign material definitions to the model parts. Within this group the parameters can be divided into high level (HL) parameters that define whether a part exists or not and middle level (ML) parameters that define the geometry and material properties.
2.) Meshing parameters that define the mesh of the models for FEM calculations. All these parameters are considered low level (LL) parameters.
3.) Load case parameters that define the load cases for the different analysis modules. Also all these parameters are considered low level (LL) parameters.

Next a list is given will all the input parameters.

Geometric model parameters

Skin	Level
:skin-shell?	HL
:skin-visco-layer?	HL
:skin-thickness-list	ML
:skin-material-list	ML

Frames	
:frames?	HL
:edge-frames?	HL
:frame-position-list	ML
:frame-web-height	ML
:frame-web-thickness-list	ML
:frame-web-material-list	ML
:frame-flange-top-radius	ML
:frame-flange-top-material	ML
:frame-flange-bottom-radius	ML
:frame-flange-bottom-material	ML

Stringers	
:stringers?	HL
:stringer-position-list	ML
:stringer-material	ML
:stringer-shape	ML
:stringer-thickness	ML
:stringer-radius	ML
:circular?	ML
:stringer-inside?	ML

Interior panels	Level
:interior-panel?	HL
:interior-visco-layer?	HL
:interior-shell?	HL
:interior-skin-thickness-list	ML
:interior-skin-material-list	ML

Insulation blankets	
:insulation?	HL
:insulation-material	ML

Floor	
:top-floor?	HL
:top-floor-thickness-list	ML
:top-floor-material-list	ML
:bottom-floor?	HL
:bottom-floor-thickness-list	ML
:bottom-floor-material-list	ML

floor-beams	
:top-floor-beams?	HL
:top-floor-beams-radius	ML
:top-floor-beams-material	ML
:top-floor-beams-offset	ML
:bottom-floor-beams?	HL
:bottom-floor-beams-radius	ML
:bottom-floor-beams-material	ML
:bottom-floor-beams-offset	ML

Geometric model parameters *continued*

Air

:air-inside?	HL

Piezo-electric-patches

:layer-1?	HL
:layer-2?	HL
:layer-3?	HL
:layer-1b?	HL
:layer-2b?	HL
:layer-3b?	HL

Piezo-electric-patches *continued*

Each layer has the same parameters. Here only the parameters for layer 1 are mentioned.

:x1-list	ML
:y1-list	ML
:t1-list	ML
:l1-list	ML
:b1-list	ML
:layer-1-material-list	ML

Meshing parameters

	Level		Level
:air-inside-mesh-nr	LL	:inbetween-frame-mesh-nr-part-n	LL
:air-mesh-factor	LL	:inbetween-stringer-mesh-nr-part-n	LL
:frame-z-mesh	LL		

Load case parameters

	Level		Level
Mechanical analysis		**High frequency sound transmission loss analysis**	
:cabin-pressure	LL	:stringer-pitch-reference	LL
:fuselage-bending-moment	LL	:frame-pitch-reference	LL
:fuselage-shear-force	LL	:stiffening-correction-factor	LL
Eigenmode analysis		:fsplit1	LL
:frequency?	LL	:fsplit2	LL
Thermal insulation analysis		**Low frequency sound transmission loss analysis**	
:thermal?	LL	:nr-of-eigenmodes	LL
:radiation?	LL	:max-freq	LL
:convection?	LL	:transmission-loss?	LL
:heat-flux	LL	:t1	LL
:mass-flow-rate-list	LL	:sampling-frequency	LL
:outside-temp-at-infinity	LL	:acoustic-source-point	LL
:outside-surface-emissivity	LL	:acoustic-standoff-point	LL
:air-outside-initial-temperature	LL	:nr-of-increments	LL
:skin-initial-temperature	LL		
:interior-skin-initial-temperature	LL		
:filling-initial-temperature	LL		
:delta-temp-max	LL		
:initial-time-period	LL		
:total-time-period	LL		
:minimum-time-increment	LL		
:maximum-time-increment	LL		
:temp-change-rate	LL		

F Additional information on the fuselage parameterisation

F.1 FEM representations of various fuselage elements

All FEM analyses are performed with ABAQUS. Therefore, all fuselage elements are modelled with ABAQUS [1] specific FEM elements.

Stringers

The stringers are simplified by modelling the stringers as beam elements (ABAQUS: B31 elements). The beam elements are positioned between two nodes of the surface of the fuselage skin, or in case of a solid fuselage skin between two nodes of the inner surface of the solid skin. ABAQUS has the option to define an arbitrary thin walled cross section. The arbitrary cross section is defined by specifying the corner coordinates of each segment of the centre line together with the thickness for each segment. By choosing the beam lengthwise axis through the centre line of the beam element and the normal direction 'n_1' perpendicular to the fuselage skin the correct geometrical properties are defined. This is illustrated in figure F.1.

The stringer is modelled in longitudinal direction with the same amount of mesh elements as the number of mesh elements in the neighbouring skin.

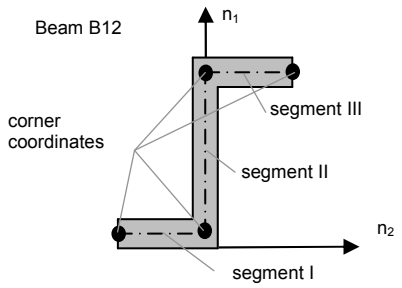

Figure F.1: *Modelling stringers with beam element that have a 'Z' cross section.*

Frames

The frames are also simplified. The frame web is modelled with shell elements (ABAQUS: S4R elements) and the frame top and bottom flanges are modelled with circular beam elements (ABAQUS: B31 elements). This is illustrated in figure F.2. The number of elements in height direction of the frame web is controlled with the input parameter *':frame-z-mesh'*. The circular cross section of the top and bottom flanges beam elements are determined such that the cross sectional area is equal to the real flanges. Since the cross section of the flanges is circular the orientation of the cross section is not of importance.

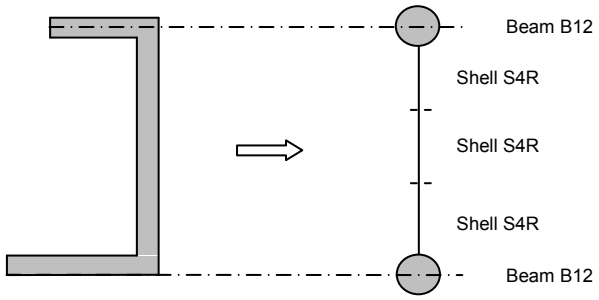

Figure F.2: *Equivalent beam and shell model of the frames.*

Air inside fuselage

The air inside the fuselage is only modelled for the acoustical analysis. The number of elements in the height direction from the top of the frames untill the 'end-lines' is controlled with the input parameter ':air-inside-mesh-nr'. Figure G.3 gives two examples where the input parameter ':frame-z-mesh' = 3 and parameter ':air-inside-mesh-nr' = 4 for a fuselage primitive with identical 'end-lines' and a fuselage primitive with different 'end-lines'.

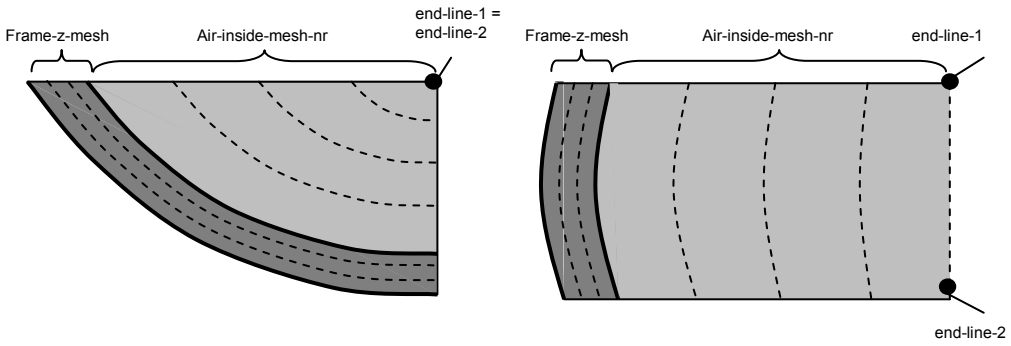

Figure F.3: *Mesh examples in radial direction.*

The acoustical analysis is performed with a steady state dynamic frequency analysis. Because the speed of sound in air is smaller than that in metals or composites, fewer mesh elements are required for the air compared to the structural parts like the fuselage skin. Therefore a more rough mesh is chosen for the air in circumferential and longitudinal direction compared to the fuselage skin. For the same reason, only one air element is chosen in the frame height direction for the air between the frames.

The air inside the fuselage is modeled with 8 node acoustic solid brick elements (ABAQUS: 3D8A). For the case where the 'end-lines' are coincident the air elements in the corner are modeled with 6 node acoustic solid triangle elements (ABAQUS: 3D6A).

Because of the different nature of acoustic and structural elements the edge surfaces of the air and the skin need to be coupled. This is done with the ABAQUS specific '*TIE' option. The ABAQUS specific '*TIE' option connects a slave node to a master node. Figure F.4 illustrates the connection scheme of the air inside the fuselage with the skin and frame elements.

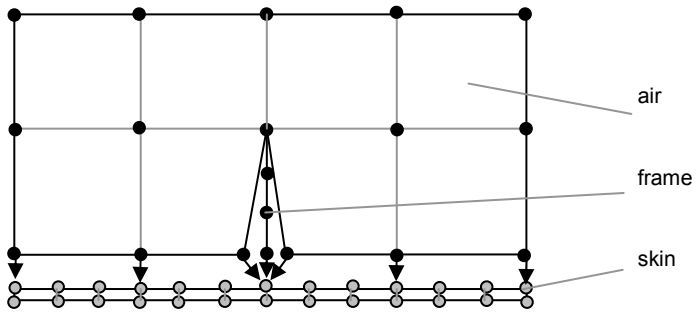

Figure F.4: *Mesh connection of air elements to the frame and skin elements.*

Interior panels

The interior panels are modeled with solid brick elements (ABAQUS: 3D8). The in-plane mesh is automatically copied from the in-plane mesh of the skin. Similar to the ':skin-thickness-list' parameter for the fuselage skin the ':interior-panel-thickness-list' controls the number of elements in the thickness direction.

Insulation blankets

The insulation blankets are also modeled by solid brick elements (ABAQUS: 3D8), that fill the space between the frames, skin and interior panel. Similar to the air elements the insulation blanket elements are coupled to the skin, frame and interior elements with the ABAQUS specific '*TIE' option. Like for the air inside the fuselage primitive, also for the insulation blankets a more rough mesh is chosen.

Floor panels

The floors are always modeled with shell elements (ABAQUS: S4R). Because shell elements have no actual thickness, they fit perfectly between two fuselage primitives. The floor thickness is defined in the element properties. The floor mesh is automatically coupled to the mesh of the air, the mesh of the interior panel and the mesh of the insulation blankets. When required the floor is coupled to the neighbouring elements with the ABAQUS specific '*TIE' option.

Floor beams

The floor beams are modeled with beam elements (ABAQUS: B31). For simplicity reasons, the floor beam elements have circular cross section. Therefore the orientation of these elements is of no importance.

Model mirroring

To be able to handle a-symmetric load cases, the model is mirrored in the symmetry plane with the ABAQUS specific '*MIRROR' option. The two halves are connected again with each other with the ABAQUS specific '*TIE' option.

Node and element numbering system

Each group of fuselage parts has its own identification number. The identification numbers specify the range of mesh element numbers that can be used for the different fuselage parts like the skin, frames, stringers, insulation blankets etc. These identification numbers are used to identify the elements in the post processing step of the DEE.

Throughout the model, the node numbers are increased by 1 in the u-direction and in v-direction by the amount of nodes that exist in u-direction. In the thickness direction the node numbers are increased by the amount of nodes in u-direction multiplied with the amount of nodes in v-direction. The mesh element numbers are chosen identical to the first node number of the specific mesh element plus the group identification number. The user is free to choose the group identification numbers. Care should be taken that no overlapping (similar element numbers for different mesh elements) will occur for large models.

Model restrictions and simplifications

To keep the model as simple as possible no interior equipment like passenger seats, luggage bins, galleys, toilets, curtains etc are modeled. Also the passengers themselves influence the sound absorption within a passenger cabin. These aspects could be taken into account by adding an impedance property to the floor and interior panels that represent similar sound absorption behaviour. Typical values can be found in literature.

Assembling fuselage primitives

To make an assembly of different fuselage primitives, the neighbouring nodes of different fuselage primitives are connected with the '*TIE' option.

F.2 ICAD material library

To be able to assign all the required material properties to the different elements by just assigning the material reference name in the input file, a material library is constructed within the ICAD environment.

There are many different kinds of materials. Therefore, to be able to automate the material assigning process, a fixed format is required for each type of material. First of all, materials can be divided into solid and fluid materials. Solid materials are used for the structural elements and fluid materials for the air and insulation blankets. The selection between these two materials is made with the Bolean IF THEN parameter; *':fluid?'*. By setting this parameter equal to *'true'* the material is a fluid material, otherwise a solid material.

When a material is recognised to be a fluid, it will require two material properties; the bulk modulus and the density. Another IF THEN parameter specifies whether the fluid is used to model air or an insulation blanket. When this parameter identifies the material to be an insulation blanket also the sound absorption coefficient is required.

For solid materials always the density and the elasticity properties have to be specified. The elasticity properties are specified in a list. If this list contains only an E-modulus and a density, the material is considered to be isotropic. For orthotropic or an-isotropic materials a list of 9 elasticity parameters (E_1, E_2, E_3, ν_{12}, ν_{13}, ν_{23}, G_{12}, G_{13}, G_{23}) has to be specified.

Solid materials can be made piezoelectric by assigning the Bolean IF THEN parameter *':piezo?'* to *'true'*. Then the piezoelectric strain coefficients and the dielectric constants are required.

F.3 Exporting the meshed ICAD model

The FEM model is exported with the ICAD specific option: 'write report'. The 'write report' option can be used to generate many different types of output files. For example: IGES files, STEP files, CATIA files, Pro Engineer files and text files. In this DEE the text file writer is used to generate a 'ready to run' ABAQUS text input file. The text file writer is a routine that can be programmed, what to write in the text file. The ABAQUS text input file is generated in separate pieces that are later translated into one complete input file. The different files are:

- Heading file, that contains the title and some lines to reduce the size of the ABAQUS output data that will be written to the standard output files of ABAQUS every time an ABAQUS analysis is performed.
- Node files, that contain the node numbers with their coordinates. The node numbering follows the routine as described in section F.1.
- Element files, that contain the element numbers with their corresponding node numbers. The element number is specified with the first node number of the mesh element. So for post-processing, the same identification system can be used for elements output as for node output.
- MPC files, that contain the TIE commands to connect the air and blanket elements to the structural elements.
- Boundary condition files, that contain node sets with their constraining degrees of freedom.
- History file, that contains the analysis definition and the output request.
- Mirror file, that contains commands to mirror the fuselage primitive.
- MPC files, that contain TIE commands to link different fuselage primitives within a fuselage assembly..
- Join file, that contains a routine that will concatenate the files mentioned above to one ABAQUS input file.
- Output data files, that are required for the Python and Matlab post processing routines. The output files for the Python routines contain node numbers that are used in the output selection procedure and the output files for the Matlab post processing scripts contain material property data.

When all text files are generated, a DOS translate routine joins the files to one complete, ready to run, ABAQUS input file.

F.4 Reference

[1] ABAQUS user manual, version 6.4

G Results of the DEE application on the aluminium test cylinder

G.1. Design of experiments and the resulting evaluations

For the analysis and optimisation of the stiffened aluminum cylinder a design of experiments has been performed with the Latin hypercube routine of the G_OPT program developed by Lanzi [1]. First, a set of 60 sample points is generated. For a second optimisation step another 40 sample points are generated.

The four design variables that are chosen for the optimisation of the stiffened aluminium cylinder concept are:
1.) The skin thickness [t_{skin}], also indicated as *SkinThickness*
2.) The number of frames [n_{fr}], also indicated as *NrFrames*
3.) The number of stringers [n_{str}], also indicated as *NrStringers*
4.) The stringer factor [k_{str}], also indicated as *StringerFactor*

The DEE is used to determine the performance of each requirement and objective functions. Eight requirements are considered:
1.) The tensile stress criteria of the cylinder skin [R_{skt}], also indicated as *RskinTen*
2.) The buckling criteria of the cylinder skin [R_{skb}], also indicated as *RskinBuck*
3.) The tensile stress criteria of the stringers [R_{strt}], also indicated as *RstringerTen*
4.) The Euler buckling criteria of the stringers [R_{strb}], also indicated as *RstringerBuck*
5.) The Hoop stress criteria of the cylinder skin [R_{Hoop}], also indicated as *Rhoop*

Three objective functions are considered:
1.) The weight of the aluminium test cylinder [W_{cil}], also indicated as *Weight*
2.) The thermal insulation characterised by the temperature difference [θ], also indicated as *DeltaT*.
3.) The acoustic insulation characterised by the overall sound transmission loss [OTL]

The design variables together with the evaluations of the requirements and the objective functions are shown in table G.1.1 for the first optimisation step and in table G.1.2 for the second optimisation step.

Table G.1.1: *Design of experiments and evaluations of the structural requirements and objective functions for 60 sample points used in the first optimisation step.*

	Design variables				Evaluations							
Nr	t_{sk} (mm)	n_{fr} (-)	n_{str} (-)	k_{str} (-)	R_{skb} (-)	R_{strb} (-)	R_{skt} (-)	R_{strt} (-)	R_{Hoop} (-)	W_{cil} (Kg)	θ (K)	TL (dB)
1	1.4501	1	12	0.8402	0.2422	0.2023	0.0806	0.0536	0.1978	8.4085	5.08e-4	28.7260
2	0.5155	4	14	1.1349	2.4723	0.0094	0.1521	0.0729	0.3854	6.8004	1.78e-4	28.7264
3	0.7168	3	6	0.6605	8.3701	0.1658	0.1719	0.0752	0.4064	5.6167	2.23e-4	28.7376
4	0.5125	1	16	0.5715	2.4295	0.2582	0.1883	0.0929	0.4843	4.3923	1.72e-4	28.7090
5	0.8504	0	6	1.0321	4.7721	1.0816	0.1427	0.1165	0.3550	4.3205	3.08e-4	29.0755
6	1.0268	4	14	0.6123	0.4857	0.0495	0.1091	0.0516	0.2565	7.9994	3.65e-4	28.9983
7	1.2502	3	6	1.1324	1.5739	0.0563	0.0988	0.0487	0.2364	8.1888	4.13e-4	28.3296
8	0.8213	0	16	1.0814	0.5517	0.3107	0.1126	0.0892	0.2996	5.6016	2.97e-4	29.0926
9	1.3345	3	16	1.1884	0.1476	0.0158	0.0758	0.0435	0.1875	10.0810	4.43e-4	28.2061
10	0.8253	0	8	0.5143	3.1276	3.4422	0.1498	0.1241	0.3680	3.9538	2.99e-4	29.0792
11	1.4865	3	8	0.5109	0.5669	0.2169	0.0858	0.0411	0.2025	8.8285	4.95e-4	29.8952
12	0.6107	2	10	1.0062	3.7709	0.0595	0.1644	0.0881	0.4153	5.4310	1.97e-4	28.7916
13	1.4927	0	8	0.5279	0.5586	3.3369	0.0857	0.0709	0.2078	6.7454	5.35e-4	29.3327
14	1.3029	1	16	0.5016	0.1923	0.4288	0.0902	0.0460	0.2199	7.5368	4.58e-4	28.5400
15	0.5095	4	8	1.1928	9.7237	0.0182	0.1885	0.0823	0.4560	5.9746	1.75e-4	28.6905
16	1.4782	0	6	1.1930	0.9649	0.8512	0.0850	0.0703	0.2090	7.0553	5.31e-4	30.2943
17	0.5184	3	12	0.5516	4.6541	0.1020	0.2020	0.1078	0.4840	5.1276	1.53e-4	28.7421
18	1.4772	3	16	0.7972	0.1237	0.0402	0.0755	0.0424	0.1816	9.8838	4.92e-4	30.3085
19	0.9830	4	10	0.9930	1.0396	0.0252	0.1122	0.0593	0.2656	7.9887	3.49e-4	28.6976
20	0.9542	2	14	0.7632	0.5657	0.0826	0.1128	0.0554	0.2768	6.9366	3.20e-4	28.8561
21	1.3859	2	6	0.8122	1.2166	0.2019	0.0919	0.0598	0.2212	7.9970	4.74e-4	28.4097
22	1.1759	1	10	1.1756	0.6073	0.1161	0.0955	0.0520	0.2367	7.4796	4.13e-4	28.7517
23	1.0815	2	10	0.5684	0.8819	0.2400	0.1119	0.0619	0.2697	6.8346	3.66e-4	29.0608
24	0.6096	4	16	0.7696	1.3813	0.0217	0.1488	0.0724	0.3612	6.7397	2.13e-4	28.7971
25	0.6325	2	16	1.1771	1.0397	0.0218	0.1281	0.0641	0.3407	6.6282	2.05e-4	28.6724
26	1.0533	0	14	0.8049	0.4248	0.7326	0.1037	0.0849	0.2602	5.8057	3.81e-4	29.0491
27	1.4912	4	12	1.1153	0.2115	0.0171	0.0749	0.0403	0.1785	10.5338	5.27e-4	29.4793
28	0.5046	0	12	0.7897	4.4208	0.7868	0.1930	0.1530	0.5137	3.2957	1.80e-4	28.6587
29	1.4601	4	12	0.5926	0.2506	0.0670	0.0828	0.0435	0.1939	9.6134	5.17e-4	29.5933
30	1.3205	0	16	1.0999	0.1552	0.3307	0.0785	0.0639	0.2003	7.7161	4.77e-4	29.4211
31	0.5176	1	6	0.6559	21.0448	0.6428	0.2325	0.1376	0.5731	3.7564	1.74e-4	28.7383
32	1.0318	1	10	0.8464	0.9408	0.2343	0.1122	0.0610	0.2760	6.4650	3.61e-4	28.9611
33	0.5664	0	12	1.1560	2.7981	0.3415	0.1588	0.1234	0.4385	4.1077	2.03e-4	28.8923
34	1.2027	4	6	0.6061	1.8945	0.1335	0.1063	0.0488	0.2475	8.1063	4 28e-4	28.7663
35	0.7781	1	12	0.5885	1.4943	0.3931	0.1452	0.0938	0.3577	5.2337	2.69e-4	28.9880
36	1.3562	0	6	0.7959	1.2982	1.9556	0.0943	0.0755	0.2306	6.2469	4.89e-4	29.1633
37	1.4664	4	8	0.9229	0.5538	0.0407	0.0834	0.0416	0.1965	9.6738	5.19e-4	30.0338
38	1.3190	0	12	0.5959	0.3355	1.7041	0.0913	0.0755	0.2238	6.3920	4.76e-4	29.4621
39	1.4507	0	16	0.7630	0.1313	0.7402	0.0777	0.0640	0.1924	7.5779	5.21e-4	28.7687
40	1.0594	4	14	1.1164	0.3813	0.0129	0.0945	0.0480	0.2297	9.0247	3.76e-4	29.0651
41	0.6130	4	8	0.8962	6.4761	0.0369	0.1763	0.0765	0.4155	6.1049	2.14e-4	28.7802
42	0.9927	1	6	0.7000	3.2546	0.6085	0.1276	0.0825	0.3107	5.7644	3.47e-4	28.6708
43	0.5411	2	14	0.8444	2.4924	0.0549	0.1679	0.0810	0.4329	5.3637	1.72e-4	28.8414
44	1.2625	3	12	0.7959	0.3621	0.0550	0.0912	0.0537	0.2184	8.5878	4.18e-4	29.0454
45	0.8938	2	6	0.9716	4.1951	0.1325	0.1364	0.0854	0.3305	6.0729	2.99e-4	28.9854
46	1.4535	2	12	0.5368	0.2574	0.2300	0.0842	0.0571	0.2020	8.4758	4.97e-4	29.0052
47	0.5093	1	8	1.1954	9.6590	0.1117	0.1947	0.0852	0.5128	4.4319	1.71e-4	28.6893
48	0.9939	2	14	1.1138	0.4528	0.0351	0.1006	0.0509	0.2543	7.7211	3.35e-4	28.7161
49	1.4184	2	12	1.0723	0.2455	0.0512	0.0793	0.0550	0.1936	9.1409	4.85e-4	30.0823
50	0.5915	0	8	0.8011	7.3263	1.2677	0.1904	0.1539	0.4797	3.2705	2.12e-4	28.8725
51	0.8709	3	10	0.7181	1.5663	0.0783	0.1316	0.0597	0.3136	6.6625	2.78e-4	29.0794
52	1.2171	1	6	1.0259	1.7221	0.2788	0.1028	0.0680	0.2512	6.9443	4.27e-4	28.8279
53	1.4574	2	8	1.0724	0.5514	0.0825	0.0832	0.0465	0.2016	8.7616	4.98e-4	29.3561
54	0.5177	3	16	0.5321	2.4326	0.0766	0.1875	0.0964	0.4558	5.3642	1.53e-4	28.7388
55	0.9009	1	16	0.5228	0.5393	0.3694	0.1229	0.0623	0.3036	5.9085	3.14e-4	28.8769
56	0.6881	4	12	0.8649	1.8880	0.0250	0.1454	0.0727	0.3494	6.8212	2.41e-4	28.5683
57	0.5051	4	8	0.6196	12.1141	0.0807	0.2209	0.0899	0.5141	5.3780	1.74e-4	28.6625
58	1.2142	2	6	0.5079	1.8653	0.5315	0.1066	0.0681	0.2544	7.0534	4.14e-4	28.6802
59	0.8896	3	16	0.9356	0.4739	0.0241	0.1088	0.0604	0.2698	7.7228	2.85e-4	29.0393
60	0.9230	4	6	1.0378	3.7892	0.0416	0.1299	0.0580	0.3060	7.2726	3.27e-4	28.8139

Table G.1.2: *Design of experiments and evaluations of the structural requirements and objective functions for another 40 data points used in the second optimisation step.*

	Design variables				Evaluations							
Nr	t_{sk} (mm)	n_{fr} (-)	n_{str} (-)	k_{str} (-)	R_{skb} (-)	R_{strb} (-)	R_{skt} (-)	R_{strt} (-)	R_{Hoop} (-)	W_{cil} (Kg)	θ (K)	TL (dB)
1	0.7478	0	14	0.5951	1.1779	1.3309	0.1451	0.1186	0.3648	4.1635	2.70^{e}-4	28.8919
2	0.9941	0	12	0.7167	0.7228	1.1164	0.1146	0.0942	0.2847	5.2223	3.60^{e}-4	28.7215
3	0.9553	0	16	0.7397	0.4200	0.7344	0.1103	0.0899	0.2796	5.4693	3.46^{e}-4	28.8344
4	0.9592	0	12	0.5038	0.8549	2.3561	0.1236	0.1023	0.3048	4.7547	3.47^{e}-4	28.7173
5	0.9406	0	16	0.5285	0.4771	1.5237	0.1186	0.0977	0.2953	4.9816	3.41^{e}-4	28.7020
6	0.6853	0	12	0.7481	1.9901	0.9551	0.1549	0.1253	0.3961	3.9848	2.47^{e}-4	28.5508
7	0.6761	0	16	0.7249	1.0711	0.7210	0.1449	0.1164	0.3773	4.2773	2.44^{e}-4	28.4969
8	0.6790	0	16	0.5055	1.1857	1.5968	0.1566	0.1277	0.3953	3.8465	2.45^{e}-4	28.5121
9	0.9764	0	14	0.6198	0.5576	1.2662	0.1152	0.0948	0.2862	5.1586	3.54^{e}-4	28.8428
10	0.7166	0	12	0.5029	1.9453	2.2713	0.1598	0.1314	0.3969	3.7438	2.59^{e}-4	28.7360
11	0.7954	0	14	0.7443	0.9353	0.8242	0.1322	0.1073	0.3369	4.6251	2.88^{e}-4	29.0468
12	0.8440	0	12	0.6242	1.1757	1.4539	0.1346	0.1105	0.3345	4.4580	3.05^{e}-4	29.0414
13	0.7943	0	16	0.6000	0.7369	1.1323	0.1335	0.1089	0.3375	4.5173	2.87^{e}-4	29.0474
14	0.9857	0	14	0.7382	0.5214	0.8798	0.1111	0.0909	0.2784	5.4062	3.57^{e}-4	28.6214
15	0.9175	0	14	0.5036	0.6929	1.9764	0.1252	0.1034	0.3099	4.7083	3.32^{e}-4	28.8204
16	0.6519	0	14	0.6908	1.6368	0.9323	0.1569	0.1265	0.4043	3.9334	2.35^{e}-4	28.5576
17	0.6610	0	12	0.6024	2.3316	1.5088	0.1662	0.1355	0.4176	3.6633	2.38^{e}-4	28.5112
18	0.6514	0	14	0.5144	1.7877	1.7832	0.1668	0.1363	0.4188	3.6195	2.35^{e}-4	28.5607
19	0.8138	0	16	0.7084	0.6573	0.7865	0.1265	0.1026	0.3234	4.8171	2.94^{e}-4	29.0361
20	0.8465	0	12	0.7335	1.1231	1.0282	0.1309	0.1070	0.3279	4.6335	3.06^{e}-4	29.0324
21	0.9779	0	16	0.6314	0.4108	1.0515	0.1115	0.0915	0.2790	5.3447	3.54^{e}-4	28.8321
22	0.6544	0	16	0.6025	1.2436	1.0753	0.1553	0.1256	0.3988	3.9401	2.36^{e}-4	28.5437
23	0.7853	0	14	0.5010	1.0724	1.9398	0.1433	0.1178	0.3560	4.1533	2.84^{e}-4	29.0013
24	0.8525	0	14	0.6539	0.8019	1.1085	0.1281	0.1048	0.3212	4.7031	3.09^{e}-4	29.1018
25	0.8269	0	16	0.5068	0.6890	1.6503	0.1331	0.1093	0.3323	4.4646	2.99^{e}-4	28.0596
26	0.9921	0	12	0.6179	0.7492	1.5314	0.1172	0.0967	0.2899	5.0645	3.59^{e}-4	28.6522
27	0.7392	0	12	0.6685	1.6697	1.2334	0.1488	0.1214	0.3739	4.0887	2.67^{e}-4	28.8504
28	0.8623	0	12	0.5378	1.1419	2.0333	0.1349	0.1113	0.3338	4.4030	3.12^{e}-4	29.0018
29	0.8889	0	14	0.5788	0.7355	1.4428	0.1262	0.1039	0.3137	4.7219	3.22^{e}-4	29.0377
30	0.6573	0	14	0.6217	1.6539	1.1783	0.1596	0.1295	0.4069	3.8340	2.37^{e}-4	28.5287
31	0.7437	0	14	0.6659	1.1595	1.0353	0.1427	0.1161	0.3622	4.2716	2.69^{e}-4	28.8639
32	0.7275	0	16	0.6569	0.9103	0.9087	0.1403	0.1135	0.3597	4.3539	2.63^{e}-4	28.7966
33	0.7754	0	12	0.5692	1.5197	1.7571	0.1468	0.1206	0.3649	4.0891	2.80^{e}-4	28.9677
34	0.8955	0	16	0.6768	0.5137	0.8889	0.1184	0.0967	0.2994	5.0937	3.24^{e}-4	28.9417
35	0.8864	0	16	0.5989	0.5459	1.1565	0.1221	0.1000	0.3063	4.8981	3.21^{e}-4	29.0096
36	0.9980	0	14	0.5380	0.5401	1.7219	0.1154	0.0953	0.2854	5.1037	3.61^{e}-4	28.8617
37	0.8948	0	14	0.7344	0.6811	0.8682	0.1205	0.0984	0.3040	5.0213	3.24^{e}-4	28.9609
38	0.9124	0	12	0.6859	0.9268	1.2040	0.1243	0.1021	0.3089	4.8359	3.30^{e}-4	28.9515
39	0.9490	0	14	0.6798	0.5907	1.0437	0.1163	0.0953	0.2904	5.1506	3.44^{e}-4	29.8299
40	0.6904	0	14	0.7448	1.3695	0.8000	0.1476	0.1191	0.3811	5.1891	2.49^{e}-4	28.5836

G.2. Response surfaces of the design requirements and the objective function for the aluminium test cylinder

This appendix gives an overview of the response surfaces for the different design requirements. The structural requirements are independent of the design variable; interior panel core thickness. Each response surface represents the requirements as function of two design variables. The remaining two design variables are fixed. The response surfaces are created with the G_OPT program developed by Lanzi [1] using the data from table G.1.

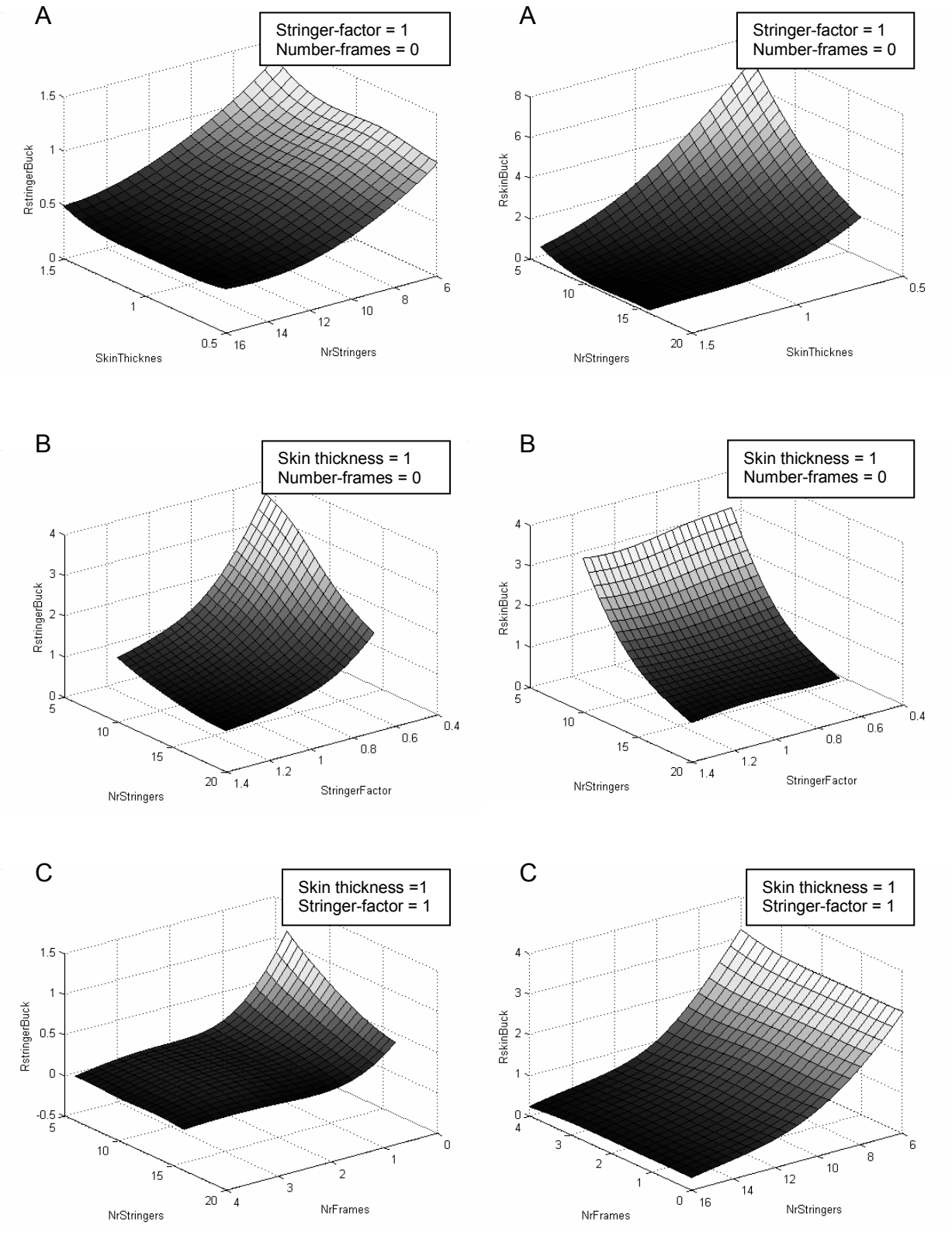

Figure G.2.1: *Response surfaces for the R stringer buckling requirement. (Validation set errors: Max=58.4879, Mean=29.5286, Rsqr=0.83311, Rmea=1.1667, APE=21.8125)*

Figure G.2.2: *Response surfaces for the R skin buckling requirement. (Validation set errors: Max=15.4884, Mean=10.8904, Rsqr=0.95619, Rmea=0.43655, APE=11.7277)*

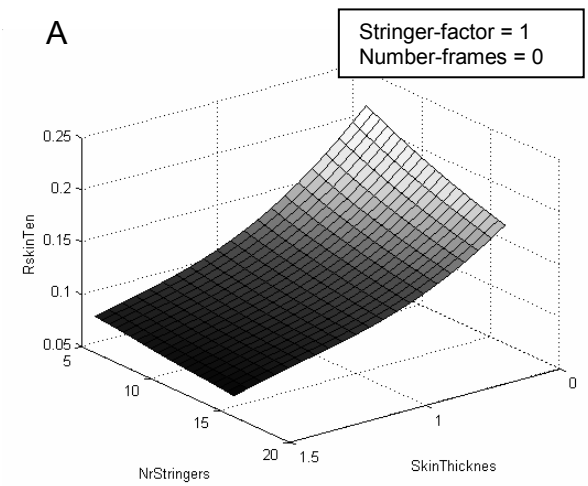

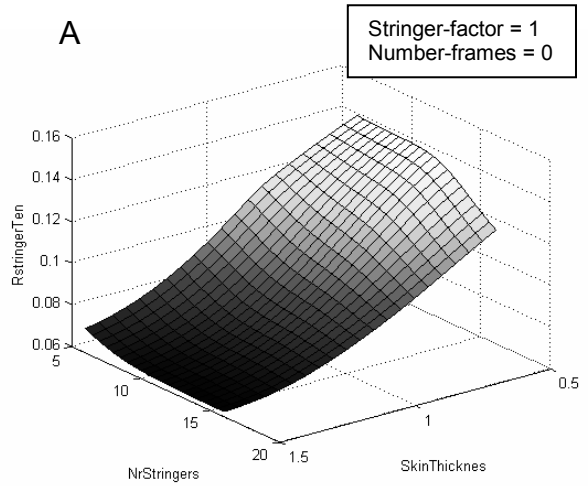

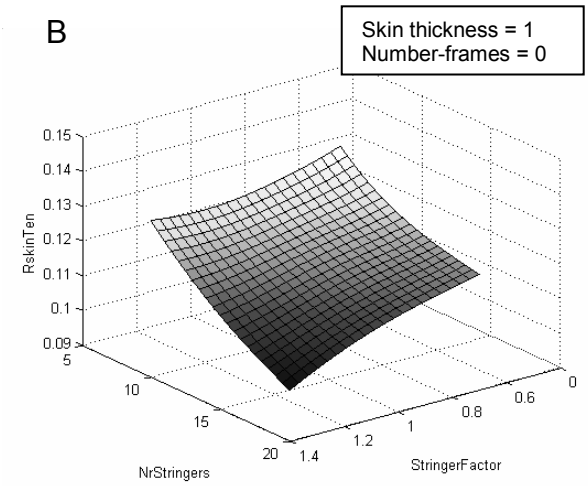

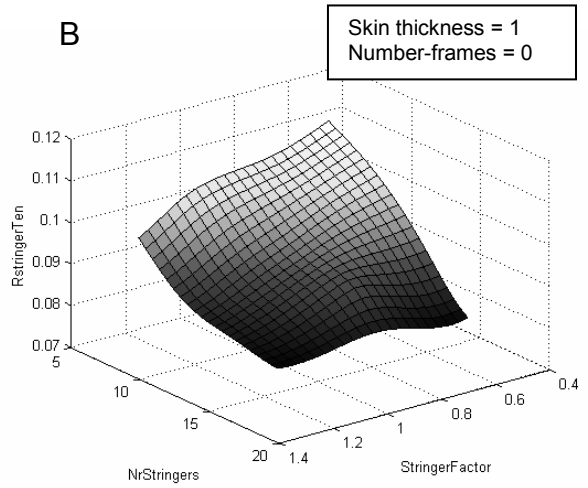

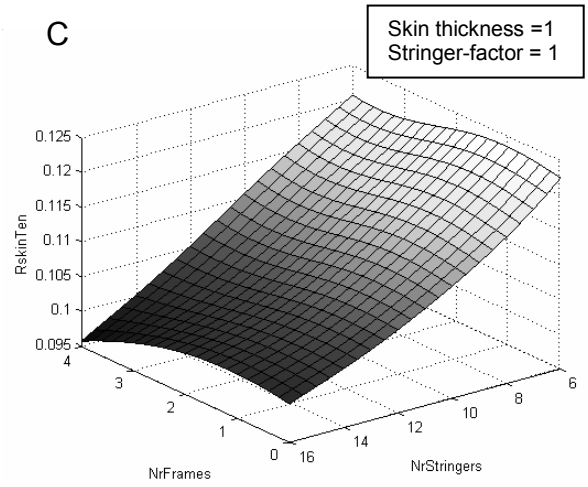

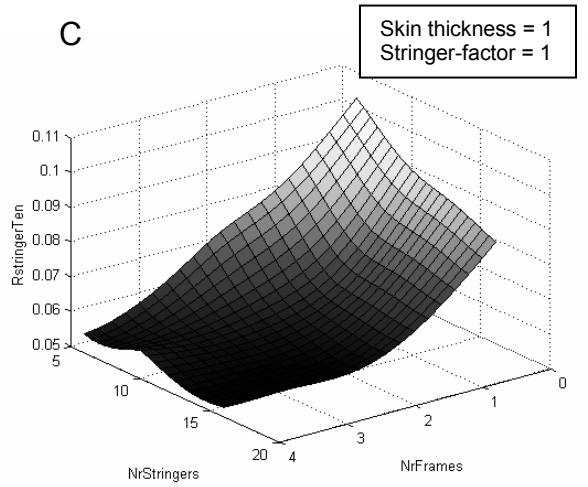

Figure G.2.3: *Response surfaces for the R skin tensile requirement. (Validation set errors: Max=3.3384, Mean=1.3631, Rsqr=0.9861, Rmea=0.19704, APE=1.5004)*

Figure G.2.4: *Response surfaces for the R stringer tensile requirement. (Validation set errors: Max=13.7226, Mean=6.2395, Rsqr=0.95247, Rmea=0.50396, APE=6.4388)*

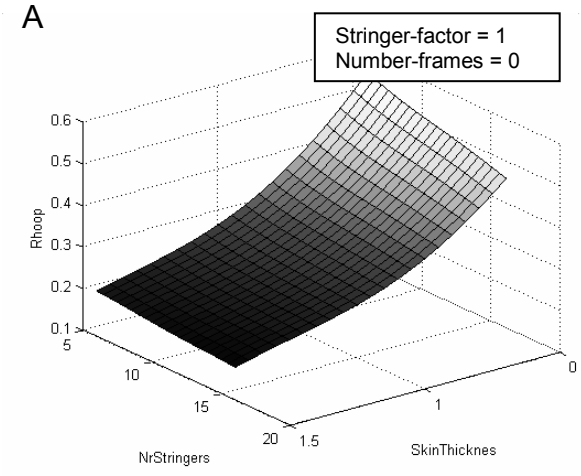

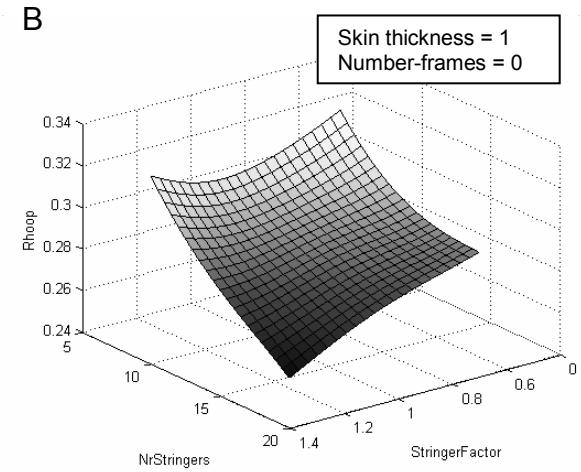

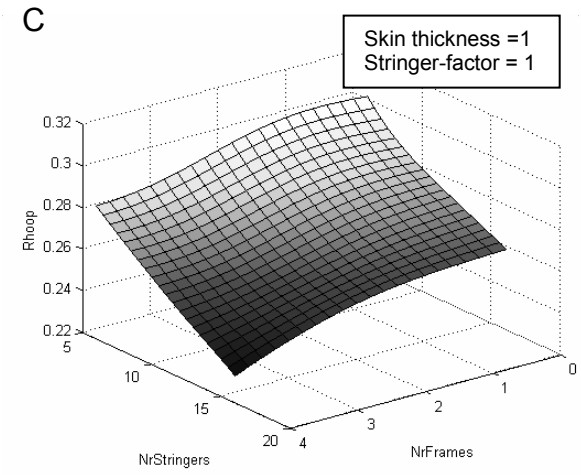

Figure G.2.5: *Response surfaces for the R hoop requirement. (Validation set errors: Max=3.1252, Mean=1.4721, Rsqr=0.99637, Rmea=0.10085, APE=1.475)*

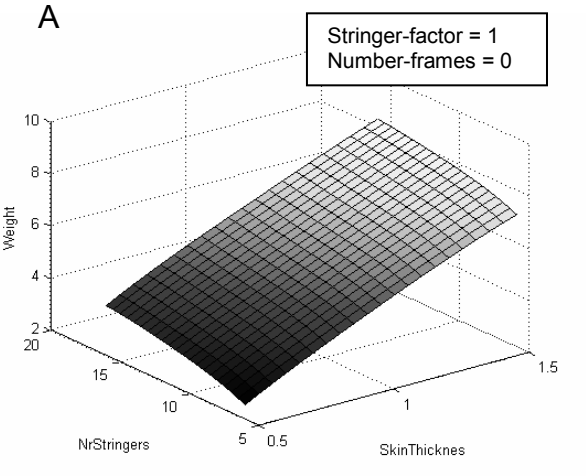

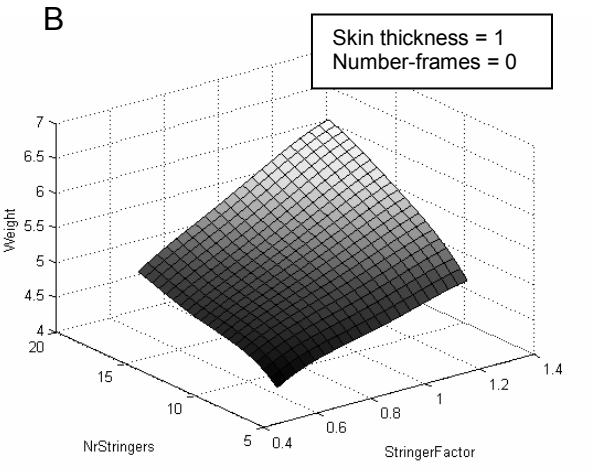

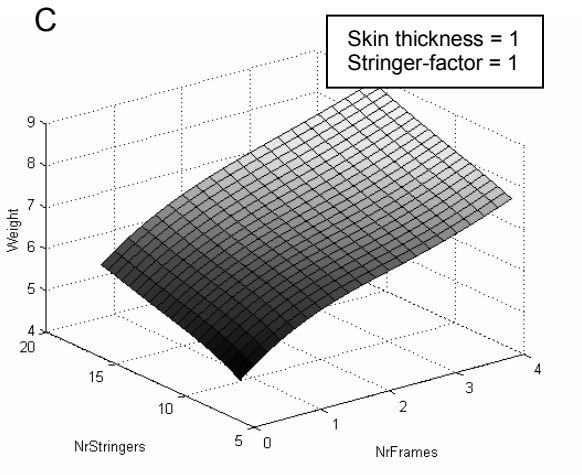

Figure G.2.6: *Response surfaces for the cylinder weight. (Validation set errors: Max=1.7973, Mean=0.84737, Rsqr=0.99716, Rmea=0.078534, APE=0.84497)*

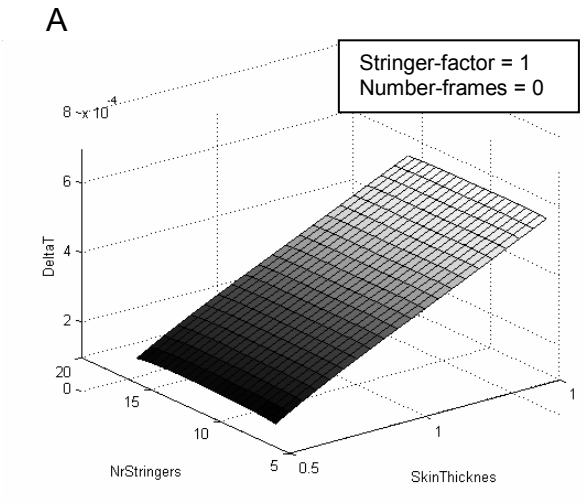

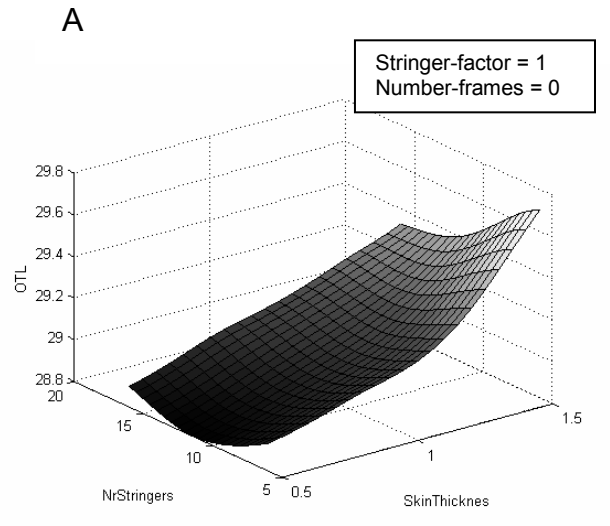

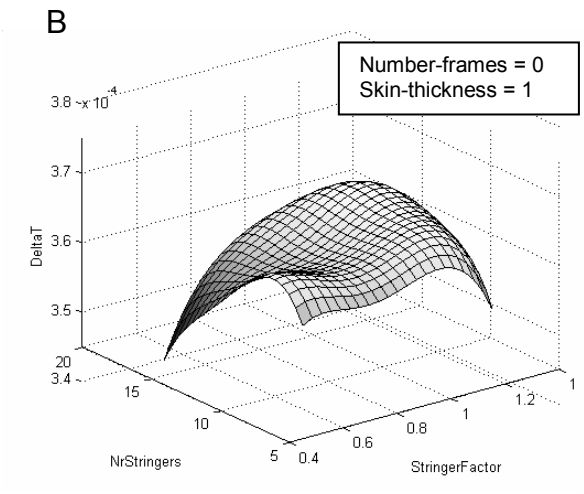

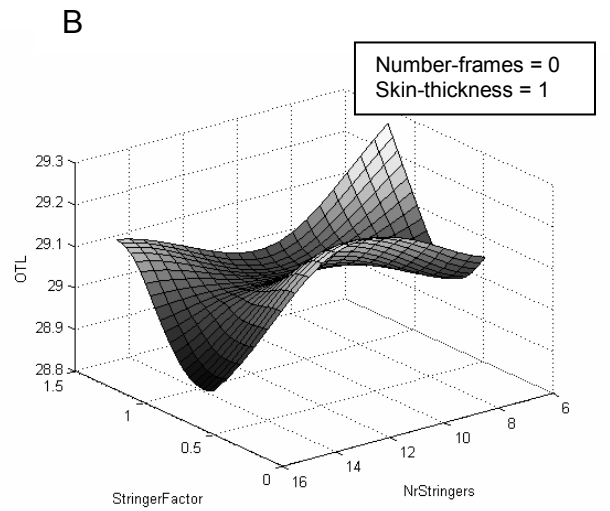

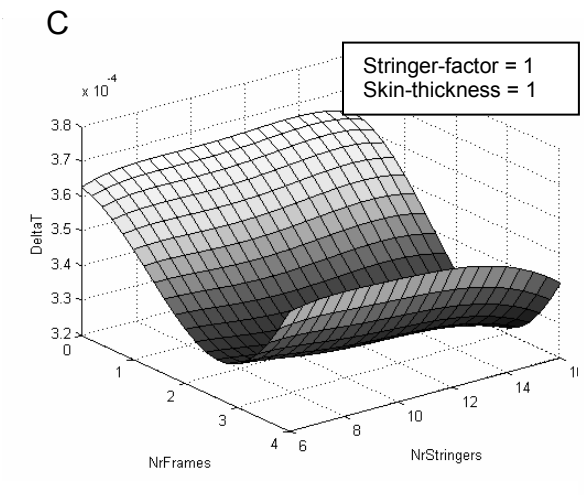

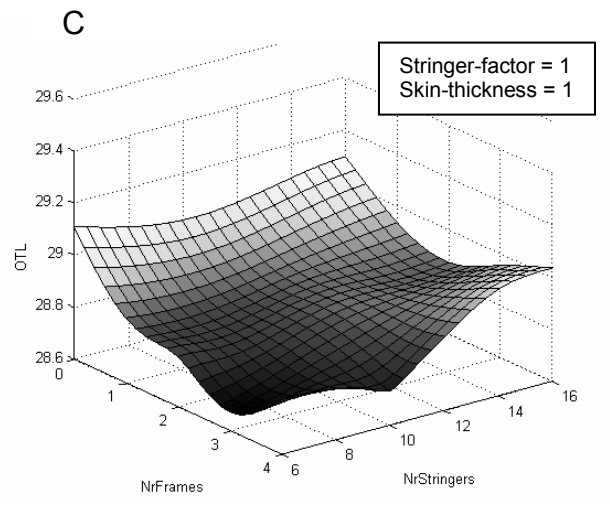

Figure G.2.7: *Response surfaces for the thermal insulation. (Validation set errors: Max=3.5963, Mean=1.5723, Rsqr=0.99758, Rmea=0.089429, APE=1.3061)*

Figure G.2.8: *Response surfaces for the acoustical insulation OTL. (Validation set errors: Max=1.9808, Mean=0.89194, Rsqr=-0.18008, Rmea=1.9183, APE=0.89282)*

G.3. Multi Objective Optimisations

The multi objective optimisations are performed with the Multi Objective Genetic Algorithm optimisation option of the G_OPT program developed by Lanzi [1]. This optimisation procedure determines a Pareto set of configurations for which two selected objectives are optimal. Table G.3.1 gives the Pareto set for minimum total fuselage section weight and maximum overall sound transmission loss. Table G.3.2 gives the minimum total fuselage section weight with maximum thermal insulation. The corresponding representations of the fuselage configurations are given in table G.3.1 and G.3.2.

Table G.3.1: *First 20 points of the Pareto set for minimum total fuselage section weight and maximum overall acoustic insulation (OTL).*

	Design variables				Objectives		Constraints				
Pareto set nr	SkinThickness	NrFrames	NrStringers	StringerFactor	OTL	Weight	RskinBuck	RstringerBuck	RskinTen	RstringerTen	Rhoop
1	0.7063	0	16	0.6284	28.7331	4.2080	1.0002	0.9989	0.1444	0.1162	0.3704
2	0.7063	0	16	0.6294	28.7329	4.2100	0.9997	0.9955	0.1444	0.1162	0.3703
3	0.7076	0	16	0.6284	28.7384	4.2138	0.9950	0.9994	0.1442	0.1161	0.3698
4	0.7090	0	16	0.6284	28.7436	4.2195	0.9898	0.9998	0.1440	0.1160	0.3692
5	0.7104	0	16	0.6294	28.7487	4.2272	0.9842	0.9968	0.1438	0.1158	0.3685
6	0.7118	0	16	0.6294	28.7539	4.2330	0.9791	0.9973	0.1436	0.1157	0.3680
7	0.7131	0	16	0.6294	28.7592	4.2387	0.9740	0.9977	0.1434	0.1155	0.3674
8	0.7145	0	16	0.6294	28.7645	4.2444	0.9689	0.9981	0.1432	0.1154	0.3668
9	0.7159	0	16	0.6304	28.7695	4.2521	0.9634	0.9951	0.1429	0.1152	0.3662
10	0.7173	0	16	0.6294	28.7752	4.2559	0.9590	0.9990	0.1428	0.1151	0.3657
11	0.7186	0	16	0.6294	28.7805	4.2616	0.9540	0.9994	0.1426	0.1150	0.3651
12	0.7200	0	16	0.6294	28.7858	4.2674	0.9491	0.9999	0.1424	0.1149	0.3645
13	0.7214	0	16	0.6304	28.7908	4.2751	0.9438	0.9968	0.1422	0.1147	0.3639
14	0.7227	0	16	0.6314	28.7958	4.2828	0.9385	0.9937	0.1419	0.1146	0.3632
15	0.7241	0	16	0.6314	28.8011	4.2885	0.9337	0.9941	0.1417	0.1144	0.3627
16	0.7255	0	16	0.6304	28.8068	4.2923	0.9294	0.9981	0.1416	0.1143	0.3622
17	0.7269	0	16	0.6304	28.8121	4.2980	0.9246	0.9985	0.1414	0.1142	0.3616
18	0.7282	0	16	0.6304	28.8175	4.3037	0.9199	0.9989	0.1412	0.1141	0.3611
19	0.7296	0	16	0.6304	28.8228	4.3094	0.9153	0.9993	0.1410	0.1140	0.3605
20	0.7310	0	16	0.6314	28.8277	4.3172	0.9102	0.9962	0.1408	0.1138	0.3599

Table G.3.2: *First 20 points of the Pareto set for minimum total fuselage section weight and maximum temperature difference between the inside and outside surface of the fuselage wall (Delta T or θ).*

	Design variables				Objectives		Constraints				
Pareto set nr	SkinThickness	NrFrames	NrStringers	StringerFactor	DeltaT	Weight	RskinBuck	RstringerBuck	RskinTen	RstringerTen	Rhoop
1	0.7049	0	16	0.6353	2.54e-4	4.2161	1.0018	0.9746	0.1442	0.1160	0.3703
2	0.7049	0	16	0.6402	2.54e-4	4.2259	0.9993	0.9580	0.1440	0.1158	0.3699
3	0.7076	0	16	0.6373	2.55e-4	4.2315	0.9904	0.9688	0.1438	0.1157	0.3690
4	0.7131	0	16	0.6294	2.58e-4	4.2387	0.9740	0.9977	0.1434	0.1155	0.3674
5	0.7145	0	16	0.6441	2.58e-4	4.2739	0.9616	0.9476	0.1425	0.1148	0.3656
6	0.7173	0	16	0.6402	2.59e-4	4.2775	0.9536	0.9615	0.1423	0.1147	0.3648
7	0.7200	0	16	0.6353	2.60e-4	4.2792	0.9463	0.9791	0.1421	0.1147	0.3640
8	0.7214	0	16	0.6363	2.61e-4	4.2868	0.9409	0.9761	0.1419	0.1145	0.3634
9	0.7227	0	16	0.6363	2.61e-4	4.2926	0.9361	0.9765	0.1417	0.1144	0.3629
10	0.7269	0	16	0.6333	2.63e-4	4.3039	0.9233	0.9880	0.1413	0.1141	0.3614
11	0.7296	0	16	0.6304	2.64e-4	4.3094	0.9153	0.9993	0.1410	0.1140	0.3605
12	0.7324	0	16	0.6333	2.65e-4	4.3268	0.9047	0.9896	0.1405	0.1136	0.3592
13	0.7324	0	16	0.6412	2.65e-4	4.3425	0.9011	0.9620	0.1402	0.1134	0.3587
14	0.7324	0	16	0.6431	2.65e-4	4.3464	0.9002	0.9552	0.1401	0.1134	0.3586
15	0.7324	0	16	0.6451	2.65e-4	4.3504	0.8993	0.9485	0.1401	0.1133	0.3584
16	0.7324	0	16	0.6461	2.65e-4	4.3523	0.8989	0.9451	0.1400	0.1133	0.3584
17	0.7365	0	16	0.6422	2.66e-4	4.3616	0.8871	0.9596	0.1396	0.1130	0.3570
18	0.7420	0	16	0.6343	2.68e-4	4.3687	0.8728	0.9889	0.1392	0.1127	0.3553
19	0.7420	0	16	0.6353	2.68e-4	4.3707	0.8725	0.9854	0.1391	0.1127	0.3553
20	0.7420	0	16	0.6363	2.68e-4	4.3727	0.8720	0.9818	0.1391	0.1127	0.3552

G.4 Reference

[1] Lanzi, L., Optimisation of composite stiffened panels under post buckling constraints, PhD thesis, Polytecnico di Milano, 2004

H structural and acoustic modes of the aluminium test cylinders

In this section the natural frequencies of the four aluminium test cylinders, discussed in chapter 8 and 9, are determined for the low frequency range (0-500Hz). First, the natural frequencies of the four test cylinder structures are determined, followed by the natural frequencies of the air cavity inside the cylinder, which are identical for the cylinders without frames. Finally the coupled natural frequencies of the structure and the air cavity together are determined.

H.1 Natural frequencies of the four test cylinder structures

In this section the natural frequencies of the simple supported non-stiffened cylinder, the cylinders with 6 and with 12 stringers and the cylinder with 12 stringers and 2 frames are determined with the DEE. The DEE makes use of ABAQUS for the structural eigenmode analysis. First, the representation of the FEM model will be discussed, followed by the numerical results of the eigenmode analysis.

Description of the FEM models

The skin of the aluminium test cylinder is modelled with 8 node solid elements. A single element is used in the thickness direction of the skin. The number of elements in circumferential and longitudinal direction is chosen large enough to be able to represent the structural modes below 500 Hz correctly.

The stringers are modelled with beam elements. Because for the real cylinders the stringers are positioned on the outside of the cylinder, the beam elements are positioned on the outside nodes of the solid 8 node cylinder skin elements. The beam elements are given the cross section properties of the used z-stiffeners. This means that the cross-section orientation of the beam elements has to be taken into account. However for the test cylinders the cross-section orientation of all beam elements belonging to the same stringer is identical, which means that the orientation can be defined once for each group of beam elements belonging to the same stringer.

The frames are modelled as a combination of shell elements for the frame webs and beam elements for the frame flanges. For simplicity reasons, the beam elements for the frames have circular cross sections with an area equal to the real frame flanges. Circular cross sections have been chosen because in that case the orientation of the beam elements is not of importance.

The different elements of the aluminium test cylinders are given the material properties as given in table 8.2.1 mentioned in chapter 8.

The edges of the aluminium test cylinders are simple supported, meaning that all translational degrees of freedom on the edge nodes of the cylinder skin are fixed. This automatically means that the nodes of the beam elements that represent the stringers are also simple supported at the cylinder edges.

Results of the natural frequency analysis of the cylinder structures

The natural frequencies and mode shapes of the 4 different test cylinders are given in table H.1. For the non-stiffened cylinder the eigenmodes can be identified with the number of sin waves in circumferential direction and the number of half sin waves in longitudinal direction. This makes it possible to present the eigenmodes of the non-stiffened cylinder as presented in figure H.1. For the stiffened cylinders the mode shapes will be more complex.

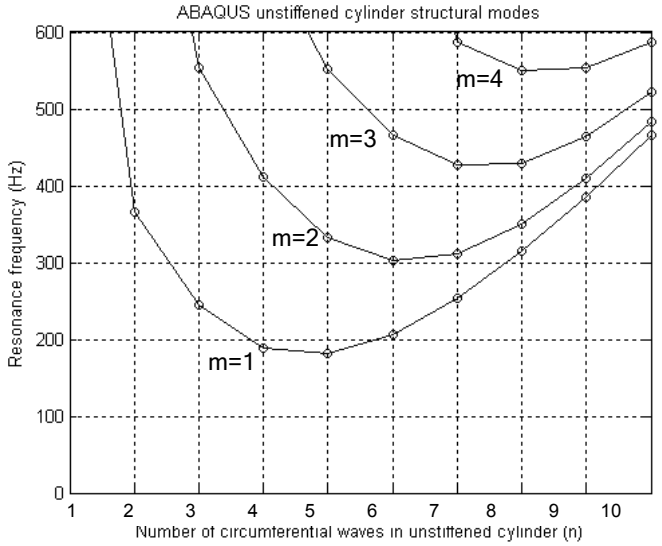

Figure H.1: *Numerical determined natural frequencies of the simple supported non-stiffened aluminium test cylinder. Each line represents mode shapes with identical number of longitudinal half sin-waves.*

H.2 Natural frequencies of the air cavity

The natural frequencies of the air cavity within the test cylinders are identical for the three test cylinders without frames. The air cavity for the cylinder with frames is different because of the presence of the frames. This means that only two FEM models are required to determine the natural frequencies of the air cavities for all test cylinders. The DEE discussed in chapter 6 is used again to determine the natural frequencies of this two air cavity models.

Table H.1: *Numerically determined structural natural frequencies of the non-stiffened cylinder, the cylinder with 6 and 12 stringers and the cylinder with 12 stringers and 2 frames. For the non-stiffened cylinder the mode shapes can be identified by the number of half sin waves in longitudinal direction (m) and the number of sin waves in circumferential direction (n).*

	Unstiffened Cylinder		Cylinder with 6 stringers	Cylinder with 12 stringers	Cylinder with 12 stringers and 2 frames
nr	[Hz]	Mode (m, n)	[Hz]	[Hz]	[Hz]
1	180.66	1, 5	104.67	101.52	482.69
2	180.94	1, 5	105.53	102.65	482.81
3	189.19	1, 4	105.56	102.65	487.43
4	189.19	1, 4	107.17	105.45	487.43
5	206.43	1, 6	107.20	105.48	490.53
6	206.43	1, 6	107.87	107.87	490.53
7	243.97	1, 3	179.99	107.87	496.23
8	245.69	1, 3	183.18	109.18	496.50
9	253.45	1, 7	187.25	109.20	510.08
10	253.49	1, 7	187.26	109.78	519.25
11	301.82	2, 6	205.12	109.78	519.25
12	301.82	2, 6	205.13	109.94	519.38
13	311.18	2, 7	229.17	179.27	529.22
14	311.41	2, 7	230.16	185.13	529.93
15	314.38	1, 8	236.25	185.89	541.80
16	314.38	1, 8	236.56	185.89	550.12
17	331.66	2, 5	236.63	205.31	550.12
18	332.63	2, 5	239.19	205.31	550.51
19	350.23	2, 8	239.23	219.84	550.76
20	350.23	2, 8	241.19	220.61	552.29
21	366.07	1, 2	252.18	229.44	556.17
22	366.07	1, 2	252.75	230.44	556.67
23	385.84	1, 9	276.20	230.44	564.19
24	385.85	1, 9	313.96	234.61	564.19
25	409.56	2, 9	331.89	234.62	570.63
26	409.59	2, 9	333.51	241.20	570.63
27	411.79	2, 4	333.84	241.20	571.00
28	411.79	2, 4	341.70	247.52	571.00
29	427.16	3, 7	342.10	247.64	576.42
30	427.73	3, 7	349.86	251.81	580.14
31	429.64	3, 8	355.74	251.81	580.14
32	429.64	3, 8	362.85	253.24	585.70
33	463.80	3, 9	369.02	254.12	585.87
34	463.86	3, 9	369.44	254.82	587.21
35	465.47	3, 6	385.54	276.20	589.52
36	465.47	3, 6	405.47	276.20	589.52
37	466.56	1, 10	405.53	331.19	593.01
38	466.56	1, 10	405.76	338.36	593.02
39	483.57	2, 10	411.16	339.08	594.41
40	483.57	2, 10	411.17	351.49	595.60
41	521.88	3, 10	415.84	351.49	595.60
42	521.88	3, 10	417.65	352.36	598.74
43	550.26	3, 5	425.05	352.36	598.74
44	550.54	4, 8	425.40	385.54	
45	550.55	4, 8	430.53	385.99	
46	552.08	3, 5	441.13	402.70	
47	552.93	4, 9	441.22	402.70	
48	553.06	4, 9	442.02	402.96	
49	553.23	2, 3	442.37	402.98	
50	555.85	1, 11	447.74	405.35	

Description of the FEM models

The acoustic cavity is modelled with 8 node 3D solid cubic acoustic elements and for the centre elements 6 node 3D triangular elements are used. For the model of the air cavity for the cylinder with frames, the model has gaps at the frame positions. The air properties are given in table H.2. The edges of the air cavity are considered solid walls.

Table H.2: *Properties of the air cavity within the four test cylinders*

Speed of sound c_s	343 m/s
Density ρ	1.225 kg/m^3
Bulk modulus of elasticity B	144120 N/m^2

Results of the natural frequency analysis of the air cavity models

The natural frequencies and mode shapes of the acoustic modes for the air cavity without gaps at frame positions are given in table H.3. The natural frequencies for the air cavity with gaps at the frame positions are given in table H.4.

Table H.3: *Numerically determined natural frequencies of the air cavity within the three aluminium test cylinders without frames.*

Mode (s,n,m)	Frequency	Mode (s,n,m)	Frequency	Mode (s,n,m)	Frequency
0,0,1	176.36	0,2,1	674.89	1,0,2	847.52
0,0,2	350.07	0,0,4	678.69	0,3,0	887.24
0,1,0	399.78	0,2,2	726.84	0,3,1	889.08
0,1,1	434.36	0,1,4	763.65	0,2,4	891.51
0,0,3	518.44	1,0,0	795.11	0,1,5	900.01
0,1,2	522.74	0,2,3	802.52	1,0,3	907.13
0,1,3	638.61	1,0,1	808.65	0,3,2	931.29
0,2,0	656.23	0,0,5	827.82	0,3,3	962.51

Table H.4: *Numerically determined natural frequencies of the air cavity for aluminium test cylinder stiffened with 12 stringers and 2 frames.*

Mode	Frequency	Mode	Frequency	Mode	Frequency
1	174.18	9	519.01	17	724.09
2	345.65	10	638.27	18	724.85
3	398.92	11	638.85	19	755.49
4	399.46	12	654.77	20	755.69
5	432.75	13	656.41	21	801.65
6	433.00	14	670.18	22	803.56
7	517.99	15	673.68	23	803.92
8	518.79	16	674.48	24	815.56

The mode shapes of the air cavity of the cylinders without frames can be identified by the number of sin waves in circumferential direction (n), the number of half sin waves in longitudinal direction (m) and the number of half sin waves in radial direction (p). By comparing the results of table H.4 with table H.3, it can be concluded that the existence of the frames only has a small influence on the acoustic natural frequencies. From table H.3 and H.4 it can be concluded that the natural frequencies of the air cavity with the frame gaps, are a bit lower than the natural frequencies of the

air cavity without the frame gaps. As an example figure H.2A and B show corresponding acoustic modes for the air cavity without the frame gaps (726.82 Hz) and with the frame gaps (724.08 Hz).

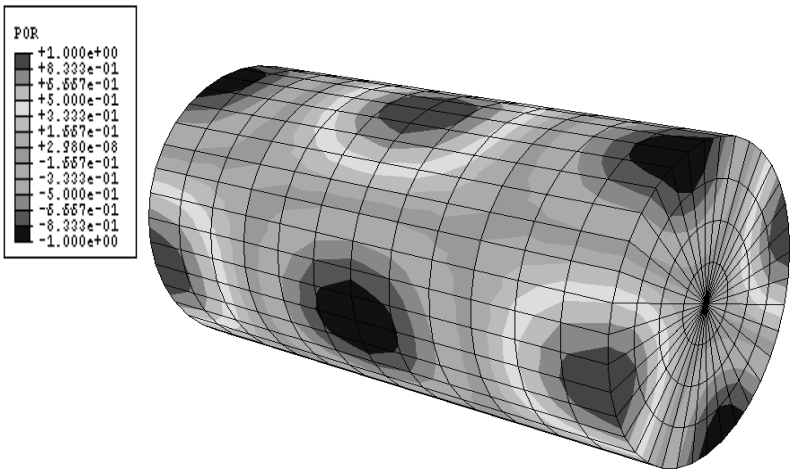

Figure H.2A: *Example of an acoustic mode at 726.82 Hz for the cylinders without frames. (See also colour section).*

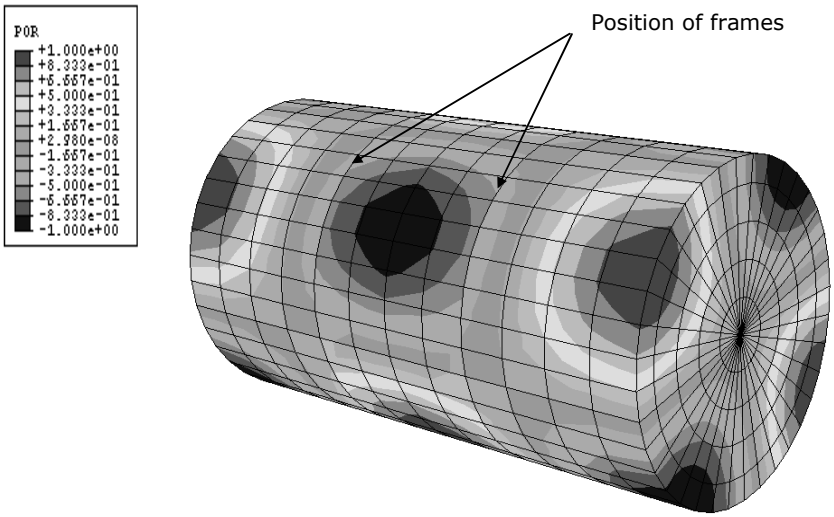

Figure H.2B: *Example of an acoustic mode at 724.08 Hz for the cylinder with 2 frames. (See also colour section).*

H.3 Coupled acoustic-structural natural frequencies

ABAQUS uses an approximate method to determine the coupled structural and acoustic eigenmodes by super-positioning the structural and acoustic eigenmodes. To be able to analyse coupled acoustic-structural models, the acoustic elements have to be connected to the structural elements by using the ABAQUS specific '*TIE' option. The coupled eigenmodes for the four test cylinders are shown in table H.5. It can be concluded that, besides some small shifts in frequency, almost all structural and acoustical natural frequencies that were found in separate structural and acoustical analysis are also found in the coupled structural-acoustic natural frequency analysis. To find out which modes are responsible for the largest dips in the sound transmission loss, steady state dynamic analyses are performed, which is discussed in section 9.3.

Table H.5: *Numerically determined coupled acoustic-structural natural frequencies of the non-stiffened cylinder, the cylinder with 6 and 12 stringers and the cylinder with 12 stringers and 2 frames.*

	Unstiffened Cylinder	Cylinder with 6 stringers	Cylinder with 12 stringers	Cylinder with 12 stringers and 2 frames
1	0.0000	0.0000	0.0000	0.0000
2	176.27	104.62	101.46	174.02
3	178.59	105.49	102.60	345.32
4	178.71	105.52	102.60	394.15
5	186.58	107.15	105.42	396.84
6	186.76	107.18	105.46	429.09
7	204.09	107.86	107.86	431.56
8	204.25	176.27	107.86	479.60
9	240.27	177.90	109.18	479.65
10	241.68	181.59	109.20	484.44
11	250.79	185.14	109.78	484.52
12	250.94	185.29	109.78	487.19
13	298.19	202.99	109.94	487.28
14	298.43	203.20	176.28	493.08
15	307.89	226.81	177.24	493.41
16	307.89	227.76	183.82	508.47
17	311.17	235.97	184.09	515.10
18	311.40	236.25	184.22	516.78
19	327.58	236.31	203.26	517.50
20	328.23	238.95	203.47	517.73
21	346.44	238.99	218.03	517.84
22	346.69	241.02	218.78	518.92
23	349.87	249.40	229.19	522.42
24	357.90	249.52	230.17	529.19
25	358.68	274.33	230.18	541.47
26	382.05	310.75	234.37	543.08
27	382.30	327.52	234.38	543.19
28	389.33	329.64	241.03	546.92
29	397.34	330.40	241.03	547.01
30	405.30	338.43	247.41	549.25
31	405.36	338.44	247.54	549.32
32	405.55	346.09	251.26	552.96
33	405.93	349.88	251.50	553.58
34	422.13	349.89	251.75	561.45
35	422.36	354.97	251.75	561.53
36	424.52	365.80	253.19	565.05
37	424.82	366.11	274.31	565.29
38	425.61	381.94	274.32	568.23
39	432.96	389.30	326.88	568.31
40	458.50	397.31	336.22	574.80
41	458.74	404.28	336.88	576.71
42	459.15	404.29	345.78	576.82
43	459.56	404.74	346.72	582.54
44	462.09	410.29	347.04	582.64
45	462.37	410.33	347.60	585.24
46	478.63	414.51	349.88	586.67
47	478.92	415.31	382.25	587.74
48	514.65	419.46	382.37	587.76
49	516.30	420.24	389.18	590.46
50	516.50	425.64	396.52	590.50

I Results of the DEE application for a stiffened skin fuselage concept

I.1. Design of experiments and the resulting evaluations

For the analysis and optimisation of the stiffened skin fuselage concept a design of experiments has been performed with the Latin hypercube routine of the G_OPT program developed by *Lanzi [1]* to generate a set of 100 data points. In a second optimization step another 50 data points are generated.

The five design variables that are chosen for the optimisation of the stiffened skin fuselage concept are:

1.) The skin thickness [t_{skin}], also indicated as *SkinThickness*
2.) The number of frames [n_{fr}], also indicated as *NrFrames*
3.) The number of stringers [n_{str}], also indicated as *NrStringers*
4.) The stringer factor [k_{str}], also indicated as *StringerFactor*
5.) The interior panel core thickness [t_{inc}], also indicated as *InteriorCoreThickness*

The DEE is used to determine the performance of each requirement. Five structural requirements are considered:

1.) The tensile stress criteria of the fuselage skin [R_{skt}], also indicated as *RskinTen*
2.) The buckling criteria of the fuselage skin [R_{skb}], also indicated as *RskinBuck*
3.) The tensile stress criteria of the stringers [R_{strt}], also indicated as *RstringerTen*
4.) The Euler buckling criteria of the stringers [R_{strb}], also indicated as *RstringerBuck*
5.) The hoop stress criteria [R_{Hoop}], also indicated as *Rhoop*

Also six objective functions are determined:

1.) The temperature difference between the inside and outside surface of the fuselage wall [θ], also indicated as *DeltaT*.
2.) The overall sound transmission loss in frequency range 1 [0-500Hz], [TLHF1]
3.) The overall sound transmission loss in frequency range 2 [500Hz-5kHz], [TLHF2]
4.) The overall sound transmission loss in frequency range 3 [5-20kHz], [TLHF3]
5.) The structural weight of the fuselage section [W_{struc}]
6.) The total weight of the fuselage section including the structure, insulation blanket and interior panels [W_{tot}].

The design variables together with the evaluations of the requirements and the objective functions are presented in table I.1 and I.2.

Table I.1: *Design of experiments and evaluations of the structural requirements and objective functions for 100 data points used in the first optimisation step.*

	Design variables					Evaluations										
Data point nr	Skin thickness	Nr of frames	Nr of stringers	Stringer area factor	Interior panel core thickness	Rhoop	Rskin tensile	Rstringer tensile	Rskin buckling	Rstringer buckling	θ	TLHF 1	TLHF 2	TLHF 3	Wtotal	Wstructure
1	1.9501	12	70	0.9860	36	0.698	0.724	0.612	0.948	0.409	93.48	37.52	68.54	119.16	1464.3	943.1
2	1.0237	22	20	1.0195	11	1.102	1.510	1.324	93.512	0.424	73.22	24.19	72.35	136.01	1016.6	627.3
3	1.0835	11	100	0.8662	9	1.166	0.992	0.815	1.985	0.378	95.90	38.54	72.20	116.58	1151.3	772.5
4	1.7660	22	100	1.4058	10	0.659	0.597	0.495	0.451	0.033	85.68	37.00	71.95	123.85	1589.5	1206
5	1.2482	25	70	0.7205	36	0.969	1.082	0.924	3.427	0.167	70.65	32.62	69.28	115.37	1303.0	781.1
6	1.9954	25	30	0.8731	17	0.671	0.848	0.732	6.002	0.314	81.35	28.53	79.27	125.84	1342.6	922.7
7	1.0016	12	30	1.4958	38	1.236	1.309	1.105	35.773	0.402	77.01	28.35	61.05	135.89	1142.6	609.6
8	1.9506	11	80	0.5081	8	0.731	0.822	0.701	0.856	1.706	113.75	38.27	91.92	114.14	1234.0	861.2
9	1.4241	11	20	0.5472	28	0.987	1.262	1.089	41.596	6.446	89.47	27.24	77.97	119.75	1095.6	616.7
10	1.7530	9	70	1.3361	4	0.765	0.711	0.591	1.134	0.353	121.17	37.80	81.25	115.60	1311.5	959.4
11	1.4032	25	100	0.5358	8	0.863	0.983	0.840	1.221	0.215	78.70	35.89	70.62	105.97	1234.3	860.7
12	1.1503	10	80	0.8858	40	1.184	1.043	0.863	2.990	0.566	81.50	37.71	54.43	122.70	1263.7	720.0
13	1.3735	25	40	1.3821	37	0.901	0.976	0.833	7.863	0.083	72.83	28.55	67.46	120.00	1354.1	826.9
14	1.5690	14	20	1.2393	18	0.825	1.040	0.904	27.981	0.747	92.62	26.21	86.26	131.07	1149.2	723.2
15	1.9934	22	90	0.6286	30	0.619	0.738	0.635	0.567	0.225	81.19	37.51	67.51	103.29	1475.2	986.2
16	1.4362	16	70	1.3235	28	0.928	0.814	0.671	1.930	0.117	84.63	35.33	68.87	115.24	1388.8	910.0
17	1.9255	25	100	1.4151	35	0.665	0.573	0.472	0.369	0.027	78.95	37.27	64.03	122.26	1765.4	1249
18	1.0457	12	30	0.5017	7	1.197	1.593	1.382	40.410	4.053	94.71	27.75	81.85	112.65	913.9	545.5
19	1.0998	22	60	1.4766	11	0.959	0.941	0.792	5.179	0.051	74.47	31.01	70.12	124.75	1251.3	862.1
20	1.8489	22	40	1.4634	8	0.651	0.765	0.659	3.387	0.097	88.05	29.58	76.21	112.63	1343.0	970.2
21	1.7013	18	20	0.9234	40	0.785	1.009	0.879	23.593	0.841	83.43	26.26	76.11	124.80	1295.5	752.4
22	1.7375	20	70	0.8586	5	0.777	0.821	0.696	1.361	0.196	97.23	34.20	77.01	126.54	1291.9	934.6
23	1.8630	8	20	0.6215	5	0.808	0.979	0.843	19.149	9.068	124.42	28.09	84.74	138.53	1083.7	726.5
24	1.5139	14	90	0.6040	25	0.838	0.927	0.790	1.222	0.625	88.16	38.10	66.27	125.05	1262.9	800.1
25	1.0054	9	90	1.4495	23	1.226	0.850	0.673	2.330	0.182	84.90	38.68	67.14	116.48	1320.7	868.1
26	1.1303	9	50	1.3626	7	1.114	1.046	0.879	8.154	0.486	102.23	33.22	79.16	109.94	1079.4	710.7
27	1.1190	25	20	0.5176	38	1.128	1.558	1.355	82.118	1.423	69.00	25.17	70.58	122.35	1151.1	618.3
28	1.0173	18	70	0.5617	10	1.142	1.343	1.154	6.426	0.576	81.60	33.13	77.27	140.58	1042.0	657.9
29	1.9889	14	100	1.4510	28	0.658	0.556	0.456	0.332	0.082	93.48	40.48	70.15	117.53	1688.6	1210
30	1.9377	20	40	1.3895	32	0.729	0.766	0.650	3.126	0.136	85.14	30.59	71.46	115.16	1450.5	950.8
31	1.2334	14	100	1.4498	5	0.954	0.722	0.580	1.076	0.070	98.15	37.59	84.02	111.84	1378.2	1020
32	1.4371	20	20	0.5003	7	0.956	1.258	1.088	40.715	2.312	89.80	25.24	86.99	120.11	1063.5	695.1
33	1.9152	16	20	0.6437	17	0.763	0.948	0.819	17.481	2.185	97.12	26.18	82.96	126.42	1215.2	795.2
34	1.3833	10	100	1.4890	38	1.001	0.684	0.541	0.823	0.134	87.16	40.79	62.29	117.10	1561.3	1028
35	1.9581	10	30	0.6480	34	0.773	0.903	0.775	6.636	3.582	96.93	30.91	74.49	129.22	1287.8	777.3
36	1.0526	18	100	0.8878	29	1.092	0.987	0.819	2.094	0.126	74.08	36.71	76.84	116.08	1293.7	809.2
37	1.3426	25	90	1.3010	23	0.869	0.759	0.628	1.246	0.034	71.71	34.47	69.22	108.87	1480.6	028.3
38	1.0119	8	40	0.9767	24	1.346	1.364	1.153	20.048	1.657	86.21	32.24	72.00	121.52	1032.7	574.8
39	1.4393	18	50	0.5603	24	0.888	1.110	0.958	5.487	0.869	81.92	31.67	72.93	115.31	1182.6	725.1
40	1.5130	25	50	1.0483	20	0.825	0.933	0.796	4.136	0.121	74.67	30.46	78.34	122.66	1309.2	873.0
41	1.4092	11	60	0.7271	4	0.955	1.043	0.885	3.617	1.048	110.54	35.02	81.39	107.70	1078.9	726.5
42	1.5845	8	40	1.0665	36	0.929	0.956	0.810	5.822	1.393	93.45	34.01	70.53	121.20	1257.1	735.4
43	1.0029	20	70	1.4896	40	1.188	0.940	0.766	4.507	0.050	71.67	33.35	69.24	139.24	1391.5	847.7
44	1.0759	16	30	0.5042	39	1.252	1.570	1.353	37.742	2.301	76.04	27.46	68.40	128.35	1101.8	563.5
45	1.0492	25	80	0.8762	4	1.044	1.081	0.916	3.768	0.096	75.87	32.76	74.49	111.15	1173.8	821.0
46	1.7147	9	60	1.4200	26	0.788	0.742	0.621	1.711	0.376	98.04	36.83	70.82	119.25	1382.1	914.2
47	1.6744	22	50	0.5757	40	0.734	0.961	0.835	3.493	0.510	78.10	31.63	68.44	115.14	1347.3	804.2
48	1.9907	9	30	1.1518	5	0.695	0.817	0.702	5.816	1.328	22.59	31.40	81.60	123.74	1194.2	836.7
49	1.6441	16	100	0.9736	38	0.839	0.739	0.610	0.657	0.150	85.39	38.99	66.22	125.69	1507.7	975.3
50	1.9040	10	90	1.0326	17	0.763	0.685	0.566	0.569	0.396	107.47	39.97	73.99	121.56	1421.3	1001

Table I.1 continued: *Design of experiments and evaluations of the structural requirements and objective functions for 100 data points used in the first optimisation step.*

	Design variables					Evaluations										
Data point nr	Skin thickness	Nr of frames	Nr of stringers	Stringer area factor	Interior panel core thickness	Rhoop	Rskin tensile	Rstringer tensile	Rskin buckling	Rstringer buckling	θ	TLHF 1	TLHF 2	TLHF 3	Wtotal	Wstructure
51	1.0122	18	100	1.4410	21	1.095	0.756	0.706	1.759	0.056	75.13	36.46	67.08	118.46	1419.5	977.5
52	1.0281	14	70	1.0687	19	1.127	1.019	0.995	4.861	0.281	81.22	34.45	63.25	123.83	1167.9	736.5
53	1.0780	20	20	1.4048	24	1.189	1.332	1.357	79.416	0.326	73.99	24.48	79.92	121.70	1097.6	639.8
54	1.2368	16	40	1.1007	37	1.082	1.081	1.082	11.260	0.396	79.33	29.87	60.70	115.61	1224.9	697.5
55	1.1217	16	20	1.3487	5	1.162	1.301	1.327	71.845	0.563	93.23	24.58	90.92	117.67	990.5	632.5
56	1.0846	25	30	0.5177	17	1.127	1.456	1.480	35.917	1.056	68.90	25.94	70.09	114.27	1067.0	646.2
57	1.4654	16	50	1.4198	8	0.910	0.840	0.828	4.134	0.183	96.88	31.80	74.39	107.17	1235.1	861.8
58	1.8823	25	70	1.4741	22	0.676	0.621	0.606	0.909	0.048	78.55	33.86	71.45	117.11	1575.7	1129
59	1.6263	25	80	1.0786	37	0.774	0.728	0.715	1.118	0.080	75.72	34.89	63.84	119.20	1520.7	993.7
60	1.9438	10	100	0.6024	26	0.761	0.729	0.708	0.498	1.338	100.32	41.23	75.48	119.85	1373.8	906.1
61	1.6747	8	60	0.5590	20	0.879	0.922	0.904	2.410	4.234	104.36	37.16	72.19	118.85	1173.9	737.9
62	1.2066	20	100	1.0084	13	1.009	0.829	0.793	1.427	0.105	81.67	36.03	63.60	113.83	1314.1	914.5
63	1.9414	9	20	1.2663	32	0.720	0.829	0.845	15.516	1.971	97.90	28.14	77.78	117.25	1283.5	783.7
64	1.0226	22	40	0.9110	26	1.081	1.273	1.308	19.274	0.305	68.40	28.22	71.80	132.11	1133.6	665.0
65	1.8718	18	50	0.8941	24	0.705	0.785	0.789	2.413	0.378	88.04	32.26	75.32	128.79	1349.9	892.8
66	1.4527	9	100	1.2919	16	0.900	0.669	0.638	0.773	0.318	100.35	40.78	73.62	116.01	1402.5	987.3
67	1.4330	22	100	0.5329	32	0.817	0.915	0.916	1.133	0.340	74.94	37.10	66.96	127.50	1324.5	824.3
68	1.0520	12	60	0.5023	22	1.175	1.345	1.340	8.750	2.280	83.27	33.81	78.27	123.11	1034.8	587.5
69	1.8179	18	90	0.9791	22	0.708	0.674	0.661	0.649	0.171	88.55	37.30	70.17	115.14	1463.5	1017
70	1.5558	9	100	0.6877	12	0.853	0.814	0.799	0.860	1.230	106.70	40.83	78.28	120.19	1221.2	827.2
71	1.9501	16	70	1.2635	11	0.718	0.645	0.627	0.885	0.161	102.01	35.60	77.60	111.24	1434.1	1045
72	1.7015	9	30	0.8765	20	0.805	0.927	0.936	9.500	2.804	101.54	30.68	76.19	109.86	1164.2	728.2
73	1.2785	16	30	0.9040	8	1.048	1.180	1.183	21.192	0.803	93.77	26.98	81.90	112.63	1047.9	674.5
74	1.7601	14	40	0.8701	6	0.737	0.854	0.869	4.439	0.857	107.27	31.07	82.45	121.04	1176.7	814.1
75	1.4285	22	20	1.4459	6	0.823	1.032	1.075	34.923	0.266	83.81	25.23	89.96	117.34	1128.5	765.6
76	1.5102	8	80	0.5908	36	0.965	0.936	0.912	1.692	2.733	92.12	39.83	77.51	120.23	1253.3	731.6
77	1.8720	25	60	0.6025	20	0.701	0.816	0.812	1.712	0.369	78.66	32.46	67.24	118.13	1354.9	919.0
78	1.5455	25	90	0.8632	20	0.795	0.782	0.768	1.040	0.114	75.12	35.41	72.38	112.07	1398.5	962.3
79	1.3306	22	60	0.7672	9	0.854	0.998	1.005	4.043	0.297	80.34	31.25	76.24	120.53	1171.7	793.1
80	1.0359	22	100	1.2386	37	1.017	0.802	0.767	1.795	0.055	69.18	35.98	64.64	133.66	1462.2	934.7
81	1.9590	18	100	0.6306	13	0.667	0.702	0.696	0.475	0.364	94.42	38.25	73.69	127.82	1381.9	983.0
82	1.4158	18	20	1.4046	39	0.911	1.062	1.089	37.019	0.408	79.74	26.08	74.00	113.92	1243.5	705.5
83	1.5338	20	20	0.5304	32	0.919	1.127	1.130	33.743	2.233	80.41	25.85	89.90	103.53	1203.1	702.9
84	1.4442	12	60	1.0630	17	0.891	0.869	0.859	2.988	0.476	94.26	34.92	77.28	121.26	1220.4	799.9
85	1.0038	18	80	1.1887	4	1.097	0.931	0.899	3.622	0.121	86.75	34.15	75.08	110.51	1186.4	833.1
86	1.8580	16	70	1.4007	40	0.760	0.646	0.623	0.968	0.129	88.28	36.20	58.69	128.34	1575.1	1032
87	1.1108	10	70	1.4979	37	1.204	0.855	0.807	3.477	0.268	81.80	36.55	68.26	131.03	1343.8	816.3
88	1.3056	9	30	1.4548	27	1.009	1.038	1.045	17.746	0.984	89.62	29.60	76.78	118.33	1146.0	672.4
89	1.8797	20	30	0.5016	4	0.756	0.906	0.907	7.626	1.639	99.38	27.77	86.27	125.67	1184.0	832.0
90	1.0488	18	70	0.8047	38	1.124	1.123	1.107	5.226	0.325	72.94	33.82	59.42	110.06	1232.1	699.2
91	1.4301	20	20	1.0130	22	0.957	1.117	1.134	38.282	0.631	80.62	25.53	62.24	115.42	1159.0	712.1
92	1.5250	14	90	1.0617	6	0.813	0.733	0.715	0.984	0.223	103.13	37.66	76.89	122.29	1305.5	942.8
93	1.1780	20	100	0.5124	18	1.069	1.081	1.060	1.998	0.463	77.93	36.11	70.19	115.42	1173.4	747.4
94	1.5104	25	20	0.9771	37	0.866	1.059	1.085	32.469	0.447	74.22	26.17	71.67	122.29	1278.8	751.7
95	1.2289	8	20	1.1043	8	1.151	1.262	1.278	58.410	3.475	106.27	26.89	85.49	115.86	957.7	584.3
96	1.5119	25	20	0.8518	4	0.849	1.072	1.100	32.798	0.582	82.77	25.48	85.60	119.23	1129.4	777.0
97	1.9273	16	60	0.5835	38	0.753	0.812	0.798	1.612	0.927	89.33	34.83	67.19	134.04	1387.2	855.1
98	1.6339	14	80	1.4993	16	0.771	0.642	0.622	0.950	0.127	95.78	36.93	77.47	108.18	1457.1	1042
99	1.7655	22	50	1.0475	40	0.693	0.784	0.796	2.672	0.191	79.18	31.75	68.54	120.23	1444.8	901.8
100	1.9659	16	30	1.4207	14	0.730	0.767	0.766	5.872	0.320	99.62	29.37	86.05	123.78	1306.5	902.4

Table I.2: *Design of experiments and evaluations of the structural requirements and objective functions for another 50 data points used in the second optimisation step.*

	Design variables					Evaluations										
Data point nr	Skin thickness	Nr of frames	Nr of stringers	Stringer area factor	Interior panel core thickness	Rhoop	Rskin tensile	Rstringer tensile	Rskin buckling	Rstringer buckling	θ	TL HF1	TLHF 2	TLHF 3	Wtotal	Wstructure
1	1.6875	9	90	0.6458	8	0.7964	0.8461	0.7178	0.9068	1.3182	114.4	39.93	56.90	108.86	1203.5	830.5
2	1.4537	10	100	0.7956	4	0.9528	0.8609	0.7145	0.9770	0.5865	113.7	40.07	76.71	108.44	1197.1	844.3
3	1.4700	14	80	0.6160	6	0.8499	0.9718	0.8300	1.7458	0.7058	102.3	36.48	79.10	109.59	1145.8	783.0
4	1.6529	13	100	0.5371	4	0.8337	0.8834	0.7472	0.7959	0.8122	111.3	39.13	77.61	108.73	1192.0	839.8
5	1.5895	8	80	0.5511	4	0.9103	0.9581	0.8095	1.4961	2.7154	120.9	39.17	79.16	108.94	1106.1	753.9
6	1.5576	13	100	0.7260	7	0.8699	0.8438	0.7079	0.8448	0.4174	105.1	39.04	77.45	111.59	1239.7	871.8
7	1.4504	9	80	0.7987	8	0.9040	0.9160	0.7746	1.6939	0.9424	109.0	38.50	71.92	106.07	1157.9	784.6
8	1.4542	10	90	0.5347	8	0.9675	1.0015	0.8466	1.4422	1.5452	108.4	39.14	70.82	105.41	1117.3	744.1
9	1.6705	12	80	0.7925	5	0.7848	0.8326	0.7042	1.1639	0.5423	111.8	37.44	78.58	114.32	1223.6	866.2
10	1.6279	8	100	0.6535	4	0.8864	0.8491	0.7111	0.7853	1.4744	121.4	41.31	77.60	108.43	1183.4	831.1
11	1.6701	12	80	0.5007	7	0.7924	0.9274	0.7944	1.3104	1.4347	108.5	37.47	80.44	119.23	1160.3	792.1
12	1.6945	14	100	0.7916	4	0.7473	0.7687	0.6475	0.6455	0.3044	107.8	38.85	77.72	108.92	1290.5	938.3
13	1.4866	10	90	0.6169	5	0.9449	0.9495	0.7992	1.3044	1.2228	113.0	39.14	81.73	109.92	1134.7	777.2
14	1.4982	8	100	0.7449	7	0.9498	0.8643	0.7180	0.9298	1.0692	114.4	41.17	77.02	111.13	1191.9	823.9
15	1.4698	14	100	0.5298	5	0.8487	0.9540	0.8131	1.0710	0.6904	103.3	38.56	81.27	109.65	1153.1	795.5
16	1.6952	12	100	0.5393	8	0.7794	0.8595	0.7309	0.7342	0.9407	108.4	39.61	54.95	108.18	1215.1	842.1
17	1.6903	10	100	0.7911	6	0.8424	0.7805	0.6504	0.6605	0.6059	115.0	40.40	76.11	113.20	1268.5	905.5
18	1.4981	9	80	0.7807	5	0.8786	0.9014	0.7636	1.5669	0.9696	114.6	38.52	82.34	110.16	1151.6	794.0
19	1.6125	13	80	0.7972	8	0.8484	0.8594	0.7221	1.2917	0.4639	105.2	37.05	64.70	107.00	1230.9	857.8
20	1.5758	8	100	0.5449	8	0.9163	0.9175	0.7699	0.9062	2.1153	114.2	41.30	65.09	105.51	1154.9	781.7
21	1.5748	8	80	0.5148	8	0.9204	0.9796	0.8289	1.5603	3.1904	114.3	39.21	66.98	106.56	1112.6	739.5
22	1.6903	8	80	0.7777	6	0.8594	0.8410	0.7032	1.1520	1.2667	119.2	39.33	77.84	114.12	1199.8	836.9
23	1.6007	14	90	0.5728	8	0.7926	0.8999	0.7699	1.0661	0.7247	102.3	37.80	64.32	105.96	1197.3	824.2
24	1.5628	14	90	0.7545	5	0.8018	0.8499	0.7206	1.0467	0.3877	105.0	37.70	79.52	112.43	1224.5	866.9
25	1.4898	14	100	0.5228	8	0.8412	0.9481	0.8084	1.0370	0.7704	99.6	38.63	68.49	103.95	1170.1	796.9
26	1.6840	10	90	0.5355	5	0.8545	0.8957	0.7585	0.9662	1.5595	116.2	39.39	77.49	115.70	1164.6	807.2
27	1.5855	14	80	0.5593	4	0.7993	0.9386	0.8043	1.4580	0.8541	106.9	36.62	78.86	109.01	1153.2	800.9
28	1.6695	9	90	0.7750	4	0.8000	0.8108	0.6833	0.8817	0.8538	119.3	39.85	78.80	109.21	1216.1	863.5
29	1.4584	9	100	0.5071	6	0.9034	0.9742	0.8300	1.1239	1.9309	112.2	40.57	77.91	108.01	1109.5	746.7
30	1.5089	11	90	0.7448	7	0.8986	0.8850	0.7425	1.1741	0.6427	108.6	38.76	78.03	111.14	1193.9	825.9
31	1.6016	10	80	0.6683	7	0.8895	0.9100	0.7659	1.3872	1.2033	112.2	38.21	79.79	118.36	1168.4	800.5
32	1.5748	11	100	0.5827	6	0.8699	0.8958	0.7546	0.8815	0.9483	111.2	39.81	75.98	110.06	1179.5	816.8
33	1.6768	13	90	0.7446	7	0.8205	0.8225	0.6919	0.8919	0.4679	107.9	38.22	79.40	119.30	1254.2	886.0
34	1.4511	9	80	0.5364	6	0.9089	1.0225	0.8717	1.9048	2.1572	112.2	38.47	80.16	108.79	1082.8	719.9
35	1.4644	11	100	0.6319	8	0.9231	0.9220	0.7733	1.0431	0.7938	106.5	39.70	69.60	104.59	1174.9	801.7
36	1.5232	13	100	0.7026	4	0.8848	0.8655	0.7271	0.9114	0.4706	108.9	38.97	76.91	107.77	1209.1	856.8
37	1.4595	13	80	0.7758	7	0.9202	0.9240	0.7801	1.6978	0.4703	104.1	36.82	78.76	114.51	1180.0	812.0
38	1.4765	11	80	0.5199	4	0.9227	1.0206	0.8679	1.8372	1.6505	112.0	37.58	78.58	107.09	1091.2	738.8
39	1.4704	8	100	0.6083	4	0.9672	0.9356	0.7811	1.0540	1.7147	118.0	41.11	76.67	106.12	1127.1	774.7
40	1.6758	13	90	0.6581	4	0.8219	0.8511	0.7192	0.9277	0.6255	111.7	38.18	78.60	109.28	1215.2	863.0
41	1.5320	14	80	0.5302	8	0.8254	0.9755	0.8365	1.6223	0.8981	100.6	36.60	68.66	104.00	1150.2	777.0
42	1.6635	8	80	0.5218	6	0.8774	0.9354	0.7917	1.3379	3.1561	118.7	39.29	77.75	112.56	1128.3	765.7
43	1.5930	10	90	0.5291	7	0.8965	0.9375	0.7936	1.1280	1.5739	111.8	39.30	78.76	116.35	1148.0	780.1
44	1.6980	11	80	0.6404	4	0.8175	0.8747	0.7406	1.1914	1.0326	116.4	37.86	79.99	109.81	1180.5	828.3
45	1.6302	8	90	0.7844	7	0.8851	0.8306	0.6919	0.9478	1.0793	116.5	40.37	79.08	131.51	1214.8	846.9
46	1.5839	13	90	0.5229	5	0.8667	0.9395	0.7990	1.1507	1.0305	108.7	38.06	79.21	113.81	1157.2	799.7
47	1.4558	13	90	0.5709	7	0.9276	0.9795	0.8300	1.4119	0.8516	103.8	37.92	77.83	114.25	1145.9	777.8
48	1.5459	10	90	0.7776	5	0.9092	0.8632	0.7204	1.0898	0.6938	114.3	39.21	80.18	115.01	1195.9	838.4
49	1.4916	12	80	0.7821	4	0.8621	0.9063	0.7655	1.5813	0.5439	109.6	37.20	78.64	106.73	1168.4	816.0
50	1.6637	14	100	0.6408	6	0.7631	0.8288	0.7033	0.7264	0.4813	104.9	38.83	75.59	111.79	1244.3	881.7

I.2. Response surfaces of the design requirements and objective functions

This appendix gives an overview of the response surfaces for the different structural requirements and objective functions. The structural requirements are independent of the design variable '*interior panel core thickness*'. Each depicted response surface represents the requirement or objective as function of two design variables. The remaining three design variables are fixed. The response surfaces are created with the G_OPT program developed by Lanzi [1] using the data from table I.1.

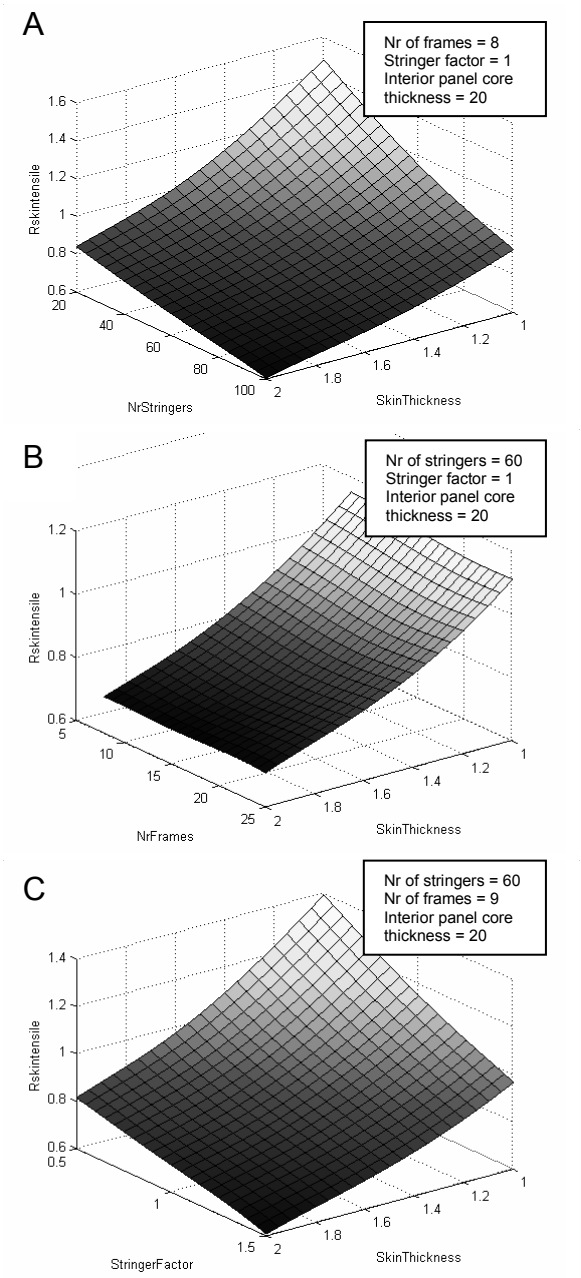

Figure I.2.1: *Response surfaces for the R skin tensile requirement. (Validation set errors: Max=2.4432, Mean=1.412, Rsqr=0.99645, Rmea=0.10536, APE=1.4191)*

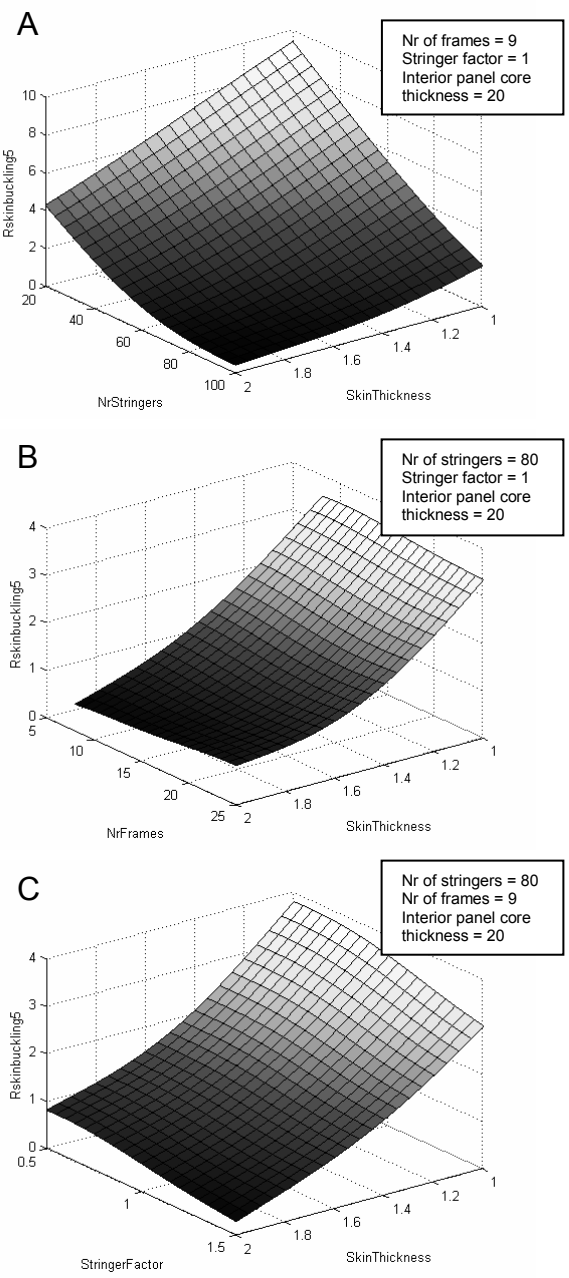

Figure I.2.2: *Response surfaces for the R skin buckling requirement, which is a combination of compressive and shear buckling. (Validation set errors: Max=3.4052, Mean=1.7353, Rsqr=0.99306, Rmea=0.17674, APE=1.9565)*

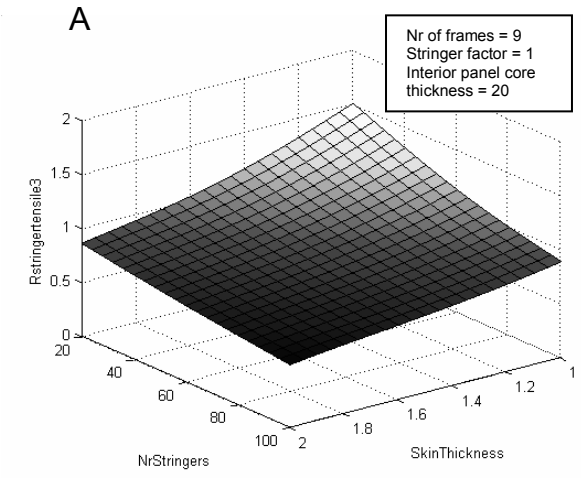

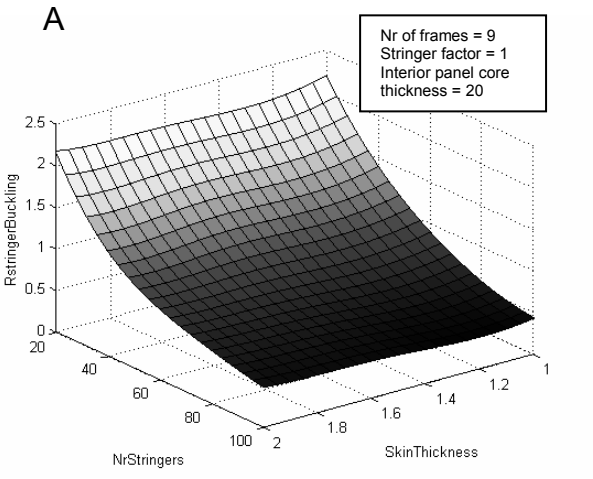

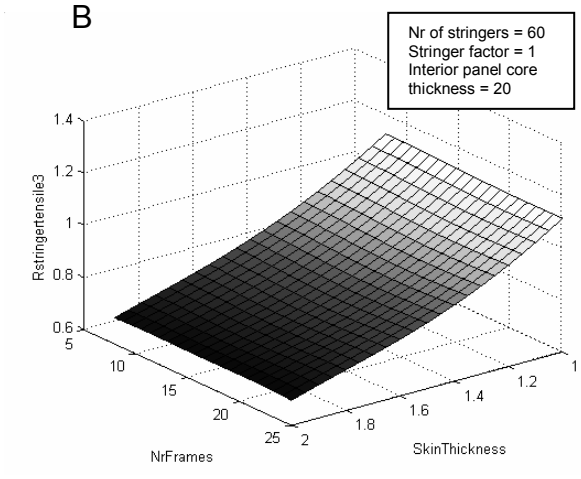

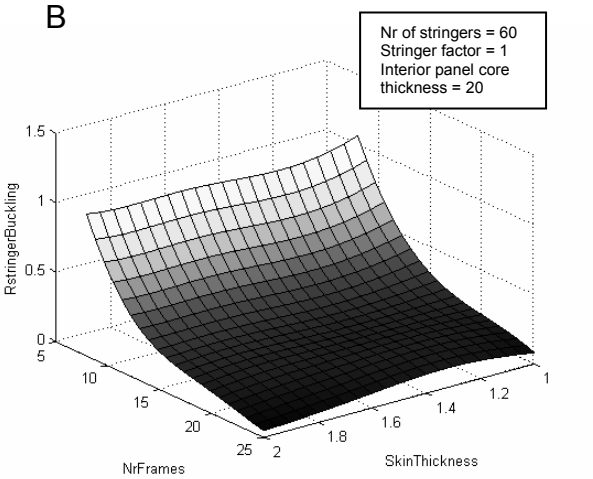

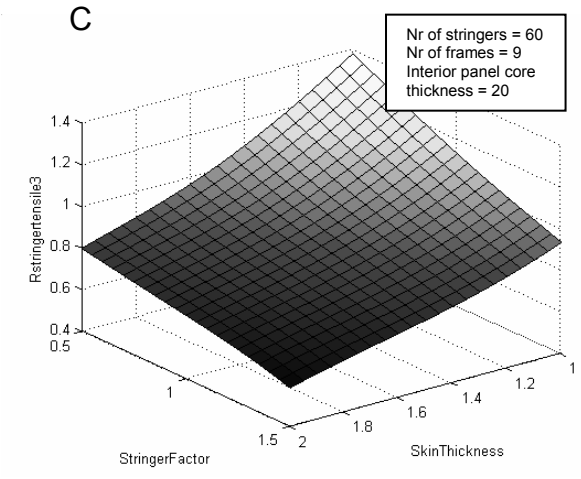

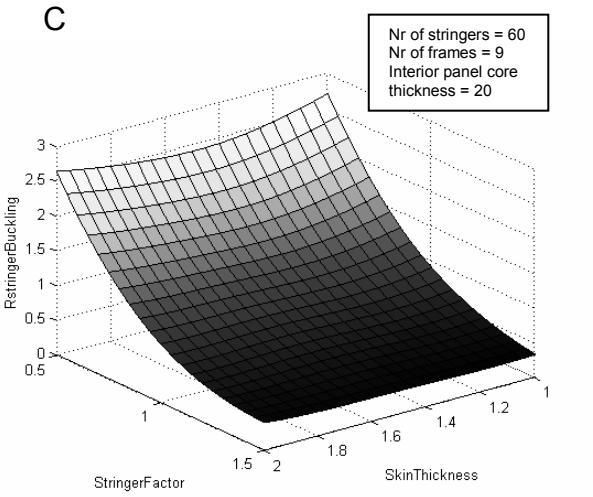

Figure I.2.3: *Response surfaces for the R stringer tensile requirement. (Validation set errors: Max=2.8574, Mean=1.308, Rsqr=0.99458, Rmea=0.14688, APE=1.432).*

Figure I.2.4: *Response surfaces for the R stringer Euler buckling requirement. (Validation set errors: Max=26.2379, Mean=13.6764,Rsqr=0.93404, Rmea=0.56011, APE=14.236).*

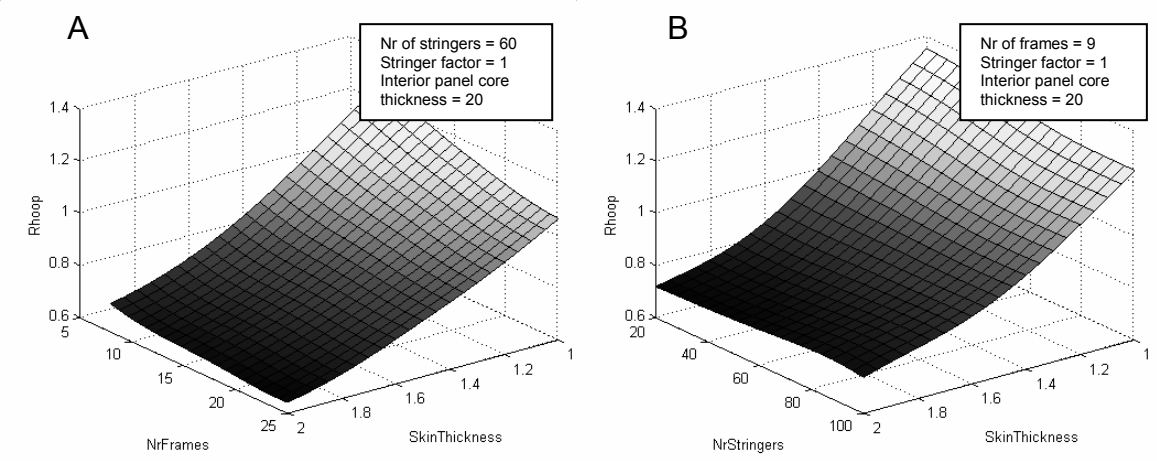

Figure I.2.5: *Response surfaces for the R hoop requirement (Validation set errors: Max=6.7972, Mean=2.9173, Rsqr=0.96647, Rmea=0.35387, APE=2.9173).*

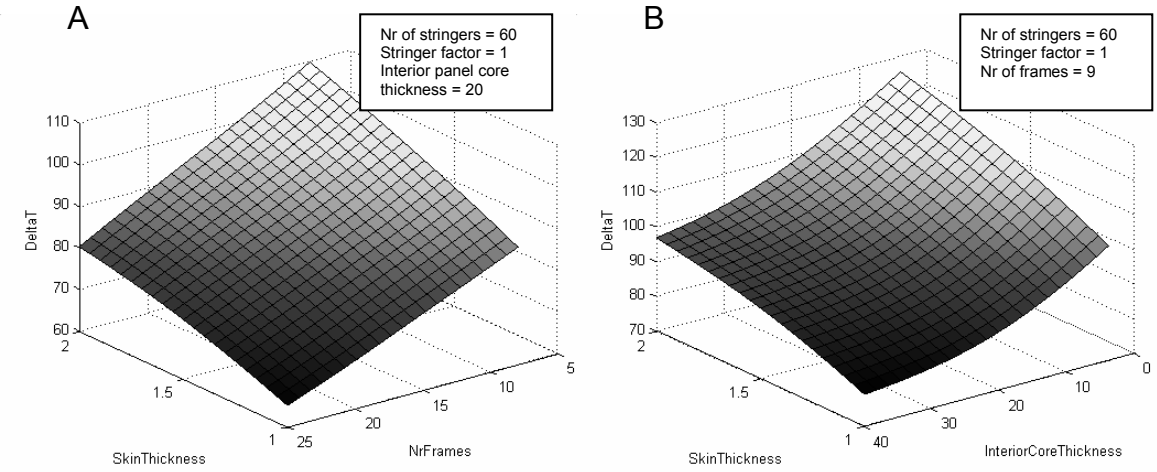

Figure I.2.6: *Response surfaces for the temperature difference requirement, which is independent of the number of stringers and the stringer factor.(validation set errors: Max=1.7553, Mean=0.86908, Rsqr=0.99491, Rmea=0.13883, APE=0.85957).*

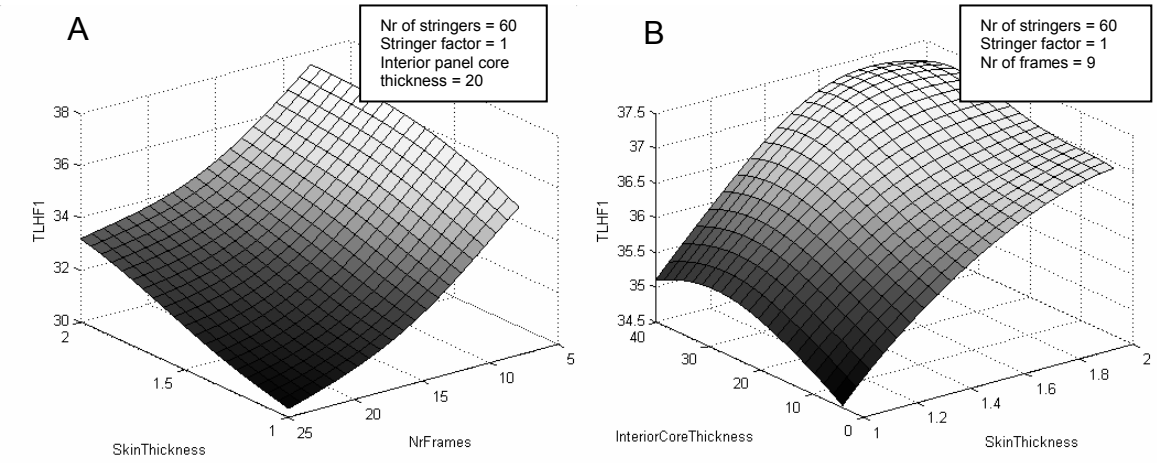

Figure I.2.7: *Response surfaces for the overall sound transmission loss requirement in the frequency range 1, [0-500Hz]. (validation set errors: Max=1.9122, Mean=0.73769, Rsqr=0.99606, Rmea=0.12251, APE=0.69819).*

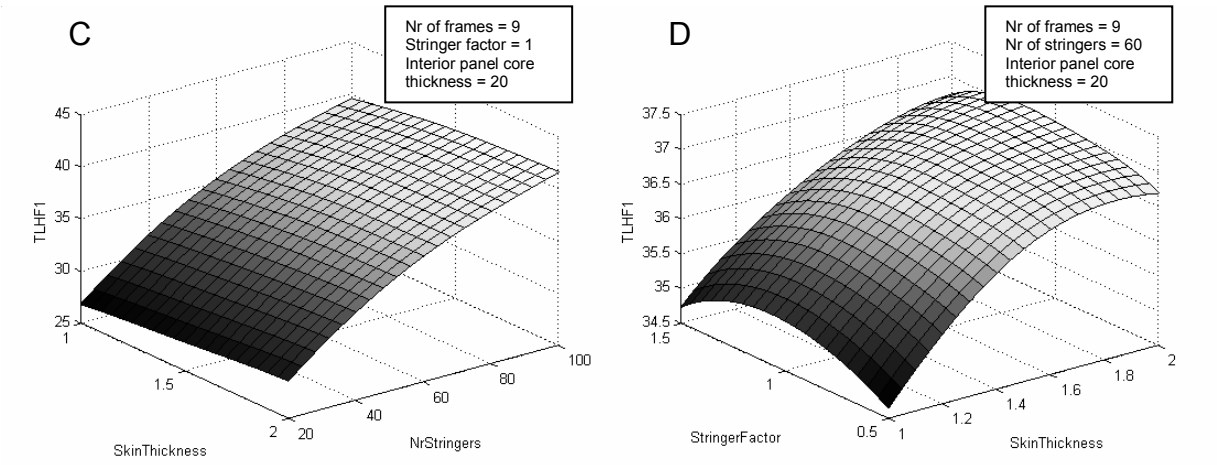

Figure I.2.7continued: *Response surfaces for the overall sound transmission loss requirement in the frequency range 1, [0-500Hz]. (validation set errors: Max=1.9122, Mean=0.73769, Rsqr=0.99606, Rmea=0.12251, APE=0.69819).*

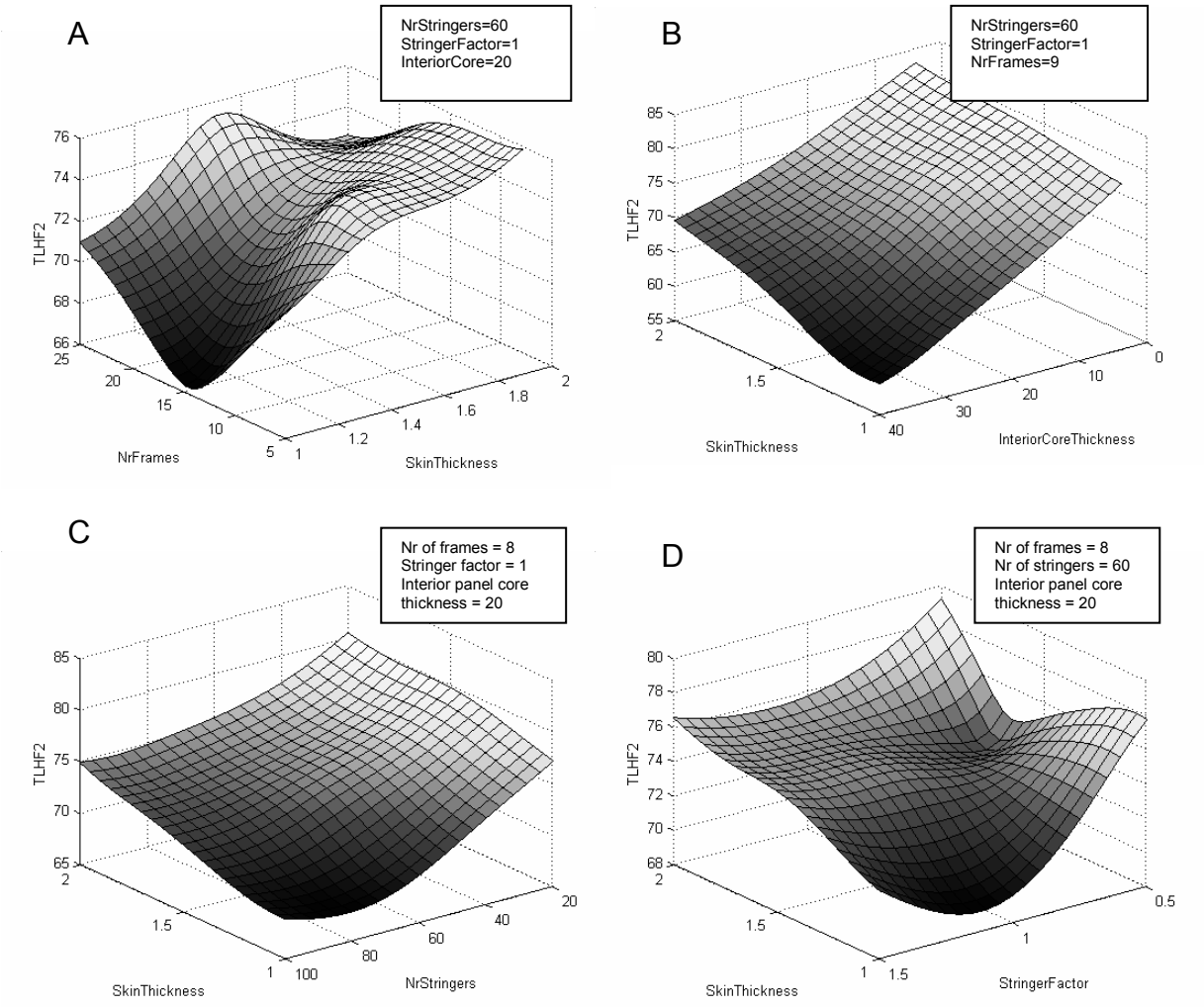

Figure I.2.8: *Response surfaces for the overall sound transmission loss requirement in frequency range 2, [500-5000Hz]. (Validation set errors: Max=10.4894, Mean=4.0135, Rsqr=0.69814, Rmea=1.2748, APE=4.0815).*

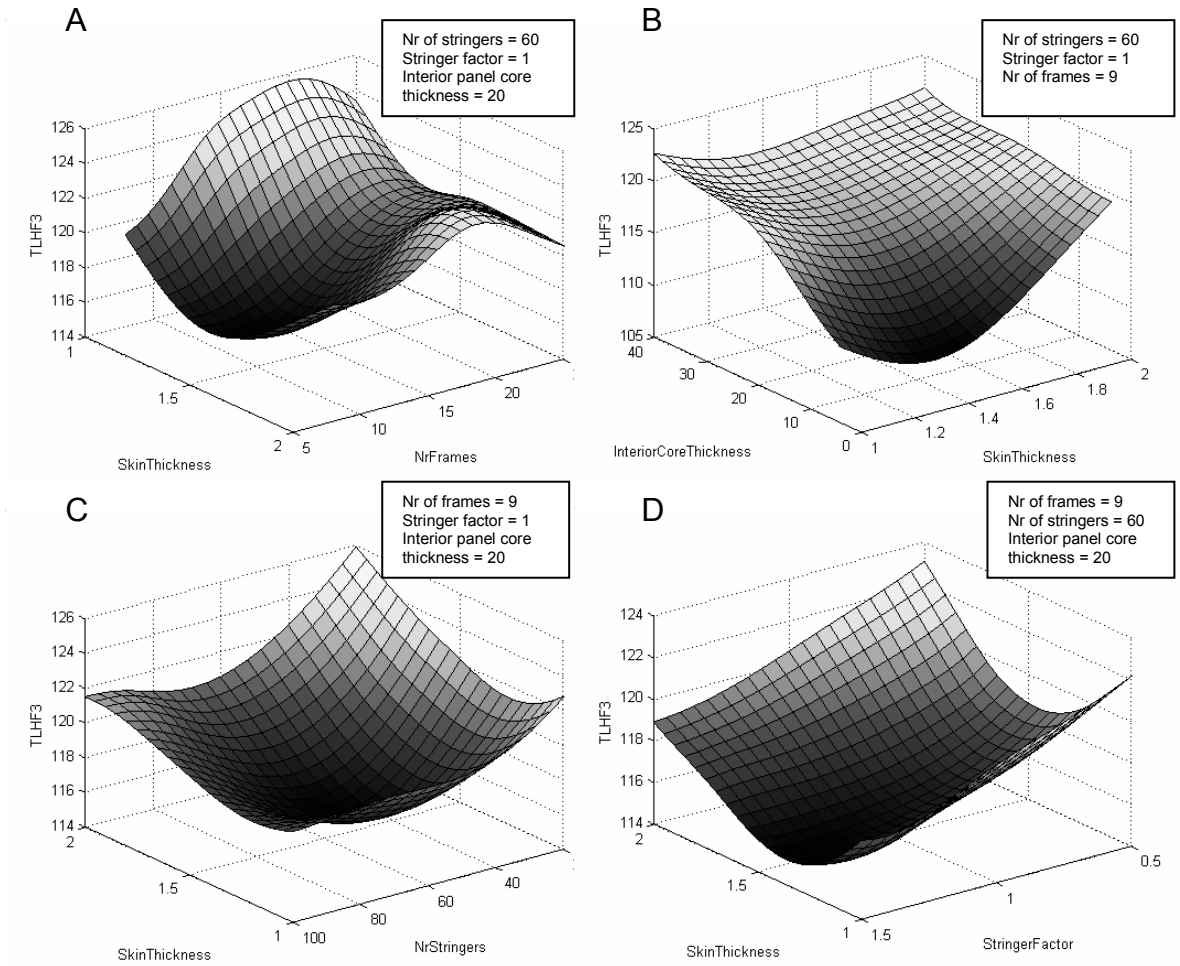

Figure I.2.9: *Response surfaces for the overall sound transmission loss requirement in frequency range 3, [5000-20000Hz]. (Validation set errors: Max=9.4275, Mean=5.1055, Rsqr=0.088034, Rmea=1.6561, APE=5.1611).*

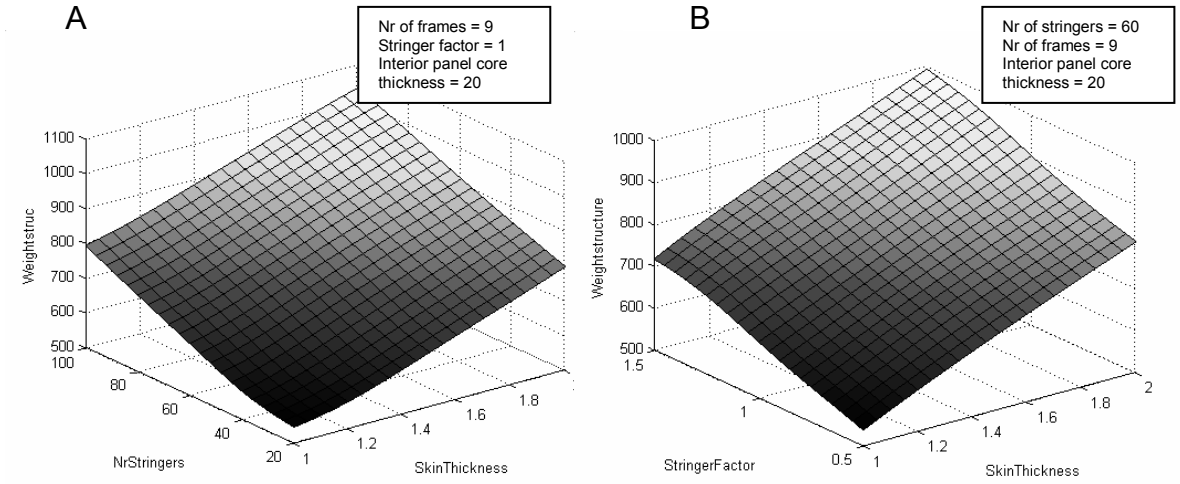

Figure I.2.10: *Response surfaces for the structural fuselage section weight objective function, which is independent of the interior panel core thickness because the insulation blanket and interior panels are not included. (Validation set errors: Max=2.6984, Mean=1.5963, Rsqr=0.9924, Rmea=0.19281, APE=1.6437).*

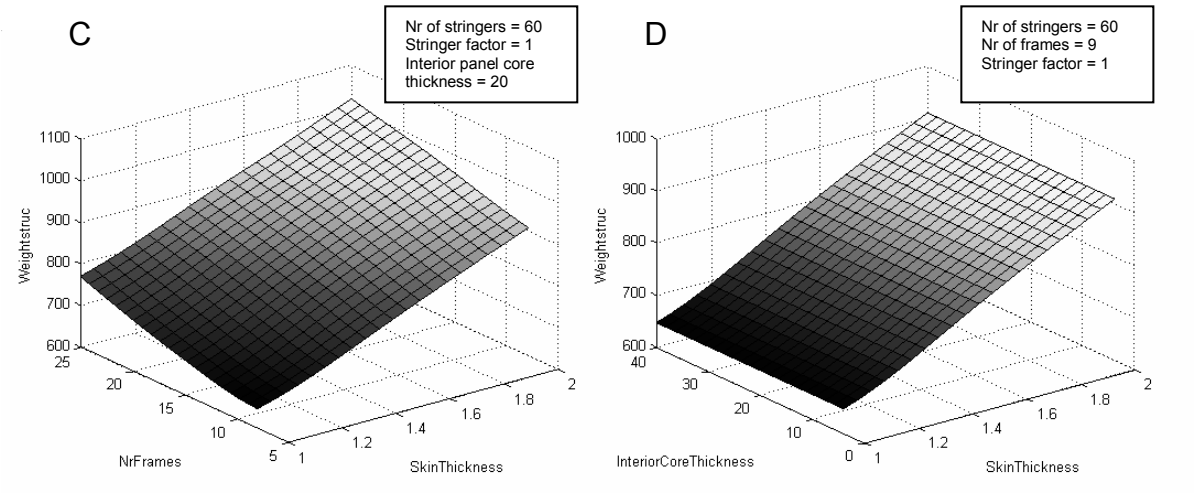

Figure I.2.10 continued: *Response surfaces for the structural fuselage section weight objective function, which is independent of the interior panel core thickness because the insulation blanket and interior panels are not included. (Validation set errors: Max=2.6984, Mean=1.5963, Rsqr=0.9924, Rmea=0.19281, APE=1.6437).*

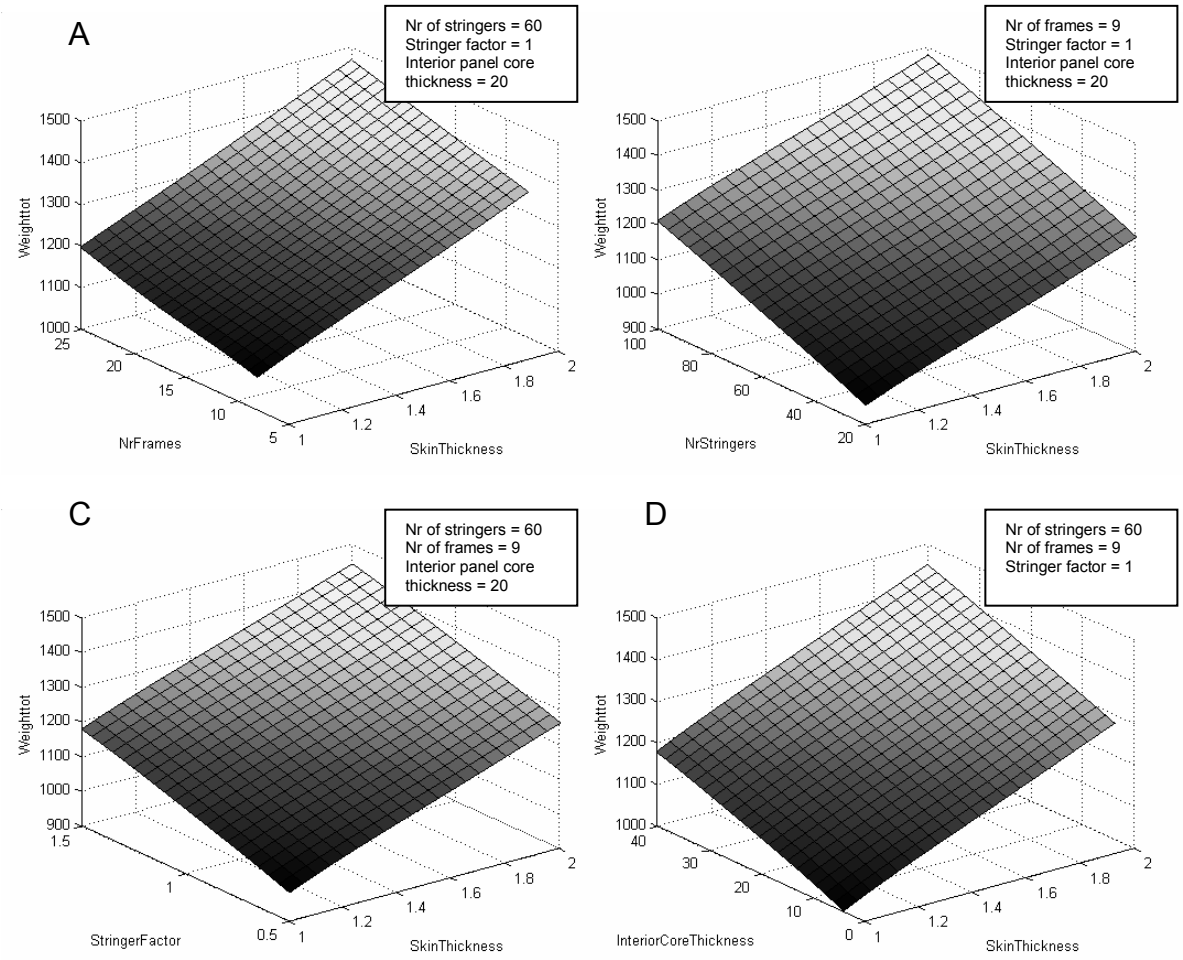

Figure I.2.11: *Response surfaces for the structural fuselage section weight objective function, which is independent of the interior panel core thickness because the insulation blanket and interior panels are not included. (validation set errors: Max=0.99618, Mean=0.39267, Rsqr=0.99882, Rmea=0.068576, APE=0.38815).*

I.3. Sequential programming optimisations

Table I.3.1: *Four optimised solutions for minimum structural fuselage weight determined with the sequential programming (SQP) option of the G_OPT program using four different program settings. Only continuous variables can be considered. Therefore the design variable Interior Core thickness, Number of frames and the number of stringers have to be fixed. Four fixed sets are considered with a constant interior panel core thickness of 4 mm.*

	Solution 1	Solution 2	Solution 3	Solution 4
G_OPT program settings				
Tol value on design variable	1e-5	1e-5	1e-5	1e-5
Tol value on obj function	1e-5	1e-5	1e-5	1e-5
Max number of iterations	25	25	25	25
Fixed design variables				
NrFrames	12	12	13	11
NrStringers	90	100	100	100
InteriorCorethickness	4	4	4	4
Start design variables				
Skin Thickness	1.9	1.9	1.9	1.9
StringerFactor	0.8	0.8	0.8	0.8
Design variables				
SkinThickness	1.6268	1.4842	1.4830	1.4826
StringerFactor	0.7089	0.6614	0.6610	0.6609
Final performances				
Rhoop	0.8216	0.9045	0.8981	0.9138
Rskintensile	0.8476	0.8895	0.8926	0.8875
Rstringertensile	0.7178	0.7507	0.7539	0.7483
Rskinbuckling	1.0000	1.0000	1.0000	1.0000
Rstringerbuckling	0.6415	0.6453	0.5435	0.7666
θ	111.5	108.2	106.2	110.1
TLHF1	38.72	39.32	38.94	39.70
TLHF2	81.55	79.63	78.88	80.32
TLHF3	116.22	117.71	117.38	118.08
Weighttot	1207.21	1176.13	1184.06	1166.80
Objective function				
Weightstruc	840.87	818.40	823.52	812.65

I.4. Multi Objective Optimisations

The multi objective optimisations are performed with the Multi Objective Genetic Algorithm optimisation option of the G_OPT program developed by Lanzi [1]. This optimisation procedure determines a Pareto set of configurations for which two selected objectives are optimal. Table I.4.1 gives the Pareto set for minimum total fuselage section weight and maximum thermal insulation. Table I.4.2 gives the minimum total fuselage section weight with maximum sound transmission loss in the low frequency range and table I.4.3 and I.4.4 give the Pareto set for minimum total fuselage section weight and maximum sound transmission loss in the middle and high frequency range. The corresponding representations of the fuselage configurations given in table I.4.1-4 are illustrated in figure 10.9 of chapter 10. Table I.4.5 gives the first 20 configurations of the Pareto set for minimum fuselage section weight and maximum thermal and sound transmission loss of the low, middle and high frequency range.

Table I.4.1: *First 20 points of the Pareto set for minimum total fuselage section weight and maximum temperature difference between the inside and outside surface of the fuselage wall (θ).*

	Design variables					Objectives		Constraints				
Pareto set nr	Skin thickness	Nr of frames	Nr of stringers	Stringer area factor	Interior panel core thickness	θ	Wtotal	Rhoop	Rskin tensile	Rstringer buckling	Rstringer tensile	Rskin buckling
1	1.5176	12	100	0.5235	6	106.2	1151.29	0.8998	0.9323	0.7935	0.9289	1.0021
2	1.5216	12	100	0.5471	6	106.3	1160.46	0.8934	0.9214	0.7835	0.9258	0.9329
3	1.5412	9	100	0.6922	4	115.3	1173.74	0.9019	0.8438	0.7094	0.8806	0.9832
4	1.5412	10	100	0.6333	4	113.2	1164.18	0.8975	0.8691	0.7340	0.8908	0.9847
5	1.5569	9	100	0.7078	4	115.7	1183.04	0.8926	0.8322	0.6993	0.8593	0.9443
6	1.5686	13	100	0.5235	4	107.2	1162.30	0.8763	0.9077	0.7734	0.8400	0.8723
7	1.6078	8	100	0.7510	4	118.8	1200.23	0.8812	0.7928	0.6639	0.7729	0.9984
8	1.6314	8	100	0.7510	4	119.2	1206.38	0.8720	0.7839	0.6566	0.7467	0.9996
9	1.6784	8	90	0.8255	5	119.8	1225.84	0.8339	0.7872	0.6594	0.9177	0.9347
10	1.6784	8	90	0.8294	5	119.8	1226.97	0.8337	0.7861	0.6583	0.9164	0.9259
11	1.6902	8	90	0.8451	4	121.3	1228.88	0.8324	0.7751	0.6485	0.8939	0.8935
12	1.6941	8	90	0.8922	4	121.5	1243.34	0.8285	0.7605	0.6348	0.8697	0.7996
13	1.7922	8	90	0.8450	4	123.2	1255.39	0.8020	0.7398	0.6183	0.7603	0.9086
14	1.8078	8	80	0.8608	5	122.8	1245.33	0.7847	0.7692	0.6450	0.9673	1.0046
15	1.8588	8	80	0.9471	4	125.1	1274.91	0.7706	0.7285	0.6082	0.8262	0.8322
16	1.8706	8	70	1.1431	4	125.7	1292.75	0.7515	0.7168	0.5981	0.9609	0.6361
17	1.9451	8	70	0.9667	5	125.5	1279.76	0.7388	0.7313	0.6127	0.9500	0.9335
18	1.9725	8	80	1.1471	4	127.2	1351.87	0.7450	0.6385	0.5271	0.4905	0.5632
19	1.9765	8	80	0.9000	4	126.9	1293.09	0.7498	0.6960	0.5804	0.6758	0.9635
20	1.9765	8	80	0.9588	4	127.1	1307.68	0.7477	0.6827	0.5678	0.6312	0.8401

Table I.4.2: *First 20 points of the Pareto set for minimum total fuselage section weight and maximum sound transmission loss in the low frequency range [0-500Hz].*

	Design variables					Objectives		Constraints				
Pareto set nr	Skin thickness	Nr of frames	Nr of stringers	Stringer area factor	Interior panel core thickness	TLHF1	Wtotal	Rhoop	Rskin tensile	Rstringer buckling	Rstringer tensile	Rskin buckling
1	1.4706	9	100	0.6922	6	40.5321	1166.80	0.9289	0.8776	0.7371	0.9947	0.9746
2	1.4863	11	100	0.6255	5	39.7182	1161.96	0.9119	0.9014	0.7619	0.9927	0.8543
3	1.4980	9	100	0.6883	7	40.6151	1178.66	0.9091	0.8696	0.7315	0.9474	0.9886
4	1.5020	11	100	0.5784	7	39.7668	1161.98	0.9022	0.9165	0.7774	0.9594	0.9842
5	1.5176	8	100	0.7667	4	41.0286	1181.45	0.9205	0.8224	0.6870	0.8917	0.9514
6	1.5294	12	100	0.5510	4	39.3948	1152.20	0.8978	0.9120	0.7748	0.9123	0.9223
7	1.5373	8	100	0.7510	5	41.0931	1187.74	0.9074	0.8229	0.6886	0.8638	0.9924
8	1.5451	8	100	0.7588	8	41.1860	1210.02	0.8897	0.8243	0.6904	0.8524	0.9738
9	1.5451	9	100	0.6882	5	40.6716	1179.51	0.8950	0.8463	0.7121	0.8747	0.9939
10	1.5686	8	100	0.7549	30	41.7626	1329.49	0.9169	0.8365	0.6955	0.8209	0.9857
11	1.5686	12	100	0.5392	4	39.4640	1158.75	0.8812	0.8988	0.7646	0.8441	0.9601
12	1.5725	8	100	0.7941	20	41.5176	1292.32	0.8801	0.8175	0.6822	0.8131	0.8934
13	1.5765	8	100	0.7824	22	41.5775	1299.92	0.8845	0.8217	0.6856	0.8093	0.9206
14	1.5922	8	100	0.7510	27	41.7389	1319.48	0.8950	0.8297	0.6914	0.7915	0.9973
15	1.5922	8	100	0.7588	33	41.8634	1351.31	0.9194	0.8254	0.6848	0.7913	0.9779
16	1.6000	8	100	0.7549	6	41.2343	1211.56	0.8743	0.8007	0.6708	0.7821	0.9881
17	1.6000	8	100	0.7667	31	41.8497	1346.22	0.9065	0.8214	0.6822	0.7817	0.9595
18	1.6078	8	100	0.7510	7	41.2698	1218.21	0.8669	0.8017	0.6720	0.7729	0.9984
19	1.6078	8	100	0.7863	22	41.6306	1309.26	0.8708	0.8102	0.6758	0.7712	0.9140
20	1.6157	8	100	0.8059	26	41.7635	1337.76	0.8792	0.8034	0.6679	0.7602	0.8708

Table I.4.3: *Pareto set for minimum total fuselage section weight and maximum sound transmission loss in the middle frequency range [500-5000Hz].*

	Design variables					Objectives		Constraints				
Pareto set nr	Skin thickness	Nr of frames	Nr of stringers	Stringer area factor	Interior panel core thickness	TLHF2	Wtotal	Rhoop	Rskin tensile	Rstringer buckling	Rstringer tensile	Rskin buckling
1	1.5059	14	100	0.5078	4	79.81	1148.87	0.9028	0.9454	0.8056	0.9543	0.7910
2	1.5647	13	100	0.5039	5	80.81	1160.38	0.8772	0.9192	0.7841	0.8425	0.9285
3	1.6353	13	90	0.5235	4	82.87	1165.02	0.8362	0.9120	0.7791	0.9807	0.9816
4	1.7294	14	90	0.5000	4	83.63	1191.30	0.7977	0.8810	0.7544	0.8106	0.9482
5	1.7451	13	90	0.5314	4	84.64	1196.40	0.7932	0.8631	0.7376	0.8135	0.9954
6	1.8353	14	80	0.5353	5	85.45	1219.34	0.7481	0.8566	0.7335	0.9334	0.9988
7	1.8549	12	90	0.5941	4	86.73	1235.18	0.7512	0.7992	0.6803	0.7240	0.9893
8	1.8706	14	80	0.5627	4	86.02	1230.79	0.7395	0.8329	0.7124	0.8871	0.9322
9	1.9059	12	90	0.6098	4	87.19	1252.96	0.7457	0.7748	0.6587	0.6813	0.9626
10	1.9333	12	90	0.6176	4	87.35	1262.30	0.7395	0.7617	0.6471	0.6592	0.9509
11	1.9451	13	90	0.5588	4	87.28	1256.31	0.7371	0.7725	0.6589	0.6234	0.9984
12	2.0000	11	90	0.6608	4	87.74	1282.99	0.7347	0.7201	0.6087	0.6094	0.9949

Table I.4.4: *First 20 points of thePareto set for minimum total fuselage section weight and maximum sound transmission loss in the high frequency range [5000-20.000Hz].*

	Design variables					Objectives		Constraints				
Pareto set nr	Skin	Nr of frames	Nr of stringers	Stringer area factor	Interior panel core thickness	TLHF3	Wtotal	Rhoop	Rskin tensile	Rstringer buckling	Rstringer tensile	Rskin buckling
1	1.5020	10	100	0.6255	14	122.92	1205.93	0.8859	0.9028	0.7641	0.9534	1.0026
2	1.5020	12	100	0.5275	20	123.33	1220.14	0.8844	0.9468	0.8064	0.9596	0.9891
3	1.5020	12	100	0.5549	4	118.51	1146.13	0.9111	0.9229	0.7834	0.9635	0.9090
4	1.5020	13	100	0.5275	28	124.51	1266.03	0.8850	0.9448	0.8032	0.9637	0.8555
5	1.5020	14	100	0.5118	32	124.76	1286.64	0.8886	0.9489	0.8069	0.9629	0.7802
6	1.5020	14	100	0.5235	33	124.81	1295.03	0.8914	0.9433	0.8012	0.9635	0.7493
7	1.5058	9	100	0.7039	13	122.98	1218.54	0.8840	0.8684	0.7310	0.9350	0.9486
8	1.5059	12	100	0.5471	22	123.71	1237.17	0.8809	0.9362	0.7962	0.9550	0.9316
9	1.5059	12	100	0.5471	26	124.19	1256.87	0.8881	0.9362	0.7948	0.9550	0.9316
10	1.5059	12	100	0.5510	20	123.34	1228.50	0.8786	0.9346	0.7952	0.9555	0.9204
11	1.5059	13	100	0.5196	12	120.93	1186.32	0.8810	0.9483	0.8091	0.9549	0.8778
12	1.5059	13	100	0.5314	23	123.89	1243.94	0.8726	0.9420	0.8026	0.9562	0.8449
13	1.5059	13	100	0.5353	21	123.45	1235.37	0.8710	0.9407	0.8018	0.9566	0.8341
14	1.5059	14	100	0.5039	38	125.01	1312.91	0.9185	0.9438	0.8002	0.9539	0.8016
15	1.5059	14	100	0.5157	29	124.61	1274.58	0.8752	0.9466	0.8061	0.9548	0.7700
16	1.5059	14	100	0.5431	34	124.83	1306.88	0.8919	0.9326	0.7909	0.9561	0.7002
17	1.5098	12	100	0.5235	6	119.31	1149.18	0.9038	0.9359	0.7964	0.9437	1.0015
18	1.5137	12	100	0.5235	11	121.02	1176.90	0.8852	0.9409	0.8020	0.9363	1.0018
19	1.5137	12	100	0.5314	17	122.66	1209.60	0.8768	0.9399	0.8010	0.9377	0.9782
20	1.5137	12	100	0.5314	23	123.82	1239.30	0.8804	0.9399	0.7996	0.9377	0.9782

Table I.4.5: *First 20 points of the Pareto set for minimum total fuselage section weight and maximum θ, TLHF1, TLHF2 and TLHF3.*

	Design variables					Objectives					Constraints				
Pareto set nr	Skin thickness	Nr of frames	Nr of stringers	Stringer area factor	Interior panel core thickness	θ	TLHF1	TLHF2	TLHF3	Wtotal	Rhoop	Rskin tensile	Rstringer buckling	Rstringer tensile	Rskin buckling
1	1.4706	8	100	0.7549	6	113.54	40.97	80.17	119.09	1177.25	0.9373	0.8503	0.7105	0.9685	0.9741
2	1.4745	9	100	0.7627	10	107.17	40.63	77.56	120.71	1213.03	0.9060	0.8555	0.7170	0.9836	0.8030
3	1.4863	11	100	0.5706	25	91.84	40.10	71.42	123.89	1247.26	0.9069	0.9356	0.7923	0.9876	1.0058
4	1.4863	12	100	0.6412	5	107.05	39.33	79.32	118.28	1175.67	0.9016	0.8981	0.7592	0.9972	0.6896
5	1.4941	20	100	0.5039	32	78.01	37.72	67.06	125.08	1319.04	0.8185	0.9474	0.8129	0.9725	0.3737
6	1.5020	8	100	0.8216	36	91.49	41.68	69.01	122.32	1361.59	0.9748	0.8339	0.6874	0.9082	0.8249
7	1.5020	13	100	0.6647	24	89.77	39.26	68.78	123.86	1288.52	0.8637	0.8839	0.7478	0.9635	0.5383
8	1.5020	14	100	0.5627	27	87.00	39.07	68.30	124.54	1278.28	0.8658	0.9271	0.7885	0.9644	0.6534
9	1.5098	8	100	0.8216	20	100.35	41.40	73.23	121.83	1284.66	0.9096	0.8292	0.6905	0.8961	0.8260
10	1.5137	13	100	0.5941	38	85.45	39.74	68.37	124.74	1337.31	0.9189	0.9067	0.7636	0.9448	0.6863
11	1.5176	9	100	0.7627	7	111.41	40.67	79.57	119.45	1207.87	0.8923	0.8350	0.7000	0.9138	0.8095
12	1.5216	8	100	0.7706	40	90.47	41.67	69.17	123.10	1367.59	0.9900	0.8352	0.6887	0.8855	0.9425
13	1.5216	8	100	0.8294	38	91.20	41.72	68.60	122.53	1378.14	0.9758	0.8210	0.6757	0.8770	0.8113
14	1.5216	10	100	0.6608	6	110.53	40.22	80.44	119.50	1179.55	0.8929	0.8718	0.7357	0.9240	0.9097
15	1.5216	10	100	0.6765	7	109.42	40.24	79.78	119.93	1190.22	0.8859	0.8677	0.7319	0.9248	0.8700
16	1.5294	11	100	0.6608	28	91.22	40.28	70.21	123.65	1301.61	0.8861	0.8815	0.7421	0.9194	0.7718
17	1.5294	12	100	0.5431	11	101.35	39.47	77.56	120.98	1187.30	0.8732	0.9258	0.7887	0.9115	0.9449
18	1.5294	12	100	0.6686	27	90.28	39.83	69.22	123.90	1305.50	0.8687	0.8753	0.7383	0.9198	0.6348
19	1.5294	13	100	0.5941	21	91.85	39.26	70.58	123.41	1259.58	0.8511	0.9042	0.7689	0.9161	0.6876
20	1.5333	9	100	0.6882	20	99.16	40.95	73.92	122.98	1256.85	0.8876	0.8694	0.7313	0.8919	0.9927

I.5. Reference

[1] Lanzi, L.,Optimisation of composit stiffened panels under post buckling constraints, PhD thesis, Polytecnico di Milano, 2004

J Results of the DEE application on a sandwich fuselage concept

J.1. Design of experiments and the resulting evaluations

For the analysis and optimisation of the sandwich fuselage concept a design of experiments has been performed with the Latin hypercube routine of the G_OPT program developed by *Lanzi [1]* to generate a set of 100 data points. In a second optimisation step another 50 data points are generated.

The four design variables that are chosen for the optimisation of the sandwich fuselage concept are:

1.) The skin facing thickness [t_f], also indicated as SkinFacingThickness.
2.) The skin core thickness [t_c], also indicated as SkinCoreThickness.
3.) The number of frames [n_{fr}], also indicated as NrFrames.
4.) The interior panel core thickness [t_{inc}], also indicated as InteriorCoreThickness.

The DEE is used to determine the performance of each requirement. Four structural requirements are considered:

1.) The hoop stress criteria [R_{Hoop}}, also indicated as Rhoop.
2.) The sandwich buckling criteria, [R_{swb}], also indicated as RsandBuckling.
3.) The tensile stress criteria in the sandwich skin [R_{swt}], also indicated as Rtensile.
4.) The wrinkling criteria [R_{wr}], also indicated as RsandWrinkling.

Also the evaluations of the six objective functions are determined:

1.) The temperature difference between the inside and outside surface of the fuselage wall [θ], also indicated as DeltaT.
2.) The overall sound transmission loss in frequency range 1 [0-500Hz], [TLHF1].
3.) The overall sound transmission loss in frequency range 2 [500-5000Hz], [TLHF2].
4.) The overall sound transmission loss in frequency range 3 [5000-20000Hz], [TLHF3].
5.) The weight of the fuselage section structure [W_{struc}], also indicated as WeightStruc.
6.) The weight of the fuselage section including the structure, insulation blanket and interior panels [W_{tot}], also indicated as WeightTot.

The design variables together with the evaluations of the requirements and the objective functions for the first 100 data points are shown in table J.1. The results for the 50 data points used for the second optimisation step are shown in table J.2.

Table J.1: *Design of experiments and evaluations*

	Design variables				Evaluations									
Data point nr	Skin facing thickness	Skin core thickness	Nr of frames	Interior panel core thickness	Rhoop	Rsandwich tensile	Rsandwich buckling	Rwrinkling	θ	TLHF1	TLHF2	TLHF3	Wtotal	Wstructure
1	1.9252	11	5	21	0.7934	0.1362	0.2916	0.7156	107.88	34.90	84.25	132.03	1374.3	945.2
2	0.6040	26	2	5	0.8715	0.4067	0.9828	2.1956	114.87	40.76	85.80	112.95	926.3	593.4
3	1.4155	30	1	39	0.3543	0.1816	0.4099	0.9532	90.32	42.16	71.08	124.80	1416.2	907.7
4	0.5052	11	8	35	2.8646	0.4934	1.1220	2.6476	76.27	31.91	68.64	116.94	962.0	455.6
5	1.2316	30	8	9	0.3705	0.2078	0.4386	1.0931	109.22	30.59	78.82	117.66	1237.5	888.6
6	0.6060	11	1	40	2.4852	0.4156	0.9445	2.2166	79.95	41.71	74.88	106.92	981.8	448.6
7	0.8104	5	4	11	4.3114	0.3239	0.7261	1.7109	95.93	39.82	93.05	108.24	874.8	490.8
8	1.9673	29	1	5	0.2678	0.1320	0.2900	0.6891	127.25	42.13	86.48	119.04	1424.3	1096.6
9	1.7518	25	8	39	0.3474	0.1489	0.3109	0.7753	90.88	33.30	69.14	134.73	1531.3	1018.6
10	1.3837	14	1	6	0.8165	0.1871	0.4068	0.9775	124.88	40.74	92.26	116.41	1103.1	754.9
11	0.5638	23	4	28	1.0623	0.4402	0.9611	2.3628	89.13	33.88	74.14	117.12	1018.3	561.1
12	1.6000	8	1	30	1.3101	0.1647	0.3478	0.8562	101.31	42.69	77.28	130.18	1256.5	775.9
13	1.3299	12	8	4	1.0120	0.1957	0.4236	1.0259	116.22	31.64	86.81	110.22	1107.7	767.9
14	1.4001	6	7	36	1.9536	0.1886	0.4075	0.9834	88.34	35.02	78.03	103.26	1238.4	723.3
15	1.8481	29	4	27	0.2834	0.1417	0.3020	0.7369	99.49	39.54	74.77	141.13	1513.4	1069.3
16	0.6444	20	7	6	1.0786	0.3836	0.8479	2.0590	106.44	31.70	84.90	109.44	931.1	587.4
17	0.7045	26	8	30	0.6964	0.3533	0.7661	1.8888	87.66	30.58	70.99	122.52	1124.9	660.0
18	0.5593	6	8	9	5.2025	0.4591	1.0491	2.4316	86.45	42.06	75.82	123.27	812.8	439.8
19	1.9774	23	7	15	0.3466	0.1320	0.2767	0.6871	109.79	31.58	80.60	145.39	1468.9	1083.1
20	1.3198	24	4	11	0.4575	0.1965	0.4202	1.0284	113.13	33.66	82.41	122.87	1206.0	841.1
21	0.5660	29	1	40	0.8436	0.4286	1.0631	2.3234	83.97	40.23	69.34	120.38	1114.2	597.9
22	1.7830	18	4	40	0.5001	0.1477	0.3119	0.7668	93.97	43.24	74.08	125.73	1471.2	946.5
23	1.2918	17	7	22	0.6918	0.1998	0.4284	1.0490	98.74	30.33	80.52	122.66	1215.3	785.6
24	0.6392	15	1	21	1.6237	0.3891	0.9049	2.0825	94.00	46.86	88.85	112.07	925.6	498.2
25	1.0914	7	4	31	2.1727	0.2398	0.5256	1.2613	89.60	38.07	80.89	122.02	1092.5	604.8
26	1.7847	22	1	20	0.3929	0.1454	0.3175	0.7591	110.89	40.65	104.95	142.65	1381.6	968.1
27	0.7421	28	6	17	0.6050	0.3334	0.7134	1.7846	98.65	36.79	76.71	125.68	1076.9	683.2
28	0.7418	29	1	23	0.6533	0.3338	0.8031	1.7904	97.64	41.79	77.47	129.36	1086.1	661.5
29	1.7978	9	4	5	1.0458	0.1471	0.3151	0.7658	126.09	38.00	97.47	110.75	1225.9	878.8
30	1.0963	18	7	40	0.7435	0.2336	0.5017	1.2307	86.94	32.32	71.14	131.72	1245.3	719.6
31	1.2656	28	5	35	0.3965	0.2047	0.4353	1.0738	90.50	34.31	70.61	128.10	1347.2	858.2
32	1.0710	19	2	31	0.7116	0.2390	0.5355	1.2601	94.32	59.54	77.54	126.41	1169.1	692.9
33	1.8643	5	4	35	1.6716	0.1427	0.3051	0.7442	98.28	39.46	81.07	112.68	1371.4	861.3
34	0.5706	12	6	19	2.2902	0.4386	0.9852	2.3335	87.86	36.96	81.52	114.02	899.7	479.9
35	1.8169	12	8	27	0.7666	0.1448	0.3079	0.7538	99.33	31.50	79.99	127.88	1393.2	932.9
36	1.1578	15	4	20	0.8897	0.2246	0.4820	1.1764	101.22	33.87	91.73	124.05	1123.1	701.8
37	0.5969	10	5	40	2.8114	0.4291	0.9605	2.2756	77.16	35.41	71.86	116.50	994.3	459.9
38	0.6013	11	1	6	2.5132	0.4194	0.9510	2.2371	105.76	43.17	81.66	114.24	802.0	449.5
39	1.9360	20	4	5	0.4150	0.1360	0.2868	0.7059	127.02	35.57	96.55	110.92	1361.7	1025.1
40	1.3199	6	6	14	2.0845	0.2007	0.4353	1.0431	103.63	36.32	91.49	113.74	1092.5	694.5
41	1.8398	5	8	4	1.6922	0.1443	0.3122	0.7516	121.65	36.64	91.02	117.60	1233.8	888.1
42	1.9804	22	1	39	0.3629	0.1316	0.2853	0.6852	96.33	48.49	75.55	140.07	1551.0	1035.9
43	1.9630	12	1	15	0.7104	0.1334	0.2842	0.6936	119.18	42.08	89.42	132.89	1338.4	942.1
44	1.2500	6	1	15	2.2098	0.2122	0.4450	1.1012	107.77	43.65	77.33	116.81	1037.8	634.5
45	0.6561	17	4	4	1.3368	0.3843	0.8472	2.0486	111.67	34.69	86.02	115.09	880.9	544.6
46	0.5258	29	5	5	0.8572	0.4654	1.0662	2.5158	110.17	43.54	80.55	106.07	942.5	612.3
47	1.2090	27	1	14	0.4556	0.2111	0.4801	1.1129	111.40	40.55	84.97	129.75	1187.6	809.5
48	0.7256	6	2	25	4.0087	0.3569	0.8029	1.8852	84.85	46.36	83.95	117.84	910.8	453.5
49	1.1451	30	4	22	0.3955	0.2243	0.4839	1.1799	99.24	43.13	75.62	124.45	1248.3	830.6
50	1.8393	20	4	19	0.4326	0.1430	0.3022	0.7426	109.57	31.27	82.03	147.95	1398.2	988.2

Table J.1 continued: *Design of experiments and evaluations*

	Design variables				Evaluations									
Data point nr	Skin facing thickness	Skin core thickness	Nr of frames	Interior panel core thickness	Rhoop	Rsandwich tensile	Rsandwich buckling	Rwrinkling	θ	TLHF1	TLHF2	TLHF3	Wtotal	Wstructure
51	1.8143	19	6	30	0.4576	0.1432	0.3032	0.7481	98.41	32.28	76.63	133.26	1449.7	980.0
52	0.6396	29	6	39	0.6906	0.3831	0.8285	2.0610	83.32	31.27	66.32	128.15	1160.7	650.0
53	1.0627	15	4	39	0.9602	0.2441	0.5239	1.2800	87.79	36.81	74.14	124.07	1187.7	664.4
54	1.3060	14	5	6	0.8658	0.1996	0.4308	1.0488	118.00	33.37	94.21	110.87	1103.6	755.2
55	1.5179	30	7	28	0.3138	0.1698	0.3542	0.8890	94.83	36.37	72.06	131.49	1426.8	977.8
56	0.9342	5	7	22	3.6866	0.2812	0.6223	1.4747	87.40	36.44	90.16	108.64	995.0	553.1
57	1.7857	15	7	10	0.6074	0.1465	0.3114	0.7641	114.68	31.69	87.43	128.22	1314.4	946.9
58	1.7541	29	5	8	0.2937	0.1485	0.3132	0.7781	116.76	33.52	73.61	124.03	1390.0	1046.0
59	0.5310	29	8	7	0.8121	0.4564	1.0102	2.4724	104.80	35.72	79.51	103.46	973.5	632.9
60	1.5132	14	3	30	0.7593	0.1726	0.3695	0.9008	98.86	35.90	83.87	133.29	1286.1	811.1
61	1.9187	10	7	40	0.8810	0.1373	0.2921	0.7147	94.38	32.78	75.86	117.70	1473.4	941.4
62	0.5611	15	3	34	1.7970	0.4441	1.0094	2.3846	83.18	36.21	80.92	107.47	978.4	481.3
63	0.8473	12	7	4	1.5144	0.3006	0.6667	1.5947	108.54	31.90	101.29	111.81	930.0	589.3
64	0.9160	22	3	19	0.6839	0.2776	0.6228	1.4706	101.32	37.14	81.96	131.52	1082.2	672.5
65	1.9877	29	8	24	0.2674	0.1315	0.2729	0.6832	99.22	32.76	73.91	134.36	1569.7	1141.9
66	0.6576	17	8	22	1.2447	0.3806	0.8434	2.0317	89.16	35.11	80.72	119.06	997.8	567.0
67	0.8525	23	4	39	0.7317	0.2989	0.6459	1.5816	86.56	34.38	70.59	124.35	1177.3	661.3
68	1.4368	8	3	39	1.4540	0.1827	0.3948	0.9560	91.48	39.20	78.57	116.87	1258.4	729.1
69	0.9892	12	6	30	1.3220	0.2603	0.5677	1.3682	89.11	33.84	81.26	119.90	1103.4	625.7
70	1.2648	20	7	4	0.5806	0.2031	0.4350	1.0677	117.30	30.80	84.44	113.19	1140.1	807.8
71	1.4831	17	1	36	0.6127	0.1741	0.3810	0.9114	95.97	43.58	78.37	145.95	1319.3	814.9
72	0.6138	18	6	34	1.2749	0.4004	0.8867	2.1561	83.59	31.88	72.32	116.14	1038.6	544.5
73	1.9865	27	6	36	0.2878	0.1308	0.2727	0.6813	93.59	36.40	70.63	134.18	1603.6	1109.4
74	1.8674	30	2	16	0.2688	0.1392	0.3066	0.7269	110.37	39.05	80.96	137.00	1459.9	1075.3
75	1.3905	16	1	21	0.6928	0.1851	0.4063	0.9707	106.41	39.84	79.39	119.72	1199.4	774.2
76	1.3672	5	3	22	2.3373	0.1934	0.4218	1.0145	100.16	41.26	86.90	116.99	1121.3	680.1
77	1.9453	29	1	31	0.2705	0.1336	0.2936	0.6973	98.31	49.09	75.81	136.81	1552.2	1086.1
78	1.4630	25	2	28	0.3990	0.1767	0.3921	0.9258	98.99	42.09	77.39	138.24	1339.9	886.1
79	1.2503	20	5	29	0.5941	0.2081	0.4445	1.0913	95.51	35.04	76.14	129.91	1247.6	783.3
80	1.8646	6	7	18	1.4532	0.1426	0.3051	0.7396	107.67	35.99	85.19	112.77	1312.4	944.0
81	0.9940	20	2	5	0.7119	0.2560	0.5794	1.3547	119.93	36.37	88.19	121.45	1015.5	677.5
82	1.2496	9	3	9	1.4705	0.2086	0.4554	1.0960	114.17	38.43	88.68	118.36	1045.0	676.0
83	1.0139	27	6	7	0.4871	0.2487	0.5289	1.3176	112.38	31.54	81.26	117.40	1114.8	773.2
84	1.9251	13	2	40	0.6645	0.1359	0.2901	0.7081	96.80	39.06	77.89	134.13	1470.7	941.3
85	1.4177	24	6	17	0.4261	0.1810	0.3834	0.9497	104.80	31.56	79.73	133.04	1283.3	886.9
86	1.9579	15	1	28	0.5570	0.1328	0.2859	0.6922	106.50	40.55	83.48	138.15	1428.6	966.1
87	1.5756	22	2	7	0.4348	0.1644	0.3609	0.8603	123.73	37.79	87.49	125.87	1247.0	901.5
88	1.9375	6	1	6	1.3956	0.1374	0.2863	0.7105	130.95	45.38	103.30	113.29	1234.9	879.9
89	0.5315	5	3	37	6.6836	0.4859	1.1078	2.5790	72.06	41.55	75.33	148.32	903.1	380.3
90	1.0775	8	1	35	1.9289	0.2429	0.5190	1.2679	89.62	43.67	80.63	111.23	1097.9	589.6
91	1.5418	10	6	27	1.0806	0.1700	0.3652	0.8868	98.36	33.60	81.30	133.00	1267.8	805.1
92	1.6401	13	3	17	0.7684	0.1597	0.3409	0.8330	111.15	36.67	86.99	132.29	1255.8	849.3
93	1.1847	24	8	32	0.4969	0.2167	0.4598	1.1382	90.84	33.48	72.09	121.46	1288.4	811.7
94	1.1569	25	8	18	0.4825	0.2214	0.4707	1.1644	99.85	30.84	77.82	125.87	1216.5	815.4
95	1.7551	5	4	16	1.7867	0.1515	0.3269	0.7913	111.79	39.94	91.43	111.15	1234.8	826.1
96	1.7102	20	8	24	0.4562	0.1527	0.3220	0.7961	100.40	30.59	73.51	127.43	1402.4	965.6
97	1.7092	25	3	37	0.3543	0.1526	0.3313	0.7956	93.98	39.61	72.90	129.97	1479.5	977.5
98	0.6693	14	4	16	1.6652	0.3790	0.8382	2.0141	96.14	36.53	83.28	110.95	922.1	520.2
99	0.9149	26	6	28	0.5554	0.2746	0.5841	1.4581	92.23	33.64	73.29	131.28	1177.5	723.7
100	0.8948	6	2	5	3.0650	0.2916	0.6518	1.5374	109.50	41.44	91.45	127.87	867.8	516.1

Table J.2: *Design of experiments and evaluations of the structural requirements and objective functions for another 50 data points used in the second optimisation step.*

	Design variables				Evaluations									
Data point nr	Skin facing thickness	Skin core thickness	Nr of frames	Interior panel core thickness	Rhoop	Rsandwich tensile	Rsandwich buckling	Rwrinkling	θ	TLHF1	TLHF2	TLHF3	Wtotal	Wstructure
1	1.3187	11	2	5	1.1188	0.1964	0.4280	1.0331	122.65	39.64	90.42	110.64	1058.0	712.0
2	1.3501	13	1	4	0.9101	0.1921	0.4164	1.0034	126.53	41.08	97.43	114.16	1072.9	734.1
3	1.2595	13	3	6	0.9695	0.2060	0.4455	1.0807	119.25	36.57	91.28	111.41	1065.2	715.8
4	1.3089	13	3	4	0.9369	0.1984	0.4287	1.0406	123.50	36.72	103.58	116.38	1072.6	733.6
5	1.3989	13	2	6	0.8762	0.1846	0.4014	0.9707	123.48	38.75	84.07	107.58	1107.5	758.3
6	1.2668	13	1	6	0.9633	0.2043	0.4444	1.0685	122.25	40.86	92.43	113.79	1054.0	704.3
7	1.3932	11	1	4	1.0697	0.1874	0.4019	0.9772	127.44	41.86	103.72	114.85	1072.1	731.4
8	1.3890	12	3	5	0.9733	0.1876	0.4050	0.9828	122.44	37.21	91.92	109.70	1097.9	753.0
9	1.2570	11	3	6	1.1744	0.2068	0.4495	1.0861	118.64	37.49	94.15	114.65	1048.3	697.0
10	1.3967	11	1	6	1.0670	0.1869	0.4008	0.9747	123.88	41.79	93.51	110.44	1083.6	732.5
11	1.2531	11	1	6	1.1806	0.2078	0.4477	1.0845	121.46	41.54	95.79	114.24	1032.8	681.4
12	1.2521	11	3	4	1.1785	0.2075	0.4514	1.0903	121.97	37.66	93.91	112.15	1036.5	695.6
13	1.2836	11	1	4	1.1549	0.2030	0.4368	1.0590	125.60	41.66	96.80	114.76	1033.3	692.4
14	1.3622	11	3	4	1.0916	0.1914	0.4145	1.0033	123.30	37.74	99.93	112.49	1075.5	734.7
15	1.2958	12	2	6	1.0294	0.1993	0.4340	1.0487	121.03	39.04	90.63	109.35	1063.0	712.7
16	1.3685	12	1	5	0.9861	0.1901	0.4099	0.9919	125.11	41.38	95.91	111.16	1076.5	731.5
17	1.2739	12	3	5	1.0516	0.2039	0.4420	1.0702	121.17	37.04	95.40	116.27	1057.3	712.1
18	1.2949	12	2	4	1.0302	0.1994	0.4344	1.0495	124.03	39.12	90.65	113.68	1052.5	712.6
19	1.2564	12	1	5	1.0656	0.2066	0.4473	1.0794	123.33	41.19	96.15	124.55	1036.9	691.7
20	1.2631	13	2	5	0.9598	0.2038	0.4456	1.0731	122.83	38.60	90.03	118.07	1054.7	710.1
21	1.3941	12	2	4	0.9636	0.1856	0.4032	0.9759	126.22	39.27	90.91	112.83	1087.6	747.8
22	1.3423	11	3	6	1.1064	0.1941	0.4206	1.0180	120.63	37.62	99.17	108.81	1078.5	727.3
23	1.2630	13	1	4	0.9660	0.2050	0.4457	1.0718	125.74	40.93	96.85	131.08	1042.1	703.1
24	1.3521	13	2	5	0.9033	0.1908	0.4156	1.0037	123.65	38.72	90.67	119.06	1086.2	741.8
25	1.3591	13	3	6	0.9063	0.1914	0.4126	1.0027	121.34	36.70	84.07	107.36	1100.4	751.2
26	1.3074	13	1	5	0.9365	0.1982	0.4303	1.0357	124.36	40.97	91.51	120.79	1063.0	718.8
27	1.3320	12	1	6	1.0105	0.1952	0.4214	1.0187	123.08	41.28	91.59	115.81	1068.7	718.5
28	1.3991	13	1	5	0.8815	0.1855	0.4015	0.9685	126.35	41.13	92.07	111.23	1095.7	751.4
29	1.3345	12	3	4	1.0087	0.1949	0.4218	1.0223	123.64	37.18	89.50	113.08	1073.7	733.8
30	1.3662	11	2	6	1.0830	0.1898	0.4129	0.9977	121.91	39.67	95.86	109.31	1079.9	728.7
31	1.3718	13	1	6	0.8971	0.1891	0.4096	0.9876	124.49	41.04	85.34	109.10	1090.9	741.6
32	1.3978	11	2	5	1.0605	0.1856	0.4035	0.9755	124.54	39.76	91.07	112.31	1086.0	740.1
33	1.3384	11	1	5	1.1099	0.1949	0.4186	1.0169	124.97	41.72	91.36	111.51	1057.8	711.8
34	1.3267	12	1	4	1.0143	0.1960	0.4231	1.0228	126.57	41.35	91.35	114.87	1056.6	716.7
35	1.3164	13	2	6	0.9250	0.1958	0.4271	1.0305	121.68	38.63	87.55	111.38	1078.3	729.0
36	1.3385	11	2	4	1.1037	0.1936	0.4217	1.0181	124.46	39.71	97.68	112.81	1059.9	719.1
37	1.3325	13	2	4	0.9151	0.1935	0.4218	1.0182	125.45	38.74	99.36	113.05	1073.8	734.9
38	1.3339	13	3	5	0.9214	0.1949	0.4206	1.0214	121.82	36.71	89.73	120.81	1086.4	742.3
39	1.3182	12	3	6	1.0200	0.1973	0.4269	1.0348	119.91	37.07	89.71	114.23	1078.0	727.7
40	1.3312	12	2	5	1.0047	0.1941	0.4224	1.0213	123.70	39.13	102.07	108.40	1070.4	725.3
41	1.2954	11	3	5	1.1427	0.2009	0.4361	1.0543	120.70	37.58	89.91	111.33	1056.9	710.8
42	1.3796	12	2	6	0.9727	0.1875	0.4074	0.9860	122.43	39.16	90.92	108.29	1093.0	742.4
43	1.3909	13	3	4	0.8879	0.1871	0.4032	0.9801	124.12	36.85	91.20	114.16	1101.5	762.8
44	1.3927	11	3	5	1.0699	0.1873	0.4052	0.9816	122.88	37.74	90.06	110.13	1091.3	745.4
45	1.2630	11	2	6	1.1641	0.2049	0.4470	1.0779	120.23	39.52	95.25	117.23	1043.4	692.0
46	1.2503	12	2	5	1.0633	0.2063	0.4500	1.0863	121.79	39.02	94.86	119.21	1041.8	696.6
47	1.2626	11	1	5	1.1725	0.2062	0.4442	1.0764	123.08	41.59	93.84	111.59	1031.0	684.8
48	1.3118	13	1	4	0.9338	0.1976	0.4288	1.0323	126.58	41.02	108.21	117.86	1059.4	720.5
49	1.3059	12	2	5	1.0223	0.1978	0.4307	1.0408	123.26	39.09	100.57	111.31	1061.5	716.4
50	1.3235	12	2	6	1.0099	0.1952	0.4248	1.0271	121.50	39.08	90.55	115.27	1072.8	722.5

J.2. Response surfaces of the design requirements and objective functions for the sandwich fuselage

This appendix gives an overview of the response surfaces for the different structural requirements and objective functions. The structural requirements are independent of the design variable '*interior panel core thickness'*. Each depicted response surface represents the requirement or objective function as function of two design variables. The remaining two design variables are fixed. The response surfaces are created with the G_OPT program developed by Lanzi [1] using the data from table J.1.

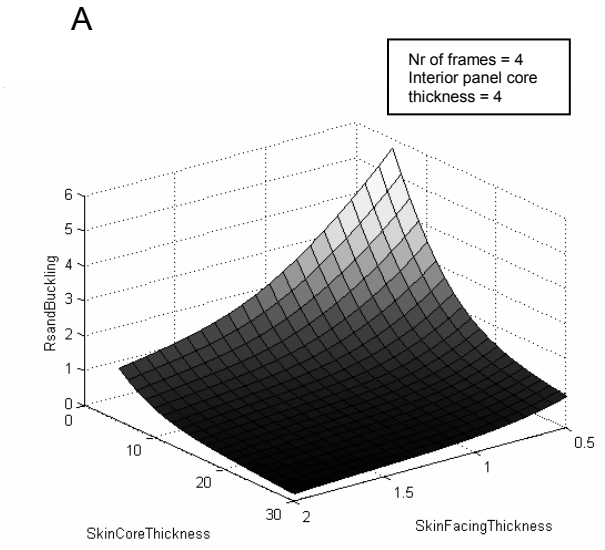

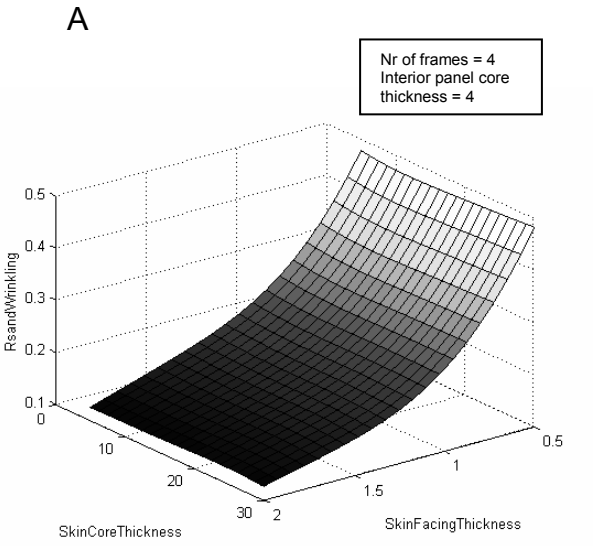

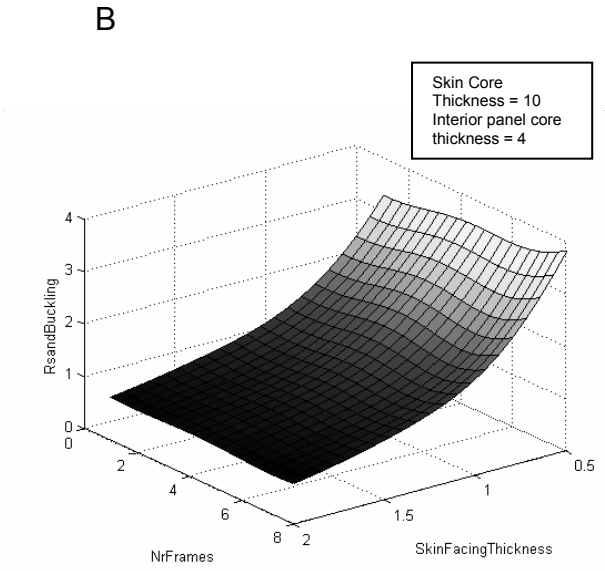

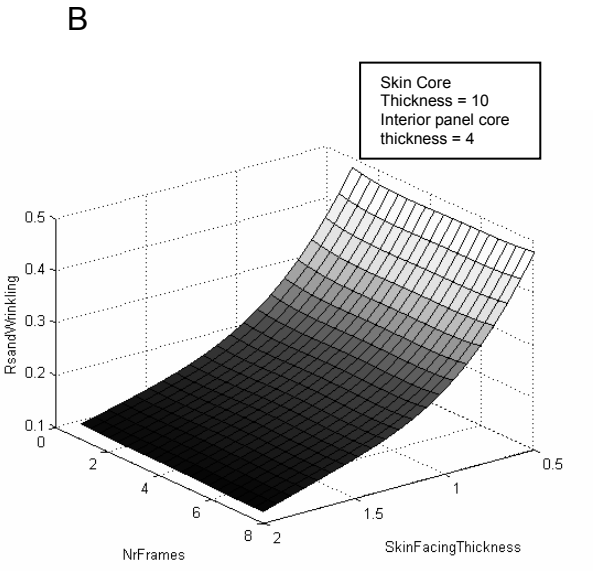

Figure J.2.1: *Response surfaces for the R sandwich buckling requirement. (Validation set errors: Max=17.6766, Mean=7.3561, Rsqr=0.96429, Rmea=0.63351, APE=8.6581)*

Figure J.2.2: *Response surfaces for the R sandwich wrinkling requirement. (Validation set errors: Max=3.3169, Mean=1.566, Rsqr=0.9983, Rmea=0.10169, APE=1.4554)*

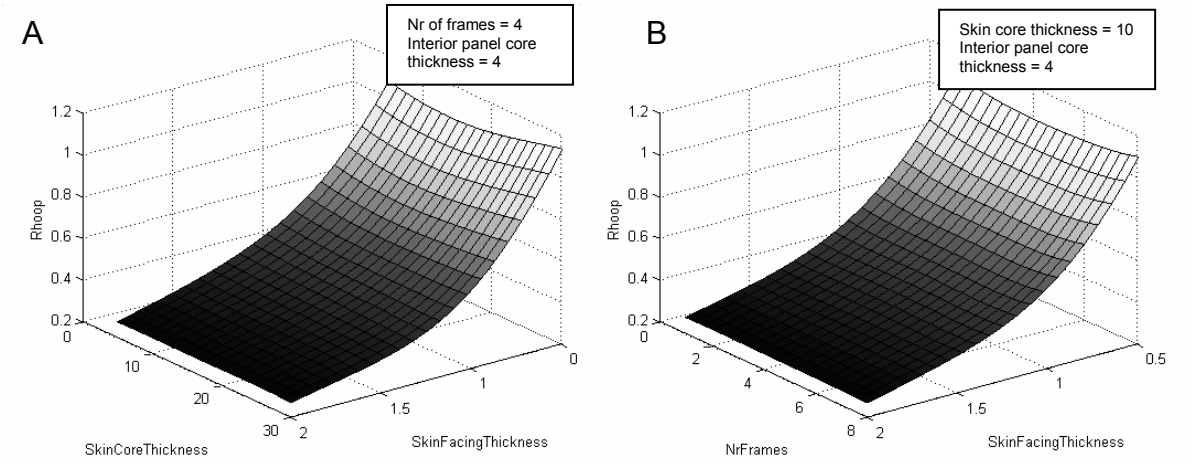

Figure J.2.3: *Response surfaces for the R hoop requirement. (Validation set errors: Max=4.1511, Mean=2.0855, Rsqr=0.99466, Rmea=0.2021, APE=2.4004).*

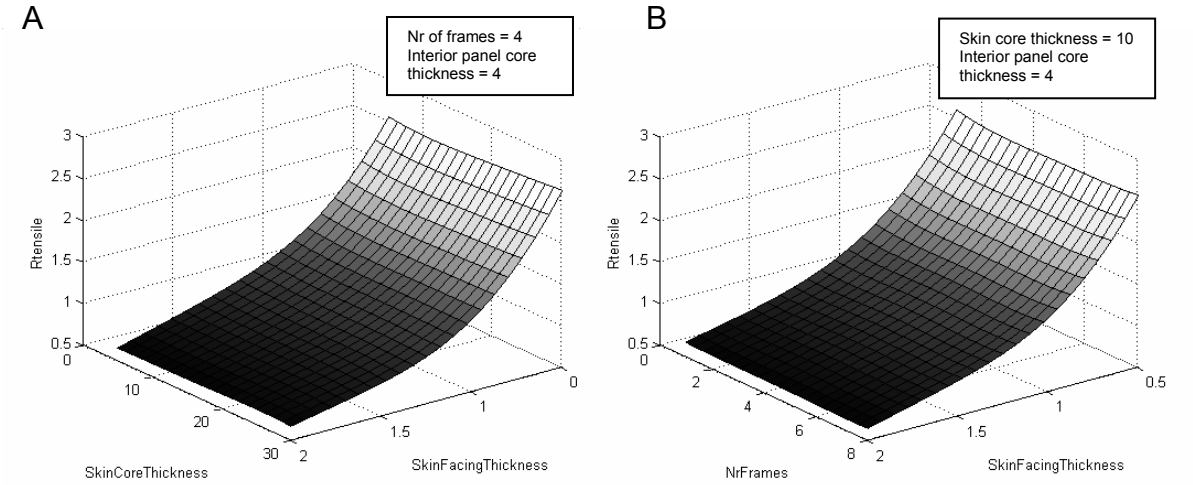

Figure J.2.4: *Response surfaces for the R sandwich tensile requirement. (Validation set errors: Max=3.6532, Mean=1.6551, Rsqr=0.99669, Rmea=0.16389, APE=1.6904).*

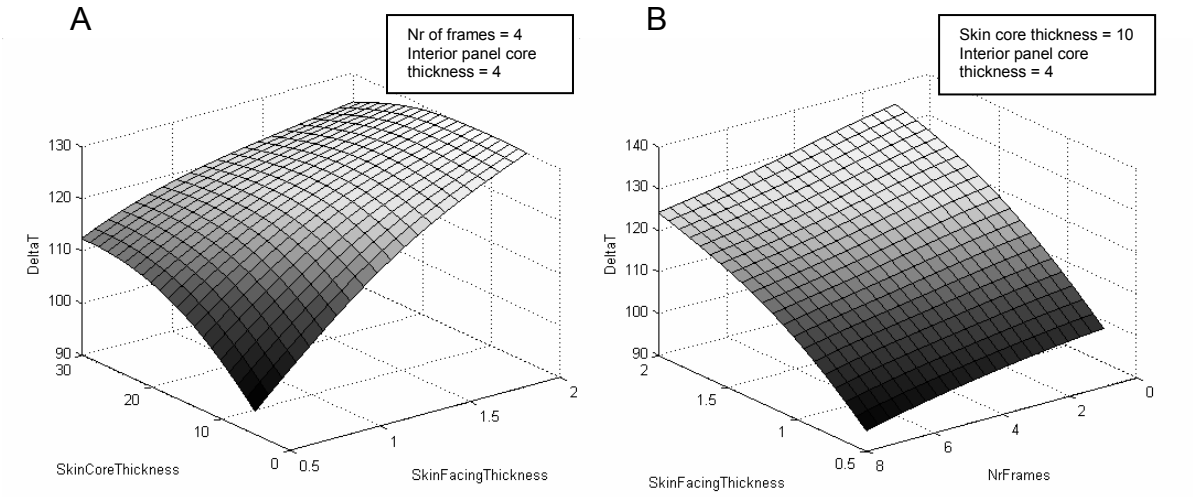

Figure J.2.5: *Response surfaces for the temperature difference requirement. (Validation set errors: Max=0.75553, Mean=0.3602, Rsqr=0.99752, Rmea=0.09404, APE=0.36338).*

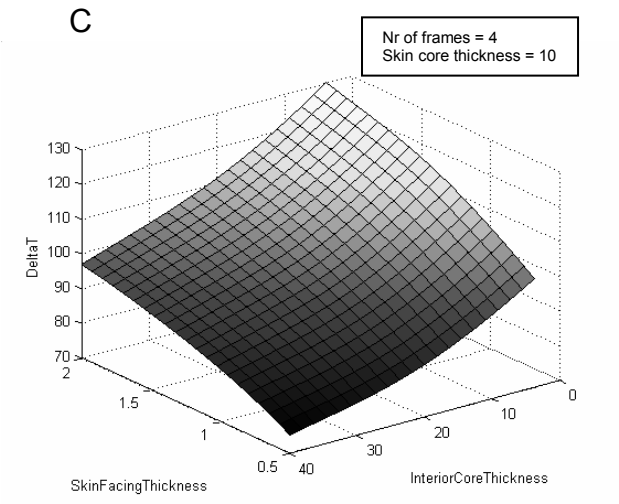

Figure J.2.5 continued: *Response surfaces for the temperature difference requirement. (Validation set errors: Max=0.75553, Mean=0.3602, Rsqr=0.99752, Rmea=0.09404, APE=0.36338).*

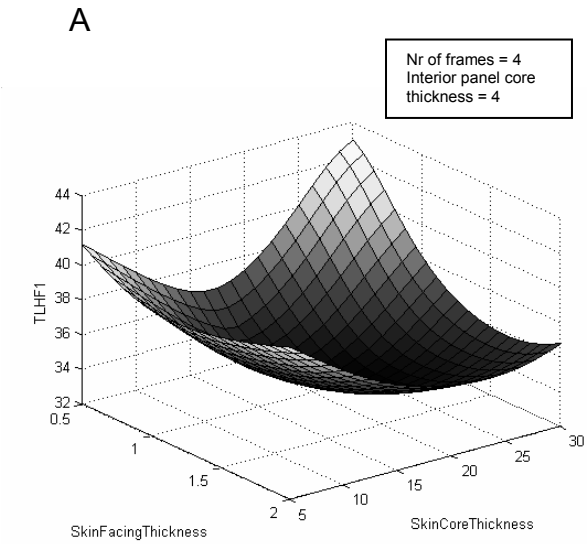

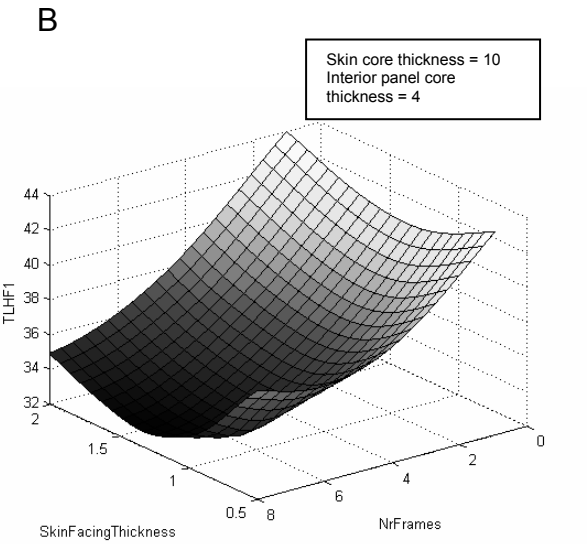

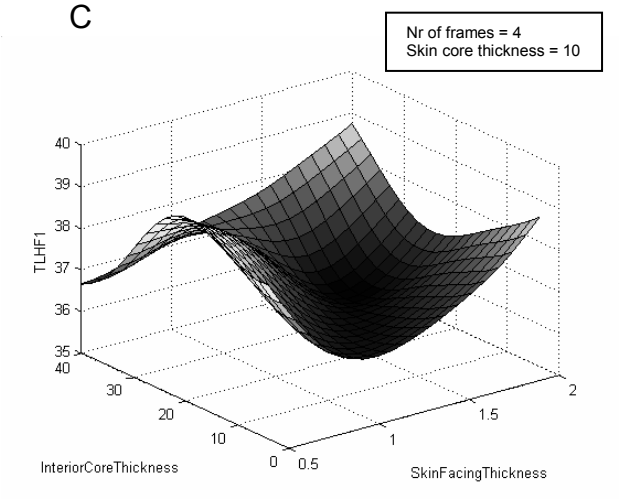

Figure J.2.6: *Response surfaces for the overall sound transmission loss requirement in the frequency range 1, [0-500Hz]. (Validation set errors: Max=6.7019, Mean=2.525, Rsqr=0.88012, Rmea=0.76349, APE=2.596).*

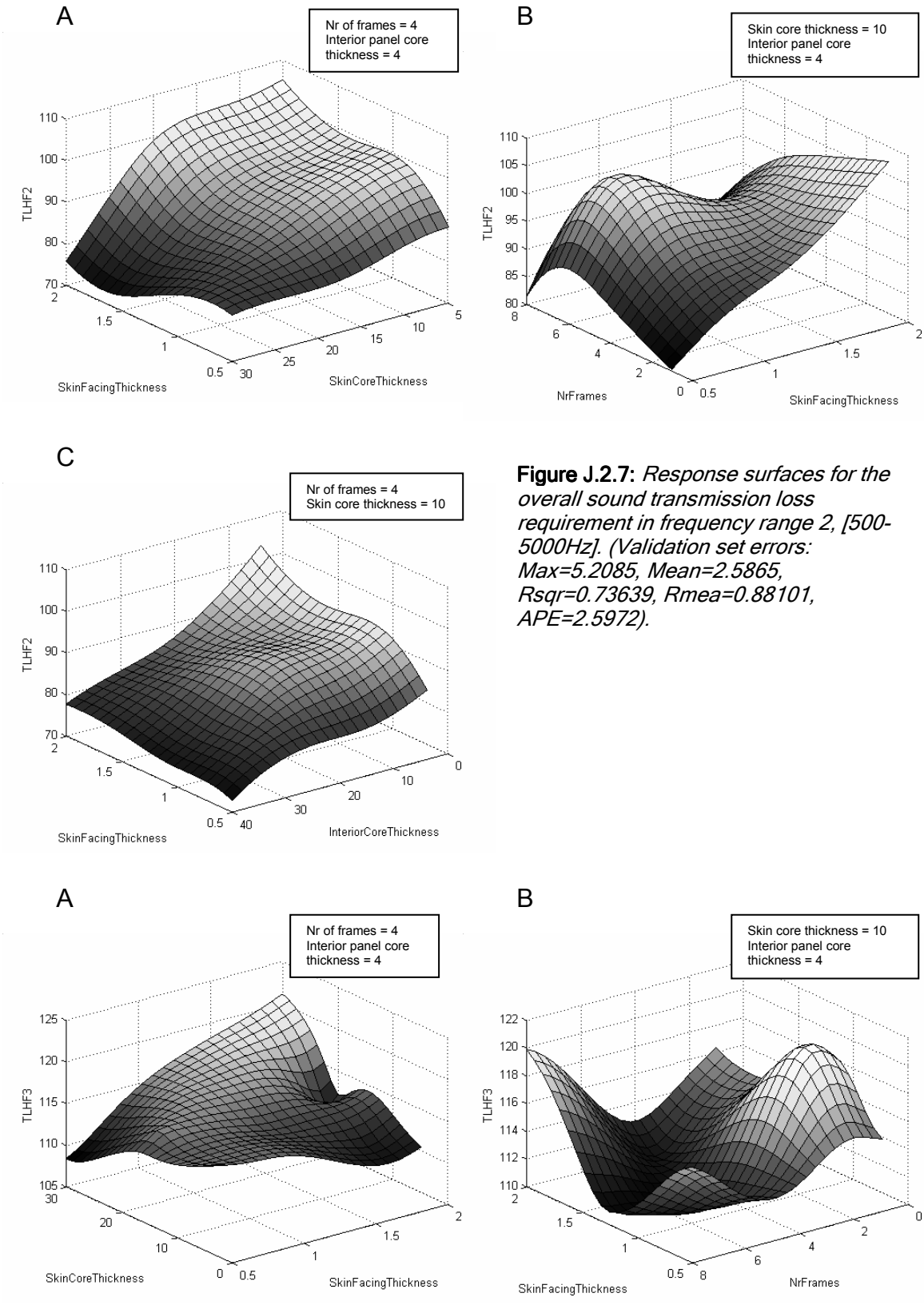

Figure J.2.7: *Response surfaces for the overall sound transmission loss requirement in frequency range 2, [500-5000Hz]. (Validation set errors: Max=5.2085, Mean=2.5865, Rsqr=0.73639, Rmea=0.88101, APE=2.5972).*

Figure J.2.8: *Response surfaces for the overall sound transmission loss requirement in frequency range 3, [5000-20000Hz]. (Validation set errors: Max=6.5654, Mean=3.6084, Rsqr=0.62293, Rmea=1.0033, APE=3.663).*

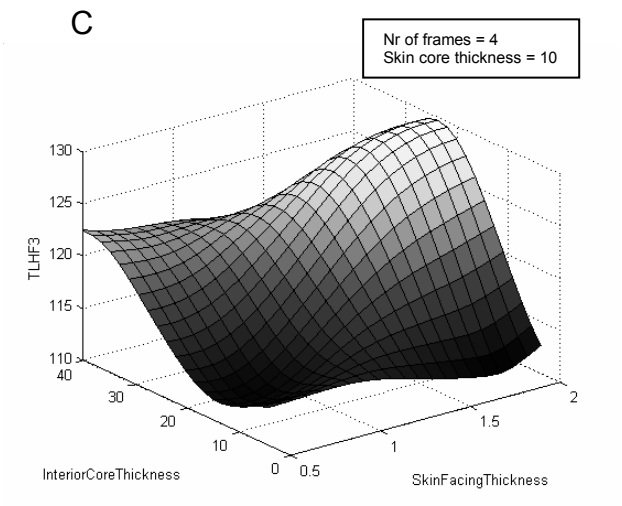

Figure J.2.8continued: *Response surfaces for the overall sound transmission loss requirement in frequency range 3, [5000-20000Hz]. (Validation set errors: Max=6.5654, Mean=3.6084, Rsqr=0.62293, Rmea=1.0033, APE=3.663).*

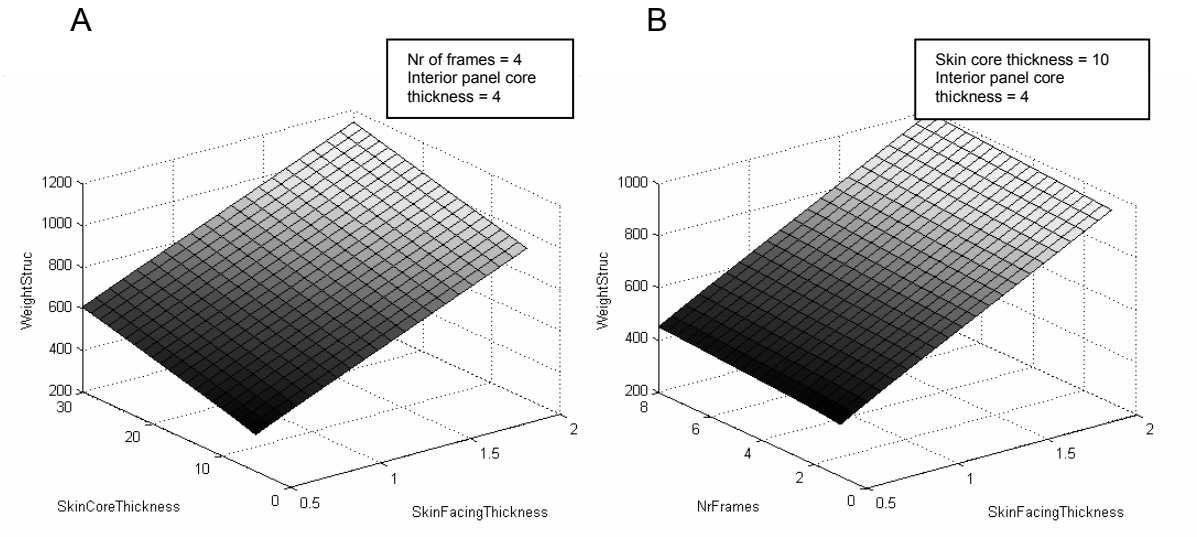

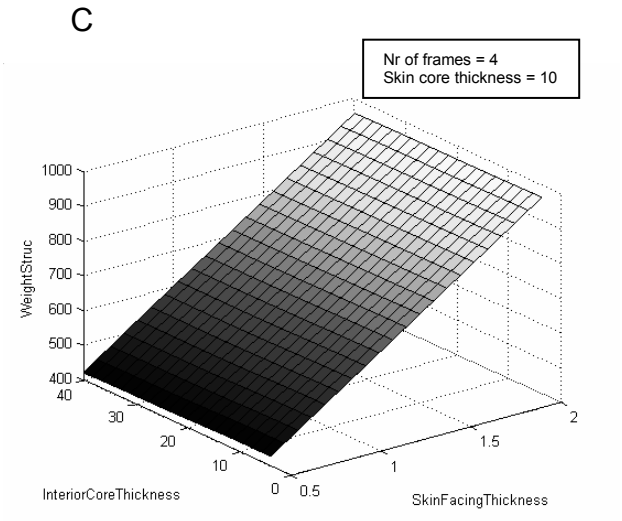

Figure J.2.9: *Response surfaces for the structural fuselage section weight objective function, which is independent of the interior panel core thickness because the insulation blanket and interior panels are not included. (Validation set errors: Max=0.97419, Mean=0.23465, Rsqr=0.99991, Rmea=0.021358, APE=0.18371).*

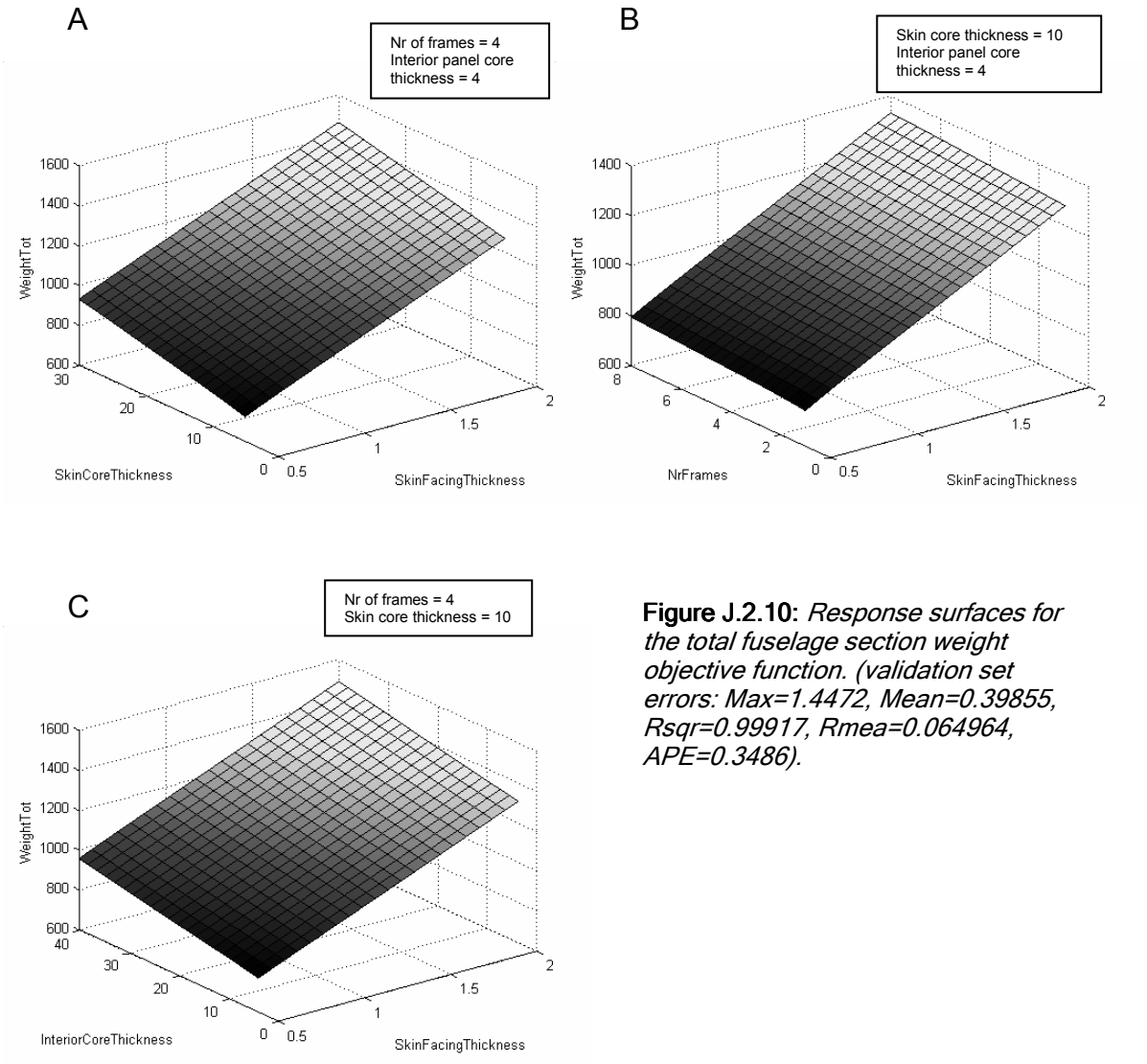

Figure J.2.10: *Response surfaces for the total fuselage section weight objective function. (validation set errors: Max=1.4472, Mean=0.39855, Rsqr=0.99917, Rmea=0.064964, APE=0.3486).*

J.3. Sequential programming optimisations

Table J.3.1: *Four optimised solutions for minimum structural fuselage weight determined with the sequential programming (SQP) option of the G_OPT program using four different program settings. Only continuous variables can be considered. Therefore the design variable Interior Core thickness, Number of frames and the number of stringers have to be fixed. Four fixed sets are considered with a constant interior panel core thickness of 4 mm.*

SQP	**Solution 1**	**Solution 2**	**Solution 3**	**Solution 4**
G_OPT program settings				
Tol value on design variable	1e-5	1e-5	1e-5	1e-5
Tol value on obj function	1e-5	1e-5	1e-5	1e-5
Max number of iterations	25	25	25	25
Fixed design variables				
SkinCoreThickness	12	12	12	13
NrFrames	1	2	3	1
InteriorCorethickness	4	4	4	4
Start design variables				
SkinFacingThickness	1.9	1.9	1.9	1.9
Design variables				
SkinFacingThickness	1.3593	1.3470	1.3613	1.3559
Final performances				
RsandBuckling	0.9825	0.9459	0.9376	0.8974
RsandWrinkling	0.1917	0.1909	0.1905	0.1915
Rhoop	0.4162	0.4167	0.4142	0.4176
RsandTensile	1.0000	1.0001	1.0004	1.0001
θ	126.88	125.45	124.21	127.09
TLHF1	41.36	39.19	37.25	41.04
TLHF2	94.13	93.03	93.31	94.25
TLHF3	116.20	116.57	115.28	116.11
Weighttot	1068.12	1070.75	1082.46	1074.75
Objective function				
Weightstruc	728.35	730.88	742.65	735.96

J.4. Multi Objective Optimisations for sandwich fuselage

The multi objective optimisations are performed with the Multi Objective Genetic Algorithm optimisation option of the G_OPT program developed by Lanzi [1]. This optimisation procedure determines a Pareto set of configurations for which two selected objectives are optimal. Table J.4.1 gives the Pareto set for minimum total fuselage section weight and maximum thermal insulation. Table J.4.2 gives the minimum total fuselage section weight with maximum sound transmission loss in the low frequency range and table J.4.3 and J.4.4 give the Pareto set for minimum total fuselage section weight and maximum sound transmission loss in the middle and high frequency range. The corresponding representations of the fuselage configurations given in tables J.4.1to J.4.4 are illustrated in figure 11.4A to 11.4D of chapter 11. Table J.4.5 gives the first 20 configurations of the Pareto set for minimum total fuselage section weight and maximum thermal and sound transmission loss in the low, middle and high frequency range.

Table J.4.1: *First 25 points of the Pareto set for minimum total fuselage section weight and maximum temperature difference between the inside and the outside surface of the fuselage wall (Delta T).*

	Design variables				Objectives		Constraints			
Pareto set nr	Skin facing thickness	Skin core thickness	Nr of frames	Interior panel core thickness	θ	Wtotal	Rsandwich buckling	Rwrinkling	Rhoop	Rsandwich tensile
1	1.3588	12	1	4	126.88	1067.94	0.9828	0.1917	0.4164	1.0004
2	1.3588	14	1	4	127.35	1083.62	0.8224	0.1906	0.4170	0.9958
3	1.3647	12	1	4	126.97	1070.02	0.9791	0.1909	0.4145	0.9960
4	1.3706	13	1	4	127.33	1079.95	0.8894	0.1895	0.4127	0.9891
5	1.3765	12	1	4	127.17	1074.18	0.9719	0.1893	0.4107	0.9874
6	1.3824	12	1	4	127.27	1076.26	0.9683	0.1885	0.4089	0.9831
7	1.4000	13	1	4	127.79	1090.36	0.8735	0.1855	0.4035	0.9679
8	1.4118	12	1	4	127.74	1086.68	0.9505	0.1847	0.3999	0.9624
9	1.4235	12	1	4	127.93	1090.85	0.9435	0.1832	0.3964	0.9545
10	1.4294	12	1	4	128.02	1092.93	0.9400	0.1824	0.3947	0.9505
11	1.4353	12	1	4	128.11	1095.02	0.9365	0.1817	0.3930	0.9466
12	1.4412	12	1	4	128.20	1097.11	0.9330	0.1810	0.3914	0.9428
13	1.4471	12	1	4	128.29	1099.19	0.9296	0.1803	0.3897	0.9390
14	1.4529	12	1	4	128.38	1101.28	0.9261	0.1796	0.3881	0.9352
15	1.4588	12	1	4	128.47	1103.36	0.9227	0.1789	0.3865	0.9314
16	1.4706	12	1	4	128.64	1107.54	0.9158	0.1775	0.3833	0.9240
17	1.4765	12	1	4	128.73	1109.63	0.9124	0.1768	0.3818	0.9204
18	1.4765	13	1	4	128.91	1117.48	0.8327	0.1761	0.3819	0.9175
19	1.4824	12	1	4	128.81	1111.72	0.9090	0.1761	0.3802	0.9168
20	1.4824	13	1	4	128.99	1119.56	0.8296	0.1754	0.3803	0.9138
21	1.4882	12	1	4	128.90	1113.80	0.9056	0.1754	0.3787	0.9132
22	1.5059	12	1	4	129.15	1120.07	0.8954	0.1735	0.3742	0.9026
23	1.5118	12	1	4	129.23	1122.16	0.8921	0.1728	0.3727	0.8991
24	1.5235	12	1	4	129.40	1126.34	0.8854	0.1715	0.3698	0.8923
25	1.5471	11	1	4	129.53	1126.82	0.9632	0.1698	0.3643	0.8824

Table J.4.2: *First 20 points of the Pareto set for minimum total fuselage section weight and maximum sound transmission loss in the low frequency range [0-500 Hz].*

	Design variables				Objectives		Constraints			
Pareto set nr	Skin facing thickness	Skin core thickness	Nr of frames	Interior panel core thickness	TLHF1	Wtotal	Rsandwich buckling	Rwrinkling	Rhoop	Rsandwich tensile
1	1.3294	19	1	29	47.56	1244.12	0.5920	0.1922	0.4289	1.0104
2	1.3294	19	1	32	48.22	1260.19	0.5826	0.1920	0.4283	1.0084
3	1.3353	12	1	27	43.57	1178.94	0.9277	0.1928	0.4148	1.0074
4	1.3353	13	1	30	44.49	1202.84	0.8182	0.1923	0.4150	1.0057
5	1.3353	19	1	30	47.79	1251.52	0.5893	0.1914	0.4268	1.0057
6	1.3353	20	1	33	48.15	1275.82	0.5534	0.1909	0.4276	1.0025
7	1.3412	12	1	28	43.72	1186.29	0.9156	0.1919	0.4125	1.0026
8	1.3412	12	1	30	44.01	1196.85	0.8979	0.1917	0.4114	1.0016
9	1.3412	13	1	28	44.00	1194.34	0.8334	0.1917	0.4143	1.0025
10	1.3412	13	1	29	44.23	1199.62	0.8249	0.1916	0.4138	1.0020
11	1.3412	14	1	30	44.90	1213.00	0.7552	0.1913	0.4153	1.0017
12	1.3412	15	1	28	44.87	1210.48	0.7205	0.1913	0.4183	1.0026
13	1.3412	16	1	29	45.84	1223.88	0.6767	0.1911	0.4199	1.0024
14	1.3412	16	1	30	46.14	1229.19	0.6718	0.1910	0.4196	1.0021
15	1.3412	16	1	31	46.32	1234.53	0.6665	0.1910	0.4192	1.0017
16	1.3412	17	1	30	46.76	1237.32	0.6416	0.1909	0.4215	1.0021
17	1.3412	17	1	31	46.96	1242.66	0.6373	0.1908	0.4213	1.0016
18	1.3471	12	1	25	42.90	1172.64	0.9426	0.1916	0.4122	1.0007
19	1.3471	12	1	26	43.18	1177.88	0.9328	0.1914	0.4117	0.9999
20	1.3471	12	1	29	43.82	1193.65	0.9044	0.1910	0.4102	0.9980

Table J.4.3: *First 20 points of the Pareto set for minimum total fuselage section weight and maximum sound transmission loss in the middle frequency range [500-5000 Hz].*

	Design variables				Objectives		Constraints			
Pareto set nr	Skin facing thickness	Skin core thickness	Nr of frames	Interior panel core thickness	TLHF2	Wtotal	Rsandwich buckling	Rwrinkling	Rhoop	Rsandwich tensile
1	1.3588	12	1	4	94.12	1067.94	0.9828	0.1918	0.4164	1.0004
2	1.3765	12	1	4	94.39	1074.18	0.9719	0.1893	0.4107	0.9874
3	1.3824	12	1	4	94.48	1076.26	0.9683	0.1885	0.4088	0.9831
4	1.3882	12	1	4	94.57	1078.35	0.9647	0.1877	0.4070	0.9789
5	1.3941	12	1	4	94.66	1080.43	0.9611	0.1870	0.4052	0.9747
6	1.3941	13	1	4	94.83	1088.28	0.8767	0.1863	0.4053	0.9721
7	1.4000	12	1	4	94.75	1082.51	0.9575	0.1862	0.4034	0.9706
8	1.4235	12	1	4	95.12	1090.85	0.9435	0.1832	0.3964	0.9545
9	1.4294	12	1	4	95.21	1092.93	0.9400	0.1824	0.3947	0.9505
10	1.4353	12	1	4	95.31	1095.02	0.9365	0.1817	0.3930	0.9466
11	1.4647	12	1	4	95.78	1105.45	0.9192	0.1782	0.3849	0.9277
12	1.4882	11	1	4	96.01	1105.92	1.0001	0.1762	0.3788	0.9165
13	1.4941	11	1	4	96.11	1108.01	0.9963	0.1755	0.3773	0.9129
14	1.4941	12	1	4	96.27	1115.89	0.9022	0.1748	0.3772	0.9096
15	1.5000	11	1	4	96.22	1110.10	0.9926	0.1749	0.3758	0.9094
16	1.5059	13	1	4	96.57	1127.92	0.8172	0.1728	0.3743	0.8996
17	1.5118	12	1	4	96.56	1122.16	0.8921	0.1728	0.3727	0.8991
18	1.5176	11	1	4	96.53	1116.37	0.9815	0.1729	0.3713	0.8991
19	1.5176	13	1	4	96.77	1132.10	0.8110	0.1715	0.3713	0.8927
20	1.5647	11	1	4	97.40	1133.09	0.9524	0.1680	0.3602	0.8726

Table J.4.4: *First 20 points of the Pareto set for minimum total fuselage section weight and maximum sound transmission loss in the high frequency range [5000-20.000 Hz].*

	Design variables				Objectives		Constraints			
Pareto set nr	Skin facing thickness	Skin core thickness	Nr of frames	Interior panel core thickness	TLHF3	Wtotal	Rsandwich buckling	Rwrinkling	Rhoop	Rsandwich tensile
1	1.3353	18	2	12	124.87	1155.51	0.6333	0.1905	0.4190	0.9995
2	1.3353	19	2	11	125.20	1158.34	0.5980	0.1905	0.4194	0.9998
3	1.3353	20	2	14	128.25	1182.04	0.5702	0.1907	0.4209	1.0010
4	1.3412	16	2	11	122.37	1136.36	0.7086	0.1900	0.4160	0.9963
5	1.3412	19	2	14	127.24	1176.06	0.6000	0.1898	0.4183	0.9960
6	1.3471	12	2	14	120.87	1122.18	0.9838	0.1912	0.4139	1.0009
7	1.3471	13	2	7	118.19	1094.11	0.8678	0.1904	0.4148	0.9979
8	1.3471	15	2	8	119.71	1114.97	0.7469	0.1895	0.4141	0.9935
9	1.3471	15	2	10	121.00	1125.31	0.7521	0.1895	0.4140	0.9936
10	1.3471	15	2	12	122.13	1135.66	0.7574	0.1896	0.4140	0.9936
11	1.3471	16	1	35	136.20	1258.09	0.6396	0.1899	0.4159	0.9951
12	1.3471	16	3	18	128.47	1181.64	0.7271	0.1918	0.4132	1.0027
13	1.3471	17	1	36	137.59	1271.66	0.6016	0.1896	0.4177	0.9936
14	1.3471	18	2	10	123.62	1149.24	0.6258	0.1889	0.4150	0.9912
15	1.3471	18	2	11	124.34	1154.45	0.6275	0.1889	0.4152	0.9913
16	1.3471	18	3	17	129.92	1192.51	0.6375	0.1916	0.4145	1.0024
17	1.3471	20	2	14	128.41	1186.19	0.5662	0.1892	0.4173	0.9930
18	1.3471	21	2	15	130.06	1199.46	0.5373	0.1894	0.4182	0.9945
19	1.3530	12	1	6	116.77	1076.56	0.9887	0.1925	0.4157	1.0046
20	1.3530	13	2	6	117.63	1091.03	0.8623	0.1896	0.4133	0.9935

Table J.4.5: *First 20 points of the Pareto set for minimum total fuselage section weight and maximum Delta T, TLHF1, TLHF2 and TLHF3.*

	Design variables				Objectives					Constraints			
Pareto set nr	Skin facing thickness	Skin core thickness	Nr of frames	Interior panel core thickness	θ	TLHF1	TLHF2	TLHF3	Wtotal	Rsandwich buckling	Rwrinkling	Rhoop	Rsandwich tensile
1	1.3059	20	1	31	97.41	48.80	77.97	134.44	1254.71	0.5636	0.1951	0.4379	1.0257
2	1.3235	15	2	26	100.24	42.54	81.12	127.72	1199.86	0.7777	0.1933	0.4226	1.0125
3	1.3235	19	2	20	105.69	39.90	83.33	129.68	1201.03	0.6170	0.1924	0.4259	1.0097
4	1.3235	21	2	16	109.93	38.27	85.28	130.35	1196.35	0.5458	0.1924	0.4258	1.0108
5	1.3294	14	1	25	101.97	43.27	77.18	123.43	1182.46	0.7957	0.1932	0.4213	1.0120
6	1.3294	16	2	12	114.85	37.56	85.81	122.81	1137.41	0.7156	0.1915	0.4197	1.0045
7	1.3294,	16	2	18	107.66	38.53	83.04	124.85	1168.58	0.7292	0.1916	0.4208	1.0044
8	1.3294	17	2	5	124.57	37.43	90.40	118.96	1108.95	0.6553	0.1913	0.4205	1.0037
9	1.3294	18	2	16	110.05	37.96	84.75	126.80	1174.27	0.6423	0.1913	0.4218	1.0038
10	1.3294	20	2	14	112.42	37.55	85.78	128.16	1179.96	0.5722	0.1914	0.4227	1.0051
11	1.3294	20	2	33	95.49	47.79	76.30	135.03	1278.91	0.6170	0.1924	0.4248	1.0080
12	1.3294	21	2	15	111.16	37.92	85.57	129.80	1193.23	0.5432	0.1916	0.4236	1.0065
13	1.3353	12	2	10	116.91	38.93	85.80	119.36	1097.53	0.9693	0.1927	0.4183	1.0097
14	1.3353	13	2	31	96.78	42.61	81.23	128.01	1214.20	0.8564	0.1922	0.4156	1.0066
15	1.3353	14	2	24	101.85	40.88	81.30	125.63	1185.66	0.8306	0.1916	0.4179	1.0031
16	1.3353	14	2	30	97.52	43.16	81.05	129.16	1216.89	0.8060	0.1921	0.4169	1.0061
17	1.3353	15	1	23	103.79	42.11	77.50	121.62	1182.17	0.7507	0.1923	0.4219	1.0083
18	1.3353	15	2	12	114.82	37.82	85.49	122.00	1131.51	0.7625	0.1911	0.4176	1.0018
19	1.3353	15	2	23	102.79	40.61	81.42	125.95	1188.51	0.7786	0.1914	0.4189	1.0022
20	1.3353	16	2	7	121.75	37.57	89.24	119.69	1113.54	0.7013	0.1907	0.4179	1.0002

J.5. Reference

[1] Lanzi, L.,Optimisation of composit stiffened panels under post buckling constraints, PhD thesis, Polytecnico di Milano, 2004

Samenvatting

Het ontwerpen van een vliegtuigromp is een ingewikkeld proces waarbij vele ontwerp eisen komen kijken zoals stijfheid & sterkte, vermoeiing, schade tolerantie, brandbestendigheid en thermische & acoustische isolatie. Ook zaken als inspectiemogelijkheden, onderhoud, produceerbaarheid en repareermogelijkheden spelen een rol. Het is moeilijk om al deze aspecten gelijk vanaf het begin van het ontwerp proces mee te nemen.

In dit onderzoek is geprobeerd om een antwoord te vinden op de vraag of een multidisciplinaire ontwerpmethode kan leiden tot een (lichter) ontwerp vergeleken met de normaal toegepaste stapsgewijze aanpak.

Om een antwoord te vinden op deze vraag is een geautomatiseerde multidisciplinaire ontwerpmethode ontwikkeld voor vliegtuigrompen. Vanwege het feit dat er zoveel aspecten komen kijken bij een ontwerp van een vliegtuigromp, zijn in dit onderzoek alleen de aspecten stijfheid & sterkte en thermische & acoustische isolatie meegenomen. In de toekomst kan deze ontwerpmethode gemakkelijk worden uitgebreid met meer ontwerpaspecten.

De multidisciplinaire ontwerpmethode is vormgegeven als een 'Design and Engineering Engine' (DEE). De DEE is een ontwerpgereedschap dat bestaat uit verschillende computerprogrammas die aan elkaar zijn gekoppeld. Het hart van de DEE bestaat uit de 'Multi Model Generator' (MMG) wat in feite een parametrische beschrijving is van de vliegtuigromp geometrie waarvan verschillende modellen voor de analyse modules worden afgeleid. De MMG bestaat uit standaard bouwstenen waaruit elk type vliegtuigromp kan worden gegenereerd. De invoer voor de MMG is een invoerfile waarin alle parameters zijn gedefinieerd die de vluigtuigromp configuratie bepalen. De uitvoer van de MMG zijn de verschillende modellen die nodig zijn voor de betreffende analyse modules. De huidige DEE heeft 4 analyse modules;

1.) De constructie module is in staat om twee verschillende constructie concepten door te rekenen; de verstijfde huid constructie en de sandwich constructie. De spanningen in de constructiedelen worden berekend met het FEM pakket ABAQUS. Deze spanningen worden dan geevalueerd met sterkte en knik criteria welke afhankelijk zijn van het constructie concept..
2.) De acoustische isolatie module bestaat uit drie delen. Het eerste deel is gebasseerd op literatuur formules die vertaald zijn in een MATLAB script. De literatuur formules vertegenwoordigen de isolatie concepten die kunnen voorkomen in de wand van een vliegtuigromp. De isolatie concepten die worden beschouwd zijn de massa vergelijking, invloed van verstijvers en spanten, cylinder resonantie effecten, het dubbele wand principe, isolatie dekens en visco elastische damping lagen. Het tweede deel bestaat uit een FEM analyse van de eigenfrequenties en een FEM analyse om het frequentie afhankelijke drukverschil over de vliegtuigrompwand te bepalen. Omdat dit deel vrij veel computertijd in beslag neemt wordt dit deel alleen toegepast voor het geconvergeerde optimale

ontwerp, terwijl de literatuur formules worden gebruikt tijdens de vele configuratie doorrekenstappen. Het derde deel bestaat uit een aktief geluid controle systeem dat gebruik maakt van piezoelektrische actuatoren. Dit deel is ontwikkeld in samenwerking met TNO TPD binnen het "Smart Panel' project. Helaas is dit deel niet geheel operationeel omdat het gebruik maakt van regel-algoritmes ontwikkeld door TNO TPD die niet beschikbaar zijn in de DEE vanwege eigendoms rechten.

3.) De thermische isolatie module voert een tijdsafhankelijke warmte FEM analyse uit op de wand van de vliegtuigromp. Het binnenoppervlak wordt verwarmd met een constante warmte stroom. Na een bepaalde periode bereikt de FEM oplossing een evenwicht in het temperatuurveschil tussen de binnen en buitenkant van de wand. De grootte van dit temperatuurverschil is als maat genomen voor de thermische isolatie van de vliegtuigromp.

4.) De gewichtsmodule gebruikt de geometrische dimensies en materiaal eigenschappen om het gewicht van elk onderdeel van de wand van de vliegtuigromp te bepalen en berekend daarmee het totaal gewicht.

Een genetisch algoritme is gebruikt voor de optimalisatie van de vliegtuigromp configuratie. Als eerste wordt er een 'Design of Experiments' gedaan voor het bepalen van een populatie met oplossingen, voor een groep combinaties van de te optimaliseren variabelen. Van deze oplossingen worden responsieoppervlakken bepaald die weer worden gebruikt in de genetische optimalisatie routines. Validatie berekeningen worden uitgevoerd om het gevonden optimum te controleren. Wanneer nodig, zal een tweede optimalisatie stap worden uitgevoerd waarbij de optimalisatie variabelen worden gekozen in de buurt van het gevonden optimum uit de eerste optimalisatie stap.

Uiteindelijk zijn twee vliegtuigrompen doorgerekend met de DEE; een verstijfde huid vliegtuigromp en een sandwich romp. Beide concepten zijn blootgesteld aan dezelfde belastingen en randvoorwaarden. Voor de gegeven belastingen en randvoorwaarden laat de DEE zien dat de sandwich rompontwerp iets minder zwaar is dan het verstijfde rompontwerp. Wanneer minimum gewicht in ogenschouw wordt genomen als ontwerpdoel volgt uit onderzoek met de DEE dat het multidisciplinaire rompontwerp nagenoeg gelijk is aan de stapsgewijze ontworpen vliegtuig romp.

Door het gebruik van koolstof versterkte composieten in plaats van aluminium blijkt dat een aanzienlijke gewichtbesparing mogelijk is voor de verstijfde vliegtuigromp constructie.

Om de literatuur formules te valideren, die betrekking hebben op de invloed van frames en verstijvers op de geluid transmissie, is een aantal experimenten uitgevoerd. Vier experimenten zijn uitgevoerd om de het geluidsdrukverschil over de cylinderwand te bepalen van een onverstijfde cylinder, een cylinder met 6 verstijvers, een cylinder met 12 verstijvers en een cylinder met 12 verstijvers en 2 frames. Uiteindelijk kan worden geconcludeerd dat de literatuur formules alleen kunnen worden gebruikt boven de ringfrequentie. Voor vliegtuigrompen met een radius van ongeveer 2 m, ligt de ring frequentie op +/- 400 Hz. Voor een nauwkeurige analyse moet uitgebreider onderzoek worden gedaan. Voor het aantonen van het multidisciplinaire optimalisatie principe voldoen de literatuur formules.

In dit onderzoek is aangetoond dat het DEE ontwerp principe goed werkt. Het is een flexibel ontwerpgereedschap dat gemakkelijk kan worden uitgebreid met nieuwe analyse modules. In toekomstig onderzoek zouden de analyse modules kunnen worden vervangen met meer geavanceerde en meer accurate modules.

Uiteindelijk heeft de multidisciplinaire ontwerp methode voor de in dit onderzoek geanalyseerde voorbeeldrompen niet geleid tot een spectaculaire gewichtsbesparing vergeleken met de normaal toegepaste stapsgewijze ontwerpmethode. De reden hiervoor ligt in het feit dat er voor de gekozen ontwerp variabelen, weinig correlatie bestaat tussen de stijfheid & sterkte en de thermische & acoustische insolatie. Wellicht kan er door het inbrengen van andere ontwerpeisen zoals schadebestendigheid en vermoeing in de DEE en het kiezen van andere ontwerpvariabelen meer voordeel worden gehaald uit de multidisciplinaire ontwerpmethode.

About the author

Lars Adriaan Krakers
Born 25th of January 1972 in Hengelo ov, The Netherlands

1984-1990	VWO, Lyceum De Grundel, Hengelo ov.
1990-1999	Aerospace Engineering at the Delft University of Technology. Master project at the chair of Production Technology concerning the acoustical and structural efficiency of a composite fuselage with an integrated elastomer layer, in the context of the cost reduction concept'
1999-2009	PhD research at Delft University of Technology During the PhD participated in two projects: – European research project: MOB 'Multidisciplinary design and Optimization of a Blended wing body'. (Contract number G4RD 1999-0172) – 'Smart Panel' project initiated by TNO TPD about active noise control with piezo electric actuators.
2004-2006	NIMR post doctoral research on the DuPeam project, 'Ductile Piezoelectric actuator materials', which was performed at the TU Delft
2006-current	Hydraulic engineer at Flowserve pump division, Hengelo ov

List of publications

Krakers, L.A., Tooren, M.J.L. van, Beukers, A., Bergsma, O.K., Multidisciplinary fuselage design: integration of mechanics & acoustics, SAMPE conference, Paris, France, 2000.

Krakers, L.A., Tooren, M.J.L. van, Beukers, A design engine to evaluate sound damping of flat panels in the low frequency range, ECCM conference, Brugge, Belgium, 2002.

Krakers, L.A., M.J.L. van Tooren, M.J.L. van, Beukers, A., La Rocca, G., Lisandrin, P., A design & engineering engine to investigate acoustics in preliminary fuselage design, 9th AIAA/CEAS conference, Hilton Head Island USA, 2003

Krakers, L.A., Tooren, M.J.L. van, Beukers, Berkhof, A.P., Goeje M.P. de, Active noise control in fuselage design, Acoustics conference, Cadiz, Spain, 2003.

Krakers, L.A., Tooren, M.J.L., van, Zaal, K., Vermeeren, C., Integration of acoustics and mechanics in a stiffened shell fuselage, part III, Applied composite materials, vol 12, nr 1, p 21-35, Springer, 2005.

Tooren, M.J.L., Krakers, L.A., Beukers, A., Integration of acoustics and mechanics in a sandwich fuselage, part IV, Applied composite materials, vol 12, nr 1, p 37-51, Springer, 2005.

Beukers, A., Tooren, M.J.L., Krakers, L.A., Application of a viscoelastic layer, part V, Applied composite materials, vol 12, nr 1, p 53-57, Springer, 2005.

Tooren, M.J.L. van , Krakers, L.A., A generalised stress singularity approach for material failure prediction and its application to adhesive strength prediction, Journal of adhesion science and technology, 2006.

Tooren, M.J.L van, Krakers, L.A., Multidisciplinary fuselage design, Proceedings AIAA Aerospace Sciences Meeting and Exhibit, p 1-11, 2007, Reno, Nevada, USA

Colour section

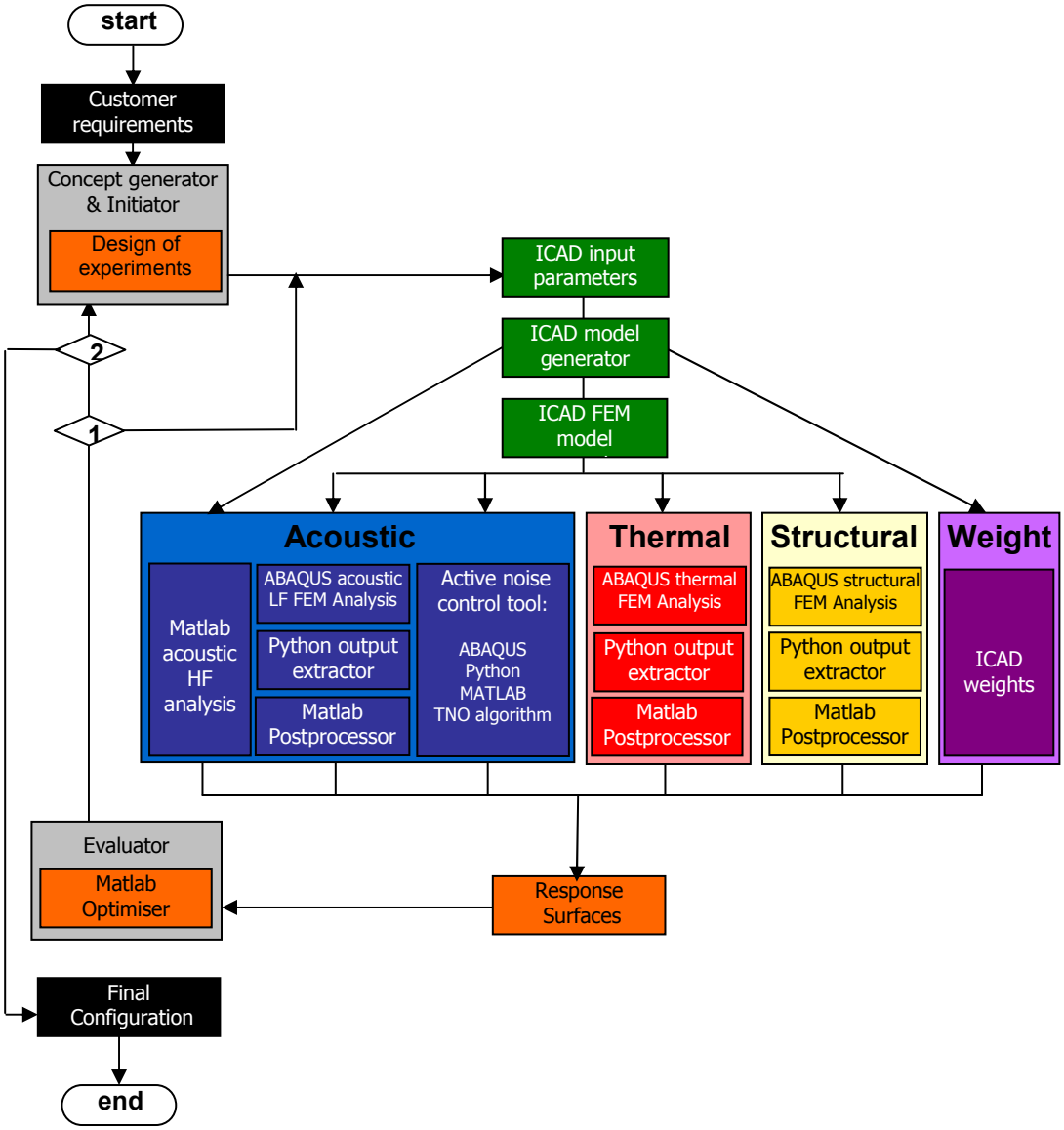

Figure 6.2: *Schematic overview of the DEE used for the design of pressurised fuselage taking into account the structural and the thermal & acoustical insulation aspects.*

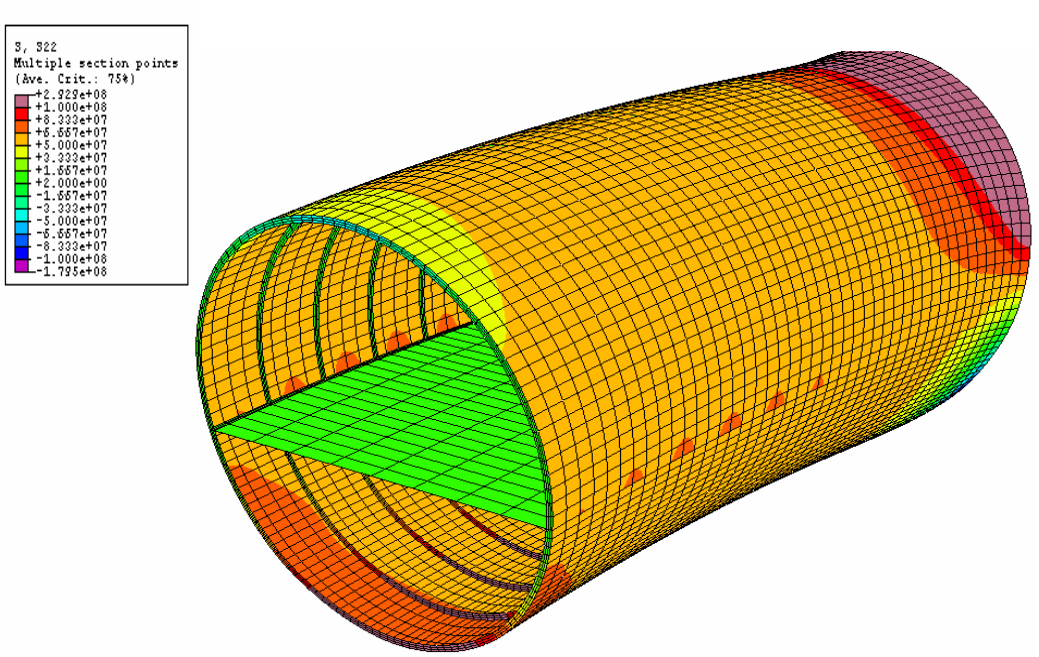

Figure 6.22: *Example of the stress distribution of a stringer stiffened fuselage loaded with an internal pressure, a bending moment and a shear load.*

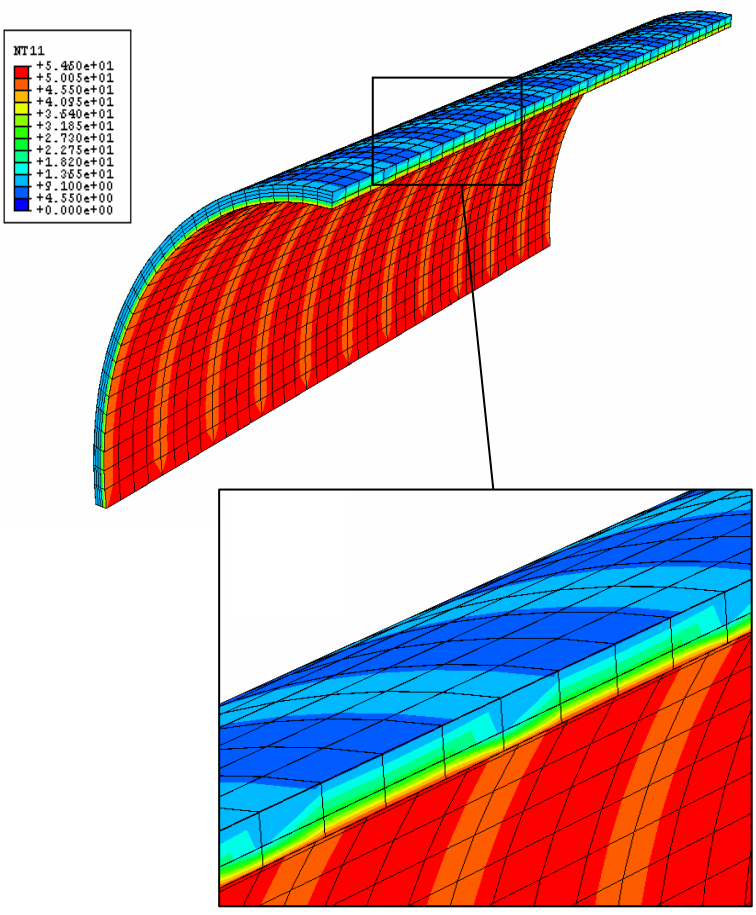

Figure 6.26: *Illustration of FEM results of the thermal insulation module corresponding to the results in figure 6.25.*

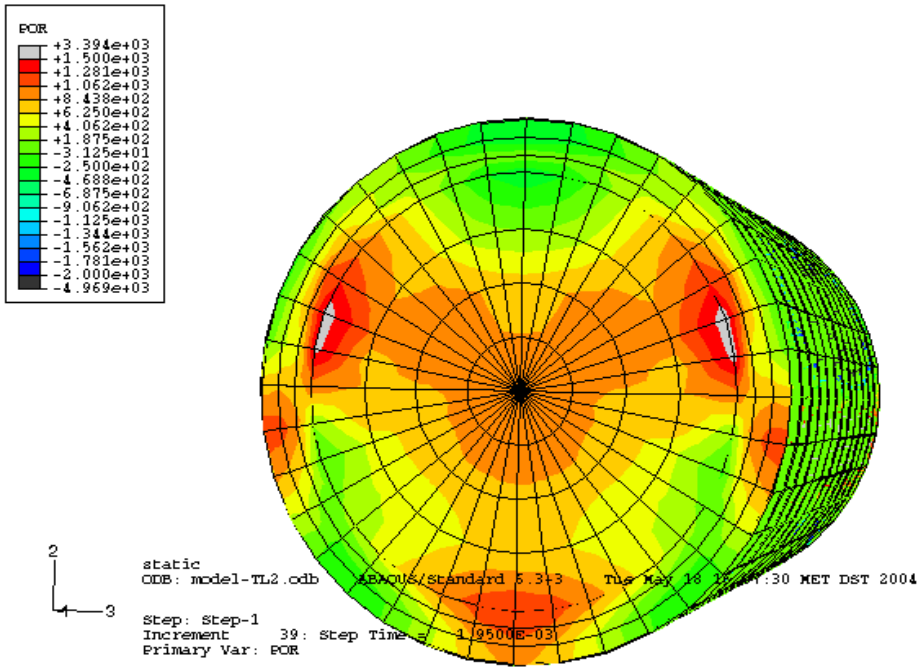

Figure 6.27: *Resultant pressure distribution at a time step of the acoustical FEM analysis in the low frequency range.*

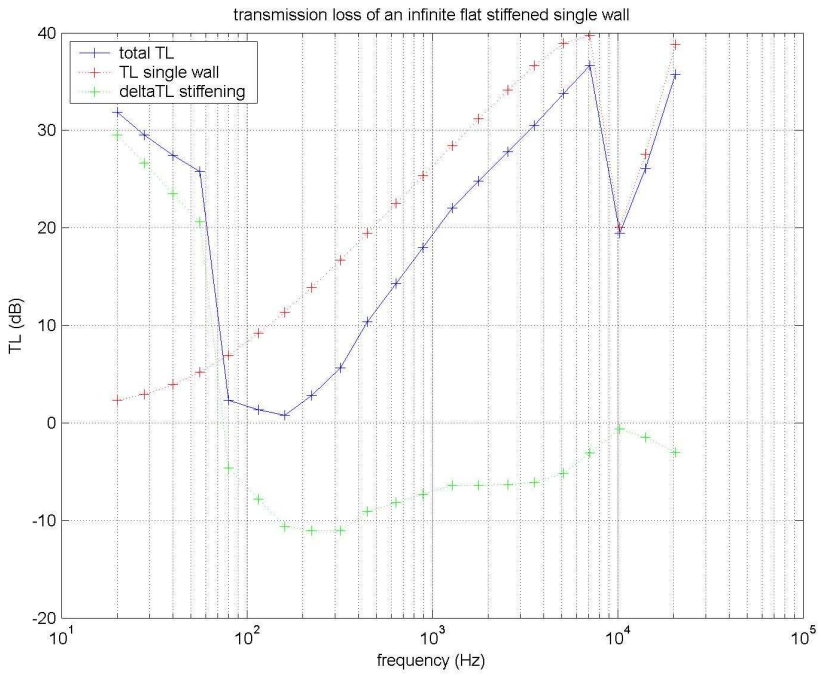

Figure 6.29: *Illustration of the TL determined with literature formulas*

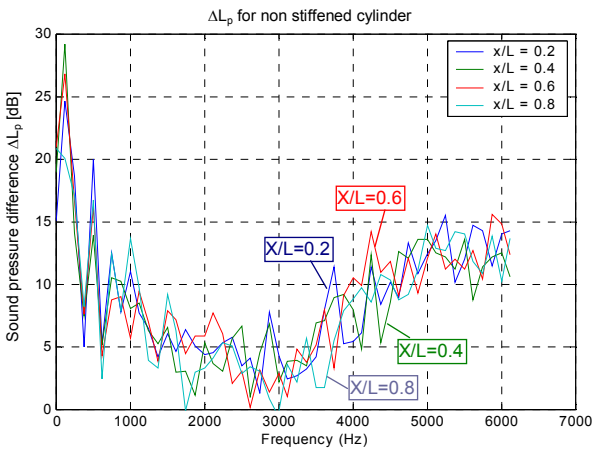

Figure 8.15: *Sound pressure difference for the inside microphone at r/R = 0.87, φ_m = 0 and variable x/L_{cil} position.*

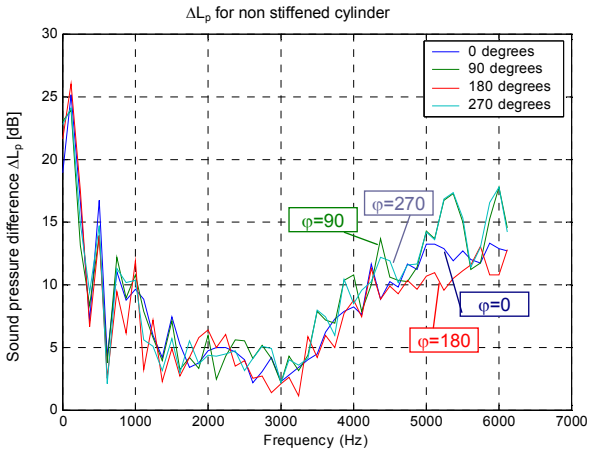

Figure 8.16: *Sound pressure difference for the inside microphone at r/R = 0.87, average x/L_{cil} and variable φ_m position.*

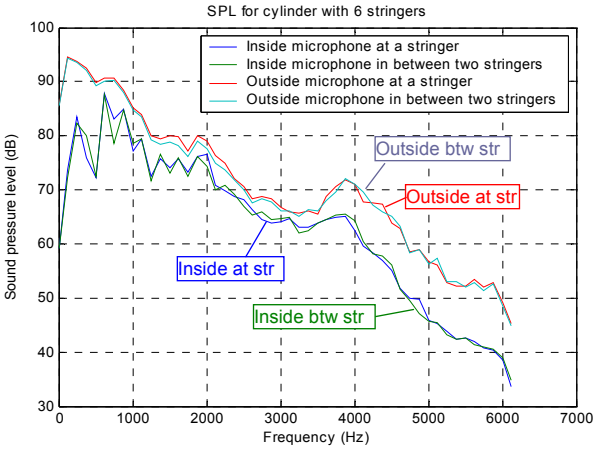

Figure 8.22: *Sound pressure levels for the inside and outside microphone at and in between stringers at r/R = 0.87, φ_m = 0 and averaged x/L_{cil} position.*

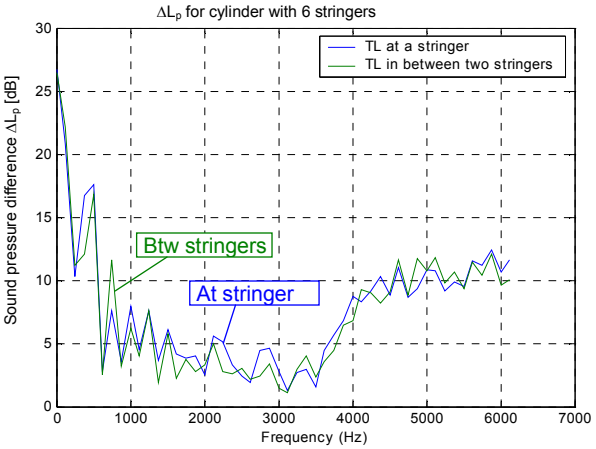

Figure 8.23: *Sound pressure difference at and in between stringers at r/R = 0.87, φ_m = 0 and averaged x/L_{cil} position.*

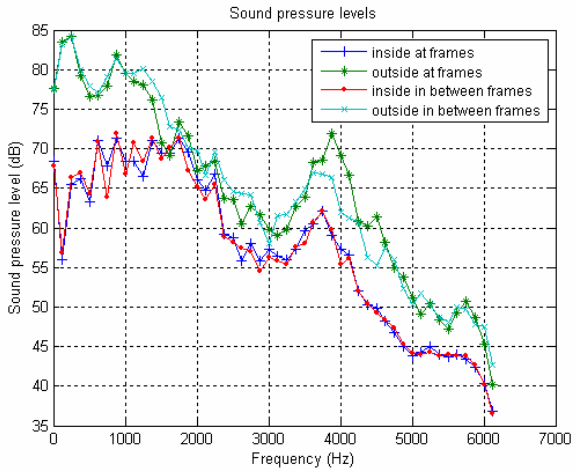

Figure 8.30: *Average sound pressure levels at and in between frame positions. (Averaged over x/L_{cil} = 0.33 and 0.67, at and in between stringers at r/R = 0.87).*

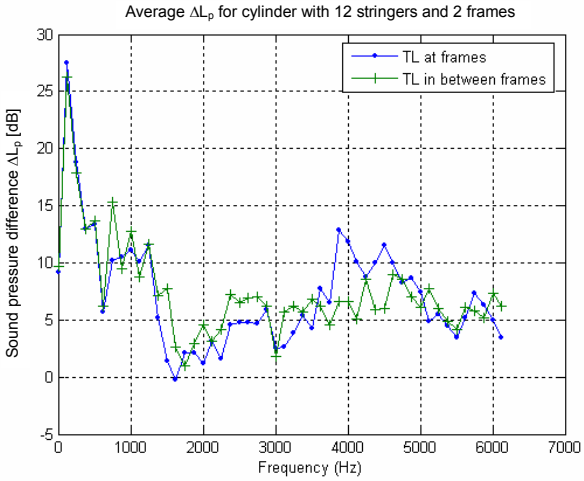

Figure 8.31: *Average sound pressure difference at and in between frame positions (Averaged over x/L_{cil} =0.33 and 0.67 at and in between stringers at r/R =0.87).*

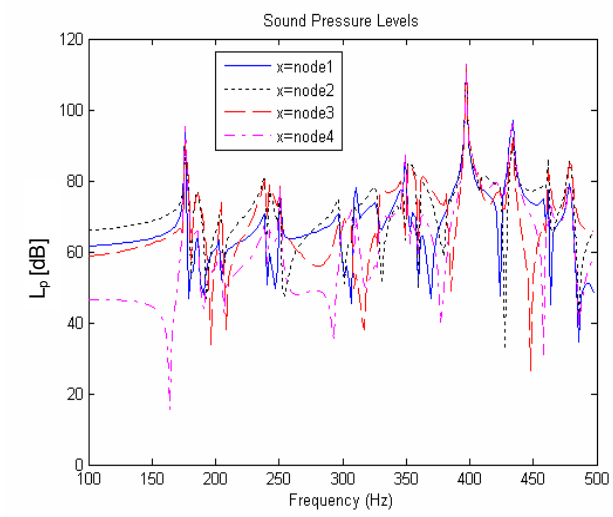

Figure 9.2: *Numerically determined sound pressure levels at node 1, 2, 3 and 4 for the non-stiffened cylinder exited by a concentrated point load. The excitation and recording nodes are defined in figure 9.1.*

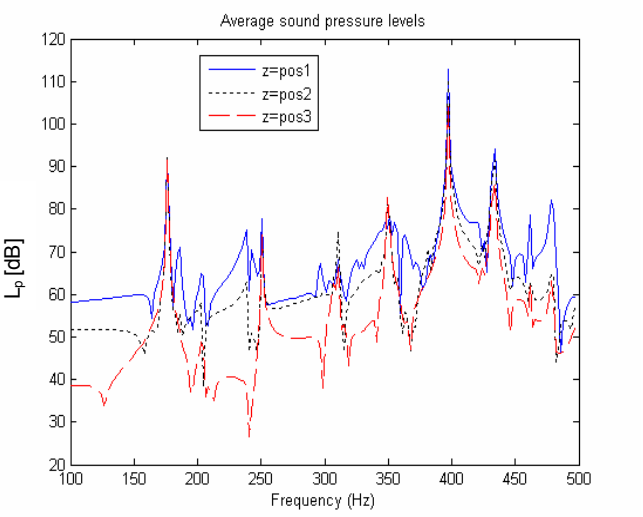

Figure 9.3: *The averaged sound pressure levels at three z-positions for the non-stiffened cylinder exited by a concentrated point load. The L_p are averaged over the x-positions. The excitation and recording nodes are defined in figure 9.1.*

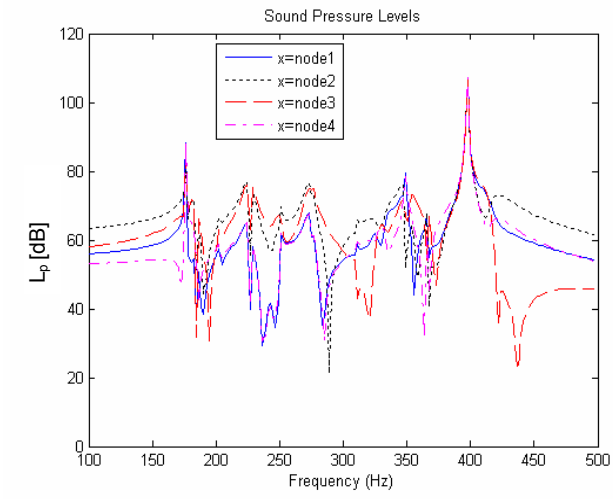

Figure 9.4: *Numerically determined sound pressure levels at node 1, 2, 3 and 4 for the cylinder with 6 stringers exited by a concentrated point load. The excitation and recording nodes are defined in figure 9.1.*

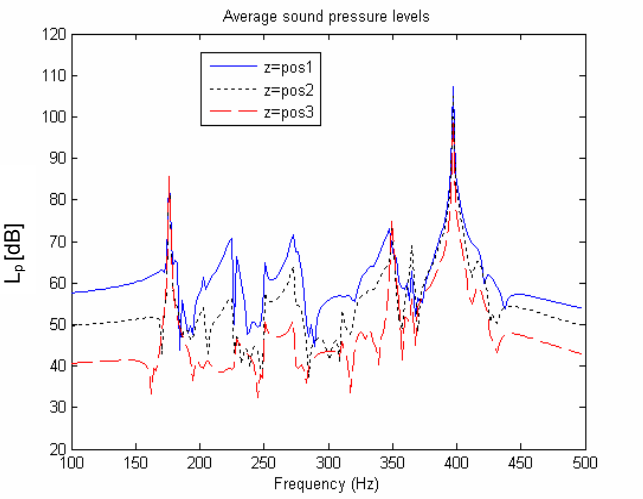

Figure 9.5: *The averaged sound pressure levels at three z-positions for the cylinder with 6 stringers exited by a concentrated point load. The SPL are averaged over the x-positions. The excitation and recording nodes are defined in figure 9.1.*

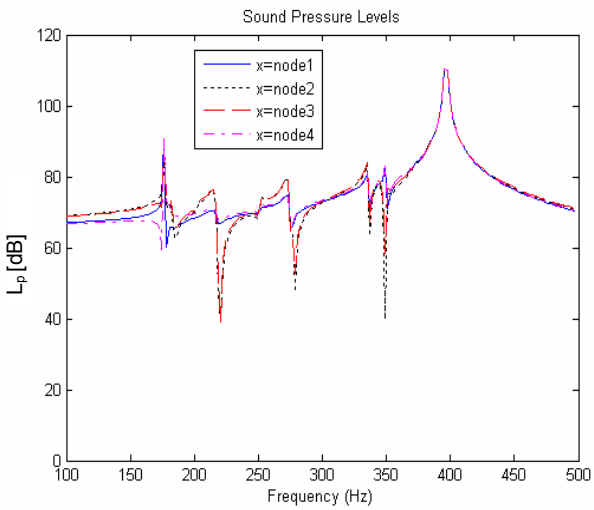

Figure 9.6: *Numerically determined sound pressure levels at node 1, 2, 3 and 4 for the cylinder with 12 stringers exited by a concentrated point load of 1N at node 108. The excitation and recording nodes are defined in figure 9.1.*

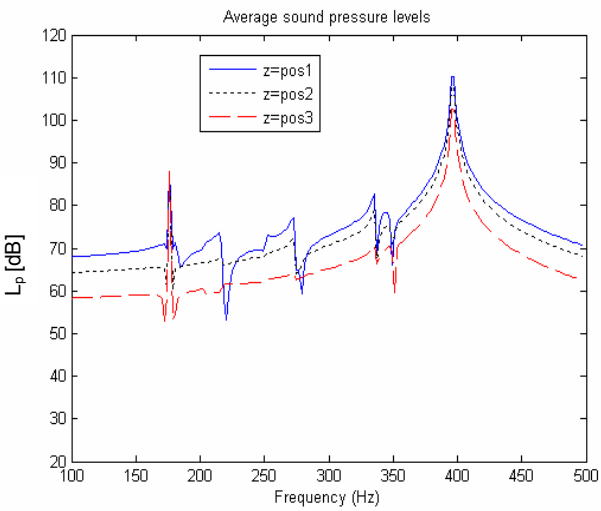

Figure 9.7: *The averaged sound pressure levels at three z-positions for the cylinder with 12 stringers exited by a concentrated point load of 1N at node 108. The L_p are averaged over the x-positions. The x- and z-positions of the recording nodes and the excitation node are defined in figure 9.1.*

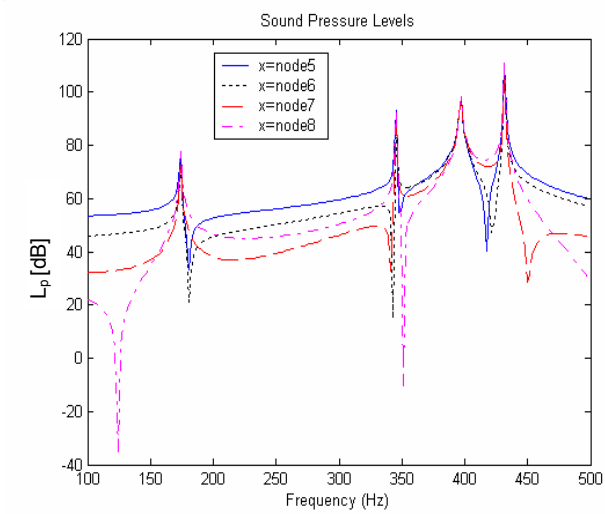

Figure 9.8: *Numerically determined sound pressure levels at node 5, 6, 7 and 8 for the cylinder with 12 stringers and 2 frames exited by a concentrated point load of 1N at node 108. The excitation and recording nodes are defined in figure 9.1.*

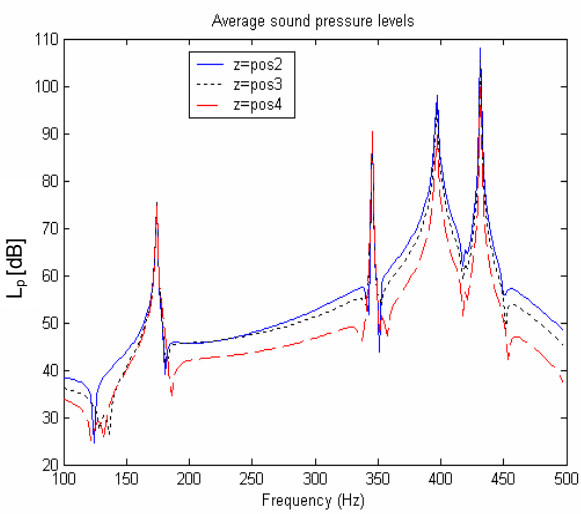

Figure 9.9: *The averaged sound pressure levels at three z-positions for the cylinder with 12 stringers and 2 frames exited by a concentrated point load of 1N at node 108. The L_p are averaged over the x-positions. The x- and z-positions of the recording nodes and the excitation node are defined in figure 9.1.*

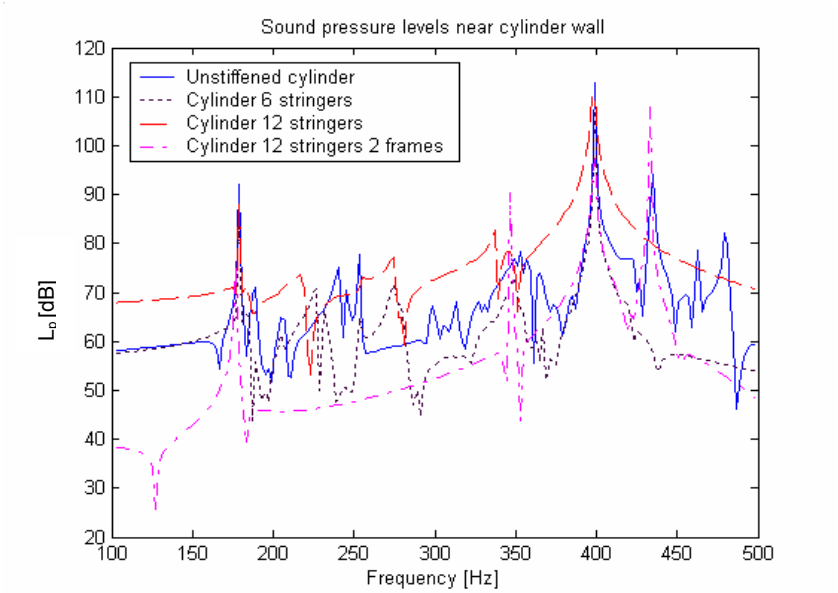

Figure 9.10: *Comparison of the numerically determined sound pressure levels in the frequency range of [100-500 Hz] for the non-stiffened cylinder and the cylinders stiffened with 6 and 12 stringers and the cylinder stiffened with 12 stringers and 2 frames.*

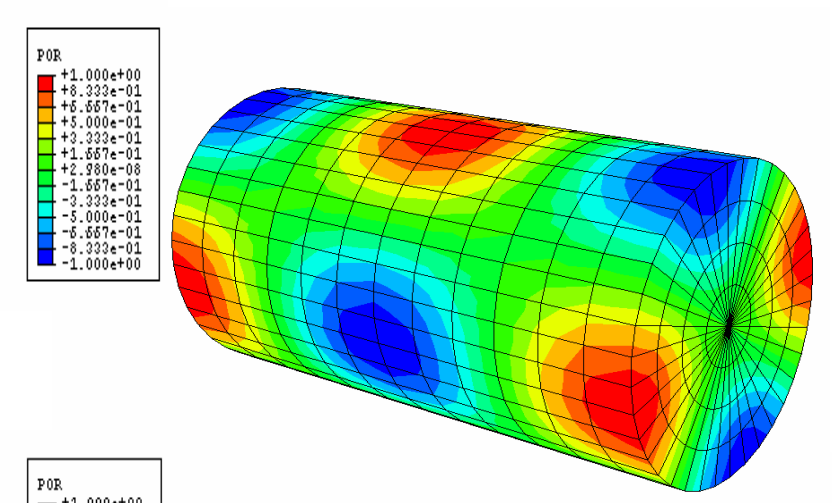

Figure H.2A: *Example of an acoustic mode at 726.82 Hz for the cylinders without frames.*

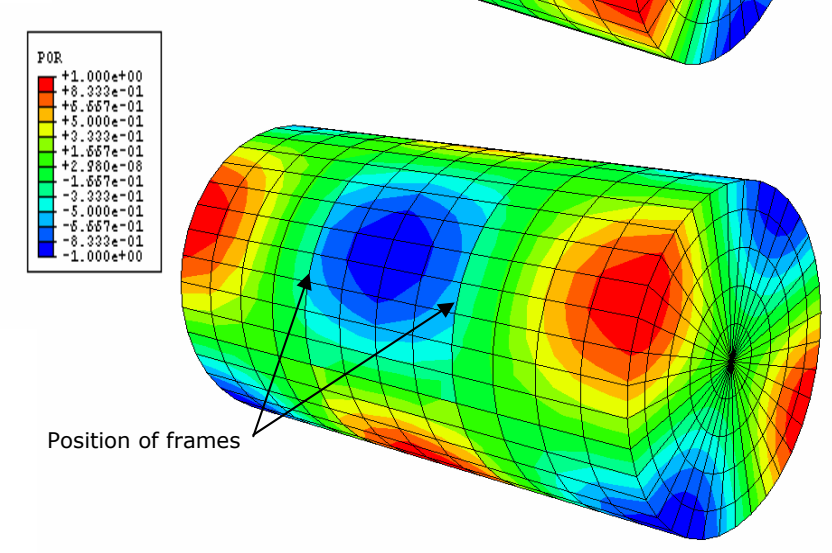

Figure H.2B: *Example of an acoustic mode at 724.08 Hz for the cylinder with 2 frames.*

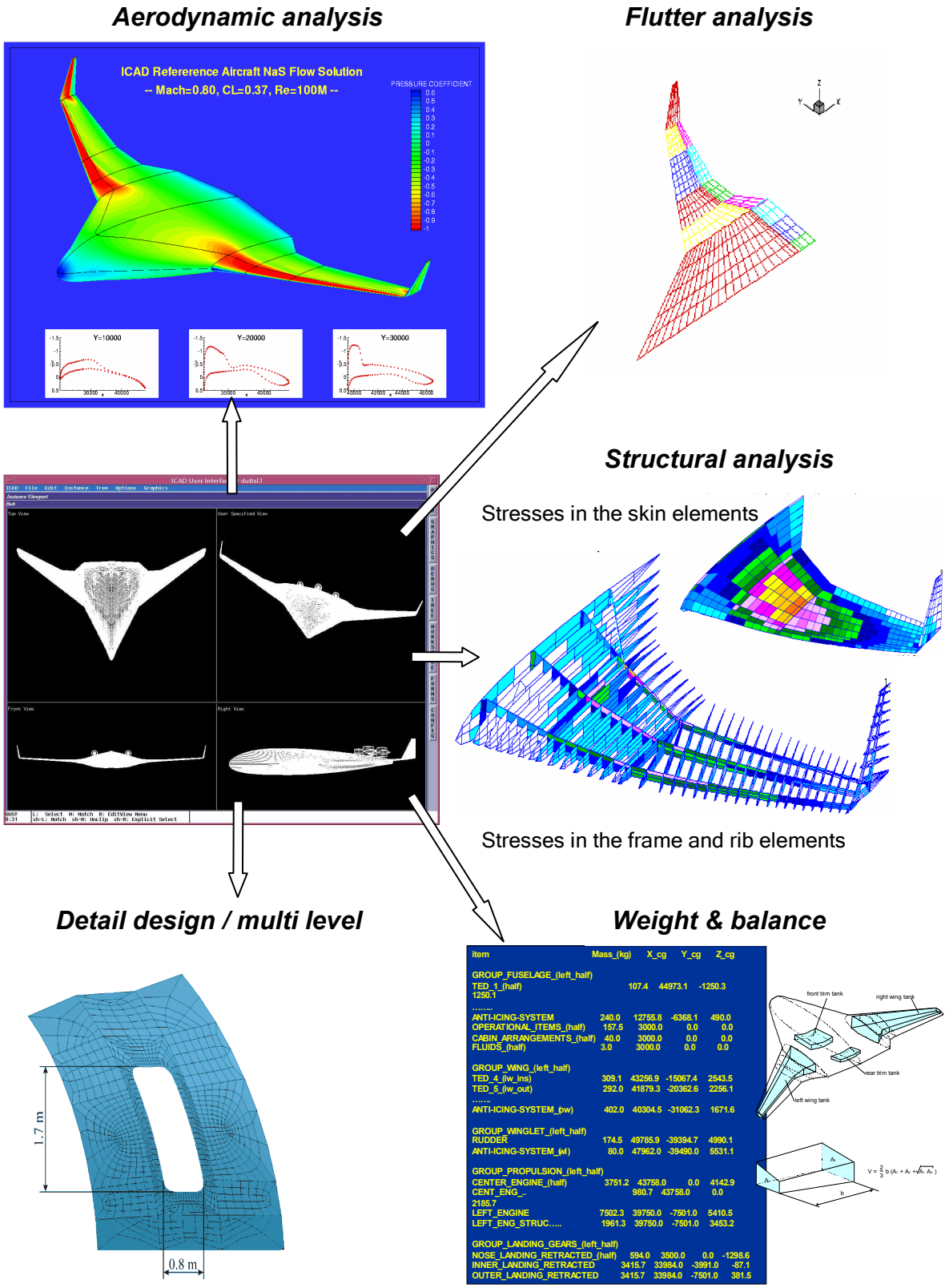

Figure 12.4: *Example of the aircraft DEE with the different disciplines; aerodynamics, structure, flutter, weight and balance and detailed design, which has been developed for the European research project MOB.*